



Cumhuriyet Science Journal
Faculty of Science, Cumhuriyet University
58140 - Sivas - Türkiye
Phone: +90(346) 487 13 72
Fax: +90(346) 219 11 86
e-mail: csj@cumhuriyet.edu.tr
<http://csj.cumhuriyet.edu.tr/en>
<http://dergipark.org.tr/en/pub/csaj>

Cumhuriyet Science Journal Vol: 43 No: 3 Year 2022

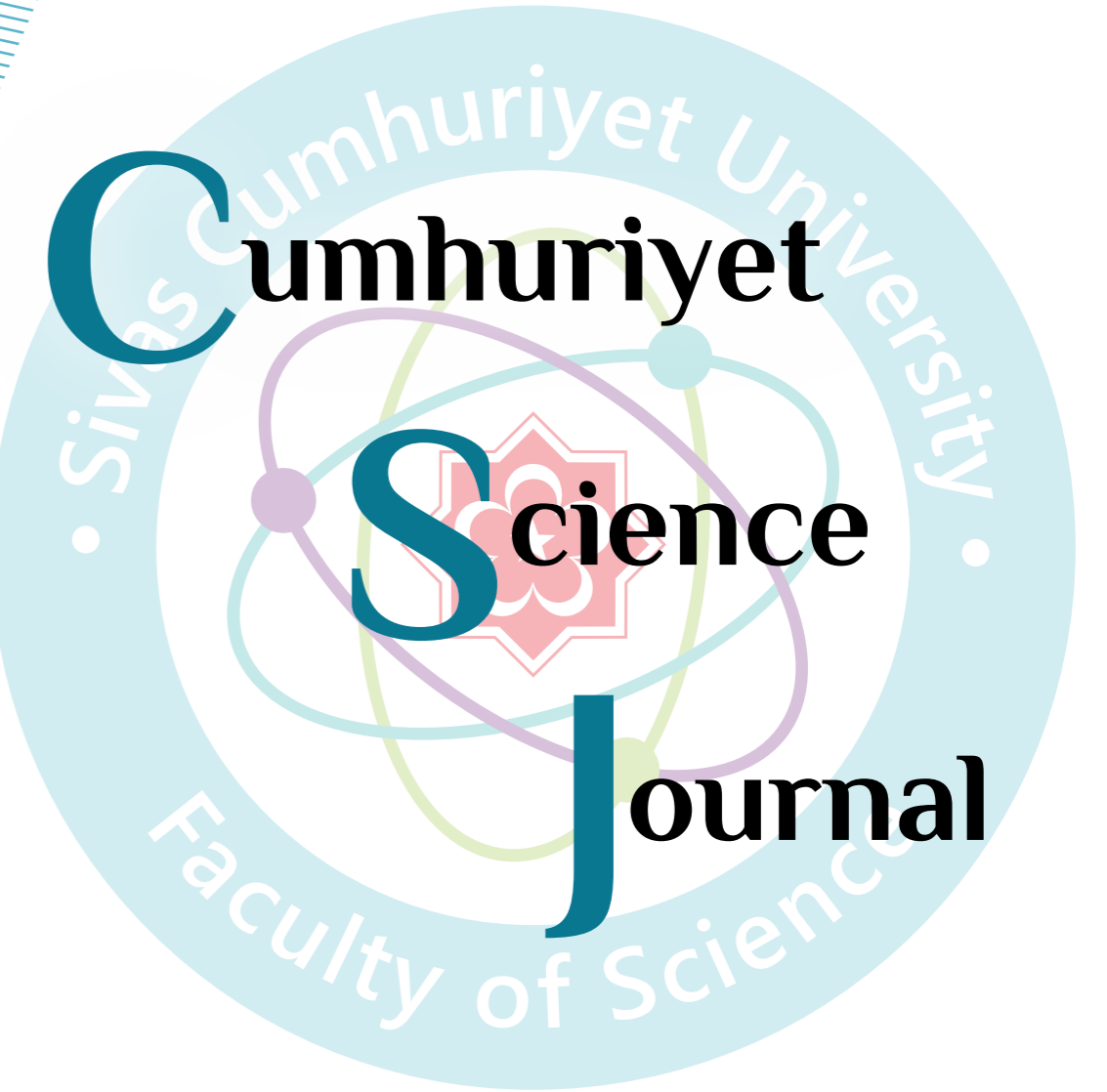


Sivas Cumhuriyet University

ISSN : 2680-2587

e-ISSN : 246-2587X

dergipark.org.tr/tr/pub/csaj
e-mail: csj@cumhuriyet.edu.tr



Cumhuriyet Science Journal (CSJ) is an official publication of Sivas Cumhuriyet University, Science Faculty. The high quality research papers related to the natural sciences are published as online four times a year. CSJ is an open access, free of charge journal and all articles in CSJ have undergone peer review and upon acceptance are immediately and permanently free for everyone to read and download.

Volume: 43

Number: 3

Year: 2022



ISSN:2587-2680
e-ISSN:2587-246X
Period:Quarterly
Founded:2002
Publisher:Sivas Cumhuriyet
University

Cumhuriyet Science Journal (CSJ)

Journal Previous Name: Cumhuriyet Üniversitesi Fen-Edebiyat Fakültesi Fen Bilimleri Dergisi

Old ISSN: 1300-1949

Owner on behalf of the Sivas Cumhuriyet University, Faculty of Science

Prof. Dr. İdris ZORLUTUNA (Sivas Cumhuriyet University)

Editor in Chief

Prof. Dr. İdris ZORLUTUNA (Sivas Cumhuriyet University)

Managing Editor

Assoc. Prof. Dr. Adil ELİK (Sivas Cumhuriyet University)

Editors

Prof. Dr. Baki KESKİN

bkeskin@cumhuriyet.edu.tr

Subjects: Mathematics and Statistics

Institution: Sivas Cumhuriyet University

Assoc. Prof. Dr. Adil ELİK

elik@cumhuriyet.edu.tr

Subjects: Chemistry and Chemical Engineering,
Environmental Sciences, Basic Sciences (General)

Institution: Sivas Cumhuriyet University

Prof. Dr. Nilüfer TOPSAKAL

ntopsakal@cumhuriyet.edu.tr

Subjects: Applied Mathematics

Institution: Sivas Cumhuriyet University

Prof. Dr. Serkan AKKOYUN

sakkoyun@cumhuriyet.edu.tr

Subjects: Physics and Physical Engineering

Institution: Sivas Cumhuriyet University

Prof. Dr. Halil İbrahim ULUSOY

hiulusoy@cumhuriyet.edu.tr

Subjects: Chemistry, Analytical Chemistry, Drug Analysis, Pharmacy

Institution: Sivas Cumhuriyet University

Prof. Dr. Fatih UNGAN

fungan@cumhuriyet.edu.tr

Subjects: Optics, Phonotics and Fiber optics

Institution: Sivas Cumhuriyet University

Assoc. Prof. Dr. Nail ALTUNAY

naltunay@cumhuriyet.edu.tr

Subjects: Bioanalytical Chemistry, Chemometric Analysis

Institution: Sivas Cumhuriyet University

Section Editors

Prof. Dr. Natalia BONDARENKO

bondarenkonp@info.sgu.ru

Subjects: Applied Mathematics and Physics

Institution: Samara University

Prof. Dr. Marcello LOCATELLI

marcello.locatelli@unich.it

Subjects: Analytical Chemistry

Institution: University "G. d'Annunzio" of Chieti-Pescara

Prof. Dr. Konstantin P. KATIN

kpkatin@yandex.ru

Subjects: Theoretical Chemistry, Computational design of nanostructures, nanodevices and nanotechnologies

Institution: National Research Nuclear University

Assoc. Prof. Dr. Duran KARAKAŞ

dkarakas@cumhuriyet.edu.tr

Subjects: Inorganic Chemistry, Theoretical Chemistry

Institution: Sivas Cumhuriyet University

Assoc. Prof. Dr. Yaşar ÇAKMAK

ycakmak@cumhuriyet.edu.tr

Subjects: Applied Mathematics

Institution: Sivas Cumhuriyet University

Assoc. Prof. Dr. Sevgi DURNA DAŞTAN

sdurna@cumhuriyet.edu.tr

Subjects: Molecular Biology

Institution: Sivas Cumhuriyet University

Assist. Prof. Dr. Yener ÜNAL

uyener@cumhuriyet.edu.tr

Subjects: Statistics

Institution: Sivas Cumhuriyet University

Abstracted&Indexing

ULAKBİM TR-Dizin

Index Copernicus (ICI Journals Master List)

Clarivate Analytics Zoological Record

Crossref

WorldCat

Akademik Dizin

Arastirmax Bilimsel Yayın İndeksi

Bielefeld Academic Search Engine (BASE)

Directory of Research Journal Indexing (DRJI)

Google Scholar

Research Gate

Idealonline

Editorial Board

Prof. Dr. Sezai ELAGÖZ (ASELSAN)
Prof. Dr. Mustafa SOYLAK (Erciyes University)
Prof. Dr. Chuan Fu Yang (Nanjing University of Science and Technology)
Prof. Dr. Münevver SÖKMEN (KGTU)
Prof. Dr. Hüseyin MERDAN (TOBB ETU)
Prof. Dr. Mehmet AKKURT (Erciyes University)
Prof. Dr. Mustafa KAVUTÇU (Gazi University)
Prof. Dr. Francois VOS (The University of Queensland)
Prof. Dr. Abuzar KABIR (International Forensic Research Institute)
Prof. Dr. Mustafa TÜZEN (GOP University)
Prof. Dr. Songül KAYA MERDAN (METU)
Prof. Dr. Jose Javier Valiente-Dobon (INFN-LNL, Padova University)
Prof. Dr. Yeşim SAĞ AÇIKEL (Hacettepe University)
Prof. Dr. Mehmet ŞİMŞİR (Sivas Cumhuriyet University)
Prof. Dr. Atalay SÖKMEN (KGTU)
Prof. Dr. Ricardo I. JELDRES (Universidad de Antofagasta)
Prof. Dr. Mustafa YILDIRIM (Sivas Cumhuriyet University)
Prof. Dr. Ali DELİCEOĞLU (Erciyes University)
Prof. Dr. Tuncay BAYRAM (Karadeniz Technical University)
Prof. Dr. Gökhan KOÇAK (Erciyes University)
Prof. Dr. Nadjat Laouet (Freres Mentouri Constantine-1 University)
Assoc. Prof. Dr. Savaş KAYA (Sivas Cumhuriyet University)

Layout Editors:

Lecturer Aykut HASBEK

Copyeditors:

Assist. Prof. Dr. Doğa Can SERTBAŞ
Assist. Prof. Dr. Hacı Ahmet KARADAŞ
Research Assistant Özgür İNCE

Proofreader:

Assist. Prof. Dr. Yener ÜNAL
Lecturer Aykut HASBEK

Publication Type: Peer Reviewed Journal

Cite Type: Cumhuriyet Sci. J.

Contact Information

Faculty of Science Cumhuriyet University
58140 Sivas- TURKEY
Phone: +90 (346) 487 13 72
Fax: +90 (346) 219 11 86
e-mail: csj@cumhuriyet.edu.tr
<http://dergipark.gov.tr/csj>

CONTENTS			PAGES
1	Mehmet SARİMAHMUT, Sindi VEKSHARİ, Merve DEMİRBAG KARAALİ, Serap CELİKLER <i>In vitro Evaluation of Antigenotoxic Effects of Phloridzin</i>	Research Article	358 - 364
2	Serife CAN CAKA, Pınar ÖZTOPCU VATAN, Selda KABADERE, Mustafa YAMAÇ, Ruhi UYAR <i>Determination of Antiproliferative Effects of Exopolysaccharides from Six Mushroom Species on Glioma Cells</i>	Research Article	365 - 369
3	Ayşe KARA, Ömer Faruk ALGUR, Ahmet MAVİ, Ali YILDIRIM, Meryem ŞENGÜL KÖSEOĞLU <i>Effects of Some Herbs on the In-vitro Growth of Helicobacter pylori and Their Antioxidant Properties</i>	Research Article	370 - 378
4	Cuneyt CESUR, Belgin COŞGE ŞENKAL, Tansu USKUTOĞLU <i>Fatty Acid Composition of Seed Oil from Cocklebur (Xanthium Strumarium Subsp. Strumarium) Grown in Turkey</i>	Research Article	379 - 383
5	Göknil COŞKUN, Akın AKLAMUZ, Ufuk İNCE, Mert ÜLGEN <i>Synthesis, Structure Elucidation and Biological Activity of New Hybrid Hydrazone-Amide Compounds</i>	Research Article	384 - 390
6	Mehmet Abdullah ALAGÖZ, İnci Selin DOĞAN, Sıla SENER, Zeynep ÖZDEMİR <i>Synthesis, Molecular Docking and Molecular Dynamics Simulation Studies of Some Pyridazinone Derivatives as Lipase Inhibitors</i>	Research Article	391 - 397
7	El Hassen MOKRANI, Amine ABDELAZIZ, Naamane AKAKBA, Soumia TENIOU, Rym Gouta DEMMAK, Abderrahmane BENSEGUENI <i>Molecular Docking and Drug-likeness Prediction of New Potent Tubulin Colchicine Binding Site Inhibitors for Potential Antitumor Drug</i>	Research Article	398 - 403
8	Bydaa ATRON, Hanaou AHAMADA, Ayşe Hümeýra TAŞKIN KAFA, Cem ÇELİK, Mürşit HASBEK <i>Antifungal and Antibiofilm Activities of Some Essential Oils Against Candida spp</i>	Research Article	404 - 408
9	Fatma KILIÇ DOKAN <i>Investigation of the Effect of Different Synthesis Methods on the Photocatalytic Activity of TiO₂: Comparison of Rutile and Anatase TiO₂</i>	Research Article	409 - 415
10	Ersen YILMAZ, Mehmet ATEŞ, Muhammed ERBAY <i>Green Synthesis of Gold Nanoparticles Using Aqueous Extract of Asphodelus Aestivus, Coating with Chitosan Biopolymer and Cytotoxicity Studies</i>	Research Article	416 - 422
11	Shwan AHMED, Aysel SARI <i>Serum Vitamin D Among Patients with Type 2 Diabetes Mellitus</i>	Research Article	423 - 431
12	Uğur TUTAR, Cem ÇELİK <i>Antibiofilm and Antimicrobial Properties of 1-allyl-3-(2-diisopropylaminoethyl) Benzimidazolium Chloride and its Silver(I)-NHC Complex</i>	Research Article	432 - 436
13	Eyüp BAŞARAN, Reşit ÇAKMAK, Ercan ÇINAR, Ozge CEVİK <i>Some Heterocyclic Hydrazone Compounds: Synthesis, Spectral Characterization and Anticancer Activity Study</i>	Research Article	437 - 442
14	Fikret YILMAZ, Semra ERGEN <i>Comparison of Oliver-Pharr and Work of Indentation Approach to Determine the Mechanical Properties of Melt-Spun Al-12%Wt.Si-0.5%Sb Alloy</i>	Research Article	443 - 448
15	Burcu ÇINARCI, Temha ERKOÇ <i>A Study On the Kernels of Irreducible Characters of Finite Groups</i>	Research Article	449 - 453
16	Ergin BAYRAM <i>Constant Mean Curvature Surfaces Along a Spacelike Curve</i>	Research Article	454 - 459
17	Pakize UYGUN <i>(k,μ)-Paracontact Manifolds and Their Curvature Classification</i>	Research Article	460 - 467

18	Sevil ÇULHA ÜNAL <i>Solutions of Time Fractional fKdV Equation Using the Residual Power Series Method</i>	Research Article	468 - 476
19	Fatih HEZENCİ <i>A Note on Fractional Midpoint Type Inequalities for Co-ordinated (s1, s2)-Convex Functions</i>	Research Article	477 - 491
20	Şerife YILMAZ <i>Robust Stability and Stable Member Problems for Multilinear Systems</i>	Research Article	492 - 496
21	Huriye KADAKAL <i>Generalization of Some Integral Inequalities for Arithmetic Harmonically Convex Functions</i>	Research Article	497 - 503
22	Neslihan SARIGÜL <i>Does Electron Spectrum Affect TLD-100 Dose Response in 6 MV Photon Beam Irradiation?</i>	Research Article	504 - 509
23	Mehpeyker KOCAKOÇ, Recep TAPRAMAZ <i>Rx, Ry and Rz Rotation Operators of Spin 4 Systems in Quantum Information Theory</i>	Research Article	510 - 514
24	Dilek TOKTAMIŞ <i>The Effect of Experimental Cycles on the Traps Depths of Dosimetric Traps of Natural Calcite Minerals</i>	Research Article	515 - 519
25	Hiwa Mohammad QADR <i>Investigation of Gamma Ray Buildup Factor for some Shielding Absorber</i>	Research Article	520 - 525
26	Ümit IŞIK, Uğur ÇEVİK, Dicle BAL AKKOCA, Kahraman OĞUZ, Nevzat DAMLA <i>Chemical and Radiological Characterizations of the Desert Dust Coming from Northern Africa to Batman (Southeastern Turkey)</i>	Research Article	526 - 533
27	Tenzile ERBAYRAM, Ümmügülsüm YILDIRIM, Yunus AKDOĞAN <i>A new Lifetime Distribution Based on the Transmuted First Two Lower Records</i>	Research Article	534 - 542
28	Hasan Aykut KARABOĞA, Serkan AKOGUL, İbrahim DEMİR <i>Classification of Students' Mathematical Literacy Score Using Educational Data Mining: PISA 2015 Turkey Application</i>	Research Article	543 - 549

In vitro Evaluation of Antigenotoxic Effects of Phloridzin

Mehmet Sarimahmut ^{1,a,*}, Sindi Vekshari ^{1,b}, Merve Demirbağ Karaali ^{1,c}, Serap Çelikler ^{1,d}

¹ Department of Biology, Faculty of Science and Arts, Bursa Uludağ University, Bursa, Türkiye

*Corresponding author

Research Article

History

Received: 14/12/2021

Accepted: 27/08/2022

Copyright



©2022 Faculty of Science,
Sivas Cumhuriyet University

ABSTRACT

Phytochemicals have a vast number of properties contributing to human health by acting on numerous different mechanisms. Phloridzin, a phytochemical mainly found in *Malus* species, possesses diverse biological activities including anti-diabetic and antioxidative activities. Here, our aim is to explore antigenotoxic potential and proliferative effects of phloridzin on human lymphocytes *in vitro* by employing chromosome aberration, micronucleus and comet assays. Mitomycin C, both an anticancer and genotoxic agent, was utilized to induce genotoxicity. Phloridzin significantly suppressed the genotoxic effects of mitomycin C at 125-500 µg/mL concentrations in all assays used ($p < 0.05$). We also revealed that phloridzin and mitomycin C combination had a significantly negative effect on mitotic index ($p < 0.05$), whereas in general, gender differences did not play a role in manifestation of neither antigenotoxic nor antiproliferative activities of the combination. These results suggest that phloridzin is an antigenotoxic compound and its consumption may interfere with the activity of anticancer drugs that exert their effects based on genotoxic mechanisms.

Keywords: Phloridzin, Genotoxicity, Mitomycin C, Chromosome aberration.

^a msarimahmut@uludag.edu.tr

^b <https://orcid.org/0000-0003-2647-5875>

^c mervedemirbag@gmail.com

^d <https://orcid.org/0000-0002-2874-0241>

^b sindiidnis01@gmail.com

^d <https://orcid.org/0000-0001-7975-3950>

^d scelikler@uludag.edu.tr

^d <https://orcid.org/0000-0002-4177-3478>

Introduction

Numerous plants have been used in the field of medicine for therapeutic purposes. For many decades, phytochemicals, bioactive components of plant origin, have been under investigation because of the beneficial effects in maintenance of human health [1]. Many studies report that a diet rich in phytochemicals is directly associated with reduced risk of chronic diseases including cancer [2-4].

Phloridzin, a phytochemical belonging to the group of dihydrochalcones, is the predominant phenolic compound in *Malus* species [5]. Phloridzin is formed by the glycosylation of phloretin and was detected in several other plants such as Australian native sarsaparilla (*Smilax glycyphylla*), sweet tea (*Lithocarpus polystachyus*), and at trace amounts in strawberry fruit [6-8]. Phloridzin is found at highest levels in seeds, moderate levels in core and the skin and lowest level in the cortex of apple fruits [9]. Phloridzin and its derivatives are renowned for their activity to inhibit sodium-linked glucose transporters which in turn lowers blood glucose levels [9]. Accordingly, numerous studies have been conducted to understand the significance of phloridzin in treating type 2 diabetes [10,11]. Moreover, phloridzin has been studied for antioxidative, anti-inflammatory, hepatoprotective and cardioprotective activities [12-15]. Although phloridzin has been examined for its biological activities from various aspects, antigenotoxic properties of this molecule have

not been studied so far. Our aim is to determine the potential genotoxic and antigenotoxic effects of phloridzin *in vitro* in human lymphocytes by employing chromosome aberration test, micronucleus and comet assays.

Materials and Methods

Chemicals and Lymphocyte Culture

Phloridzin (catalogue number PHL80513) was purchased from Merck, Germany. Phloridzin was dissolved in ethanol and diluted with distilled H₂O. The stock solution was kept at -20°C for further use. Mitomycin C (MMC) was purchased from Kyowa Hakko Kogyo, Japan and its stock solution was freshly prepared at 250 µg/mL concentration before each experiment. MMC was diluted 1:1000 upon addition to lymphocyte culture to a final concentration of 0.25 µg/mL.

Lymphocyte culture was set up by adding 0.5 mL of heparinized blood to 5 mL of RPMI 1640 medium (Sigma, St. Louis, MO, USA) supplemented with 20% fetal calf serum (Biochrom, AG), 1% penicillin/streptomycin (Merck, Darmstadt, Germany), 2% L-Glutamine (Merck, Darmstadt, Germany) and 2 to 10 µg/mL concentration of phytohemagglutinin (Biochrom AG, Germany). The culture media was stored at -20°C.

Human peripheral blood lymphocytes were obtained from 2 female and 2 male healthy, non-smoking

volunteers with no recent history of medication. Peripheral blood samples (5 mL) were collected under sterile conditions by venipuncture into heparinized tubes. Whole blood (0.5 mL) was then added to 5 mL culture medium and incubated at 37°C.

Ethanol was used as solvent control (1:1000). Phloridzin concentrations were determined as 125, 250 and 500 µg/mL after a preliminary study. All phloridzin doses were used in simultaneous combinations with a single dose of MMC (0.25 µg/mL) [16]. Treatments started 48 h (24 h for comet assay) after the beginning of incubation at 37°C. Lymphocyte cultures were treated with phloridzin and/or MMC for 24 h before harvest in all assays.

Chromosome Aberration (CA) Test

Briefly, 2 h prior to harvesting, 50 µl of demecolcine (10 µg/mL) was added to each culture medium. The cells were incubated with a hypotonic solution (0.075 M KCl) and then fixed in cold methanol:glacial acetic acid (3:1). Following a series of 3 washing steps with the fixative, metaphase spreads were prepared by dropping the concentrated cell suspension onto ice-cold slides. Air-dried slides were stained with Giemsa (pH 6.8) stain for 15 min and examined under a light microscope. A total of well-spread, 100 metaphases were scored in each group for CA analysis and the frequency of CA per cell was recorded. The CAs were scored according to Environmental Health Criteria 51 for short-term tests for mutagenic and carcinogenic chemicals [17]. Mitotic index (MI) was calculated according to following formula:

$$MI = (\text{number of cells in mitosis} / \text{total number of cells}) \times 100.$$

Micronucleus (MN) Assay

The assay was carried out as described by Fenech and Morley [18] with minor modifications. Cytochalasin B (6 µg/mL) was added at 44 h to block cytokinesis. Lymphocyte cultures were harvested after 72 h. MN value was scored as the frequency of binucleated lymphocytes containing MN per 1000 binucleated cells. Nuclear division index (NDI) was calculated among the 500 lymphocytes that were scored in MN assay according to the following equation:

$$NDI = (\text{MONO} + (2 \times \text{BN}) + (3 \times \text{TRI}) + (4 \times \text{TETRA})) / 500.$$

Here, MONO, BN, TRI and TETRA depict the number of mononucleated, binucleated, trinucleated and tetranucleated lymphocytes, respectively.

Comet Assay

Alkaline single cell gel electrophoresis was carried out according to the procedure originally developed by Singh et al. [19] with minor modifications. Shortly, the cells were centrifuged at 500 rpm for 4 min at the end of treatment. Subsequently, the cells were suspended with pre-warmed 100 µl low melting agarose and immediately pipetted onto slides precoated with normal melting agarose. Then the slides were immersed in cold lysis buffer (2.5 M NaCl, 100 mM Na₂EDTA, 10 mM Tris, 1% Triton X-100 and 10%

DMSO) and kept overnight in the dark at 4°C. The slides were then placed in an alkaline electrophoresis buffer (300 mM NaOH and 1 mM Na₂EDTA; pH > 13) and the embedded cells were exposed to this alkali solution for 15 min to allow for DNA unwinding.

Electrophoresis was performed at 0.75 V/cm (25 V, 300 mA) for 25 min. After electrophoresis, the slides were neutralized with 0.4 M Tris at pH 7.5. The slides were stained with ethidium bromide (2 µg/mL) and 100 cells per group were examined under a microscope with fluorescence attachment (Novel N-800M). Imaging was performed by using software (Kameram 21, Argenit, Istanbul). Comet tail length, tail DNA %, Olive tail moment, percentage of damaged cells (PDC) and DNA damage index (DDI) parameters were evaluated for each cell. DDI was calculated according to the following formula [20]:

$$DDI = (1 \times \Sigma \text{Type1}) + (2 \times \Sigma \text{Type2}) + (3 \times \Sigma \text{Type3}) + (4 \times \Sigma \text{Type4}) / (\Sigma \text{Type0} + \Sigma \text{Type1} + \Sigma \text{Type2} + \Sigma \text{Type3} + \Sigma \text{Type4})$$

PDC was calculated according to the following formula [20]:

$$\% \text{ Damaged Cells} = \Sigma \text{Type2} + \Sigma \text{Type3} + \Sigma \text{Type4}$$

Statistical Analysis

All statistical analyses were performed using the SPSS 23.0 statistical software for Windows. Results were expressed as mean ± standard deviation. Kolmogorov-Smirnov normality test was applied to evaluate the distribution characteristics of the variables. Parametric one-way analysis of variance (ANOVA) or non-parametric Kruskal-Wallis analyses were selected throughout the study depending on the normality test results. Intergroup differences were determined by Tukey HSD or Tamhane's T2 post hoc tests following one-way ANOVA analysis. Paired sample *t*-tests were employed to determine whether there was a significant difference between genders in each treatment group in all assays. Two-sided *p* < 0.05 was considered to be statistically significant.

Results

Potential Genotoxic and Antigenotoxic Effects of Phloridzin

Mean frequencies of observed chromosome gaps, breaks, rings, exchanges and the total number of CAs per cell were given in Table 1. Phloridzin alone caused a statistically significant increase in total CA frequencies compared to solvent control group at 500 µg/mL concentration (*p* < 0.05). Mean value for total CA aberration per cell in MMC treatment group was slightly higher than that of control groups, but the difference was not significant (*p* > 0.05). On the other hand, significantly elevated total CA frequencies were detected in all combination treatments in contrast to negative and solvent controls, and also compared to MMC treatment alone (*p* < 0.05). Fig. 1A displays the results of total CA frequencies by gender. In general, there were no significant differences between genders across all treatment groups (*p* > 0.05) except MMC and 500 µg/mL phloridzin combination (*p* < 0.05).

Table 1. CA and MI values of lymphocyte cultures treated with phloridzin and/or MMC.

Dose ($\mu\text{g/mL}$)	N ^b	Chromosome Gap (%)	Chromosome Breakage (%)	Chromosome Ring (%)	Chromosome Exchange (%)	Total Aberration / Cell	MI (%)
NC	4	0.56 \pm 0.06	0.45 \pm 0.09	0.03 \pm 0.01	1.24 \pm 0.43	0.57 \pm 0.12	5.91 \pm 1.26
SC	4	0.63 \pm 0.18	0.58 \pm 0.04	0.11 \pm 0.02 ^c	1.47 \pm 0.60	0.70 \pm 0.17	6.55 \pm 0.04
125 $\mu\text{g/mL}$ Phl ^a	4	1.09 \pm 0.18	0.45 \pm 0.04	0.13 \pm 0.01 ^c	2.63 \pm 0.87	1.08 \pm 0.24	6.80 \pm 0.83
250 $\mu\text{g/mL}$ Phl	4	1.33 \pm 0.04 ^c	0.75 \pm 0.06	0.05 \pm 0.02	2.97 \pm 1.26	1.28 \pm 0.32 ^c	7.12 \pm 0.93
500 $\mu\text{g/mL}$ Phl	4	1.39 \pm 0.28	0.87 \pm 0.23 ^c	0.12 \pm 0.04	4.39 \pm 1.08 ^{cf}	1.70 \pm 0.38 ^{cd}	7.73 \pm 0.85
MMC	4	1.03 \pm 0.56	0.81 \pm 0.25	0.07 \pm 0.01 ^c	1.89 \pm 1.03	0.95 \pm 0.45	5.26 \pm 0.81
MMC + 125 $\mu\text{g/mL}$ Phl	4	1.49 \pm 0.14 ^{cd}	1.10 \pm 0.26 ^{cd}	0.15 \pm 0.03	5.55 \pm 0.92 ^{cde}	2.07 \pm 0.26 ^{cde}	2.40 \pm 0.74 ^{cd}
MMC + 250 $\mu\text{g/mL}$ Phl	4	1.73 \pm 0.18 ^{cd}	1.11 \pm 0.03 ^{cd}	0.13 \pm 0.06	5.67 \pm 0.7 ^{cde}	2.16 \pm 0.19 ^{cde}	2.60 \pm 1.27 ^{cde}
MMC + 500 $\mu\text{g/mL}$ Phl	4	1.65 \pm 0.14 ^{cd}	0.91 \pm 0.15 ^c	0.13 \pm 0.03	5.99 \pm 0.59 ^{cde}	2.17 \pm 0.16 ^{cde}	2.23 \pm 0.98 ^{cde}

MI: Mitotic index; NC: Negative control; SC: Solvent control; a: Phloridzin; b: Number of donors; c: $p < 0.05$ compared to negative control; d: $p < 0.05$ compared to solvent control; e: $p < 0.05$ compared to MMC alone.

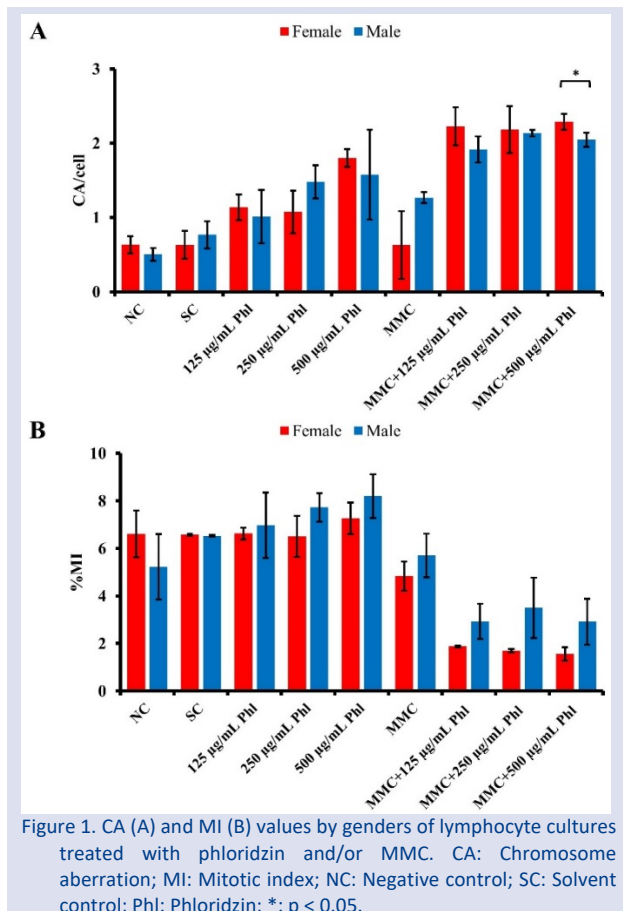


Figure 1. CA (A) and MI (B) values by genders of lymphocyte cultures treated with phloridzin and/or MMC. CA: Chromosome aberration; MI: Mitotic index; NC: Negative control; SC: Solvent control; Phl: Phloridzin; *: $p < 0.05$.

The mean MN (%) frequencies scored in four donors were given in Table 2. Phloridzin treatments alone did not cause a significant MN formation compared to solvent control at all doses ($p > 0.05$). MMC treatment alone induced MN induction approximately 4 to 7-fold compared to control groups ($p < 0.05$, Table 2). In contrast, MMC combination with phloridzin (125-500 $\mu\text{g/mL}$) resulted in significantly diminished MN frequencies ($p < 0.05$, Table 2 and Fig. 2A). The effectiveness of phloridzin in MMC induced MN reduction was more evident at higher doses. MN frequencies by genders in response to treatments were presented in Fig. 2A. The findings reveal that there is no significant difference in MN frequencies across genders in treatment groups ($p > 0.05$). A significant difference between genders was detected in negative control group ($p < 0.05$); however, that difference did not appear in solvent control group.

Table 2. MN and NDI values of lymphocyte cultures treated with phloridzin and/or MMC.

Dose ($\mu\text{g/mL}$)	N ^b	NDI	MN (%)
NC	4	2.72 \pm 0.61	4.08 \pm 3.42
SC	4	2.79 \pm 0.64	7.87 \pm 2.17
125 $\mu\text{g/mL}$ Phl ^a	4	2.77 \pm 0.93	10.07 \pm 0.59
250 $\mu\text{g/mL}$ Phl	4	3.65 \pm 0.24	13.59 \pm 2.60 ^c
500 $\mu\text{g/mL}$ Phl	4	3.19 \pm 0.70	11.34 \pm 1.07
MMC	4	2.55 \pm 0.19	28.85 \pm 7.72 ^{cd}
MMC + 125 $\mu\text{g/mL}$ Phl	4	3.31 \pm 0.09	9.30 \pm 1.81 ^e
MMC + 250 $\mu\text{g/mL}$ Phl	4	2.52 \pm 0.21	4.44 \pm 5.42 ^e
MMC + 500 $\mu\text{g/mL}$ Phl	4	2.95 \pm 0.26	5.54 \pm 1.92 ^e

NDI: Nuclear division index; MN: Micronucleus; NC: Negative control; SC: Solvent control; a: Phloridzin; b: Number of donors; c: $p < 0.05$ compared to negative control; d: $p < 0.05$ compared to solvent control; e: $p < 0.05$ compared to MMC alone.

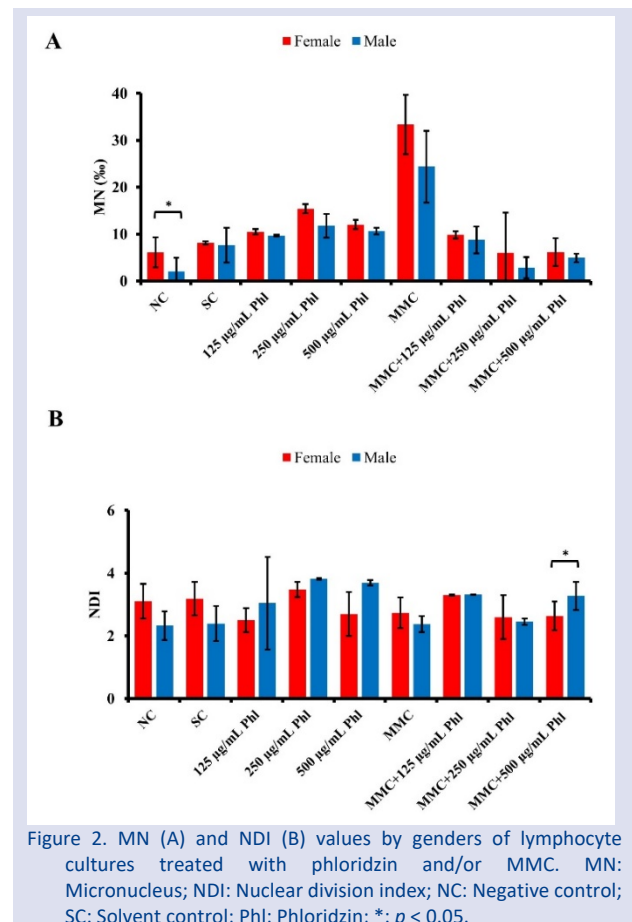


Figure 2. MN (A) and NDI (B) values by genders of lymphocyte cultures treated with phloridzin and/or MMC. MN: Micronucleus; NDI: Nuclear division index; NC: Negative control; SC: Solvent control; Phl: Phloridzin; *: $p < 0.05$.

The findings of comet assay were expressed as the changes in the comet tail length, percentage of DNA in tail, Olive tail moment, DDI and PDC (Table 3). There were no

significant changes detected among any of the comet parameters compared to solvent control ($p > 0.05$) after phloridzin treatment except an increase in tail DNA percentage at 500 $\mu\text{g}/\text{mL}$ concentration ($p < 0.05$). MMC dramatically raised the values of all DNA damage associated comet parameters ($p < 0.05$). On the other hand, when phloridzin was used in combination with MMC, it significantly suppressed the DNA damage induced by MMC at all doses ($p < 0.05$). Moreover, both 125 and 250 $\mu\text{g}/\text{mL}$ concentrations were effective in suppressing the DNA damage to the level observed in the

control groups. Only combination treatment with 500 $\mu\text{g}/\text{mL}$ phloridzin induced DNA damage at a level that is both significantly higher than solvent control and lower than MMC alone according tail DNA % and PDC values ($p < 0.05$). The effects of gender differences on DDI and PDC were represented in Fig. 3A and B, respectively. In the context of gender differences in response to treatments, there was no significant change between genders in DDI and PDC values ($p > 0.05$) apart from the DDI values after 500 $\mu\text{g}/\text{mL}$ phloridzin treatment ($p < 0.05$).

Table 3. DDI and PDC values after comet assay of lymphocyte cultures treated with phloridzin and/or MMC.

Dose ($\mu\text{g}/\text{mL}$)	N ^b	Tail length (μm)	Tail DNA (%)	Olive tail moment	DDI	PDC
NC	4	3.13 \pm 0.49	2.09 \pm 0.28	0.20 \pm 0.03	0.12 \pm 0.03	0.01 \pm 0.01
SC	4	3.30 \pm 0.21	1.56 \pm 0.68	0.20 \pm 0.11	0.11 \pm 0.06	0.01 \pm 0.01
125 $\mu\text{g}/\text{mL}$ Phl ^a	4	3.21 \pm 0.35	2.46 \pm 0.28	0.37 \pm 0.09	0.21 \pm 0.04	0.03 \pm 0.01
250 $\mu\text{g}/\text{mL}$ Phl	4	3.34 \pm 1.48	2.07 \pm 0.51	0.29 \pm 0.23	0.16 \pm 0.08	0.01 \pm 0.01
500 $\mu\text{g}/\text{mL}$ Phl	4	4.23 \pm 0.45	3.37 \pm 0.14 ^d	0.38 \pm 0.18	0.18 \pm 0.07	0.02 \pm 0.02
MMC	4	5.30 \pm 1.09 ^{cd}	4.92 \pm 1.13 ^{cd}	0.70 \pm 0.20 ^{cd}	0.55 \pm 0.16 ^{cd}	0.13 \pm 0.04 ^{cd}
MMC + 125 $\mu\text{g}/\text{mL}$ Phl	4	2.65 \pm 0.97 ^e	2.33 \pm 0.70 ^e	0.23 \pm 0.04 ^e	0.15 \pm 0.04 ^e	0.01 \pm 0.01 ^e
MMC + 250 $\mu\text{g}/\text{mL}$ Phl	4	3.09 \pm 0.54 ^e	2.58 \pm 0.48 ^e	0.26 \pm 0.08 ^e	0.17 \pm 0.08 ^e	0.03 \pm 0.03 ^e
MMC + 500 $\mu\text{g}/\text{mL}$ Phl	4	2.67 \pm 0.25 ^e	3.00 \pm 0.42 ^{de}	0.36 \pm 0.12 ^e	0.25 \pm 0.05 ^e	0.05 \pm 0.01 ^{de}

DDI: DNA damage index; PDC: percentage of damaged cells; NC: Negative control; SC: Solvent control; a: Phloridzin; b: Number of donors; c: $p < 0.05$ compared to negative control; d: $p < 0.05$ compared to solvent control; e: $p < 0.05$ compared to MMC alone.

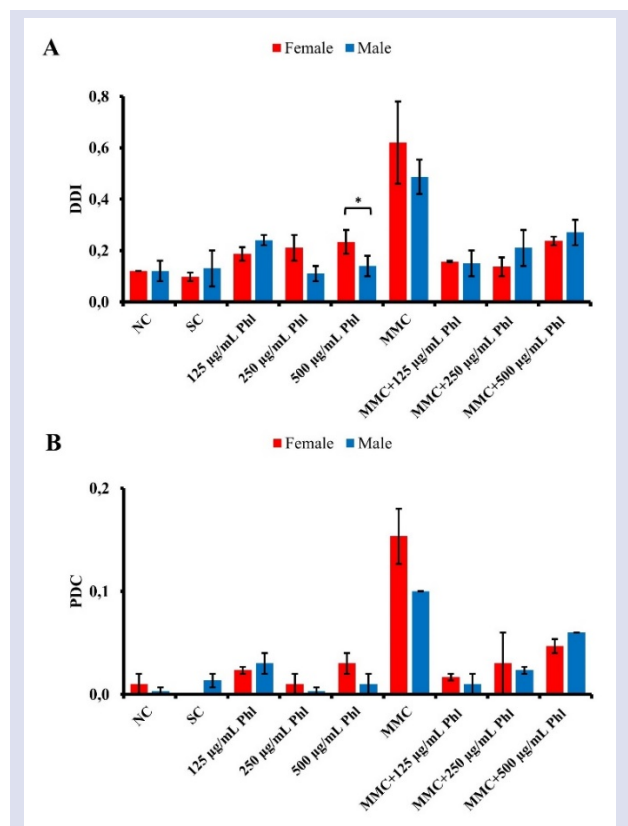


Figure 3. DDI (A) and PDC (B) values by genders after comet assay of lymphocyte cultures treated with phloridzin and/or MMC. DDI: DNA damage index; PDC: percentage of damaged cells; NC: Negative control; SC: Solvent control; Phl: Phloridzin; *: $p < 0.05$.

Effect of Phloridzin on Proliferative Activity

Change in MI values is presented in Table 1 and Fig. 1B. Phloridzin alone heightened MI values compared to control groups at all concentrations ($p > 0.05$). However, MMC alone decreased MI value compared to control groups ($p > 0.05$). Interestingly, all of the MMC and phloridzin combination treatments resulted in a remarkable decrease in MI values compared to both control groups and MMC treatment alone ($p < 0.05$, Table 1). When gender differences in response to treatments were examined, there were no significant differences throughout all of the treatments, but of note, female group suffered a steeper decline in MI after combination treatments ($p > 0.05$, Fig. 1B).

NDI remained more or less the same in all treatment groups compared to solvent control (Table 2). Data displayed in Fig. 2B on gender differences in response to treatments of phloridzin and/or MMC were analogous to those presented in Table 2. There was a statistically significant difference between male and female groups only in MMC and 500 $\mu\text{g}/\text{mL}$ phloridzin combination ($p < 0.05$, Fig. 2B).

Discussion

Phytochemicals have been utilized for both their therapeutic and preventive characteristics in traditional and modern medicine [21]. Also, research suggests that apple consumption is involved in lowering the risk of severe chronic diseases in general [22]. Thus, it becomes

meaningful to intensify the research on elucidating the phytochemicals responsible for the aforementioned effects in order to maximize health benefits. High phytochemical content provides apple with its antioxidant properties and the consumption of apple juice is reported to have antigenotoxic potential [23]. Apple is rich in phloridzin that is mainly found in *Malus* species [24]. Therefore, we investigated the potential genotoxic and antigenotoxic effects of phloridzin *in vitro* in human lymphocytes by employing several genotoxicity assays.

Slightly increased values of total CA, MN, DDI and PDC in almost all selected doses of phloridzin suggest that this molecule might have genotoxic effects above a certain threshold concentration. This observation becomes more pronounced when 500 µg/mL phloridzin treatment is considered since it led to significant increase in total CA per cell and tail DNA % parameters compared to solvent control ($p < 0.05$). Phenolic compounds such as curcumin, vanillic acid and vitamin C at certain concentrations might be regarded as other examples for a phytochemical to exert genotoxic effects alone [25-27]. This phenomenon was also observed when Fox et al. [28] employed a novel cell based ATAD-5 luciferase assay to detect genotoxic compounds and identified resveratrol, genistein and baicalein as DNA damage inducers. Moreover, Lu [29] et al. showed that epigallocatechin gallate, an exemplary antioxidant found in green tea, induced DNA damage via interaction of its weakly-bound electrons with DNA bases (especially guanine) through a reductive mechanism. Therefore, it is crucial to acknowledge that while antioxidants can minimize the detrimental effects of ROS, they alone may have the capability to induce DNA damage at certain concentrations.

In our study, MMC was selected as a genotoxic agent as it generates oxidative stress and induces DNA damage via DNA alkylation [30]. As expected, MMC treatment resulted in increased genotoxic effects in all genotoxicity assays (Tables 1-3). Combination of phloridzin with MMC mitigated the genotoxic activity of this agent significantly in all assays regardless of the selected phloridzin concentration ($p < 0.05$, Tables 1-3). The extent to which phloridzin mitigated genotoxic effects caused by MMC varied between the assays used. In both MN and comet assays, DNA damage was suppressed to the level observed in the control groups (Tables 2 and 3). However, phloridzin was not as effective in mitigating the genotoxic effects as it was in MN and comet assays at reducing CAs. The resulting total CAs per cell after MMC and phloridzin combinations were significantly higher than that of solvent control ($p < 0.05$, Table 1). This difference can be examined by looking further into the applied methods. CA presence is acknowledged as an evidence of major structural and/or numerical aberrations at chromosomal level [31]. Other types of CAs—chromosome or chromatid gaps and breaks arise from unrepaired double strand DNA damage whereas chromosome rings and exchanges originate from mis-repaired DNA damage [32]. In contrast, MN originates from whole or acentric chromosome fragments which manifests genomic instability at chromosomal level caused by not only DNA damage, but also distortions in components of mitotic apparatus such as mitotic spindle or centrosomes [33]. Comet

assay focuses on analysis of repairable DNA damage whether it is a single- or double-strand breakage, but this test is unable to give information at chromosomal level such as in CA and MN [34]. Therefore, the differences in our results can be explained by the fact that CA, MN and comet assays measure the genotoxic effect of an agent indirectly in different manners and due to the different evaluation sensitivity of the assays. Limited observation of significant change involving gender differences in response to treatments suggests that phloridzin genotoxicity or antigenotoxicity is not dependent upon gender.

Antigenotoxic effects of phloridzin can be attributed to its antioxidative properties of harboring free radical scavenging activities and inhibitory action against lipid peroxidation [35]. Furthermore, similar studies have demonstrated that phloridzin was responsible in reducing the amount of potentially genotoxic substances such as heterocyclic amines found in processed foods and reactive carbonyl species generated under oxidative stress [36,37].

From MI and NDI analyses, it seems in general that phloridzin alone has a positive impact on cell proliferation in an insignificant manner. In addition, proliferative effects of phloridzin on keratinocyte cultures was demonstrated in another study [38]. Phloridzin and MMC combination led to a significant decrease in MI values ($p < 0.05$, Table 1) and somewhat increased NDI values (Table 2). There are several studies in the literature exemplifying that MI and NDI values were not affected in the same manner. For instance, acacia honey and food additives monopotassium glutamate and magnesium diglutamate were found to decrease MI values, but not significantly affect NDI values which are in correlation with our findings [39,40]. MI and NDI values following phloridzin and its combination treatments did not differ between genders considerably except at 500 µg/mL phloridzin and MMC combination (Fig. 2B). Overall, the lack of gender differences in response to treatments suggests that proliferative effects of phloridzin is independent from gender.

To conclude, our study has demonstrated that phloridzin is able to inhibit genotoxic effects of antineoplastic agent, MMC. It is also noticeable that phloridzin has reduced the proliferation of lymphocytes when used in combination with MMC. In general, gender differences did not take part in how phloridzin induced genotoxic and proliferative effects whether it is used alone or in combination with MMC. As a result, the ability of phloridzin to interfere with the action of MMC and possibly with other DNA damaging agents suggests that caution should be exercised when phloridzin is consumed together with chemotherapeutic agents.

Acknowledgment

The authors would like to thank Ahmet Sari Mahmout for English editing and proofreading of the manuscript.

Conflicts of interest

The authors report no conflict of interest.

References

- [1] Zhang L., Virgous C., Si H., Synergistic anti-inflammatory effects and mechanisms of combined phytochemicals, *J. Nutr. Biochem.*, 69 (2019) 19–30.
- [2] Chikara S., Nagaprasanthan L.D., Singhal J., Horne D., Awasthi S., Singhal S.S., Oxidative stress and dietary phytochemicals: Role in cancer chemoprevention and treatment, *Cancer Lett.*, 413 (2018) 122–134.
- [3] Zhang Y.J., Gan R.Y., Li S., Zhou Y., Li A.N., Xu D.P., Li H.B., Antioxidant phytochemicals for the prevention and treatment of chronic diseases, *Molecules*, 20 (12) 2015 21138–21156.
- [4] Dembinska-Kiec A., Mykkänen O., Kiec-Wilk B., Mykkänen H., Antioxidant phytochemicals against type 2 diabetes, *Br. J. Nutr.*, 99 (E-S1), 2008, ES109–ES117.
- [5] Gosch C., Halbwirth H., Stich K., Phloridzin: biosynthesis, distribution and physiological relevance in plants, *Phytochemistry*, 71 (2010) 838–843.
- [6] Hilt P., Schieber A., Yildirim C., Arnold G., Klaiber I., Conrad J., Beifuss U., Carle R., Detection of phloridzin in strawberries (*Fragaria x ananassa* Duch.) by HPLC–PDA–MS/MS and NMR spectroscopy, *J. Agric. Food. Chem.*, 51 (2003) 2896–2899.
- [7] Cox S.D., Jayasinghe K.C., Markham J.L., Antioxidant activity in Australian native sarsaparilla (*Smilax glycyphylla*), *J. Ethnopharmacol.*, 101 (2005) 162–168.
- [8] Dong H., Ning Z., Yu L., Li L., Lin L., Huang J., Preparative separation and identification of the flavonoid phlorhizin from the crude extract of *Lithocarpus polystachyus* Rehd, *Molecules*, 12 (2007) 552–562.
- [9] Baldissarroto A., Malisardi G., Scalambra E., Andreotti E., Romagnoli C., Vicentini C.B., Manfredini S., Vertuani S., Synthesis, antioxidant and antimicrobial activity of a new phloridzin derivative for dermo-cosmetic applications, *Molecules*, 17 (11) (2012) 13275–13289.
- [10] Ehrenkranz J.R., Lewis N.G., Kahn C.R., Roth J., Phlorizin: A review, *Diabetes Metab. Res. Rev.*, 21 (2005) 31–38.
- [11] David-Silva A., Esteves J.V., Morais M.R.P., Freitas H.S., Zorn T.M., Correa-Giannella M.L., Machado U.F., Dual SGLT1/SGLT2 inhibitor phlorizin ameliorates non-alcoholic fatty liver disease and hepatic glucose production in type 2 diabetic mice, *Diabetes Metab. Syndr. Obes.*, 13 (2020) 739–751.
- [12] Rezk B.M., Haenen G.R., van der Vijgh W.J., Bast A., The antioxidant activity of phloretin: the disclosure of a new antioxidant pharmacophore in flavonoids, *Biochem. Biophys. Res. Commun.*, 295 (1) (2002) 9–13.
- [13] Chang W.T., Huang W.C., Liou C.J., Evaluation of the anti-inflammatory effects of phloretin and phlorizin in lipopolysaccharide-stimulated mouse macrophages, *Food Chem.*, 134 (2) (2012) 972–979.
- [14] Hirose M., Shibasaki T., Nakada T., Kashihara T., Yano S., Okamoto Y., Isaji M., Matsushita N., Taira E., Yamada M., Phlorizin prevents electrically-induced ventricular tachyarrhythmia during ischemia in langendorff-perfused guinea-pig hearts, *Biol. Pharm. Bull.*, 37 (7) (2014) 1168–1176.
- [15] Khalifa M.M., Bakr A.G., Osman A.T., Protective effects of phloridzin against methotrexate-induced liver toxicity in rats, *Biomed. Pharmacother.*, 95 (2017) 529–535.
- [16] Kaya F.F., Topaktaş M., Genotoxic effects of potassium bromate on human peripheral lymphocytes in vitro, *Mutat. Res. - Genet. Toxicol. Environ. Mutagen.*, 626 (1–2) (2007) 48–52.
- [17] IPCS, Guide to Short Term Tests for Detecting Mutagenic and Carcinogenic Chemicals, Geneva: World Health Organization, (1985).
- [18] Fenech M., Morley A.A., Measurement of micronuclei in lymphocytes, *Mutat. Res. Genet. Toxicol. Environ. Mutagen.*, 147(1–2) (1985) 29–36.
- [19] Singh N.P., McCoy M.T., Tice R.R., Schneider E.L., A simple technique for quantitation of low levels of DNA damage in individual cells, *Exp. Cell Res.*, 175 (1988) 184–191.
- [20] Anderson D., Yu T.W., Phillips B.J., Schmezer P., The effect of various antioxidants and other modifying agents on oxygen-radical-generated DNA damage in human lymphocytes in the COMET assay, *Mutat. Res.*, 307 (1994) 261–271.
- [21] Jamshidi-Kia F., Lorigooini Z., Amiri-Khoei H., Medicinal plants: Past history and future perspective, *J. HerbMed Pharmacol.*, 7 (1) (2018) 1–7.
- [22] Hyson D.A., A comprehensive review of apples and apple components and their relationship to human health, *Adv. Nutr.*, 2 (5) (2011) 408–420.
- [23] Handan B.A., De Moura C.F.G., Cardoso C.M., Santamarina A.B., Pisani L.P., Ribeiro D.A., Protective Effect of Grape and Apple Juices against Cadmium Intoxication in the Kidney of Rats, *Drug Res.*, 70 (11) (2020) 503–511.
- [24] Vasantha Rupasinghe H.P., Yasmin A., Inhibition of oxidation of aqueous emulsions of omega-3 fatty acids and fish oil by phloretin and phloridzin, *Molecules*, 15 (1) (2010) 251–257.
- [25] Cao J., Jiang L.P., Liu Y., Yang G., Yao X.F., Zhong L.F., Curcumin-induced genotoxicity and antigenotoxicity in HepG2 cells, *Toxicol.*, 49 (8) (2007) 1219–1222.
- [26] Erdem M.G., Cinkilic N., Vatan O., Yilmaz D., Bagdas D., Bilaloglu R., Genotoxic and anti-genotoxic effects of vanillic acid against mitomycin C-induced genomic damage in human lymphocytes in vitro, *Asian Pac. J. Cancer Prev.*, 13 (10) (2012) 4993–4998.
- [27] Błasiak J., Trzeciak A., Dżiki A., Ułańska J., Pander B., Synergistic Effect of Vitamin C on DNA Damage Induced by Cadmium, *Gen. Physiol. Biophys.*, 19 (4) (2000) 373–379.
- [28] Fox J.T., Sakamuru S., Huang R., Teneva N., Simmons S.O., Xia M., Tice R.R., Austin C.P., Myung K., High-throughput genotoxicity assay identifies antioxidants as inducers of DNA damage response and cell death, *Proc. Natl. Acad. Sci. U.S.A.*, 109 (14), 2012, 5423–5428.
- [29] Lu L.Y., Ou N., Lu Q.B., Antioxidant induces DNA damage, cell death and mutagenicity in human lung and skin normal cells, *Sci. Rep.*, 3(1) 2013 1–11.
- [30] Verweij J., Pinedo H.M., Mitomycin C: mechanism of action, usefulness and limitations, *Anticancer Drugs*, 1 (1) (1990) 5–13.
- [31] Choy W.N., Genetic toxicology and cancer risk assessment, New York: Marcel Dekker, Inc., (2001).
- [32] Preston R.J., Dean B.J., Galloway S., Holden H., McFee A.F., Shelby M., Mammalian in vivo cytogenetic assays: Analysis of chromosome aberrations in bone marrow cells, *Mutat. Res.*, 189 (1987) 157–165.
- [33] Kirsch-Volders M., Elhajouji A., Cundari E., Van Hummelen P., The in vitro micronucleus test: a multi-endpoint assay to detect simultaneously mitotic delay, apoptosis, chromosome breakage, chromosome loss and non-disjunction, *Mutat. Res. Genet. Toxicol. Environ. Mutagen.*, 392(1–2) (1997) 19–30.
- [34] D'Costa A., Kumar M.P., Shyama S.K., Genotoxicity Assays: The Micronucleus Test and the Single-cell Gel Electrophoresis Assay. In: Meena S.N., Naik M.M., (Eds).

- Advances in Biological Science Research. Cambridge: Academic Press, (2019) 291–301.
- [35] Sun L., Sun J., Thavaraj P., Yang X., Guo Y., Effects of thinned young apple polyphenols on the quality of grass carp (*Ctenopharyngodon idellus*) surimi during cold storage, *Food Chem.*, 224 (2017) 372–381.
- [36] Cheng K.W., Wu Q., Zheng Z.P., Peng X., Simon J.E., Chen F., Wang M., Inhibitory effect of fruit extracts on the formation of heterocyclic amines, *J. Agric. Food Chem.*, 55 (25) (2007) 10359–10365.
- [37] Shao X., Bai N., He K., Ho C.T., Yang C.S., Sang S., Apple polyphenols, phloretin and phloridzin: New trapping agents of reactive dicarbonyl species, *Chem. Res. Toxicol.*, 21 (10) (2008) 2042–2050.
- [38] Lee J., Jung E., Kim Y.S., Park D., Toyama K., Date A., Lee J., Phloridzin isolated from *Acanthopanax senticosus* promotes proliferation of $\alpha 6$ integrin (CD 49f) and $\beta 1$ integrin (CD29) enriched for a primary keratinocyte population through the ERK-mediated mTOR pathway, *Arch. Dermatol. Res.*, 305 (8) (2013) 747–754.
- [39] Aliyu M., Odunola O.A., Farooq A.D., Mesaik A.M., Choudhary M.I., Azhar M., Asif M.M., Erukainure O.L., Antioxidant, mitogenic and immunomodulatory potentials of acacia honey, *Nutr. Ther. Metab.*, 32 (2) (2014) 68–78.
- [40] Avuloglu-Yilmaz E., Yuzbasioglu D., Unal F., In vitro genotoxicity assessment of monopotassium glutamate and magnesium diglutamate, *Toxicol. In Vitro*, 65 (2020) 104780.

Determination of Antiproliferative Effects of Exopolysaccharides from Six Mushroom Species on Glioma Cells

Şerife Can^{1,a}, Pınar Öztopcu-Vatan^{2,b}, Selda Kabadere^{3,c,*}, Mustafa Yamaç^{2,d}, Ruhi Uyar^{3,e}

¹ Dr. Burhan Nalbantoglu State Hospital Microbiology Laboratory, Lefkosa, Turkish Republic of Northern Cyprus

² Department of Biology, Faculty of Science and Letters, Eskisehir Osmangazi University, Eskisehir, Türkiye

³ Department of Physiology, Faculty of Medicine, Eskisehir Osmangazi University, Eskisehir, Türkiye

*Corresponding author

Research Article

History

Received: 23/04/2022

Accepted: 27/08/2022

Copyright



©2022 Faculty of Science,
Sivas Cumhuriyet University

ABSTRACT

Glial tumors are the largest and danger group of central nervous system tumors. The use of natural products now has been contemplated of exceptional value in the control of cancer. Mushrooms have been used for many centuries, not just as a food, but also to treat many illnesses. Therefore, we aimed to evaluate the effect of exopolysaccharides (EPS) obtained from six different edible mushrooms on the survival of glioma cells. In this study the effects of 0.4, 1, 2, 4 and 6 µg/mL doses of EPSs from six mushroom species *Coprinus comatus*, *Fistulina hepatica*, *Panus neostrigosus*, *Laetiporus sulphureus*, *Polyporus squamosus*, and *Lenzites betulinus* were investigated on the rat glioma cell line (C6) in two different periods by MTT assay. According to our results 0.4 and 1 µg/mL of EPSs from six mushroom species were not effective or less effective, but 2, 4 and 6 µg/mL doses killed glioma cells about 27 to 71 % for 24 hours, 35 to 78 % for 48 hours As a result, these mushroom EPSs showed different cytotoxicity to glioma cells time and dose-dependently. These findings can be suggested that the anti-tumor effects of EPSs can be potential use in clinical applications to treat glioma. Further studies are needed to understand these effects more clearly on glioma.

Keywords: Glioma, In vitro, Mushroom, Exopolysaccharides, Cytotoxicity.

^a can.serife@yahoo.com

^c kabadereselda@gmail.com

^e ruhiuyar66@gmail.com

^{id} <https://orcid.org/0000-0003-2265-9124>

^{id} <https://orcid.org/0000-0002-9589-0063>

^{id} <https://orcid.org/0000-0002-7608-7531>

^b poztopcu@ogu.edu.tr

^d myamac@ogu.edu.tr

^{id} <https://orcid.org/0000-0003-4339-4129>

^{id} <https://orcid.org/0000-0002-7262-0036>

Introduction

Evidence of cancer dates back at least to 35.000 BC in a Neanderthal skull and Egyptian and Incan mummies [1] and cancer is one of the major worldwide fatal diseases. Chemotherapy, radiotherapy, and surgical methods exist for the treatment of cancer in modern medicine however, most cancer therapeutic methods severely affect the host normal cells. Glioblastoma multiforme (GBM), also known as glioblastoma or grade IV astrocytoma, is a worldwide and aggressive brain tumor. Although important improvements achieved in the conventional treatment of GBM over recent years, the median survival of GBM patients is still approximately two years [2]. Hence, the use of natural products now has been contemplated of exceptional value in the control of cancer [3].

Edible and medicinal mushrooms have been used since the Neolithic age as a natural bioactive metabolite source [4], and the theoretical and practical background for the use of mushrooms' for medicinal purposes comes from especially traditional eastern medicine. [5]

It is estimated that the fungal kingdom includes 1.5 million species which has a potential natural source for new bioactive metabolite(s). It is well-known that mushrooms contain various bioactive compounds with medicinal properties as cell wall components such as polysaccharides, polysaccharopeptides and polysaccharide-protein complexes or as secondary metabolites such as polysaccharides, phenolic

compounds, terpenes, and steroids [6,7]. Polysaccharides are reported as the most important bioactive compounds found in mushrooms which have antioxidant, antidiabetic, antimicrobial, anti-inflammatory, and immunomodulatory activities [6,8], and has reported as potential antitumoral compounds [5].

In various Asian countries, mainly polysaccharides (especially β-glucans) from different mushroom species are used for developing pharmaceutical preparations for clinical and commercial purposes such as GLPS polysaccharide fraction from *Ganoderma lucidum*, grifolan from *Grifola frondosa*, lentinan from *Lentinus edodes*, PSK and PSP from *Trametes versicolor*, and schizophyllan from *Schizophyllum commune* [7,9]. Different clinical studies have also confirmed the cancer inhibitory effects of different mushroom species such as *Agaricus brasiliensis*, *Cordyceps sinensis*, *Ganoderma lucidum*, *Grifola frondosa*, *Flammulina velutipes*, *Hypsizygus marmoreus*, *Lentinus edodes*, *Phellinus linteus*, *Schizophyllum commune*, *Trametes versicolor*, and *Tremella mesenterica* [9]. A lot of compounds from mushrooms have proceeded through phase I, II, and III clinical studies [10], and most of the preparations derived from mushroom polysaccharides have been prescribed and used extensively and successfully in modern clinical practice to treat different cancer types in China, Japan, South Korea, Taiwan, and other Asian countries [5,11].

The biologically active polysaccharides in mushrooms can be found in the fruit bodies, cultured mycelium, and culture broth [9]. Collecting or producing the fruit bodies is a season-depending, time-consuming, and/or labor-intensive process. On the other hand, a submerged culture of mushrooms can be a promising alternative for easy, fast, and efficient production of bioactive metabolites [12]. In this view of point, the anticancer activities of exopolysaccharides (EPS) from submerged culture of six mushroom species, *Coprinus comatus*, *Fistulina hepatica*, *Panus neostrigosus*, *Laetiporus sulphureus*, *Polyporus squamosus*, and *Lenzites betulinus*, were investigated on the rat glioma (C6) cells in the present study.

Material And Methods

Materials

The used fungal isolates have been stored at 4°C on a potato dextrose agar (PDA) medium. All medium components were purchased from Merck (Darmstadt, Germany). All reagents for cell culture were purchased commercially from Sigma-Aldrich Products.

Inoculum Preparation

The fungal cultures were initially grown on PDA plates at 28 °C for a week. Five active growing mycelial discs (6 mm diam) from the fungal colony were transferred into 100 mL of potato malt peptone medium (PMP; g/L; potato dextrose broth 24, malt extract 10, peptone 1). After incubation (28 °C, 100 rpm for 4 days), the fungal biomass was harvested, washed with sterile distilled water (SDW) three times and the total volume was completed with SDW to 100 mL. The inoculants were prepared via homogenization of the cells with a Waring blender (Heidolph Silent Crusher M). The prepared cell suspensions were used as inoculants (4%) for all experimental groups.

Exopolysaccharide Production

Submerged culture studies were performed in a sterilized PMP medium at 28 °C, 100 rpm for 7 days. The fungal cultures were harvested by filtration (Whatman No. 2 filter paper). To precipitate crude EPS, the obtained culture filtrates were mixed with cold ethanol (4:1, v/v), stirred, and stood overnight at 4 °C. The crude EPSs were obtained by centrifugation (7500 rpm, 10 min), discharging of supernatant, and finally, crude EPSs were lyophilized and stored at 4 °C until used.

MTT colorimetric assay

The C6 cells were purchased from ATCC and cultured as described previously [13]. At first, the C6 cells were seeded into 2×10^4 cells/well in 96 well plates for 24 hours. Fungal EPSs were dissolved in DMEM, then diluted further in DMEM again. After the incubation period the cells were then exposed to 0.4, 1, 2, 4 and 6 µg/mL fungal EPSs doses for 24 or 48 hours. Control group had only a complete

medium containing DMEM supplemented with 10 % fetal calf serum and 1 % penicillin-streptomycin solution.

MTT colorimetric assay was used to evaluate drug cytotoxicity screening [13]. The absorbance was read at 550 nm (Bio-Tek Instruments microplate reader).

Statistical Analysis

All statistical analyses were carried out by one-way analysis of variance (ANOVA) and followed up by Tukey's multiple comparison tests. A p-value less than 0.05 was considered significant.

Results

At the doses of 0.4 and 1 µg/mL, *Coprinus comatus* EPS did not show any significant effect on the viability of C6 cells after 24 or 48-hour incubation but 2, 4 and 6 µg/mL doses reduced the percentages of living cells by 59, 69 and 69 % ($p < 0.001$), for 24 hours, and 53, 70, and 69 % ($p < 0.001$) after 48 hours, respectively (Figure 1). IC₅₀ values of *Coprinus comatus* EPSs were calculated at 1.8 µg/mL for 24 hours and 1.9 µg/mL for 48 hours.

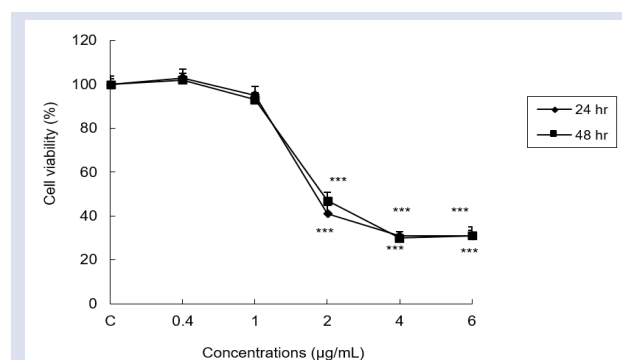


Figure 1. The effects of different doses of *Coprinus comatus* EPS (***: $p < 0.001$)

At the doses of 0.4 and 1 µg/mL, *Fistulina hepatica* EPS did not show any significant effect on the viability of C6 cells after 24-hour incubation but 2, 4 and 6 µg/mL doses reduced the percentages of living cells by 35, 37 and 38 % ($p < 0.001$), for 24 hours, and 1, 2, 4, and 6 µg/mL doses reduced the percentages of living cells by 39 ($p < 0.01$), 44, 45 and 45 % ($p < 0.001$) after 48 hours, respectively (Figure 2). Because the effect is lower, IC₅₀ values of *Fistulina hepatica* EPSs could not be calculated for 24 and 48 hours.

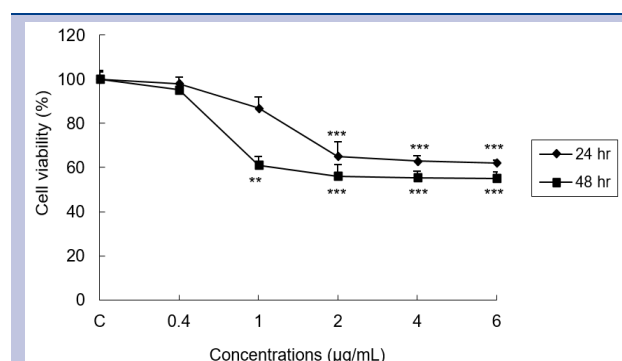


Figure 2. The effects of different doses of *Fistulina hepatica* EPS (**: $p < 0.01$; ***: $p < 0.001$)

At the doses of 0.4, 1, and 2 $\mu\text{g}/\text{mL}$ *Panus neostrigosus* EPS did not show any significant effect on the viability of C6 cells after 24 or 48-hour incubation but 4 and 6 $\mu\text{g}/\text{mL}$ doses reduced the percentages of living cells by 27 and 71 % ($p < 0.001$) for 24 hours, and 28 and 79 % ($p < 0.001$) after 48 hours, respectively (Figure 3). IC_{50} values of *Panus neostrigosus* EPSs were calculated at 4.9 $\mu\text{g}/\text{mL}$ for 24 hours and 4.7 $\mu\text{g}/\text{mL}$ for 48 hours.

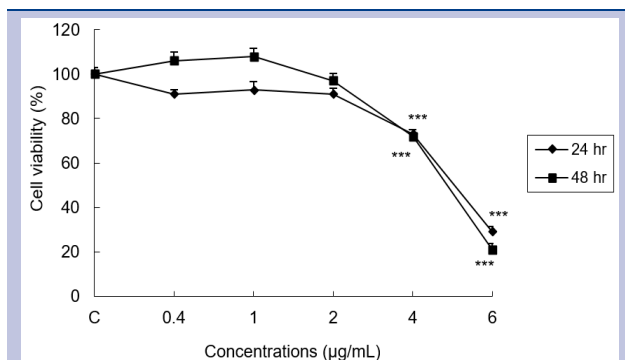


Figure 3. The effects of different doses of *Panus neostrigosus* EPS (***: $p < 0.001$).

At the doses of 0.4 and 1 $\mu\text{g}/\text{mL}$, *Laetiporus sulphureus* EPS did not show any significant effect on the viability of C6 cells after 24-hour incubation but 2, 4 and 6 $\mu\text{g}/\text{mL}$ doses reduced the percentages of living cells by 36, 54 and 63 % ($p < 0.001$) for 24 hours, 1, 2, 4 and 6 $\mu\text{g}/\text{mL}$ doses reduced the percentages of living cells by 35, 48, 74, and 78 % ($p < 0.001$) after 48 hours, respectively (Figure 4). IC_{50} values of *Laetiporus sulphureus* EPSs were calculated at 2.9 $\mu\text{g}/\text{mL}$ for 24 hours and 2.1 $\mu\text{g}/\text{mL}$ for 48 hours.

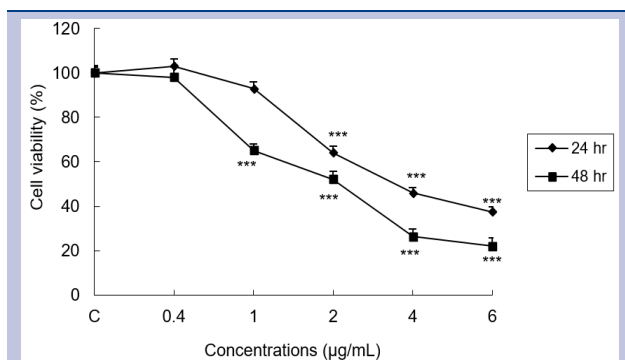


Figure 4: The effects of different doses of *Laetiporus sulphureus* EPS (***: $p < 0.001$)

At the doses of 0.4 and 1 $\mu\text{g}/\text{mL}$, *Polyporus squamosus* EPS did not show any significant effect on the viability of C6 cells after 24 incubation but 2, 4 and 6 $\mu\text{g}/\text{mL}$ doses reduced the percentages of living cells by 27, 59, and 61% ($p < 0.001$) for 24 hours 1, 2, 4 and 6 $\mu\text{g}/\text{mL}$ doses reduced the percentages of living cells by 18 ($p < 0.01$), 51, 68, and 69 % ($p < 0.001$) after 48 hours, respectively (Figure 5). IC_{50} values of *Polyporus squamosus* EPSs were calculated by 3.2 $\mu\text{g}/\text{mL}$ for 24 hours and 1.95 $\mu\text{g}/\text{mL}$ for 48 hours.

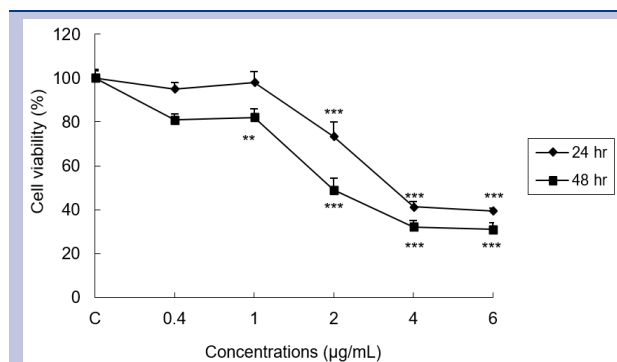


Figure 5. The effects of different doses of *Polyporus squamosus* EPS (***: $p < 0.001$).

At the doses of 0.4, 1, and 2 $\mu\text{g}/\text{mL}$ *Lenzites betulinus* EPS did not show any significant effect on the viability of C6 cells after 24-hour incubation but 4 and 6 $\mu\text{g}/\text{mL}$ doses reduced the percentages of living cells by 42 ($p < 0.01$) and 47 % ($p < 0.001$) for 24 hours 2, 4 and 6 $\mu\text{g}/\text{mL}$ doses reduced the percentages of living cells by 42, 59 and 58 % ($p < 0.001$) after 48 hours, respectively (Figure 6). The IC_{50} value of *Lenzites betulinus* EPS was calculated at 2.9 $\mu\text{g}/\text{mL}$ for 48 hours.

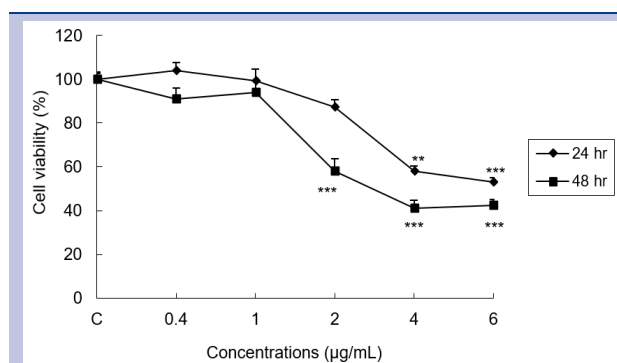


Figure 6: The effects of different doses of *Lenzites betulinus* EPS (**: $p < 0.01$; ***: $p < 0.001$).

Discussion

According to Zhang et al, the antitumor activity of the mushroom was reported firstly by Lucas by discovering the inhibitory effect of a substance from *Boletus edulis* against Sarcoma S-180 tumor cells which is also the first report for bioactivity of Basidiomycetes mushrooms [14, 15]. Because of their preventive effect on oncogenesis and tumor metastasis and stimulating effect on the host immune system, mushroom polysaccharides are widely used especially in Asian countries with chemotherapy [5,12]. Other than antimicrobial [16], antioxidant [17] antiviral[18], antiallergic [19], anti-inflammatory [5], antidiabetic [20], hepatoprotective [21], and radioprotective [22] activities and immunological activities of polysaccharides derived from mushrooms are well-documented [23,24,25] and most extensively studied⁵.

According to the present results *Coprinus comatus* EPS was found to be the most effective mushroom species on

C6 cells. IC₅₀ doses of *Coprinus comatus* EPSs were calculated by 1.8 µg/mL for 24 hours and 1.9 µg/mL for 48 hours and calculations were close to each other depending on time. Similarly, Nowakowski et al [13] mentioned that according to MTT assay results, ethanolic extracts of *Coprinus comatus* were one of the most effective of all the mushroom species they tried on some human glioma cells (U87MG, LN-18 cell lines). In another study, the cytotoxic effects of ethanol and ethyl acetate extracts of *Coprinus comatus* on LNCaP prostate cancer cells were investigated and the IC₅₀ value was found to be 28.3 µg/mL. Also, higher concentrations of *C. comatus* extracts killed more than 50% of the cells. In addition, it also had anti-androgenic effects on androgen-dependent LNCaP cells [26]. According to our results, IC₅₀ values of *Panus neostrigosus*, *Laetiporus sulphureus* and *Polyporus squamosus* EPSs were calculated by 4.9, 2.9 and 3.2 µg/mL for 24 hours and 4.7, 2.1 and 1.95 µg/mL for 48 hours. When we compare these three mushroom species in terms of effect for 24 and 48 hours, *Laetiporus sulphureus* EPS (2.9 µg/mL) and *Polyporus squamosus* EPS (1.95 µg/mL) were found to be the most effective on C6 cells, respectively. The IC₅₀ value of *Lenzites betulinus* EPS was calculated just in 48 hours and it was found 2.9 µg/mL. Since *Fistulina hepatica* EPS at the dose of 6 µg/mL reduced the percentages of living cells by 45 % (p<0.001) after 48 hours, IC₅₀ values of *Fistulina hepatica* EPSs could not be calculated for 24 and 48 hours

In different studies, it has been discovered that various polysaccharides obtained from mushrooms have suppressive effects on cell proliferation in cancer cells [27]. It has been determined that they show this effect through apoptosis. Although studies on brain tumors related to the aforementioned fungi are very scarce, studies related to cancer in recent years are increasing. In our study, the proliferation suppressive effect of six different EPSs on glioma cells was investigated. It was determined that the most effective EPSs among them was the *Coprinus comatus* EPS in two different periods. It is thought that there may be different reasons for this difference. The biological effectiveness of the mushroom EPSs can vary depending on their chemical composition, solubility, degree of branching, molecular weight, the charge of polymers, and structure in aqueous media [9,28].

As a result, these mushroom EPSs were time and dose-dependently toxic to glioma cells. Our results can be suggested that the cytotoxic effects of EPS can be potential use in clinical application to treat glioma. Although our data are promising in terms of cancer prevention, there are not enough studies related to this topic. Our future studies will focus on the characterization of polysaccharides and investigation of other cancer cell lines.

Conflicts of Interest

The author declares no conflicts of interest. No competing financial interests exist.

References

- [1] Barillot E., Calzone L., Hupe P., Vert J.P., Zinovyev A., Computation system biology of cancer, USA: CRC Press, Taylor and Francis Group. A Chapman and Hall Book, (2013).
- [2] Jemal A., Siegel R., Ward E., Hao Y., Xu J., Thun M.J., Cancer statistics CA, *A Cancer Journal for Clinicians*, 59(4) (2009) 225-49.
- [3] Zjawiony J.K., Biologically active compounds from Aphyllophorales (Polypore) Fungi, *Journal of Natural Products*, 67(2) (2004) 300-310.
- [4] Wasser S.P., Medicinal mushroom science: Current Perspectives, Advances, Evidences, and Challenges, *Biomedical Journal*, 37(6) (2014) 345-356.
- [5] Savelkoul H.F.J., Chanput W., Wichers H.J., Immunomodulatory effects of mushroom β-glucans. In: Diet, Immunity and Inflammation, (Eds. PC Calder and P Yaqoob): 416–434. Woodhead Publishing Series in Food Science, Technology and Nutrition, (2013).
- [6] Sanchez C., Bioactives from Mushroom and Their Application. In: Food Bioactives, (Ed M Puri): 23–57. Springer International Publishing, (2007).
- [7] Khan A.A., Gani A., Khanday F.A., Masoodi F.A., Biological and pharmaceutical activities of mushroom β-glucan discussed as a potential functional food ingredient, *Bioactive Carbohydrates and Dietary Fibre*, 16 (2018) 1–13.
- [8] Chaturvedi V.K., Agarwal S., Gupta K.K., Ramteke P.W., Singh M.P., Medicinal mushroom: boon for therapeutic applications, *3 Biotech*, 8 (2018) 334.
- [9] Wasser S.P., Medicinal mushrooms as a source of antitumor and immunomodulation Polysaccharides, *Applied Microbiology and Biotechnology*, 60 (2002) 258–274.
- [10] Wasser S.P., Medicinal mushrooms in human clinical studies. Part I. Anticancer, oncoimmunological, and immunomodulatory activities: A review, *International Journal of Medicinal Mushrooms*, 19 (2017) 279–317.
- [11] Vitak T., Yurkiv B., Wasser S., Nevo E., Sybirna N., Effect of medicinal mushrooms on blood cells under conditions of diabetes mellitus, *World Journal of Diabetes*, 8(5) (2017) 187–201.
- [12] Dudekula U.T., Doriya K., Devarai S.K., A critical review on submerged production of mushroom and their bioactive metabolites, *3 Biotech*, 10 (2020) 337.
- [13] Nowakowski P., Markiewicz Z.R., Gromkowska-Kępką K, Naliwajko S.K., Moskwa J., Bielecka J., Grabia M., Borawska M., Socha K., Mushrooms as potential therapeutic agents in the treatment of cancer: Evaluation of anti-glioma effects of *Coprinus comatus*, *Cantharellus cibarius*, *Lycoperdon perlatum* and *Lactarius deliciosus* extracts, *Biomedicine & Pharmacotherapy*, 133 (2021) 111094.
- [14] Zhang M., Cui S.W., Cheung P.C.K., Wang Q., Antitumor polysaccharides from mushrooms: a review on their isolation process structural characteristics and antitumor activity, *Trends in Food Science and Technology*, 18 (2007) 4–19.
- [15] Lucas E.H., Tumor inhibition in *Boletus edulis* and other *Holobasidiomycetes*, *Antibiotic Chemotherapy*, 7 (1957) 1-15.
- [16] Lindequist U., Niedermeyer T.H.J., Ju"lich W.D., The pharmacological potential of Mushrooms, *Evidence-Based Complementary and Alternative Medicine*, 2 (2005) 285–299.

- [17] Deng C., Hu Z., Fu H.T., Hu M.H., Xu X., Chen J.H., Chemical analysis and antioxidant activity in vitro of a β -D-glucan isolated from *Dictyophora indusiate*, *International Journal of Biological Macromolecules*, 51 (2012) 70–75.
- [18] Minari M.C., Rincao V.P., Soares S.A., Ricardo N.M., Nozawa C., Linhares R.E., Antiviral properties of polysaccharides from *Agaricus brasiliensis* in the replication of bovine herpesvirus 1, *Acta Virologica*, 55 (2011) 255–259.
- [19] Wasser S.P., Weis A.L., Medicinal properties of substances occurring in higher Basidiomycetes mushrooms: current perspectives (review), *International Journal of Medicinal Mushrooms*, 1 (1999) 31–62.
- [20] Yamaç M, Kanbak G, Zeytinoğlu M, Bayramoğlu G, Şentürk H, Uyanoğlu M. Hypoglycemic effect of *Lentinus strigosus* (schwein.) Fr. crude exopolysaccharide in streptozotocin induced diabetic rats, *Journal of Medicinal Food*, 11(3) (2008) 513–517.
- [21] Uyanoglu M., Yamac M., Canbek M., Sentürk, H., Kartkaya K., Oglakçı A., Turgak O., Kanbak G., Curative effect of crude exopolysaccharides of some macrofungi on alcohol-induced liver damage, *Ultrastructural Pathology*, 37(3) (2013) 218–226.
- [22] Pillai T.G., Devi U.P., Mushroom beta glucan: potential candidate for post irradiation Protection, *Mutation Research*, 751 (2013) 109–115.
- [23] Kidd P.M., The use of mushroom glucans and proteoglycans in cancer treatment, *Alternative Medicine Review*, 5 (2000) 4–27.
- [24] Borchers A., Keen C.L., Gershwin M.E., Mushrooms, tumors, and immunity: an Update, *Experimental Biology and Medicine*, 229 (2004) 393–406.
- [25] Ren L., Perera C., Hemar Y., Antitumor activity of mushroom polysaccharides: a Review, *Food and Function*, 3 (2012) 1118–1130.
- [26] Zaidman B.Z., Wasser S.P., Nevo E., Mahajna J., *Coprinus comatus* and *Ganoderma lucidum* interfere with androgen receptor function in LNCaP prostate cancer cell, *Molecular Biology Reports*, 35 (2008) 107–117.
- [27] Wong J.H., Ng T.B., Chan H.H.L., Liu Q., Man G.C.W., Zhang C.Z., Guan S., Ng C.C.W., Fang E.F., Wang H., Liu F., Ye X., Rolka K., Naude R., Zhao S., Sha O., Li C., Xia L., Mushroom extracts and compounds with suppressive action on breast cancer: evidence from studies using cultured cancer cells, tumor-bearing animals, and clinical trials, *Applied Microbiology and Biotechnology*, 104 (2020) 4675–4703.
- [28] Zekovic D.B., Kwiatkowski S., Vrvic M.M., Jakovljevic D., Moran C.A., Natural modified (1-3)- β -glucans in health promotion and disease alleviation, *Critical Reviews in Biotechnology*, 25 (2005) 205–230.

Effects of Some Herbs on the In-vitro Growth of *Helicobacter pylori* and Their Antioxidant Properties

Ayşe Aydan Kara ^{1,a,*}, Ömer Faruk Algur ^{1,b}, Ahmet Mavi ^{2,c}, Ali Yıldırım ^{2,d}, Meryem Şengül Köseoğlu ^{1,e}

¹ Department of Biology, Faculty of Science, Atatürk University, Erzurum, Türkiye

² Department of Secondary Science and Mathematics Education, Kazım Karabekir Faculty of Education, Atatürk University, Erzurum, Türkiye

*Corresponding author

Research Article

History

Received: 13/04/2022

Accepted: 07/09/2022

Copyright



©2022 Faculty of Science,
Sivas Cumhuriyet University

ABSTRACT

Helicobacter pylori is one of the important causes of chronic gastritis, peptic ulcer, stomach cancer in humans. The importance of these diseases has led to the development of effective drug treatment regimens against them. The basis of this study is the determination of the effects of some medicinal plants on the in-vitro growth of *H. pylori* and their antimicrobial and antioxidant potential. For this purpose, different parts of 15 plant species were extracted using solvents. Water, ethanol, chloroform, acetone extracts of plants were used and antimicrobial activities of these extracts against both *H. pylori* and other test microorganisms were investigated using the agar disc diffusion methods. The antioxidant properties of the extracts, which were found to be effective in terms of antimicrobial activity, were determined by the thiocyanate method. As a result, acetone extracts of plants; it was determined that it showed higher antimicrobial activity than water, ethanol, chloroform extracts. The most effective two plants against *H. pylori* for water, ethanol, chloroform, acetone were *Capsella bursa-pastoris*, *Acorus calamus*; *Acorus calamus*, *Achillea millefolium*; *Acorus calamus*, *Pimpinella anisum*, *Acorus calamus*, *Achillea millefolium*, respectively. Acetone extracts of *Hypericum perforatum*, *Rosmarinus officinalis*, *Achillea millefolium*; *Acorus calamus*, *Pimpinella anisum* plants were found to have antioxidant properties.

Keywords: *Helicobacter pylori*, In-vitro Studies, Plant extract, Antimicrobial activity, Antioxidant activity.

^a aydan@atauni.edu.tr
^c amavi@atauni.edu.tr
^e sengulm@atauni.edu.tr

^b <https://orcid.org/0000-0002-1889-3498>
^d <https://orcid.org/0000-0003-1207-9783>
^f <https://orcid.org/0000-0001-6050-0304>

^b ofalgur@yahoo.com
^d aliyildirim@mu.edu.tr

^d <https://orcid.org/0000-0001-6447-3454>
^e <https://orcid.org/0000-0002-0735-3728>

Introduction

Helicobacter pylori is gram-negative, highly motile, spiral-shaped bacterium [1, 2]. *H. pylori* has 5 to 7 polar sheathed flagella. These basic characteristics of morphology and motility are thought to be advantageous to these organisms due to their localization in the mucous layer of the gastrointestinal tracts of humans [3, 4]. *H. pylori* colonizes the gastric epithelial surface. *H. pylori* has microaerophilic growth capability and urease activity so the bacterium withstands the stomach's hostile ambiance [4-6]. *H. pylori* is known as the etiologic agent of acute or chronic gastritis and a predisposing factor in peptic ulcer disease, gastric carcinoma [3, 7]. The Natural reservoir of *H. pylori* is humans. The bacterium can be transmitted with the fecal-oral route. Half of the adults in developed countries and 80-90 % of the population in developing countries are infected with these bacteria. *H. pylori* is treated with combined antibiotic therapy [8, 9]. It is known that antibiotic regimens used in *H. pylori* treatment have some side effects and also some of the treated patients develop antibiotic resistance [4, 10, 11]. Due to the various side effects of synthetic drugs used in the treatment of diseases caused by *H. pylori* and other pathogenic bacteria, researches on the use of herbal extracts have intensified in recent years. Herbal extracts are also recommended because they contain natural antioxidant ingredients. Therefore, the fact that a plant material has both antimicrobial and antioxidant effects, it is increased its value even more. There are many plants in the world and in our country that are known to be good for

various stomach diseases and are used with traditional methods. This study, it was aimed to determine the antimicrobial effects and antioxidant properties of some medicinal plants in our country, which are used with the belief that they are good for stomach problems, on *H. pylori* which is a stomach pathogen.

Materials and Methods

Plant Material

15 plant samples that have been preferred for gastrointestinal system disorders by researchers [12, 13] were obtained either as purchased from the local market or collected from the Erzurum region of Turkey. Taxonomic determinations were done using the serial "Flora of Turkey and East Aegean Islands" [12] as well as comparing them with the specimens in the herbarium. Scientific and local names, parts used and folk uses of these plants were summarized in Table 1.

Preparation of Plants Extracts

10 g of powdered parts of the plants (used parts, see Table 1) were separately incubated with 100 ml acetone, chloroform, ethanol, water for 24 hours at room temperature on a shaker (G24 environmental shaker incubator). Final suspensions were filtered using Whatman filter paper (no.1) and extracts were stored at refrigerator until used [5, 14, 15].

Table 1. Plants used in the study

Plant Name (family)	Local name	Part used	Traditional Uses
<i>Achillea millefolium</i> L. (Compositae)	Civanperçemi, Akbaşlı	Flowers, Branches with the leaf	Infection, hemorrhoids, stomach cramp, ulcer, rheumatism
<i>Acorus calamus</i> L. (Araceae)	Eğir kökü, Azakeğeri	Rhizoms	Dysentery, cirrhosis, rachitis, stomach ulcer
<i>Capsella bursa-pastoris</i> L. (Cruciferae)	Çobançantası, Çingildaklıot	Flowers, Leaves, Branches	Wounds, bleedings, hemorrhoids, tension, stomach and intestine bleedings
<i>Carum carvi</i> L. (Umbelliferae)	Frenk kimyonu, Karaman kimyonu	Fruits	Cough, stomach and intestine diseases
<i>Foeniculum vulgare</i> Miller (Umbelliferae)	Rezene, Arapsaçı	Fruits	Cough, bronchitis, diarrhea, stomach and intestine pains, wound, tiredness
<i>Glycyrrhiza glabra</i> L. (Leguminosae)	Meyan kökü, Piyan	Roots	Stomach and duodenal ulcer, tuberculosis, gastritis, bronchitis, kidney diseases
<i>Hypericum perforatum</i> L. (Guttiferae)	Sarı kantaron, Binbirdelikotu	Branches with the flower	Asthma, bronchitis, rheumatism, stomach ulcer, tuberculosis, diarrhea, hemorrhoids, antidepressant
<i>Linum usitatissimum</i> L. (Linaceae)	Keten tohumu, Zeyrek tohumu	Seeds	Boil, diabetes, constipation, rheumatism, stomach ulcer, cough, shingles
<i>Matricaria chamomilla</i> var. <i>recutita</i> L. (Compositae)	Mayıs papatyası, Papatya çiçeği	Flowers	Cancer, hemorrhoids, tonsillitis, stomach ulcer, epilepsy, sinusitis, hepatitis, neuralgia, gastritis, enteritis
<i>Melissa officinalis</i> L. (Labiatae)	Oğulotu, Limon nanesi	Leaves	Anemia, asthma, stomach and intestine pains, tension, palpitation of the heart, neurasthenia
<i>Mentha piperita</i> L. (Labiatae)	Kültür nanesi, İngiliz nanesi	Leaves	Stomach ulcer, bronchitis, melancholy, eczema, antiseptic, megrim, liver diseases, epilepsy
<i>Pimpinella anisum</i> L. (Umbelliferae)	Anason, Mesirotu	Fruits	Infection, megrim, angina, gastritis, bronchitis
<i>Rosmarinus officinalis</i> L. (Labiatae)	Biberiye, Kuşdili	Leaves	Antiseptic, hepatitis, asthma, stomach spasm, constipation
<i>Thymus</i> L. (Labiatae)	Kekik, Saterotu	Leaves	Headache, bronchitis, chronic gastritis, stomach ulcer, asthma, cough, antiseptic, bronchitis, rheumatism
<i>Urtica dioica</i> L. (Urticaceae)	Isırganotu, Dızlağan	Leaves	Infection, ulcer, diabetes, cancer, arthritis, edema, allergy, stomach and intestine diseases, rheumatism, nephrolithiasis, gall bladder, anemia

Antimicrobial Activity

Microorganisms

8 species of bacteria (*Helicobacter pylori* ATCC 49503, *Staphylococcus aureus* ATCC 33862, *Bacillus subtilis* ATCC 6633, *Enterobacter cloacae* ATCC 13047, *Escherichia coli* ATCC 25922, *Proteus mirabilis* ATCC 7002, *Pseudomonas aeruginosa* ATCC 10145, *Klebsiella pneumoniae* (Clinic isolate), two species of fungi (*Candida albicans* ATCC 60193 and *Saccharomyces cerevisiae* NRRLY 12632) were used in this study. The microorganisms were obtained from the Faculty of Medicine at Karadeniz Technical University, Trabzon, Turkey and the Faculty of Medicine at Atatürk University, Erzurum, Turkey and North University Street, Illinois, USA.

Disc diffusion method

Antimicrobial Activity was carried out by Kirby-Bauer disc diffusion method [15-17]. 100 µl of water, chloroform, ethanol, acetone extracts of 15 plants were transferred onto 6mm diameter antimicrobial susceptibility blank discs (Oxoid). Discs were dried at 37°C in the incubator [14, 18]. The antibiotics [Ampicilin (10µg/disc), OFX; ofloxacin (10 µg/disc), SCF: sulbactam (30 µg) + cefoperazone (75 µg) = (105µg/disc) and NET: netilmicin (30 µg/disk) for bacteria, NYS::nystatin (30 µg/disk) for

fungi] were used as a positive controls. Only solvent-treated discs were used as a negative control. It was taken from the cultures of microorganisms grown in the mediums with inoculating loop and suspended in phosphate- buffered saline (PBS). The dilutions were prepared to be 10⁸ CFU/mL according to McFarland turbidity standard no.0.5. These dilutions were used as inoculum [15, 19]. The samples taken from these dilutions using sterile cotton swab sticks were spread over the surface of proper agar plates (*Brucella* Agar supplemented with %5 human blood for *H. pylori*, Potato Dextrose Agar (PDA) for fungi and Nutrient Agar (NA) for other test bacteria) [20]. Then the absorbed discs were placed on the inoculated agar plates. *Brucella* Agar plates were incubated under microaerophilic conditions in anaerobic jars with campygen gas generating kit (Oxoid) at 37°C for 3-5 days [5]. The other plates were incubated at 37°C for 18-24 hours for bacteria and 3 days for fungi. The antimicrobial activity was evaluated by measuring the diameter of the inhibition zone against test microorganisms. Each assay was repeated twice [21].

Minimum inhibitory concentration (MIC)

It was found that acetone extracts of plants showed stronger antimicrobial activity against *H. pylori* among the extracts of plants prepared using 4 different solvents. Therefore, only the MIC values of the acetone extracts of

the plants were determined. Diameters of the inhibition zone showing the antimicrobial activities of acetone extracts of the plants against *H. pylori* were measured. Then MIC values of the extracts forming the broadest diameter of the inhibition zone against *H. pylori* among acetone extracts of plants were determined. For this purpose, those with diameters of the inhibition zone of 17 mm and higher from acetone extracts of the plants (*Achillea millefolium*, *Pimpinella anisum*, *Rosmarinus officinalis*, *Thymus*, *Hypericum perforatum*) against *H. pylori* were chosen. Powdered parts of the plants were incubated with acetone at room temperature on a shaker. Final suspensions were filtered using Whatman filter paper (no.1). The extracts were evaporated to dryness at 40°C in a rotary evaporator [5, 22]. MIC values of the extracts were determined by modifying the agar dilution methods. [11, 23, 24]. To determine the MIC values, Brucella Agar, which was sterilized by autoclave, was cooled to 60°C and 5% human blood was added. Then 24-well plates were placed on a hot plate and maintained at 60 °C. In the next step, 1 mL Brucella Agar was added to each well in 24-well plates. On the other hand, 100 mg of the dried extracts were dissolved in 1 mL of Dimethyl sulfoxide (DMSO) and 100 µL of it was taken and diluted with 900 µL of Brucella Agar. Thus, a 10 mg/mL dilution was prepared and the volume of 1 mL from here was transferred to the first well. Then, by transferring the volume of 1 ml from one well to the other, it was provided to prepare two-fold serial dilutions with a concentration of 5 mg/mL in the first well and 0.0024 mg/mL in the 12 well. All tests were done at least in duplicate. The same procedures were applied for ampicillin as positive control and DMSO solution as the negative control. 24-well plate is closed and solidified at room temperature. It was taken from the cultures of *H. pylori* grown in the medium (Brucella Agar supplemented with %5 human blood) with inoculating loop and suspended in phosphate-buffered saline (PBS). The dilution was prepared to be according to 10⁸ CFU/mL McFarland turbidity standard no.0.5. This dilution was used as inoculum. 10 µL of this dilution was injected into each well with a micropipette. 24 well-plates were incubated under microaerophilic conditions in anaerobic jars with campygen gas generating kit (Oxoid) at 37°C for 3-5 days. Microbial growth in each well was determined by observing and comparing wells with the positive and negative controls. The lowest extract concentration in which there was no visible growth was evaluated as MIC [5, 11, 15, 19, 20, 23, 24].

Antioxidant Activity

Thiocyanate method

Since acetone extracts of plants showed stronger antimicrobial activity against *H. pylori*, antioxidant activities of the acetone extract of 5 plants (*Achillea millefolium*, *Pimpinella anisum*, *Rosmarinus officinalis*, *Hypericum perforatum*) forming the broadest inhibition zone against *H. pylori* among acetone extracts of plants were determined thiocyanate method.

The antioxidant activities of the extracts were determined according to the thiocyanate method [25]. First, powdered parts of the plants were incubated with acetone at room temperature on a shaker. Final suspensions were filtered using Whatman filter paper (no.1). The extracts were evaporated to dryness at 40°C in a rotary evaporator [5, 22]. Then, stock solutions of the extracts with a concentration of 1 mg/mL were prepared. The volume of the stock solution corresponding to the desired amounts was placed in the veneer cups with automatic pipettes and the volume was adjusted to 2.5 ml with buffer solution. Then, 2.5 mL of the linoleic acid emulsion was added to each test tube. As a control, a buffer solution (2.5 mL) containing solvent in the amounts used in the experiments (maximum 300 µL) and a mixture of 2.5 mL linoleic acid emulsion was used. Incubation was carried out at 40 °C. At different intervals, 100 µL of each of the samples were taken into test tubes containing 4.7 mL of ethanol, and 100 µL of s Fe²⁺ solution and 100 µL of SCN⁻ solution were added. The blank sample was obtained by adding 100 µL of Fe²⁺ solution and 100 µL of SCN⁻ solution to a test tube containing 4.8 mL of ethanol. The absorbances of the samples at 500 nm were read against the blank sample. The incubation was terminated when the control sample reached maximum absorbance. BHT was used as a standard antioxidant in all tests.

Results and Discussion

Antimicrobial Activity

Disc diffusion method

The antimicrobial activities of water, ethanol, chloroform, acetone extracts of 15 plant species obtained by the extraction methods given in the method section were determined against *Helicobacter pylori*, 7 other test bacteria species, 2 fungus species. The antimicrobial activity was evaluated by measuring the diameter of an inhibition zone.

The antimicrobial activities of water extracts of 14 plant species on *H. pylori* and other microorganisms were given in Table 2 and Table 3, respectively. *Linum usitatissimum* wasn't used because water extract of it was not prepared.

Extract of *Capsella bursa-pastoris* plant showed the maximum antimicrobial activity against *H. pylori* in the water extracts and formed diameter of the inhibition zone of 33 mm. This was followed by extracts of *Acorus calamus*, *Glycyrrhiza glabra*, *Achillea millefolium* and *Mentha piperita*, respectively. It was remarkable that water extract of *Capsella bursa-pastoris*, which was effective on *H. pylori*, was also effective on most other test microorganisms (Table 2). This plant extract formed diameter of the inhibition zone of 20 mm against *K. pneumoniae* and 16 mm against *B. subtilis*. Among the water extracts, the plants with the broadest spectrum of antimicrobial activity were *Capsella bursa-pastoris* and *Thymus*. Extracts of these plants showed an inhibition

effect on 6 of the test microorganisms. *C. albicans* was not inhibited by the water extract of any plant. Among the test microorganisms, *H. pylori*, *K. pneumoniae* and *B. subtilis* were found to be the most sensitive bacteria to water extracts (Table 3).

The antimicrobial activities of extracts of ethanol, chloroform, acetone of 15 plant species against *H. pylori* and other microorganisms were given in Table 2 and Table 3, respectively.

The extract belonging to *Acorus calamus* plant showed the maximum antimicrobial activity against *H. pylori* in ethanol extracts and formed diameter of the inhibition zone of 30 mm as can be seen Table 2. This was followed by extracts of *Achillea millefolium*, *Rosmarinus officinalis*, *Thymus*, respectively. When the effect of ethanol extracts on other test microorganisms was examined (Table 3), it was determined that although *Acorus calamus* was the most inhibitory effect against *H. pylori*, it was effective only against *B. subtilis* among other microorganisms. *Achillea millefolium* and *Rosmarinus officinalis* extracts, which were also effective against *H. pylori*, showed an inhibition effect against only 3 microorganism species. Among the ethanol extracts, the plants with the broadest spectrum of antimicrobial activity were *Thymus* and *Foeniculum vulgare* as can be seen Table 3. Extracts of these plants showed an inhibition effect against 7 of the test microorganisms. Among the test microorganisms, the most sensitive microorganisms species to ethanol extracts were respectively *B. subtilis*, *S. aureus*, *K. pneumoniae* whereas *P. aeruginosa* was not affected by any extracts.

Chloroform extract of *Acorus calamus* plant showed the maximum antimicrobial activity against *H. pylori* in chloroform extracts and formed diameter of the inhibition zone of 32 mm. This was followed by *Pimpinella anisum*, *Achillea millefolium* and *Carum carvi* extract respectively (Table 2). The effects of chloroform extracts against other test microorganisms were found different (Table3).

Table 2. Antibacterial activities of extracts of the plant against *H. pylori* ATCC 49503

Plants	Diameter of inhibition zone (mm)			
	Water	Ethanol	Chloroform	Acetone
<i>A. calamus</i> L.	21	30	32	37
<i>A. millefolium</i> L.	17	20	21	30
<i>C. bursa-pastoris</i> L.	33	12	10	9
<i>C. carvi</i> L.	8	15	17	15
<i>F. vulgare</i> Miller	—	16	14	9
<i>G. glabra</i> L.	18	10	12	12
<i>H. perforatum</i> L.	—	10	11	19
<i>L. usitatissimum</i> L.	Not tested	10	16	13
<i>M. chamomilla</i> var. <i>recutita</i> L.	—	15	15	13
<i>M. officinalis</i> L.	—	16	16	14
<i>M. piperita</i> L.	15	12	14	14
<i>P. anisum</i> L.	—	16	25	27
<i>R. officinalis</i> L.	—	20	14	24
<i>Thymus</i> L.	10	17	16	20
<i>U. dioica</i> L.	—	9	11	10
Negative Control	—	—	—	—
Ampicillin	45	—	—	—

Among the chloroform extracts, it was determined that the plant with the broadest spectrum of antimicrobial activity was *Foeniculum vulgare*. This extract formed an inhibition effect against 7 of the test bacteria and also inhibited *C. albicans* fungus species.

Table 3. Antimicrobial activity of extracts of the plant against other test microorganisms [Diameter of inhibition zone (mm)]

Plants	Microorganisms																																				
	<i>B. subtilis</i>				<i>S. aureus</i>				<i>E. cloacae</i>				<i>E. coli</i>				<i>K. pneumoniae</i>				<i>P. aeruginosa</i>				<i>P. mirabilis</i>				<i>C. albicans</i>				<i>S. cerevisiae</i>				
	W	E	C	A	W	E	C	A	W	E	C	A	W	E	C	A	W	E	C	A	W	E	C	A	W	E	C	A	W	E	C	A	W	E	C	A	
<i>A. calamus</i> L.	13	16	14	18	—	—	9	12	—	—	—	—	—	—	—	—	—	—	—	—	—	—	—	—	—	—	—	—	—	—	—	—	—	—	—	—	—
<i>A. millefolium</i> L.	—	15	17	22	8	9	10	12	—	—	—	—	—	—	—	—	—	—	—	—	—	—	—	—	—	—	—	—	—	—	—	—	—	—	—	—	—
<i>C. bursa-pastoris</i> L.	16	—	—	—	—	7	—	10	—	—	—	9	—	—	—	—	—	—	—	—	—	—	—	—	—	—	—	—	—	—	—	—	—	—	—	—	—
<i>C. carvi</i> L.	—	17	17	22	—	11	11	17	—	—	—	—	—	—	—	—	—	—	—	—	—	—	—	—	—	—	—	—	—	—	—	—	—	—	—	—	—
<i>F. vulgare</i> Miller	—	19	18	12	—	21	11	9	—	7	8	—	—	9	12	7	—	7	8	—	—	—	—	—	—	—	—	—	—	—	—	—	—	—	—	—	—
<i>G. glabra</i> L.	11	11	12	9	—	—	—	—	—	8	—	—	—	—	—	—	—	—	—	—	—	—	—	—	—	—	—	—	—	—	—	—	—	—	—	—	—
<i>H. perforatum</i> L.	—	15	15	10	—	8	8	10	—	—	—	—	—	—	—	—	—	—	—	—	—	—	—	—	—	—	—	—	—	—	—	—	—	—	—	—	—
<i>L. usitatissimum</i> L.	*	11	11	—	*	—	9	—	*	—	—	—	*	—	8	—	*	—	—	—	*	—	—	—	*	—	—	—	—	—	—	—	—	—	—	—	—
<i>M. chamomilla</i> var. <i>recutita</i> L.	—	18	18	12	—	11	11	13	—	—	—	—	—	—	—	—	—	—	—	—	—	—	—	—	—	—	—	—	—	—	—	—	—	—	—	—	—
<i>M. officinalis</i> L.	—	10	—	9	—	—	—	—	—	—	—	—	—	—	—	—	—	—	—	—	—	—	—	—	—	—	—	—	—	—	—	—	—	—	—	—	—
<i>M. piperita</i> L.	—	8	—	7	—	—	—	—	—	—	—	—	—	—	—	—	—	—	—	—	—	—	—	—	—	—	—	—	—	—	—	—	—	—	—	—	—
<i>P. anisum</i> L.	—	19	20	24	—	8	13	15	—	—	—	—	—	—	—	—	—	—	—	—	—	—	—	—	—	—	—	—	—	—	—	—	—	—	—	—	—
<i>R. officinalis</i> L.	—	15	15	25	—	9	11	13	—	—	—	—	—	—	—	—	—	—	—	—	—	—	—	—	—	—	—	—	—	—	—	—	—	—	—	—	—
<i>Thymus</i> L.	7	14	10	8	10	10	—	11	12	11	—	11	—	—	—	—	—	—	—	—	—	—	—	—	—	—	—	—	—	—	—	—	—	—	—	—	—
<i>U. dioica</i> L.	—	13	11	6	—	9	7	—	—	—	—	—	—	—	—	—	—	—	—	—	—	—	—	—	—	—	—	—	—	—	—	—	—	—	—	—	—
Negative Control	—	—	—	—	—	—	—	—	—	—	—	—	—	—	—	—	—	—	—	—	—	—	—	—	—	—	—	—	—	—	—	—	—	—	—	—	—
Antibiotics	28 (OFX)				22 (SCF)				10 (OFX)				18 (Amp.)				12 (OFX)				22 (NET)				13 (Amp.)				18 (Nistatin)				20 (Nistatin)				

—: No inhibition, *: Not tested, W: Water Extract, E: Ethanol Extract, C: Chloroform Extract, A: Acetone Extract

Among the test microorganisms, the most sensitive species to chloroform extracts were respectively *B. subtilis*, *S. aureus* and *K. pneumoniae*, Whereas *P. aeruginosa* was not affected by any extracts.

Acetone extracts of *Acorus calamus* plant showed maximum antimicrobial activity in acetone extracts as in chloroform and ethanol extracts of plants and formed diameter of the inhibition zone of 37 mm. This was followed by extracts of *Achillea millefolium*, *Pimpinella anisum*, *Rosmarinus officinalis*, *Thymus*, *Hypericum perforatum*, respectively (Table 2).

When looking at the effect of acetone extracts against other test microorganisms (Table 3), it was determined that *Acorus calamus*, which was the most effective against *H. pylori*, had an inhibition effect against only 3 microorganism species. *Achillea millefolium*, *Pimpinella anisum*, *Rosmarinus officinalis*, *Hypericum perforatum* extracts, which were also effective against *H. pylori*, showed an inhibition effect on 4, 6, 5, 2 microorganism species, respectively. It was determined that *Thymus* was the plant with the broadest spectrum of antimicrobial activity among acetone extracts and this extract formed an inhibition effect against 7 of the test microorganisms. Among the test microorganisms, *B. subtilis*, *K. pneumoniae* and *S. aureus* were found to be the most sensitive species to acetone extracts, respectively. No microorganism was effective against *P. aeruginosa*.

It was determined in our study that acetone extracts of plants had the stronger antimicrobial activity and water extracts had the weaker antimicrobial activity when compared in terms of different solvents. When various research results were examined, it was seen that water extracts generally had low antimicrobial activity compared to other solvents. [17, 26].

However, it is of great importance that the water extracts of a plant exhibit antimicrobial activity since boiled in water or infusion of the plant is generally preferred in the traditional use of medicinal plants. There have been some findings showing that water extracts of some plants have stronger antimicrobial activity than their extracts in various solvents [15, 27-29]

It was determined in our study that water extract of *Capsella bursa-pastoris* was quite effective against both *H. pylori* and other test microorganisms. In this respect, *Capsella bursa-pastoris* was found important for research. Although they weren't as effective against *H. pylori* as *Capsella bursa-pastoris*, water extracts of *Acorus calamus*, *Glycyrrhiza glabra*, *Achillea millefolium* were also effective against *H. pylori*.

Various researchers investigating the antimicrobial effect of plant extracts have used a wide variety of solvents for different parts of different plants [2, 5, 10, 14, 17, 20, 23, 30, 31]. It is not possible to make a preference ranking valid for all plants and plant parts among these solvents. However, ethanol, chloroform and acetone were preferred as solvents in our research considering the working intensity in the literature and generally looking at the positive results.

When the solvents used in our study were evaluated for its potential to extract bioactive substances in the plants, acetone was found to be superior to other

solvents. Indeed, regardless of the inhibition zone diameter sizes, in general, 29 of 140 samples (20.71 %) of water extracts, 61 of 150 samples (40.66 %) of ethanol extracts, 59 of 150 samples (39.33%) of chloroform extracts, 64 of 150 samples (42.66%) acetone extracts were also found to have an antimicrobial effect (Table 2 and Table 3). This finding is interesting because there have been few studies researching the conclusion that acetone extracts are superior in antimicrobial activity [26]. This researcher has stated that acetone, methanol, ethanol, water extracts of plants have ranked as acetone> methanol-chloroform-water> methylene dichloride> methanol> ethanol> water in terms of antimicrobial effect. In this study, it was also stated in this study that acetone was preferred as a solvent because it can dissolve hydrophilic and lipophilic structures in plants, can be volatile and can be mixed with water, has low toxicity, and can be mixed with polar and non-polar solvents [26]. However, as stated above, acetone extracts have been often found to be inferior to other extracts in terms of antimicrobial effect. As a matter of the fact, when different research results are examined, it has been determined that extracts of ethanol in some of them [31], extracts of petroleum ether in some of them [17], extracts of chloroform and ethyl ether in other some of them [30] have shown stronger antimicrobial activity. In this case, it is considered that it is not possible to offer an ideal type of solvent for the plant or plant part to be used in terms of antimicrobial effects.

If a generalization was made regardless of the wide of the inhibition zones and the solvent type, it was determined that the plants with the broadest spectrum of antimicrobial activity are *Thymus* and *Foeniculum vulgare*. The broad spectrum of activity of a substance with antimicrobial effect is important in terms of its practical use and evaluation. Therefore, in our research, the antimicrobial effects of extracts, which had an inhibition effect against *H. pylori*, were also examined on other test microorganisms. It was found to be promising in this regard the plants whose names were mentioned above.

When the test microorganisms were evaluated in general, *B. subtilis*, *K. pneumoniae*, *S. aureus* and *H. pylori* bacteria species were the most sensitive species to extracts of plants. *B. subtilis* and *S. aureus* are Gram-positive, *K. pneumoniae* and *H. pylori* are Gram-negative bacteria. It was difficult to comment on whether the extracts were more effective against Gram-positive or Gram-negative bacteria based on these results. Most of the other test bacteria were chosen among Gram-negative bacteria because *H. pylori* was the target organism in this study and it has gram-negative characteristics. Two Gram-positive bacteria and two yeasts were included in this study to facilitate the estimation of the spectrums of antimicrobial activity of the extracts. Many researchers have also preferred similar test microorganisms when they have worked with *H. Pylori* [10, 32, 33]. However, according to the literature, the effect of both various plant extracts and other antimicrobials on Gram-negative bacteria is less than

Gram-positive bacteria due to the less permeability of the Gram-negative cell wall [34]. The fact that the plant extracts used in our study inhibited Gram-negative bacteria; it made us think these extracts contain powerful antimicrobials.

In this study, *Bacillus subtilis* and *Staphylococcus aureus* species, which were determined as the most sensitive bacteria to extracts of plants, have identified as sensitive species also according to the results of previous research [34]. The single-layer and more permeable cell wall of Gram-positive bacteria including also *S. aureus* and *B. subtilis*, increases their susceptibility to various antimicrobials. [18]. It was seen that the maximum inhibition zone diameters of extracts of the plants used against *H. pylori* in our study were 33 mm (*Capsella bursa-pastoris*), 30 mm (*Acorus calamus*), 32 mm (*Acorus calamus*) and 37 mm (*Acorus calamus*) for water, ethanol, chloroform, acetone, respectively. In some literature studies investigating the antimicrobial activities of plants against *H. pylori*; 26 mm of Black myrobalan (*Terminalia chebula*) plant [15], 42 mm of bearberry (*Arctostaphylos uva-ursi*) and 17 mm of cowberry (*Vaccinium vitis-idaea*) plants. [27], 13 mm of rose oil [19], 40 mm of *Quercus brantii var.persica* [28] have been found to produce inhibition zone diameters against *H. pylori*. has been found to produce inhibition zone diameters against *H. pylori*. In this case, the inhibition zone diameter sizes obtained in our research are quite high and comparable with the above values.

Diameters of the inhibition zone observed in bacterial species which were found to be sensitive both in our research and in previous studies [21] showed that the antimicrobial activities of the extracts used in our study were at an average level. As a matter of fact, acetone extracts of the plants which caused the broadest inhibition according to the results obtained from our study formed a maximum inhibition zone diameter of 25 mm against *B. subtilis* (*Rosmarinus officinalis*), 17 mm against *S. aureus* (*Carum carvi*), 11 mm against *E. coli* (*Thymus*), 16 mm against *K. pneumoniae* (*Melisa officinalis*). However, it is difficult to say which plant extract is stronger in terms of antimicrobial activity based on these findings. Because, although diameters of the inhibition zone are used for comparison purposes, methodical differences, solvent quality and small differences in the amount absorbed on the disk lead to big errors in this regard. For this reason, MIC values are used, which allow a better comparison of antimicrobial activity.

There were also two types of fungi among the test microorganisms used in our study. Among water, ethanol, chloroform, acetone extracts of the plants in our study, The number of those showing antimicrobial effects against *C. albicans* and *S. cerevisiae* yeast species were determined respectively as 0,4; 3,2; 3,3; 3,3. The maximum inhibition zone diameter (12 mm) against *C. albicans* was produced by acetone extract of *Pimpinella anisum* and the maximum inhibition zone diameter (12 mm) against *S. cerevisiae* was produced by water extract of *Capsella bursa*. None of the water extracts formed an

inhibition zone against *C. albicans*. The inhibition zone diameter sizes determined in our study for *C. albicans* and *S. cerevisiae* have been similar to the inhibition diameter values in studies with these species in the literature [35, 36]. Essentially, a researcher has stated that the antifungal properties of herbal extracts are weak from their antibacterial properties and this is due to the structural difference in the cells. According to this investigator, antimicrobial agents must bind to sterols in the cell membrane to inhibit the eukaryotic fungal cell, whereas such binding is not required for non-sterol-bearing procaryotic bacterial cells [18].

Extracts of the plants used in this study were not effective against *Pseudomonas aeruginosa* bacteria species. This result is not surprising. Because *P. aeruginosa* is a species that has a high potential to gain resistance among bacteria and therefore falls outside the spectrum of effect of many antibiotics [1]. As a parallel with the findings obtained from our research, it has been identified as one of the *P. aeruginosa* resistant species in previous studies on the antimicrobial properties of extracts of various plants [15].

Minimum Inhibitory Concentration (MIC)

MIC values were determined also besides diameter sizes of the inhibition zone caused by extracts of plants against test microorganisms in our study. It was found that acetone extracts of plants showed stronger antimicrobial activity against *H. pylori* among the extracts of plants prepared using 4 different solvents. Then MIC values of the extracts forming the broadest inhibition zone against *H. pylori* among acetone extracts of plants were determined. For this purpose, those with a diameter of inhibition zone of 17 mm and broader from acetone extracts of the plants (*Achillea millefolium*, *Pimpinella anisum*, *Rosmarinus officinalis*, *Thymus*, *Hypericum perforatum*) against *H. pylori* were chosen.

The MIC assays of acetone extracts of the six plants against *H. pylori* were given in Table 4. When Table 4 was examined, it was seen that the MIC values of the acetone extracts of the plants varied between 0.019 to 0.625 mg / mL. On the other hand, it was understood that *Acorus calamus* plant had the best (lowest) MIC value (0.019 mg / mL) among acetone extracts of 6 plants.

The MIC values obtained as a result of our research are close to the MIC values determined for extracts of various plants in the literature. Indeed, Ohsaki et al. [33] has found that plant of *Myroxylon peruiferum* has been effective against *H. pylori* with MIC values of 0.078 mg/mL, Sharifi et al. [28] found that plant of *Quercus brantii var.persica* has been effective against *H. pylori* with MIC values of 0.002 mg/mL. These values are smaller (better) than the MIC values obtained in our research. However, there have been also researchers who have been determined MIC values greater (with less inhibitory effect) than our values. For example, Takashima et al. [32] has determined MIC values of 0.3-85.0 mg/mL against *H. pylori* in his study with *Derris malaccensis*. In this case, we can say that the MIC values obtained from extracts of

plants used in our study are at an average level when compared with the values in the literature.

Table 4. Minimum inhibitory concentrations (MIC) of acetone extracts of some plants against *H. pylori* ATCC 49503

Plants	Diameterofinhibit ion zone (mm)	MIC (mg/mL)
<i>Acorus calamus</i> L.	36-37	0.019
<i>Achillea millefolium</i> L.	28-30	0.039
<i>Hypericum perforatum</i> L.	17-19	0.625
<i>Pimpinella anisum</i> L.	25-27	0.156
<i>Rosmarinus officinalis</i> L.	22-24	0.156
<i>Thymus</i> L.	18-20	0.312
Ampicillin	38-45	0.00039

Antioxidant Activity

Thiocyanate method

Since acetone extracts of plants showed stronger antimicrobial activity against *H. pylori*, antioxidant activities of the acetone extract of 5 plants (*Achillea millefolium*, *Pimpinella anisum*, *Rosmarinus officinalis*, *Hypericum perforatum*) forming the broadest inhibition zone against *H. pylori* among acetone extracts of plants were determined. Thiocyanate method and the results were summarized in Figure 1-5.

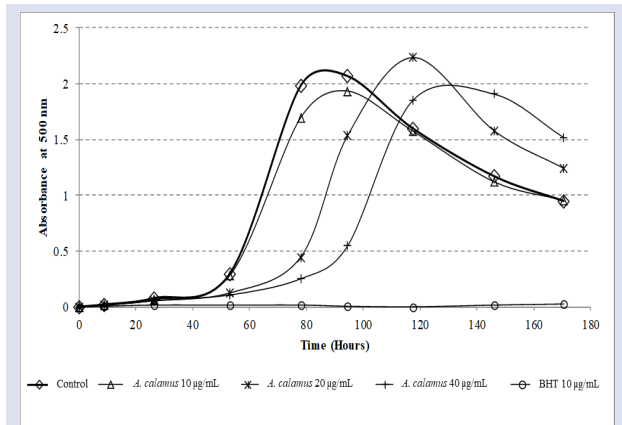


Figure 1. Antioxidant activity of acetone extract of *Acorus calamus*

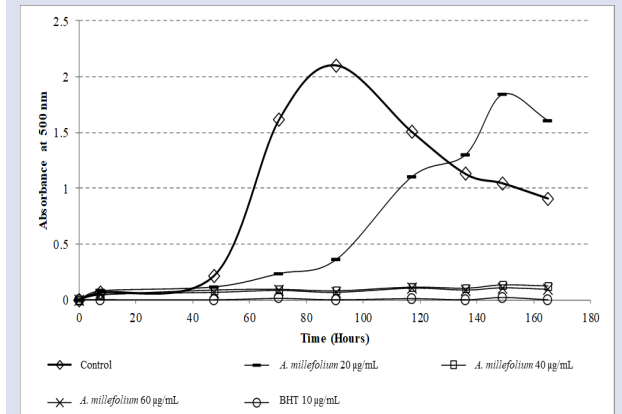


Figure 2. Antioxidant activity of acetone extract of *Achillea millefolium*

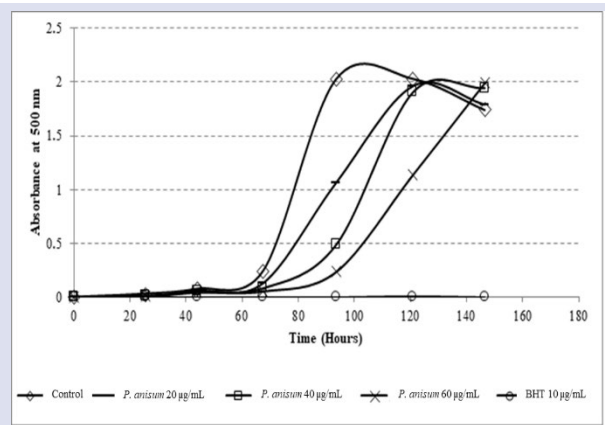


Figure 3. Antioxidant activity of acetone extract of *Pimpinella anisum*

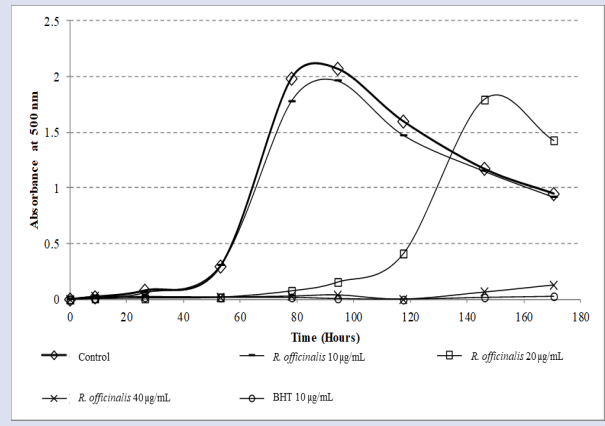


Figure 4. Antioxidant activity of acetone extract of *Rosmarinus officinalis*

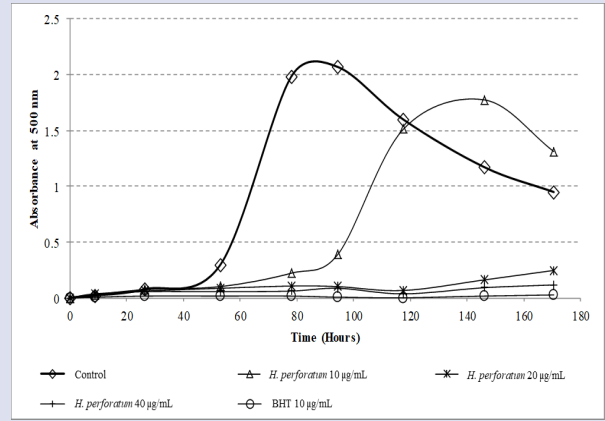


Figure 5. Antioxidant activity of acetone extract of *Hypericum perforatum*

Statistical analyzes of antioxidant activity values were carried out with the SPSS 9.0 package program by performing a two-way analysis of variance. Among acetone extracts of the plants, the extract of *Hypericum perforatum* showed stronger antioxidant activity. This was followed by *Rosmarinus officinalis*, *Achillea millefolium*, *Acorus calamus*, *Pimpinella anisum*, respectively. In all extracts with antioxidant activity, a linear relationship was observed between the concentration of the extract and the antioxidant activity. In other words, as the extract concentration increased, the antioxidant activity increased. The concentration of 40 mg/mL of *Hypericum perforatum* plant showed the maximum antioxidant

activity. This effect of the *Hypericum perforatum* plant followed a parallel course to BHT 50 over for 150 hours as can be seen in Figure 5. It was observed that the concentration of 10 mg/mL of the same plant was ineffective and followed a similar chart to the control. The same was true for other extracts. Generally, a decrease in antioxidant activity was observed in low-concentration extracts around 50-100 hours. On the other hand, in terms of antioxidant activity values of plants, it was determined that the control and extract samples were statistically different from each other ($p < 0.05$).

Antioxidants are present in aerobic organisms against undesired oxidation of biomolecules. Antioxidants are substances that prevent or delay oxidation at the initial and/or developmental stages. Therefore, the presence of compounds with antioxidant activity in biological systems is important for life, and many biological functions such as antimutagenic, anticarcinogenic, anti-aging originate from these antioxidants [37, 38].

In recent years, in researches on the antimicrobial properties of plant extracts, taking into account the benefits mentioned above, the antioxidant properties of the studied plant are also included in the study and researches on this subject is gaining intensity [22, 39, 40].

On the other hand, if a herbal product has both antimicrobial and pro-oxidant (oxidation-promoting) qualities, it is certainly not possible to use it in practice. For these reasons, the antioxidant properties of acetone extract of 5 plants (*Hypericum perforatum*, *Rosmarinus officinalis*, *Achillea millefolium*; *Acorus calamus*, *Pimpinella anisum*) determined to be the most effective in terms of antimicrobial properties in our study were also investigated. For this reason, these 5 plants are recommended for the treatment of diseases due to their antimicrobial properties against *H. pylori* and other test microorganisms and their antioxidant properties mentioned above. Acetone extracts of these 5 plants showed antioxidant properties when Figure 1-5 were examined, it was seen that antioxidant activities of plant extracts increase with increasing concentration. It has been stated that this situation has been due to the increase in the amount of active substance in the extracts with the increasing amount of extract [37]. Since the antioxidant activity in plant extracts is affected by many different factors, it is also stated that it is difficult to determine the main source of antioxidant activity and the contribution of other factors. However, it has been stated that phenolic compounds and flavonoid group substances generally found in various plant extracts have a significant effect on their antioxidant properties [37].

Conclusion

It was determined in our study that the effects of some medicinal plants on the in-vitro growth of *H. pylori* and their antimicrobial and antioxidant potential. As a result, *Hypericum perforatum*, *Rosmarinus officinalis*, *Achillea millefolium*; *Acorus calamus*, *Pimpinella anisum* plants are recommended for the treatment of diseases due to

their antimicrobial properties against *H. pylori* and other test microorganisms and their antioxidant properties. *Acorus calamus* and *Achillea millefolium*, especially should also be tested for in vivo studies. With more detailed studies, it is also necessary to determine the antioxidant properties of other plant extracts (Water, chloroform, ethanol) and to reveal their in-vivo usability.

Conflicts of Interest

The authors state that there is no conflict of interests.

References

- [1] Madigan M. T., Martingo J. M., Brock Mikroorganizmaların Biyolojisi, 11. Baskı. Ankara, (2010) 866-867.
- [2] Widelski J., Okin'czyc P., Paluch E., Mroczek T., Szperlik J., Z'uk M., Sroka Z., Sakipova Z., Chinou I., Skalicka-Woz'niak K., Malm A., Korona-Głowniak I., The Antimicrobial Properties of Poplar and Aspen–Poplar Propolis and Their Active Components against Selected Microorganisms, including *Helicobacter pylori*, *Pathogens*, 11 (2022) 191.
- [3] Mobley H. L. T., Mendz G. L., Hazell, S. L., *Helicobacter pylori* Physiology and Genetics, Washington, (2001).
- [4] Guerra-Valle M., Orellana-Palma P., Petzold G., Plant-Based Polyphenols: Anti-*Helicobacter pylori* Effect and Improvement of Gut Microbiota, *Antioxidants*, 11 (2022) 109.
- [5] Tabak M, Armon R., Neoman I., Cinnamon extracts inhibitory effect on *Helicobacter pylori*, *J. Ethnopharmacol*, 67 (1999) 269-277.
- [6] Korona-Głowniak I., Głowniak-Lipa A., Ludwiczuk A., Baj T., Malm A., The In Vitro Activity of Essential Oils against *Helicobacter Pylori* Growth and Urease Activity, *Molecules*, 25 (2020) 586.
- [7] Yan J., Peng C., Chen P., Zhang W., Jiang C., Sang S., Zhu W., Yuan Y., Yanjun Hong Y., Yao M., In-vitro anti-*Helicobacter pylori* activity and preliminary mechanism of action of *Canarium album* Raeusch. fruit extracts, *J. Ethnopharmacol*, 283 (2022) 114578.
- [8] Ali S. M., Khan A. A., Ahmed I, Musaddiq M., Ahmed K. S., Polasa H., Rao L W., Habibullah C. M., Sechi L. A., Ahmed N., Antimicrobial activities of Eugenol and Cinnamaldehyde against the human gastric pathogen *Helicobacter pylori*, *Ann. Clin. Microbiol. Antimicrob*, 4 (2005) 20.
- [9] Villalva M., Silvan J. M., Guerrero-Hurtado E., Gutierrez-Docio A., Navarro del Hierro J., Alarcón-Cavero T., Prodanov M., Martin D., Martinez-Rodriguez A. J., Influence of In Vitro Gastric Digestion of Olive Leaf Extracts on Their Bioactive Properties against *H. pylori*, *Foods*, 11 (2022) 1832.
- [10] Fabry W., Okemo P., Mwatha W. E., Chhabra S. C., Ansorg R., Susceptibility of *Helicobacter pylori* and *Candida spp.* to the East African plant *Terminalia spinosa*, *Arzneimittel-Forschung/Drug Research*, 46 (1) (1996b) 539-540.
- [11] Yeşilada E., Gürbüz İ., Shibata H., Screening of Turkish anti-ulcerogenic folk remedies for anti -*Helicobacter pylori* activity, *J. Ethnopharmacol*, 66 (1999) 289-293.
- [12] Davis, P. H., Flora of Turkey and the East Aegan Islands. Edinburgh, (1988).
- [13] Baytop T (1999). Türkiye'de Bitkiler ile Tedavi, İstanbul, (1999) 480.

- [14] Aslan A., Güllüce M., Ögütçü H., Bazı likenlerin antimikrobiyal aktiviteleri üzerine bir araştırma, *Biyoteknoloji (Kükem) Dergisi*, 22 (2) (1999) 19-26.
- [15] Malekzadeh F., Ehsanifar H., Shahamat M., Levin M., Colwell R. R., Antibacterial activity of black myrobalan (*Terminalia chebula* Retz) against *Helicobacter pylori*, *Int. J. Antimicrob. Ag.*, 18 (2001) 85-88.
- [16] Bauer A.W., Kirby W. M. M., Sherris J. C., Turk, M., Antibiotic susceptibility testing by a standardized single disk method, *American. J. Clin. Pathol.*, 36 (1966) 493-496.
- [17] Ingolfsdottir K., Hjalmarsdottir M.A., Sigurdsson A., Gudjonsdottir G. A., Brynjolfsdottir A., Steingrimsson O., In vitro susceptibility of *Helicobacter pylori* to protolichesterinic acid from the Lichen *Cetraria islandica*, *Antimicrob. Agents Chemother*, 41(1) (1997) 215-217.
- [18] Ali-Shtayeh S., Yaghmour M. R., Faidi Y. R., Salem K., Antimicrobial activity of 20 plants used in folkloric medicine in the Palestinian area, *J. Ethnopharmacol*, 60 (1998) 265-271.
- [19] Boyanova L., Neshev G., Inhibitory effect of rose oil products on *Helicobacter pylori* growth invitro: preminilary report, *J. Med. Microbiol.*, 48 (1999) 705-706.
- [20] Kadota S., Basnet P., Ishii E., Tamura T., Namba, T., Antibacterial activity of tricarabdal a from *Rabdasia trichocarpa* against *Helicobacter pylori*, *Zbl Bakt.*, 286 (1997) 63-67.
- [21] Srinivasan D., Nathan S., Suresh T., Perumalsamy P.L., Antimicrobial activity of certain Indian medicinal plants used in folcloric medicine, *J. Ethnopharmacol.*, 74 (2001) 217-220.
- [22] Yıldırım A., Mavi A., Kara A. A., Determination of antioxidant and antimicrobial activities of *Rumex crispus* L. Extracts, *J. Agric. Food Chem.*, 49 (2001) 4083-4089.
- [23] Valsaraj R., Pushpangadan P., Smitt V. W., Adhersen A., Nyman U., Antimicrobial screening of selected medicinal plants from India, *J. Ethnopharmacol.*, 58 (1997) 75-83.
- [24] Kubo J., Lee J. R., Kubo I., Anti-*Helicobacter pylori* agents from the cashew apple, *J. Agric. Food Chem.*, 47 (1999) 533-537.
- [25] Yen G. C., Chen H. Y., Antioxidant activity of various tea extracts in relation to their antimutagenicity, *J. Agric. Food Chem.*, 43 (1995) 27-32.
- [26] Eloff J. N., A sensitive and Quick microplate method to determine the minimal inhibitory concentration of plant extracts for bacteria, *Planta Med.*, 64 (1998) 711-713.
- [27] Annuk H., Hirno S., Türi E., Mikelsaar M., Arak E., Wadström T., Effect on cell surface hydrophobicity an susceptibility of *Helicobacter pylori* to medicinal plant extracts, *FEMS Microbiol. Lett.*, 172 (1999) 41-45
- [28] Sharifi A., Azizi M., Moradi-Choghakabodi P., Aghaei S., Aziz A., In vitro anti-*Helicobacter pylori* activity of aqueous extract from Persian Oak testa, *Chin. Herb. Med.*, 11(4) (2019) 394-399.
- [29] Shen X., Zhan W., Peng C., Yan J., Chen P., Jiang C., Yuan Y., Chen D., Zhu W., Yao M., In vitro anti-bacterial activity and network pharmacology analysis of *Sanguisorba officinalis* L. against *Helicobacter pylori* infection, *Chin Med.*, 16(33) (2021) 2-19.
- [30] Ibrahim N. H., Awaad A. S., Alnafisah R. A., Alqasoumi S. I., El-Meligy R. M., Mahmoud A. Z., In-vitro activity of *Desmostachya bipinnata* (L.) Stapf successive extracts against *Helicobacter pylori* clinical isolates, *Saudi Pharm J.*, 26 (2018) 535-540.
- [31] Cáceres A., Fletes L., Aguilar L., Ramirez O., Figueroa L., Taracena A. M., Samayoa B., Plants used in Guatemala for the treatment of gastrointestinal disorders. 3. confirmation of activity against enterobacteria of 16 plants, *J. Ethnopharmacol.*, 38 (1993) 31-38.
- [32] Takashima J., Chiba N., Yoneda K., Ohsaki A., Derrisin, a new rotenoid from *Derris malaccensis* Plain and Anti-*Helicobacter pylori* activity of its related constituents, *J. Nat. Prod.*, 65 (2002) 611-613.
- [33] Ohsaki A., Takashima J., Chiba, N., Kawamura M., Microanalysis of selective potent anti- *Helicobacter pylori* compound in a Brazilian medicinal plant, *Myroxylon peruiferum* and the activity of analogues., *Bioorg. Med. Chem. Lett.*, 9 (1999) 1109-1112.
- [34] Urzua A., Caroli M., Vasquez L., Mendoza L., Wilkens M., Tojo E., Antimicrobial study of the resinous exudate and of diterpenoids isolated from *Eupatorium salvial* (Asteraceae), *J. Ethnopharmacol*, 62 (1998) 251-254.
- [35] Panizzi L., Caponi C., Catalano S., Cioni P. L., Morelli I., In vitro antimicrobial activity of extracts and isolated constituents of *Rubus ulmifolius*, *J. Ethnopharmacol*, 79 (2002) 165-168.
- [36] Heisey R. M., Gorham, B. K., Antimicrobial effects of plant extracts on *Streptococcus mutans*, *Candida albicans*, *Trichophyton rubrum* and other microorganism, *Lett Appl Microbiol.*, 14 (1992) 136-139.
- [37] Mavi, A., *Polygonum cognatum* Meissn (Madımak) ve *Rumex crispus* L (Evelik) bitkilerinin antioksidant aktivitelerinin mukayesesi, Yüksek Lisans, Atatürk Üniversitesi, Fen Bilimleri Enstitüsü, (2000).
- [38] Gulcin İ., Antioxidants and antioxidant methods: an updated overview, *Archiv. Toxicol.*, (2020).
- [39] Mwamatopea B, Tembo D, Chikowe I, Kampirad E., Nyirendae C., Total phenolic contents and antioxidant activity of *Senna singueana*, *Melia azedarach*, *Moringa oleifera* and *Lannea discolor* herbal plants, *Scientific African*, 9 (2020).
- [40] Akhtara M. S., Rafiullah M., Shehataa W. A., Hossain A., Alib M., Comparative phytochemical, thin layer chromatographic profiling and antioxidant activity of extracts from some Indian herbal drugs, *J. Bioresour. Bioprod.*, 7 (2022) 128-134.

Fatty Acid Composition of Seed Oil from Cocklebur (*Xanthium Strumarium* Subsp. *Strumarium*) Grown in Turkey

Cüneyt Cesur^{1,a}, Belgin Coşge Şenkal^{2,b}, Tansu Uskutoğlu^{2,c,*}

¹ Karamanoğlu Mehmetbey University, Energy Systems Engineering, Karaman, Türkiye

² Yozgat Bozok University, Faculty of Agriculture, Department of Field Crops, Yozgat, Türkiye

*Corresponding author

Research Article

History

Received: 18/08/2021

Accepted: 04/06/2022

Copyright



©2022 Faculty of Science,
Sivas Cumhuriyet University

ABSTRACT

Vegetable oils are not only used for human consumption but also used for industrial purposes (soaps, biodiesel, painting, cosmetics, etc.). One of the most important criteria in determining the usage areas of vegetable oils is the fatty acid composition it contains. Turkey supplies its edible oil needs with both seed and vegetable oil imports. To meet this vegetable oil need of Turkey, vegetable oils obtained from different plants are of great importance. This study, it was aimed to determine the oil content, fatty acid composition, and some properties of cocklebur (*Xanthium strumarium* subsp. *strumarium*) seeds collected from the natural area. 100 fruit weight (g), seed weight (g), and hull ratio (%) were determined as 32.23±2.66, 7.17±0.99, and 77.70±2.84, respectively. Cocklebur seeds contain 24.19% seed oil. Its oil is rich in linoleic (%76.97) and oleic (%11.91) acids.

Keywords: Cocklebur, Biodiesel, Fatty acids, Linoleic acid.

^a cuneytcesur@kmu.edu.tr

^b <https://orcid.org/0000-0002-1607-363X>

^c tansuuskutoglu@gmail.com

^c <https://orcid.org/0000-0001-6631-1723>

^b belgin.senkal@yobu.edu.tr

^b <https://orcid.org/0000-0001-7330-8098>

Introduction

The most important problems facing humanity in the 21st century are climate change and global warming. This situation leads to problems such as ongoing desertification, water, and wind erosion [1]. In addition, both population and urbanization and the increase of industrial facilities create serious pressure on agricultural areas [2,3]. All these negativities cause water resources to shrink. Environmental pollution is generally based on fossil fuels, and searching for environmentally friendly alternative energy sources is more important [4]. In addition to reducing these negativities for the sustainability of life, new production areas and plants are brought to the agricultural production pattern.

Plants maintain their vitality by producing essential nutrients and some vital organic compounds such as carbohydrates, proteins, and fats oils. These products also constitute the most important sources of nutrients in humans and animals. Oil crops are plants that contain oil in their seeds or fruits and are of economic importance in terms of the fatty acid composition of this oil. Oil is a triglyceride ester which is consist of trivalent alcohol and three fatty acids connecting with ester linkages. The most important ingredient of the oil is fatty acids which are hydrocarbon chains and result in a straight carboxyl group (-COOH). The number of carbons and double bonds in these chains determines the physical and chemical properties of the oil [5]. The usage areas of oils depending on the physical and chemical properties of oils. Vegetable oils are not only used as food sources but also use in industrial purposes [6].

Because of environmental damage caused by fossil fuels, the use of renewable energy which is obtained from plant material is increasing with each passing day and it became more important. Understanding that fossil fuels will run out one day, it increased attention on renewable energy sources. Plants such as corn, safflower, soybean, canola, etc. are used to produce biodiesel, and also that oil plants are used as human food. Oil which is used as raw material for biodiesel is constituted supply and demand irregularities in the oil consumption as food. Today, the oil market is needed as human food, especially in some countries is subject to serious shortcomings [7]. To overcome this situation, fatty oil which isn't suitable for human consumption should be used in the biodiesel industry. This will reduce the pressure on edible oil production.

Xanthium L. belongs to Asteraceae family, and represented by 3 species (*X. orientale* / rough cocklebur, *X. spinosum* / cocklebur, and *X. strumarium* / large cocklebur), and 3 subspecies (*X. orientale* subsp. *italicum*, *X. strumarium* subsp. *brasilicum*, *X. strumarium* subsp. *strumarium*) in total it has 6 taxa in Turkey [8]. *Xanthium* L. species are annual and seen as it has no commercial properties. Therefore, it is diagnosed as a weed and while farmers are trying to get rid of cocklebur due to its detrimental effect on crops, at the same time, farmers waste not only their strength but also their time and money [9].

Cocklebur seed contains 25-42% oil. Looking at the oil composition, linoleic acid accounts for 77% of the total oil

content. The human body cannot synthesize a couple of rare fatty acids and one of them is linoleic acid. This fatty acid is of great importance in maintaining cardiovascular health and cholesterol balance [10]. In this respect, there may be used as food oils because of containing high linoleic acid content [5, 11, 12].

Cocklebur is used in traditional and modern medicine because its seed oil has various biological activities such as antibacterial, antitumor, etc. Because of these properties, cocklebur plant oil is used treatment of some diseases such as allergies, diabetes, appendix, sinusitis, cancer, high blood pressure, and dysentery [13-15].

The oil contained in cocklebur plant seeds is at least useable in industries. In the world, plant cultivation has two serious obstacles: water and soil. For cultivation, sometimes the soil is not suitable and sometimes the soil is good but the water is missing one. Cocklebur has a feature that can minimize the effect of bad soil structure and lack of water. In addition, the plant can grow easily in these infertile areas. This feature will allow the opening of lands with limited opportunities for agricultural production. On the other hand, the cocklebur plant not only developing of biological diversity but also constitutes the vegetation in the area which is open to erosion. The plant can create vegetation in danger of erosion area and it can contribute to the prevention of environmental degradation.

This study, it was aimed to determine the oil content, fatty acid composition, and some properties of cocklebur seeds collected from the natural area.

Materials and Methods

In autumn 2014, plant material (Figure 1) (*X. strumarium* subsp. *strumarium*) was collected in Muslubelen gateway, which is located in Yozgat coordinate 39° 41' 34.64"N-34° 50' 54.86" E and 1443 m altitude. All measurements and oil extraction from seeds were carried out in the laboratories of Yozgat Bozok University, Faculty of Agriculture.

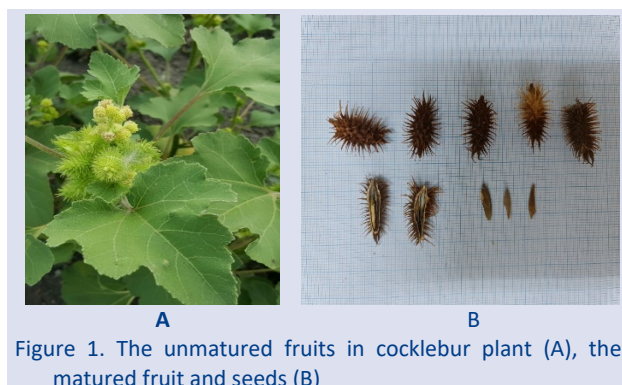


Figure 1. The unmatured fruits in cocklebur plant (A), the matured fruit and seeds (B)

Seed Properties of Cocklebur

100 fruit weight (g), seed weight (g), hull weight (g), and hull ratio (%) were determined in the plant material collected from the natural area at full maturity. Fruit width (mm), fruit length (mm), seed width (mm), seed length

(mm), and seed thickness (mm) of randomly selected 10 fruits were measured. All measurements and weighings were made in triplicate.

Extraction Procedure

Cocklebur seeds (2 g) were ground with a laboratory-type blender. The oil was extracted using petroleum benzene in a Soxhlet apparatus for 3 h. After the solvent was removed using a rotary evaporator. The extracted oils were kept in brown bottles, flushed with nitrogen, and stored at - 18 °C until analyses.

Derivatization of the Seed Oils

Trans-methyl derivatives were prepared for Gas chromatography–Mass spectrometry (GC-MS) (Agilent 6890 N Network GC system combined with Agilent 5973 Network Mass Selective Detector) analysis of the seed oil samples. Trans-methyl derivatives of samples were prepared according to the method described by Orhan et al. [16]. GC-MS operating conditions were performed as specified in Official Methods of Analysis of Association of Analytical Chemistry (AOAC) [17].

Results and Discussion

Seed Properties of *X. Strumarium* Subsp. *Strumarium*

Each cocklebur fruit contains two seeds. Some seed properties of cocklebur are given in Table 1. One of the most important properties sought in oil plants is the hull ratio. Since the filling of the grain and the decrease in the hull ratio increase the oil yield, a low hull ratio is desired. Commercial variety of safflower, grown in Turkey, seeds hull content about 40 - 51 % [18-20]. Although it varies according to the area of use (oil or confectionary sunflower), the hull ratio in sunflower is around 40-50% [21-22]. When the cocklebur is examined, it will be seen that this rate is around 77%. However, this plant is still wild species. This ratio can be improved with breeding studies.

Table 1. Some properties of cocklebur seed

Seed Properties	Unit	Value
100 Fruit weight		32.23±2.66
Seed weight	(g)	7.17±0.99
Hull weight		23.95±2.49
Hull ratio	(%)	77.70±2.84
Fruit length		15.83±1.75
Fruit width		6.94±1.18
Seed length	(mm)	13.35±1.39
Seed width		1.54±0.24
Seed thickness		3.81±0.49

Fatty acid analysis of the seed oil by GC–MS

Cocklebur plant seeds that are collected in nature contain an average of 24,19 % raw oil. When the seed oil was investigated, linoleic acid, oleic acid, palmitic acid, and stearic acid were determined as major oil

components. The cocklebur seed oil contains 76.97% linoleic acid and 11.38% oleic acid. Because of that, the cocklebur seed oil is in the oleic-linoleic acid group. The crops in this group are considered as source of first-class cooking oil [5]. It is seen as a quality oil component oleic acid, linoleic acid, and linolenic acid total of three of the acid is 89.10% in the cocklebur seed oil. In addition, its oil contains 0.08% heptadecanoic acid and 0.31% gadeloic acid. The composition of the cocklebur also contains 9.23% saturated fatty acids. The distribution of saturated fatty acids palmitic acid, stearic acid, and eicosenoic acid were determined 6.51%, 3.80%, and 0.20% respectively (Table 2).

Table 2. The chemical composition of cocklebur seed oil

No	Compounds	Retention Index	(%)
1	Palmitic acid [C _{16:0}]	1298	6.51
2	Heptadecanoic acid [C _{16:1}]	1416	0.08
3	Stearic acid [C _{18:0}]	1622	3.80
4	Oleic acid [C _{18:1}]	1638	11.38
5	Linoleic acid [C _{18:2}]	1710	76.97
6	Linolenic acid [C _{18:3}]	1778	0.75
7	Eicosenoic acid [C _{20:0}]	1916	0.20
8	Gadeloic acid [C _{20:1}]	1952	0.31
		Total :	100.00
Total Saturated Fatty Acids			
Σ [C _{16:0}] + [C _{18:0}] + [C _{20:0}]			10.51
Total Unsaturated Fatty Acids			
Σ [C _{16:1}] + [C _{18:1}] + [C _{18:2}] + [C _{18:3}] + [C _{20:1}]			89.49

Fatty acid containing a double bond is called a single (mono) unsaturated fatty acid and the fatty acid-containing multiple bonds are called multiple (poly) unsaturated fatty acids. These fatty acids are rich in oil called unsaturated fats. Oleic acid, linoleic acid, and linolenic acid are the most important unsaturated fatty acids found in vegetable oils. Especially oleic acid and linoleic acid are the two major unsaturated fatty acids that are found in vegetable oils [23]. These fatty acids contain two and three double bonds in the carbon chain, respectively. These fatty acids are referred to as vitamin F and these essential fatty acids are important in human nutrition [24]. While the total of oleic acid and linoleic acid are 88.88% in Cocklebur, this ratio changes in other oil plants such as 82.66% in olives, 81.46% in peanuts, 82.98% for rapeseed, 85.20% in sesame, 88.82% in sunflower, 91.5% in the safflower, 77.86% in soy, has a rate of 25.99% in linen and 35.23% in camelina [5].

Erucic acid oils used only in industrial areas and genetic studies led to the development of species that have low erucic acid content. While this rapeseed developed by breeding programs adopted for quality edible oil erucic acid maximum limit of 2% [25], in the analysis of cocklebur seeds erucic acid has not been observed.

Oil Content and the Fatty Acid Composition of Cocklebur Seeds and Comparison with other Oil Crops

It had determined that the oil rate of the cocklebur seeds was 24.19%. It has been observed that this oil ratio may have economic importance when compared with other oil crops, such as soybean, rapeseed, sunflower, linen, cotton, etc. (Table 3). The oils obtained from the seeds of the plants in Table 3 are evaluated differently. It is seen that the oil content of these plants varies between 16-50%, and the oil content of cocklebur seeds has an average value. Like poppyseed oil, the cocklebur seed oil is light yellow in color. It is similar to sunflower oil in taste and smell.

Table 3. Comparison of cocklebur seed oil content with other oil crops

Plant	Oil content (%)	References
Soybean (<i>Glycine max</i> L.)	18-24	[26]
Rapeseed (<i>Brassica napus</i> ssp.)	36-50	[27]
Sunflower (<i>Helianthus annuus</i> L.)	33-50	[28]
Linen (<i>Linum usitatissimum</i> L.)	35-50	[29]
Cotton (<i>Gossypium</i> spp.)	16-20	[30]
Crambe (<i>Crambe abyssinica</i> Hochst.)	25-40	[31]
Camelina (<i>Camelina sativa</i> Crantz)	30-45	[31]
Cocklebur (<i>X. strumarium</i> subsp. <i>strumarium</i>)	24.19	This study

Cocklebur plant in terms of distribution of fatty acids seems to have considerable potential. The quality edible oils class and oleic acid-rich plants are olives, peanut, sesame, and rapeseed. When these plants are compared to cocklebur, their' oleic acid is seen to be lower (Figure 2).

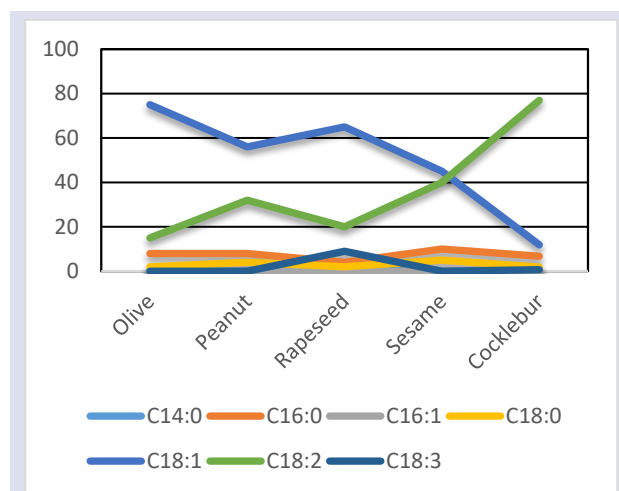


Figure 2. The oleic acid-rich plants

In this study, it was determined that cocklebur seed oil contains higher linoleic acid (76.97%) compared to many

oil crops. Linoleic acid ratios were reported as 15% in olive, 32% in peanut, 20% in rapeseed, 40% in sesame, 70% in sunflower, 77% in safflower, 12% in flax, and 20% in camelina. Oils rich in linoleic acid and oleic acid are the most consumed cooking oils [5]. The total amount of oleic acid and linoleic acid in cocklebur seed oil is 88.88%. This rate is seen to be 88.66% in olive oil and 88.82% in sunflower oil, which is commonly used cooking oil.

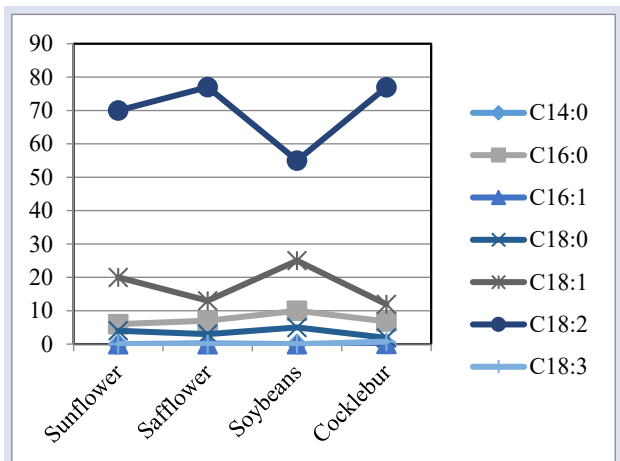


Figure 3. Linoleic acid-rich plants

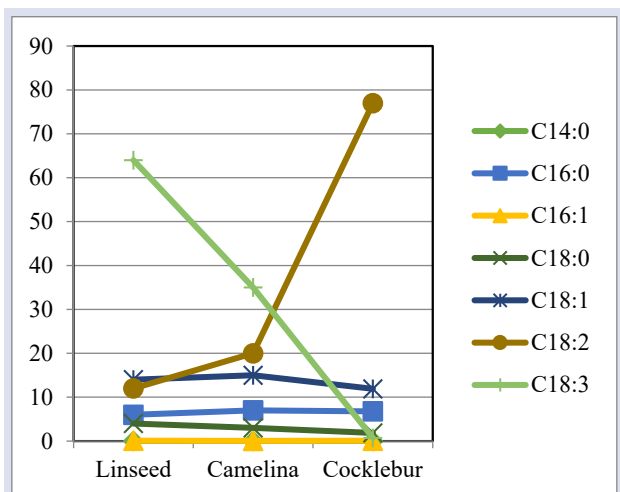


Figure 4. Linolenic acid-rich plants

Linolenic acid is one of the few essential fatty acids like linoleic acid. While linolenic acid is not found in olive, peanut, sesame, safflower, and sunflower oils, it can be found up to 5% in soybean oil. (Figure 4). In cocklebur, the ratio was determined as 0.74%. Linolenic acid shelf-life and durability are lower because they oxidize quickly. Therefore, linolenic acid contained in oils dries quickly and is more suitable for use in industrial areas. It has been widely used in products such as paints, varnishes, and lacquer. Plants with a high percentage of linolenic acid play an important role in the production of biodiesel which is used in renewable energy sources and has increasing importance in recent years.

The primary use of vegetable oils is in the food industry. However, vegetable oils with low edible oil

quality are used economically in other industrial areas apart from food. In this context, it is of great importance to expanding the cultivation of oil plants, which have economic value for different industries. As is seen in Figure 5, erucic acid isn't found in cocklebur oil which is harmful in terms of edible oil. Erucic acid was harmful in the 1960s because it was making unwanted effects on the heart, animal growth rate, and muscle. Until 1982, World Health Organization (WHO) determined the maximum rate of erucic acid in edible oils which is up to 10%. After 1982, they revised this rate up to 5%. Thus, the lack of erucic acid in the oil of cocklebur is a suitable value for edible oil [27].

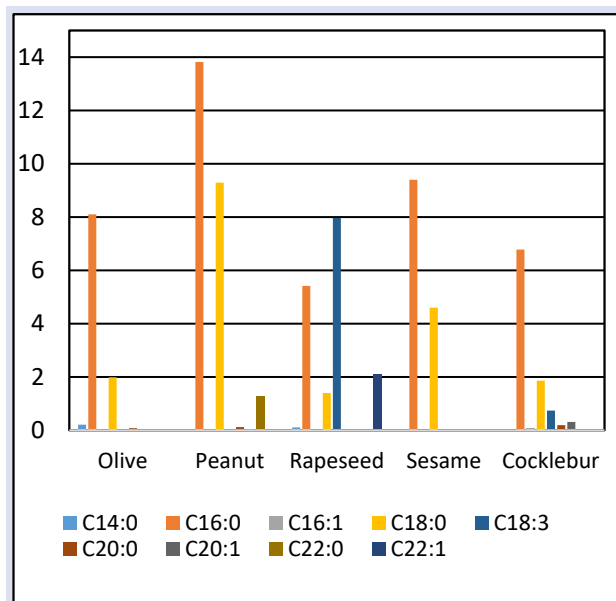


Figure 5. Comparison of minor fatty acid components of cocklebur seed oil with some oil crops

Plants that contain a high amount of oil in their seeds or fruits and that can be used economically are called oil crops. The fatty acid composition of oils is the most important factor that determines their commercial use. Cocklebur, which contains 24% oil in its seeds, is a plant with the potential to be economically evaluated. According to its fatty acid composition, cocklebur oil can be evaluated in medicinal, herbal medicine, and possible pharmaceutical use. However, more detailed studies are needed to determine whether the oil can be used for human consumption and because of the physiological characteristics of the plant, cultivating the plant will provide huge economic and agricultural benefits.

Conflicts of Interest

The authors state that did not have a conflict of interests.

References

- [1] Saygın S.D., Madenoğlu S., Erpul G., Türkiye’de Toprak Erozyonu ve Çölleşme, *TÜRKTOB*, 4(15) (2015) 64-69.
- [2] Dong F., Gao X., Yu X., Long R., Driving Mechanisms and Peak Level of CO₂ Emissions in China: Evidence from a Simultaneous Equation Model, *Sustainability*, 273 (2018) 3306-3317.
- [3] Kyzioł-Komosinska J., Rosik – Dulewska C., Dzieniszewska A., Pajak M., Low – Moor Peats as Biosorbents for Removal of Onionicdyes from Water, *Fresenius Environ. Bull.*, 27(1) (2018) 6-20.
- [4] Mancini M., Volpe M.L., Gatti B., Malik Y., Moreno A.C., Leskovar D., Cravero V., Characterization of Cardoon Accessions as Feedstock for Biodiesel Production, *Fuel*, 235 (2019) 1287-1293.
- [5] Baydar H., Erbas S., Yağ Bitkileri Bilimi ve Teknolojisi. Isparta: S.D.U. Ziraat Fakültesi Yayınları, (2014).
- [6] Ardabili A.G., Farhoosh R.M., Khodaparast H., Chemical Composition and Physico Chemical Properties of Pumpkin Seeds (*Cucurbita pepo* subsp. *pepo* var *styriaca*) Grown in Iran, *J. Agric. Sci. Technol.*, 13 (2011) 1053-1063.
- [7] Eryılmaz T., Yesilyurt M.K., Cesur C., Gökdoğan O., Biodiesel Production Potential from Oil Seeds in Turkey, *Renew. Sustain. Energy Rev.*, 58 (2016) 842-851.
- [8] Güner A., Aslan S., Ekim T., Vural M., Babaç M.T., Türkiye Bitkileri Listesi (Damarlı Bitkiler). İstanbul: Nezahat Gökyiğit Botanik Bahçesi ve Flora Araştırmaları Derneği Yayını, (2012).
- [9] Bozic D., Barac M., Saric-Krsmanovic M., Pavlovic D., Ritz C., Vrbnicanin S., Common Cocklebur (*Xanthium strumarium*) Response to Nicosulfuron. *Not. Bot. Horti. Agrobot. Cluj Napoca.*, 43(1) (2015) 186–191.
- [10] Arslan B., The Determination of Oil Content and Fatty Acid Compositions of Domestic and Exotic Safflower (*Carthamus tinctorius* L.) Genotypes and Their Interactions, *Agronomy*, 6 (2007) 415-420.
- [11] Nagaraj G., Safflower Seed Composition and Oil Quality Review. III. International Safflower Conference, Beijing, (1993) 58–71.
- [12] Bowles V., Mayerhofer G., Davis R., Good A.G., Hall J.C.A., Phylogenetic Investigation of *Carthamus* Combining Sequence and Microsatellite Data, *Plant Syst. Evol.*, 287 (2010) 85–97.
- [13] Haque M.E., Rahman S., Rahmatullah M., Jahan R., Evaluation of Anti-Hyperglycemic and Anti-Nociceptive Activity of *Xanthium indicum* Stem Extract in Swissalbino Mice, *BMC Complement Altern. Med.*, 13 (2013) 296-300.
- [14] Peng W., Ming O.L., Han P., Zhang O.Y., Jiang Y.P., Zheng C.J., Han T., Qin L.P., Anti-allergic Rhinitis Effect of Caffeoylxanthiazonoside Isolated from Fruits of *Xanthium strumarium* L. in Rodent Animals, *Phytomedicine*, 21 (2014) 824–829.
- [15] Chen W.H., Liu W.J., Wang Y., Song X.P., Chen G.Y., A New Naphthoquinone and Other Antibacterial Constituents from the Roots of *Xanthium sibiricum*, *Nat. Prod. Res.*, 29(8) (2015) 739–744.
- [16] Orhan I.E., Senol F.S., Ozturk N., Celik S.A., Kan A.P.Y., Phytochemical Contents and Enzyme Inhibitory and Antioxidant Properties of *Anethum graveolens* L. (dill) Samples Cultivated Under Organic and Conventional Agricultural Conditions, *Food Chem. Toxicol.*, 59 (2013) 96-103.
- [17] AOAC, Official Methods of Analysis of Association of Analytical Chemistry. 15th edn. Washington DC: (1990) 963.
- [18] Ada R., Dimension, Geometric, Agricultural and Quality Characteristics of Safflower Seeds, *Turkish J. Field Crop.*, 19 (1) (2014) 7-12.
- [19] Kılı F., Kanar Y., Tekeli F., Evaluation of Seed and Oil Yield with Some Yield Components of Safflower Varieties in Kahramanmaraş (Turkey) Conditions. *Int. J. Environ.*, 7 (2) (2016) 136-140.
- [20] Demir I., Kara K., The Effect of Different Environmental Conditions on Yield and Oil Rates of Safflower (*Carthamus tinctorius* L.), *Fresenius Environ. Bull.*, 27 (2) (2018) 989-995.
- [21] Ahmad S., Environmental Effects on Seed Characteristics of Sunflower (*Helianthus annuus* L.), *J Agron Crop Sci.*, 187(3) (2001) 213-216.
- [22] Ergen Y., Sağlam C., Yield and Yield Characters of Different Confectionery Sunflower Varieties in Conditions of Tekirdag, *J. Tekirdag Agric. Fac.*, 2 (3) (2005) 221-227.
- [23] Baydar H., Bitkilerde Yağ Sentezi, Kalitesi ve Kaliteyi Artırmada Islahın Önemi, *Ekin*, 11 (2000) 50-57.
- [24] Nas S., Gökalp H.Y., Unsal M., Bitkisel Yağ Teknolojisi, Denizli: Pamukkale Üniversitesi Mühendislik Fakültesi Ders Kitapları, (2001).
- [25] Kurt O., Seyis F., Alternatif Yağ Bitkisi: Ketencik, *J. of Fac. of Agric. Omu*, 23 (2) (2008) 116-120.
- [26] Wilson R.F., H.R., Specht, J.E. (Ed), Seed Composition In: Boerma, Soybeans: Improvement, Production, and Uses, 3rd ed. , Madison: (2004) 621–677.
- [27] Salunkhe D.K., Chavan J.K., Adsule R.N., Kadam S.S., World Oilseeds: Chemistry, Technology, and Utilization. New York: Van Nostrand Reinhold (1992).
- [28] Panchenco A.Y., Sunflower Production and Breeding in the USSR. 2nd International Sunflower Conference, Manitoba, (1966) 15–29.
- [29] Anonymous, Flax-Lin Recolte. Available at: <https://www.grainscanada.gc.ca/flax-lin/harvest-recolte/2016/hqf16-qrl16-en.htm> Retrieved October 24, 2016.
- [30] Lukonge E., Labuschagne M.T., Hugo A., The Evaluation of Oil and Fatty Acid Composition in Seed of Cotton Accessions from Various Countries, *J. Sci. Food Agric.*, 87 (2007) 340–347.
- [31] Baydar H., Erbaş S., 2014. Yağ Bitkileri Bilimi ve Teknolojisi. Süleyman Demirel Üniversitesi Yayın No: 97 (ISBN: 978-9944-452-75-5)

Synthesis, Structure Elucidation and Biological Activity of New Hybrid Hydrazone-Amide Compounds

Göknil Pelin Coşkun ^{1,a,*}, Akın Aklamuz ^{1,b}, Ufuk İnce ^{2,c}, Mert Ülgen ^{1,d}

¹ Department of Pharmaceutical Chemistry, Faculty of Pharmacy, Acibadem Mehmet Ali Aydınlar University, İstanbul, Türkiye

² Department of Pharmaceutical Microbiology, Faculty of Pharmacy, Erciyes University, Kayseri, Türkiye

*Corresponding author

Research Article

History

Received: 22/04/2022

Accepted: 30/06/2022

Copyright



©2022 Faculty of Science,
Sivas Cumhuriyet University

ABSTRACT

Bacterial infection today occupies a tremendous place in world health. The infection diseases were kept under control after the development of penicillin and further studies were performed on the development of new antibacterial agents. However, to date, bacterial resistance caused a big failure in the treatment of infectious disease and therefore, development of new antibacterial agents became important for human health. In the present study, we have designed, synthesized and elucidated the structures of new hydrazone-amide compounds and their hybrid amide derivatives. The structures of the compounds were elucidated with spectroscopic methods and their purity were proven by TLC, HPLC-MS analysis. The antibacterial and antifungal activity studies of the novel molecules were investigated on different strains. Among the synthesized compounds, AA3a and AA4a appeared to show promising antibacterial activity. None of the compounds showed significant antifungal activity on *Candida albicans*. The drug likeness properties and boiled-egg plot analysis were performed for all of the compounds. The novel molecules showed no violation on Lipinski's rule of five and all the molecules showed good gastrointestinal absorption properties in the *in silico* studies.

Keywords: 4-ASA, Hydrazone, Hydrazone, Amide, Antibacterial activity.

^a goknilpelincoskun@gmail.com

^b <https://orcid.org/0000-0001-5168-3866>

^c Ecz.ufuk.ince@gmail.com

^d <https://orcid.org/0000-0002-7316-4802>

^e Akin.aklamuz@live.acibadem.edu.tr

^f <https://orcid.org/0000-0003-2374-3061>

^g Mert.ulgen@acibadem.edu.tr

^h <https://orcid.org/0000-0003-4913-4950>

Introduction

Infectious diseases have been a tremendous threat to human health for centuries. First success was achieved via the discovery of penicillin and bacterial infections were kept in control over a period of time. To date, many new antibiotics were presented to human health services but the treatment failed due to the low bioavailability, adverse effects and uncontrolled release of these compounds [1]. Over the past decades, unfortunately bacteria showed resistance to current antibiotics with a fast adaptation to the environment. For a certain period of time, discovery of new bacterial targets resulted with the development of more effective antibiotics; however, scientists still face with different bacterial resistances [2]. In order to overcome the resistance, bacterial life cycle must be studied in detail. A new bacterial macromolecule could be an answer to both bacterial resistance and infectious disease treatment. The design of a new drug passes through a series of process that involved in medicinal chemistry [3-5]. The drug spectrum mainly identifies with MIC dilution assays, which most likely provide a detailed insight into the drug. Besides the MIC studies, *in silico* techniques also support and shorten the discovery time of the drug candidate [6].

Medicinal chemistry studies include a series of steps starting with the identification of pharmacophore groups. The effects of many heterocyclic rings and different functional groups have been studied over a period of time. Among them, studies on hydrazone-hydrazone structures

occupies a vital place in drug discovery process. Hydrazones consist of a structure of $-HC=N-NH_2$. However, hydrazone-hydrazones have $-HC=N-NH-CO-$ structure, an additional carbonyl group. The synthetic route for hydrazone-hydrazones involves a reaction between hydrazone and substituted aldehyde/ketone. The reaction sometimes requires no catalyst; but in some circumstances, an acid may facilitate the reaction. Their synthetic procedure requires no complex conditions; therefore, these class of compounds are extensively studied over a period of time. Besides their high yield synthetic route, they possess diverse uses such as anticancer, antimicrobial, anticonvulsant, antidiabetic, anti-tuberculosis, antitumor, antidepressant, anti-inflammatory, and antiviral activities [7]. Metabolically, hydrazone-hydrazones cause a lower toxicity than hydrazides since the free amino group turns into an azomethine moiety. The *in vitro* metabolic studies also showed the hydrolytic profile of hydrazone-hydrazone structures [8, 9]. The specific physicochemical properties of the hydrazone-hydrazones made them an important functional group on antibacterial drug development, which may eliminate the microbial resistance to the current drugs [10]. Nifuroxazide is one of the leading molecule that contains a hydrazone-hydrazone functionality and it exerts antiseptic effects. Mitoguazone (anticancer), ferimzone (fungicide), dihydralazine (antihypertensive) have hydrazone functionality. We,

therefore, decided to design a series of hydrazone containing molecules at the first place.

The dual activities or more pharmacophore group has advantages on the biological activities of drugs. The design of our study started with hydrazide-hydrazone synthesis. We have included one more step for our compounds by introducing amide, another important functional group which is available in the structure of antibacterial, local anaesthetic, analgesic and anticancer drugs.

In the light of the foregoing, we have designed and synthesized a series of novel hydrazide-hydrazone compounds starting from 4-aminosalicylic acid (4-ASA) as amide hybrids. We have elucidated their structure with spectroscopic methods and purified them with column chromatography; afterwards the purity of the compounds were elucidated by LC-MS studies. Their antibacterial activities were investigated on different bacterial strains. Among the synthesized compounds, compound AA3a (hydrazide-hydrazone) and AA4a (hydrazide-hydrazone/amide hybrid) showed promising antibacterial activity.

Materials and Methods

General

All the chemicals were purchased from Merck (Darmstadt, Germany), Sigma-Aldrich (St. Louis, MO). Reactions were monitored by TLC on silica gel plates purchased from Merck (Merck Co., Darmstadt, Germany). Melting points of the synthesized compounds were determined in a Stuart SMP50 Automatic Melting Point apparatus and these are uncorrected. The purity of the compounds was confirmed by TLC, LC-MS. NMR spectra were recorded on BRUKER 400 MHz (Billerica, MA) for ¹H-NMR. Data are reported as follows: chemical shift, multiplicity (b.s.: broad singlet, d: doublet; m: multiplet, s: singlet, and t: triplet), coupling constants (Hz), integration. An Agilent 1260 Infinity II HPLC-MS spectra equipped with G7114A 1260DAD detector, G7311B 1260 Quad Pump system, G1328C 1260 manual injection unit and G6125B LC/MSD detector was used for both HPLC and mass analysis. Retention times were recorded with ACE C18 column (particle size: 3 µm, pore size: 100Å). The column temperature was adjusted to 25°C in the column compartment. The mobile phase consisted of acetonitrile-water (80:20, v/v) mixture and delivered at a flow rate of 0.8 ml/min. The injection volume was 20 µL. The UV detector was operated at 254 nm. R_f×100 values were recorded on petroleum ether/ethyl acetate/gl. acetic acid (different ratios, see Table 2). Mass spectral analysis were performed with Advion Expression CMS device, ASAP probe, Advion Chem express software. Samples were scanned as positive and negative ion and were directly applied into the device via an ASAP probe.

Synthetic procedure for methyl 4-amino-2-hydroxybenzoate (AA1)

4-aminosalicylic acid (0.01 mol) was dissolved in methanol (30 ml) and few drops concentrated sulphuric

acid was added. The mixture was heated under reflux for 20-24 h and the reaction was monitored with TLC. After the reaction was completed, the mixture was neutralized with 10% NaHCO₃ and the solid obtained was filtered and recrystallized with ethanol [11].

Synthetic procedure for 4-amino-2-hydroxybenzohydrazide (AA2)

4-ASA ester (AA1) (0.01 mole) was dissolved in ethanol (10 ml) and excess hydrazine hydrate was added. The reaction was refluxed for 4-6 hours and monitored with TLC. After the reaction was completed, the mixture was evaporated under atmospheric pressure. The crude product was recrystallized with ethanol. [12]

General procedure for the synthesis of compounds 4-amino-N'-[(E)-(4-substitutedphenyl)methylidene]-2-hydroxybenzohydrazide (AA3a-b)

4-ASA hydrazide (AA2) (0.001 mol) was dissolved in ethanol and equimolar amount of substituted benzaldehyde was added in the presence of few drops concentrated hydrochloric acid. The reaction mixture was refluxed for 6 hours and monitored with TLC. After the reaction was completed, ice-cold water was added and precipitate formed was filtered, dried and purified with column chromatography.

Synthetic procedure for N-(4-(((2Z)-2-(4-chlorobenzylidene)hydrazinyl)carbonyl)-3-hydroxyphenyl)benzamide (AA4a)

Compound AA3a (0.001 mole) was dissolved in THF and sodium carbonate (30 mg) was added. Benzoyl chloride (0.003 mole) was added dropwise in cold and the reaction mixture was kept in room temperature for 4 hours. The reaction was monitored with TLC. After the reaction was completed, the precipitate was filtered and purified with column chromatography.

Methyl 4-amino-2-hydroxybenzoate (AA1)

Gray crystal. Yield 91 %; m. p. 121°C; MW: 167.05 g/mol; R_f×100 value: 74.6; Rt value: 12.12 min. ¹H-NMR (400 MHz) (DMSO-d₆/TMS) δ ppm: 10.78 (s, 1H, Ar-OH), 7.46 (bs, 2H, Ar-NH₂), 6.14-6.00 (m, 3H, Ar-H), 3.79 (s, 3H, COOCH₃). MS (vAPCI): [M⁺1]: 168.

4-Amino-2-hydroxybenzohydrazide (AA2)

Orange solid. Yield 98 %; m. p. 197°C; MW: 167.06 g/mol; R_f×100 value: 4.7; Rt value: 6.40 min. ¹H-NMR (400 MHz) (DMSO-d₆/TMS) δ ppm: 12.45 (bs, 1H, NH-NH₂), 9.51 (s, 1H, Ar-OH), 7.43 (bs, 2H, Ar-NH₂), 6.18-5.70 (m, 3H, Ar-H), 4.39 (bs, 2H, NH-NH₂). MS (vAPCI): [M⁺1]: 168.

4-Amino-N'-[(E)-(4-chlorophenyl)methylidene]-2-hydroxybenzohydrazide (AA3a)

White solid. Yield 97 %; m. p. 250-252°C; MW: 289.06 g/mol; R_f×100 value: 62.2; Rt value: 19.20 min. ¹H-NMR

(400 MHz) (DMSO- d_6 /TMS) δ ppm: 12.43 (bs, 1H, -NH-N=CH-), 11.60 (s, 1H, -NH-N=CH-), 8.39 (s, 1H, Ar-OH), 7.75-5.49 (m, 8 H, Ar-H and *Ar-NH₂). MS (vAPCI): [M+1]: 290. *Ar-NH₂ was exchanged with deuterium

4-Amino-N'-[(E)-(4-bromophenyl)methylidene]-2-hydroxybenzohydrazide (AA3b)

Yellow solid. Yield 75%; m. p. 240-242 °C; MW: 333.01 g/mol; Rfx100 value: 63.1; Rt value: 14.01 min. ¹H-NMR (400 MHz) (DMSO- d_6 /TMS) δ ppm: 12.39 (bs, 1H, -NH-N=CH-), 11.80 (s, 1H, -NH-N=CH-), 8.39 (s, 1H, Ar-OH), 7.87-5.93 (m, 8 H, Ar-H and *Ar-NH₂). MS (vAPCI): [M+1]: 334. *Ar-NH₂ was exchanged with deuterium

N-(4-[(2Z)-2-(4-chlorobenzylidene)hydrazinyl]carbonyl)-3-hydroxyphenylbenzamide (AA4a)

Yellow solid. Yield 80.05 %; m. p. 235-237°C; MW: 393.08 g/mol; Rfx100 value: 65; Rt value: 9.12 min. ¹H-NMR (400 MHz) (DMSO- d_6 /TMS) δ ppm: 12.97 (bs, 0.3H, CONH), 12.31 (s, 1H, Ar-OH), 10.80-10.55 (m, 2H, -NH-N=CH-), 8.16-6.87 (m, 12H, Ar-H). MS (vAPCI): [M+1]: 394.

Antimicrobial Activity Test

The six compounds were tested for their antimicrobial activities against *Staphylococcus aureus* ATCC 29213, *Enterococcus faecalis* ATCC 29212 (Gram-positive bacteria), *Escherichia coli* ATCC 25922, *Pseudomonas aeruginosa* ATCC 27853 (Gram-negative bacteria) and *Candida albicans* ATCC 10231 (fungus). This test was

performed according to the Clinical Laboratory Standards Institute (CLSI) M100-S28 protocol for bacteria [10] and CLSI M27-A3 protocol for fungi [14]. Mueller Hinton Broth (MHB) and RPMI-1640 mediums were used for determination of antibacterial and antifungal activity of the compounds, respectively.

The compounds were dissolved in 10% DMSO. The serial dilutions of each compound at the range of 512-2 μ g/mL were prepared in 96-well microplates, after placing broth mediums in each well. Suspension of each microorganism was prepared using McFarland 0.5 standard and as a result 10⁵ cfu/ml densities were reached. Microplates were incubated for 24 hours at 37°C for bacteria and for 48 hours at 35°C for fungus. The reference drugs were tested against these microorganisms. Besides, growth control of microorganisms and sterilization control of the mediums were tested. 10% DMSO as solvent in this study was tested for its potential antimicrobial activity. The wells with the lowest concentration without microbial growth were determined as minimum inhibition concentration (MIC). The detection was made by visual evaluation using dye MTT [15]. The test repeated 3 times.

In Silico Properties

Drug likeness properties were studied using SwissADME program. The SMILE codes of the compounds were inserted and the ADME predictions were run via the program. The results displayed in Table 1.

Table 1. Some properties of synthesized compounds from SwissADME

	HBA	HBD	TPSA	Log P _{o/w}	SC	-Log K _p	GIA	RoF (V)	Ghose	Leadlikeness (V)
4-ASA	3	3	83.65	0.84	Soluble	6.30	High	0	No	No
AA 1	3	2	72.55	1.31	Soluble	6.15	High	0	Yes	No
AA 2	3	4	101.37	0.82	Soluble	7.09	High	0	No	No
AA 3a	3	3	87.71	1.97	Moderate	5.96	High	0	Yes	Yes
AA 3b	3	3	87.71	1.80	Moderate	6.18	High	0	Yes	Yes
AA 4a	4	3	90.79	2.70	Poor	5.18	High	0	Yes	No

MW: Molecular weight, **HBA:** H-bond acceptor, **HBD:** H-bond donor, **TPSA:** Topologic polar surface area (\AA^2) **Log P_{o/w}:** Consensus Log P_{o/w} (Average of all five predictions), **SC:** Solubility Class (Water), **GIA:** Gastrointestinal absorption, **Log K_p:** skin permeation (-cm/s), **RoF (V):** Rule of Five (violation number), **Ghose:** Ghose Filter, **Leadlikeness (V):** Suitability score (violation number).

Results and Discussion

Chemistry

4-Aminosalicylic acid (4-ASA) was chosen as a starting compound for this study. Its ester and hydrazide derivatives were synthesized accordingly; confirming with the literature data [11, 12]. The corresponding hydrazide derivatives were then converted into their hydrazide-hydrazone structures. Briefly, 4-ASA hydrazide was treated with substituted benzaldehydes in the presence of hydrochloric acid. The hydrazide-hydrazones are generally known to be produced in high yield with no catalyst needed. First attempts for hydrazone synthesis were done only in room temperature. However, the reaction only

proceeded in the presence of concentrated hydrochloric acid. Although, there are several solvents available for hydrazone synthesis, we decided to perform the synthesis in absolute ethanol as it has less toxicity than other solvents. The amide formation of the hydrazone structures were tricky. The first attempt was to add benzoyl moiety in the beginning of the synthesis. However, when doing so, the amide was hydrolyzed easily in the esterification process. Furthermore, benzoylation of hydroxyl group could be another problem for the following steps. Eventually, we decided to synthesize amide in the last step. The formation of amide was

performed using Schotten Baumann reaction. For this, hydrazide-hydrazone was dissolved in tetrahydrofuran (THF) and small amount of sodium carbonate was added to provide basic conditions. The benzoyl chloride was added dropwise and the reaction was kept in room temperature for several hours. The chlorine substituted derivative underwent amide formation but the reaction could not be completed in the case of bromine substituted derivative. It was assumed that the steric hindrance resulting from bromine could be the main cause (Figure 2). All the reaction processes were monitored by thin layer chromatography (TLC) with the mobile phases listed below (Table 2). The compounds were purified with crystallization and column chromatography. The purity of the compounds were also confirmed by LC-MS.

Table 2. TLC mobile phase conditions

Compound	Mobile Phase	Rfx100 Value
AA1	S1: Ethyl acetate:petroleum ether +100µl g. acetic acid	AA1:74.6
AA2	(5/5, v/v)	AA2: 4.7
AA3a-b	S2: Ethyl acetate:petroleum ether +100µl g. acetic acid	AA3a:62.2 AA3b:63.1
AA4a	S3: Ethyl acetate:petroleum ether +100µl g. acetic acid	AA4a:65
	(6/4, v/v)	

The structures of original hydrazide-hydrazone and amide hybrids were elucidated by $^1\text{H-NMR}$ and MS spectral techniques. The results proved the proposed structures of the compounds. $^1\text{H-NMR}$ spectra showed the formation of ester and hydrazide derivatives from 4-ASA. Methyl protons of AA1 were recorded at 3.79 ppm with 3 integration values. The disappearance of carboxylic acid proton was also another proof for the presence of ester. The hydrazide formation was confirmed by observing the presence of $-\text{CO-NH-NH}_2$ protons. The methyl protons of AA1 disappeared and two broad singlet peaks were recorded at 7.43 and 4.39 ppm respectively. As $-\text{NH-}$ proton is close to carbonyl group, it shifted down field and recorded at 7.43 ppm, 1H integration. $-\text{NH}_2$ protons were recorded at 4.39 ppm, 2H integration. The formation of hydrazide-hydrazone was monitored with azomethine proton in NMR spectra. The $^1\text{H-NMR}$ results indicated the formation of hydrazide-hydrazone with the disappearance of NH_2 protons from compound AA2. The peak recorded at 4.39 ppm disappeared and singlet peaks were recorded at 11.60-11.80 ppm for AA3a and AA3b respectively. However, aromatic amine protons were exchanged with deuterium as this is a common condition for protons bonded with heteroatoms. Same situation was observed for AA4a, as the amide proton was recorded as 0.3 H integration value. The chemical shift for this proton was strong because of carbonyl and aromatic rings. Therefore, the formation of the amide hybrid was proved by a peak recorded at 12.97 ppm.

For all the synthesized compounds, mass spectral analysis were performed both with LC-MS and Mass Spectra (Volatile Atmospheric Pressure Chemical

ionization (vAPCI). The molecular ion peaks were recorded as calculated (M+1) (See Supplementary file).

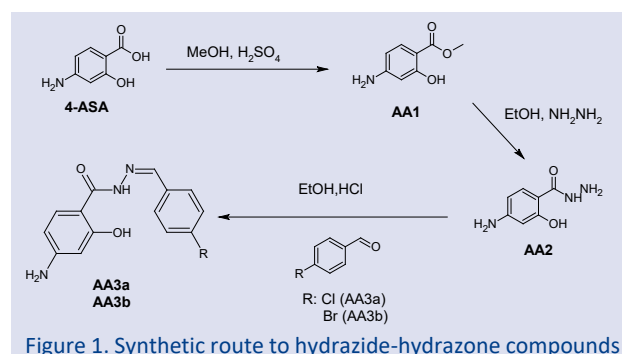


Figure 1. Synthetic route to hydrazide-hydrazone compounds

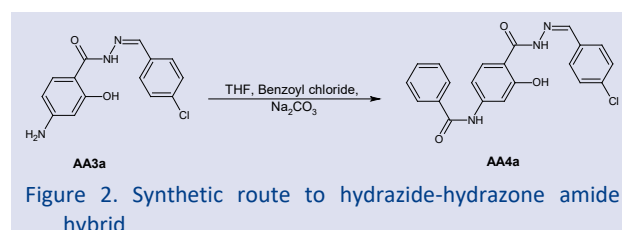


Figure 2. Synthetic route to hydrazide-hydrazone amide hybrid

Biological Activity

Several studies were reported for the biological activities of hydrazide-hydrazone structures [16-35]. The hydrazone group has an advantage of blocking the free amine for metabolic stability. Thus, the potential toxicity of the hydrazones could be compared to hydrazone derivatives. We therefore decided to study their antibacterial and antifungal activities on different bacterial and fungal strains. The MIC values were determined for each compound and ampicillin, gentamicin, vancomycin for antibacterial and fluconazole for antifungal activity were used as reference drugs. The results were listed in Table 3.

The antibacterial results obtained in the present study gave a general overview for certain functional groups of the synthesized compounds. It was understood from the results that compounds have moderate antimicrobial activity to both Gram positive and Gram negative bacteria. All of the synthesized compounds and 4-ASA showed weak activity to *S. aureus* ATCC 29213 with MIC value of 256 µg/ml. Thus, the modifications on the functional groups caused no difference for *S. aureus* strain. On the other hand, compounds showed promising activity against *E. faecalis* ATCC 29212 with the MIC value ranging from 64-256 µg/ml. Introduction of carboxylic acid, ester and hydrazide groups showed no difference in the activity against *E. faecalis*. However, chlorine substitution of hydrazide-hydrazone made a difference on the activity. This could be due to proper lipophilicity of the compound. When chlorine is replaced with bromine atom, the activity decreases. As bromine atom is larger than chlorine, the bromine derivative might have difficulty in reaching cellular targets. Besides, amide hybrid altered the activity profile in a negative way. With those results, we can conclude that larger molecules may lower the antibacterial activity on Gram-positive bacteria.

For Gram-negative bacterial strains, compounds showed weak antibacterial activity (except for compound AA4a). The functional group modifications from carboxylic acid to ester, hydrazide and hydrazide-hydrazone favoured the antibacterial activity. There is also a decrease on the antibacterial activity of compound AA3b, which has a bromine atom, on *E. coli* strain. This could also be a result of the bulky bromine group. On the contrary, the hybrid molecule showed the best antibacterial activity on *P. aeruginosa* strains.

It was assumed that the peptidoglycan barrier made no significant difference in terms of antibacterial activity. In a way, the target macromolecule of the compounds could not be enzymes in peptidoglycan biosynthesis. Because, cell wall difference made no change in the antibacterial activity. This could partly explain the small difference between Gram-positive and Gram-negative antibacterial activity. However, in both cases, hydrazine and amide functional groups caused dramatic increases in the activity. It is difficult to analyse the structure-activity relationship with few substitutional changes but the bulky group made a notable decrease in the activity on bacterial strains.

The diverse biological activities of hydrazone compounds led us to investigate the *C. albicans* strains. In our present study, there are no significant antifungal activity detected for all of the compounds. This could be the result of no interaction with lanosterol 14 α -demethylase enzyme in ergosterol synthesis. Thus, the MIC values of all compounds on *C. albicans* ATCC 10231 were at the range of 128-512 μ g/ml.

Table 3: *In vitro* MICs (μ g/mL) observed of the compounds and reference antimicrobial drugs

COMPOUNDS		MICROORGANISMS				
		S. a.	E. f.	E. c.	P. a.	C. a.
1	4-ASA	256	128	256	256	128
2	AA-1	256	128	128	128	256
3	AA-2	256	128	128	128	>512
4	AA-3a	256	64	128	128	128
5	AA-3b	256	128	256	128	128
6	AA-4a	256	256	256	64	256
	Ampicilin	2	2	16	NT	NT
	Gentamycin	1	2	1	1	-
	Vancomycin	1	2	NT	NT	NT
	Fluconazole	NT	NT	NT	NT	1

S.a.: *Staphylococcus aureus* ATCC 29213; E.f.: *Enterococcus faecalis* ATCC 29212; E.c.: *E. coli* ATCC 25922; P.a.: *Pseudomonas aeruginosa* ATCC 27853; C.a.: *Candida albicans* ATCC 10231
NT: Not Tested

Drug Likeness Properties

A SwissADME program was used for calculation of physicochemical properties of the synthesized compounds and 4-ASA [36]. The details were listed in Table 1. The parameters that are most likely to be considered in drug development were calculated virtually. H-bond acceptor (HBA), H-bond acceptor (HBD), polar

surface area (PSA/TPSA), partition coefficient (Log Po/w), skin permeability (Log Kp), Rule of five (violation number-RoF) and Gastrointestinal absorption (GIA) were calculated and evaluated for the suitability. According the Lipinski's rule of five, all of the compounds showed no violation and presented to have good bioavailability. All of the novel molecules passed the Ghose filter. However, lead likeness were applicable interestingly only for hydrazide-hydrazone compounds. The boiled-egg plot was also investigated for the absorption of compounds from gastrointestinal system and penetration of them from the brain. All of the compounds showed good absorption on gastrointestinal tract but their brain permeability was poor (Figure 3).

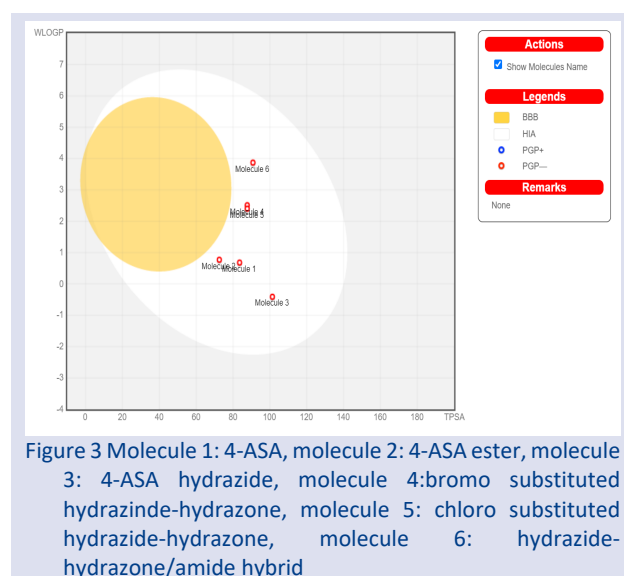


Figure 3 Molecule 1: 4-ASA, molecule 2: 4-ASA ester, molecule 3: 4-ASA hydrazide, molecule 4: bromo substituted hydrazide-hydrazone, molecule 5: chloro substituted hydrazide-hydrazone, molecule 6: hydrazide-hydrazone/amide hybrid

Conclusion

In the present study, we have synthesized and elucidated the structures of novel hydrazide-hydrazone compounds and a hydrazide-hydrazone/amide hybrid drug candidate. The structures of the compounds were elucidated using spectroscopic methods and purity of the compounds were confirmed by chromatographic methods. The compounds having hydrazide-hydrazone and the amide hybrid showed promising antibacterial activity on tested bacterial strains. The antibacterial mechanism of action could possibly be depending on the physicochemical properties of the compounds. Further studies should be carried out in order to find out the correct mechanism of the new lead molecules.

Acknowledgements

This study was granted by TUBITAK 2209-A 2021/1 1919B012100499.

Conflicts of interest

There are no conflicts of interest in this work.

References

- [1] Zheng H., Li H., Deng H., Fang W., Huang X., Qiao J., Tong Y., Near Infrared Light-Responsive And Drug-Loaded Black Phosphorus Nanosheets For Antibacterial Applications, *Colloids Surf B Biointerfaces*, 214 (2022) 112433.
- [2] Theuretzbacher U., Resistance drives antibacterial drug development, *Curr. Opin. Pharmacol*, 11(5) (2011) 433-8.
- [3] Kaplan Ö., Gökşen N. Biosynthesis of silver nanoparticles from Teucroside and investigation of its antibacterial activity, *Cumhuriyet Sci. J.*, 42 (1) (2021) 60-67.
- [4] Aşan Özsağlam M. , Tacer S. , Boulechfar S., Zellagui A. An Investigation of the Bactericidal and Fungicidal Effects of Algerian Propolis Extracts and Essential Oils., *Cumhuriyet Sci. J.*, 43 (1) (2022) 14-19.
- [5] Akgül Ö., Akgünlü Ç., Biler H., Ateş A., Ermertcan Ş. Antimicrobial activity screening of a series of taurine derivatives, *Cumhuriyet Science J*, 42 (4) (2021) 781-788.
- [6] Lister P.D., The role of pharmacodynamic research in the assessment and development of new antibacterial drugs, *Biochem Pharmacol*, 71(7) (2006) 1057-65.
- [7] Boulebdia H., Zinea Y., Khodjaa I.A., Mermer A., Demir A., Debache A., Synthesis and radical scavenging activity of new phenolic hydrazone/hydrazide derivatives: Experimental and theoretical studies, *J. Mol. Struct.*, 1249 (2022) 131546.
- [8] Komurcu S.G., Rollas S., Ulgen M., Gorrod J.W., Cevikbas A., Evaluation of some arylhydrazones of p-aminobenzoic acid hydrazide as antimicrobial agents and their in vitro hepatic microsomal metabolism, *Boll Chim. Farm.*, 134(7) (1995) 375-9.
- [9] Ulgen M., Durgun B.B., Rollas S., Gorrod J.W., The in vitro hepatic microsomal metabolism of benzoic acid benzylidenehydrazide, *Drug Metabol Drug Interact*, 13(4) (1997) 285-94.
- [10] P. Vijaya G., Sundaraselvan., Synthesis, characterization, PASS analysis and ADMET properties of oxazolone ring containing hydrazone derivatives, *Materials Today: Proceedings*, 48 (2022) 502–507.
- [11] Chen J., Lu W., Chen H., Bian X., Yang G., A New Series of Salicylic Acid Derivatives as Non-saccharide α -Glucosidase Inhibitors and Antioxidants, *Biol. Pharm. Bull*, 42(2) (2019) 231-246.
- [12] Yamada H., Kojo M., Nakahara T., Murakami K., Kakima T., Ichiba H., Yajima T., Fukushima T., Development of a fluorescent chelating ligand for scandium ion having a Schiff base moiety, *Spectrochim. Acta A. Mol. Biomol. Spectrosc.*, 90 (2012) 72-7.
- [13] Clinical and L.S. Institute, Performance standards for antimicrobial susceptibility testing, Clinical and Laboratory Standards Institute Wayne, PA. (2017).
- [14] Wayne, P., Clinical and Laboratory Standards Institute: Reference method for broth dilution antifungal susceptibility testing of yeasts; approved standard, *CLSI Document M27-A3 and Supplement S.*, 3 (2008) 6-12.
- [15] Shi L., Ge H.M., Tan S.H., Li H.Q., Song Y.C., Zhu H.L., Tan R.X., Synthesis and antimicrobial activities of Schiff bases derived from 5-chloro-salicylaldehyde, *Eur. J. Med. Chem.*, 42 (4) (2007) 558-64.
- [16] Rollas S., Küçükgül S.G., Biological activities of hydrazone derivatives, *Molecules*, 12(8) (2007) 1910-39.
- [17] Küçükgül S.G., Mazi A., Sahin F., Oztürk S., Stables J., Synthesis and biological activities of diflunisal hydrazide-hydrazones, *Eur. J. Med. Chem.*, 38 (11-12) (2003) 1005-13.
- [18] Şenkardes S., Kaushik-Basu N., Durmaz İ., Manvar D., Basu A., Atalay R., Küçükgül S.G., Synthesis of novel diflunisal hydrazide-hydrazones as anti-hepatitis C virus agents and hepatocellular carcinoma inhibitors, *Eur. J. Med. Chem.*, 27(108) (2016) 301-308.
- [19] Rollas S., Kucukguzel S.G., Hydrazone, amide, carbamate, macromolecular and other prodrugs of doxorubicin, *Open Drug Delivery Journal*, 2 (2008) 77-85.
- [20] Küçükgül S.G., Koç D., Çıkla-Süzgün P., Özsavcı D., Bingöl-Özakpınar Ö., Mega-Tiber P., Orun O., Erzincan P., Sağ-Erdem S., Şahin F., Synthesis of Tolmetin Hydrazone-Hydrazones and Discovery of a Potent Apoptosis Inducer in Colon Cancer Cells, *Arch. Pharm. (Weinheim)*, 348(10) (2015) 730-42.
- [21] Küçükgül S.G., Rollas S.. Synthesis, characterization of novel coupling products and 4-arylhydrazono-2-pyrazoline-5-ones as potential antimycobacterial agents, *Farmaco*, 57(7) (2002) 583-7.
- [22] Han M.I., Guler G., Temel Y., Sadik K., Kucukguzel S.G., Synthesis and antibacterial activity of new hydrazide-hydrazones derived from Benzocaine, *Marmara Pharm. J.*, 21(4) (2017) 961-966.
- [23] Çıkla-Süzgün P., Küçükgül S.G., Recent Advances in Apoptosis: THE Role of Hydrazones, *Mini Rev. Med. Chem.*, 19(17) (2019) 1427-1442.
- [24] Şenkardes S., Han M.I., Kulabaş N., Abbak M., Çevik Ö., Küçükgül İ., Küçükgül S.G., Synthesis, molecular docking and evaluation of novel sulfonyl hydrazones as anticancer agents and COX-2 inhibitors, *Mol. Divers*, 24(3) (2020) 673-689.
- [25] Çıkla P., Özsavcı D., Bingöl-Özakpınar Ö., Şener A., Çevik Ö., Özbaş-Turan S., Akbuğa J., Şahin F., Küçükgül S.G., Synthesis, cytotoxicity, and pro-apoptosis activity of etodolac hydrazide derivatives as anticancer agents, *Arch. Pharm. (Weinheim)*, 346(5) (2013) 367-79.
- [26] Hamzacebi M.C., Rollas S., Kucukguzel, S.G., Kocyigit-Kaymakcioglu B., Synthesis and structure elucidation of hydrazones derived from N-(2,4-dimethylphenyl)-3-oxobutanamide, *ARKIVOC (Gainesville, FL, United States)*, (12) (2008) 188-194.
- [27] Kucukguzel S.G., Rollas S., Kucukguzel I., Kiraz M., Synthesis and antimycobacterial activity of some coupling products from 4-aminobenzoic acid hydrazones, *Eur. J. Med. Chem.*, 34(12) (1999) 1093-1100.
- [28] Koc H.C., Atlihan I., Mega-Tiber P., Orun O., Kucukguzel S.G., Synthesis of some novel hydrazide-hydrazones derived from etodolac as potential anti-prostate cancer agents, *J. Res. Pharm.*, 26(1) (2022) 1-12.
- [29] Cıkla P., Kucukguzel G., Kucukguzel I., Rollas S., De Clercq E., Pannecouque C., Andrei G., Snoeck R., Sahin F., Bayrak O.F., Synthesis and evaluation of antiviral, antitubercular and anticancer activities of some novel thioureas derived from 4-aminobenzohydrazide hydrazones, *Marmara Pharm. J.*, 14(1) (2010) 13-20.
- [30] Tatar E., Senkardes S., Sellitepe H.E., Kucukguzel S.G., Karaoglu S.A., Bozdeveci A., De Clercq E., Pannecouque C., Ben Hadda T., Kucukguzel I., Synthesis, and prediction of molecular properties and antimicrobial activity of some acylhydrazones derived from N-(arylsulfonyl)methionine, *Turkish J. Chem.*, 40(3) (2016) 510-534.

- [31] Han M.I., Bekci H., Cumaoglu A., Kucukguzel, S.G., Synthesis and characterization of 1,2,4-triazole-containing hydrazide-hydrazones derived from (S)-naproxen as anticancer agents, *Marmara Pharm. J.*, 22(4) (2018) 559-569.
- [32] Senkardes S., Kiyimaci M.E., Kale K., Kozanoglu I.M., Kaskatepe B., Kucukguzel S.G., Synthesis, structural elucidation and biological activities of some novel sulfonyl hydrazones as antibacterial agents, *J. Res. Pharm.*, 25(2) (2021) 135-141.
- [33] Aydin S., Kaushik-Basu N., Arora P., Basu A., Nichols D.B., Talele T.T., Akkurt M., Celik I., Buyukgungor O., Kucukguzel S.G., Microwave assisted synthesis of some novel flurbiprofen hydrazide-hydrazones as anti-HCV NS5B and anticancer agents, *Marmara Pharm. J.*, 17(1) (2013) 26-34.
- [34] Han M.I., Atalay P., Tunç C.Ü., Ünal G., Dayan S., Aydın Ö., Küçükğüzel Ş.G., Design and synthesis of novel (S)-Naproxen hydrazide-hydrazones as potent VEGFR-2 inhibitors and their evaluation in vitro/in vivo breast cancer models, *Bioorg. Med. Chem.*, 1(37) (2021) 116097.
- [35] Senkardes S., Tatar E., Nepravishta R., Cela D., Paci M., Bingöl-Ozakpınar O., Sekerler T., De Clercq E., Pannecouque C., Kucukguzel S.G., Synthesis and Biological Activity of N-(arylsulfonyl) Valine Hydrazones and Assistance of NMR Spectroscopy for Definitive 3D Structure, *Lett. Drug Design&Discov.*, 16(9) (2019) 974-983.
- [36] SwissTargetPrediction. Swiss Institute of Bioinformatics, (2021), Retrieved 12 April, 2022 from <http://www.swisstargetprediction.ch/>

Synthesis, Molecular Docking and Molecular Dynamics Simulation Studies of Some Pyridazinone Derivatives as Lipase Inhibitors

Mehmet Abdullah Alagöz ^{1,a,*}, İnci Selin Doğan ^{2,b}, Sıla Özlem Şener ^{3,c}, Zeynep Özdemir ^{1,d}

¹ Department of Pharmaceutical Chemistry, Faculty of Pharmacy, İnönü University, Malatya, Türkiye

² Department of Pharmaceutical Chemistry, Faculty of Pharmacy, Karadeniz Technical University, Trabzon, Türkiye

³ Department of Pharmacognosy, Gülhane Faculty of Pharmacy, Health Sciences University Ankara, Türkiye

*Corresponding author

Research Article

History

Received: 24/06/2022

Accepted: 26/08/2022

Copyright





©2022 Faculty of Science,
Sivas Cumhuriyet University

ABSTRACT


Human health and illness are dependent on lipases, which play a key role in maintaining cell integrity, storing fat for energy and serving as signaling molecules. In this study, 4 compounds that carry 6-phenylpyridazin-3(2H)-one main nucleus, which can be effective as lipase inhibitors, were synthesized and their structures were elucidated. The biological activity of synthesized compounds was evaluated via the porcine pancreatic lipase type II (PLL) inhibitor assay. Orlistat, a lipase inhibitor, was used as a positive control. Compound **8d** was found to be the most effective compound, with an IC_{50} value of 32.66 ± 2.8265 ($\mu\text{g/mL}$). In addition, molecular docking and molecular dynamics simulations studies were carried out to examine the interactions of the compounds with the target in detail. The results obtained as a result of these *in silico* studies were found to be compatible with the lipase inhibition effects of the compounds. It was observed that the compounds may have potential lipase inhibitory effects as a result of the substitutions of the 3-(6-oxo-3-phenylpyridazin-1(6H-yl)propanehydrazide structure.


Keywords: Pyridazinone, Molecular docking, Molecular dynamics simulations studies, Lipase inhibition.


 mehmet.alagoz@inonu.edu.tr


 <https://orcid.org/0000-0001-5190-7196>


 selinci@gmail.com

 <https://orcid.org/0000-0003-4949-1747>

 silaozlem.sener@sbu.edu.tr

 <https://orcid.org/0000-0001-7679-7165>

 zeynep.bulut@inonu.edu.tr

 <https://orcid.org/0000-0003-4559-2305>

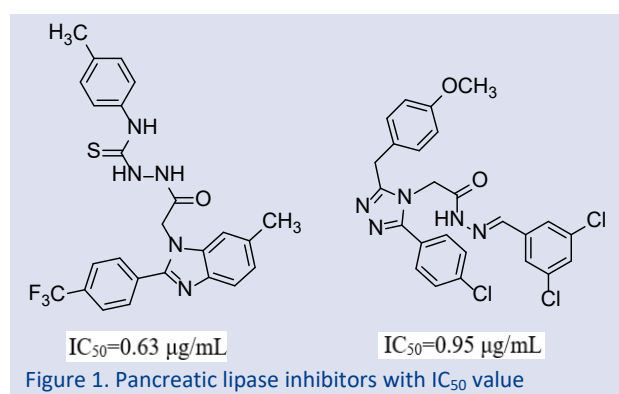
Introduction

Lipids play an important role in regulating the physicochemical properties and functions of cellular membranes, membrane repair, and cellular signaling. It is an efficient energy storage unit. In particular, they play a critical role in the metabolism of drug molecules. Changing the amounts of various lipid species by activating or deactivating their biosynthetic or degradation processes has been demonstrated to be either beneficial or harmful [1].

Lipases have an important role in both human health and disease. Lipases operate in dietary lipid digestion, transport, and processing. Lipases also hydrolyze a range of lipid substrates to control membrane integrity, lipid signaling, and the creation and dynamics of lipid rafts [2]. Most lipases are members of the serine hydrolase superfamily, which uses the nucleophilic active-site serine catalyze the hydrolysis of various lipid substrates. Because of the common biochemistry across this enzyme class, as well as particular chemical scaffolds that target serine hydrolases, various lipase inhibitors have been developed [3,4].

Pyridazinone derivatives have been suggested to offer such intriguing bioactivity as an antitumoral, antibacterial-antifungal, anticonvulsant, analgesic, anti-inflammatory, antiplatelet, and anticancer impact [5-12]. Also, many of the pyridazinone derivatives have been synthesized by our research group as an inhibitor of cholinesterases which are from the serine hydrolase enzyme family [13-

17]. It has been reported that compounds with heterocyclic ring containing nitrogen and oxygen atoms, such as oxadiazolone, benzo[1,3]oxazinon and benzoxazole, inhibit PLL. [18-20]. Cetilistat, which has a benzo[1,3]oxazin-4-one structure, inhibits pancreatic lipase, and is used in the clinic. In addition, it has been reported that compounds containing benzylidenehydrazide and thiosemicarbazide group (Figure 1) have significant lipase inhibition effects [21-23].



In the light of this information, four pyridazinone derivative compounds (**8a-d**) were designed, synthesized and their lipase inhibitory properties were investigated with the MTT assay. Molecular docking simulations were employed to determine the compounds to interactions to

the targeted enzyme. By comparing the outcomes of in vitro enzyme inhibition and molecular docking investigations, the relationships between structure and activity was established [24].

Materials and Methods

Chemistry

Aldrich, Fluka, and Emanuel Merck supplied all of the compounds employed in this investigation. Scheme 1 entails the synthesis of 4-oxo-4-phenylbutanoic acid (3), 6-(p-tolyl)-4,5-dihydropyridazin-3(2H)-one (4), 6-(p-tolyl)pyridazin-3(2H)-one (5), ethyl 3-(6-oxo-3-(p-tolyl)pyridazin-1(6H)-yl)propanoate (6) In this study, **8b** and **8d** were synthesized for the first time. TLC on Merck Kieselgel F254 plates was used to track the progression of the reaction. Using the Electrothermal 9200 melting points device, the melting points were ascertained. The structures of these pyridazinone derivatives were confirmed by $^1\text{H-NMR}$ and $^{13}\text{C-NMR}$ spectra obtained with a Bruker avance 300 MHz NMR spectrometer at İBTAM (İnönü University) and mass spectra obtained with an Agilent LC/MS instrument.

Synthesis of Compounds

Synthesis of 6-(p-tolyl)pyridazin-3(2H)-one (5)

Glyoxylic acid (2) (0.05 mol) and 4-methylacetophenone (1) (0.15 mol) were heated for 2 hours at 100°C . The reaction mixture was cooled to 40°C at the conclusion of this interval, and then 20 mL water and 5 mL ammonium hydroxide solution (25%) were added to the reaction mixture until the medium pH reached 8. The reaction mixture was then extracted using dichloromethane. The separated aqueous layer was

treated with hydrazine hydrate (0.05 mol), and the reaction mixture was refluxed for 2 hours. The reaction mixture was cooled to room temperature when the reaction was completed. The precipitate that formed was filtered to yield chemicals [13,14].

Synthesis of ethyl 3-(6-oxo-3-(p-tolyl)pyridazin-1(6H)-yl)propanoate (6)

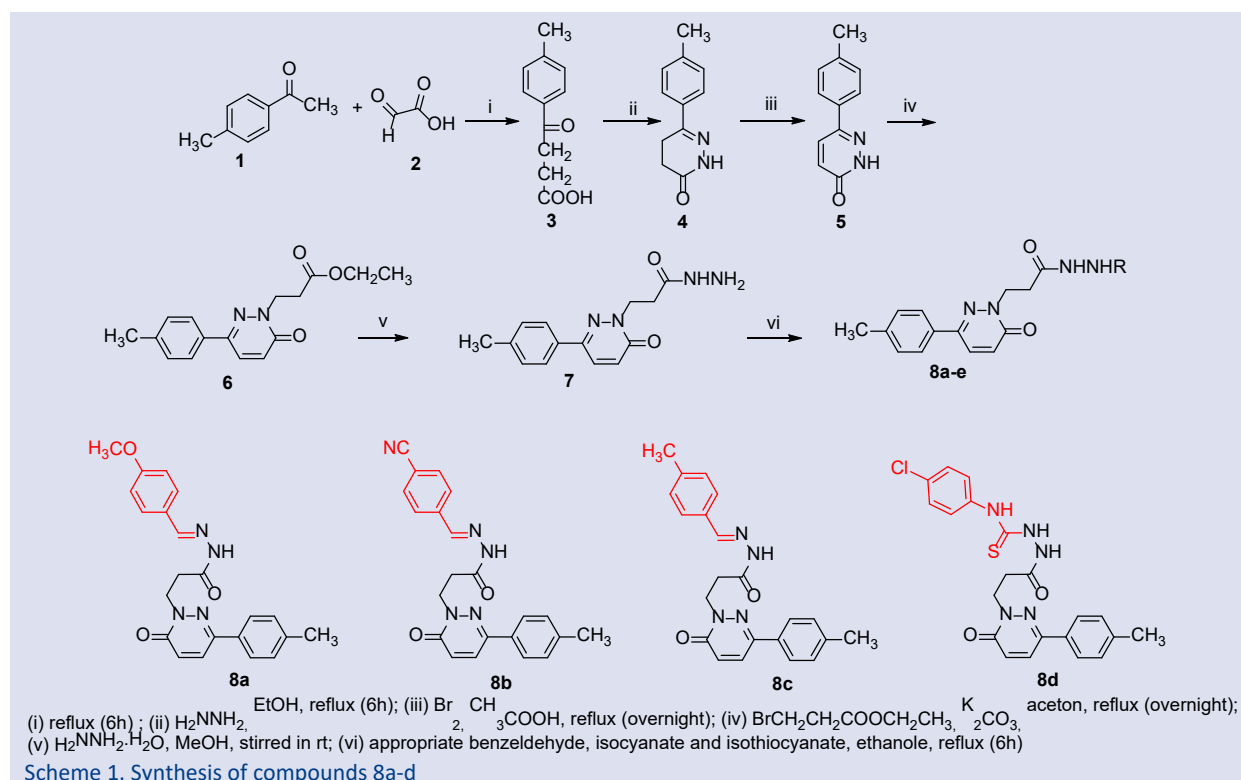
Overnight in acetone (40 mL), 0.01 mol 6-(p-tolyl)pyridazin-3(2H)-one (5), 0.02 mol (2.2252 mL) ethyl bromopropionate, and 0.02 mol (2.7636 g) potassium carbonate were refluxed. After cooling, the organic salts were filtered out, the solvent was removed, and the residue was refined by recrystallization with methanol to get the esters [15].

Synthesis of 3-(6-oxo-3-(p-tolyl)pyridazin-1(6H)-yl)propanehydrazide (7)

Hydrazine hydrate (99%, 3 mL) was added to a 25 mL methanol solution containing 0.01 mol ethyl 3-(6-oxo-3-(p-tolyl)pyridazin-1(6H)-yl)propanoate (6) and stirred for 3 hours at room temperature. The resulting precipitate was filtered, washed with water, dried, and recrystallized from ethanol [16,17].

General procedure for the title compounds (8a-d)

In ethanol (15 mL), 0.01 mol of 3-(6-oxo-3-(p-tolyl)pyridazin-1(6H)-yl)propanehydrazide (7) and 0.01 mol of substituted benzaldehyde/substituted phenylisocyanate/substituted phenylisothiocyanate were mixed. refluxed for 6 hours; at the conclusion of the reaction The precipitate from methanol/water was filtered, dehydrated, and crystallized [16,17]. Compounds **8a** and **8c** were previously synthesized by our research team [15].



(*E/Z*)-*N'*-(4-cyanobenzylidene)-3-(6-oxo-3-(*p*-tolyl)pyridazin-1(6*H*)-yl)propanehydrazide (**8b**); White powder, MP: 271-3 °C, Yield 81%, ¹H-NMR (DMSO-d₆, 400 MHz) δ ppm; δ (ppm) 2.28 (3H; s; -CH₃, 33%), 2.33 (3H; s; -CH₃, 67%) 2.79 (2H; t; *J*=7.78 Hz; -N-CH₂-CH₂-C=O, %33), 3.20 (2H; t; *J*=7.78 Hz; -N-CH₂-CH₂-C=O, %67), 4.42 (2H; t; *J*=7.78 Hz; -N-CH₂-CH₂-C=O), 6.98 (1H; s; -N=CH-, 67%), 7.04 (1H; s; -N=CH-,33%), 7.19-7.23 (2H, m, pyridazinone protons)7.68-8.18 (8H; m; phenyl protons), 11.67 (1H; s; -NH-N,67%). 11.77 (1H; s; -NH-N,33%). ¹³C-NMR (DMSO-d₆, 100 MHz) δ ppm; 172.89, 167.14, 159.30, 144.32, 142.64, 141.16, 135.97, 134.55, 133.74, 133.39, 131.33, 130.80, 130.68, 130.44, 129.96, 129.32, 127.99, 118.88, 112.45, 47.94, 33.31, 31.16. LC/MS (API): m/z calculated for C₂₂H₁₉N₅O₂ : 385.15 found: 386.10.

N-(4-chlorophenyl)-2-(3-(6-oxo-3-(*p*-tolyl)pyridazine-1(6*H*)-yl)propanoyl)hydrazine-1-carbothioamide (**8d**); White powder, MP: 228-30 °C, Yield 84%, ¹H-NMR (DMSO-d₆, 400 MHz) δ ppm; 2.35 (3H; s; -CH₃), 2.72 (2H; t; *J*=7.88 Hz; -N-CH₂-CH₂-C=O), 4.36 (2H; t; *J*=7.88 Hz; -N-CH₂-CH₂-C=O), 7.00- 8.08 (10H; m; phenyl and pyridazinone protons), 8.36 (1H;s;O=C-NH-NH-), 9.06 (1H;s; -NH-NH-C=S-NH), 9.90 (1H; s; -NH-NH-C=S-NH), ¹³C-NMR (DMSO-d₆, 100 MHz) δ ppm; 181.34, 168.27, 159.41, 149.88, 143.18, 138.58, 134.67, 132.87, 131.10, 130.72, 130.20, 130.08, 129.39, 128.41, 128.13, 128.01, 47.94, 32.61, 24.98. LC/MS (API): m/z calculated for C₂₁H₂₀ClN₅O₂S : 441.10 found: 442.10.

Biological Activity

Lipase Inhibitory Effect Assay

p-nitrophenyl butyrate was employed as the substrate for the porcine pancreatic lipase type II (PLL) inhibitory assay in the improved method [25]. Compounds (8a-8d) and orlistat (as a positive control) were produced at concentrations of 6.25, 12.5, 25, 50, and 100 µg/mL. The following equation was used to compute the proportion of PLL inhibitory effect:

$$\text{PLL Inhibition (\%)} = \frac{[(A-B)-(C-D)]}{(A-B)} * 100$$

A: absorbance in the presence of the substrate (control group),

B: absorbance in the absence of the substrate and compound (blank),

C: absorbance in the presence of the substrate and compound (experimental group),

D: absorbance in the presence of a compound (blank of C).

The IC₅₀ values of pyridazinone derivatives are given in Table 1.

Molecular Docking Studies

Molecular docking was conducted utilizing Maestro 11.8. Using 2D Sketcher, the structures of the ligands were created. The ligands were minimized using the Schrodinger utility MacroModel. 3D structures of ligands were constructed utilizing Maestro11.8 software LigPrep software and with OPLS 2005 force field, then were optimized with conjugated gradient method. Lipase

complex (triacylglycerol lipase/colipase complex) 1ETH pdb encoded protein downloaded from www.rcsb.org [26-28].

Schrödinger's modules, Protein Preparation Wizard Prime, Impact, Epik, Propka, and Prime were used for removing ligands and solvent molecules in protein, adding hydrogens and assigning charges. After the target region of the proteins was determined, the grid box was created with the grid generation panel. It has been reported in the literature that the target site of the protein is the catalytic triad of Ser153, Asp177 and His264 [29]. Grid map was created in this region. Then prepared ligands were docked in this grid map 50 times in SP mode with Glide (Maestro 11.8) [30,31].

Molecular Dynamics Simulation Studies

The molecular dynamics (MD) simulations of the compounds were carried out using the Desmond software of the Maestro 12.8 (Schrodinger, NewYork) program. Protein ligand complexes were placed in a 10 Å thick cubic box. TIP3P water model was used in the simulation box. The system was neutralized using Na⁺ and Cl⁻ ions. The concentration of the system was adjusted with 0.15M NaCl solution. Desmond's default relaxation protocol has been applied to the simulation system. These results suggest that compound 8d may interact with the protein in a similar way to orlistat.

ADMET predictions

Before the calculations, the structures of the compounds were drawn with 2D Sketcher and prepared with LigPrep. Some ADME properties (molecular weights, logP, volume, QPP Caco, Qplog Khsa, Percent Human Oral Absorption, Rule of Five) of the compounds were calculated with QikProp (Maestro) software. The estimated mutagenic, tumorigenic and irritant properties of the compounds were calculated with the DataWarrior 4.07.02 program [32].

Results and Discussion

Chemistry

The synthesis of the compounds was synthesized with a yield between 70% and 87% according to the literature are shown in Scheme 1. Compounds 8b and 8d were synthesized for the first time. Compounds 8a and 8c are registered in the literature. The molecular structures of these compounds were confirmed by ¹H-NMR, ¹³C-NMR, and LC/MS. Compounds have *E/Z* isomers due to the C=N groups in their structures. Therefore, the peaks of the isomers may be seen at different ppm values and at different percentages. The signals of the protons in the CH₃, -N-CH₂-CH₂-C=O, -N-CH₂-CH₂-C=O, -N=CH, and, -NH-N groups of compounds 8b were 67% and 33%, in the *E* and *Z* isomers.

Biological Activity

Orlistat, an inhibitor of pancreatic and other lipases, was utilized to investigate the PLL inhibition of produced drugs. By inhibiting at a concentration of 32.66 ± 2.8265 $\mu\text{g/mL}$, the chemical 8d was shown to be the most potent. Compounds 8a and 8b have IC_{50} values of 92.70 ± 3.2231 $\mu\text{g/mL}$ and 93.15 ± 4.2592 $\mu\text{g/mL}$, respectively, which are indicative of a modest lipase inhibitory action. At a dosage of 52.06 ± 3.7526 $\mu\text{g/mL}$, the compound 8c inhibited the lipase enzyme.

Table 1. PLL inhibition of synthesized compounds 8a-d

Compounds	PLL Inhibition* (IC_{50} ($\mu\text{g/mL}$) \pm SD**)
8a	92.70 ± 3.2231
8b	93.15 ± 4.2592
8c	52.06 ± 3.7526
8d	32.66 ± 2.8265
Orlistat	13.49 ± 1.2262

*Porcine pancreatic lipase **Standard deviation

Molecular Docking Studies

Molecular docking studies were carried out to examine the interactions of the compounds and orlistat with the active site of the target protein. Docking results and activity results were found to be compatible. While the docking scores of the synthesized compounds are between -5.042 and -6.202 kcal/mol, the docking score of orlistat is -6.692 kcal/mol. The docking score of compound 8d (IC_{50} : 32.66 ± 2.8265) with the best PLL inhibition was calculated as -6.202 kcal/mol. The docking scores are given in Table 2.

Table 2. Docking scores of compounds 8a-d and orlistat against target protein

Compounds	Docking Scores (kcal/mol)
8a	-5.182
8b	-5.042
8c	-5.819
8d	-6.202
Orlistat	-6.692

As a result of docking studies, the interactions of ligands with residues in the active region of the protein were also investigated (Figure 2).

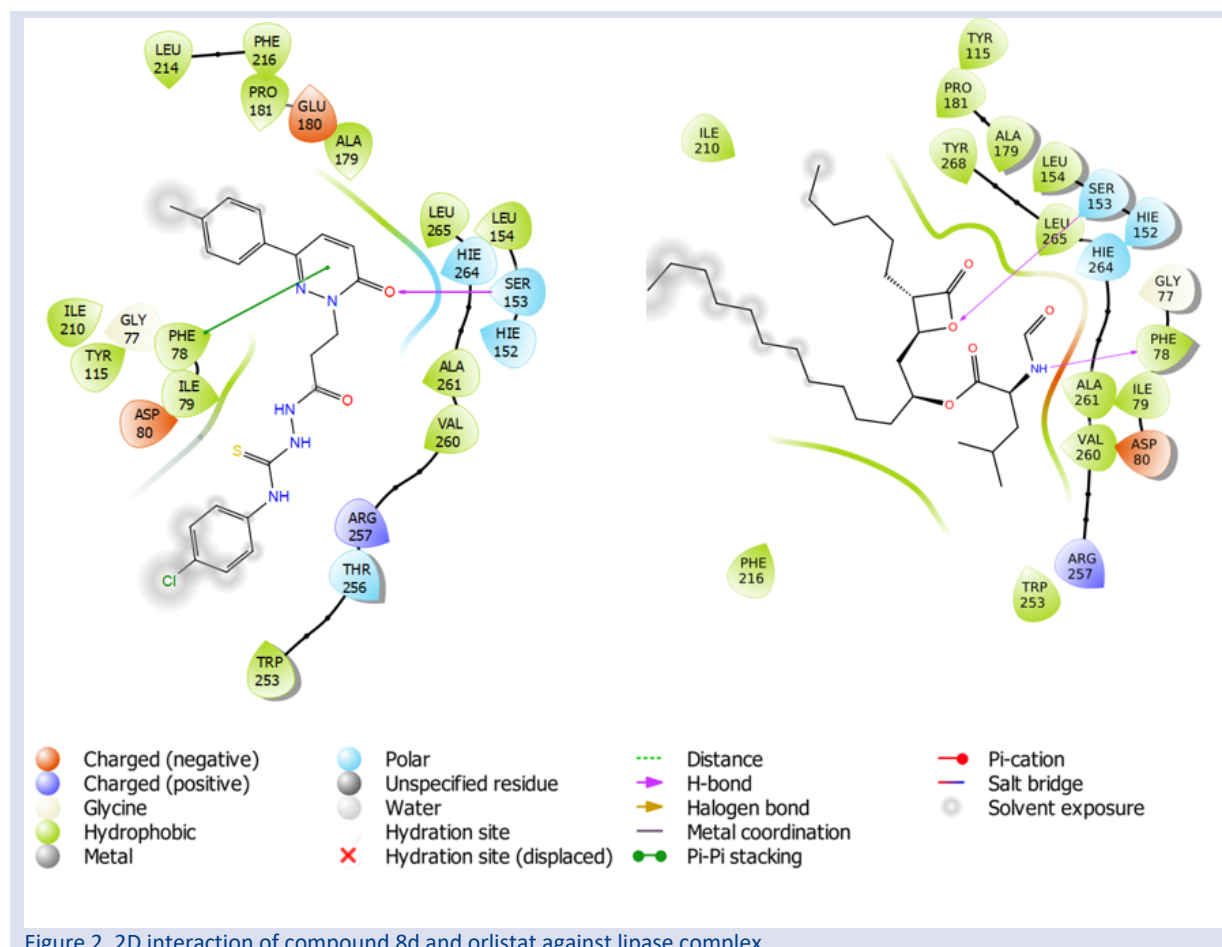


Figure 2. 2D interaction of compound 8d and orlistat against lipase complex

Orlistat made hydrogen bonds with SER153 and PHE78 in the active site of the protein. In addition, hydrophobic interaction with TYR115, PRO181, ALA179, TYR268,

LEU154, LEU265, ALA261, VAL260, TRP 253 and PHE 216, polar interaction with SER153, HIS152, HIS264, charged (-) interaction with ASP80 and charged (+) interaction with

ARG257. It was observed that compound 8d, which has the best activity among the synthesized compounds, interacts similarly with orlistat and hydrogen bonds with SER153 and pi-pi stacking PHE 78. When we examined its 3D placement, we found that compound 8d and orlistat with the active site of the 1ETH pdb-encoded protein (Figure 3).

It was observed that compounds 8a and 8b with the lowest activity did not make hydrogen bonds with SER153, which is among the most important residues for activity. According to the molecular docking results, it is thought that the strong interaction with SER153 located in the active region of the protein is related to both the docking score and the activity.

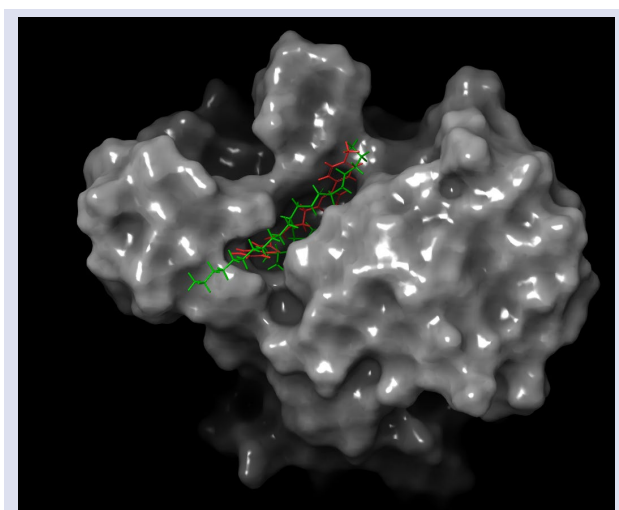


Figure 3. 3D placement of orlistat (green) and compound 8d (red) with the active site of the 1ETH pdb-encoded protein

Molecular Dynamics Simulation Studies

Also, MD trajectory analysis of orlistat and compound 8d which showed the best lipase inhibition activity, with target protein for 50 ns was performed (Figure 4). Changes of the order of 1-3 Å are perfectly acceptable for small, globular proteins [33]. According to the analysis results, it is seen that the root mean square deviations (RMSD) values of the alpha carbons (C α , blue line, left Y axis) of the enzyme (1ETH) vary between roughly 1.2 – 2.4 Å. Compound 8d has a RMSD value between 3.2 – 6.4 Å, orlistat has a RMSD value of 2.4 – 6.4 Å for 50 ns. These results are similar to compound 8d in orlistat (Figure 4). When the plot of compound 8d is examined, it is seen that RMSD value (red line, right Y axis) increased from 3.2 Å to 5.6 Å in about 2 ns and reached 6.4 Å in the following time. In this 48 ns period, the range of RMSD value under 1 Å.

Examining the plot of orlistat, the RMSD value ranges from 2.4 to 4.8 Å up to 35 ns. In this 35 ns period, the range

of RMSD is less than 3 Å. However, after the 35th ns, the RMSD value increased up to 6.4 Å and decrease again from the 42nd ns.

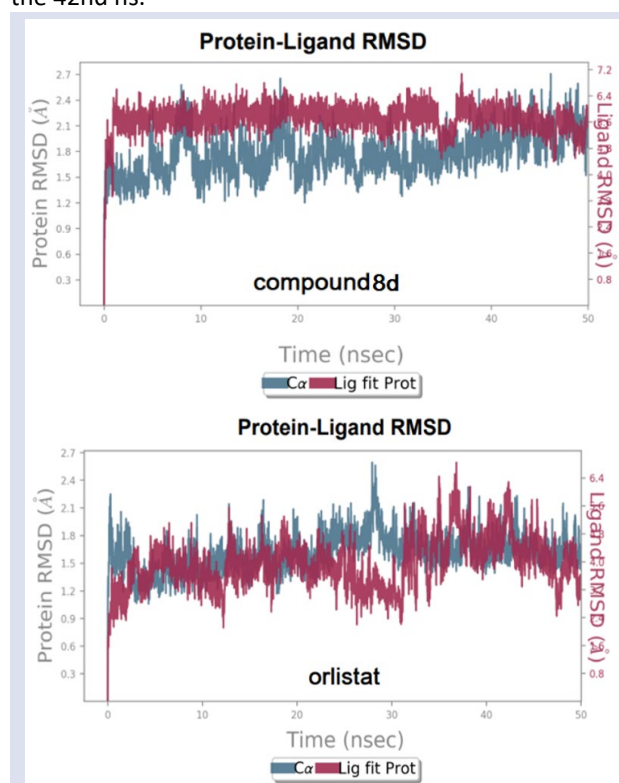


Figure 4. The Root Mean Square Deviations (RMSD) plots. RMSDs for compound 8d and orlistat.

ADMET Predictions

In addition to interacting with target macromolecules, it is very important for drugs to reach their target sites in order to have an effect. Many synthesized molecules cannot be used as drugs due to their unsuitable physicochemical properties. Although the compounds show high activity, they may have significant toxic effects, limiting their use. Therefore, it is important to determine the absorption, distribution, metabolism, excretion, and toxicity (ADMET) properties of drug candidate compounds. In our study, various ADME and toxicological parameters of the synthesized compounds were calculated (Table 3). The logP values of the compounds range from 3.84 to 4.96. The volume values of the compounds were found close to each other. Caco permeability values and serum albumin binding values of the compounds were found to be suitable. The compounds have very high oral absorption values, which are important for the use of drugs. None of the compounds showed predicted mutagenic, teratogenic, and irritant effects. All compounds comply with Lipinski's rule of five.

Table 3. Some predicted ADME and toxicological, properties of compounds.

Comp.	Mol MW	logP	Volume	QPP Caco	QPlog Khsa	P. H. O.A.	Rule of five	Mutagenic	Teratogenic	Irritant
8a	390.44	4.79	1300.37	642.75	0.77	100.00	0	none	none	none
8b	385.42	3.84	1238.10	301.95	0.47	93.84	0	none	none	none
8c	374.44	4.97	1281.20	625.93	0.92	100.00	0	none	none	none
8d	441.93	4.96	1378.13	349.10	0.78	100.00	0	none	none	none
orlistat	495.74	6.56	1919.70	338.82	0.97	100.00	1	none	none	none

Conclusions

Orlistat was used as a test for the PLL inhibition of produced drugs. By inhibiting at $32.66 \pm 2.8265 \mu\text{g/mL}$, compound 8d was revealed to be the most effective compound. Molecular modeling and MD studies were performed to examine the interaction of compounds 8a-d and orlistat with the target protein. The compounds were docked successfully, and the resulting activities were in sync. The most active chemical 8d has been demonstrated to interact with orlistat in a similar way. In this study, it was observed that the compounds obtained as a result of the substitutions of the 3-(6-oxo-3-phenylpyridazin-1(6H)-yl) propanehydrazide structure may have potential lipase inhibitory effects. It is planned to develop new, more effective and targeted (lipase complex) compounds by using the data obtained in further studies. The suitable ADMET properties of Compound 8d support its potential as a drug.

Conflicts of interest

The author declare that they have no conflict of interests

References

- [1] Tang Q.J., Zhang L., Zheng J., Song J., Chen X., Cao W., Xue C., He X., Ma M., Zhao Y., Drug-guided screening for pancreatic lipase inhibitors in functional foods, *Food Funct*, 12 (2021) 4644-4653.
- [2] Zechner R., Zimmermann R., Eichmann T.O., Kohlwein S.D., Haemmerle G., Lass A. Madeo F., Fat Signals lipases and lipolysis in lipid metabolism and signaling, *Cell metab.*, 15(2012) 279–291.
- [3] Bachovchin D.A., Cravatt B.F., The pharmacological landscape and therapeutic potential of serine hydrolases, *Nat Rev Drug Discov.*, 3 (2012) 52-68.
- [4] Faucher F., Bennett J.M., Bogyo M., Lovell, S., Strategies for Tuning the Selectivity of Chemical Probes that Target Serine Hydrolases, *Cell Chem. Biol.*, 27 (2020) 937-952.
- [5] Ahmad E.M., Kassab A.E., El-Malah A.A., Hassan M.S.A., Synthesis and biological evaluation of pyridazinone derivatives as selective COX-2 inhibitors and potential anti-inflammatory agents, *Eur. J. Med. Chem.*, 171 (2019) 25-37.
- [6] Gong J., Zheng Y., Wang Y., Sheng W., Li Y., Liu, X. A new compound of thiophenylated pyridazinone IMB5043 showing potent antitumor efficacy through ATM-Chk2 pathway, *PLoS ONE*, 13 (2018) e0191984.
- [7] Ramadan S.K., Shaban S.S., Hashem A.I., Facile and expedient synthesis and anti-proliferative activity of diversely pyrrolones bearing 1,3-diphenylpyrazole moiety, *Synth. Commun.*, 55 (2020) 185-196.
- [8] Dubey S., Bhosle P.A., Pyridazinone: An important element of pharmacophore possessing broad spectrum of activity, *Med. Chem. Res.*, 24 (2015) 3579-3598.
- [9] Özdemir Z., Başak-Türkmen N., Ayhan İ., Çiftçi O., Uysal M., Synthesis of new 6-[4-(2-fluorophenylpiperazine-1-yl)]-3(2H)-pyridazinone-2-acethyl-2-(substitutedbenzal) hydrazine derivatives and evaluation of their cytotoxic effects in liver and colon cancer cell lines, *Pharm. Chem. J.*, 52 (2019) 923–929.
- [10] Ciftci O., Özdemir Z., Acar C., Sözen M., Başak-Türkmen N., Ayhan İ., Gözükar H., The novel synthesized pyridazinone derivatives had the antiproliferative and apoptotic effects in SHSY5Y and HEP3B cancer cell line, *Lett. Org. Chem.*, 15 (2018) 323–33.
- [11] Asif M., Abid Imran M., Study of heterocyclic-fused pyridazinone analogues having phosphodiesterase-IV inhibitor activities as anti-inflammatory agents, *J. Med. Chem. Sci.*, 3 (2020) 109-117.
- [12] Alagöz M.A., Özdemir Z., Uysal M., Carradori S., Gallorini M., Ricci A., Zara S., Mathew B., Synthesis, Cytotoxicity and Anti-Proliferative Activity against AGS Cells of New 3(2H)-Pyridazinone Derivatives Endowed with a Piperazinyl Linker, *Pharmaceuticals*, 14 (2021) 183.
- [13] Önkol T., Gökçe M., Orhan İ., Kaynak F., Design, synthesis and evaluation of some novel 3(2H)-pyridazinone-2-yl acetohydrazides as acetylcholinesterase and butyrylcholinesterase inhibitors, *Org. Commun.*, 6 (2013) 55-67.
- [14] Özçelik A.B., Gökçe M., Orhan İ., Kaynak F., Şahin, M.F., Synthesis and antimicrobial, acetylcholinesterase and butyrylcholinesterase inhibitory activities of novel ester and hydrazide derivatives of 3(2H)-pyridazinone, *Arzneim.-Forschung*, 60 (2010), 452-458.
- [15] Bozbey İ., Özdemir Z., Uslu H., Özçelik A.B., Şenol F.S., Erdoğan-Orhan İ., Uysal, M., *Mini Rev Med Chem*, 20 (2020) 1042.
- [16] Özdemir Z., Yılmaz H., Sarı S., Karakurt A., Şenol F.S., Uysal M., Design, synthesis, and molecular modeling of new 3(2H)-pyridazinone derivatives as acetylcholinesterase/butyrylcholinesterase inhibitors, *Med. Chem. Res.*, 26 (2017), 2293-308.

- [17] Özçelik A.B., Özdemir Z., Sari S., Utku S., Uysal, M., A New Series of Pyridazinone Derivatives as Cholinesterases Inhibitors: Synthesis, In Vitro Activity and Molecular Modeling Studies, *Pharmacol Rep.*, 71 (2019) 1253-1263.
- [18] Kopelman P., Bryson A., Hickling R., Rissanen A., Rossner S., Toubro S., Valensi P., Cetilistat (ATL-962), a novel lipase inhibitor: a 12-week randomized, placebo-controlled study of weight reduction in obese patients, *Int. J. Obes.*, 31 (2007) 494–499.
- [19] Point V., Kumar K.V.P.P., Marc S., Delorme V., Parsiegla G., Amara S., Carrière F., Buono G., Fotiadu F., Canaan S., Leclaire J., Cavalier J.F., Analysis of the discriminative inhibition of mammalian digestive lipases by 3-phenyl substituted 1,3,4-oxadiazol-2(3H)-ones, *Eur. J. Med. Chem.* 58 (2012) 452–463.
- [20] Jayanna N.D., Vagdevi H.M., Dharshan J.C., Kekuda T.R.P., Hanumanthappa B. C., Gowdarshivannanavar B.C., Synthesis and biological evaluation of novel 5,7-dichloro-1,3-benzoxazole derivatives, *J. Chem.* 2013 (2012) 1–9.
- [21] Kumar A., Chauhan S., Pancreatic lipase inhibitors: The road voyaged and successes, *Life Sci.*, 271 (2021) 119115.
- [22] Montes E., Karaali N., Yilmaz F., Ülker S., Kahveci B., Microwave-assisted synthesis and biological evaluation of some benzimidazole derivatives containing a 1,2,4-triazol ring, *Arch. Pharm.*, 346 (2013) 556–561.
- [23] Bekircan O., Montes E., Ülker S., Kucuk C., Synthesis of some new 1,2,4-triazole derivatives starting from 3-(4-chlorophenyl)-5-(4-methoxybenzyl)-4H-1,2,4- triazol with anti-lipase and anti-urease activities, *Arch. Pharm.* 347 (2014) 387–397.
- [24] Evren A.E., Çelik İ., Acar Çevik U., Synthesis, molecular docking, in silico ADME and antimicrobial activity studies of some new benzimidazole-triazole derivatives, *CSJ*, 42 (2021) 795-805.
- [25] Sridhar S.N.C., Bhurta D., Kantiwal D., George G., Monga V., Paul A.T., Design, synthesis, biological evaluation and molecular modelling studies of novel diaryl substituted pyrazolyl thiazolidinediones as potent pancreatic lipase inhibitors, *Bioorganic Med. Chem. Lett.*, 27 (2017) 3749-3754.
- [26] Foteini-Nafsika D., Luis A.M., Angel G., Barrie K., Steve P.W., Overcoming challenges in developing small molecule inhibitors for GPVI and CLEC-2, *Platelets*, 32 (2021) 744-752.
- [27] Bivi N., Hu H., Chavali B., Chalmers M.J., Reutter C.T., Durst G.L., Riley A., Sato M., Allen M.R., Burr D.B., Dodge J.A., Structural features underlying raloxifene's biophysical interaction with bone matrix, *Bioorganic Med. Chem.*, 24 (2016) 759-767.
- [28] Sable R., Jois S. Surfing the Protein-Protein Interaction Surface Using Docking Methods: Application to the Design of PPI Inhibitors, *Molecules*, 20 (2015) 11569-11603.
- [29] Hu B., Cui F., Yin F., Sun Y., Li Y., Caffeoylquinic Acids Competitively Inhibit Pancreatic Lipase through Binding to the Catalytic Triad, *Int. J. Biol. Macromol.*, 80 (2015) 529-535.
- [30] Halgren T., Murphy R., Friesner R., Beard H., Frye L., Pollard W., Banks J., Glide: A New Approach for Rapid, Accurate Docking and Scoring. 2. Enrichment Factors in Database Screening, *J. Med. Chem.*, 47 (2004). 1750-1759.
- [31] Kuzu B., Hepokur C., Alagöz M.A., Burmaoglu S., Algul O., Synthesis, Biological Evaluation and In Silico Studies of Some 2-Substituted Benzoxazole Derivatives as Potential Anticancer Agents to Breast Cancer, *Chemistry Select*, 7 (2022) e20210355.
- [32] Ersan R.H., Kuzu B., Yetkin D., Alagoz M.A., Dogen A., Burmaoglu S., Algul O., 2-Phenyl substituted Benzimidazole derivatives: Design, synthesis, and evaluation of their antiproliferative and antimicrobial activities, *Med. Chem. Res.*, (2022)
- [33] Kolinski A., Klein P., Romiszowski P., Skolnick J., Unfolding of globular proteins: monte carlo dynamics of a realistic reduced model, *Biophys. J*, 85 (2003) 3271–3278.

Molecular Docking and Drug-likeness Prediction of New Potent Tubulin Colchicine Binding Site Inhibitors for Potential Antitumor Drug

Mokrani El Hassen ^{1,a,*}, Abdelaziz Mohamed Amine ^{1,b}, Akakba Naamane ^{1,c}, Teniou Soumia^{1,d}, Rym Gouta Demmak^{1,e}, Bensegueni Abderrahmane ^{1,f}

¹ Laboratory of Applied Biochemistry, Department of Biochemistry and Cellular and Molecular Biology, Faculty of Natural and Life Sciences, University Mentouri Brothers Constantine 1, Constantine, Algeria.

*Corresponding author

Research Article

History

Received: 29/01/2022

Accepted: 27/08/2022

Copyright



©2022 Faculty of Science,
Sivas Cumhuriyet University

ABSTRACT

Cancer is a real public health problem that figures among the main causes of morbidity and mortality in the world. The Colchicine Binding Site (CBS) is an important pocket for potential tubulin polymerization destabilizers. Colchicine binding site inhibitors (CBSI) exhibit their biological effects by inhibiting tubulin assembly and suppressing microtubule formation. In order to identify new potent CBSI, molecular docking and drug likeness prediction were performed. In this context, a collection of 850 similar compounds to combretastatinA-4 from PubChem database was docked into the CBS. Out of these, compounds S1 and S2 were found to have highest negative binding energy of -9.462 and -9.017 Kcal/mol respectively. Furthermore, these two compounds were predicted to have satisfying drug likeness properties, indicating that they might be promising lead compounds for further antitumor drug research.

Keywords: Cancer, Colchicine binding site, Glide, Molecular docking, Tubulin.

^a mohsen.mokrani@umc.edu.dz
^c mohsenmokrani@yahoo.fr
^e demmak_rym@hotmail.com

^b <https://orcid.org/0000-0002-2725-2940>
^d <https://orcid.org/0000-0003-0021-0334>
^f <https://orcid.org/0000-0002-2793-5653>

^b abdz.amine@gmail.com
^d soumia.teniou@hotmail.com
^e abensegueni@yahoo.fr

^b <https://orcid.org/0000-0002-4320-2927>
^d <https://orcid.org/0000-0003-3330-0045>
^e <https://orcid.org/0000-0003-3467-6749>

Introduction

Cancer is one of the leading causes of morbidity and death in the world [1]. The International Agency for Research on Cancer estimated 19 292 789 new cases and close to 10 million deaths in 2020 alone [2-3]. It is well known that cancer results from erratic cell division. This process is carried by different structures such as the mitotic spindle, which is composed of polymerized tubulin to form microtubules [4-6].

Tubulin is a dimeric protein containing an α and β chain and possessing multiple binding sites. Chemotherapeutic agents targeting vinca alkaloids and taxanes binding sites (Figure 1-A) were used clinically for over 50 years [7]. Although having good potency at first, they often trigger multidrug resistance in patients, which significantly reduces the therapeutic effects of these molecules [8]. Colchicine Binding Site (CBS) targeting agents in tubulin, commonly known as Colchicine Binding Site Inhibitors (CBSI), were recently gaining traction as potential multi-resistance evading drugs for their ability to bind well to different kinds of tubulin isomers [9]. The CBS cavity is located on the β subunit directly facing the α -subunit. This site is composed of three zones. The first zone includes Val α 181, Ser α 178, Val β 313, Met β 257 and Asn β 256. The second zone is a hydrophobic pocket composed of Lys β 350, Asn β 348, Ile β 368, Val β 313, Ala β 315, Ala β 314, Leu β 253, Lys β 252, Leu β 250, Ala β 248, Leu β 246, Leu β 240 and Cys β 239. The last zone is situated deeper in the CBS cavity and contains Thr β 237, Val β 236, Tyr β 200, Glu β 198, Phe β 167, Asn β 165, Gln β 134 and Ile β 4 (Figure 1-B) [10].

This work aims at identifying new potent CBSIs using molecular docking approach followed by a computational drug likeness prediction.

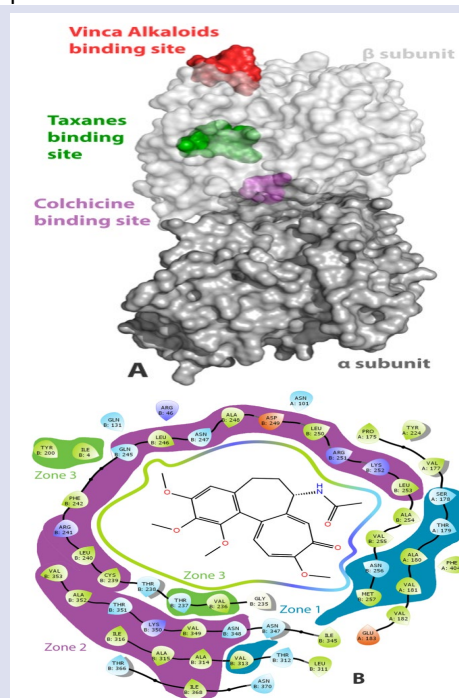


Figure 1. (A) Surface representation of tubuline subunits and its binding sites. (B) Representation of Colchicine binding site amino acids

Materials and Methods

The identification of new potent CBSIs requires the use of several programs which are:

Schrödinger Suites is one of the most known software for computer aided drug design. This program ranks molecules using GlideScore scoring function which is an empirical scoring function that estimates the free binding energy in Kcal/mol. In this study, we used Glide SP [11] for docking calculation. We also used LigPrep for ligand preparation, Epik [12] and Maestro for protein preparation.

ADMETlab2.0 (<http://admet.scbdd.com/>) is a web server that provides ADMET predictions based on a comprehensive database from 288967 entries [13]. It was used to predict physicochemical, pharmacokinetic and toxicity properties of the most promising compounds from molecular docking.

PyMOL is an open-source software for 3D visualization. Tubulin surface generation and visualization of 3D poses of the docked compounds were performed using PyMOL 2.4.0.

PDBaser is an open-source python tool that we designed on top of Biopython [14] and Openbabel [15] to provide a fast and intuitive way to separate ligands and chains from protein PDB files [16]. We used this tool in order to facilitate the preparation process.

Validation Of Docking Protocol

The performance of Glide protocol was evaluated before starting docking study on CBS. The Root Mean Square Deviation (RMSD) was calculated for 100 protein-ligand crystal structures from Protein Data Bank (PDB). It is a metric that measures average distances between the docking binding mode and the experimental conformation of a ligand. A docking protocol reproduce correctly the experimental conformation of a ligand in its binding site when RMSD value is less than or equal to 2Å [17].

Protein Preparation

A Tubulin-CBSI complex was downloaded from PDB (ID: 6BR1). This protein was prepared for docking study using Schrödinger's protein preparation wizard. This program serves to define the protonation state of some CBS's residues, to control their side chain orientation and to all hydrogen atoms [18]. The Colchicine binding site was defined using a grid box which was generated from position of the co-crystallized ligand occupying the CBS (E3Y) using default settings.

Ligand Preparation

850 analogs compounds to combretastatin A-4 (CA-4), a potent CBSI (Figure S1, Supplementary file), were downloaded from PubChem database in sdf format. These molecules were prepared for docking using LigPrep. It is one of Schrödinger's modules that serve to prepare and optimize the structures of ligand to meet the

requirements of the simulation programs without necessitating any further user intervention. In our study, LigPrep was used to generate for each compound a number of structures (up to 32) with various tautomers, protonation states at $\text{pH } 7.0 \pm 2$ and enantiomers (when undefined). After this preparation, the geometries of each ligand were optimized and the final chemical library contained 1151 molecules [19].

Molecular Docking Calculations

Docking calculations of the prepared molecules against CBS were done with the default parameters of Glide Standard Precision (SP). The resulting poses were clustered according to their GlideScore, which were given as a binding free energy, ΔG (kcal/mol).

Drug Likeness and Toxicity Prediction

The physicochemical, pharmacokinetic and toxicity properties of the best CBSI obtained in this study were predicted using ADMETLab at <http://admet.scbdd.com/>. These properties consist of Lipinski and Veber's Rule, Gastrointestinal absorption (GI), Blood-Brain Barrier permeability (BBB), cell permeability (CACO-2), Cytochrome P450 (CYP) inhibition, and toxicity (hERG inhibition, Ames test, carcinogenicity). The same parameters of Colchicine were also studied for comparison.

Results and Discussion

Validation of Docking Protocol

Before carrying out molecular docking study, docking protocol was evaluated by calculating the RMSD value of 100 protein-ligand complexes from PDB. The predicted binding mode was considered correct if the RMSD was below 2.0 Å. In our results, Glide reproduced well the experimental data. Indeed, 86 % of RMSD values were less than 2Å (Table 1) which indicates that this program can reproduce correctly the binding mode of a co-crystal ligand. For example, Figure 2 shows that there was a negligible deviation between experimental pose (in green) and docked conformation (in blue) of the ligand E3Y from the complex 6BR1 in the PDB.

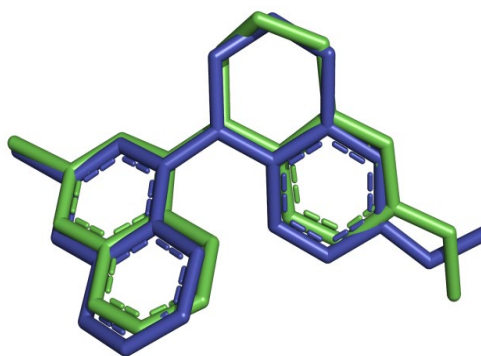


Figure 2. Superposition of the crystal conformation of the ligand extracted from 6BR1 (colored in green) against the best predicted pose (colored in blue).

Table 1. List of 100 complexes protein-ligand used to test the reliability of the docking protocol

Protein	Ligand	RMSD	Protein	Ligand	RMSD	Protein	Ligand	RMSD
6OHS	MJY	1.876	2OLE	KR2	1.7138	4E00	OF1	0.4476
2XF0	4UB	0.4289	2OS3	BB2	1.9188	4E01	OF1	0.8993
3C56	PH4	1.459	2P98	YE7	0.5281	4EY7	E20	0.9358
5IX0	6EZ	0.3958	2P9A	YE6	2.6817	4FLL	YZ6	1.663
6MD7	JE1	0.7884	2Q95	A05	0.8423	4IKR	PVP	1.3035
1CEB	AMH	0.8469	2Q96	A18	0.2668	4IKS	TFD	4.8465
1G27	BB1	1.4265	2QT9	524	0.8796	4IU6	FZ1	1.9144
1G2A	BB2	1.1678	2QTB	474	1.345	4JE7	BB2	2.2446
1G36	R11	0.9716	2R3O	2SC	1.0854	4O09	2R6	0.4272
1LOX	RS7	0.772	2R4B	GW7	0.3121	4PES	2PJ	0.8403
1LQY	BB2	1.2246	2RGU	356	1.8357	4U69	Q07	1.2069
1LRY	BB2	1.9926	2FZD	TOL	0.943	4WY1	3VO	0.2048
1N7I	LY1	0.4849	2RJP	886	0.5776	5AUV	AGI	0.4577
1N8Q	DHB	0.1285	2RJQ	BAT	1.7085	5CA1	NZO	0.4506
1Q1Y	BB2	0.9882	2VOZ	C41	1.7057	5CVK	56E	6.6885
1QZF	CB3	7.5903	3C43	315	1.0281	5DC5	B3N	2.6629
1QZY	TDE	1.7746	3D01	PG5	4.2033	5EDH	5MF	0.5759
1RBP	RTL	1.1126	3D4L	P6G	1.1565	5F00	5T8	0.2391
1RTI	HEF	0.8429	3EBH	BES	1.0669	5JF1	BB2	1.7818
1S17	GNR	3.0068	3F8S	PF2	2.2045	5LB6	UN9	0.5594
1SZZ	BB2	1.7339	3G0B	T22	1.0045	5OR6	A4K	1.0859
1X7J	GEN	0.2432	3G0D	XIH	0.3508	5PZQ	93V	1.1727
1YVM	TMG	0.5978	3HAB	677	0.7651	5S1O	WQA	0.7486
1ZVX	FIN	1.5694	3IU8	T03	0.6359	5UMW	RBF	5.072
2ABI	1CA	0.3414	3IU9	T07	0.9728	6HOT	CIY	0.4124
2ADU	R20	0.9403	3K6L	2BB	1.0032	6IND	AKO	1.2239
2AI7	SB7	0.4472	3KWF	B1Q	0.4655	6M8C	IRH	0.7043
2AIA	SB8	1.2518	3L0L	HC3	0.4431	5LYJ	7BA	1.4671
2AIE	SB9	0.8716	3M6P	BB2	2.4957	6BR1	E3Y	0.5614
2AJ8	SC3	0.9461	3OAP	9CR	1.0484	6PZ0	FMN	0.8904
2BUC	008	1.1211	3PKC	Y08	1.4013	6PZR	P7D	1.2664
2EW5	Y12	2.3255	3PN4	BB2	1.2453	6THZ	NB5	1.3521
2EW6	Y13	1.4993	4D09	788	4.0803			
2NQ7	HM5	1.1931	4DR9	BB2	2.3316			

Molecular Docking Calculations

In order to identify new potent CBSI, 1151 analogs compounds to combretastatin-a-4 were docked into the CBS using Glide SP. The results show that 795 compounds were found to exhibit a higher CBS inhibitory potency than that of CA-4, the reference molecule, whose score is -

5.173 Kcal/mol (Table S1 in supplementary file). Out of these, compounds S1 and S2 were found to have highest negative binding energy of -9.462 and -9.017 Kcal/mol respectively (Table 2).

Table 2. PubChem ID, Docking scores, ranking, Hbond, eModel and Ligand efficiency of the most promising CBSI (S1 and S2). The same data for CA-4 were done for comparison.

Compound	PubChem ID	Glide Score (Kcal/mol)	Hbond	eModel	Ligand efficiency	Ranking
S1	145336937	-9.462	-0.330	-68.181	-0.411	1
S2	138585723	-9.017	-0.307	-59.575	-0.474	2
CA-4	-5.173	-0.110	-16.433	-0.255	796

Poses Analysis

The binding mode of these potent inhibitors into the CBS was predicted using the poses given by Glide. As shown in figure 3, compounds S1 and S2 cover the entire CBS in a rational orientation, thus leading to an important inhibitory potency. In addition, compound S1 makes two hydrogen bonds with Thr α 179 whereas S2 and CA-4 make one such bond with the same residue. However, an additional hydrogen bond is observed between S2 and Ala β 315, whereas S1 and CA-4 have bare contacts with this residue.

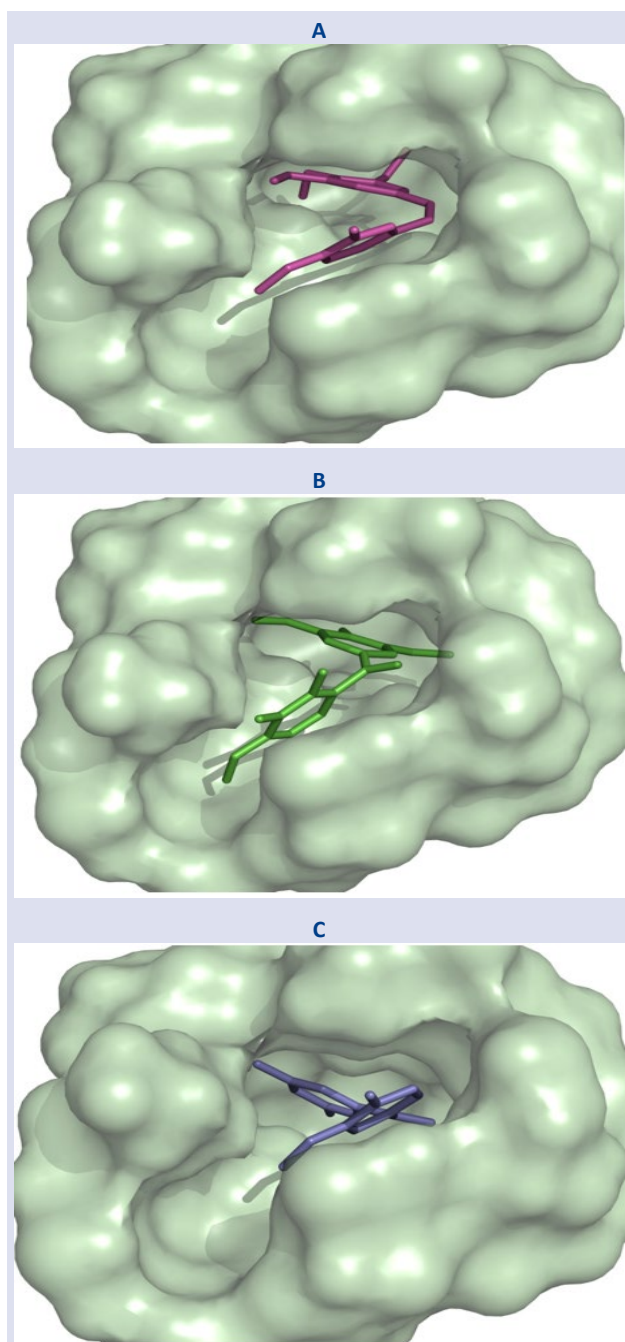


Figure 3. Positioning of CA-4 (A), S1 (B) and S2 (C) into the Tubuline Colchicine Binding Site.

It should be noted that both S1 and S2 form a hydrogen bond with a structural water molecule, which connects these inhibitors to Val β 236. The difference of the inhibitory potency between these two compounds and CA-4 may be explained by the different number of hydrogen bonds between them and the protein. Indeed, whereas S1 and S2 are involved in three such bonds, CA-4 is involved in only one (Figure 4).

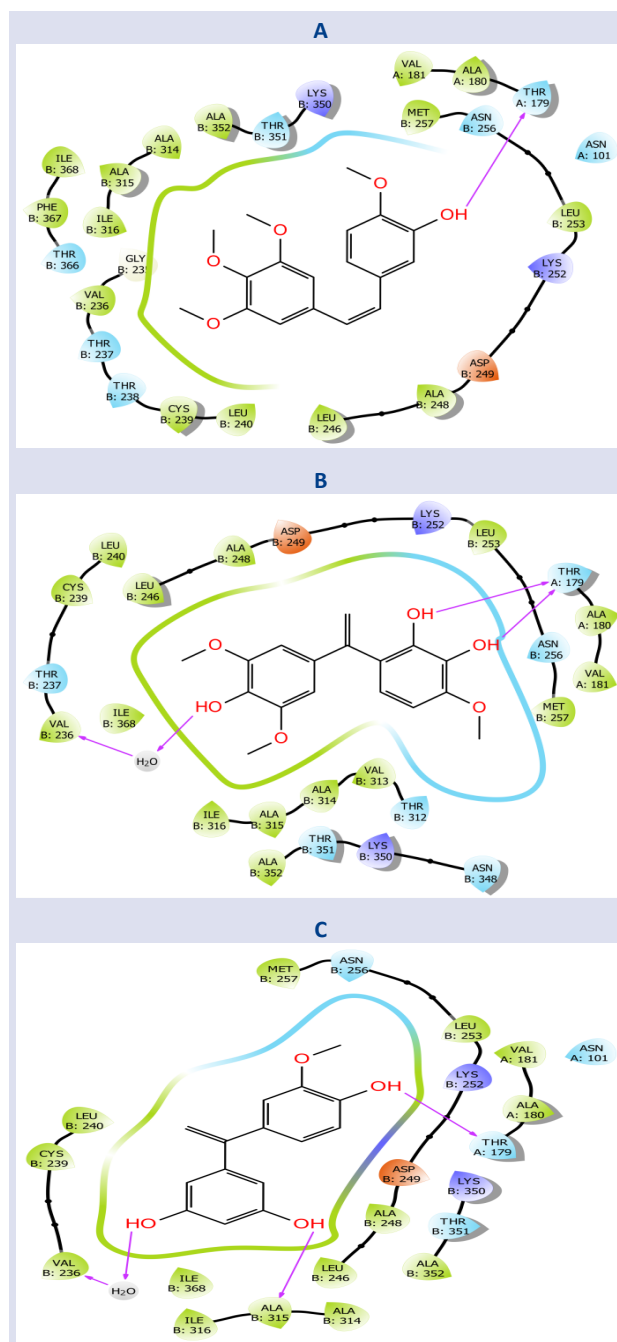


Figure 4. Binding mode prediction of CA-4 (A), S1 (B) and S2 (C) into the Tubuline Colchicine Binding Site. Purple arrows head from the donor to the acceptor of hydrogen bonds.

Drug Likeness and Toxicity Prediction

Physicochemical, pharmacokinetic and toxicity parameters of the most promising CBSI, S1 and S2 were predicted using ADMETLab. The same properties of Colchicine were also predicted for comparison. As shown in Table 3, compounds S1 and S2 are predicted to have a higher BBB penetration than that of colchicine. In addition, they have a high CACO-2 cell permeability and intestinal absorption, which allows them to reach the bloodstream. With no Lipinski and Veber's rule violation, both S1 and S2 follow the criteria for orally available drugs. Furthermore, these two promising compounds did not show potential toxicity, which guarantees their use in vivo. However, these two compounds inhibit same CYP which are important for the metabolism of numerous drugs in the liver. It should be noted that this problem can be resolved during their optimization.

Table 3. Drug likeness prediction and toxicity of S1, S2 and Colchicine.

Properties	Colchicine	S1	S2
BBB permeability	Suitable average	Suitable	Suitable
GI absorption	High	High	High
CYP inhibition	None	CYP1A2	CYP3A4, CYP2D6, CYP1A2
CACO-2	-4.712	-5.110	-5.023
Lipinski	Suitable	Suitable	Suitable
Veber	Suitable	Suitable	Suitable
Toxicity	None	None	None

Conclusion

In brief, molecular docking approach using Glide was employed to predict the binding energies and the interaction modes of 1150 compounds from the PubChem database. After the validation of docking protocol, compounds S1 and S2 were identified as new potent CBSI. Still more remarkably, these two compounds were predicted to have good drug likeness and toxicity properties indicating that they might be promising lead candidates for further anticancer drug discovery.

Acknowledgment

The authors greatly acknowledge the Directorate General of Scientific Research and Technological Development, Algeria, for their support.

Conflicts of interest

The authors state that did not have conflict of interests

References

- [1] Üstün E., Şahin N., Molecular Docking Studies of N-Heterocyclic Carbene Molecules with Thioredoxin Reductase and DNA, *Cumhuriyet Sci. J.*, 42(3) (2021) 656-662.
- [2] Sung H., Ferlay J., Siegel RL., Laversanne M., Soerjomataram I., Jemal A., Bray F., Global Cancer Statistics 2020: GLOBOCAN Estimates of Incidence and Mortality Worldwide for 36 Cancers in 185 Countries, *CA: Cancer. J. Clin.*, 71 (3) (2021) 209-249.
- [3] International Agency for Research on Cancer, Global cancer observatory, GLOBOCAN 2020. Available at <https://gco.iarc.fr/>. Retrieved September 10, 2021.
- [4] Taperaa M., Kekeçmuhammed H., Tüzün B., Sarıpınar E., Koçyiğit UM., Yıldırım E., Doğan M., Zorlu Y. Synthesis, Carbonic Anhydrase Inhibitory Activity, Anticancer Activity and Molecular Docking Studies of New Imidazolyl Hydrazone Derivatives, *J. Mol. Struct.*, 1269 (2022) 133816.
- [5] Sarkı G., Tüzün B., Ünlüer D., Kantekin H. Synthesis, characterization, chemical and biological activities of 4-(4-methoxyphenethyl)-5-benzyl-2-hydroxy-2H-1,2,4-triazole-3(4H)-one phthalocyanine derivatives, *Inorg. Chim. Acta.*, Available online 30 July 2022, 121113.
- [6] Koçyiğit UM., Doğan M., Muğlu H., Taslimi P., Tüzün B., Yakan H., Bal H., Güzel E., Gülçin I. Determination of biological studies and molecular docking calculations of isatin-thiosemicarbazone hybrid compounds, *J. Mol. Struct.*, 1264 (2022) 133249.
- [7] Cutts JH., Beer CT., Noble RL., Biological properties of Vincalokoblastine, an alkaloid in *Vinca rosea* Linn, with reference to its antitumor action, *Cancer. Res.*, 20 (1960) 1023-31.
- [8] Person F., Wilczak W., Hube-Magg C., Burdelski C., Möller-Koop C., Simon R., Noriega M., Sauter G., Steurer S., Burdak-Rothkamm S., Jacobsen F., Prevalence of β III-tubulin (TUBB3) expression in human normal tissues and cancers, *Tumor. Biol.*, 39(10) (2017) 1010428317712166.
- [9] Stengel C., Newman SP., Leese MP., Potter BV., Reed MJ., Purohit A., Class III β -tubulin expression and in vitro resistance to microtubule targeting agents, *Br. J. Cancer.*, 102(2) (2009) 316-324.
- [10] Massarotti A., Coluccia A., Silvestri R., Sorba G., Brancale A., The Tubulin Colchicine Domain: a Molecular Modeling Perspective, *Chem.Med.Chem.*, 7(1) (2012) 33-42.
- [11] Halgren TA., Murphy RB., Friesner RA., Beard HS., Frye LL., Pollard WT., Banks JL., Glide: A New Approach for Rapid, Accurate Docking and Scoring. 2. Enrichment Factors in Database Screening, *J. Med. Chem.*, 47(7) (2004) 1750-1759.
- [12] Shelley JC., Cholleti A., Frye LL., Greenwood JR., Timlin MR., Uchimaya M., Epik: A Software Program For Pk A Prediction And Protonation State Generation For Drug-Like Molecules, *J.Comput. Aided. Mol. Des.*, 21(12) (2007) 681-691.
- [13] Jie Dong DSC., Wang NN., Yao ZJ., Zhang L., Cheng Y., Ouyang D., Lu AP., ADMETlab: a platform for systematic ADMET evaluation based on a comprehensively collected ADMET database, *J. Cheminformatics.*, 10 (2018) 29.
- [14] Hamelryck T., Manderick B., PDB File Parser And Structure Class Implemented in Python, *Bioinformatics.*, 19(17) (2003) 2308-2310.
- [15] O'Boyle NM., Banck M., James CA., Morley C., Vandermeersch T., Hutchison GR., Open Babel: An open chemical toolbox, *J. Cheminformatics.*, 3(1) (2011) 33-3.

- [16] PDBaser: A python tool for fast protein - ligand extraction, Available at <https://github.com/mimminou/PDBASER>. Retrived March 10, 2021.
- [17] Hioual KS., Chikhi A., Bensegueni A., Merzoug A., Boucherit H., Teniou S., Mokrani EH., Merabti B., Successful challenge: A Key Step In Infectious Diseases Treatment Using Computer-Aided Drug Design, *Int. J. Biol. Sci. App.*, 1(1) (2014) 11-14.
- [18] Sandeli AK., Khiri-Meribout N., Benzerka S., Gürbüz N., Dündar M., Karcı H., Bensouici C., Mokrani EH., Ozdemir I., Koç A., Ozdemir N., Debache A., Ozdemir I., Silver (I)-N-heterocyclic carbene complexes: Synthesis and characterization, biological evaluation of Anti-Cholinesterase, anti-alpha-amylase, anti-lipase, and antibacterial activities, and molecular docking study, *Inorg. Chim. Acta.*, 525 (2021) 120486.
- [19] Mokrani EH., Bensegueni A., Chaput L., Beauvineau C., Djeghim H., Mouawad L., Identification Of New Potent Acetylcholinesterase Inhibitors Using Virtual Screening And In Vitro Approaches, *Mol. Inform.*, 38 (2019) 1800118.

Antifungal and Antibiofilm Activities of Some Essential Oils Against *Candida* spp

Bydaa Atron ^{1,a,*}, Hanaou Ahamada ^{1,b}, Ayşe Hümeýra Taşkin Kafa ^{1,c}, Cem Celik ^{1,d}, Mursit Hasbek ^{1,e}

¹ Department of Medical Microbiology, Faculty of Medicine, Sivas Cumhuriyet University, Sivas, Turkey.

*Corresponding author

Research Article

History

Received: 12/04/2022

Accepted: 04/08/2022

Copyright



©2022 Faculty of Science,
Sivas Cumhuriyet University

ABSTRACT

Candida species are commonly encountered strains associated with a wide range of infections. Unlike bacterial pathogens, fungal pathogens treatment is difficult and the development of resistance has been increasing at an alarming rate. In this study, the antifungal and antibiofilm effect of thyme oil, rosemary oil, mint oil, citronella oil, was tested on *Candida albicans*, *Candida tropicalis*, *Candida kefyr*, *Candida glabrata*, *Candida parapsilosis* isolated from clinical samples. The agar disc diffusion method was employed to determine the antifungal effect of the essential oils, and the inhibition of biofilm formation was assessed using microtiter biofilm inhibition assay. The results indicated that all the essential oils inhibited *Candida* strains and their biofilm in varying degrees. The highest antifungal activity in all isolates was observed in the thyme oil (>50mm), while rosemary oil showed the highest antibiofilm effect (>77%) in all tested strains. These findings led us to assume that the active components found in essential oils might be potential antifungal agents, adding to the repertoire of therapeutic options for the treatment of candidiasis.

Keywords: Antibiofilm, Antifungal, Citronella oil, Mint oil, Thyme oil.

^a bidaahamad@gmail.com

^c biologist85@gmail.com

^e mhasbek@hotmail.com

^{id} <https://orcid.org/0000-0002-7571-9277>

^{id} <https://orcid.org/0000-0002-7282-4928>

^{id} <https://orcid.org/0000-0002-5217-8607>

^b hanaou.ahamada@yahoo.com

^d cemcelik58@gmail.com

^{id} <https://orcid.org/0000-0002-0000-2239>

^{id} <https://orcid.org/0000-0002-7141-5874>

Introduction

Candida species are fungi that exist as commensals in human and animal mucous membranes. *Candida* spp has long been a leading cause of hospital-acquired infections. Human fungal infections have risen in recent years [1].

Candida albicans is the most commonly isolated in human candidiasis [2]. *Candida* spp. produces dangerous opportunistic infections, particularly in immunocompromised patients (HIV infections), because the immune system normally suppresses the spread of *Candida* [3].

Antifungal drugs are used to treat infections that are caused by fungi. They include the azoles group such as: clotrimazole, fluconazole, itraconazole, ketoconazole and polyenes which include: amphotericin B and nystatin [4].

Azoles have a fungistatic effect that inhibits the growth of fungal cell [5]. However, they are often related to excessive toxicity to the host tissues and drug resistance hence fungal infection becomes a serious clinical problem. Infections caused by *Candida* biofilm is particularly difficult to eradicate because the biofilm is more resistant to antifungal agents than planktonic cells [6]. Biofilm formation is considered to be important virulence factor as it protects microbes against adverse environmental factors, antibiotics, reduces the effectiveness of host immune mechanisms, and facilitates the acquisition of nutrients [7]. Some species of the *Candida* genus cause infections related to biofilm formation and it associated with higher patients mortality, probably correlated with the poor permeability of the matrix to the antifungal drugs [8].

Plants and their derivatives have been used previously in traditional medicine in the treatment of many diseases. Essential oils (EO) are naturally formed by the aromatic plant as a secondary metabolite. They are volatile, composed of a complex mixture of organic compounds, and characterized by a strong fragrance [9]. Essential oils are known for their activities against bacteria, fungi, viruses, and cancers. They are employed as analgesics, anti-inflammatory medications, spasmolytics, and local anesthetics [10].

The literature provides a lot of information regarding the effect of essential oils on the growth of *C. albicans* but, a little data on their impacts on biofilm formation and on the other *Candida* species. In this study, we tested the antimicrobial and antibiofilm effect of six essential oils obtained commercially, against ten strains of *Candida* clinical isolates and a standard strain.

Materials and Methods

Essential Oils

Essential oils are used in traditional and alternative medicine methods with the relevant literature review selected from the oils used and obtained commercially. The oils included; thyme oil (*Thymus vulgaris*), rosemary oil (*Salvia rosmarinus*), mint oil (*Mentha piperita*), citronella oil (*Cymbopogon nardus*).

Microorganisms

A total of Ten fungal strains of *Candida* cultures were prospectively obtained from the Clinical Microbiology

Laboratory of Sivas Cumhuriyet University Practice and Research Hospital in Sivas, Turkey. clinical isolates of *Candida albicans*, *Candida tropicalis*, *Candida kefyr*, *Candida glabrata*, *Candida parapsilosis*, and a standard strain *Candida albicans* ATCC 10231 were used for quality control of the study. Yeasts were cultured from clinical samples that included urine, sputum, vaginal swabs, blood, oral swabs and abscesses. Those samples were refrigerated until further processing.

Inoculum Preparation

The yeast to be used in the study, were reproduced by incubating overnight at 37°C in yeast peptone agar. Yeast suspension 0.5 McFarland (1×10^6 CFU/ml) to be at McFarland turbidity standard has been prepared. Inoculum suspensions of all Mueller Hinton Agar (MHA) media homogeneously spread on the surface.

Sensitivity Test Of The Essential Oils

The agar disc diffusion method was used to determine the sensitivity to the essential oils. The disc (6 mm in diameter) was placed on inoculated agar. Discs with this diameter can absorb 10-15 µl of liquid [11].

As the negative control, DMSO, which is the solvent of the EO, was used. Incubation of the inoculated plates was performed at 37 °C. The inhibition zone was measured to assess the antimicrobial activity against the *Candida* spp. All the tests were conducted three times. All plates were incubated at 37°C for 18-24 hours [12].

Microtiter Biofilm Inhibition Assay

The inhibition of biofilm formation was assessed using microtiter biofilm inhibition assay. Briefly, 100 µL of *Candida* strains 0.5 McFarland (1×10^6 CFU/ ml) were inoculated into 96-well microtiter plate wells and 100 µL of Essential oil (EO) were added into all the wells. The final volume was 200 µL per well on the microtiter plate. Since the densities of essential oils vary, the oils were weighed on precision scales to determine the volume. Stock solutions are prepared by dissolving essential oils in DMSO at 50 % and 25 %. The final DMSO concentration in the microplate wells was set at 1%. Incubation of the microplates was conducted at 37 °C for 48 h. The positive control was the suspension without EO. Following the 48 h incubation, the suspension was discarded, left to dry, then washes three times by phosphate buffer saline (PBS). A volume of 200 µL of 0.1% crystal violet was added of the 96-well. Incubated at room temperature for 30 min. Then, crystal violet was discarded and wells were washed with PBS three times. The plate was left to dry at room temperature for 30 min. Then, 95% ethanol was used to solubilize the crystal violet and the absorbance was read through a microplate reader (BMG LABTECK, Offenburg, Germany) at 550 nm. All experiments were performed in

triplicate [11]. Percent inhibition of biofilm was calculated using the equation described by Onsare and Arora [13].

$$\% \text{ Inhibition} = 100 - ((\text{OD } 570 \text{ sample}) / (\text{OD } 570 \text{ control}) \times 100)$$

Results

In this study, the anti-candidal activity of the four essential oils was investigated against ten clinical isolates of *Candida* spp.

Antifungal Activity Assays

The in vitro results of anti-candidal activity of the essential oils by the disc diffusion method are shown in Table 1. The different levels of oil activity were observed in the inhibition zone. The essential oils inhibited the growth of *Candida* strains, producing a zone diameter of inhibition from 8.0 mm to ≥ 50 mm based on the susceptibility of the *Candida* species. As the highest anti-candidal activity of the essential oils were observed in the thyme oil.

Table 1. Antifungal activity results of essential oils (Inhibition zone diameters)

Strains	Essential oils			
	Thyme Oil	Rosemary Oil	Mint Oil	Citronella
<i>C.tropicalis</i> (1)	≥ 50 mm	12 mm	17 mm	25 mm
<i>C.tropicalis</i> (2)	≥ 50 mm	19 mm	14 mm	34 mm
<i>C.parapsilosis</i> (1)	≥ 50 mm	24 mm	14 mm	32 mm
<i>C.parapsilosis</i> (2)	≥ 50 mm	27 mm	16 mm	20 mm
<i>C. albicans</i> (1)	≥ 50 mm	≥ 50 mm	≥ 50 mm	29 mm
<i>C. albicans</i> (2)	≥ 50 mm	≥ 50 mm	≥ 50 mm	38 mm
<i>C. kefyr</i>	≥ 50 mm	≥ 50 mm	≥ 50 mm	21 mm
<i>C.glabrata</i> (1)	≥ 50 mm	≥ 50 mm	≥ 50 mm	21 mm
<i>C.glabrata</i> (2)	≥ 50 mm	≥ 50 mm	≥ 50 mm	32 mm
<i>C. albicans</i> ATCC 10231	≥ 50 mm	≥ 50 mm	≥ 50 mm	33 mm

The potential of the oils to prevent biofilm cell formation was investigated through the biofilm inhibition assay. The most effective oil was Rosemary oil. Which was observed to reduce the biofilm of all the strains under study. The biofilm of *C.parapsilosis* showed the highest reduction value, while *C.glabrata* had the least one. Mint oil had a significant reduction as well. The reduction activity was highest in the isolates of *C.tropicalis*. Similarly to rosemary oil, the lowest reduction value was seen in *C.glabrata* isolates. Furthermore, citronella oil was mostly effective against *C.parapsilosis* and least effective against the strains of *C.tropicalis*. Thyme Oil was found to be the weakest oil in the terms of biofilm reduction. It had activity on *C.tropicalis* and *C.parapsilosis*. However, It showed a little to no effect against *C.glabrata* and *C. albicans*.

The results are shown in the following table.

Table 2. biofilm inhibition assay results of essential oils (%)

Strains	Essential oils							
	Thyme Oil		Rosemary oil		Mint oil		Citronella	
	Reduction in biofilm formation (%)		Reduction in biofilm formation (%)		Reduction in biofilm formation (%)		Reduction in biofilm formation (%)	
	1/2	1/4	1/2	1/4	1/2	1/4	1/2	1/4
<i>C. tropicalis</i> (1)	14±0.30	18±0.013	78±0.31	76±0.31	61±0.27	57±0.29	28±0.40	18±0.47
<i>C. tropicalis</i> (2)	52±0.13	62±0.24	85±0.16	78±0.41	70±0.10	78±0.36	64±0.39	61±0.39
<i>C. parapsilosis</i> (1)	47±0.22	49±0.17	86±0.21	84±0.40	54±0.32	67±0.37	54±0.42	58±0.40
<i>C. parapsilosis</i> (2)	6±0.27	13±0.07	83±0.11	77±0.38	56±0.12	66±0.46	32±0.45	30±0.50
<i>C. albicans</i> (1)	2±0.13	13±0.22	60±0.9	80±0.33	37±0.13	60±0.46	37±0.44	31±0.46
<i>C. albicans</i> (2)	21±0.13	27±0.08	65±0.44	88±0.35	38±0.43	63±0.43	25±0	15±0.59
<i>C. kefir</i>	11±0.08	9±0.17	52±0.50	77±0.35	60±0.41	30±0.37	16±0.6	39±0.53
<i>C. glabrata</i> (1)	9±0.10	NE	59±0.30	77±0.28	54±0.18	30±0.53	35±0.45	14±0.59
<i>C. glabrata</i> (2)	5±0.18	80±0.04	52±0.42	78±0.27	35±0.33	35±0.30	23±0.53	42±0.47
<i>C. albicans</i> ATCC 10231	2±0.17	NE	34±0.09	78±0.30	58±0.21	58±0.53	40±0.35	39±0.37

NE: No effect

Discussion

Plants as sources of antimicrobial compounds have sparked increased interest in recent years. The plant-derived antimicrobial agents have been reported to be safe and without side effects and antimicrobial properties of plant volatile oils have been recognized [14].

Previous studies have indeed demonstrated the antimicrobial activity of essential oils, mainly focusing on *C. albicans* [15]. However, in this study, we tested the antifungal activities of the EO against 5 clinical strains including *C. albicans*. The observation in this study is consistent with previous reports that EOs from thyme, rosemary, mint oil, citronella possess anti-candidal activity and exhibit anti-biofilm action as well [16] [17] [18].

Candida biofilm structure is particularly difficult to eradicate since biofilm is much more resistant to antifungal agents than planktonic cells. In this context, a more effective strategy seems to assess the prevention of biofilm formation than its eradication plus the direct effect on the planktonic cells.

Mint essential oil is one of the most well-known and extensively utilized essential oils. *Mentha piperita*, (family Lamiaceae) is a species found in many parts of the world which has a financial worth because of its flavoring, odor, and medicinal qualities in foods and cosmetic industrial products. In addition, the leaves and flowers of *M. piperita* have medicinal properties [19]. Several studies have shown that mint oil extracted from *M. piperita* exhibited strong inhibitory activity against many organisms [20]. In our study, the Mint oil exhibited antifungal and antibiofilm activities against both the standard and clinical strains of *Candida* species, with inhibition zone diameters ranging from 17 mm to more than 50 mm. Bona and his colleagues observed similar results [21]. The most sensitive strains to Mint oil (with inhibition zone ≥ 50 mm) were: *C. albicans*, *C. kefir*, and *C. glabrata*. Mint oil showed a reduction in

biofilm formation of the tested strains. The highest inhibitory effect was observed in *C. tropicalis* isolates (78%), while the lowest effect was observed in *C. glabrata* strains (35%). The antibiofilm effect of mint oil on *Candida* isolates growth reported in this study support those of previous studies [22,23]. In a study carried out by Samber and others, they investigated the synergistic anti-candidal activity and mode of action of *Mentha piperita* essential oil and its major components against *Candida* spp and mode of action as well. According to their results, the mint EO and its lead compounds influence antifungal activity by reducing ergosterol levels, inhibiting PM-ATPase, and leading to intracellular acidification and cell death [24].

Citronella oil is mostly derived from *Cymbopogon nardus*. It has long been used in traditional practices by many ancient cultures. It's widely used in the perfume industry and soap manufacturing [25]. Citronella oil is well-known for its antibacterial properties. It has been recommended as home remedy for the treatment of oral and vaginal fungal infections by numerous books and articles and products containing these essential oils for the treatment of such infections are being used in many parts of the world [26]. The results of the present study have shown that the inhibitory effect of EO from citronella was less than that of thyme oil, rosemary oil, and Mint oils in planktonic and biofilm-forming isolates. The Inhibition zone diameters were between (20-38 mm). The least susceptible strains were *C. kefir* and *C. glabrata* (21 mm), while *C. albicans* strains were the highest susceptible to citronella. The antibiofilm inhibition of Citronella showed different values among the tested strains. The highest reduction was observed in *C. tropicalis* (64%) and *C. parapsilosis* (58%), while the lowest reduction was observed in *C. albicans* strains (15%) which is lower than the reduction that was achieved in a previous study [27]. The difference could be due to the use of standard instead

of clinical strains. Furthermore, the geographical location from which the plants were collected can influence resulting outcome. When comparing antibiofilm inhibition of Citronella to other EOs used in this study, Citronella oil along with thyme oil, rosemary oil, and mint oil has a high reduction in biofilm formation of *C. tropicalis* and *C. parapsilosis* isolates. *C. albicans* isolates were less susceptible to Citronella than the others. Our result disagrees with that of a previously published work submitted by Trindade and his colleagues. They suggest that Citronella EO has a strong in vitro antifungal and antibiofilm activity on *C. albicans* [28].

Rosemary is a plant that originates in the Mediterranean region and belongs to the *Lamiaceae* family. It might, however, be found all over the planet. It is a perennial and aromatic plant. Rosemary can be used as a spice in cooking, as a natural preservative in the food industry, and as an ornamental and medicinal plant [29]. In our result, rosemary oil showed an inhibition zone in all tested clinical isolates and standard (12-50 mm). The highest effect of rosemary oil (≥ 50) was seen against *C. albicans*, *C. kefyr* and *C. glabrata*. Our results regarding *C. albicans* agree with that of previous work by Matsuzaki et al, which suggests that Rosemary EO has significant antifungal activity against *Candida albicans* [30].

Rosemary oil also inhibits biofilm formation in all tested clinical isolates and the standard isolate. Significant effect (>83%) is seen particularly against *C. tropicalis*, *C. parapsilosis* and *C. albicans*. The antifungal activity of rosemary essential oil in this study was similar to the known literature with a little difference, which could be for many reasons such as a different growing environment of Rosemary, and different extraction methods of essential oils [31].

Thyme essential oil is used as a flavor in a wide variety of foods, beverages, confectionery products, and perfumery to synthesize soaps and lotions. It possesses some antiseptic, bronchiolitis, antispasmodic, and antimicrobial properties [32]. It was documented that thyme EO has an inhibitory impact on *Candida albicans* virulence factors.

Alves et al suggested that Thyme EO is very effective in inhibiting *C. albicans* germ tube formation. Also, it was found to disrupt *C. albicans* biofilms [33].

Rajkowska and others demonstrated the role of the effect of thyme essential oils on candida cell distribution and biofilm formation. Their results showed a statistically significant reduction in biofilm formation [34].

In this present study, thyme oil showed a high effect (inhibition zone ≥ 50 mm) against all tested clinical isolates and the standard. However, in biofilm inhibition, thyme oil shows a significant effect (> 60%) in only *C. tropicalis* and *C. glabrata*. Antifungal activities of thyme oil found in this study are consistent with several reports where thyme oil shows a high effect on *Candida* species [35].

Taken together these results show that *thyme*, *rosemary*, *mint*, and *citronella* essential oils have anti-candidal and anti-biofilm potential.

Conclusion

In this study, the inhibitory effect of thyme oil, rosemary oil, mint oil, and citronella oil on *Candida* spp were tested. In conclusion, rosemary and mint oils were found to be the most effective. they can be used as effective anti-biofilm against *Candida* spp. However, if essential oils are to be used for medicinal purposes, molecular mechanisms, mode of action, stability, toxicity, and efficiency of active components derived from essential oils must be explored and assessed further. The results of this work support the research for new alternatives or complementary therapies against candidal infections.

Conflicts of interest

There are no conflicts of interest in this work.

References

- [1] Bongomin F., Gago S., Oladele R O., Denning DW., Global and multi-national prevalence of fungal diseases-estimate precision, *Journal of Fungi*, 3 (4) (2017) 57-69.
- [2] Cleveland A., Harrison L., Farley M., Hollick R., Stein B., Chiller T., Declining Incidence of Candidemia and the Shifting Epidemiology of Candida Resistance in Two US Metropolitan Areas, 2008–2013: Results from Population-Based Surveillance., *PLOS ONE*, 10(3) (2015) e0120452..
- [3] Nobile C., Johnson A., *Candida albicans* Biofilms and Human Disease, *Annual Review Of Microbiology*, 69(1) (2015) 71-92.
- [4] Calogiuri G., Garvey L. H., Nettis E., Romita P., Di Leo E., Caruso R., Foti C., Skin allergy toazole antifungal agents for systemic use: A review of the literature, *Recent Patents On Inflammation & Allergy Drug Discovery*, 13 (2) (2019) 144–157.
- [5] Di Bonaventura G., Spedicato I., Picciani C., D'Antonio D., Piccolomini R., In vitro pharmacodynamic characteristics of amphotericin B, caspofungin, fluconazole, and voriconazole against bloodstream isolates of infrequent *Candida* species from patients with hematologic malignancies, *Antimicrobial Agents and Chemotherapy*, 48(11) (2004) 4453–4456..
- [6] Silva S., Rodrigues C., Araújo D., Rodrigues M., Henriques M., *Candida* Species Biofilms' Antifungal Resistance, *Journal Of Fungi*, 3(1) (2017) 8-11
- [7] Chandra J., Mukherjee, P., *Candida* Biofilms: Development, Architecture, and Resistance, *Microbiology Spectrum*, 3(4) (2015) 70-85.
- [8] Nett J., Andes D., Contributions of the Biofilm Matrix to *Candida* Pathogenesis. *Journal Of Fungi*, 6(1) (2020) 21-33.
- [9] Rajkowska K., Nowicka-Krawczyk P., Kunicka-Styczyńska A., Effect of Clove and Thyme Essential Oils on *Candida* Biofilm Formation and the Oil Distribution in Yeast Cells, *Molecules*, 24(10) (2019) 42-54.
- [10] Ali B., Al-Wabel N., Shams S., Ahamad A., Khan S., Anwar F., Essential oils used in aromatherapy: A systemic review, *Asian Pacific Journal of Tropical Biomedicine*, 5(8) (2015) 601-611.
- [11] Bauer, A. W., W. M. M. Kirby, J. C. Sherris, and M. Turck. Antibiotic susceptibility testing by a standardized single

- disk method, *American Journal of Clinical Pathology*, 36 (1966) 493-496.
- [12] Raveau R., Fontaine J., Lounès-Hadj Sahraoui A. Essential Oils as Potential Alternative Biocontrol Products against Plant Pathogens and Weeds: A Review, *Foods*, 9(3) (2020) 349-365.
- [13] Onsare, J., and Arora, D. Antibiofilm potential of flavonoids extracted from *Moringa oleifera* seed coat against *Staphylococcus aureus*, *Pseudomonas aeruginosa* and *Candida albicans*, *Journal of Applied Microbiology*, 118 (3) (2015) 313–325.
- [14] Jayathilaka E., Rajapaksha D., Nikapitiya C., De Zoysa M., Whang I., Antimicrobial and Anti-Biofilm Peptide Octominin for Controlling Multidrug-Resistant *Acinetobacter baumannii*, *International Journal Of Molecular Sciences*, 22(10) (2021) 53-55.
- [15] Bachmann S., VandeWalle K., Ramage G., Patterson T., Wickes B., Graybill J., Lopez-Ribot J., In vitro activity of caspofungin against *Candida albicans* biofilms, *Antimicrobial Agents and Chemotherapy*, 46 (2002) 3591-3596
- [16] Chandra J., Mukherjee P., Leidich S., Faddoul F., Hoyer L., Douglas J., Ghannoum M., Antifungal resistance of candidal biofilms formed on denture acrylic in vitro, *Journal of Dental Research*, 80(1) (2001) 903-908
- [17] Shuford J., Piper K., Steckelberg J., Patel N R., vitro biofilm characterization and activity of antifungal agents alone and in combination against sessile and planktonic clinical *Candida albicans* isolates, *Diagnostic Microbiology and Infectious Disease*, 57(3) (2007) 277-279
- [18] Chouhan S, Sharma K., Guleria S., Antimicrobial activity of some essential oils -present status and future perspectives, *Medicines*, 4(3) (2017) 58-71.
- [19] Bona E., Cantamessa S., Pavan M., Novello G., Massa N., Rocchetti, A., Sensitivity of *Candida albicans* to essential oils: are they an alternative to antifungal agents?, *Journal Of Applied Microbiology*, 121(6) (2016) 1530-1545.
- [20] Kizil S., Hasımlı N., Tolan V., Kilinc E. Yuksel U., Mineral content, essential oil components and biological activity of two *Mentha* species (*M. piperita* L., *M. spicata* L, *Turkish Journal Of Field Crops*, 15(2) (2010) 148-153.
- [21] Saharkhiz M., Motamedi M., Zomorodian K., Pakshir K., Miri R., Hemyari, K., Chemical Composition, Antifungal and Antibiofilm Activities of the Essential Oil of *Mentha piperita*, *ISRN Pharmaceutics*, 20(12) (2012) 1-6.
- [22] Benzaid C., Belmadani A., Djeribi R., Rouabhia M., The effects of *Mentha piperita* essential oil on *C. albicans* growth, transition, biofilm formation, and the expression of the secreted aspartyl proteinases genes, *Antibiotics*, 8(1) (2019) 10.
- [23] Samber, N., Khan, A., Varma, A., & Manzoor, N. Synergistic anti-candidal activity and mode of action of *Mentha piperita* essential oil and its major components, *Pharmaceutical Biology*, 53(10) (2015) 1496–1504.
- [24] Sharma R., Rao R., Kumar S., Mahant S., Khatkar S., Therapeutic Potential of Citronella Essential Oil: A Review, *Current Drug Discovery Technologies*, 16(4) (2019) 330–339.
- [25] Nakahara K., Alzoreky N.S., Yoshihashi T., Nguyen T., Trakoontivakorn G. Chemical composition and antifungal activity of essential oil from *Cymbopogon nardus* (Citronella Grass), *Japan International Research Center for Agricultural Sciences*, 37 (2013) 249–52.
- [26] Khan M. S. A., Ahmad I., Antibiofilm activity of certain phytocompounds and their synergy with fluconazole against *Candida albicans* biofilms, *Journal of Antimicrobial Chemotherapy*, 67(3) (2011) 618–621.
- [27] González-Trujano M., Peña E., Martínez A., Moreno J., Guevara-Fefer, P., Déciga-Campos, M., López-Muñoz F., Evaluation of the antinociceptive effect of *Rosmarinus officinalis* L. using three different experimental models in rodents, *Journal of Ethnopharmacology*, 11(3) (2007) 476–482.
- [28] Trindade, L.A., Cordeiro, L.V., de Figueiredo Silva, D. et al. The antifungal and antibiofilm activity of *Cymbopogon nardus* essential oil and citronellal on clinical strains of *Candida albicans*, *Braz J. Microbiol.*, 53(3) 1231-1240.
- [29] Matsuzaki, Y., Tsujisawa, T., Nishihara, T., Nakamura, M. and Kakinoki, Y. Antifungal activity of chemotype essential oils from rosemary against *Candida albicans*, *Open Journal of Stomatology*, 3(2) (2013) 176-182.
- [30] Alves, M., Gonçalves, M., Zuzarte, M., Alves-Silva, J., Cavaleiro, C., Cruz, M., & Salgueiro, L. Unveiling the Antifungal Potential of Two Iberian Thyme Essential Oils: Effect on *C. albicans* Germ Tube and Preformed Biofilms, *Frontiers In Pharmacology*, 10(2) (2019) 146-158
- [31] Rajkowska, K., Nowicka-Krawczyk, P., & Kunicka-Styczyńska, A. Effect of Clove and Thyme Essential Oils on *Candida* Biofilm Formation and the Oil Distribution in Yeast Cells, *Molecules (Basel, Switzerland)*, 24(10) (2019) 154-165
- [32] Meccatti V. M., Oliveira J. R. D., Figueira W., Lagareiro Netto A., Zamarioli, L. S., Marcucci, C., Camargo E., Carvalho A., Oliveira D., *Rosmarinus officinalis* L. (rosemary) extract has antibiofilm effect similar to the antifungal nystatin on *Candida* samples, *Anais Da Academia Brasileira de Ciências*, 93(2) (2021) e20190366.
- [33] Ghasemi G., Alirezalu A., Ghosta Y., Jarrahi A., Safavi S. A., Abbas-Mohammadi M., Barba J., Munekata S., Domínguez R., Lorenzo M., Composition, Antifungal, Phytotoxic, and Insecticidal Activities of *Thymus kotschyianus* Essential Oil, *Molecules*, 25(5) (2020) 152-164.
- [34] Nabavi M., Marchese A., Izadi M., Curti V., Daglia M., Nabavi F., Plants belonging to the genus *Thymus* as antibacterial agents: From farm to pharmaca, *Food Chemistr*, 173 (2015) 339–347.
- [35] Rajkowska K., Nowicka-Krawczyk P., Kunicka-Styczyńska A., Effect of Clove and Thyme Essential Oils on *Candida* Biofilm Formation and the Oil Distribution in Yeast Cells, *Molecules*, 24(10) (2019) 1954.

Investigation of the Effect of Different Synthesis Methods on the Photocatalytic Activity of TiO₂: Comparison of Rutile and Anatase TiO₂

Fatma Kiliç Dokan^{1,a,*}

¹ Department of Chemistry and Chemical Processing Technologies, Mustafa Çıkrıkçıoğlu Vocational School, Kayseri University, Kayseri, Türkiye

*Corresponding author

Research Article

History

Received: 22/04/2022

Accepted: 11/07/2022

Copyright



©2022 Faculty of Science,
Sivas Cumhuriyet University

fatmakilic@kayseri.edu.tr

<https://orcid.org/0000-0002-5355-2904>

ABSTRACT

In this study, the effect of the synthesis method (solid state, sol-gel and hydrothermal) on the photocatalytic activity of the anatase and rutile phases of TiO₂ was evaluated. As a result of XRD, FESEM and BET analysis of pure phase TiO₂ powders in anatase and rutile phases, the changes in particle structures, surface areas and morphologies were examined and the differences in both synthesis method and phase structures were evaluated with Photodegradation experiments. The results of the X-ray diffraction (XRD) analysis showed that the TiO₂ compound synthesized in the anatase phase and by the synthesized hydrothermal method exhibited a much smaller crystal size than the other synthesis methods and the rutile phase. Surface morphology examinations of the samples were made with scanning electron microscopy (FESEM), particle sizes were determined in the range of 90-200 nm, and their surface areas were examined by Brunauer–Emmett–Teller (BET) analysis. The adsorption-desorption isotherms shown also support the XRD data of the highest surface area. The photocatalytic behavior of the compounds was investigated using methylene blue degradation. As a result of all the syntheses and characterization studies, it has been shown that TiO₂ obtained by hydrothermal method exhibits the best photocatalytic activity.

Keywords: Anatase TiO₂, Hydrothermal method, Photocatalytic activity, Rutile TiO₂

Introduction

In different experimental research in recent years, titanium dioxide (TiO₂) has become one of the most important experimental items, mainly because of its outstanding values, including stability, non-toxic, recyclability, low cost and unique photochemical and photophysical advantages, and mainly in water-hydrogen separation, it is used as a widely applied waste treatment material. Such as water treatment, biological sensor, solar cell etc. [1-5]

Different sized inorganic materials certain structural properties structures, including nanotubes, nanorods, flower-like, fan-shaped, microspheres (hollow, solid, or porous), etc. attracted great attention due to its innovations. [6-9]

TiO₂ exists in crystalline and amorphous form. It also has three basic polymeric crystal structures: anatase, rutile, and brookite. Anatase and rutile are tetragonal, brookite is orthorhombic.

All contain the octahedral TiO₆ structure, but the bond bonding is different, indicating the difference in phases; For example, the unit cell constants of rutile are a=4.59, c=2.96, while the unit cell constants of anatase are a=3.79 and c=9.51. Rutile structure is formed by the combination of 2 to 12 linear chains. The tetragonal structure is formed by the combination of oxygen atoms at the corners of these linear chains. In the anatase structure, there are no oxygen atoms at the corners and all 4 sides are tetragonal [10]. Figure 1 shows that each Ti⁴⁺ ion in the crystal is surrounded by six O²⁻. The octahedral structure in rutile

crystals is not regular and shows slightly orthorhombic bending. The octahedral structure in anatase TiO₂ is greatly disturbed to a symmetry less than orthorhombic in shape, the bond length between Ti-Ti in the anatase form (3.79 Å and 3.04 Å) is greater than that of the rutile form (3.57 Å and 2.96 Å); The bond length between Ti-O (1.934 Å and 1.980 Å) is shorter than that of the rutile phase (1.949 Å and 1.980 Å) [10].

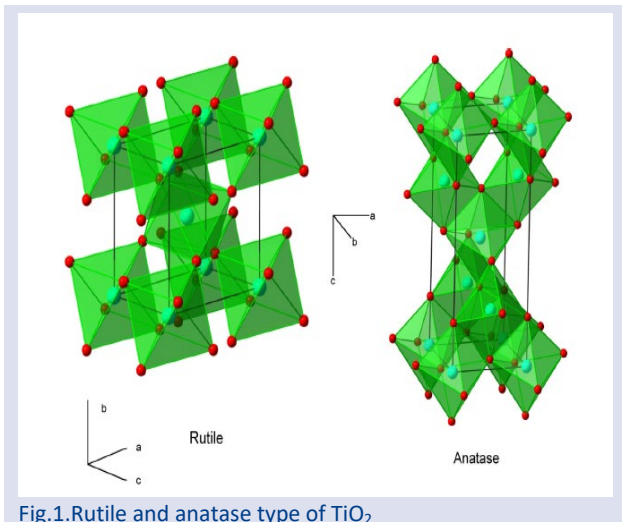
This difference in the lattice structure is the most important reason why Anatase TiO₂ is more active than rutile TiO₂ in reactions, and this causes different electronic band structure and bulk densities between the two forms of TiO₂. Rutile TiO₂ has the highest refractive index among these three phases. For this reason, it is generally used in paint raw materials and in the cosmetics industry [11] Anatase crystal form shows the highest photocatalytic activity among other crystal forms [12] For this reason, Anatase TiO₂ constitutes a large part of the studies. However, there are studies that show higher photocatalytic performance than pure Anatase, which is a mixture of Anatase and Rutile at different rates. TiO₂ nanoparticles, which are commercially used and called Degusa P-25, consist of a ratio of 3:1 (Anatase - Rutile).

Anatase TiO₂ is widely used in heterogeneous catalyst, photocatalyst, solar cells, gas sensors and wastewater treatment systems. Rutile TiO₂ has the highest refractive index among these three phases. For this reason, it is generally used in paint raw materials and in the cosmetics industry [13] Anatase crystal form shows the highest

photocatalytic activity among other crystal forms [14]. For this reason, Anatase TiO₂ constitutes a large part of the studies. However, there are studies that show higher photocatalytic performance than pure Anatase, which is a mixture of Anatase and Rutile at different rates. TiO₂ nanoparticles, which are commercially used and called Degusa P-25, consist of a ratio of 3:1 (Anatase - Rutile). Apart from the effect of different ratios in the crystal structure on the photocatalytic activity, the change in the size of the TiO₂ particles also has serious effects on the photocatalytic performance.

Particle size is a very important factor affecting the performance of photocatalytic materials. The size and type of the material directly affects the surface structure, resulting in an efficient photocatalytic material. [15-17].

In this letter, we report a solid state, sol-gel and hydrothermal approach for the synthesis of anatase and rutile TiO₂. This work will contribute to the fundamental research of different synthesis methods and the investigation and detailing of the photocatalytic activity properties on two different forms of TiO₂.



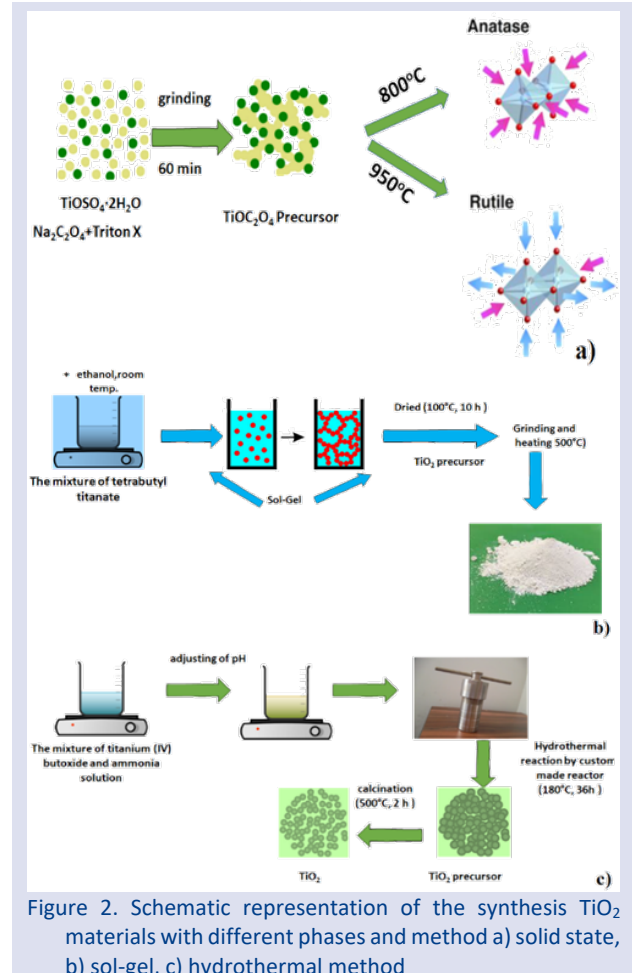
Materials and Methods

Synthesis of Rutile and Anatase type TiO₂

Three methods were chosen to synthesize different type of TiO₂ photocatalyst. Conventional solid state, sol-gel and new optimized hydrothermal synthesis. Dehydrate titanyl sulfate (TiOSO₄·2H₂O), sodium oxalate (Na₂C₂O₄) and Triton -X as surfactant were used for solid state method. After grinding at room temperature for a total of 60 minutes, the precursor (TiOC₂O₄) was prepared. TiO₂ photocatalytic material was obtained because of heat treatment at 800°C. The material was sintered at 950°C to obtain the rutile form with the same method (fig 2.a). [18-20]

A stoichiometric amount of tetra butyl titanate was mixed vigorously into 20 mL of ethanol, and the solution was stirred continuously until gel formation. The gel was dried at 100°C, calcined at 500°C and ground to obtain TiO₂ particles (fig 2.b). [20-22]

TiO₂ synthesis was carried out with the new and optimized hydrothermal method by our team. The titanium IV butoxide and ammonia mixture was brought to the optimum pH point and mixed for 1 h at 70°C, then the stainless steel was autoclaved and heated at 180°C for 36 h. The resulting precipitate was washed 3 times to remove impurities and finally, heat treatment was carried out at 500°C for 2 hours (fig 2.c). [23]



Characterization

Surface morphologies and particle distributions of TiO₂ materials synthesized by different synthesis methods (solid state, sol-gel and hydrothermal method) with different crystal phases were evaluated by Field emission scanning electron microscopy (FE-SEM, Gemini 550). The chemical components of the materials were determined by X-ray diffraction (XRD, Cu-Kα radiation, Bruker AXS D8). The bonding structures of the material were investigated in the Fourier transform infrared spectra (FT-IR) (Perkin-Elmer-spotlight 400) wavelength range of 4000–500 nm. Pore size distribution, pore volume and specific surface area were defined by the Brunauer-Emmett-Teller (BET, Gemini IV micromeritic) method.

Results

In this study, it is aimed to make comparisons by synthesizing anatase and rutil phases with all synthesis methods.

Generally, the photocatalytic activity of TiO₂ varies very significantly with the crystal phase structure, crystal size, surface area and pore structure [24]. X-ray diffraction (XRD) analysis was performed to the identification of the crystallographic structure of the samples and results can be seen in fig.3 and fig.4. In Fig 3(a-c) XRD results of the rutile phases are synthesis via different methods patterns are demonstrated. It was determined by indexing that the peaks belong to the rutile phase (JCPDS card no. 21-1276).

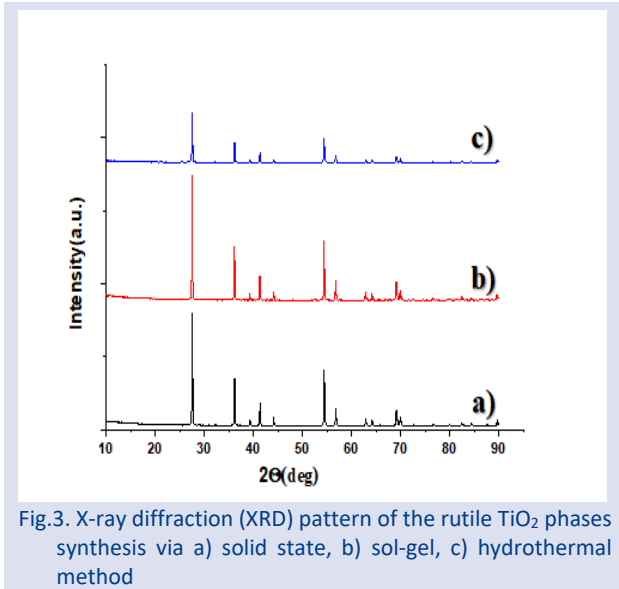


Fig.3. X-ray diffraction (XRD) pattern of the rutile TiO₂ phases synthesis via a) solid state, b) sol-gel, c) hydrothermal method

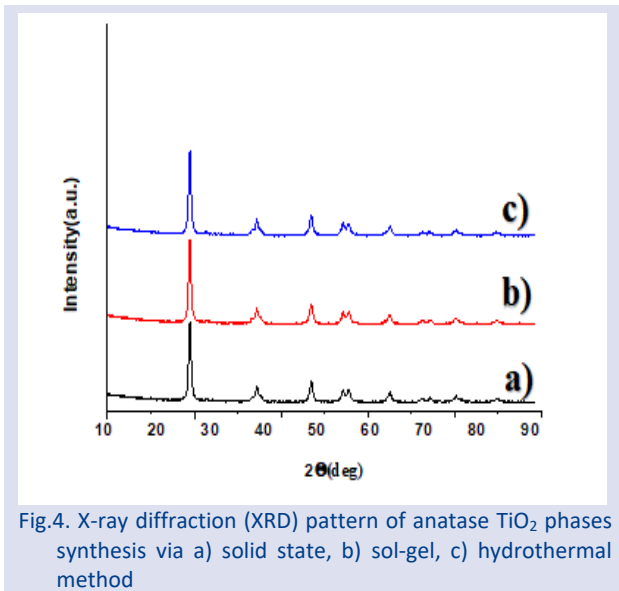


Fig.4. X-ray diffraction (XRD) pattern of anatase TiO₂ phases synthesis via a) solid state, b) sol-gel, c) hydrothermal method

The crystal structure properties of the compounds are summarized in Table 1, which shows an increase in the crystal size because of synthesis method. In Fig 4(a-c) XRD results of the anatase phases are synthesis via different methods patterns are demonstrated. All peaks that were relatively sharp compared to other peaks were first indexed as anatase TiO₂. (JCPDS No. 84-1285).

In Table 1, the crystallite sizes of all compounds synthesized by different methods are given and it is

estimated from the half-bandwidth of the X-ray spectral peak by the Scherrer equation [25], which is given with Eq. 1.

$$D = \frac{0,94\lambda}{\beta \cos\theta} \quad (1)$$

If we examine the formula, where λ is the wavelength, θ is the x-ray diffraction angle, β is the full width of the peaks at half maximum (FWHM) in radians. This β value was calculated from the xrd pattern with the help of the topas program. While the anatase-hydrothermal TiO₂ crystallite size is 98 nm, the rutile-solid state TiO₂ is 145 nm (Table 1). It is important that we examine table 1 to observe the effect of different synthesis methods on the crystal size.

The structure and morphology of the synthesized material were scrutinized with FESEM images (rutile) in Fig. 5 and fig 6. The FESEM image of the as-obtained TiO₂ indicates a fine spherical shape with uniform size in Fig. 5(a-c). It is observed that the spherical shape of the TiO₂ is consist of micro sphere structures.

FESEM images of the TiO₂ (anatase) exhibit that the particles had spherical morphology in low (Fig. 6 a-c) and spherical shape of the TiO₂ are consist of nano sphere structures.

Table 1. Surface area, average crystallite size, lattice parameters values for rutile and anatase TiO₂ synthesized via different methods

Sample	Surface area (m ² /g)	Average crystallite size, D (nm)	Granule size (nm)	Lattice parameters (Å°)		
				a	b	c
Rutile TiO ₂ -solid state method	11	145	200-300	4,59		2.95
Rutile TiO ₂ -sol-gel method	17	132	180-230	4.58		2.94
Rutile TiO ₂ -Hydrothermal method	28	130	150-200	4.56		2.93
Anatase TiO ₂ -solid state method	24	134	100-150	3.79		9.53
Anatase TiO ₂ - sol-gel method	32	124	80-120	3.78		9.52
Anatase TiO ₂ -Hydrothermal method	44	98	70-100	3.78		9.51

It is remarkable that the FESEM measurements are harmony with the synthesis methods. That is, the particle sizes of the samples synthesized by the solid-state method are the largest, and the sizes of the samples synthesized by hydrothermal are smaller than the others, and these measurements were taken via image pro plus 5 program, and the values are shown in Table 1.

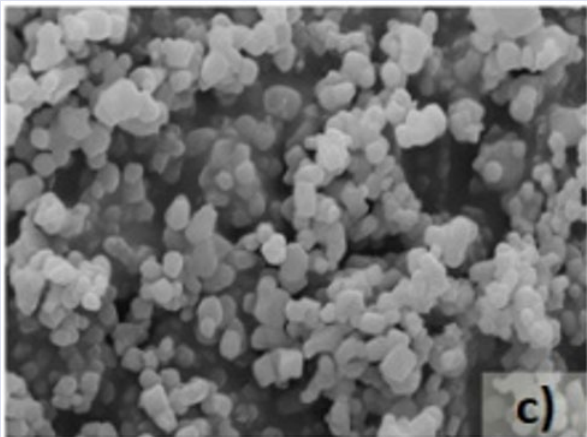
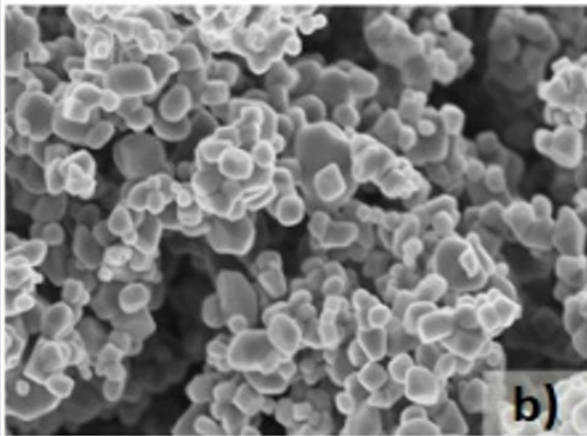
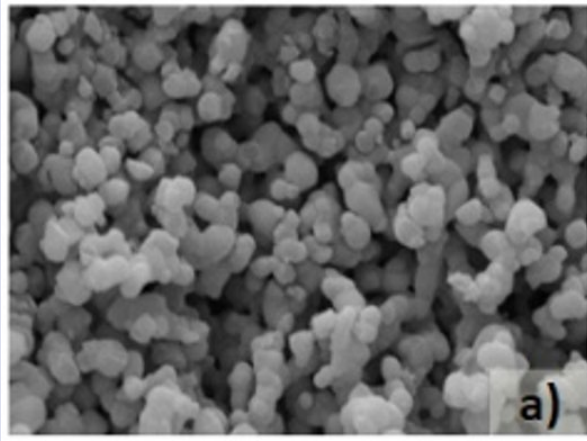


Fig. 5. FESEM images of the rutile TiO_2 phases synthesis via a) solid state, b) sol-gel, c) hydrothermal method

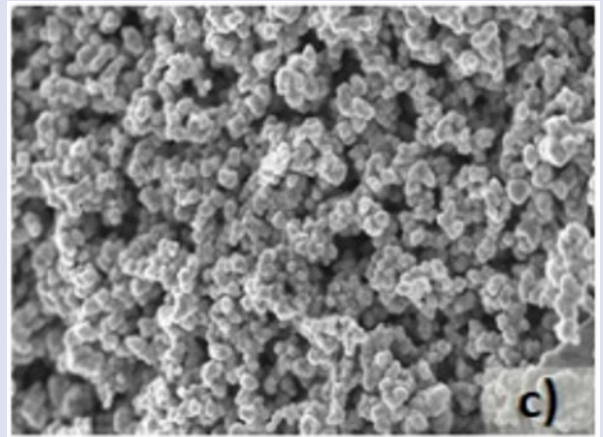
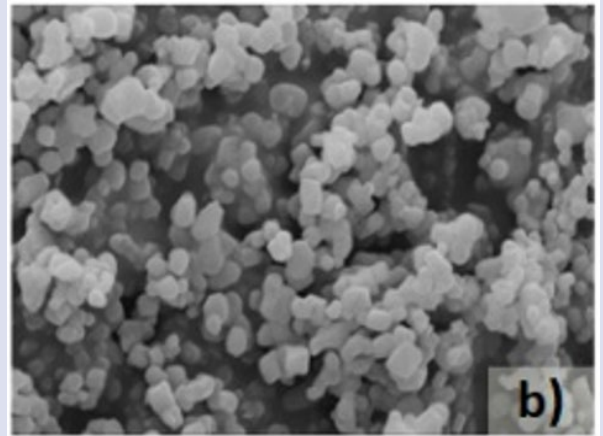
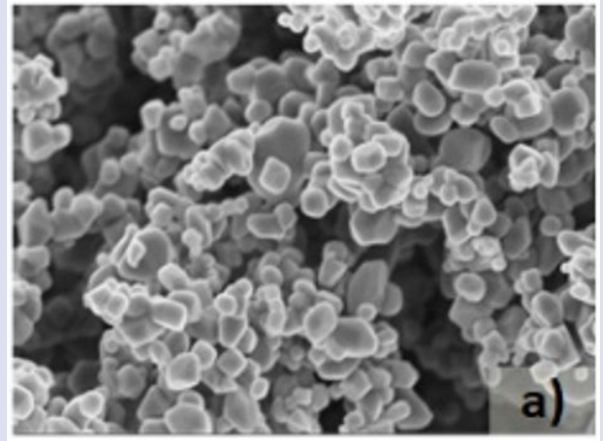


Fig. 6. FESEM images of the anatase TiO_2 phases synthesis via a) solid state, b) sol-gel, c) hydrothermal method

The crystal size values obtained from the XRD data, and the particle sizes calculated from the FESEM images are in harmony and all values are given in Table 1. To analyze the porosity of all samples N_2 adsorption-desorption isotherms were evaluated (Fig 7).

Examining the isotherm for rutile samples shows a very small, adsorbed amount of N_2 gas, indicating a non-porous property. Compared with the isotherms for anatase show a more adsorbed amount of N_2 gas indicates the existence of micropores. Average BJH adsorption pore volume values and BJH desorption pore size values are shown in Table 1.

Many different studies have suggested that TiO_2 in anatase structure generally has superior photocatalyst properties. The most important reason for this is that the anatase structure has a wider band gap, longer charge carrier lifetime, longer diffusion path length and higher charge carrier mobility. [26-33]

Therefore, the high photocatalytic performance can be attributed to the outstanding structure of rutile or anatase type TiO_2 .

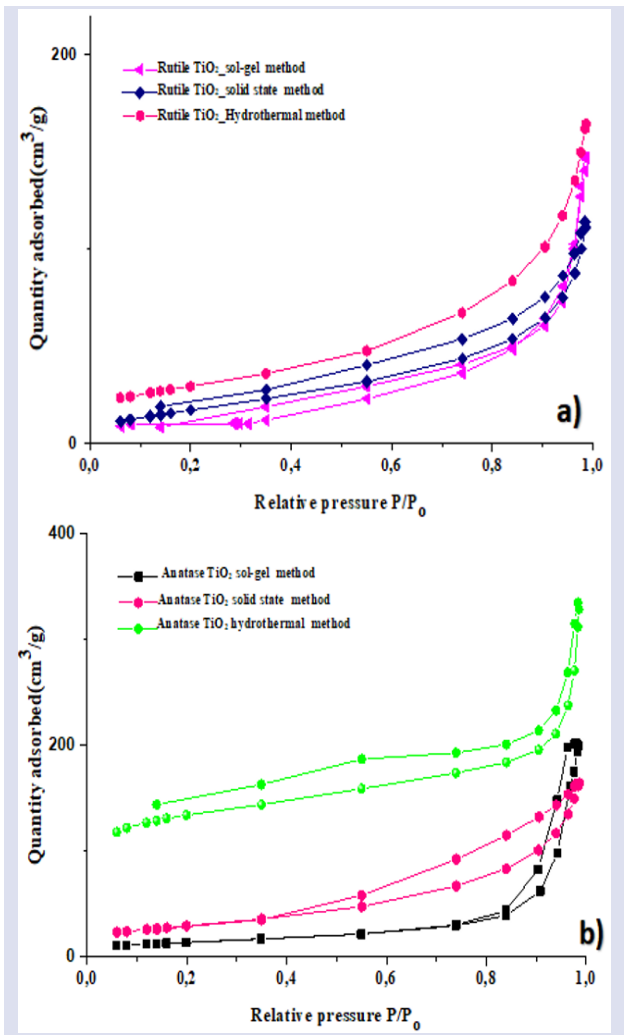


Fig. 7. Nitrogen adsorption-desorption isotherm for a)rutile and b)anatase TiO₂ synthesized via different methods.

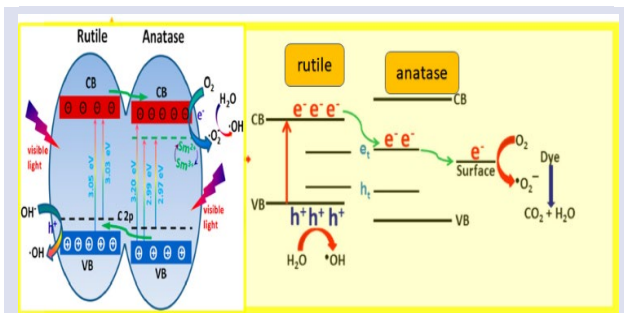


Figure 8. Schematic representation of the Difference in TiO₂ photocatalytic mechanism between rutile and anatase.

Photocatalytic activity measurements of the prepared samples were investigated by photodegradation of methylene blue (MB) using a 300 W xenon lamp. For the study, 50 mg of photocatalyst was dispersed in 100 mL of aqueous solution containing 5 ppm MB and kept in the dark for 30 min to stabilize the adsorption/desorption of the photocatalysts on the MB surface, and the photocatalytic reaction was carried out at 365 nm (15 W, under UV light).

Examining the behavior of the material without any catalyst in Figure 9.a-b, it very clearly shows that the

degradation of MB is extremely slow, which means that the reduction reaction is not kinetically favorable.

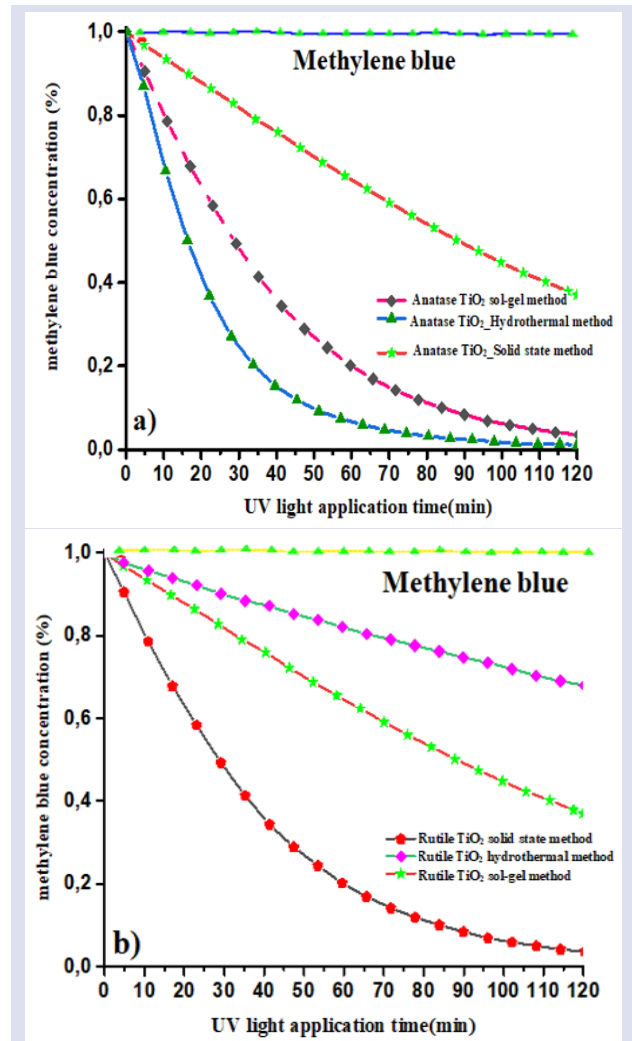


Figure.9. Degradation of methylene blue a) anatase and b) rutile TiO₂ synthesized via different methods

After adding the studied materials, a slight increase in the MB decay rate can easily be seen.

Due to the anatase structure of TiO₂, it is the most widely used semiconductor photocatalyst for the removal of organic pollutants by converting them into small molecules. Photocatalytic degradation rates of some organic pollutants are quite low. TiO₂ has a band gap of about 3.0-3.2 eV and can only be excited by light with a wavelength below 387 nm. This prevents the use of sunlight and visible light and therefore reduces the photocatalytic activity of TiO₂[34-38].

In our study, both the synthesis methods and the effects of rutile and anatase structures on the photocatalytic mechanism were investigated. Although many studies have compared rutile anatase in the literature, the synergistic effect of different synthesis methods on this mechanism has not been investigated.

When Table 1 is examined, the crystal size of the rutile phase synthesized by the hydrothermal method is small, the surface area is large and the particle size is much smaller than the other samples synthesized via sol-gel and

solid-state methods, this is an expected result because the best method used to obtain nano-sized homogeneously dispersed particles is the hydrothermal method. A different result from our expectation in the table is that the particle size of the materials obtained by the sol-gel method is larger than that obtained by the solid-state method, the possible reason for this may be the particle growth due to agglomeration during the synthesis.

Discussion and Conclusion

In this study, rutile and anatase phase TiO₂ were synthesized by different synthesis methods and the photocatalytic activities of all materials were investigated. The best result was obtained in the anatase phase synthesized by the hydrothermal method, and the lowest result was obtained in the rutile phase synthesized by the solid-state method. From the study outputs, it can be said that anatase material with a high surface area and a low crystal size is the best photocatalytic material.

Conflicts of Interest

The author declares no conflicts of interest.

Acknowledgment

The author would like to thank Nilgün Kayaci and Senem Sanduvac for their help .

References

- [1] Ebrahimi M., Zakery A., Karimipour M., Molaei M., Nonlinear optical properties and optical limiting measurements of graphene oxide - Ag@TiO₂ compounds, *Opt. Mater.*, 57 (2016) 146-152.
- [2] Le L., Xu J., Zhou Z., Wang H., Xiong R., Shi J., Effect of oxygen vacancies and Ag deposition on the magnetic properties of Ag/N co-doped TiO₂ single-crystal films, *Mater. Res. Bull.*, 102 (2018) 337-341.
- [3] An G., Ma W., Sun Z., Liu Z., Han B., Miao S., Miao Z., Ding K., Preparation of titania/carbon nanotube composites using supercritical ethanol and their photocatalytic activity for phenol degradation under visible light irradiation, *Carbon* 45(9) (2007) 1795-1801.
- [4] Wang T., Wei J., Shi H., Zhou M., Zhang Y., Chen Q., Zhang Z., *Physica E.*, 86 (2017) 103-110.
- [5] Liu H., Dong X., Wang X., Sun C., Li J., Zhu Z., A green and direct synthesis of graphene oxide encapsulated TiO₂ core/shell structures with enhanced photoactivity, *Chem. Eng. J.*, 230 (2013) 279-285.
- [6] Wang X., Li Y., Rare-Earth-Compound Nanowires, Nanotubes, and Fullerene-Like Nanoparticles: Synthesis, Characterization, and Properties., *Chem Eur J.*, 9 (22) (2003) 5627-5635.
- [7] Miao-Miao Y., Zhong-Lin C., Wen-Shou W., Liang Z., Ji-Min S., Template-free Hydrothermal Preparation of Mesoporous TiO₂ Microspheres on a Large Scale., *Chemistry Letters*, 37 (9) (2008) 938-939.
- [8] Wang W.S, Zhen L, Xu C.Y, Zhang B.Y, Shao W.Z., Room Temperature Synthesis of Hollow CdMoO₄ Microspheres by a Surfactant-Free Aqueous Solution Route., *J Phys Chem.*, 110 46 (2006) 23154–23158.
- [9] Zhang Q., Ge J.P., Goebel J., Hu Y.X., Lu Z.D., Yin Y., Rattle-type silica colloidal particles prepared by a surface-protected etching process., *Nano Res.*, 2 (2009) 583–591.
- [10] Fujishima A., Rao T.N., Tryk D.A., TiO₂ Photocatalysts and Diamond Electrodes, *Electrochimica Acta*, 45 (28) (2000) 4683-4690.
- [11] Zhao, J., Bowman L., Zhang X., Vallyathan V., Young S.H., Castranova V., ve Ding M., Titanium Dioxide (TiO₂) Nanoparticles Induce JB6 Cell Apoptosis Through Activation of the Caspase-8/Bid and Mitochondrial Pathways, *J.Toxicol. Environ. Health Part A.*, 72 (19) (2009) 1141-1149.
- [12] Liu X., Zhou K., Wang L., Wang B., Li Y., Oxygen Vacancy Clusters Promoting Reducibility and Activity of Ceria Nanorods, *J. Am. Chem. Soc.*, 131 (9) (2009) 3140-3141.
- [13] Zhao J., Bowman L., Zhang X., Vallyathan V., Young S.H., Castranova V., Ding M., Titanium Dioxide (TiO₂) Nanoparticles Induce JB6 Cell Apoptosis Through Activation of the Caspase-8/Bid and Mitochondrial Pathways, *J. Toxicol. Environ. Health Part A.*, 72 (19) (2009) 1141-1149.
- [14] Liu L., Zhao H., Andino J.M., Li Y., Photocatalytic CO₂ Reduction with H₂O on TiO₂ Nanocrystals: Comparison of Anatase, Rutile, and Brookite Polymorphs and Exploration of Surface Chemistry, *ACS Catalysis*, 2 (8) (2012) 1817-1828.
- [15] Cao S., Tao F.F., Tang Y., Li Y., Yu J., Size-and shape-dependent catalytic performances of oxidation and reduction reactions on nanocatalysts, *Chem. Soc. Rev.*, 45 (2016) 4747–4765.
- [16] Hwang, Y.J., Yang, S., Lee, H., Surface analysis of N-doped TiO₂ nanorods and their enhanced photocatalytic oxidation activity, *Appl. Catal. B Environ.*, 204 (2017) 209–215.
- [17] Tian, J., Zhao, Z., Kumar, A., Boughton, R.I., Liu, H., Recent progress in design, synthesis, and applications of one-dimensional TiO₂ nanostructured surface heterostructures: A review. *Chem. Soc. Rev.*, 43 (2014) 6920–6937.
- [18] Zhang Z., Wang C., Zakaria R., Ying J.Y., Role of Particle Size in Nanocrystalline TiO₂-Based Photocatalysts, *J. Phys. Chem.*, 102 (1998) 10871–10878.
- [19] Ohtani B., Kakimoto M., Nishimoto S., Kagiya T., Photocatalytic Reaction of Neat Alcohols by Metal-Loaded Titanium(IV) Oxide Particles, *J. Photochem. Photobiol.*, A, 70 (3) (1993) 265–72.
- [20] Wang R., Hashimoto K., Fujishima A., Chikuni M., Kojima E., Kitamura A., Shimohigoshi M., Watanabe T., Photogeneration of Highly Amphiphilic TiO₂ Surfaces, *Adv. Mater.*, 10 (2) (1998) 135–38.
- [21] Shklover V., Nazeeruddin M.K., Zakeeruddin S.M., Barbe C., Kay A., Haibach T., Steurer W., Hermann R., Nissen H.U., Gratzel M., Structure of Nanocrystalline TiO₂ powders and Precursor to Their Highly Efficient Photosensitizer, *Chem. Mater.*, 9 (1997) 430–39.
- [22] Paratsinis S.E., Bai H., Biswas P., Kinetics of Titanium(IV) Chloride Oxidation, *J. Am. Ceram. Soc.*, 73 (7) (1990) 2158–63.
- [23] Dokan F.K, Kuru M., A new approach to optimize the synthesis parameters of TiO₂ microsphere and development of photocatalytic performance, *J. Mater. Sci.: Mater. Electron*, 32 (2021) 640–65.

- [24] Yu J., Yu J.C., M. Leung K.P., Ho W., Cheng B., Zhao X., Zhao J., Effects of acidic and basic hydrolysis catalysts on the photocatalytic activity and microstructures of bimodal mesoporous titania, *J. Catal.*, 217 (2003) 69.
- [25] Kong M., Li Y., Chen X., Tian T., Fang P., Zheng F., Zhao X., Tuning the relative concentration ratio of bulk defects to surface defects in TiO₂ nanocrystals leads to high photocatalytic efficiency, *J. Am. Chem. Soc.*, 133 (2011) 16414–16417.
- [26] Sun Q., Xu Y., Evaluating Intrinsic Photocatalytic Activities of Anatase and Rutile TiO₂ for Organic Degradation in Water, *J. Phys. Chem. C*, 114 (2010) 18911–18918.
- [27] Kavan L., Gratzel M., Gilbert S. E., Klemenz C., Scheel H.J., Electrochemical and Photoelectrochemical Investigation of Single-Crystal Anatase., *J. Am. Chem. Soc.*, 118 (1996) 6716–6723.
- [28] Batzill M., Fundamental aspects of surface engineering of transition metal oxide photocatalysts, *Energy Environ. Sci.*, 4 (2011) 3275.
- [29] Fujishima A., Zhang X., Tryk D., TiO₂ photocatalysis and related surface phenomena, *Surf. Sci. Rep.*, 63 (2008) 515–582.
- [30] Yamakata A., Ishibashi T., Onishi H., Time-resolved infrared absorption study of nine TiO₂ photocatalysts., *Chem. Phys.*, 339 (2007) 133–137.
- [31] Xu M., Gao Y., Moreno E.M., Kunst M., Muhler M., Wang Y., Idriss H., Wöll C., Photocatalytic Activity of Bulk TiO₂ Anatase and Rutile Single Crystals Using Infrared Absorption Spectroscopy, *Phys. Rev. Lett.*, 106 (2011) 138302.
- [32] Luttrell T., Halpegamage S., Tao J., Kramer A. Kramer, Sutter E., Batzill M., Why is anatase a better photocatalyst than rutile? - Model studies on epitaxial TiO₂ films, *Sci. Rep.*, 4 (2014) 4043.
- [33] Sanjinés R., Tang H., Berger H., Gozzo F., Margaritondo G., Lévy F., Electronic structure of anatase TiO₂ oxide, *J. Appl. Phys.*, 75 (1994) 2042.
- [34] Kočí K., Obalová L., Matějová L., Plachá D., Lacný Z., Jirkovský J., Šolcová O., Effect of TiO₂ particle size on the photocatalytic reduction of CO₂, *Appl. Catal. B Environ.*, 89 (2009) 494–502.
- [35] Qi K., Cheng B., Yu J., Ho W., Review on the improvement of the photocatalytic and antibacterial activities of ZnO, *J. Alloys Compd.*, 727 (2017) 792–820.
- [36] Mamaghani A.H., Haghghat F., Lee C.-S., Hydrothermal/solvothermal synthesis and treatment of TiO₂ for photocatalytic degradation of air pollutants: Preparation, characterization, properties, and performance, *Chemosphere*, 219 (2019) 804–825.
- [37] Huang C.Y., Guo R.T., Pan W.G., Tang J.Y., Zhou W.G., Liu X.Y., Qin H., Jia P.Y., One-dimension TiO₂ nanostructures with enhanced activity for CO₂ photocatalytic reduction, *Appl. Surf. Sci.*, 464 (2019) 534–543.
- [38] Liu N., Chen X., Zhang J., Schwank J.W., A review on TiO₂-based nanotubes synthesized via hydrothermal method: Formation mechanism, structure modification, and photocatalytic applications, *Catal. Today*, 225 (2014) 34–51.

Green Synthesis of Gold Nanoparticles Using Aqueous Extract of *Asphodelus Aestivus*, Coating with Chitosan Biopolymer and Cytotoxicity Studies

Ersen Yılmaz^{1,a,*}, Mehmet Ateş^{2,b}, Muhammed Erbay^{3,c}

¹ Tunceli Vocational School, Munzur University, Tunceli, Türkiye

² Rare Earth Elements Application Center, Munzur University, Tunceli, Türkiye

³ Tunceli State Hospital Laboratory, Tunceli, Türkiye

*Corresponding author

Research Article

History

Received: 23/02/2022

Accepted: 09/06/2022

Copyright



©2022 Faculty of Science,
Sivas Cumhuriyet University

ABSTRACT

The green synthesis of gold nanoparticles (Au-NPs) was carried out by pouring the aqueous extract of East Anatolian origin *Asphodelus aestivus* plant onto aqueous gold metal ions and reducing them via single-step one-pot method. The absorption peak of the synthesized nanoparticles gave a maximum at 575 nm. All the X-ray diffraction peaks at $2\theta = 38.25, 44.46, 64.64$ and 77.20 that index to (111), (200), (220), and (311) planes verify the successful synthesis of Au-NPs. Mostly spherical shape particles showed a homogeneous distribution with size range 20 ± 5 nm are measured using TEM. From the FTIR spectrum, the peaks are seems to be related to phenolic compounds, flavonoids, benzophenones, terpenoids and anthocyanins which assume that they could act as the reducing agents. The plant extraction, one-pot, single-step method used is environmentally safe without the role of synthetic materials which is highly potential in mild and green synthesis applications. The Au-NPs were coated with chitosan biopolymer in aquatic solution medium and verified by SEM. Then, cytotoxic investigations of the biosynthesized Au-NPs were carried out by HUVEC cells. Au-NPs were showed toxic effects on cell culture, even if in a small amount. However, chitosan biopolymer coating increased cell viability.

Keywords: Gold nanoparticle, Biosynthesis, *Asphodelus aestivus*, Biopolymer coating, Cytotoxicity

^a chemer80@gmail.com

^b <https://orcid.org/0000-0002-8567-1668>

^b atesnrg@gmail.com

^c <https://orcid.org/0000-0002-2764-6579>

^c muhammed.erbay23@gmail.com ^d <https://orcid.org/0000-0003-2335-1009>

Introduction

Nanotechnology is a technology that deals with nano-scale materials and applications. It deals with mostly metals, semi-metals and noble metals ranging from 1 to 100 nm [1]. Among these materials, noble-metal nanoparticles have attracted more attention due to their catalytic, optical and opto-electronic properties [2]. Gold nanoparticles have been studied and continue to be investigated especially for their effective properties in medical imaging [3] and drug delivery [4]. The unique optical property of Au-NPs make them very useful in bioimaging by acting as marking agent [5].

It is important to improve the synthesis conditions of such important nanomaterials, to obtain them under conditions that do not contain harmful chemicals, and also to define their physical and chemical properties well. Using naturally derived products such enzyme [6], fungus [7], algae [8] and plant [9] as reducing agents serves this purpose [10]. Plant-mediated synthesis is quick and easy, allowing for size control, and most importantly, allowing chemical reduction in mild conditions, making it stand out from other chemical methods. However, the use of different parts of the plant such as root, stem and leaf makes this method powerful [11].

Fenugreek or *Asphodelus aestivus* is the common name of the plant species that form the *Asphodelus* genus from the *Asphodelaceae* family. While its green leaves are just emerging from the soil in March and April, the grass

harvested from the mountains is sold as a vegetable and consumed in large quantities. Using this plant, pastry, soup, stew and rice are made. It has a unique fragrance. *Asphodelus aestivus* is native to the Mediterranean region, northern Africa, and the Middle East [12]. It is a plant that often grows in mountainous regions in the east of Anatolia. Its taste is between spinach and leek and it is almost impossible to distinguish it from spinach after cooking. It is called "natural antibiotic" among local people. Biochemicals such as phenolic acid, flavonoids, alkaloids, and terpenoids that are existed in plant crude extract are play role in the reduction of nanoparticles [13]. The phenolic compounds possess anti-tumor, anti-allergic, and antiviral properties are high potential antioxidants and these kind of compounds are believed to take part in synthesis reactions of different types of gold nanoparticles. Also, different type of flavonoids, benzophenones, [14] and anthocyanins that exist in the plant could be closely related in the reduction synthesis of nanoparticles [15].

Polymer coatings are being useful in various applications. From regular coatings to nanoparticle incorporated coatings, these polymer coatings ensure a strong functionalities to the selected host materials. It is applicable to wide range of materials from metals, ceramics, polymers to nanoparticles [16]. Some studies revealed that surface modified nanoparticles with

biopolymers like PEG, Chitosan could temporarily avoid the mononuclear phagocyte system and substantially extend the circulation time of the nanoparticles [17]. In addition, the key feature in the preparation of nanoparticles is to prevent agglomeration by using coating agents like carbohydrate based polymers, e.g. dextran, chitosan (CS), starch [18]. Recently, surface optimization of nanoparticles has become a challenge for the researchers.

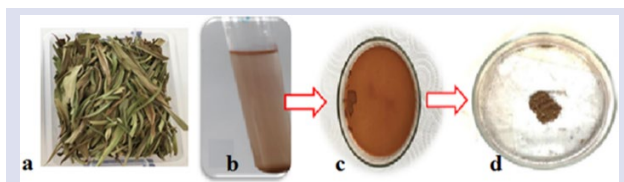


Figure 1. Summary photos of Au-NPs biosynthesis where (a) is dried *Asphodelus aestivus* stem and leaves, (b) aqueous HAuCl₄ and plant extract mixture, (c) Au-NPs left to dry in a petri dish, (d) Au-NPs scraped and collected

In the literature review, we found that Au-NP biosynthesis with the *Asphodelus aestivus* plant had not been previously performed or reported. Here, we performed the biosynthesis and characterization of Au-NPs by using aqueous gold solution and aqueous extract of *Asphodelus aestivus* plant extract (See Fig1.). Then, the synthesized Au-NPs were coated with chitosan biopolymer and cytotoxicity experiments were done.

Materials and Methods

Chemicals

Asphodelus aestivus were collected from the mountainous regions of Tunceli/Turkey. Analytical grade (HAuCl₄, 99.98%) was purchased from Sigma-Aldrich, USA, and used as gold precursor. Ethanol, conc. HCl, Acetone, medium mol weight Chitosan, F-12 nutrient mix, Trypsin-EDTA solution, Fetal Bovine Serum, Phosphate buffered saline (PBS), 3-[4,5-Dimethylthiazol-2-yl] -2,5-diphenyltetrazolium bromide (MTT) salt, Trypan Blue and Nitric Acid (HNO₃) was purchased from Sigma-Aldrich, USA. All reagents used were of analytical grade. All glassware used was cleaned and washed with distilled water and dried before used.

Preparation of *Asphodelus aestivus* Extract

The fresh plant was washed with mains water to remove dirt and washed again with distilled water before being dried in oven (Nuve Laboratory Oven) at 35°C. All the dried plant (stem and leaves) were ground into fine powder using an electric blender (Sinbo) and stored at room temperature for further use. The extract was prepared by taking 0.2 g of the fine powder and added to 100 mL of distilled boiling water. When the temperature cooled to 70 °C in about 10 minutes, the crude extract was filtered with Whatman filter paper No 1.

Synthesis of Au-NPs

In a Erlenmeyer flask, 10 mL of the filtered extract was reacted with 5 mL, 5 miliMolar of tetrachloroaurate at 25 °C and gently shaken. The time taken for the color change after the reaction and the pH were recorded. The reaction solution changes quickly from pale brown to pale purple. This color change indicated the formation of [Au / *Asphodelus aestivus*]. This Au-NPs nanoparticle emulsion synthesized was kept at 5 °C.

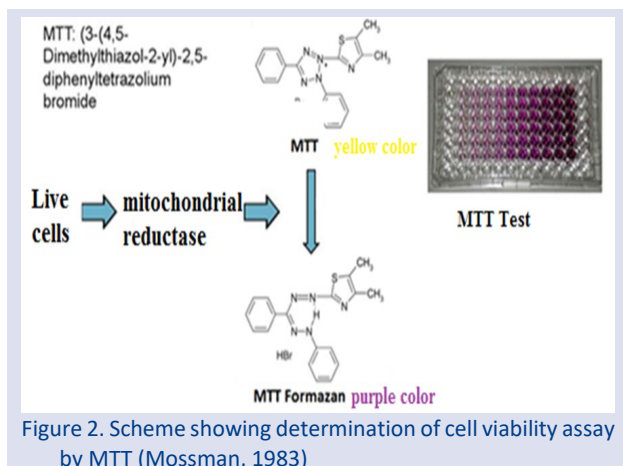
Characterization of Au-NPs

The formation of Au-NPs was confirmed by using UV-vis spectroscopy at intervals in the range of 200 to 600 nm and 2 nm resolution (Optima SP-3000 UV-VIS Spectrometer). It was diluted with distilled water before measurement and pure water was used as control solution [24]. All data obtained were converted into graphs using Origin Pro 9.1 SRO software (OriginLab Corp, Northampton, MA, USA). The nanoparticle emulsion was centrifuged for enrichment/concentration and the concentrated emulsion formed was poured into a petri dish. The petri dish was oven dried at 40 °C for one day. The obtained dry sample was collected and analyzed for its crystal structure and composition using X-ray spectroscopy. The XRD spectrum was recorded using the device operating at 40 kV and a current of 15 mA with Cu-Kα1 radiation. The device was operated in the range of 2θ 20-80° with 2/minute (Rigaku MiniFlex 600). The size and shape of the Au-NPs in the study were characterized by using the JOEL-1011 TEM instrument, which provides 0.2 nm resolution with 50-10⁶ magnification under voltage accelerating from 40-100 kV. The stability of Au-NPs was measured using Zetasizer Malvern Nano ZS and Dynamic Light Scattering (DLS). FT-IR spectra of Ag-NPs were recorded using JASCO-6700 spectrophotometer in the range 4000-400 cm⁻¹ wavelength with 16 scans and 4 cm⁻¹ resolution.

MTT Assay for Cell Viability

The MTT test, which is used for cell viability testing, is easy to use, has high reliability, reproducibility, and is widely used to determine both cell viability and cytotoxicity tests. The main basis of this technique is experiments involving the use of tetrazolium salts and measuring the color change. In our study, in the MTT cell viability test, Mossman method [19] was followed with some modifications. HUVEC cells were seeded at a density of 5 x 10³ cells /hole in a 96-hole plate (Figure 2). After 4 hours of incubation, 5% FBS or 10% FBS containing Au-NPs at concentrations ranging from 6.25 µg / mL to 100 µg / mL were replaced with DMEM and the cells were incubated at 37 °C for 24 and 48 hours. At the end of the exposure period, the toxicity of Au-NPs was evaluated by a standard colorimetric cellular viability assay using MTT dye. Cytotoxicity analyzes were made as a service purchase from Hacettepe University Advanced Technologies Application and Research Center. Within the scope of this experimental research, ISO 10993 tests and cytotoxicity tests of Au-NPs with standard L929 cell line

were performed for biological evaluation. In the analyzes, absorbance measurements at 570 nm were evaluated using a SpectraMax microplate reader (Molecular Devices, Sunnyvale, CA).



Use of Chitosan Biopolymer for Coating

The method we used in a previous study was followed for the coating of Au-NPs with chitosan [1]. 1.00 g of 75-85% deacetylated chitosan with medium MW (200-500 kDa) was dissolved in 50 mL of 0.5% (v / v) acetic acid containing solution. 40 mg of Au-NP nanoparticle suspended in 25 mL of ethyl alcohol was added to this solution. This mixture was stirred with a magnetic stirrer for 24 hours at high intensity and centrifuged at 15000 rpm for 20 minutes. The pellet was washed with ethanol and the product was dried. In this study, the effect of coating with chitosan on the stability and cytotoxicity of Au-NPs were analyzed.

Statistical Analysis

In statistical evaluation, One-Way ANOVA-Dunnet test was applied in SPSS 15.0 computer program and values below $P < 0.05$ were considered significant. In addition, regression analysis was performed using the SPSS 15.0 program in order to reveal the dose-effect relationship in this study.

Results and Discussion

Asphodelus aestivus extract (0.02 g, 10 mL) acts as both the reducing and stabilizing agent and Chloroauric acid (5 mM) acts as the gold precursor. The reduction of Chloroauric acid was indicated by the colour changes of Asphodelus aestivus extract as shown in Figure 1. The reaction was rapid as the pale greenish colour of the Asphodelus aestivus extract turns into pale purple colour within 5 minutes indicating formation of Au-NPs.

The possible chemical reduction reaction is,

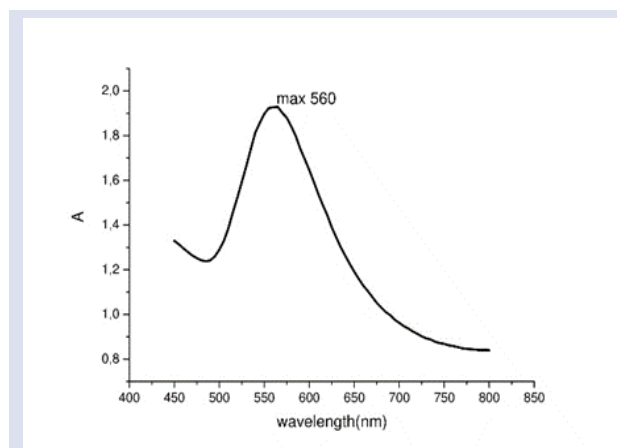


Figure 3. UV-vis absorbance bands for Au-NPs forms using A. aestivus extract

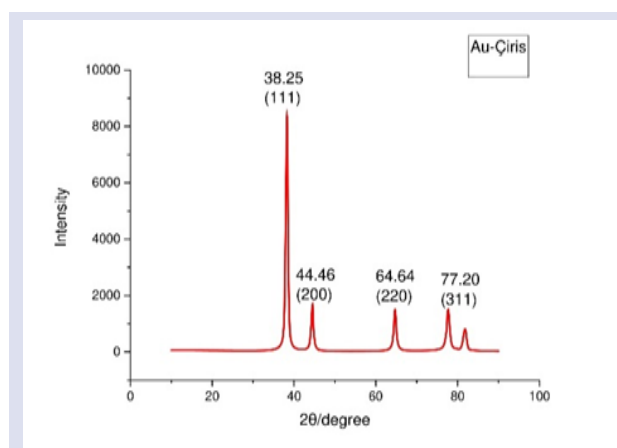


Figure 4. XRD spectra for Au-NPs forms using A. aestivus extract

UV-Visible Spectroscopy Study

The formation of Au-NPs was confirmed by the UV-vis spectra in Figure 3. After the addition of HAuCl_4 solution, a sharp peak occurs in the 555-565 nm range. This peak is confirmed by other characterizations that show the formation of Au-NPs.

X-Ray Diffraction Analysis

The sharp peaks in the powder X-ray diffraction pattern in Figure 3 show that the synthesized Au-NPs are in crystalline form. All 4 distinct peaks correspond to the standard Bragg reflections (111), (200), (220) and (311) of the surface center cubic (fcc) lattice. The particle size of Au-NPs can be calculated with little error using the Debye-Scherrer equation.

$$d = \frac{k\lambda}{(\beta \cos \theta)} \quad (2)$$

where d is the average crystallite size, k Scherrer constant (0.9), λ X-ray wavelength (0.154 nm), β the expanding line in radians and θ Bragg angle [18,22]. Using the Debye-Scherrer equation, the average crystallite size of synthesized Au-NPs is calculated as 12 nm. This calculated value is also supported by TEM findings.

Transmission Electron Microscopy (TEM) Study

In order to determine the size of AgNPs obtained by the biosynthesis method in the laboratory environment, the average particle size and clustering were determined by Transmission Electron Microscope (TEM) analysis. According to the TEM images of the NPs obtained, it can be said that the particles are formed in nano-size (<100 nm). According to the TEM analysis results, it has confirmed that the morphology of Au-NPs is basically global. This finding is also consistent with the sharp shape of the UV-Vis peak. When Au-NPs are examined in terms of size distributions, these particles are in a spherical shape, and the size ranges were found to show a homogeneous distribution in the 5-15 nm range (Figure 5). This result also supports the results calculated from XRD analysis.

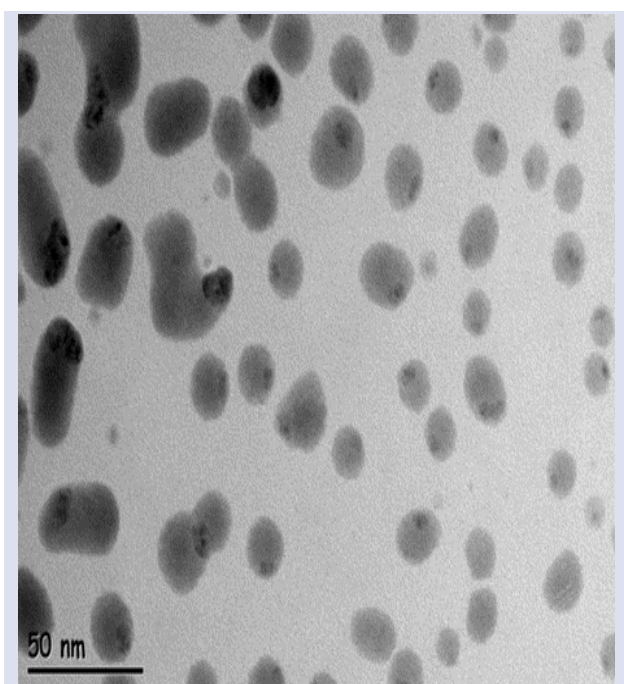


Figure 5. TEM image of Au-NPs forms using *A. aestivus* extract

Zeta Potential Study

The stability of the synthesized Au-NPs was measured using zeta potential analysis. The value of the zeta potential provides information about the particle stability. As the zeta potential increases, the particles are prevented from coming together to form aggregates due to a greater electrostatic repulsion between the particles and the stability in the colloidal suspension increases. The behavior of particles in polar liquids is determined by the zeta potential values, not by the electrical charge on their surface.

The zeta potential results of the nanoscale Au particles we synthesized in our research are given in Figure 6. Au-NPs obtained from *A. aestivus* extract were measured as -24.1 mV and are moderately stable.

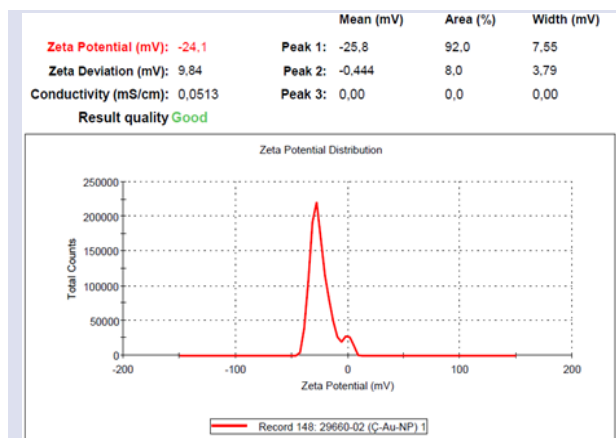


Figure 6. Zeta potential image of Au-NPs form by using *A. aestivus* extract

Dynamic Light Scattering (DLS) Study

In order to understand whether the nanoscale materials in the liquid medium are physically stable or not, the distribution of the particles is examined. Particle size and particle distributions can be obtained in dynamic light scattering (DLS) analysis. In this method, the most important parameter is the Pdl (Poly dispersity index) value. If the Pdl value is between 0.1 and 0.25, it can be said that the desired narrow distribution has been achieved.

Pdl values of AuNPs obtained from *A. aestivus* extract were obtained as 0.386. When the data obtained in this context are evaluated; Since the Pdl value of the Au-NPs obtained by the biosynthesis method is between 0.25 and 0.5, the particles are in narrow and wide distribution range. When the DLS values are read on Figure 7, it is seen that the AuNPs obtained from the *A. aestivus* plant are formed in the range of 130-135 nm at 2 % and between 6-15 nm at 98 %.

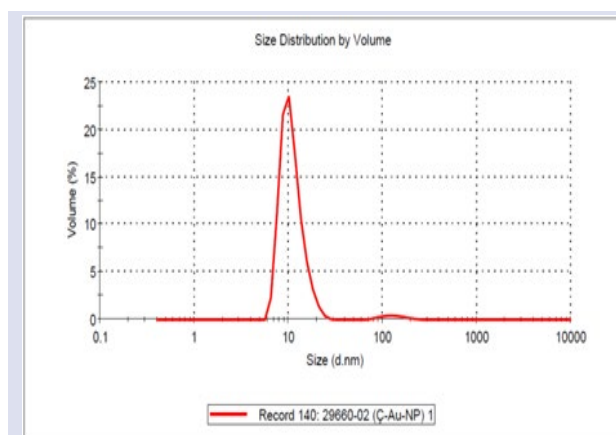


Figure 7. DLS image of Au-NPs form by using *A. aestivus* extract

Scanning Electron Microscopy (SEM) Study

After conducting TEM, DLS, Zeta Potential analyzes of the synthesized Au-NPs, the particles in liquid form were dried and turned into powder form for SEM, XRD and FT-IR analyzes. Scanning Electron Microscope (SEM) images

of AuNPs obtained from *A. aestivus* extract are given in Figure 8.

Powdered metal-based nano-sized particles generally tend to show aggregation [1]. A clustering is clearly seen in SEM images obtained at different magnifications of AuNPs obtained by the biosynthesis method.

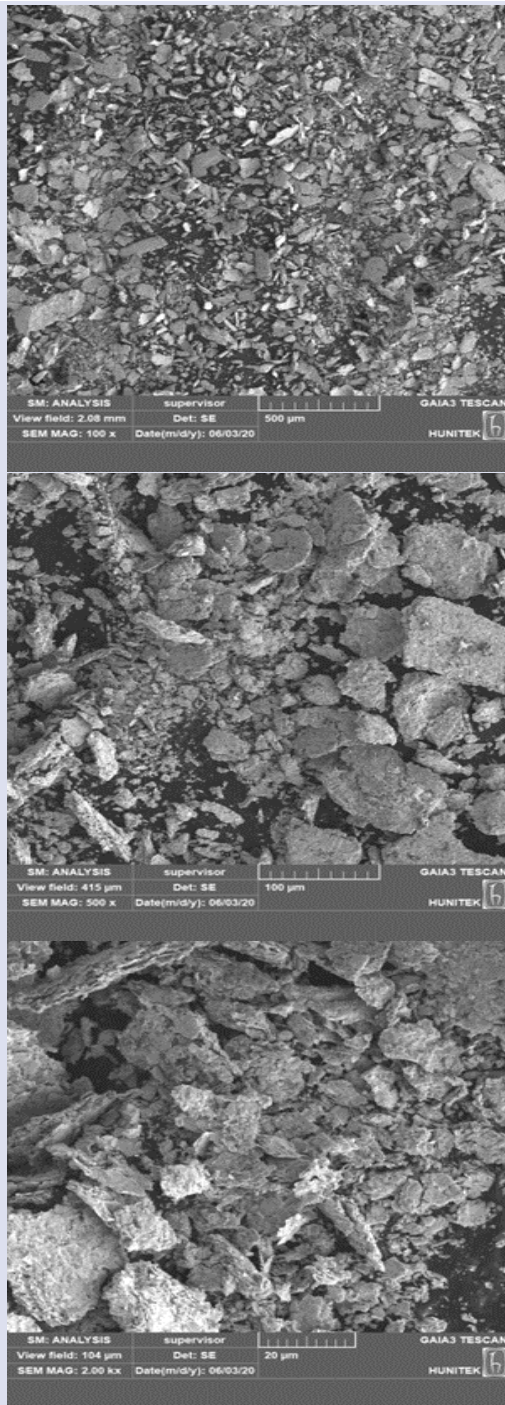


Figure 8. SEM images of the Au-NPs at three different (100x, 500x, 2kx) magnifications

Fourier Transform Infrared Spectroscopy Study

FTIR spectroscopy was performed to identify potential functional groups that allow the reduction of gold nanoparticles. Figure 9 shows the spectra from Au-NPs synthesized using the *A. aestivus* extract.

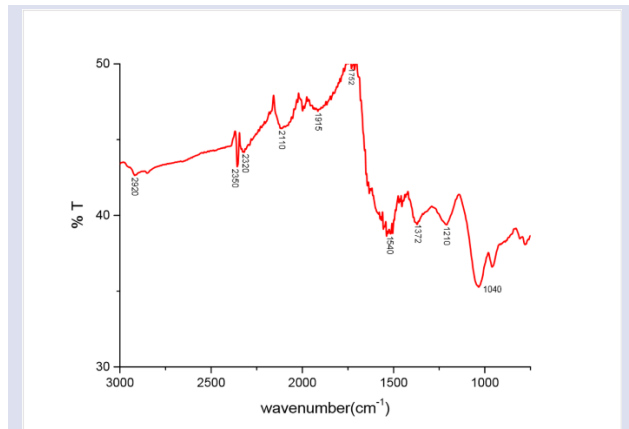


Figure 9. FT-IR graph of Au-NPs form by using *A. aestivus* extract

At the region of 2920 cm⁻¹ the presence of C-H bond in xanthone [20] and other compounds in the plant extract is significant. Peak at 1752 cm⁻¹ shows the C=O stretchings. Peaks between 1500 and 1600 cm⁻¹ are C-C aromatic bond peaks indicating the presence of aromatic components in the extract. Peaks seen in the region between 1400-1500 cm⁻¹ are related to the aromatic backbone in the extract. Peaks between 1300-1000 cm⁻¹ were attributed to C-O-C stretch. When all the IR findings are evaluated together, it can be said that aromatic compounds such as xanthenes, flavonoids, benzophenones are involved in the reduction and stabilization of gold nanoparticles.

Chitosan Capping Study

The zeta potential plot of nanoparticles obtained via biosynthesis is given in Figure 10.

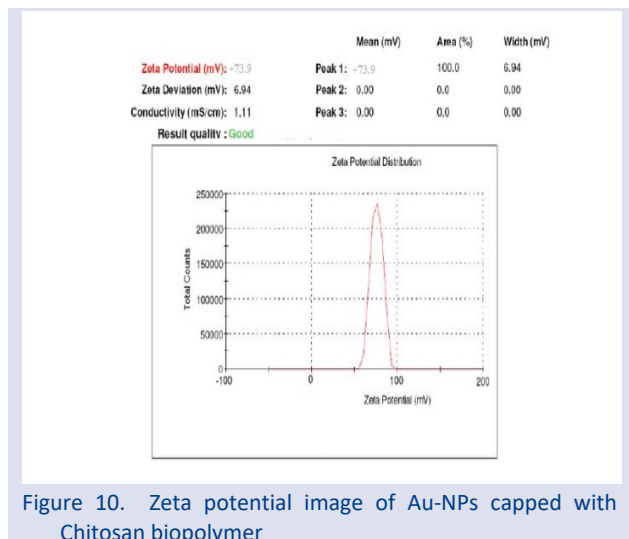


Figure 10. Zeta potential image of Au-NPs capped with Chitosan biopolymer

After biopolymer capping, the surface properties of the biosynthesized gold nanoparticles and the associated zeta potential have been changed from negative to positive and increased in absolute value. In the light of these data, it can be said that the stability of nanoparticles increased after chitosan capping.

In the SEM image given in Figure 11 below, the biosynthesized gold nanoparticles coated with chitosan

are seen. As with the synthesized uncoated powder particles, it can be said that polymer coated Gold nanoparticles also tend to form clusters.

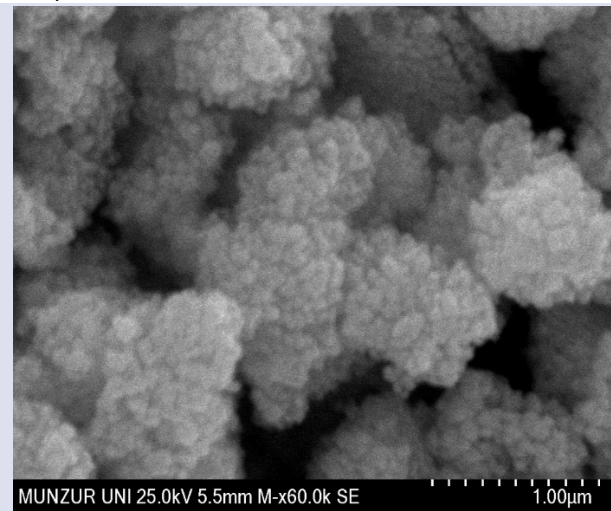


Figure 11. SEM image (60k.x) of the biosynthesized Au-NPs coated with Chitosan biopolymer

Cytotoxicity Study

HUVEC cells have been accepted as a general model for toxicity determination of NPs [21]. Because these tests are important methods for colorimetric cell viability experiments especially in the study of eukaryotic cell activity and they are widely used in cell proliferation and cytotoxicity analyzes. In this context in the study, the in-vitro cytotoxicity of AuNPs and their polymer coated derivatives obtained from *A. aestivus* plants was evaluated using the MTT test on HUVEC cells for 24 and 48 hours. First, HUVEC cells were incubated depending on the dose ($\mu\text{g} / \text{ml}$) of AuNPs and the polymer coated forms. Results were evaluated as % viability \pm confidence interval. The obtained results were given in the form of a table with percentage (%) against concentration of live cells (Figure 12 and 13).

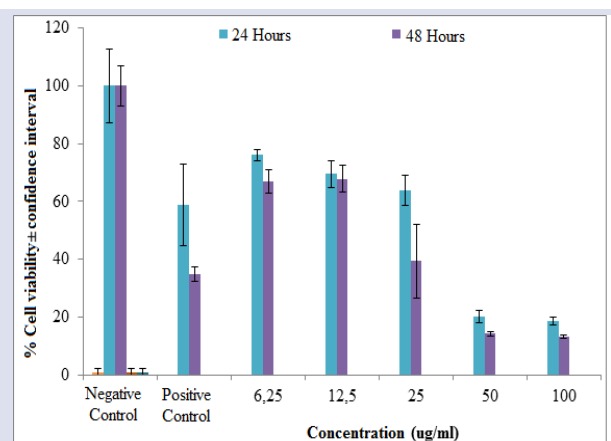


Figure 12. HUVEC viability in the presence of Au-NPs assessed by MTT assay [(% viability \pm confidence interval (95%, absolute))]

Percentage viability values of both plant extract and biopolymer-coated AuNPs on the HUVEC cell decreased due to the increase in both time and concentration.

However, by coating Au-NPs with Chitosan, cell viability appears to be higher than the uncoated forms in terms of both time and concentration.

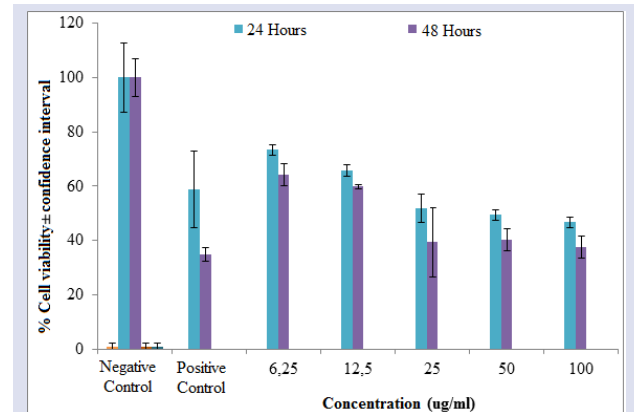


Figure 13. HUVEC viability in the presence of Chitosan coated Au-NPs assessed by MTT assay [(% viability \pm confidence interval (95%, absolute))]

This is an expected result for a coating made with a biocompatible polymer. Cell viability increased significantly with chitosan coating, especially at high concentrations.

Conclusion

In this study, an economical, green, sustainable, rapid, mild and efficient method for synthesis of Au-NPs using *A. aestivus* extract has been demonstrated. At the same time, coating with Chitosan biopolymer was done by similar methods. Based on UV-visible spectrum, DLS and TEM analysis results, Au NPs of a small size were produced. While $\pm 30\text{mV}$ zeta value is required for a suspension to be physically stable [23], the measured -24mV value of the synthesized Au-NPs can be said to be stable. It is understood that the groups determined by FT-IR are favorable reducing and stabilizing agents. The synthesized nanoparticles were further stabilized by coating with chitosan biopolymer. The two types of nanoparticles synthesized showed little cytotoxic effect. Coating with chitosan reduced cytotoxicity, especially at high particle doses. It was determined that the coating with Chitosan increased the stability and decreased cytotoxicity. Of these particles synthesized and identified it is expected to have extensive other applications.

Acknowledgment

This master thesis research project was supported by the grant funded by the Munzur University Scientific Research Projects Coordination Unit (MUNIBAP Reference Grant no. YLMUB019-03).

Conflicts of interest

The authors state that did not have conflict of interests

References

- [1] Yılmaz E., Ates M., Sahilli Y.Ç., Synthesizing, chitosan coating and detecting the nanotoxic effect of the lead selenide (PbSe) quantum dots, *Digest Journal of Nanomaterials and Biostructures*, 13(4) (2018) 1173-1182.
- [2] Rao K.J., Paria S., Aegle marmelos Leaf Extract and Plant Surfactants Mediated Green Synthesis of Au and Ag Nanoparticles by Optimizing Process Parameters Using Taguchi Method, *ACS Sustainable Chemistry and Engineering*, 3(3) (2015) 483-491.
- [3] Wu Y., Ali M.R.K., Chen K., Fang N., El-Sayed M.A., Gold nanoparticles in biological optical imaging, *Nano Today*, 24 (2019) 120-140.
- [4] Male D., Gromnicova R., McQuaid C., In: Al-Jamal K.T. (Eds). Gold Nanoparticles for Imaging and Drug Transport to the CNS, *International Review of Neurobiology*. Massachusetts: Academic Press (130) (2016) 155-198.
- [5] Yong K.T., Swihart M.T., Ding H., Prasad P.N., Preparation of Gold Nanoparticles and their Applications in Anisotropic Nanoparticle Synthesis and Bioimaging, *Plasmonics*, 4(2) (2009) 79-93.
- [6] Sanket S., Das S.K., Role of Enzymes in Synthesis of Nanoparticles. In: Thatoi H., Mohapatra S., Das S.K. (Eds). Bioprospecting of Enzymes in Industry, Healthcare and Sustainable Environment. Berlin: Springer, (2021) 139-153.
- [7] Guilger-Casagrande M., de Lima R., Synthesis of Silver Nanoparticles Mediated by Fungi: A Review, *Frontiers in bioengineering and biotechnology*, 7 (2019) Article: 287.
- [8] Khanna P., Kaur A., Goyal D., Algae-based metallic nanoparticles: Synthesis, characterization and applications, *Journal of Microbiological Methods*, 163 (2019) 105656.
- [9] Kumar, S.V., Rajeshkumar, S., Plant-Based Synthesis of Nanoparticles and Their Impact. In: Tripathi D.G., Ahmad P., Sharma S., Chauhan D.K., Dubey N.K., (Eds). *Nanomaterials in Plants, Algae, and Microorganisms*. Massachusetts: Academic Press, 1 (2018) 33-57.
- [10] Mittal A.K., Chisti Y., Banerjee U.C., Synthesis of Metallic Nanoparticles Using Plant Extracts, *Biotechnology Advances*, 31/2 (2013) 346-356.
- [11] Lee K.X., Shameli K., Miyake M., Kuwano N., Khairudin N.B.A., Mohamad S.E.B., Yew Y.P., Green synthesis of gold nanoparticles using aqueous extract of *Garcinia mangostana* fruit peels, *Journal of Nanomaterials*, (2016) Article ID 8489094.
- [12] Davis P.H., *Flora of Turkey and the East Aegean Islands*. Edinburgh: Edinburgh University Press, 8 (1984) 543-544.
- [13] Chung IM., Park I., Seung-Hyun K., Thiruvengadam M., Rajakumar G., Plant-Mediated Synthesis of Silver Nanoparticles: Their Characteristic Properties and Therapeutic Applications, *Nanoscale Research Letter*, 11 (2016) Article 40.
- [14] Shakeel A., Annu S.I., Salprima Y.S., Biosynthesis of gold nanoparticles: A green approach, *Journal of Photochemistry and Photobiology B: Biology*, 161 (2016) 141-153.
- [15] Singh P., Kim Y.-J., Zhang D., Yang D.-C., Biological Synthesis of Nanoparticles from Plants and Microorganisms, *Trends in Biotechnology*, 34 (7) (2016) 588-599.
- [16] Nathanael A.J., Oh T.H. Biopolymer Coatings for Biomedical Applications, *Polymers*, 12(12) (2020) 3061.
- [17] Wang Y., Dave R. N., Pfeffer R., Polymer coating/encapsulation of nanoparticles using a supercritical anti-solvent process, *The Journal of Supercritical Fluids*, 28(1) (2004) 85-99.
- [18] Neuberger T., Schopf B., Hofmann H., Hofmann M., von Rechenberga B., Superparamagnetic Nanoparticles for Biomedical Applications: Possibilities and Limitations of a New Drug Delivery System, *Journal of Magnetism and Magnetic Materials*, 293 (2005) 483-496.
- [19] Mossman T., Rapid colorimetric assay for cellular growth and survival: application to proliferation and cytotoxicity assays, *Journal of Immunological Methods*, 65 (1983) 55-63.
- [20] Shameli K., Ahmad M.B., Shabanzadeh P., Effect of curcuma longa tuber powder extract on size of silver nanoparticles prepared by green method. *Research on Chemical Intermediates*, 40 (2014) 1313-1325.
- [21] Cao Y., Gong Y., Liu L., The use of human umbilical vein endothelial cells (HUVECs) as an in vitro model to assess the toxicity of nanoparticles to endothelium: a review, *Journal of Applied Toxicology*, 37(12) (2017) 1359-1369.
- [22] Mahdavi M., Namvar F., Ahmad M.B., Mohamad R., Green biosynthesis and characterization of magnetic iron oxide (Fe₃O₄) nanoparticles using seaweed (*Sargassum muticum*) aqueous extract, *Molecules (Basel, Switzerland)*, 18(5) (2013) 5954-5964.
- [23] Faried M., Shameli K., Miyake M., Hajalilou A., Synthesis of silver nanoparticles via green method using ultrasound irradiation in seaweed *Kappaphycus alvarezii* media, *Research on Chemical Intermediates*, 42 (2016) 7991-8004.
- [24] Sharma R.K., Tahiliani S., Jain N., Priyadarshi R., Chhangani S., Purohit S.D., Joshi P., *Cynodon dactylon* Leaf Extract Assisted Green Synthesis of Silver Nanoparticles and Their Anti-Microbial Activity, *Advanced Science, Engineering and Medicine*, 5(8) (2013) 858-863.

Serum Vitamin D Among Patients with Type 2 Diabetes Mellitus

ShwanSulaiman Ahmed ^{1,a}, Aysel Sari ^{2,b,*}

¹ Department of Biochemistry, Faculty of Science, Firat University, Elazığ, Türkiye

² Department of Biochemistry, Faculty of Science, Firat University, Elazığ, Türkiye

*Corresponding author

Research Article

History

Received: 25/03/2022

Accepted: 02/07/2022

Copyright



©2022 Faculty of Science,
Sivas Cumhuriyet University

ABSTRACT

Vitamin D supplements are a beneficial health issue to benefit from insulin therapy. In those with T2DM, serum vit-D was checked and resuscitated. Serum vit-D was evaluated with its rich content. Serum vit D levels were statistically significantly lower in T2DM patients than in the control group. It was found to be significant in terms of the relationship between fasting blood sugar and vit-D and HbA1C. Vit-D in sugar will be used as a benefit from vit-D in patients with blood T2DM patients. The mean±SD vit-D level was 19.22±9.23 for the whole population with a fasting blood glucose level of 110 mg/dl or less, and 12.21±6.15 for people with a fasting blood glucose level above 130 mg/dl, and p<0.001. The relationship between vit-D level and fasting blood sugar is statistically significant with negative pearson correlation coefficient. Vit-D mean±SD 20.46±8.56 for the entire population with an HbA1C level equal to or lower than 6.5%, and 12.84±6% for individuals with a fasting blood glucose level above 6.5%, is 26 and p<0.001. The strong relationship between vit-D and fasting blood glucose and HbA1C is due to the fact that vit-D tends to specifically stimulate insulin production in β-pancreatic cells via the nuclear vit-D receptor (VDR) and that vit-D minimizes inflammation. Vit-D supplements are a beneficial health challenge to benefit from insulin therapy. Serum vit-D was checked in patients with T2DM. The serum has been evaluated with its rich content of vit-D. Serum vit-D levels were statistically significantly lower in T2DM patients compared to the control group. It was found to be significant in terms of the relationship between fasting blood sugar and vit-D and HbA1C. Vit-D in sugar will be used as a benefit from vit-D in blood T2DM patients.

Keywords: Vitamin D, Serum, Type 2 Diabetes Mellitus, Human.

^a shwanamed1938@gmail.com

^b <https://orcid.org/0000-0000-0000-0000>

^b ayselsari@hotmail.com

^b <https://orcid.org/0000-0002-4966-2254>

Introduction

Diabetes mellitus (DM) is an important chronic disease that occurs when the pancreas cannot produce enough insulin. It is a condition in which the body cannot adequately use the insulin it produces. It is the hormone insulin that regulates blood sugar. As a result of increased glucose or hyperglycemia, a typical effect of uncontrolled diabetes, many systems in the human body deteriorate over time. It is known that nerves and vessels are actually damaged [1]. DM is a heterogeneous disease characterized by hyperglycemia. There are two main types of diabetes patients. Type 1 diabetic (T1DM) is distinguished from other types of diabetes by the acute lack of insulin secretion. The other is Type 2 diabetic (T2DM), the cause is a mix of insulin resistance. Diabetes difficulties are becoming more regular and increasing rapidly in T2DM patients [2]. Lifestyle and genetic factors are the main causes of T2DM. People can control some factors such as obesity and diet, but other factors such as genetics, age and female gender are beyond personal control [3].

Although the effect of this is accepted, it is known that T2DM is caused by the body's insufficient use of insulin. T2DM accounts for the majority of the world's diabetic population [1]. Although the symptoms of T2DM are similar to those of T1DM, this type of diabetes has only been seen in adults, but is now increasing in children [4].

Briefly, T2DM is defined by insulin resistance, high glucose levels, and a relative absence of insulin. In general, symptoms that should be considered first include increased hunger, thirst, weight loss, urination, feeling tired, and sores [1]. In the first years, many people have no symptoms and are diagnosed in routine tests [5]. Various health problems related to T2DM are: Cushing's syndrome, acromegaly, hyperthyroidism, it is effective in some types of cancer. In addition, cancer patients have a higher risk of death if they have diabetes [6]. T2DM has a role in testosterone deficiency in men [7].

The type of fat in the diet is important, trans fatty acids or saturated fats increase the risk, but monounsaturated and polyunsaturated fats reduce the risk [3].

Both types of diabetes (WHO) defined their symptoms as a single glucose increase. In the fasting state, plasma glucose is equal to or greater than 126mg/dl. Random blood glucose greater than 200 mg/dl. Glycosed hemoglobin (HbA1C) ≥6.5% is another way to diagnose diabetes [5]. The degree of diagnosis of diabetes depends on the relationship between glucose tolerance test results, fasting glucose or HbA1C. Random or fasting blood glucose is preferred over the glucose tolerance test (GTT). This is because (FBS and RBS) is more accessible and easier for individuals. HbA1C has focal points where fasting is not required and the result is more stable than (FBS and RBS).

However, this is a disadvantage as the test is more expensive than blood glucose measurement[8].

T2DM is defined by the high glucose level in the blood associated with insulin resistance and proportional insulin deficiency. Both types of diabetes may be widely recognized depending on the conditions present [9]. The onset of T2DM can be delayed or prevented by adequate diet and normal exercise [10]. It is known that bad lifestyles such as being overweight, malnutrition, physical inactivity, stress and urbanization, which are important factors in the development of obesity and T2DM, are effective. The risk of diabetes can be reduced by more than half with drastic lifestyle actions [11].

The advantage of physical activity arises regardless of the individual's initial weight or subsequent weight loss [12]. With a high level of physical activity, the risk of DM can be reduced by approximately 28% [13]. Evidence to serve dietary changes alone is limited [14]. Some evidence for an eating routine includes high amounts of green vegetables, and some are important data for limiting the intake of the sweet drink[15]. There is indeed an association between increased consumption of sugar-sweetened fruit juice and diabetes, although there is no evidence of an association with 100% fruit juice [16].

In 2019, a study discovered evidence of the advantage of dietary fiber [17]. A healthy diet and exercise play a very important role in diabetes[8]. Better results are obtained with more exercise[18]. Exercise improves glucose control, lowers blood lipid levels, and decreases body fat content [14]. Lowering HbA1C and insulin resistance are positively affected when aerobic exercise is performed [19]. This type of eating routine of calorie restriction is widely recommended for weight loss. In addition, other recommendations include a diet containing vegetables, fruits, reduced saturated fat and low-fat dairy products [20]. DM is popular in both the developing and developed population and remains so around the world [21].

There are several forms of vit-D. Vit-D3 and vit-D2, also known as cholecalciferol and ergocalciferol, are the two main forms of vit-D. forms such as vit-D1 (a mixture of lumisterol and ergocalciferol compounds), vit-D4 (22-dihydroxyergocalciferol) and vit-D5 (cytocalciferol). In 1931, vit-D2 was chemically characterized. In 1935, the chemical formation of vit-D3 (7-dehydrocholesterol) was identified as the product of UV radiation. It is a diverse chemical form of vit-D in steroids that breaks one of the steroid ring bonds. The main structural difference between vit-D2 and vit-D3 is that vit-D2 has a double bond between carbon 22 and carbon 23 in the side chain, furthermore it contains a methyl group at carbon [22].

Wrong or excessive dietary factors are a factor in the risk of developing T2DM. Excessive use of sugar is associated with increased risk [23]. Processed carbohydrates play a key role in increasing the risk when consumed excessively [24]. Vit-D becomes active by eating foods containing vit-D and taking sunlight naturally. Vit-D is effective on skeletal health, cardiovascular disease, T2DM and various other diseases. As many studies have shown, patients with T2DM have been

reported to have low serum vit-D [2]. In the liver, ergocalciferol and cholecalciferol hydroxylate molecules are converted to 25-hydroxy [25(OH)D2 and 25(OH)D3], the main metabolite of vit-D [25]. 25(OH)D hydroxylate to 1,25-dihydroxy vit-D [1.25(OH)2D2 and 1,25(OH)2D3] in the kidney and this active form binds to the vit-D receptor and its biological activities improve [1]. The protective role of vit-D in T2DM is known, and induction of the insulin receptor gene is known. The relationship of 25(OH)D with β -cell function and insulin resistance in T2DM patients has been expressed in many studies.1,25(OH) 2D The active form of vit-D increases the insulin sensitivity (IS) of insulin target tissues. It increases the biosynthetic limit of β -cells. It aids in transformation. In this process, it converts from proinsulin to insulin, reduces fat and increases muscle mass. Thus, it improves insulin sensitivity (IS) [26]. However, the basic mechanism for how 25(OH)D affects the evolution and development of T2DM is not entirely clear in middle-aged subjects. Ranges of vit-D in human body; deficiency is <20 ng/ml, insufficient between 20 to 29 ng/ml, normal 30 to 100ng/ml, toxic >100 ng/ml [27].

Vit-D2 is usually found in fungi, while vit-D3 is found in animal sources [28]. Form vit-D2 ergosterol by UV irradiation. The calcitriol form of the vit-D receptor is the most potent natural ligand that mediates most of the physiological effects of the vitamin [29]. It modulates the response of organs to microbial pathogens by activating the innate immune system [30].

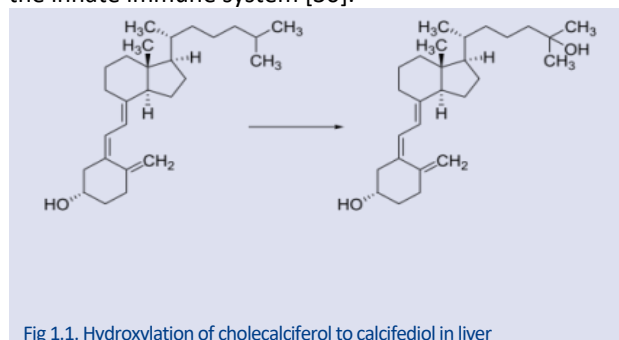


Fig 1.1. Hydroxylation of cholecalciferol to calcifediol in liver

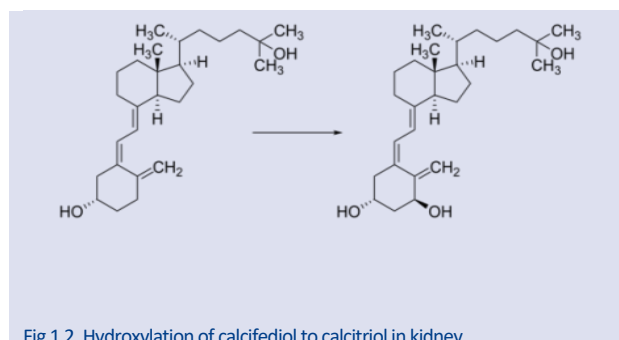


Fig 1.2. Hydroxylation of calcifediol to calcitriol in kidney

Generally, 25(OH)D serum concentration is used to evaluate the vit-D form. It is converted to 25(OH)D giving an accurate picture of vit-D status in serum. The serum level of 1.25(OH)D is characteristically not used to assess vit-D form as it is also controlled by certain hormones in the human body [31].

Vit-D deficiency is mainly due to insufficient exposure to sunlight [30]. Insufficient dietary intake of vit-D may

cause its deficiency [32]. This deficiency affects bone mineralization and causes bone diseases, including rickets, in children. It may also contribute to an increased risk of osteomalacia and osteoporosis in adults [26,32]. Weakness of the muscles increases the risk of falling, as well as the risk of fractures in adults. There are one billion people in the world who are either deficient or deficient in vit-D [26]. People who appear to be overweight or obese are at increased risk for vit-D deficiency [33]. Clothing that conceals a significant portion of human skin is associated with a lower vit-D value and an increased popularity of hypovitaminosis D [34]. In countries far from the equator, the amount and intensity of sunlight varies more seasonally [35].

Vit-D tends to specifically stimulate insulin production in β -pancreatic cells via the nuclear vit-D receptor (VDR). This method helps in minimizing vit-D inflammation. It is an important process in inducing insulin resistance [2,7]. Treatment of vit-D deficiency depends on the degree of deficiency. The lower the concentration of serum 25(OH)D prior to treatment, the higher the dose required to rapidly achieve an appropriate serum vit-D level [26].

The aim of the study is to emphasize the experimental results and to emphasize the necessity of periodically measuring the Vit D value in T2DM patients as a result of this significant increase in the HbA1C value in T2DM patients. In this context, studies related to the fact that vit-D, Ca and Mg are responsible for increasing intestinal absorption and that it is very important to measure Ca and Mg values periodically in T2DM patients with Vit D deficiency are to follow up with contributing experimental results.

Materials and Method

Individuals visiting the endocrine and diabetes unit of the teaching hospital and the emergency teaching hospital and appropriate sampling techniques were used. There were 70 diabetes patients in the study. The following cases were excluded in this sampling process. Those with chronic liver disease, those with chronic kidney disease, those with thyroid disease, patients using folic acid and multivitamin (A-Z) or vit-B12 and iron, patients taking Ca and Mg supplements, patients using insulin, pregnant women, inflammatory conditions and T2DM patients. Diabetics and control group the results obtained in this study were compared. He was fasted overnight for testing before blood samples were taken. The study group was selected between the ages of 35 and 75. Informed consent was obtained from each participant before starting the study. Required ethical permission was obtained and all procedures and questionnaires were studied in accordance with the procedure. Patients are equal to or less than 5 years according to the duration of diabetes. Selected from people over 5 years. Patients were evaluated according to their smoking habits. BMI for each participant was determined by dividing weight in kilograms (kg) by height in meters squared. BMI from 18.5 to 24.9 kg/m² was considered normal weight. A BMI of 25

to 29.9 kg/m² was considered overweight. BMI equal to or greater than 30kg/m² was considered obese. BMI uses heights and weights to assess the fall of an adult who is underweight, healthy weight, overweight or obese. BMI= weight(kg)/height²m²[36]. Diabetes status (Glycemic control): Glycated Hemoglobin was measured for all diabetic patient:HbA1c less than 6.5% was considered good control. HbA1c equal to, or more than 6.5% was considered fair control.

Lipid Profile Status

Total serum cholesterol and lipids were performed according to the guidelines of the national cholesterol education program. Total serum cholesterol below 200 mg/dl was considered normal. Total serum cholesterol equal to or greater than 200 mg/dl was considered as hypercholesterolemia. S.TG lower than 150 mg/dl was considered normal. S.TG equal and above 150 mg/dl was considered high. S.HDL-C below 40 mg/dl was considered low level. S.HDL-C between 40 and 60 mg/dl was accepted as normal level. S.HDL-C more than 60 mg/dl was considered high level. S.LDL-C of less than 130 mg/dl was considered optimal. Equal to S.LDL-C and greater than 130 mg/dl were considered as a high risk factor. Serum vit-D<10ng/ml was considered deficient. Serum vit-D was considered insufficient between 10 and 30 ng/dl. Serum vit-D >30ng/ml was accepted as the normal range.

Collection and Processing of Blood Sample

Participants who attended the morning endocrine and diabetes unit from T2DM patients diagnosed according to the WHO protocol fasted for 12 to 14 hours. Venous blood samples (6 ml) were taken between 8:30 and 11:30 in the morning from the antecubital vein using a vacutainer. 2 ml were immediately collected into a vacuum tube containing K3 EDTA as anticoagulant for HbA1c estimation. The remaining 4 ml were collected in vacutainer system gel separator tubes. Serum was separated from whole blood after coagulation using centrifugation (HITACHI centrifuge, model O5P-21) for 8 min at 6000rpm. Serum glucose was immediately processed to measure total cholesterol, triglycerides, HDL, LDL and vit-D.

Biochemical Analysis

Most of the tests were performed by the cobas c 311 and cobas6000 devices for laboratory analyze, and here we review all these tests. The sugar level is detected by using glucose HK Gen.3 300 tests Roche(Hitachi) cobas c311, cobas c501/502 with reference no. 04404483 190. The cholesterol level is detected by using cholesterol gen.2 400 tests roche (hitachi) cobas c311, cobas c501/502 with reference no. 03039773 190. The triglyceride level is detected by using triglyceride. 250 tests roche (hitachi) cobas c311, cobas c 501/502 with reference no. 20767107 322. The HDL level is detected by using tests roche (hitachi) cobas c311, cobas c 501/502 with reference no. 07528566 190. The LDL level is detected

by using tests roche (hitachi) cobas c311, cobas c 501/502 with reference no.07005717 190. The detection of serum vit-D3 is performed by using vit-D3 total 25-hydroxy vit-D3 kit (roche) with reference number 05894913 190 and modular analytics cobas e 601, cobas e 602 and E170 cobas e 411. Determination of HbA1c level was done by (HPLC D10) auto analyzer device [37, 38, 39, 40].

Statistical Analysis

Statistical package version (23) for the social sciences program was used in the analysis of our data. The t-test was used to compare the ratios. A p value of ≤ 0.05 is considered statistically significant, while a p value of 0.01 is considered statistically highly significant. One-way anova was used for comparison between more than two groups. The correlation coefficient between study parameters was determined using the pearson correlation.

Results And Discussion

General Characteristic of Studied Participants for Frequency Distribution

In this study, 70 T2DM patients and 25 healthy controls were compared. Research participants were 46 men and 49 women. The study included 79 subjects, 83.2% of whom were non-smokers and 73.7% of 70 subjects who did not exercise, whereas 16 smokers were 16.8% and 25 physically active 26.3%. 17.9% of 17 people are aged 40 or younger and 82.1% of 78 people are older than 40. Diabetes duration of 33.7% of 32 patients is 5 years or less, 40% of 38 patients have diabetes duration of more than 5 years. 16.8% of 16 patients are less than 25kg/m², 32.6% of 31 patients are with 25 between 29.9kg/m² and 50.6% of 48 people are over 30kg/m² (Table 3.1).

Table 3.1. General characteristic of studied participants for frequency distribution

Subject characteristics (n=95)		Frequency Distribution	
		Frequency (n)	Percentage (%)
Subject categorizes	Control	25	26.3
	Diabetic	70	73.7
Age (years)	≤ 40 years	17	17.9
	> 40 years	78	82.1
Gender	Male	46	48.4
	Female	49	51.6
BMI	< 25 kg/m ²	16	16.8
	25-29.9 kg/m ²	31	32.6
	> 30 kg/m ²	48	50.6
Duration of diabetes (years)	≤ 5 years	32	33.7
	> 5 years	38	40.0
	No Duration(control)	25	26.3
Family history of diabetes	Positive	61	64.2
	Negative	34	35.8
Exercise	Yes	25	26.3
	No	70	73.7
Smoking	Yes	16	16.8
	No	79	83.2

General Characteristics of Biochemical Indicators for Frequency Distribution

The biochemical indicators for this study were: 37.9% of 36 subjects had glucose less than or equal to 110 mg/dl, and 62.1% of 59 subjects had glucose greater than 110 mg/dl. 34.7% of 33 people had an HbA1c below 6.5% and 65.3% of 62 people had an HbA1c equal to or more than 6.5%. 34.7% of 33 subjects had vit-D less than 10 ng/ml, 53.7% of 51 subjects had between 10 and 29.9, and 11.6% of 11 subjects had equal or more than 30ng/ml. 27.4% of 26 subjects had less than or equal to 1.7 mg/dl and 72.5% of 69 subjects had more than 1.7 mg/dl. 22.1% of 21 subjects were less than 9 mg/dl and 77.9% of 74 subjects were equal to or more than 9 mg/dl. 68.4% of 65 people had cholesterol less than 200 mg/dl and 31.6% of 30 people had 200 mg/dl or more. It is more than 150 mg/dl. The HDL value of 32 people was 33.7% lower than 40mg/dl and 66.3% equal and more than 40mg/dl in 63 people. LDL value of 71 people is 74.7% lower than 130mg/dl and 25.3% of 41 people have equal or more than 130mg/dl (Table 3.2).

Table 3.2. General characteristics of biochemical indicators for frequency distribution

Biochemical indicators	Frequency Distribution		
	Frequency (n)	Percentage (%)	
Glucose	≤ 110 mg/dl	36	37.9
	> 110 mg/dl	59	62.1
HbA1c (%)	< 6.5 %	33	34.7
	≥ 6.5 %	62	65.3
Vitamin D	< 10 ng/ml	33	34.7
	10-29.9 ng/ml	51	53.7
	≥ 30 ng/ml	11	11.6
Cholesterol (mg/dl)	< 200	65	68.4
	≥ 200	30	31.6
Triglyceride	≤ 150 mg/dl	34	35.8
	> 150 mg/dl	61	64.2
HDL	< 40 mg/dl	32	33.7
	≥ 40 mg/dl	63	66.3
LDL	< 130 mg/dl	71	74.7
	≥ 130 mg/dl	41	25.3

Patients and Subjects Characteristics according to Control, and Diabetic Patients

In this table, we compare all the characteristics according to the control and diabetes patients. The mean \pm SD for control age was 42.48 \pm 8.11 and 52.12 \pm 9.09 for diabetic patients, $p < 0.001$. 11 (44.0%) of the controls were male, 14 (56.0%) were female, 35 (50.0%) of the diabetic patients were male and 35 (50.0%) were female, and the p value was not significant. The mean \pm SD of the control BMI were 26.90 \pm 4.09 and 30.52 \pm 4.56 for diabetic patients with $p < 0.01$. 20 (80.0%) of the controls had a positive family history of diabetes, 5 (20.0%) had a negative family history, 41 (58.6%) had a positive family history, and 29 (41.4%) had a negative diabetes history $p < 0.05$. . 32 of the patients (45.7%) had diabetes duration

of 5 years or less, 38 (54.3%) had diabetes duration of more than 5 years. Nine of the controls (36.0%) were physically active and 16 of the controls (64.0%) were physically inactive, 16 of the patients (22.9%) were physically active, and 54 (77.1%) of the patients were physically active without making any sense. not active. Of the controls, 5 (20.0%) were smokers and 20 (80.0%) were non-smokers, 11 (15.7%) of the diabetic patients were smokers and 59 (84.3%) were non-smokers. The mean±SD of glucose was 93.48±8.48 for controls and 176.64±59.90 for diabetic patients, p<0.001. The mean±SD of HbA1c was 5.28±0.19 for controls and 8.81±1.71 for diabetic patients, with p<0.001. The mean±SD of vit-D was 21.09±8.54 for controls and 13.48±6.77 for diabetic patients, with p<0.001. The mean±SD of cholesterol was 176.16±27.63 for controls and 178.44±41.61 for diabetic patients, and the p-value was not significant. The mean±SD of triglycerate was 133.84±57.70 for controls and 203.24±80.88 for diabetic patients, p<0.001. The mean±SD of HDL was 47.00±8.10 for controls and 42.3±8.59 for diabetic patients, p<0.01. The mean±SD of LDL was 109.16±25.10 for controls and 100.65±39.40 for diabetic patients and was not significant in the p-value (Table 3.3).

Table 3.3. Patients and subjects characteristics according to control, and diabetic patients

Subjects, characteristics (n=95)	Frequency Distribution or Mean±SD		p-value	
	Controls (n=25)	Diabetic (n=70)		
Age (years)	42.48 ±8.11	52.12 ±9.09	<0.001	
Gender	Male	11(44.0%)	35(50.0%)	NS
	Female	14(56.0%)	35(50.0%)	
BMI (kg/m ²)	26.90±4.09	30.52±4.56	<0.01	
Family history of diabetes	Positive	20(80.0%)	41(58.6%)	<0.05
	Negative	5(20.0%)	29(41.4%)	
Duration of diabetes	≤5 years	No Diabetic	32(45.7%)	NS
	>5 years		38(54.3%)	
Exercise	Yes	9(36.0%)	16(22.9%)	NS
	No	16(64.0%)	54(77.1%)	
Smoking	Yes	5(20.0%)	11(15.7%)	NS
	No	20(80.0%)	59(84.3%)	
Glucose (mg/dl)	93.48±8.48	176.64±59.90	<0.001	
HbA1c (%)	5.28±0.19	8.81±1.71	<0.001	
Vit.D (ng/ml)	21.09±8.54	13.48±6.77	<0.001	
Cholesterol (mg/dl)	176.16±27.63	178.44±41.61	NS	
Triglyceride (mg/dl)	133.84±57.70	203.24±80.88	<0.001	
HDL (mg/dl)	47.00±8.10	42.3±8.59	<0.01	
LDL (mg/dl)	109.16±25.10	100.65±39.40	NS	

NS: Statistically No significant. p-value<0.05 is considered significant, p-value>0.05 is considered No significant. Independent t-test and Chi-square was performed for statistical analysis.

Vitamin D Level in T2dm Patients, and Healthy Subjects in Relations with Age Group

The vit-D mean±SD of T2DM patients aged 40 years or less was 14.39±3.20, and the vit-D mean±SD of T2DM patients older than 40 years was 13.43±6.94, which was not significant. The vit-D mean±SD of healthy individuals aged 40 and over was 17.99±8.65, and the vit-D mean±SD of healthy individuals older than 40 years was 24.46±7.34 non-significant p-value (Table 3.4).

Table 3.4. Vit- D level in T2DM patients, and healthy subjects in relations with age group

Parameter	Diabetic (n=70) Mean ±SD		p-value	Controls (n=25) Mean ±SD		p-value
	<=40 year (n=4)	>40 year (n=66)		<=40 year (n=13)	40 year (n=12)	
Vit.D	14.39±3.20	13.43±6.94	NS	17.99±8.65	24.46±7.34	NS

NS : Statistically No Significant

Vitamin D level in T2DM patients, and healthy subjects in relations with BMI group.

In the comparison between the vit-D of a T2DM patient and a healthy subject in the BMI group, the mean±SD of vit-D was 19.03±10.98, and the mean±SD for T2DM patients with a BMI of less than 25 kg/m². Vit-D mean±SD for T2DM patients with a BMI between 25-29.9kg/m² is 14.41±6.66 and for T2DM patients with a BMI equal to and above 30 kg/m², the mean±SD of vit-D is 11.84±5.51 and p<0.05 is. In healthy individuals with a BMI less than 25 kg/m², vit-D mean±SD is 26.79±7.86, in healthy individuals with a BMI between 25-29.9kg/m², vit-D mean±SD is 18.86 is . In healthy individuals with equal BMI and greater than 30kg/m², vit-D was 18.86±2.83 and mean±SD was 16.90±7.58 and p<0.05 (Table 3.5).

Table 3.5. Vit-D level in T2DM patients, and healthy subjects in relations with BMI group

Parameter	Diabetic (n=70) Mean ±SD			p-value
	<25 kg/m ² (n=6)	25-29.9 kg/m ² (n=28)	>=30 kg/m ² (n=36)	
Vit.D	19.03±10.98	14.41±6.66	11.84±5.51	<0.05
Parameter	Controls (n=25) Mean ±SD			p-value
	<25 kg/m ² (n=10)	25-29.9 kg/m ² (n=3)	>=30 kg/m ² (n=12)	
Vit.D	26.79±7.86	18.86±2.83	16.90±7.58	<0.05

NS : Statistically No Significant

Vitamin D level in T2DM Patients, and Healthy Subjects in Relations with Gender Group

Between the vit-D of T2DM patients and healthy subjects in the gender group, the mean±SD of vit-D for T2DM patients was 14.90±5.71 for male and 12.07±7.51 for female, and the p-value was not significant. For males, the mean±SD of vit-D for healthy subjects was 22.72±10.37 and for females 19.81±6.93, which was not significant in the p-value (Table 3.6).

Table 3.6. Vit-D level in T2DM patients, and healthy subjects in relations with gender group

Parameter	Diabetic (n=70)Mean ±SD			Controls (n=25)Mean ±SD		
	Male (n=35)	Female (n=35)	p-value	Male (n=11)	Female (n=14)	p-value
Vit.	14.90±5	12.07±7	N	22.72±10	19.81±6	N
D	.71	.51	S	.37	.93	S

NS : Statistically No Significant

Vitamin D Level in T2dm Patients, and Healthy Subjects in Relations with Physical Activity Group

Between vit-D of T2DM patients and healthy subjects in the physical activity group, mean±SD of vit-D for T2DM patients was 14.87±6.32 for active subjects and 13.08±6 for inactive subjects, It is 91 and there is no significant difference. For active people, mean±SD of vit-D was 21.92±9.33 in healthy subjects and 20.63±8.35 for inactive subjects, which was not significant in p-value (Table 3.7).

Table 3.7.Vit-D'nin level in T2DM patients, and healthy subjects in relations with physical activity group

Parameter	Diabetic (n=70)Mean ±SD			Controls (n=25)Mean ±SD		
	Yes (n=16)	No (n=54)	p-value	Yes (n=9)	No (n=16)	p-value
Vit.D	14.87±6.32	13.08±6.91	NS	21.92±9.33	20.63±8.35	NS

NS : Statistically No Significant

Vit- D Level in T2DM Patients, and Healthy Subjects in Relations with Smoking Group

For T2DM patients, the mean±SD of vit-D was 13.79±5.10 for smokers and 13.43±7.08 for non-smokers, which was not significant in p. For smokers, mean±SD of vit-D was 25.37±8.96 in healthy subjects and 20.02±8.32 in non-smokers, and the p-value was not significant (Table 3.8).

Table 3.8.Vit-D'nin level in T2DM patients, and healthy subjects in relations with smoking group

Parameter	Diabetic (n=70)Mean ±SD			Controls (n=25)Mean ±SD		
	Yes (n=11)	No (n=59)	p-value	Yes (n=4)	No (n=18)	p-value
Vit.D	13.79±5.10	13.43±7.08	NS	25.37±8.96	20.02±8.32	NS

NS : Statistically No Significant

Table 3.11. Vit-D'nin level in T2DM patients, and healthy subjects in relations with cholesterol

Parameter	Diabetic (n=70)Mean ±SD			Controls (n=25)Mean ±SD		
	Serum total cholesterol level<200 (n=45)	Serum total cholesterol level>=200 (n=25)	p-value	Serum total cholesterol level<200 (n=20)	Serum total cholesterol level>=200 (n=5)	p-value
Vit.D	14.49±7.22	11.68±5.57	NS	19.61±8.44	27.02±6.65	NS

NS : Statistically No Significant

Vitamin D Level in T2DM Patients, and Healthy Subjects in Relations with Family History Group

Mean±SD of vit-D for T2DM patients with negative family history was 14.50±7.36 and 12.05±5.66 for positive family history, and there was no significant difference. p-value. The mean±SD of vit-D was 21.00±7.95 for healthy subjects for negative family history and 21.46±11.70 for positive family history, the p-value was not significant (Table 3.9).

Table3.9.Vit-D'nin level in T2DM patients, and healthy subjects in relations with family history group

Parameter	Diabetic (n=70)Mean ±SD			Controls (n=25)Mean ±SD		
	Negative (n=41)	Positive (n=29)	p-value	Negative (n=20)	Positive (n=5)	p-value
Vit.D	14.50±7.36	12.05±5.66	NS	21.00±7.95	21.46±11.70	NS

Vitamin D Level in T2DM Patients in Relations with Duration Group

The mean±SD of vit-D for equal and less than five years for T2DM patients was 13.81±7.54 and 13.21±6.15 for more than five years. not significant in p-value (Table 3.10).

Table3.10.Vit-D'nin level in T2DM patients in relations with duration group

Parameter	Diabetic (n=70)Mean ±SD		p-value
	<=5 year (n=32)	>5 year (n=38)	
Vit.D	13.81±7.54	13.21±6.15	NS

NS : Statistically No Significant

Vitamin D Level in T2DM Patients, and Healthy Subjects in Relations with Cholesterol

For T2DM patients with cholesterol less than 200mg/dl, the mean±SD of vit-D is 14.49±7.22, and the p value of 11.68±5.57 is not significant if the cholesterol value is greater than or equal to 200mg/dl. The mean±SD of vit-D is 19.61±8.44 in healthy individuals with a cholesterol value of less than 200mg/dl, and 27.02±6.65 in individuals with a cholesterol value equal to or greater than 200mg/dl (Table3.11).

Vitamin D Level in T2DM Patients, and Healthy Subjects in Relations with Triglyceride Group

The mean±SD of vit-D for T2DM patients with vit-D is 14.84±7.67 for T2DM patients with triglyceride level less than 150mg/dl and the value is equal to or greater than

150mg/dl for patients with high triglyceride level being 13.02±6.45 and not significant in the p-value. In healthy subjects with a triglyceride value less than 150 mg/dl, the mean±SD of vit-D is 18.82±7.57 and for individuals with a triglyceride value equal to or greater than 150 mg/dl, it is 25.13±9.11 and in terms of p is not significant (Table 3.12).

Table3.12. Vit-D'nin level in T2DM patients, and healthy subjects in relations with triglyceride group

Parameter	Diabetic (n=70)Mean ±SD			Controls (n=25)Mean ±SD		
	Serum total Triglyceride level<150(n=18)	Serum total Triglyceride level>=150(n=52)	p-value	Serum total Triglyceride level<150(n=16)	Serum total Triglyceride level>=150(n=9)	p-value
Vit.D	14.84±7.67	13.02±6.45	NS	18.82±7.57	25.13±9.11	NS

NS : Statistically No Significant

Vitamin D Level in T2DM Patients, and Healthy Subjects in Relations with HDL Group

The mean±SD of vit-D for T2DM patients with vit-D and HDL less than 40mg/dl for T2DM patients and 40mg/dl for patients with HDL is 13.18±6.81 while it was 13.68±6.83

and it was not significant in the p-value. The mean±SD of vit-D is 21.50±8.78 in healthy individuals with HDL value less than 40mg/dl, and 21.02±8.71 in individuals with HDL value equal to or greater than 40mg/dl. and p is not significant (Table 3.13).

Table3.13. Vit-D'nin level in T2DM patients, and healthy subjects in relations with HDL group

Parameter	Diabetic (n=70)Mean ±SD			Controls (n=25)Mean ±SD		
	Serum HDL Level<40(n=28)	Serum HDL Level>=40(n=42)	p-value	Serum HDL Level<40(n=4)	Serum HDL Level>=40(n=21)	p-value
Vit.D	13.18±6.81	13.68±6.83	NS	21.50±8.78	21.02±8.71	NS

NS : Statistically No Significant

Vitamin D level in T2DM Patients, and Healthy Subjects in Relations with LDL Group

Vit-D of T2DM patients and 12.39±6.00 p if the mean ±SD of vit-D for T2DM patients with LDL value less than 130 mg/dl is 13.89±7.05 and LDL value is greater than or

equal to 130mg/dl value is not significant. In healthy individuals with LDL value below 130 mg/dl, mean±SD of vit-D is 21.51±7.90 and in individuals with LDL value equal to or more than 130 mg/dl, 19.42±11,71 and there is no significant difference (Table 3.14).

Table 3.14. Vit-D level in T2DM patients, and healthy subjects in relations with LDL group

Parameter	Diabetic (n=70)Mean ±SD			Controls (n=25)Mean ±SD		
	Serum LDL Level<130(n=51)	Serum LDL Level>=130(n=19)	p-value	Serum LDL Level<130(n=20)	Serum LDL Level>=130(n=5)	p-value
Vit.D	13.89±7.05	12.39±6.00	NS	21.51±7.90	19.42±11.71	NS

NS : Statistically No Significant

Vitamin D Level in whole Study Population in Relations with Fasting Blood Glucose Level Group

The mean±SD of vit-D for the entire study population with vit-D level equal to or lower than 110mg/dl and fasting blood glucose was 19.22±9.23, and fasting blood glucose above 130mg/dl. persons with p<0.001 and 12.21±6.15 (Table 3.15).

Vitamin D Level in whole Study Population in Relations with HbA1C Level Group

The vit-D mean±SD is 20.46±8.56 for the entire population with a vit- D level and an HbA1C level equal to or less than 6.5% in the entire study population and a blood glucose level above 6.5% for fasting subjects p<0.001 and 12.84±6.26 (Table 3.16).

Table 3.15. Vit-D'nin level in whole study population in relations with fasting blood glucose level group

Parameter	Whole study population (n=92)Mean ±SD		
	Fasting blood glucose level <=110 g/dl(n=36)	Fasting blood glucose level >110 mg/dl(n=59)	p-value
Vit.D	19.22±9.23	12.21±6.15	<0.001

NS : Statistically No Significant

Table3.16. Vitamin D level in whole study population in relations with HbA1C level group

Parameter	Whole study population (n=92) Mean ±SD		
	HbA1C level<6.5 (n=33)	HbA1C level>=6.5(n=62)	p-value
Vit.D	20.46±8.56	12.84±6.26	<0.001

NS : Statistically No Significant

Correlation Between Vitamin D and other Parameters in the Study Population

According to the Pearson correlation coefficient (r), results in the entire study population showed that there was no negative significant correlation between vit-D level [age group, cholesterol, and LDL level ($r=-0.105$, $p=0.313$) each. ($r=-0.109$, $p=0.292$), ($r=-0.091$, $p=0.383$)], vit-D level had a negative and low significant correlation with triglyceride ($r=-0.209$, $p<0.05$), vit-D level, [had a negative high significant correlation with BMI, fasting blood glucose and HbA1C ($r=-0.308$, $p<0.01$), ($r=-0.334$, $p<0.01$), ($r=-0.380$, $p<0.001$), respectively, vit-D level did not have a positive and significant relationship with HDL ($r=0.100$, $p=0.336$) (Table 3.20).

Table 3.20. Correlation between vitamin D and other parameters in the study population

Parameter	(r)	p-value
Age (year)	-0.105	0.313
BMI(Kg/m ²)	-0.308**	<0.01
Cholesterol	-0.109	0.292
Triglycerides	-0.209*	<0.05
HDL	0.100	0.336
LDL	-0.091	0.383
FBS	-0.334**	<0.01
HbA1c	-0.380**	<0.001

T2DM is a metabolic problem that occurs by reducing insulin secretion from pancreatic β -cells, hyperglycemia and insulin resistance. The increase in the prevalence of diabetes is mostly linked to poor lifestyle habits and obesity. Obesity is the main health problem mostly associated with T2DM and causes increased mortality and morbidity. The disclosure of T2DM levels represents a worldwide health problem. Even as changes in diet, obesity levels and physical activity underlying genetic hazard factors turn out to be fueling this epidemic, other environmental variables may be compelling in curing T2DM. T2DM is known to be a worldwide health problem. Other environmental variables may be compelling in curing T2DM, even if changes in diet, obesity levels, and physical activity underlying genetic hazard factors in this disease turn out to be fueling this epidemic [4]. The data in our study confirmed that there was no significant relationship between the patient and control group and each group (age, gender, activity, smoking, family history, duration) in relation to vit-D. Similar observations have been reported in similar studies [2,4]. Body mass index (BMI) is known as the body weight divided by the square of height and is properly expressed in kg/m². In this study, the Pearson correlation coefficient (r) was negative between the patient's vit-D (BMI) group. and the decrease in vit-D value was shown with the increase in BMI value due to control. Similar observations have been reported in similar studies [4]. In our study, the data confirmed that there was no statistically significant relationship between vit-D and cholesterol, triglycerate, LDL, and HDL levels, and that there was a positive Pearson correlation coefficient (r) between HDL level and vit-D level. There is a negative Pearson correlation coefficient (r) between the

vit-D of the patient and control, but the vit-D of the patient and control and (cholesterol, triglycerate, LDL) level. Similar observations have been reported in similar studies [2]. The mean \pm SD vit-D level was 19.22 \pm 9.23 for the whole population with a fasting blood glucose level of 110 mg/dl or less, and 12.21 \pm 6.15 for people with a fasting blood glucose level above 130 mg/dl, and $p<0.001$. The relationship between vit-D level and fasting blood sugar is statistically significant with negative Pearson correlation coefficient. Similar observations are also observed in similar studies [1,4]. Vit-D mean \pm SD 20.46 \pm 8.56 for the entire population with an HbA1C level equal to or lower than 6.5%, and 12.84 \pm 6% for individuals with a fasting blood glucose level above 6.5%, is 26 and $p<0.001$. The relationship between vit-D level and fasting blood sugar is statistically significant with negative Pearson correlation coefficient. Similar observations have been reported in similar studies [1,4]. The strong relationship between vit-D and fasting blood glucose and HbA1C is due to the fact that vit-D tends to specifically stimulate insulin production in β -pancreatic cells via the nuclear vit-D receptor (VDR) and that vit-D minimizes inflammation. This is an important process in inducing insulin resistance [2,4].

Conclusion

T2DM is a complex metabolic disease that has turned into an important health problem. Vit-D deficiency is a major health problem worldwide, currently associated with chronic diseases such as diabetes mellitus and cardiovascular disease. The role of vit-D in insulin resistance is important and the T2DM patient should measure the vit-D value periodically.

Conflicts of interest

The authors report no conflict of interest.

References

- [1] Adela R., Borkar R.M., Bhandi M.M., Vishwakarma Reddy P.N.C., Srinivas R., Banerjee S., Lower Vitamin D Metabolites Levels were Associated with Increased Coronary Artery Diseases in Type 2 Diabetes Patients in India, *Sci. Rep.*, 6(12) (2016) 1–13.
- [2] Yassin M.M., Masoud A.E.R.D., Serum Vitamin D Status in Type 2 Diabetic Patients from Gaza Strip, *Diabetes Metab.*, 13(3) (2019) 1865–1870.
- [3] Risérus U., Willett W.C., Hu F.B., Dietary Fats and Prevention of T2DM, *Prog. Lipid Res.*, 48(1) (2009) 44–51.
- [4] Holick M.F., Schnoes H.K., Deluca H.F., Suda T., Cousins R.J., Isolation and Identification of 1,25-Dihydroxycholecalciferol a Metabolite of Vitamin D Active in Intestine, *Biochemistry*, 10(14) (1971) 2799–2804.
- [5] Turner B., Williams S., Taichman D., Vijan S., The Clinic Type 2 Diabetes Screening and Prevention Diagnosis and Evaluation Practice Improvement CME Questions, 2010.
- [6] Giovannuc E., Harlan D.M., Archer M.C., Bergenstal R.M., Gapstur S.M., Habel L.A., Pollak M., Regensteiner J.G., Yee D., Diabetes and Cancer: A Consensus Report, *Diabetes Care*, 33(7) (2010) 1674–1685.

- [7] Saad F., Gooren L., The Role of Testosterone in The Metabolic Syndrome: A Review, *J.Steroid Biochem. Mol. Biol.*, 114 (2) (2009) 40–43.
- [8] D. O. F. Diabetes, Diagnosis and Classification of Diabetes Mellitus, *Diabetes Care*, 35(1) (2012).
- [9] Natha DM., Balkau B., Bonora E., Johnsen K B., Buse JB., Colagiuri S., Davidson MB., DeFronzo R., Genuth S., Rury R. Holman RR., Ji L., Kirkman S., Knowler WC, Schatz D., Shaw J., Sobngwi E., Steffes M., Vaccaro O., Wareham N., Zinman B., International Expert Committee Report on The Role of the A1C, Assay in the Diagnosis of Diabetes, *Diabetes Care*, 32(7) (2009) 1327–1334.
- [10] Li G., Elley C.R., Kenealy T., Lifestyle Interventions Reduced the Long Term Risk of Diabetes in Adults with Impaired Glucose Tolerance, *Evid. Based. Med.*, 13(6) (2008) 173.
- [11] Sumamo E C., Dryden D., Vandermeer B., Ha Korownyk C., Annals of Internal Medicine Review Lifestyle Interventions for Patients with and at Risk for T2DM., *Ann. Intern. Med.*, 159(8) (2013) 543–55.
- [12] O’Gorman D.J., Krook A., Exercise and The Treatment of Diabetes and Obesity, *Med. Clin. North Am.*, 95(5) (2011)953–969.
- [13] Kyu H.H., Bachman V.F., Alexander L.T., Mumford J.E., Afshin A., Estep K., Veerman J.L., Delwiche K, Iannarone M.L., Moyer M.L., Cercy K., Vos T., Murray J.L., Forouzanfar M. H., Physical Activity and Risk of Breast Cancer, Colon Cancer, Diabetes, Ischemic Heart Disease, and Ischemic Stroke Events: Systematic Review and Dose Response Meta Analysis for the Global Burden of Disease Study 2013, *BMJ.*, 354 (2016) 1–10.
- [14] Nield L, Summerbell C.D., Hooper L., Whittaker V., Moore H., Dietary Advice for The Prevention of Type 2 Diabetes Mellitus in Adults, *Cochrane Database Syst. Rev.*, 16(3) (2008) 51.
- [15] Carter P., Gray L.J., Troughton J., Khunti K., Davies M., Fruit and Vegetable Intake and Incidence of Type 2 Diabetes Mellitus: Systematic Review and Meta Analysis, *BMJ*, 341(7772) (2010) 543.
- [16] Xi B., Li S., Liu Z., Tian H., Yin X., Huai P., Tang W., Zhou D., Steffen M.L., Intake of Fruit Juice and Incidence of Type 2 Diabetes: A Systematic Review and Meta Analysis, *PLoS One*, 9(3) (2014).
- [17] Reynolds, A., Mann J., Cummings J., Winter N., Mete E., and Te Morenga L., Carbohydrate quality and Human Health: A Series of Systematic Reviews and Meta Analyses, *Lancet*, 393(10170)(2019) 434–445.
- [18] Smith A.D., Crippa A., Woodcock J., Brage S., Physical Activity and Incident T2DM: A Systematic Review and Dose Response Meta Analysis of Prospective Cohort Studies, *Diabetologia*, 59(12) (2016) 2527–2545.
- [19] Zanuso S., Jimenez A., Pugliese G., Corigliano G., Balducci S., Exercise for The Management of Type 2 Diabetes: A Review of The Evidence, *Acta Diabetol.*, 47(1)(2019)15–22.
- [20] Fox C.S., Golden S.G., Anderson C., Bray G.A., Burke L.E., Boer I.H., Deedwania P., Eckel R.H., Ershow A.G., Fradkin J., Inzucchi S.E., Kosiborod M., Nelson R.G, Patel M.J, Pignone M., Quinn L., Schauer P. R., Selvin E., Vafiadis D.K., Update on Prevention of Cardiovascular Disease in Adults with Type 2 Diabetes Mellitus in Light of Recent Evidence: A Scientific Statement from The American Heart Association and the American Diabetes Association, *Diabetes Care*, 38(9) (2015)1777–1803.
- [21] Vos T., Global, Regional, and National Incidence, Prevalence, and Years Lived with Disability for 310 Diseases and Injuries, 1990–2015: A Systematic Analysis for the Global Burden of Disease Study 2015, *Lancet*, 388(10053) (2016)1545–1602.
- [22] Bolland M.J., Grey A., Gamble G.D., Reid I.R., The Effect of Vitamin D Supplementation on Skeletal, Vascular or Cancer Outcomes: A Trial Sequential Meta Analysis, *Lancet Diabetes Endocrinol.*, 2(4) (2014)307–320.
- [23] Malik V.S., Popkin B.M., Bray G.A., Després J.P., Willett W.C., Hu F.B., Sugar Sweetened Beverages and Risk of Metabolic Syndrome and Type 2 Diabetes: A Meta Analysis, *Diabetes Care*, 33(11)(2010) 2477–2483.
- [24] Hu E.A., Pan A., Malik V., Sun Q., White Rice Consumption and Risk of T2DM: Meta Analysis and Systematic Review, *BMJ*, 344(7851)(2012)1–9.
- [25] Dhas Y., Banerjee J., Damle G., Mishra N., Association of Vitamin D Deficiency with Insulin Resistance in Middle Aged Type 2 Diabetics, *Clin. Chim. Acta.*, 492(11)(2018)95–101.
- [26] Holick M.F., “Sunlight and Vitamin D for Bone Health and Prevention of Autoimmune Diseases, Cancers, and Cardiovascular Disease., *Am. J. Clin. Nutr.*, 80(6)(2004)1678–1688.
- [27] Zhang J., Li Y., Lai D., Lu D., Lan Z., Kang J., Xu Y., Cai S., Vitamin D Status is Negatively Correlated with Insulin Resistance in Chinese Type 2 Diabetes, *Int. J. Endocrinol.*, 9 (2021) 127-132.
- [28] Keegan R.J.H., Lu Z., Bogusz J.M., Williams J.E., Holick M.F., Photobiology of Vitamin D in Mushrooms and its Bioavailability in Humans, *Dermatoendocrinol.*, 5(1)(2013)165–176.
- [29] Norman W., From Vitamin D to Hormone D: Fundamentals of Vitamin D Endocrine System Essential for Good Health, *Am. J. Clin. Nutr.*, 88(2) (2008) 491-499.
- [30] Bikle D.D., Vitamin D Metabolism, Mechanism of Action, and Clinical Applications, *Chem. Biol.*, 21(3)(2014)319–329.
- [31] Clements M.R., The Problem of Rickets in UK Asians, *J.Hum.Nutr.Diet.*, 2(2) (1989) 105–116.
- [32] Heaney R.P., Functional Indices of Vit D Status and Ramifications of Vit D Deficiency 25, *Am.Journal of Clin. Nutr.*, 80(3) (2018)1706–1709.
- [33] Costa P.R.F., Assis A.M.O., Santos C.A.S.T., Santos D.B., Obesity and Vitamin D Deficiency, *A Systematic Review and Meta Analysis*, 16(4)(2015)341-9.
- [34] Norva M., Wulf H.C., Review Article, Does Chronic Sunscreen Use Reduce Vitamin D Production to Insufficient Levels ?, *British Journal of Dermatology*, 161 (4) (2009) 732–736.
- [35] Cashman K.D., Vitamin D in Childhood and Adolescence, *Postgrad Med J.*, 83(25)(2007) 230–236.
- [36] Rocha R., Cotrim H.P., Carvalho F.M., Siqueira A.C., Braga H., Freitas L.A., Body Mass Index and Waist Circumference in Non Alcoholic Fatty Liver Disease, *J. Hum. Nutr. Diet.*, 18(5) (2005) 365–370.
- [37] Ahmed A.A., Glycemic Control in Diabetes, *Oman Med. J. Jul*, 25(3) (2010) 232–233.
- [38] Kendall D., American Diabetes Association Complete Guide to Diabetes: The Ultimate Home Diabetes Reference. 5th ed., Virginia: American Diabetes Association; 2000.
- [39] Gaziano JM., Hennekens CH., O’Donnell, C.J., Breslow J.L., Buring, JE. Fasting Triglycerides, High Density Lipoprotein, and Risk of Myocardial Infarction, *Circulation*, 96 (1997) 2520–25.
- [40] Miedema K., Standardization of HbA1c and Optimal Range of Monitoring, *Scand J. Clin. Lab., Invest Suppl.*, 240 (2005) 61-72.

Antibiofilm and Antimicrobial Properties of 1-allyl-3-(2-diisopropylaminoethyl) Benzimidazolium Chloride and its Silver(I)-NHC Complex

Uğur Tutar^{1,a,*}, Cem Çelik^{2,b}

¹ Department of Pharmaceutical Botany, Faculty of Pharmacy, Sivas Cumhuriyet University, 58140 Sivas, Türkiye

² Department of Medical Microbiology, Faculty of Medicine, Sivas Cumhuriyet University, 58140 Sivas, Türkiye

*Corresponding author

Research Article

History

Received: 26/05/2022

Accepted: 06/09/2022

Copyright



©2022 Faculty of Science,
Sivas Cumhuriyet University

ABSTRACT

Today, the number of antimicrobials used in treatment has decreased, especially due to drug resistance. We need new antimicrobials. Biofilms are an important cause of antimicrobial resistance. In this study, the antimicrobial and antibiofilm properties of the salt and silver complex of benzimidazolium-based NHC compound, which were previously synthesized and characterized, were evaluated. The antimicrobial properties were tested using the broth microdilution method, while their antibiofilm potential was determined by microtiter plate assay. Salt of the NHC compound (1a) showed antimicrobial activity on microorganisms at concentrations between 31.25-125 µg/mL. The silver complex (2a) of the NHC compound showed higher antimicrobial and antibiofilm activity than the salt compound. This activity was highest on *Candida albicans* yeast (MIC 3.9 µg/mL). Compound 2a reduced the biofilm structure of *C. albicans* yeast by 86.1% compared to the control. In addition, compound 2a showed 76.4-80.6% antibiofilm activity on gram-negative bacteria. NHC compounds are seen as a promising resource for the development of new generation antimicrobials. The NHC compound evaluated in this study was found to have significant antimicrobial and antibiofilm activity. These compounds could be an important resource for the discovery of future biofilm-acting antimicrobials.

Keywords: N-heterocyclic carbene, Silver, Antimicrobial activity, Antibiofilm activity.

ututar@cumhuriyet.edu.tr

<https://orcid.org/0000-0002-8058-0994>

cemcelik58@gmail.com

<https://orcid.org/0000-0002-7141-5874>

Introduction

Microorganisms are very important to live on our planet. These tiny creatures make the world usable for other life. Microbial decomposing communities prevent our world from turning into a garbage dump of dead organisms. They also make other important contributions to all living things [1]. However, microorganisms also cause one of the most important problems in the world, which can cause infectious diseases, impair people's health and even cause death [2]. Antibiotics are used to prevent these harms of microorganisms. The first antibiotic, salvarsan, was introduced in 1910, and in a little over 100 years, antibiotics have drastically changed modern medicine. During this period, the average human lifespan was extended by 23 years. However, since then, there has been a decrease in the number of antimicrobials used in treatment, mainly due to drug resistance and problems in the discovery of new antimicrobials [3].

Antimicrobial resistance is a global public health crisis that prevents us from successfully treating bacterial infections. Many infectious agents that can be successfully treated with one of several drug classes have acquired resistance to almost all of these drugs in some cases [4]. An important reason for the spread of antimicrobial resistance is biofilms. Biofilms are environments where microorganisms live as a community by clinging to a surface and surrounding them with a protected material. Biofilms play an important role in multidrug resistance and cause high morbidity and mortality in infections [5].

New treatment strategies and new antimicrobials are needed to overcome the threats posed by this increase in antimicrobial resistance. Currently, no drug that specifically targets bacterial biofilms is in clinical use. Moreover, the development of new antimicrobial agents is currently declining for different reasons [4,6,7].

N-heterocyclic carbene (NHC) compounds and their silver complexes have antimicrobial activities on microorganisms. Therefore, NHC compounds are seen as a promising reservoir for the development of new generation antimicrobials [8]. In this study, antimicrobial and antibiofilm activities of salt and silver complex of NHC compound, which were previously synthesized and characterized, were evaluated. It is thought that this study will contribute to the literature, especially today, where sufficient new antimicrobials cannot be developed against increasing antimicrobial resistance and there are no antibiotics that will affect biofilms.

Materials and Methods

Compounds

In this study, previously synthesized and characterized 1-Allyl-3-(2-diisopropylaminoethyl)benzimidazolium chloride (1a), Chloro[1-allyl-3-(2-diisopropylaminoethyl)benzimidazol-2-ylidene]silver(I) (2a), [9] were evaluated in terms of antimicrobial and antibiofilm properties. The

Minimal Inhibition Concentration (MIC) test was used to determine the antimicrobial activities of the compounds, and the Biofilm Inhibition Concentration (BIC) test was used to determine the antibiofilm activities.

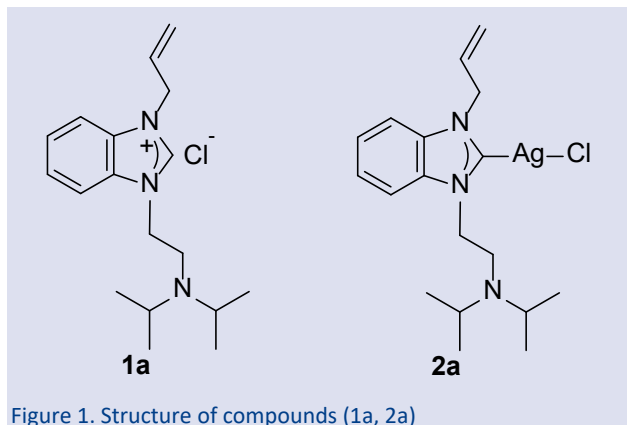


Figure 1. Structure of compounds (1a, 2a)

Microorganisms

In this study, Gram negative bacteria; *Escherichia coli* (ATCC 25922), *Acinetobacter baumannii* (ATCC 17978), Gram positive bacteria; *Staphylococcus aureus* (ATCC 29213), *Enterococcus faecalis* (ATCC 29212), and yeast strain; *Candida albicans* (ATCC 10231) obtained from the standard strains of the American Type Culture Collection were used. Standard microorganisms were stored at -80 °C and revived at room temperature before the study.

Antimicrobial activity

Microdilution method was used to determine the antimicrobial activities of the compounds according to the CLSI [10] recommendations. The minimal inhibitory concentration (MIC) values of the compounds were investigated for the studied strains using the microwell dilution method. Bacterial and fungus cultures were adjusted to 0.5 McFarland standard turbidity (1×10^8 CFU/mL microorganisms) to prepare suspensions of microorganisms.

2 mg of the compound was weighed and dissolved in 4 mL of MHB to prepare a stock solution. For the test, the compounds were dissolved in Mueller-Hinton broth (MHB) containing 10% (v/v) DMSO. Serial twofold dilutions were prepared in 96-well plates with MHB at a concentration ranging from 1.9 to 250 µg/ml.

100 microliters of the prepared solutions were added to each well and all concentrations were distributed in the wells. Then, the microorganisms used in the study (100 microliters) were added to each well to be tested. In the study, ciprofloxacin antibiotic was used for bacteria and Fluconazole was used for fungus as positive control. As negative control, wells containing strains of microorganisms prepared by dispensing 200 microliters without any compound were evaluated. The microplate reader was used to measure the optical density (OD) at 620 nm, and it was measured again following the incubation at 37 °C for 24 h. MIC was determined as the lowest concentration of 1a and 2a that inhibits the growth of test microorganisms.

Reduction in biofilm formation

Microtiter plate assay was used to test the anti-biofilm activity of compounds against microorganisms. One aliquot (100 µL) of culture (1×10^8 CFU/mL) containing 2% (w/v) glucose diluted with Tryptic Soy Broth (TSB) dispensed into a test well. Then, 100 µL of decreasing concentrations of compounds (1.9 to 250 µg/ml) were dispensed into the wells. TSB was used as negative control, and compound-free microorganism cultures alone were used as positive control. After 24 hours of incubation at 37 °C, the supernatants of the wells were decanted and each well was gently rinsed three times with 300 µL of sterile distilled water. After drying the plates for 30 minutes in air, they were stained with 0.1% (w/v) crystal violet for 30 minutes at room temperature. It was washed 3 times with distilled water and dried. The crystal violet was then dissolved in 95% ethanol and absorbance was read in a microplate reader at 570 nm. The biofilm inhibition value at SubMIC was calculated with Eq. [11] Biofilm inhibition (%) = $\{ (A_c - A_s) / A_c \} \times 100$ where A_s and A_c are the absorbance of sample and control, respectively. This test was performed in triplicate and the mean ($n = 3$) was taken.

Results and Discussion

The resistance of pathogenic microorganisms to antimicrobial treatments is increasing at an alarming rate. As a result, there are difficulties in the fight against infections. One of these difficulties is the current shortage of effective drugs. Infections caused by resistant microorganisms do not respond to conventional treatments. New antimicrobials and strategies are needed for the treatment of these infections. On the other hand, studies on finding new antimicrobials effective on resistant microorganisms have decreased considerably in recent years. For this reason, very few new antimicrobial agents have been used in the period [5]. But the spread of antibiotic resistance threatens the successful treatment of infections. New drugs need to be discovered to prevent a pre-antibiotic era from returning [12].

NHCs are typically organic compounds that mimic the chemical properties of phosphines. Since they are easy to prepare and process, they have found wide use and made a significant impact in the field of organometallic chemistry [13]. Historically, silver and its compounds have been used for medicinal applications. Silver compounds have been used especially for wound care antiseptics and for infections. Although its use has been limited by the discovery of new antibiotics, it has gained importance again with the problem of antimicrobial resistance. In recent years, NHCs and their silver complexes have been synthesized for pharmaceutical applications and are widely used as metal-based drug candidates for medical applications [13].

In our study, antimicrobial and antibiofilm activities of benzimidazolium-derived NHC compound salt and silver complex were evaluated. Salt of benzimidazolium-derived NHC compound (1a) showed antimicrobial activity on

microorganisms at concentrations between 31.25-125 µg/mL. Compound 1a showed the highest antimicrobial activity on *C.albicans*, while the activity on *S.aureus* was lower (Table 1). The silver complex of the NHC compound (2a) showed higher antimicrobial activity on the microorganisms in the study than the salt compound this activity reached the highest activity on *C. albicans* yeast

(MIC 3.9 µg/mL). The activity of compound 2a appears to be good compared to the control antifungal Fluconazole. Compound 2a also showed very strong antimicrobial activity on gram-negative bacteria at a concentration of 7.8 µg/mL. The antimicrobial activity of compound 2a on gram-positive bacteria was also found to be strong with a MIC concentration of 15.6 µg/mL (Table 1)

Table 1. Minimum Inhibitory Concentrations (MICs) of Compounds (µg/mL)

Compounds	Microorganism				
	<i>Staphylococcus aureus</i> (ATCC 29213)	<i>Enterococcus faecalis</i> (ATCC 29212)	<i>Escherichia coli</i> (ATCC 25922)	<i>Acinetobacter baumannii</i> (ATCC 17978)	<i>Candida albicans</i> (ATCC 10231)
1a	125	62.5	62.5	62.5	31,25
2a	15.6	15.6	7.8	7.8	3.9
Ciprofloxacin	<1.9	<1.9	<1.9	<1.9	
Fluconazole					<1.9

There are studies in the literature on the antimicrobial properties of silver-bound NHC compounds. Kaloğlu et al. [14] reported that NHC compounds showed antimicrobial activity at concentrations between 6.25 and 100 µg/mL in their study with gram-positive, gram-negative bacteria and yeast strains. When the study results were compared, it was seen that the silver complex we evaluated in our study had higher antimicrobial activity. Mnasri et al. [15] reported that the Ag(I) NHC complexes they synthesized showed strong antimicrobial activity against bacterial and fungal agents at 0.24 and 62.5 µg/ml concentrations. Sari et al. [16] reported that the benzimidazolium-based Ag(I)-NHC compounds they synthesized showed antimicrobial activity at different concentrations on gram-positive, gram-negative bacteria, and fungus strains. Asekunowo et al. [17] stated that Ag(I) NHC complexes showed antibacterial activity on *Staphylococcus aureus* and *Escherichia coli* at concentrations of 12.5-100 µg/mL. When the studies are evaluated, it is understood that the Ag(I)-NHC compound, whose antimicrobial activity was

evaluated in our study, has a very strong antimicrobial activity. For this reason, it would be appropriate to carry out further studies in terms of this compound being one of the new antimicrobials at the present time when new antimicrobials are needed.

Biofilm is a stable collection of microorganisms that settle on any surface in the matrix they produce. Many microorganisms in a living or non-living environment can form a biofilm. Biofilms make an important contribution to the development of resistance of microorganisms to antimicrobial drugs. This leads to the presence of bacteria in biofilms that can cause very important diseases. Today, there are no antibiotics that are effective on biofilms and aim to destroy biofilms. Accordingly, the number of resistant microorganisms is increasing, and the number of drugs that can destroy these microorganisms is gradually decreasing. Therefore, it seems very important to design new biofilm inhibitors as antimicrobial agents targeting the inhibition of biofilm formation [18].

Table 2. Reduction in Biofilm Formation on ½ MIC Value of Compounds (Concentration (µg/mL)/ Biofilm Inhibition (%))

Compounds	Microorganism				
	<i>Staphylococcus aureus</i> (ATCC 29213)	<i>Enterococcus faecalis</i> (ATCC 29212)	<i>Escherichia coli</i> (ATCC 25922)	<i>Acinetobacter baumannii</i> (ATCC 17978)	<i>Candida albicans</i> (ATCC 10231)
1a	62.5/37.7±1.1	31.25/38.6±0.9	31.25/70.5±0.5	31.25/50.8±0.3	15.6/50.8±0.2
2a	7.8/64.6±0.3	7.8/68.1±0.3	3.9/76.4±0.2	3.9/80.6±0.3	1.9/86.1±0.1

In this study, the antibiofilm activities of the salt and metal complex of the Benzimidazolium derivative NHC compound were investigated at ½ MIC concentrations. Salt of the NHC compound (1a) showed 37.7-70.5% antibiofilm activity on two gram-positive and two gram-negative bacteria and one yeast strain used in the study. Compound 1a reduced the biofilm structure formed by *E.coli* bacteria by 70.5% compared to the control. This is a remarkable result. Compound 1a also reduced the biofilm structure of *C. albicans* yeast by more than half compared to the control. Antibiofilm activity of compound 1a on gram-positive bacteria was found to be around 38%. The silver complex of NHC compound (2a) inhibited microorganism biofilms at higher rates than the salt

compound (1a). Compound 2a showed very high antibiofilm activity, especially by reducing the biofilm structure of *C. albicans* yeast by 86.1% compared to the control. In addition, compound 2a showed 76.4-80.6% antibiofilm activity on gram-negative bacteria and 64.6-68.1% on gram-positive bacteria. It was observed that compound 2a had very strong antibiofilm activity on all microorganisms used in the study (Table 2).

Üstün et al. [11] showed the antibiofilm activities of the Ag(I)-NHC compounds they synthesized on gram-positive and negative bacteria and fungal strains. Celik et al. [19] In their study, they reported that Ag(I)-NHC compounds inhibited the biofilm formation of gram-positive and gram-negative bacteria and yeast strains by

32-84% while degrading mature biofilms by 14-66%. Bernardi et al. [20] reported that they found the most effective results in inhibiting biofilms in silver and copper-linked NHC complexes. Şahin et al. [21] reported that the Ag(I) NHC compounds they synthesized found different concentrations of antibiofilm activity on two gram-positive and two gram-negative bacteria and one yeast strain. Tutar et al. [22] They reported that they found strong antibiofilm activity in their study with Ag(I) NHC complexes. Researchers have found up to 90% antibiofilm activity on gram-positive and gram-negative bacteria and yeast strains. It is very important that the newly discovered antimicrobials have antibiofilm properties. In the literature, there are limited studies on the biofilm activities of Ag(I) NHC compounds. Ag(I) NHC compound, whose antibiofilm properties we examined in our study, showed significant antibiofilm activity. Therefore, this compound is considered to have the potential for new antimicrobials.

Conclusion

Rapidly developing resistance to antimicrobials has reduced the number of drugs used for treatment, but not enough new antimicrobials have been discovered. In addition to the antimicrobial activities of the new drugs to be produced, it is very important that they also have antibiofilm properties. New substances need to be discovered for antimicrobial drugs with these properties. In this study, antimicrobial and antibiofilm activities of the salt and silver-based complex of benzimidazolium-derived NHC compound were evaluated. Significant antimicrobial and antibiofilm activity were found in these compounds on two gram-positive and two gram-negative bacteria and one yeast strain. There are publications in the literature on the antimicrobial activities of NHC compounds. However, the number of publications on the antibiofilm activities of these compounds is not high. These compounds could be an important resource in the process of producing antimicrobials of the future. Therefore, further in vitro and in vivo studies would be beneficial.

Acknowledgments

The authors thanks to Neslihan Şahin for providing the compounds, who is an academic at the Faculty of Education, Sivas Cumhuriyet University.

Conflicts of interest

The authors declared that they have no conflict of interest.

References

- [1] Stark L.A., Beneficial Microorganisms: Countering Microbephobia, *CBE Life Sci. Educ.*, 9 (4) (2010) 387-389.
- [2] Institute of Medicine (US) Committee on Emerging Microbial Threats to Health in the 21st Century. Microbial Threats to Health: Emergence, Detection, and Response. Smolinski M.S., Hamburg M.A., Lederberg J., editors. Washington (DC): National Academies Press (US); 2003.
- [3] Hutchings M.I., Truman A.W., Wilkinson B., Antibiotics: Past, Present and Future, *Curr. Opin. Microbiol.*, 51 (2019) 72-80.
- [4] McEwen S.A., Collignon P.J., Antimicrobial Resistance: a One Health Perspective, *Microbiol. Spectr.*, 6 (2) (2018) 1-26.
- [5] Frieri M., Kumar K., Boutin A., Antibiotic Resistance, *J. Infect. Public. Health.*, 10 (4) (2017) 369-378.
- [6] Conly J., Johnston B., Where Are All the New Antibiotics? The New Antibiotic Paradox, *Can. J. Infect. Dis. Med. Microbiol.*, 16 (3) (2005) 159-60.
- [7] Rabin N., Zheng Y., Opoku-Temeng C., Du Y., Bonsu E., Sintim H.O., Biofilm Formation Mechanisms and Targets for Developing Antibiofilm Agents, *Future Med. Chem.*, 7 (4) (2015) 493-512.
- [8] Liang J., Sun D., Yang Y., Li M., Li H., Chen L., Discovery of Metal-Based Complexes as Promising Antimicrobial Agents, *Eur. J. Med. Chem.*, 224 (2021) 113696.
- [9] Şahin-Yıldırım E., Şahin N., Synthesis and Structural Characterization of Chloro [1-allyl-3-(2-diisopropylaminoethyl) benzimidazol-2-ylidene] silver(I), *Ordu Univ. J. Sci. Tech.*, 10 (2) (2020) 66-75.
- [10] Clinical and Laboratory Standards Institute (CLSI), Performance Standards for Antimicrobial Susceptibility Testing, Twenty-Fourth Informational Supplement, CLSI document M100-S24, Wayne, PA, 2014.
- [11] Üstün E., Şahin N., Çelik C., Tutar U., Özdemir N., Gürbüz N., Özdemir İ., Synthesis, Characterization, Antimicrobial and Antibiofilm Activity, and Molecular Docking Analysis of NHC Precursors and Their Ag-NHC Complexes, *Dalton. Trans.*, 50 (42) (2021) 15400-15412.
- [12] Waglechner N., Culp E.J., Wright G.D., Ancient Antibiotics, Ancient Resistance, *EcoSal Plus.*, 9 (2) (2021) ESP-0027-2020.
- [13] A.Patil S., P.Hoagland A., A.Patil S., Bugarin A., N-Heterocyclic Carbene-Metal Complexes as Bio-Organometallic Antimicrobial and Anticancer Drugs, an Update (2015-2020), *Future Med. Chem.*, 12 (24) (2020) 2239-2275.
- [14] Kaloğlu M., Kaloğlu N., Günel S., Özdemir İ., Synthesis of N-Heterocyclic Carbene-Based Silver Complexes and Their Antimicrobial Properties Against Bacteria and Fungi, *J. Coord. Chem.*, 74 (17-20) (2021) 3031-3047.
- [15] Mnasri A., Mejri A., Al-Hazmy S.M., Arfaoui Y., Özdemir İ., Gürbüz N., Hamdi N., Silver-N-Heterocyclic Carbene Complexes-Catalyzed Multicomponent Reactions: Synthesis, Spectroscopic Characterization, Density Functional Theory Calculations, and Antibacterial Study, *Arch. Pharm. (Weinheim)*, 354 (9) (2021) e2100111.
- [16] Sarı Y., Akkoç S., Gök Y., Sifniotis V., Özdemir İ., Günel S., Kayser V., Benzimidazolium-Based Novel Silver N-Heterocyclic Carbene Complexes: Synthesis, Characterisation and In vitro Antimicrobial Activity, *J. Enzyme Inhib. Med. Chem.*, 31 (6) (2016) 1527-1530.

- [17] Asekunowo P.O., Haque R.A., Razali M.R., Avicor S.W., Wajidi M.F.F., Synthesis and Characterization of Nitrile Functionalized Silver(I)-N-Heterocyclic Carbene Complexes: DNA Binding, Cleavage Studies, Antibacterial Properties and Mosquitocidal Activity Against the Dengue Vector, *Aedes Albopictus*, *Eur. J. Med. Chem.*, 150 (2018) 601-615.
- [18] Nadar S., Khan T., Patching S.G., Omri A., Development of Antibiofilm Therapeutics Strategies to Overcome Antimicrobial Drug Resistance, *Microorganisms*, 10 (2) (2022) 303.
- [19] Celik C., Tutar U., Sahin N., Ozturk A., Antimicrobial, Anti-biofilm and Cytotoxic Properties of Methallyl Functionalized Benzimidazolium-Derived Ag(I)-N-Heterocyclic Carbene Complexes, *Trop. J. Pharm. Res.*, 21 (4) (2022) 817-823.
- [20] Bernardi T., Badel S., Mayer P., Groelly J., de Frémont P., Jacques B., Braunstein P., Teyssot M.L., Gaulier C., Cisnetti F., Gautier A., Roland S., High-Throughput Screening of Metal-N-Heterocyclic Carbene Complexes Against Biofilm Formation by Pathogenic Bacteria, *ChemMedChem.*, 9 (6) (2014) 1140-1144.
- [21] Şahin N., Üstün E., Tutar U., Çelik C., Gürbüz N., Özdemir İ., Antimicrobial Activity, Inhibition of Biofilm Formation, and Molecular Docking Study of Novel Ag-NHC Complexes, *J. Organomet. Chem.*, 954–955 (2021) 122082.
- [22] Tutar U., Çelik C., Şahin N., Allyl Functionalized Benzimidazolium-Derived Ag(I)-N-Heterocyclic Carbene Complexes: Anti-Biofilm and Antimicrobial Properties, *Pharm. Chem. J.*, 56 (1) (2022) 54–60.

Some Heterocyclic Hydrazone Compounds: Synthesis, Spectral Characterization and Anticancer Activity Study

Eyüp Başaran ^{1,a,*}, Reşit Çakmak ^{2,b}, Ercan Çınar ^{3,c}, Özge Çevik ^{4,d}

¹ Department of Chemistry and Chemical Processing Technologies, Vocational School of Technical Sciences, Batman University, 72060, Batman, Türkiye

² Medical Laboratory Techniques Program, Vocational School of Health Services, Batman University, 72060, Batman, Türkiye

³ Department of Nursing, Faculty of Health Sciences, Batman University, 72060, Batman, Türkiye

⁴ Department of Biochemistry, Faculty of Medicine, Adnan Menderes University, 09010, Aydın, Türkiye

*Corresponding author

Research Article

History

Received: 06/04/2022

Accepted: 07/09/2022

Copyright



©2022 Faculty of Science,
Sivas Cumhuriyet University

ABSTRACT

Cancer is currently ongoing to be a significant health problem threatening human health. Hydrazone compounds constitute a popular class of organic compounds used in novel drug discovery studies in therapy of cancer. In the current study, the preparation and structural characterization of some heterocyclic hydrazone compounds (7-12) and their anticancer capacities against HeLa cervical cancer and MCF-7 breast cancer cell lines were reported. The target compounds were characterized by some spectroscopic techniques (¹H NMR, ¹³C NMR and FT-IR). The *in vitro* cytotoxic potentials of the target molecules were assessed by using MTT assay against two cancer cell lines. L929 mouse fibroblast cell lines were employed as normal cell. The results displayed that some of the tested molecules had varying anticancer activities. Among the tested compounds, compound 8 indicated anticancer activity against HeLa cells with IC₅₀ value of 34.38 μM. On the other hand, of these tested compounds, compound 11 (IC₅₀ = 26.84 μM) displayed anticancer activity against MCF-7 cells.

Keywords: Hydrazone derivatives, Anticancer activity, Breast cancer, Cervical cancer.

^a eyup.basaran@batman.edu.tr

^{ib} <https://orcid.org/0000-0002-7840-5919>

^c ercan.cinar@batman.edu.tr

^{ib} <https://orcid.org/0000-0003-0419-7798>

^b resit.cakmak@batman.edu.tr

^{id} <https://orcid.org/0000-0003-0401-7419>

^d drozgecevik@gmail.com

^{id} <https://orcid.org/0000-0002-9325-3757>

Introduction

Cancer is a disease that occurs as a result of uncontrolled proliferation and growth of cells in the human body [1]. Cancer cells can affect a single tissue as well as spread to other tissues and show their effects [2-4]. Today, different approaches and treatments specific to each cancer type are applied in clinical practice to combat this disease. In recent years, treatment methods based on different principles such as chemotherapy, radiotherapy, surgery, stem cell therapy, immunotherapy, hormone therapy and gene therapy have been utilized in the therapy of different types of cancer. These methods are applied either alone or in combination. There is currently no ideal treatment method for each of the existing cancer types, since the treatment methods applied have advantages and disadvantages in the treatment process of each cancer patient and the treatments may differ from patient to patient [5-6]. This disease is accepted as one of the biggest health problems facing humanity. Many scientists are still carrying out researches on the treatment of this disease. Depending on the scientific developments in this subject, important developments have occurred in the discovery of novel and effective drugs to be used in the therapy of cancer, with the detection of new intracellular pathways, target enzymes and proteins, and drug-effect mechanisms associated with cancer [7,8]. Chemotherapy is one of the most commonly used treatment methods in clinical practice for

cancer patients to eradicate of cancer cells using chemotherapeutic agents. In cancer chemotherapy, the main purpose is to prevent the growth and spread of the existing tumor to other parts of the body with the chemotherapeutic agents used, and to create a cytotoxic effect that will ensure the complete eradication of the tumor as much as possible. However, the vast majority of cancer types cannot be fully treated with the chemotherapeutic agents and their combinations still used today, and the available drugs in this regard are insufficient [8-13].

Cervical cancer and breast cancer are among the cancer types with high incidence and mortality rates compared to other types of cancer. According to the report prepared with data obtained from 185 countries by the International Agency for Research on Cancer, cervical cancer is the fourth most frequently diagnosed cancer and the fourth leading cause of cancer death in women, with an estimated more than 600,000 novel cases and nearly 350,000 deaths worldwide in 2020. On the other hand, breast cancer is the type of cancer that surpasses lung cancer as the leading cause of global cancer incidence, with an estimated 2.3 million new cases representing 11.7% of all cancer cases according to the same report [14]. As with other types of cancer, suitable chemotherapeutic agents with the desired cytotoxic effect for these cancer types have still not been

discovered today [15]. Therefore, we have decided to investigate the cytotoxic effects of the synthesized molecules on cervical cancer and breast cancer cell lines in this research.

Heterocycles are the cyclic organic compounds, which contain at least one heteroatom. These compounds constitute the largest and most important family of organic compounds. Heterocyclic compounds are obtained synthetically or from plant extracts. There are many known heterocyclic compounds today. The number of these compounds increasing day by day. In studies conducted to examine the biological importance of these compounds, it was determined that most of them were bioactive molecules. These compounds have attracted great interest of many researchers recently due to their biological activities. It is known that most of them indicate antifungal, antibacterial, antidiabetic, enzyme inhibitory, antioxidant and anticancer activities [16].

Hydrazone derivatives, obtained by coupling hydrazide compounds with aldehydes and ketones, represent an important class of bioactive compounds that have attracted the attention of medicinal chemists due to their broad biological activities. Therefore, this class of organic compounds in medicinal chemistry is being used to discover the needed drugs in order to combat some diseases including various types of cancer [17-19]. Recently, it has been reported in many studies that hydrazone derivatives are molecules with anticancer activity [20-25]. On the other hand, it has been reported in some studies that organic molecules with nitro and methoxy functional groups as substituents show various biological activities [26, 27]. Therefore, we have preferred to use the starting molecules that have with nitro and methoxy functional groups as substituents in the synthesis of new heterocyclic hydrazone molecules with anticancer activity in this study.

The target of this study is to perform the synthesis and characterization of some heterocyclic hydrazone derivatives (7-12) and investigate for their anticancer properties against HeLa and MCF-7 cancer cell lines. To determine anticancer behavior of the synthesized compounds (1-12) on normal (non-cancer) cells, L929 mouse fibroblast cell lines were employed in this study. The target molecules were characterized by spectroscopic methods.

Materials and Methods

Chemistry

All chemicals required for the preparation of anticancer agents (1-12) and the determination studies of their anticancer activity were procured from Merck and Sigma Aldrich companies. These chemicals were of analytical grade, and employed without further purification. The reaction processes of the compounds were monitored by thin layer chromatography. FT-IR spectra was recorded using a Cary 630 FTIR spectrometer with the diamond ATR module at a scan range of 4000-400 cm^{-1} . ^1H - and ^{13}C NMR spectra were taken on a Bruker

AVANCE III 400 MHz spectrometer using tetramethylsilane as the internal reference at 400 and 100 MHz. Dimethyl sulfoxide (DMSO) was used as a solvent in NMR analysis. Melting points were determined on a Barnstead IA9100 electrothermal digital melting points apparatus.

General procedure for the synthesis of hydrazone derivatives

In this research, hydrazone compounds (7-12) were prepared by the condensation reaction of nicotinic acid hydrazide with benzaldehyde ester derivatives derived from two benzaldehyde derivatives as starting compounds [17, 18, 28, 29]. The esters (1-6) derived from benzaldehyde derivatives were synthesized and characterized in our previous studies [28, 29].

N'-(4-((3-Nitrobenzoyl)oxy)benzylidene)nicotinohydrazide (7)

White solid. Yield: 69%. M.p. 232-233 °C. FT-IR ν_{max} (cm^{-1}): 3263 (N-H str.), 3094, 3068 (aromatic C-H, str.), 1738 (C=O str.), 1652 (C=O str.), 1605 (C=N str.), 1530 (asymmetric, NO_2 str.), 1347 (symmetric, NO_2 str.). ^1H NMR (300 MHz, $\text{DMSO-}d_6$) δ /ppm: 12.11 (s, 1H, CONH), 9.09 (d, $J = 2.1$ Hz, 1H, Pyr-H), 8.85 – 8.73 (m, 2H, Pyr-H and Ar-H), 8.64 – 8.54 (m, 2H, Pyr-H), 8.51 (s, 1H, CH=N), 8.28 (d, $J = 7.9$ Hz, 1H, Ar-H), 7.96 – 7.87 (m, 3H, Pyr-H and Ar-H), 7.58 (dd, $J = 7.8, 4.9$ Hz, 1H, Ar-H), 7.48 (d, $J = 8.5$ Hz, 2H, Ar-H). ^{13}C NMR (75 MHz, $\text{DMSO-}d_6$) δ /ppm: 163.27 (C=O), 162.21 (C=O), 152.80 (CH=N), 152.15, 149.08, 148.45, 147.86, 136.36, 135.95, 132.80, 131.42, 130.96, 129.60, 128.96, 128.93, 124.71, 124.09, 122.92 (Pyr-C and Ar-C).

N'-(4-((3-Nitrobenzoyl)oxy)-3-ethoxybenzylidene)nicotinohydrazide (8)

White solid. Yield: 73%. Mp. 223-224 °C. FT-IR ν_{max} (cm^{-1}): 3243 (N-H str.), 3101, 3061 (aromatic C-H, str.), 2938, 2871 (aromatic C-H, str.), 1744 (C=O str.), 1649 (C=O str.), 1591 (C=N str.), 1535 (asymmetric, NO_2 str.), 1346 (symmetric, NO_2 str.). ^1H NMR (300 MHz, $\text{DMSO-}d_6$) δ /ppm: 12.12 (s, 1H, CONH), 9.14 – 9.04 (m, 1H, Pyr-H), 8.83 – 8.74 (m, 2H, Pyr-H and Ar-H), 8.69 – 8.51 (m, 3H, Pyr-H and Ar-H), 8.50 (s, 1H, CH=N), 7.94 (t, $J = 8.0$ Hz, 1H, Ar-H), 7.62 – 7.55 (m, 2H, Pyr-H and Ar-H), 7.46 – 7.40 (m, 2H, Ar-H), 3.87 (s, 3H, $-\text{OCH}_3$). ^{13}C NMR (75 MHz, $\text{DMSO-}d_6$) δ /ppm: 162.71 (C=O), 162.26 (C=O), 152.82 (CH=N), 151.57, 149.08, 148.55, 148.13, 141.03, 136.33, 135.97, 134.10, 131.56, 130.41, 129.63, 129.08, 124.69, 124.10, 123.87, 121.19, 110.57 (Pyr-C and Ar-C), 56.49 ($-\text{OCH}_3$).

N'-(4-((4-Nitrobenzoyl)oxy)benzylidene)nicotinohydrazide (9)

White solid. Yield: 78%. Mp. 252-253 °C. FT-IR ν_{max} (cm^{-1}): 3242 (N-H str.), 3109, 3071 (aromatic C-H, str.), 1728 (C=O str.), 1656 (C=O str.), 1601 (C=N str.), 1514 (asymmetric, NO_2 str.), 1343 (symmetric, NO_2 str.). ^1H NMR (300 MHz, $\text{DMSO-}d_6$) δ /ppm: 12.10 (s, 1H, CONH), 9.11 – 9.07 (m, 1H, Pyr-H), 8.78 (d, $J = 4.9$ Hz, 1H, Pyr-H),

8.51 (s, 1H, CH=N), 8.45 – 8.37 (m, 4H, Ar-H), 8.28 (d, J = 8.0 Hz, 1H, Pyr-H), 7.89 (d, J = 8.5 Hz, 2H, Ar-H), 7.60 – 7.56 (m, 1H, Pyr-H), 7.48 (d, J = 8.6 Hz, 2H, Ar-H). ¹³C NMR (75 MHz, DMSO-*d*₆) δ/ppm: 163.49 (C=O), 162.21 (C=O), 152.81 (CH=N), 152.18, 151.10, 149.08, 147.86, 135.95, 134.80, 132.79, 131.83, 129.61, 128.96, 124.50, 124.10, 122.90 (Pyr-C and Ar-C).

N'-(4-((4-Nitrobenzoyl)oxy)-3-methoxybenzylidene)nicotinohydrazide (10)

White solid. Yield: 71%. Mp. 226-227 °C. FT-IR ν_{\max} (cm⁻¹): 3184 (N-H str.), 3049, 3006 (aromatic C-H, str.), 2919, 2850 (aromatic C-H, str.), 1743 (C=O str.), 1646 (C=O str.), 1594 (C=N str.), 1523 (asymmetric, NO₂ str.), 1345 (symmetric, NO₂ str.). ¹H NMR (300 MHz, DMSO-*d*₆) δ/ppm: 12.11 (s, 1H, CONH), 9.09 (d, J = 1.6 Hz, 1H, Pyr-H), 8.79 (dd, J = 4.9, 1.4 Hz, 1H, Pyr-H), 8.49 (s, 1H, CH=N), 8.45 – 8.37 (m, 4H, Pyr-H and Ar-H), 8.28 (d, J = 8.0 Hz, 1H, Ar-H), 7.63 – 7.56 (m, 2H, Pyr-H and Ar-H), 7.44 (d, J = 8.4 Hz, 2H, Ar-H), 3.87 (s, 3H, -OCH₃). ¹³C NMR (75 MHz, DMSO-*d*₆) δ/ppm: 162.96 (C=O), 162.26 (C=O), 152.82 (CH=N), 151.55, 151.19, 149.08, 148.13, 141.07, 135.96, 134.28, 134.09, 131.85, 129.64, 124.63, 124.11, 123.85, 121.18, 110.58 (Pyr-C and Ar-C), 56.50 (-OCH₃).

N'-(4-((3,5-Bisnitrobenzoyl)oxy)benzylidene)nicotinohydrazide (11)

White solid. Yield: 65%. Mp. 250-251 °C. FT-IR ν_{\max} (cm⁻¹): 3237 (N-H str.), 3107, 3025 (aromatic C-H, str.), 1746 (C=O str.), 1650 (C=O str.), 1591 (C=N str.), 1537 (asymmetric, NO₂ str.), 1344 (symmetric, NO₂ str.). ¹H NMR (300 MHz, DMSO-*d*₆) δ/ppm: 12.10 (s, 1H, CONH), 9.14 – 9.11 (m, 4H, Pyr-H and Ar-H), 8.79 (d, J = 4.7 Hz, 1H, Pyr-H), 8.51 (s, 1H, CH=N), 8.29 (d, J = 8.0 Hz, 1H, Pyr-H), 7.91 (d, J = 8.4 Hz, 2H, Ar-H), 7.60 – 7.51 (m, 3H, Pyr-H and Ar-H). ¹³C NMR (75 MHz, DMSO-*d*₆) δ/ppm: 162.22 (C=O), 161.89 (C=O), 152.82 (CH=N), 151.95, 149.06, 148.89, 147.79, 135.95, 133.01, 132.57, 129.91, 129.61, 129.00, 124.13, 123.59, 122.83 (Pyr-C and Ar-C).

N'-(4-((3,5-Bisnitrobenzoyl)oxy)-3-methoxybenzylidene)nicotinohydrazide (12)

White solid. Yield: 68%. Mp. 247-248 °C. FT-IR ν_{\max} (cm⁻¹): 3232 (N-H str.), 3089, 3071 (aromatic C-H, str.), 2994, 2881 (aromatic C-H, str.), 1750 (C=O str.), 1653 (C=O str.), 1594 (C=N str.), 1537 (asymmetric, NO₂ str.), 1347 (symmetric, NO₂ str.). ¹H NMR (300 MHz, DMSO-*d*₆) δ/ppm: 12.12 (s, 1H, CONH), 9.14 – 9.08 (m, 4H, Pyr-H and Ar-H), 8.79 (d, J = 4.3, 1.4 Hz, 1H, Pyr-H), 8.50 (s, 1H, CH=N), 8.28 (d, J = 7.9 Hz, 1H, Pyr-H), 7.60 (d, J = 7.7 Hz, 2H, Ar-H), 7.51 – 7.41 (m, 2H, Pyr-H and Ar-H), 3.88 (s, 3H, -OCH₃). ¹³C NMR (75 MHz, DMSO-*d*₆) δ/ppm: 162.27 (C=O), 161.26 (C=O), 152.83 (CH=N), 151.43, 149.07, 148.03, 140.72, 135.99, 134.36, 131.72, 129.88, 129.63, 124.12, 123.79, 121.17, 110.69 (Pyr-C and Ar-C), 56.55 (-OCH₃).

Anticancer Assay

The cytotoxic activities of the target molecules (7-12) were evaluated by using MTT assay against two cancer cell lines (HeLa and MCF-7). In this study, L929 mouse normal

fibroblast cell lines were employed as control cells [28-30]. The percentage of cell viability was measured at 570 nm by using ELISA reader (Epoch, Biotek, USA). MTT assay was performed triplicate. Also, the effects on the cells of each compound were assessed by inverted microscope (Zeiss Axiovert). Moreover, the IC₅₀ values of the tested molecules on these cell lines were calculated by utilizing AATbio IC₅₀ calculator.

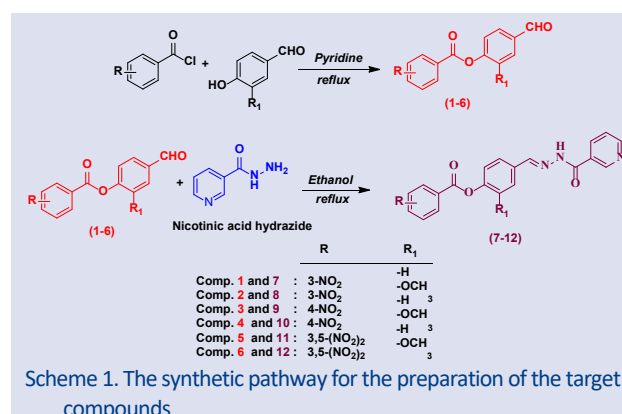
Statistical Analysis

In this research, data were gathered from three different biological replicates, and the findings were plotted as mean ± SD. One-way ANOVA was employed as statistical analysis by GraphPad Prism 7. P-value <0.05 was considered statistically important.

Results and Discussion

Chemistry

In this study, the target compounds were synthesized with high yield in two steps according to our previous studies. In the first step, six benzaldehyde ester derivatives were obtained by the reaction of two benzaldehyde derivatives (4-hydroxybenzaldehyde and 4-hydroxy-3-methoxybenzaldehyde) with substituted benzoyl chloride derivatives (3-nitrobenzoyl chloride, 4-nitrobenzoyl chloride and 3,5-dinitrobenzoyl chloride) in a pyridine medium, respectively [21,22]. In the second step, hydrazone derivatives were readily acquired via condensation reaction of nicotinic acid hydrazide with benzaldehyde ester derivatives in ethanol medium (Scheme 1). Three of the target compounds (8, 11 and 12) are new, and the others are known compounds (7, 9 and 10). All synthesis reactions were monitored by thin layer chromatography.



In this research, the target compounds (7-12) were characterized by FT-IR, ¹H- and ¹³C NMR. Their characterization data were found to be compatible with their molecule structures. In FT-IR spectra of compounds (7-12), the band representing carbonyl group (C=O) of the ester, C=O of hydrazide and imino (-C=N), appeared at 1750 – 1728 cm⁻¹, 1656 – 1646 cm⁻¹, and 1605 – 1591 cm⁻¹, respectively. In addition, asymmetric and symmetric bands of the nitro (NO₂) group in these compounds were

detected as 1537 – 1514 cm^{-1} and 1343 – 1347 cm^{-1} . In ^1H NMR spectra of (7-12), the signal due to the azomethine proton ($-\text{CH}=\text{N}$) appeared in the region 8.49 – 8.51 ppm. Signals of the CONH proton were determined in the range of approximately 12 ppm. Pyridine ring and aromatic rings protons were observed at 9.14 – 7.40 ppm. Also, methoxy ($-\text{OCH}_3$) protons found in the structures of compounds 8, 10, and 12 were observed at 3.87 – 3.88 ppm. In their ^{13}C NMR spectra, the signal due to $-\text{CH}=\text{N}$ carbon was observed at 152.80 – 152.83 ppm. The signal originating from the $\text{C}=\text{O}$ carbon of the hydrazide was observed in the region of 161.89 – 162.26 ppm, while the signal originating from the $\text{C}=\text{O}$ carbon of the ester was determined in the region 162.22 – 163.49 ppm. Furthermore, the signal due to the $-\text{OCH}_3$ carbon was detected at 56.49 – 56.55 ppm. Other carbons belonging to pyridine and aromatic rings were observed in the expected regions. On the other hand, these results were found to be compatible with the literature [31-34].

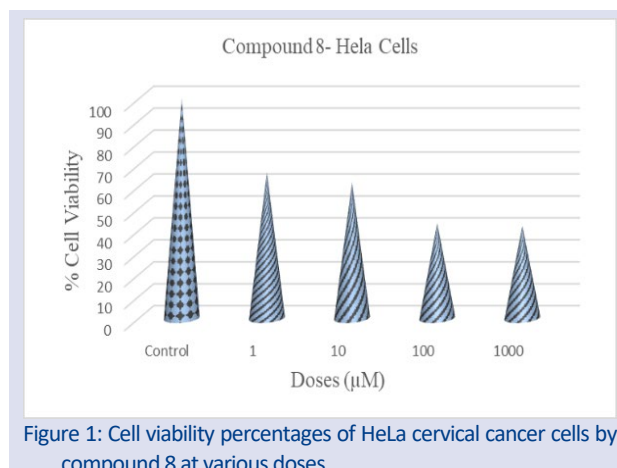
Anticancer Activity Results

In this research, the anticancer activities of synthesized hydrazone derivatives were assessed on HeLa, MCF-7 and L929 (mouse fibroblast) cell lines using MTT assay. Cisplatin was used as the standard compound. IC_{50} values of tested molecules and cisplatin are presented in Table 1.

Table 1. IC_{50} values of the synthesized hydrazone derivatives (7-12)

Compounds	HeLa (μM)	MCF-7 (μM)	L929 (μM)
7	67.78 \pm 3.98	569.12 \pm 55.10	598.60 \pm 56.72
8	34.38 \pm 2.99	107.71 \pm 10.28	204.90 \pm 20.33
9	128.5 \pm 13.65	635.41 \pm 53.45	453.02 \pm 41.08
10	240.26 \pm 21.71	246.22 \pm 21.76	59.55 \pm 6.03
11	89.1 \pm 9.45	26.84 \pm 4.35	10.76 \pm 2.78
12	364.73 \pm 30.57	215.41 \pm 25.49	324.65 \pm 34.49
Cisplatin	28.33 \pm 4.20	10.06 \pm 2.15	240.65 \pm 5.85

In this research, a total of six hydrazone compounds were synthesized for anticancer assay. When the cytotoxic activity results in Table 1 were examined, it was determined that all synthesized compounds displayed the cytotoxic activities with IC_{50} values ranging from 34.38 to 364.73 μM against HeLa cervical cancer cell lines. Amongst the tested compounds, the most ideal chemotherapeutic candidate is the 8-coded compound whose IC_{50} values were calculated as 34.38 μM and 204.90 μM in HeLa and L929 cell lines, respectively (Table 1). On the other hand, these molecules displayed anticancer activities at concentrations between 26.84 and 635.41 μM against MCF-7 breast cancer cell lines. Amongst these compounds, we found that compound **11** exhibited high cytotoxic activity on MCF-7 breast cancer cells with the IC_{50} value of 26.84. However, this compound had also cytotoxic effect on mouse fibroblast L929 cells with IC_{50} =10.76 μM . Therefore, compound **11** was not evaluated as a drug candidate because it had a toxic effect on healthy cells.



Conclusion

This study is conducted to discover novel anticancer drug candidates that are effective and have no side effects. For this purpose, we successfully synthesized six hydrazone derivatives, and then their characterization processes were performed by three spectroscopic techniques. The anticancer activities of the synthesized hydrazone derivatives on HeLa cervical and MCF-7 breast cancer cells were determined. It was determined that these molecules (7-12) displayed anticancer activities with IC_{50} values ranging from 26.84 to 635.41 μM . However, we determined that these molecules showed lower anticancer activities than the reference molecule. The results showed that two of the tested compounds (8 and 11) may be promising scaffolds for the discovery studies of new anticancer agents.

Conflicts of interest

The authors declare that they have no conflict of interest

References

- [1] De Silva D.D., Rapior S., Fons F., Bahkali A.H., Hyde, K.D., Medicinal mushrooms in supportive cancer therapies: an approach to anti-cancer effects and putative mechanisms of action, *Fungal Divers.*, 55(1) (2012) 1-35.
- [2] Atmaca H., Oğuz F., İlhan S., Drug delivery systems for cancer treatment: a review of marine-derived polysaccharides, *Curr. Pharm. Des.*, (2022).
- [3] Küpeli Akkol E., Genç Y., Karpuz B., Sobarzo-Sánchez E., Capasso, R., Coumarins and coumarin-related compounds in pharmacotherapy of cancer, *Cancers.*, 12(7) (2020) 1959.
- [4] Kashyap D., Garg V.K., Sandberg E.N., Goel N., Bishayee, A., Oncogenic and tumor suppressive components of the cell cycle in breast cancer progression and prognosis, *Pharmaceutics.*, 13(4) (2021) 569.
- [5] Luna J.I., Grossenbacher S.K., Murphy W.J., Canter, R.J., Targeting cancer stem cells with natural killer cell immunotherapy, *Expert Opin. Biol. Ther.*, 17(3) (2017) 313-324.

- [6] Weiss, T., Weller M., Roth, P., Immunological effects of chemotherapy and radiotherapy against brain tumors, *Expert Rev. Anticancer Ther.*, 16(10) (2016) 1087-1094.
- [7] Scarpa E.S., Fabrizio G., Di Girolamo M., A role of intracellular mono-ADP-ribosylation in cancer biology, *The FEBS J.*, 280(15) (2013) 3551-3562.
- [8] Mansoori B., Mohammadi A., Davudian S., Shirjang S., Baradaran, B., The different mechanisms of cancer drug resistance: a brief review, *Adv. Pharm. Bull.*, 7(3) (2017) 339-348.
- [9] Longley D.B., Johnston P.G., Molecular mechanisms of drug resistance, *J. Pathol.*, 205(2) (2005) 275-292.
- [10] Goodman L.S., Wintrobe M.M., Dameshek W., Goodman M.J., Gilman A., McLennan M.T., Nitrogen mustard therapy: Use of methyl-bis (beta-chloroethyl) amine hydrochloride and tris (beta-chloroethyl) amine hydrochloride for hodgkin's disease, lymphosarcoma, leukemia and certain allied and miscellaneous disorders, *JAMA*, 132(3) (1946) 126-132.
- [11] Barinaga M., From bench top to bedside, *Sci.*, 278(5340) (1997) 1036-1039.
- [12] Calabresi P., Welch A.D., Chemotherapy of neoplastic diseases, *Annu. Rev. Med.*, 13(1) (1962) 147-202.
- [13] Carter S.K., Slavik M., Chemotherapy of cancer, *Annu. Rev. Pharmacol.*, 14(1) (1974) 157-179.
- [14] Sung H., Ferlay J., Siegel R.L., Laversanne M., Soerjomataram I., Jemal A., Bray F., Global cancer statistics 2020: GLOBOCAN estimates of incidence and mortality worldwide for 36 cancers in 185 countries, *CA cancer J. Clin.*, 71(3) (2021) 209-249.
- [15] Cancer, UK, How Chemotherapy Drugs Work. Available at: <https://www.cancer.org/treatment/treatments-and-side-effects/treatment-types/chemotherapy/how-chemotherapy-drugs-work.html>, 2021 (accessed 28 Mar 2022).
- [16] Al-Mulla A., A review: biological importance of heterocyclic compounds, *Der Pharma Chem.*, 9(13) (2017) 141-147.
- [17] Çakmak R., Başaran E., Kaya S., Erkan S., Synthesis, spectral characterization, chemical reactivity and anticancer behaviors of some novel hydrazone derivatives: Experimental and theoretical insights, *J. Mol. Struct.*, 1253 (2022) 132224.
- [18] Başaran E., Haşimi N., Çakmak R., Çınar E., Synthesis, structural characterization, and biological evaluation of some hydrazone compounds as potential antioxidant agents, *Russ. J. Bioorganic Chem.*, 48(1) (2022) 143-152.
- [19] Tabbiche A., Bouchama A., Chafai N., Zaidi F., Chiter C., Yahiaoui M., Abiza A., New bis hydrazone: synthesis, x-ray crystal structure, DFT computations, conformational study and in silico study of the inhibition activity of SARS-CoV-2, *J. Mol. Struct.*, 1261 (2022) 132865.
- [20] Aydın S., Kaushik-Basu N., Arora P., Basu A., Nichols D.B., Talele T.T., Akkurt M., Çelik I., Büyükgüngör O., Kucukguzel Ş.G., Microwave assisted synthesis of some novel flurbiprofen hydrazone-hydrazones as anti-hcv ns5b and anticancer agents, *Marmara Pharm. J.*, 17(1) (2013) 26-34.
- [21] Şenkardeş S., Türe A., Ekrek S., Durak A.T., Abbak M., Çevik Ö., Kaşkatepe B., Küçükgülzel İ., Küçükgülzel G., Novel 2,6-disubstituted pyridine hydrazones: synthesis, anticancer activity, docking studies and effects on caspase-3-mediated apoptosis, *J. Mol. Struct.*, 1223(2021) 128962-128969.
- [22] Şenkardeş S., Han M.İ., Kulabaş N., Abbak M., Çevik Ö., Küçükgülzel İ., Küçükgülzel G., Synthesis, molecular docking and evaluation of novel sulfonyl hydrazones as anticancer agents and COX-2 inhibitors, *Mol. Divers.*, 24(3) (2020) 673-689.
- [23] Şenkardeş S., Kaushik-Basu N., Durmaz I., Manvar D., Basu A., Atalay R., Kucukguzel, S.G., Synthesis of novel diflunisal hydrazide-hydrazones as anti-hepatitis c virus agents and hepatocellular carcinoma inhibitors, *Eur. J. Med. Chem.*, 108(27) (2016) 301-308.
- [24] Aktar B.S.K., Sıcak Y., Tok T.T., Oruc-Emre E.E., Yağlıoğlu A.Ş., İyidoğan A K., Öztürk M., Demirtaş I., Designing heterocyclic chalcones, benzoyl/sulfonyl hydrazones: An insight into their biological activities and molecular docking study, *J. Mol. Struct.*, 1211 (2020) 128059.
- [25] Karaman N., Sıcak Y., Taşkın-Tok T., Öztürk M., Karaküçük-İyidoğan A., Dikmen M., Oruç-Emre E.E., New piperidine-hydrazone derivatives: Synthesis, biological evaluations and molecular docking studies as AChE and BChE inhibitors, *Eur. J. Med. Chem.*, 124 (2016) 270-283.
- [26] Çakmak R., Başaran E., Şentürk M., Synthesis, characterization, and biological evaluation of some novel Schiff bases as potential metabolic enzyme inhibitors, *Arch. Pharm.*, 355(4) (2022) 2100430.
- [27] Qin H.L., Zhang Z.W., Ravindar L., Rakesh K.P., Antibacterial activities with the structure-activity relationship of coumarin derivatives, *Eur. J. Med. Chem.*, 207 (2020) 112832.
- [28] Çınar E., Başaran E., Erdoğan Ö., Çakmak R., Boğa M., Çevik Ö., Heterocyclic Schiff base derivatives containing pyrazolone moiety: Synthesis, characterization, and *in vitro* biological studies, *J. Chin. Chem. Soc.*, 68(12) (2021) 2355-2367.
- [29] Çakmak R., Başaran E., Boğa M., Erdoğan Ö., Çınar E., Çevik Ö., Schiff base derivatives of 4-aminoantipyrine as promising molecules: synthesis, structural characterization and biological activities, *Russ. J. Bioorganic Chem.*, 48(2) (2022).
- [30] Paşa S., Erdogan Ö., Cevik Ö., Design, synthesis and investigation of procaine based new Pd complexes as DNA methyltransferase inhibitor on gastric cancer cells, *Inorg. Chem. Commun.*, 132 (2021) 108846.
- [31] Sıcak Y., Investigation of antioxidant, anticholinesterase inhibitory, tyrosinase inhibitory and urease inhibitory activities of some hydrazone derivatives, *Turk. J. Life Sci.*, 2(2) (2017) 165-170.
- [32] Bozkurt E., Sıcak Y., Oruç-Emre E.E., İyidoğan A.K., Öztürk M., Design and bioevaluation of novel hydrazide-hydrazones derived from 4-acetyl-N-substituted benzenesulfonamide, *Russ. J. Bioorganic Chem.*, 46(5) (2020) 702-714.

- [33] Sıcak Y., Oruç-Emre E.E., Öztürk M., Taşkın-Tok T., Karaküçük-İyidoğan A., Novel fluorine-containing chiral hydrazide-hydrazones: Design, synthesis, structural elucidation, antioxidant and anticholinesterase activity, and in silico studies, *Chirality*, 31(8) (2019) 603-615.
- [34] Aktar B.S.K., Sıcak Y., Tatar G., Emre E.E., Synthesis of benzoyl hydrazones having 4-hydroxy-3, 5-dimethoxy phenyl ring, their biological activities, and molecular modeling studies on enzyme inhibition activities, *Turk. J. Chem.*, 46(1) (2022) 236-252.

Comparison of Oliver-Pharr and Work of Indentation Approach to Determine the Mechanical Properties of Melt-Spun Al-12%Wt.Si-0.5%Sb Alloy

Fikret Yılmaz^{1,a,*}, Semra Ergen^{1,b}

¹ Tokat Gaziosmanpaşa University, Faculty of Arts and Science, Department of Physics, Tokat, Türkiye

*Corresponding author

Research Article

History

Received: 14/06/2021

Accepted: 06/09/2022

Copyright




©2022 Faculty of Science,
Sivas Cumhuriyet University


ABSTRACT

In this research, the hardness and reduced modulus of Al-%wt.12-%wt.0.5Sb melt-spun alloy were evaluated by using depth sensing indentation and atomic force microscopy techniques. We considered two approaches, Oliver-Pharr and Work of Indentation, to analyse the load-displacement curves. The ratio of final depth to maximum depth was found to be higher than the reported critical value of 0.70, which mean that pile-up was dominant in the melt-spun. A pile-up around the deformed surface was observed from atomic force microscope, which is consistent with the aforementioned result. The hardness calculated by Oliver-Pharr method was higher than that calculated by Work of Indentation Approach. According to the results, Work of Indentation Approach was more reliable than the Oliver-Pharr approach because of reducing pile-up affect.

Keywords: Melt-spinning Al-Si-Sb alloy, Depth-sensing indentation, Atomic force microscope, Oliver Pharr method, Work-of indentation approach.

 fikretyilmaz79@gmail.com

 <https://orcid.org/0000-0002-1835-4961>

 semraergengop@gmail.com

 <https://orcid.org/0000-0002-5515-0933>

Introduction

Today, Al-Si alloys are widely replacing iron based alloys in some areas such as automotive, aerospace and military industries due to its low weight, high corrosion resistance, high stiffness and moderate strength [1, 2]. Mechanical properties of Al-Si alloys can be further improved by using different methods such as rapid solidification techniques and/or addition of modifying agents. Uzun et al. have reported that hardness of eutectic Al-Si-Sb alloy produced by melt-spinning was about two times higher than those produced by induction melting and arc re-melting techniques [3]. On the other hand, the fact that one dimension of the alloy produced by melt-spinning is in the range of several microns makes it difficult to determine the mechanical properties by conventional hardness apparatus [4].

Recent years, determination of the mechanical properties of small volumes has become important issue since the mechanical properties at micro/nano-scale may differ from the bulk properties due to the size effects [5]. Indentation hardness testing is a commonly used non-destructive testing for evaluating the mechanical properties of materials. In a conventional hardness test, a fixed load is applied to a material with a diamond indenter and the dimensions of the residual indent is measured with the help of a microscope [6]. However, in many cases the size of the residual indents can be tiny to measure accurately with optical microscopy techniques.

Depth-sensing indentation (DSI) equipment developed during past two decades allows the

measurement of mechanical properties of materials without the need of observation of residual indent. Beside hardness (H) and reduced modulus (Er), this technique is also capable of measurement of viscoelastic parameters, yield stress, fracture parameters, strain hardening exponent and so on [5, 7, 8]. In this technique, the displacement of indenter (h) is recorded simultaneously as applied force (P) is loaded and unloaded in a specimen. Once a load-displacement (P-h) curve is obtained, H and Er of a specimen can be calculated using different empirical models proposed in literature. The two most well-known models, Oliver-Pharr and Work of indentation, will be described in detail in Section 2.

During the indentation of a material, deformations may occur at the edges of residual indent. This kind of deformations are agglomeration to outward and collapsing to inward of the indent edges, which are called pile-up and sink-in, respectively. Pile-up and/or sink-in can seriously affect the true hardness of material if they are not taken into account in calculations [9]. This kind of deformations can be directly observed by atomic force microscopy or indirectly determined by empirical values obtained from P-h curve.

It is very important to determine the mechanical properties of melt-spun alloys correctly from P-h curves. Therefore, in this research, we studied how the true hardness and reduced modulus can be calculated from P-h curves using two models and compared them in terms of pile-up effect.

Theoretical Background

Figure 1 shows a schematic load-displacement (P-h) curve and resultant indent profile of an ideal material

response. Two well-known mechanical properties, namely hardness (H) and reduced modulus (Er), can be calculated by analyzing P-h curve.

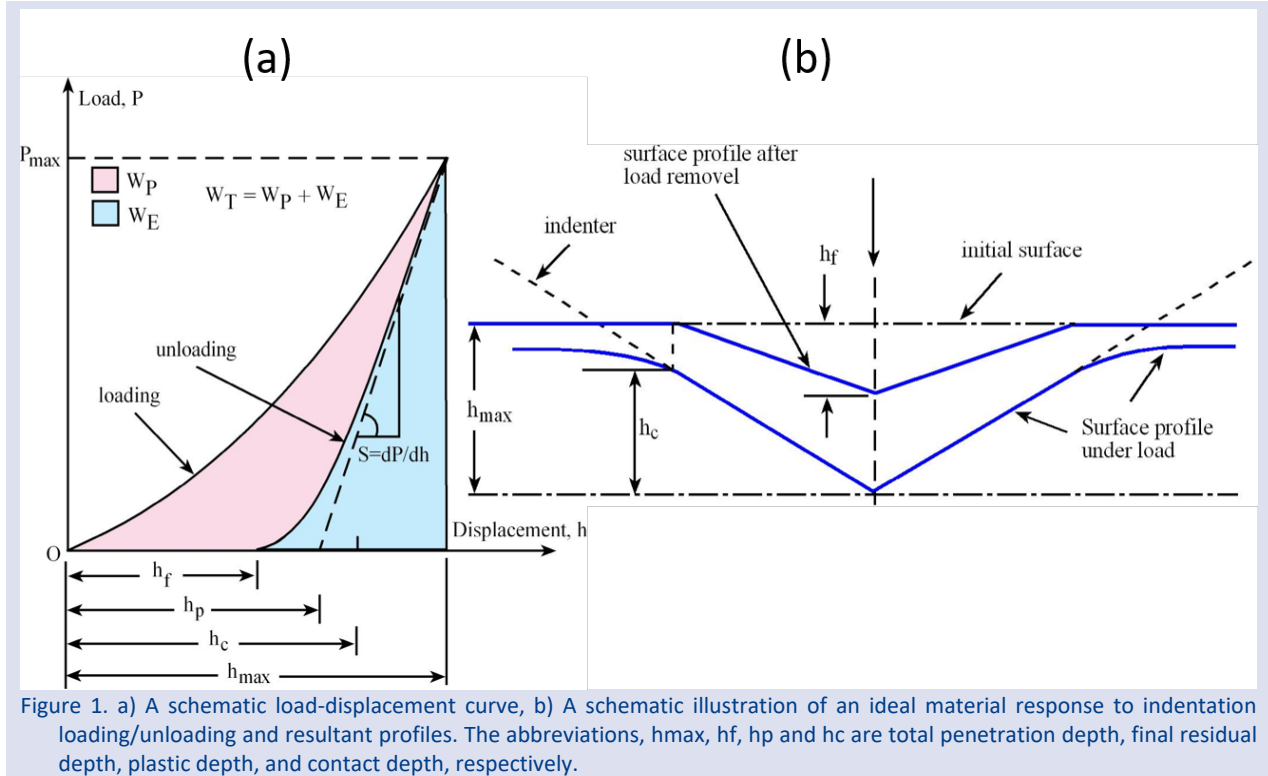


Figure 1. a) A schematic load-displacement curve, b) A schematic illustration of an ideal material response to indentation loading/unloading and resultant profiles. The abbreviations, hmax, hf, hp and hc are total penetration depth, final residual depth, plastic depth, and contact depth, respectively.

Oliver-Pharr (OP) Method

Oliver and Pharr (OP) method is the most adopted method in literature [10]. In this method, firstly unloading curve fits to the power-law relation:

$$P = K(h_{max} - h_f)^t \tag{1}$$

where P is the indentation load, K and t are the fitting parameters, h_f is the final depth. The stiffness S can be obtained by

$$S = tK(h - h_f)^{t-1} \tag{2}$$

The contact depth h_c can be estimated using:

$$h_c = h_{max} - \epsilon \frac{P_{max}}{S} \tag{3}$$

where ϵ is a constant related to an indenter geometry and 0.72 for conical indenters. Finally, the indentation hardness H_{OP} and reduced modulus Er can be determined by

$$H_{OP} = \frac{P_{max}}{A_c} \tag{4}$$

$$Er_{OP} = \frac{S}{2} \sqrt{\frac{\pi}{A_c}} \tag{5}$$

where A_c is the contact area equal to $24.5h_c^2$ for Vickers indenter.

Work of Indentation Approach (WIA)

Work of indentation approach is another analysis method which has been extensively studied since it was first proposed by Stilwell and Tabor [11]. The method has been improved by Sakai [12] who put forward a relationship between the energy of the hysteresis indentation loop and the hardness. Attaf [13] used the work of indentation approach to suggest some energy terms and Tuck [14] developed a simple formula by using the relation between work of indentation and Vickers hardness number. This method describes indentation experiment process as the use of the energy dissipated or work done during the indentation. The energies can be easily calculated thorough integrals. For instance, total work (W_T) and elastic work (W_E) are the under the areas of loading curve and unloading curve, respectively. In this case, plastic energy is equal to the difference between other energies (Figure 1a) [14, 15].

$$W_P = W_T - W_E \tag{7}$$

Tuck et al. [14] proposed a following hardness formula based on plastic work of indentation:

$$H_{WIA} = \frac{\kappa P_m^3}{9W_P^2} \tag{8}$$

where χ is a constant equal to 0.0378 for Vickers indenter. Reduced modulus can be determined using elastic and total work of indentation as follow equation [16];

$$\frac{W_E}{W_T} = 5 \left(\frac{H_{WLA}}{Er_{WLA}} \right) \quad (9)$$

Materials and Methods

Al-wt.%12Si-wt.%0.5Sb alloy from high purity of elements (Al: %99.9, Si: %99.999, Sb: 99.999 wt.%) was first melted in a graphite crucible using induction furnace and then re-melted five times to ensure homogeneity. The melt-spun alloy was produced using a melt-spinner apparatus (Edmund Bühler) with a rotating speed of 40 m/s. As-received melt-spun was 1 cm in wideness and 25 μm in thickness. Before indentation test, the surface of melt-spun was polished to 0.25 μm using diamond lap

wheels. Load-displacement curves were obtained from depth sensing indentation instrument (Shimadzu, DUH-W201S) with the load and displacement resolutions of $\pm 19.6 \mu\text{N}$ and $\pm 1 \text{ nm}$, respectively. Different loads ranging from 200 to 1200 mN were applied with a loading rate was 23,4 mN/s. AFM analysis were performed at non-contact mode for a scanning area of $80 \times 80 \mu\text{m}^2$.

Results and Discussion

Figure 2 shows microstructure of melt-spun alloy. The microstructure consists of fully equiaxed α -Al grains and homogeneously distributed fine fibrous Si eutectics (Figure 2a). Moreover, Si spheres in nano-scale size are dispersed in α -Al (Fig 2b). The fine and homogenous microstructure of Al-Si alloys is attributed to fast cooling rate, which is typical for melt-spun alloys. Similar results have been reported in literature [3, 4, 17, 18].

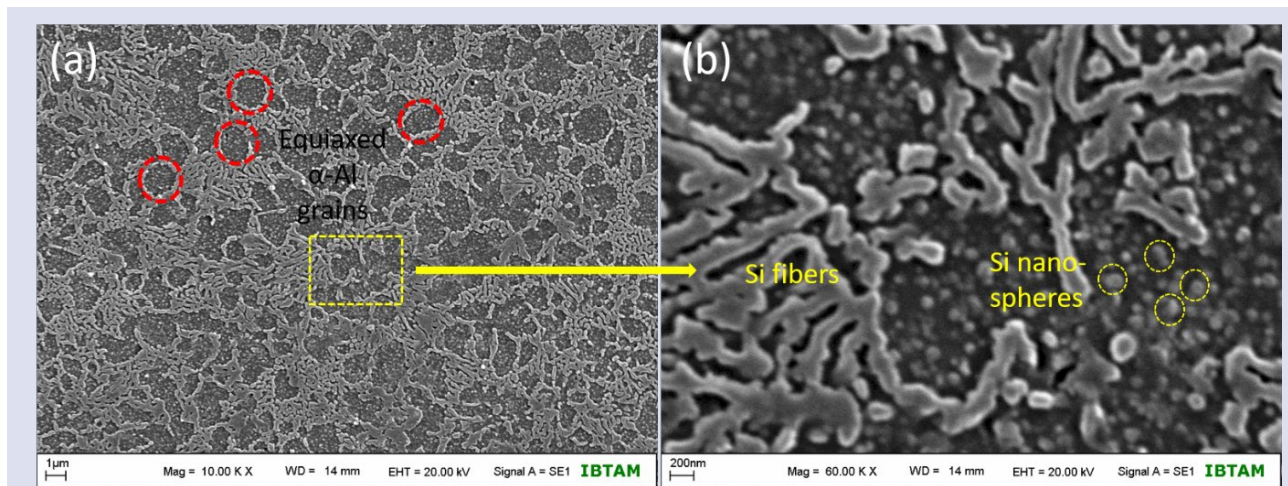


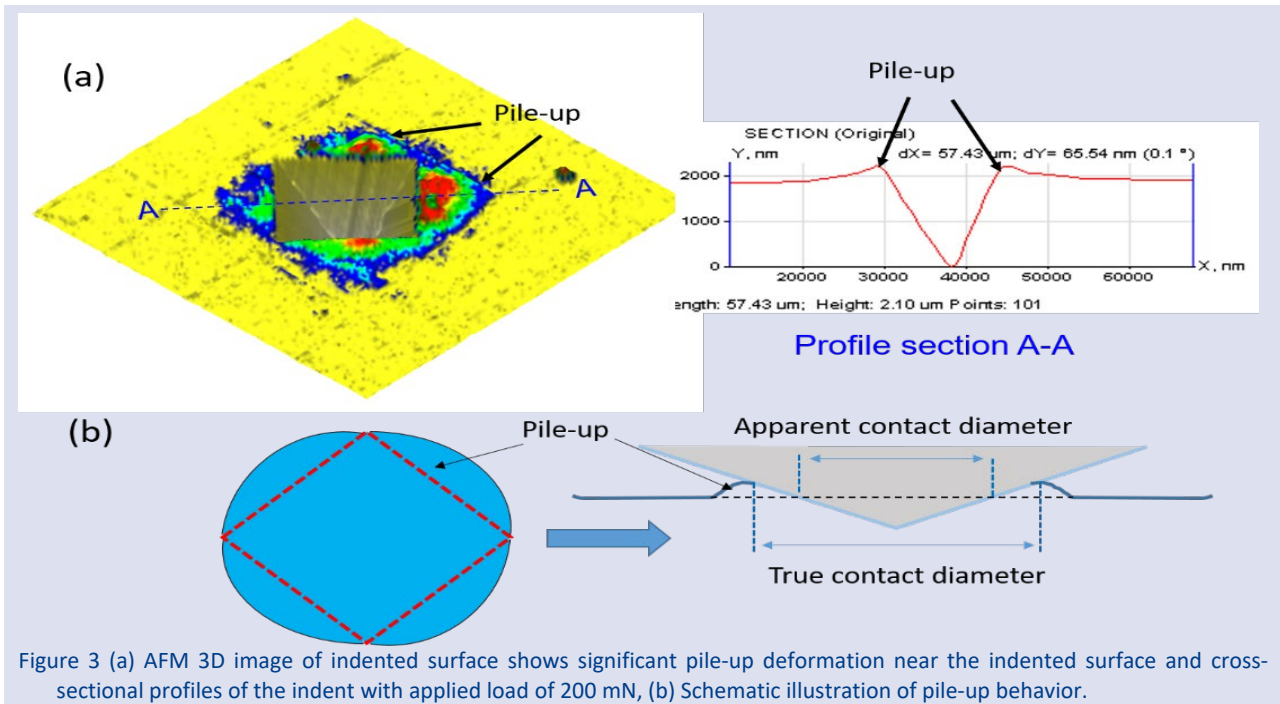
Figure 2. SEM image shows the microstructure of melt-spun ribbon. (a) homogeneously distributed equiaxed cellular α -Al grains, (b) fine silicon fibers and nano-scale silicon spheres in α -Al.

Figure 2 SEM image shows the microstructure of melt-spun ribbon. (a) homogeneously distributed equiaxed cellular α -Al grains, (b) fine silicon fibers and nano-scale silicon spheres in α -Al.

3D profile and corresponding profile section of indented area in Figure 3a clearly shows a pile-up along the four edges of the indentation imprint. The schematic illustration of pile-up phenomena is depicted in Figure 3b, which shows a difference between apparent and true contact diameter. When a pile-up is dominant at the around of deformed surface, an accuracy of hardness and reduced modulus are effected since the apparent contact depth will be smaller than true contact depth as depicted in Figure 3b. Contact depth after force removal can easily be scanned by AFM. The apparent and true contact depths are measured as 2.23 and 1.89 μm from Figure 3a. The hardness calculated using Equation 4 is approximately 2120 and 1530 MPa for apparent and true contact depths,

respectively. These results imply that a pile-up seriously affects the true hardness. Hardness can precisely determine by AFM technique, but this technique usually takes a lot of time.

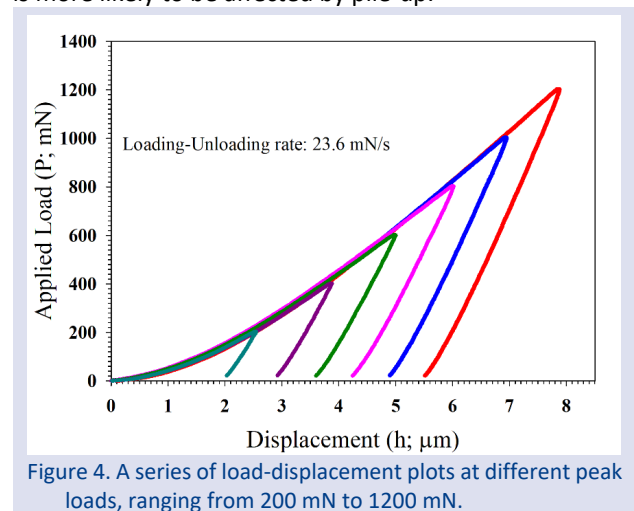
Apart from AFM technique, the ratio of final depth to maximum depth (h_f/h_{max}) is an easy measurable parameter from depth sensing indentation data that can be used to identify pile-up or sink-in behavior of a tested material. h_f/h_{max} values varying from 0.71 to 0.80 for different loads are listed in Table 1. According to Bolshakov and Pharr [19], 0.70 for h_f/h_{max} is a critical value and above this value, pile-up becomes significant for tested materials. As can be seen from Table 1, the values of h_f/h_{max} are higher than the reported critical value for each load. This result indicates the existence of pile-up around the indents, which is in agreement with AFM observations.



In order to determine the H and E_r of the melt-spun alloy, a series of load-displacement (P - h) curves were obtained from DSI test. An overlapping of loading curves means that the material is homogenous microstructure, which is compatible with SEM image (Figure 2). To obtain H and E_r , P - h curves were analyzed two well adopted approaches, Oliver-Pharr (OP) and work of indentation (WIA), which are described above in detail. Figure 5 shows the H and E_r values as a function of peak loads. From the figure, one can see that H and E_r values exhibit load dependent behavior, namely they decrease with increasing applied load. This phenomenon is called indentation size effect and observed different kinds of materials, such as metallic alloys, single crystals, ceramics, superconductors, polymers, etc. [20-22]. ISE can exist in some situations, such as work hardened surface, surface oxides, tip bluntness or poor tip-shape calibrations. Many models have been proposed in the literature to calculate load independent hardness. Perhaps the most reasonable model explaining the physical reasons behind this phenomenon was proposed by Nix and Gao [23]. This approach is based on geometrically necessary dislocations and successful to explain ISE in metallic alloys. Analysis of ISE by different models is not the object of this study, so one can find more detailed information in elsewhere [21].

From Figure 5, it is clearly seen that the hardness values calculated from OP (H_{OP}) higher than that of WIA (H_{WIA}). It is well known that the OP method does not take into account the pile-up effect observed in materials [24]. The contact depth, h_c , is therefore greatly

underestimated in the OP method, so overestimated hardness values are obtained [14]. We therefore suggest that the H_{WIA} values are more convenient than the H_{OP} values for our sample. Moreover, the hardness calculated from AFM (1530 MPa) is close to H_{WIA} (1650 MPa) than H_{OP} (1850 MPa) for applied load of 200 mN. AFM results further confirm the reliability of WIA. Reduced modulus, E_r , of the sample is given in Figure 5 b. Unlike the H values, E_r values calculated with two methods are found to be very similar to each other. This may be explained by the fact that the pile-up behavior is related to plastic deformation rather than elastic deformation. Since hardness is defined as resistance to plastic deformation, it is more likely to be affected by pile-up.



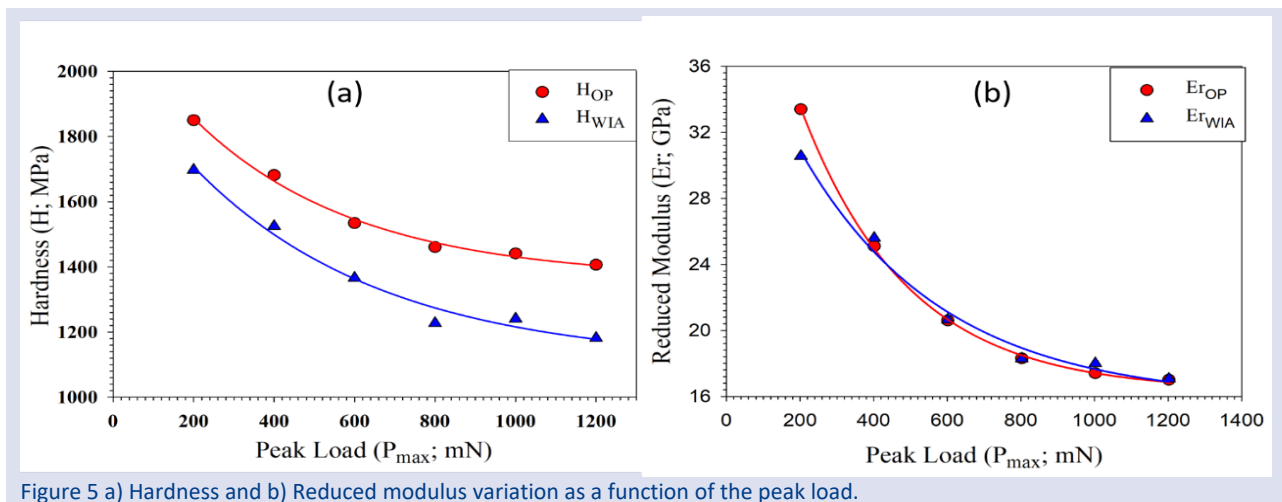


Figure 5 a) Hardness and b) Reduced modulus variation as a function of the peak load.

Conclusion

In this study, we aimed to investigate the mechanical properties of melt-spun Al - wt.%12Si - wt.%0.5Sb alloy by using depth-sensing indentation technique and compared two well-known approaches, Oliver-Pharr and work of indentation, in order to find the most suitable one. The ratios of h_f/h_{max} was found to be higher than critical value of 0.70 at various peak loads, which mean that a pile-up affect was dominant in our sample. The pile-up was further confirmed by AFM observation. Hardness and reduced modulus of the sample were calculated using Oliver-Pharr and work of indentation approaches. It was found that the values obtained by work of indentation approach were more reliable than the Oliver-Pharr approach because of reducing pile-up effect.

Conflicts of Interest

No conflict of interest was declared by the authors.

References

- [1] Choudhary C., Sahoo K.L., Mandal D., Processing and Characterisation of Modified Strain-Induced Melt Activation Processed Al-Si Alloys, *Materials Science and Technology*, 36 (2020) 181-193.
- [2] Ahn S.S., Sharief P., Lee C.H., Son H.T., Kim Y.H., Kim Y.C., Hong S., Hong S.J., Effect of Trace Elements (Co, Cr) on the Microstructure and Physical Properties of Al-Si-Cu-Mg-Fe Extruded Alloy, *Archives of Metallurgy and Materials*, 64 (3) (2019) 857-862.
- [3] Uzun O., Yılmaz F., Emeksiz C., Ergen S., Kölemen U., Correlation of Hardness and Silicon Morphology for Al-Si-Sb Alloy, *Archives of Metallurgy and Materials*, 63 (1) (2018) 467-472.
- [4] Uzun O., Yılmaz F., Kölemen U., Başman N., Sb Effect on Micro Structural and Mechanical Properties of Rapidly Solidified Al-12Si Alloy, *Journal of Alloys and Compounds*, 509 (2011) 21-26.
- [5] Qian L., Li M., Zhou Z., Yang H., Shi X., Comparison of Nano-Indentation Hardness to Microhardness, *Surface and Coatings Technology*, 195 (2005) 264-271.
- [6] Ghorbal G.B., Tricoteaux A., Thuault A., Louis G., Chicot D., Comparison of Conventional Knoop and Vickers Hardness of Ceramic Materials, *Journal of the European Ceramic Society*, 37 (2017) 2531-2535.
- [7] Menčík J., Determination of mechanical properties by instrumented indentation, *Meccanica*, 42 (2007) 19-29.
- [8] Guicciardi S., Balbo A., Sciti D., Melandri C., Pezzotti G., Nanoindentation Characterization of SiC-Based Ceramics, *Journal of the European Ceramic Society*, 27 (2007) 1399-1404.
- [9] Moharrami N., Bull S., A Comparison of Nanoindentation Pile-Up In Bulk Materials and Thin Films, *Thin Solid Films*, 572 (2014) 189-199.
- [10] Oliver W.C., Pharr G.M., An Improved Technique For Determining Hardness and Elastic Modulus Using Load And Displacement Sensing Indentation Experiments, *Journal of Materials Research*, 7 (1992) 1564-1583.
- [11] Stilwell N., Tabor D., Elastic Recovery of Conical Indentations, *Proceedings of the Physical Society*, 78 (2) (1961) 169.
- [12] Sakai M., Energy Principle of The Indentation-Induced Inelastic Surface Deformation and Hardness of Brittle Materials, *Acta Metallurgica et Materialia*, 41 (1993) 1751-1758.
- [13] Attaf M., New Ceramics Related Investigation of The Indentation Energy Concept, *Materials Letters*, 57 (2003) 4684-4693.
- [14] Tuck J.R., Korsunsky A.M., Bull S.J., Davidson R.I., On The Application of The Work-Of-Indentation Approach to Depth-Sensing Indentation Experiments In Coated Systems, *Surface and Coatings Technology*, 137 (2001) 217-224.
- [15] Beegan D., Chowdhury S., Laugier M., Work of Indentation Methods for Determining Copper Film Hardness, *Surface and Coatings Technology*, 192 (2005) 57-63.
- [16] Mukhopadhyay N., Weatherly G., Embury J., An Analysis of Microhardness of Single-Quasicrystals In The Al-Cu-Co-Si System, *Materials Science and Engineering: A*, 315 (2001) 202-210.
- [17] Birol Y., Microstructural Evolution During Annealing of a Rapidly Solidified Al-12Si Alloy, *Journal of alloys and compounds*, 439 (2007) 81-86.
- [18] Riestra M., Ghassemali E., Bogdanoff T., Seifeddine S., Interactive Effects of Grain Refinement, Eutectic Modification and Solidification Rate on Tensile Properties of Al-10Si Alloy, *Materials Science and Engineering: A*, 703 (2017) 270-279.

- [19] Bolshakov A., Pharr G., Influences Of Pile-up on The Measurement of Mechanical Properties by Load and Depth Sensing Indentation Techniques, *Journal of Materials Research*, 13 (1998) 1049-1058.
- [20] Şahin O., Uzun O., Kölemen U., Uçar N., Mechanical Characterization for B-Sn Single Crystals Using Nanoindentation Tests, *Materials Characterization*, 59 (2008) 427-434.
- [21] Yılmaz F., Uzun O., Kölemen U., Kilicaslan M.F., Basman N., Ergen S., Ozturk K., Yanmaz E., Nanoindentation Study on Gd-Deposited YBaCuO Superconductor, *Bulletin of Materials Science*, 36 (2013) 1139-1145.
- [22] Uzun O., Başman N., Alkan C., Kölemen U., Yılmaz F., Investigation of Mechanical and Creep Properties of Polypyrrole by Depth-Sensing Indentation, *Polymer Bulletin*, 66 (2011) 649-660.
- [23] Nix W.D., Gao H., Indentation Size Effects In Crystalline Materials: A Law For Strain Gradient Plasticity, *Journal of the Mechanics and Physics of Solids*, 46 (1998) 411-425.
- [24] Güçlü N., Kölemen U., Uzun O., Çelebi S., Work of Indentation Approach for Investigation of Mechanical Properties of YBCO Bulk Superconductor at Cryogenic Temperatures. *Physica C: Superconductivity*, 433 (2005) 115-122.



A Study On the Kernels of Irreducible Characters of Finite Groups

Burcu Çınarcı^{1,a}, Temha Erkoç^{1,b,*}

¹ Department of Marine Engineering, Maritime Faculty, Piri Reis University, 34940, Istanbul, Türkiye

² Department of Mathematics, Faculty of Science, Istanbul University, 34134, Istanbul, Türkiye

*Corresponding author

Research Article

History

Received: 29/03/2021

Accepted: 06/05/2022

Copyright



©2022 Faculty of Science,
Sivas Cumhuriyet University

ABSTRACT

Let G be a finite group and $\chi \in Irr(G)$, where $Irr(G)$ denotes the set of all irreducible characters of G . The kernel of χ is defined by $ker(\chi) = \{g \in G \mid \chi(g) = \chi(1)\}$, where $\chi(1)$ is the character degree of χ . The irreducible character χ of G is called as monolithic when the factor group $G/ker(\chi)$ has only one minimal normal subgroup. In this study, we have proven some results by concentrating on the kernels of nonlinear irreducible characters of G . First, we have provided an alternative proof for the classification of finite groups possessing two nonlinear irreducible characters by using their kernels. Also, we have presented the structure the solvable group G in which every nonlinear monolithic characters has same kernel

Keywords: Finite groups, Monolithic characters, Character degrees, Kernels of irreducible characters.

burcu-cinarcı@hotmail.com

<https://orcid.org/0000-0003-1202-0968>

erkocıt@istanbul.edu.tr

<https://orcid.org/0000-0001-5437-3679>

Introduction

Let G be a finite group. Since past, many studies have been carried out to investigate the structure of G whose character degrees have some special properties. For example, some authors have found all finite groups in which nonlinear irreducible characters have same degree (see Chapter 12 of [1]). On the other hand, the structure of the group G which has certain conditions on the number of its irreducible characters has been considered in much of the studies. Then in some cases the structure of the group has been fully presented. For example, Seitz has shown in [2] that if G has one nonlinear irreducible character, then $G \cong ES(2^{2a+1})$, extraspecial 2-group, or $G \cong N \rtimes K$ is Frobenius group, where N is an elementary abelian group of order q^a and the complement K is a cyclic group of order $q^a - 1$ for some prime number q . Throughout this paper, a finite group having one nonlinear irreducible character is called as a Seitz group.

Materials and Methods

Before proving our main results, we should mention some definitions and notations in the character theory of finite groups for the convenience of the reader. Our notations are standard and taken mainly from [1]. From now on, all groups are considered as finite.

Definition 2.1. The \mathbb{C} -representation of the group G is a homomorphism $\psi: G \rightarrow GL(n, \mathbb{C})$ for some integer n , where \mathbb{C} is the field of complex numbers and $GL(n, \mathbb{C})$ is the multiplicative group of non-singular $n \times n$ matrices over \mathbb{C} .

Definition 2.2. If ψ is a \mathbb{C} -representation of a group G , then the \mathbb{C} -character χ of G is the function such that $\chi(g) = tr(\psi(g))$ for all $g \in G$, where $tr(\psi(g))$ is the sum of the diagonal entries of $\psi(g)$. A character

corresponding to an irreducible representation of G is said to be irreducible.

The set of all irreducible characters and all nonlinear irreducible characters of G is denoted by $Irr(G)$ and $Irr_1(G)$, respectively. Also, $\chi(1)$ is called the degree of χ and χ is said to be a linear character when $\chi(1) = 1$. In the character theory, it is well-known that

$$|G| = |G:G'| + \sum_{\substack{\chi \in Irr(G) \\ \chi(1) > 1}} \chi(1)^2$$

and the number of linear irreducible characters of G is equal to $|G:G'|$, where G' is the commutator subgroup of G .

Definition 2.3. Let ψ be an irreducible character of the group G . The kernel of ψ is given by $ker(\psi) = \{g \in G \mid \psi(g) = \psi(1)\}$ and if $ker(\psi) = 1$, then we say that ψ is faithful.

The restriction of a character χ to a subgroup H of G is a character of H , which is denoted by χ_H . Conversely, an irreducible character μ of H determines the character μ^G of G (see Definition 5.1 of [1]). If $\mu^G = \theta$ for some character θ of G , then we have that $|G:H|\mu(1) = \theta(1)$.

Definition 2.4. For a group G and $\chi \in Irr(G)$, if $G/ker(\chi)$ has a unique minimal normal subgroup, then χ is said to be a monolithic character.

We use the notations $Irr_m(G)$ and $Irr_{1,m}(G)$ to denote all monolithic characters and all nonlinear monolithic characters of G , respectively. Monolithic characters contain some fundamental information in determining the structure of the group. For example, it is known that the group G is abelian if and only if all monolithic characters of G are linear. We want to note that if μ is an irreducible character of a p -group, then μ

must be monolithic. Also, $Irr_m(G/N) \subseteq Irr_m(G)$ for all $N \trianglelefteq G$.

Remark 2.5. For a solvable group G , we note by Lemma 2 of [5] that $D_m := \bigcap_{i=1}^n ker(\chi_i) \leq Z(G)$, where χ_i ranges over all nonlinear monolithic characters of G and $D_m \cap G' = 1$.

Remark 2.6. For a solvable group G , if $\varphi \in Irr_1(G)$ has a maximal kernel among the nonlinear irreducible characters of G , then φ is monolithic by Lemma 12.3 of [1]. Also, we may deduce that every kernel of nonlinear irreducible characters of G is a subgroup of the kernel of a nonlinear monolithic character of G . If $N \trianglelefteq G$ and G/N is nonabelian, then we have $N \leq ker(\chi)$ for some $\chi \in Irr_1(G)$.

Definition 2.7. Let G be a group. The regular character of G is given by

$$\rho(x) = \begin{cases} |G|, & x = 1 \\ 0, & 1 \neq x \in G \end{cases}$$

By Lemma 2.11 of [1], we conclude that $ker(\rho) = 1$. Here, it is convenient to note the following lemma since we will frequently use it for proving our results.

Lemma 2.8. If G is a nonabelian group and $T = \bigcap \{ker(\varphi) \mid \varphi \in Irr_1(G)\}$, then T is trivial.

Proof. Suppose that $T > 1$. By considering regular character of G , we have that $T \cap G' = 1$. Then we may write

$$|G| = |G:G'| + \sum_{\substack{\chi \in Irr(G) \\ \chi(1) > 1}} \chi(1)^2$$

and

$$|G/T| = |G:TG'| + \sum_{\substack{\chi \in Irr(G) \\ \chi(1) > 1}} \chi(1)^2.$$

Subtracting $|G/T|$ from $|G|$, we get that

$$|G| \left(\frac{|T| - 1}{|T|} \right) = |G| \left(\frac{1}{|G'|} - \frac{1}{|G'T|} \right).$$

By using $|G'T| = \frac{|G'| |T|}{|G' \cap T|}$ and simplifying above equation, we get the contradiction that $|G'|=1$. This contradiction shows that $T = 1$

Lemma 2.9. Let $G = H \times A$ be a direct product group, where A is abelian and $(|H|, |A|) = 1$. If $\chi \in Irr(H)$ and $1 \neq \xi \in Irr(A)$, then $ker_G(\chi\xi) = ker_H(\chi) \times ker_A(\xi)$.

Proof. By Theorem 4.21 of [1], we know that the character $\chi\xi$ is an irreducible character of G . Let $g \in ker_H(\chi) \times ker_A(\xi)$. Then we may write $g = ha$ for $h \in ker_H(\chi)$ and $a \in ker_A(\xi)$. This implies that

$$(\chi\xi)(g) = \chi(h)\xi(a) = \chi(1)\xi(1) = (\chi\xi)(1).$$

Thus, we obtain that $g \in ker_G(\chi\xi)$, and hence $ker_H(\chi) \times ker_A(\xi) \leq ker_G(\chi\xi)$.

Now, assume that $g \in ker_G(\chi\xi)$. Therefore, we have $(\chi\xi)(g) = \chi(h)\xi(a) = \chi(1)\xi(1)$, and so $|\chi(h)| = \chi(1)$ because ξ is a linear character of the abelian group A . Thus, $\chi(h) = u\chi(1)$ for a complex number u with $|u| = 1$. On the other hand, from Lemma 2.15 of [1], u is the $|H|$ th root of the unity. This yields that

$$\chi(1) = \chi(h)\xi(a) = u\chi(1)\xi(a),$$

and hence $u\xi(a) = 1$. Since $\xi(a)$ is the $|A|$ th root of the unity and $(|H|, |A|) = 1$, we obtain that $u = 1$ and $\xi(a) = 1$. This gives us $\chi(h) = \chi(1)$ and $\xi(a) = \xi(1)$, which shows that $g \in ker_H(\chi) \times ker_A(\xi)$. This completes the proof.

Main Results

Finite groups having two nonlinear irreducible characters have been described by Berkovich in Theorem 6 of Chapter 31 of [4]. Berkovich's proof is based on the degrees of these irreducible characters. Here, we consider the relationship between the kernels of irreducible characters and the group structure. By investigating the kernels of these two nonlinear irreducible characters, we provide an alternate proof of Berkovich's theorem as follows:

Theorem 3.1. Let $Irr_1(G) = \{\chi, \theta\}$ for the group G . Then one of the following remains true:

(1) If $ker(\theta) = ker(\chi) = 1$, then one of the following holds:

(a) $|G| = 2^{2c}$ and cyclic center $Z(G) \geq G'$ with $|G'| = 2$ and $|Z(G)| = 4$.

(b) $G \cong ES(3^{2a+1})$.

(c) $G \cong G' \rtimes K$ is a Frobenius group, where K is the cyclic Frobenius complement with $2|K| = |G'| - 1$.

(2) If $ker(\theta) = 1$ and $ker(\chi) > 1$, then G satisfies one of the following :

(d) $G \cong (C_3 \times C_3) \rtimes Q_8$ is a Frobenius group with the Frobenius complement isomorphic to Q_8 .

(e) $G/Z(G) \cong U \rtimes V$ is a Frobenius group possessing elementary abelian kernel U with a cyclic complement V . In this case, we also have $|Z(G)| = 2$, $|V| = |U| - 1$ and $Z(G) \cap G' = 1$.

(3) $ker(\theta) > 1$ and $ker(\chi) > 1$ if and only if $|G| = 2^{2a+2}$, $Z(G) \cong V_4$, $G' \leq Z(G)$ and $|G'|=2$.

Proof. By Theorem 12.15 of [1], we know that G is solvable. Suppose that $ker(\theta) = ker(\chi)$. By Lemma 2.8, we have $ker(\theta) = ker(\chi) = 1$. Thus, G' becomes the unique minimal normal subgroup of G . It can be seen by Lemma 12.3 of [1] that $\chi(1) = \theta(1)$. Furthermore, G becomes a r -group and $G/Z(G)$ is elementary abelian of order $\theta(1)^2$ or a Frobenius group. Clearly, when G is a r -group, we deduce $|G'| = r$ since $G' \leq Z(G)$ and $Z(G)$ is cyclic. Consequently, we have the equation that

$$|G| = |G:G'| + \theta(1)^2 + \chi(1)^2 = \frac{|G|}{r} + 2r^{2a}$$

for some positive integer a . Computation yields that $(r - 1)|G| = 2r^{2a+1}$ and this equality holds only when $r = 2$ or $r = 3$. Hence the cases (a) and (b) hold since the order of $G/Z(G)$ is r^{2a} . Now let G be a Frobenius group as in Lemma 12.3 of [1]. Thus, G' is the Frobenius kernel of G . On the other side, the Frobenius complement H becomes a cyclic group having the property that $2|H| = |G'| - 1$ since $|H| = \theta(1) = \chi(1)$. We see that G has the desired property in the case (c).

To prove the case (2), suppose that $ker(\theta) = 1$ and $ker(\chi) > 1$. Obviously, $G/ker(\chi)$ is a Seitz group. We also

know from Lemma 2.8 that $\ker(\chi)$ must be a minimal normal subgroup of G . Thus, we have that $|\ker(\chi)| = r^a$ for some prime r and integer a . Now first, let us consider $G/\ker(\chi)$ an extraspecial 2-group. Assume that $\ker(\chi) \not\leq G'$. Since $\ker(\chi)$ is a minimal normal subgroup of G , we know that $\ker(\chi) \cap G' = 1$. Thus G' is also a minimal normal subgroup of G . Hence $2 = |G'\ker(\chi)/\ker(\chi)| = |G'|$, and this implies $G' \leq Z(G)$. Therefore, G is nilpotent. It follows that r must be equal to 2. Otherwise, we obtain that $|Irr_1(G)| > 2$ by using the fact that $|Irr(G)| = |Irr(P)| \cdot |Irr(\ker(\chi))|$, where P is the Sylow 2-subgroup of G . Therefore, G is a 2-group and $|\ker(\chi)| = 2$. We have a contradiction that $G' = \ker(\chi)$ since $Z(G)$ is cyclic. This contradiction implies that $\ker(\chi) \leq G'$ and also $\ker(\chi)$ is the unique minimal normal subgroup of G . By using the equations

$$|G| = |G:G'| + \theta(1)^2 + \chi(1)^2 \tag{1}$$

and $|G/\ker(\chi)| = |G:G'| + \chi(1)^2$, we get that

$$\theta(1)^2 = |G| \left(1 - \frac{1}{|\ker(\chi)|}\right) = 2^{2b+1}(r^a - 1), \tag{2}$$

where $|G/\ker(\chi)| = 2^{2b+1}$ for some integer b . Since $\ker(\chi)$ is abelian group, we know from Theorem 6.15 of [1] (Ito Theorem) that $\theta(1)$ divides $|G/\ker(\chi)| = 2^{2b+1}$. Thus, $r^a - 1 = 2^\beta$ for some odd integer β . Thus, we get that $r \neq 2$. It follows that $Z(G) = 1$. Otherwise, G must be nilpotent since $\ker(\chi) \leq Z(G)$. But this is a contradiction since we obtain that $|Irr_1(G)| > 2$ by using the equation $|Irr(G)| = |Irr(P)| \cdot |Irr(\ker(\chi))|$, where P is the Sylow 2-subgroup of G . Now we determine possible values of r . If $2 \mid a$, then we see that the only possibility is that $r^a - 1 = 8$ because $r^a - 1 = (r^{a/2} - 1)(r^{a/2} + 1) = 2^\beta$ and r is an odd prime. Thus, $\ker(\chi) \cong C_3^2$ elementary abelian and also, $\ker(\chi) = F(G)$ because $F(G)$ is a r -group. Let $K \in Syl_2(G)$. Since the centralizer $C_G(\ker(\chi)) = \ker(\chi)$, we conclude that K is isomorphic to a subgroup of the group $Aut(C_3 \times C_3)$. Therefore, we get $G \cong (C_3 \times C_3) \rtimes Q_8$. Now consider the case that $2 \nmid a$. If $a > 1$, then we see that there exists an odd prime which would have to divide

$$(r - 1)(r^{a-1} + \dots + r + 1) = r^a - 1 = 2^\beta,$$

and hence there clearly is no such prime r . Thus, $a = 1$ and we have that $r - 1 = 2^\beta$ for some odd number β . The only possibility is that $r = 3$ and we obtain that $\ker(\chi)$ is a cyclic group of order 3. This is a contradiction because $Z(G) = 1$. Therefore, we need to consider that $G/\ker(\chi)$ is a Seitz Frobenius group possessing $H/\ker(\chi)$ Frobenius complement with the kernel $G'\ker(\chi)/\ker(\chi)$. Next, we claim that $\ker(\chi) \not\leq G'$. If not, $\ker(\chi)$ becomes the unique minimal normal subgroup and so $|\ker(\chi)| = r^a$ for some prime r and integer a . By using Equation (1) and $|G/\ker(\chi)| = |G:G'| + \chi(1)^2$, we know that

$$\theta(1)^2 = q^c(q^c - 1)(r^a - 1), \tag{3}$$

where $|G'/\ker(\chi)| = q^c$ and $|H/\ker(\chi)| = q^c - 1$. Now, we can consider the two cases that $F(G) = \ker(\chi)$ or $F(G) = G'$ since $\ker(\chi) \leq F(G) \leq G'$ and $G'/\ker(\chi)$ is the unique minimal normal subgroup of $G/\ker(\chi)$. Let $F(G) = \ker(\chi)$. We now have $r \neq q$ and G' is not an abelian group. It follows that $G'' = \ker(\chi)$ and so $\ker(\chi) \not\leq \ker(\lambda)$ for every $\lambda \in Irr_1(G')$. Therefore, $\ker(\chi) \not\leq \ker(\lambda^G)$ and by Clifford's Theorem (see Theorem 6.2 of [1]) we conclude that $\lambda^G = \theta$ since θ is the unique faithful irreducible character of G and G/G' is a cyclic group. Because the fact that $F(G') = \ker(\chi)$ and $G'/F(G')$ is an abelian group, from Lemma 18.1 of [3], there must be an irreducible character φ of G' satisfying the property that $\varphi(1) = |G':F(G')| = q^c$. Thus, we obtain that

$$\varphi^G(1) = |G:G'| \varphi(1) = (q^c - 1)q^c = \theta(1),$$

and hence by using Equation (3), we get $\theta(1) = q^c(q^c - 1) = (r^a - 1)$. By Clifford's Theorem, we have $\theta_{\ker(\chi)} = \xi_1 + \xi_2 + \dots + \xi_{r^a-1}$, where $\xi_i \in Irr(\ker(\chi))$ for $i \in \{1, \dots, r^a - 1\}$. This leads by Clifford's Theorem to $I_G(\xi_i) = \ker(\chi)$ for all nonprincipal irreducible characters ξ_i of $\ker(\chi)$ because $|G:I_G(\xi_i)| = r^a - 1 = \theta(1)$. Thus, we have seen that there exists $K \leq G$ such that $G = \ker(\chi) \rtimes K$ is a Frobenius group with $\ker(\chi)$ being the Frobenius kernel. K has a unique involution since $|K| = q^c(q^c - 1)$ is even. This shows $Z(K) > 1$, which leads the contradiction as we know that $G/\ker(\chi) \cong K$ is a Frobenius group.

Now, we may assume that $F(G) = G'$. We note that $r = q$ and $G' \in Syl_r(G)$ as $F(G)$ is a r -group. Thus we also know that G' is not an abelian group since $q \mid \theta(1)$. It follows that $\ker(\chi) = Z(G') = G''$ since $G'/\ker(\chi)$ is the unique minimal normal subgroup of $G/\ker(\chi)$. By using the similar thought in the previous paragraph, we have $\psi^G = \theta$ for $\psi \in Irr_1(G')$. Therefore, $\theta(1) = r^t(r^c - 1)$, where $\psi(1) = r^t$ for some integer t . By using Equation (3), we get that

$$\theta(1)^2 = r^c(r^c - 1)(r^a - 1) = r^{2t}(r^c - 1)^2,$$

and by equating these expressions, we find that $a = c = 2t$. It follows that $|\ker(\chi)| = r^c = |G'/\ker(\chi)|$ and $\psi(1) = r^{c/2}$ for every nonlinear irreducible character ψ of G' . Since by Corollary 2.30 of [1] we have that $r^c = \psi(1)^2 \leq |G':Z(\psi)|$ and that $Z(G') \leq Z(\psi)$, we deduce that $Z(G') = Z(\psi)$. As $r^c = |G'/Z(G')|$, again by Corollary 2.30 of [1], for all $x \in G' - Z(G')$ we see that $\psi(x) = 0$.

Take $x \in G' - Z(G')$; then $\psi(x) = 0$ for all $\psi \in Irr_1(G')$. Then we have a contradiction that

$$\begin{aligned} r^c &= |Z(G')| < |C_{G'}(x)| \\ &= \sum_{\psi \in Irr_1(G')} |\psi(x)|^2 + \sum_{\mu \in Lin(G')} |\mu(x)|^2 = r^c \end{aligned}$$

This proves our claim $\ker(\chi) \not\leq G'$. Thus, $\ker(\chi)$ and G' are different minimal normal subgroups of G . By Ito's Theorem, $\theta(1) \mid q^c - 1$ since $G' \times \ker(\chi) \trianglelefteq G$ is abelian, and hence it may be written the degree of θ as $\theta(1) = \frac{q^c - 1}{t}$ for some t . By using Equation (1),

$$q^c(q^c - 1)r^a = |G|$$

$$= (q^c - 1)r^a + (q^c - 1)^2 + (q^c - 1/t)^2$$

and this calculation shows that $r^a = 1 + \frac{1}{t^2}$, which is possible only if $r^a = 2$. This implies that $|ker(\chi)| = 2$. Actually, we have $ker(\chi) = Z(G)$, which yields that the case (b) holds.

Let us consider the case (3), that is, $ker(\chi) > 1$ and $ker(\theta) > 1$. Take $N := ker(\chi) \cap ker(\theta)$, then we know from Lemma 2.8 that $|N| = 1$ and both $ker(\chi)$ and $ker(\theta)$ are minimal normal subgroups of G . Since $G/ker(\chi)ker(\theta)$ is abelian, we have that $G' \leq ker(\chi)ker(\theta)$. Suppose that $G = ker(\chi)ker(\theta)$. By using Equation (1), we get that

$$|G/ker(\theta)| - |G:G'| = \theta(1)^2 = |G| - |G/ker(\chi)|$$

since $ker(\chi)$ and $ker(\theta)$ are subgroups of G' . Thus, we have $|ker(\theta)|(|ker(\chi)| - 1) = |ker(\chi)| - 1$, which leads the contradiction that $|ker(\theta)| = 1$. Therefore, we see that $G' < ker(\chi)ker(\theta)$. Suppose that $ker(\chi) \leq G'$, then we get $G'ker(\theta) = ker(\chi)ker(\theta)$, and so $|G' \cap ker(\theta)| > 1$. Thus, we have $ker(\theta) \leq G'$, which contradicts with $G' < ker(\chi)ker(\theta)$. Then $ker(\chi) \not\leq G'$. Similarly, we obtain that $ker(\theta) \not\leq G'$. Thus G' is the another minimal normal subgroup. Now, we claim that $G'ker(\theta) = G'ker(\chi) = ker(\chi)ker(\theta)$. It is easy to see that $ker(\theta) = ker(\theta) \cap G'ker(\chi) \leq G'ker(\chi)$ and $ker(\chi) = ker(\chi) \cap G'ker(\theta) \leq G'ker(\theta)$, which yields that $G'ker(\theta) = G'ker(\chi) = ker(\chi)ker(\theta)$, as desired. We also note that $|G'| = |ker(\theta)| = |ker(\chi)|$.

First, we assume that $G/ker(\chi)$ is a Seitz Frobenius group. Since $|G'ker(\chi)/ker(\chi)| = |G'ker(\theta)/ker(\theta)|$, we see that $G/ker(\theta)$ cannot be an extraspecial 2-group. Thus, $G/ker(\theta)$ is also a Seitz Frobenius group whose order is $r^n(r^n - 1)$ for some prime r and $\theta(1) = \chi(1) = r^n - 1$. Because $G' \cong G'ker(\chi)/ker(\chi) \cong ker(\theta)$, we conclude that $r^n = |G'| = |ker(\chi)|$, and hence we get $|G| = r^{2n}(r^n - 1)$. By using Equation (1), we have

$$r^{2n}(r^n - 1) = r^n(r^n - 1) + 2(r^n - 1)^2,$$

which gives a contradiction that $1 = r^n - 1 = \chi(1)$. Therefore we need to consider the case that $G/ker(\chi)$ is an extraspecial 2-group. Since we have $2 = |G'ker(\chi)/ker(\chi)| = |G'ker(\theta)/ker(\theta)|$, we deduce that $G/ker(\theta)$ is also an extraspecial 2-group, and so we get that G is a 2-group. Thus, minimal normal subgroups $ker(\chi)$, $ker(\theta)$ and G' are also subgroups of $Z(G)$ of order 2. In fact, $ker(\chi)ker(\theta) = Z(G)$ because $G/ker(\chi)$ is an extraspecial 2-group. Therefore, we obtain the case (3) that $Z(G) \cong V_4$, $|G| = 2^{2n+2}$ and $\chi(1) = \theta(1) = 2^n$, where V_4 is the Klein-4-group, and hence we are done.

Theorem 3.2. Let $Irr_{1,m}(G) = \{\chi_1, \chi_2, \dots, \chi_n\}$ for a nonabelian solvable group G . Assume that $ker(\chi_i) = ker(\chi_j)$ for $i, j \in \{1, 2, \dots, n\}$. Then $\chi_1(1) = \dots = \chi_n(1) = d$ for some integer d and one of the following holds:

(i) $G = S \times T$, where $S \in Syl_p(G)$ and $T \trianglelefteq G$ is abelian.

Also, $S/Z(S)$ is an elementary abelian p -group and $Z(S)$ is cyclic.

(ii) $G/Z(G)$ is a Frobenius group possessing an abelian Frobenius complement whose order equals d , G' is an elementary abelian p -group and $G' \cap Z(G) = 1$. Also, for $R \in Syl_p(Z(G))$ we have $G = R \times K$. In fact, $K/Z(K)$ becomes a Frobenius group.

Proof. We first note that when every nonlinear monolithic character of G is faithful, then G' becomes the unique minimal normal subgroup of G from Remark 2.6, and hence we complete the proof by Lemma 12.3 of [1]. Therefore, we can suppose that $ker(\chi_i) \neq 1$ for $i \in \{1, 2, \dots, n\}$. Since $1 < \bigcap_{i=1}^n ker(\chi_i) = ker(\chi_1)$, then by Remark 2.5, we have that $ker(\chi_1) \leq Z(G)$ and also $ker(\chi_1) \cap G' = 1$. Therefore, we conclude by Remark 2.6 that G' is a minimal normal subgroup of G . First let us consider $ker(\chi_1) < Z(G)$. Thus, we get that $G/Z(G)$ is abelian because it has no nonlinear monolithic character. So G becomes a nilpotent group. Because the fact that G is nonabelian and nilpotent, then there is a nonabelian Sylow p -subgroup $S \trianglelefteq G$ having the property with $G = S \times T$. Since $S' = G' \leq S$, then we observe that T is an abelian group. Furthermore, the factor group $G/ker(\chi_1)$ needs to be a nonabelian and p -group. This gives from Remark 2.6 that $T \leq ker(\chi_1)$. Since we know $Irr_{1,m}(G/T) = Irr_{1,m}(S)$, we obtain that S has exactly n nonlinear monolithic characters having same kernel. From Lemma 2.8, we deduce that every nonlinear irreducible characters of S needs to be faithful. Therefore, S is as in Lemma 12.3 (a) of [1], which is as desired result in (i).

From now on, we shall suppose that $ker(\chi_1) = Z(G)$. If the factor group $G/Z(G)$ is a p -group, G is nonabelian and nilpotent. Also, we note that $(|S|, |Z(G)|) \neq 1$, where S is a Sylow p -subgroup of G . Therefore, there exists $N < Z(G)$ subgroup with $G/N \cong S$. Since $Irr_{1,m}(S) \subseteq Irr_{1,m}(G)$ and $G/NZ(S) \cong S/Z(S)$, we have a contradiction that $n = |Irr_{1,m}(S/Z(S))| < |Irr_{1,m}(S)| \leq |Irr_{1,m}(G)| = n$.

Then $G/Z(G)$ becomes a Frobenius group as Lemma 12.3 (b) of [1], that is,

$$G/Z(G) \cong Z(G)G'/Z(G) \rtimes B/Z(G),$$

where $Z(G)G'/Z(G) \cong G'$ is an elementary abelian p -group. Let's pick $R \in Syl_p(Z(G))$. Because the fact that $Z(G) \cap G' = 1$, we get $G' \times R \in Syl_p(G)$. Since $G' \times R$ splits over the normal abelian group R , then we get by Gaschütz's Lemma that $G = R \times K$, where $K/Z(K)$ is a Frobenius group.

Conversely, the groups as in the theorem have nonlinear monolithic characters having equal kernel by Lemma 2.9, and hence we are done.

Conclusion

For many years, several authors have defined some new concepts and given theorems on the classifications of a finite group by using its irreducible characters. The aim of this paper is to consider the relation between the groups structure and their irreducible character kernels. Under some certain conditions related to irreducible character kernels, we have given a classification of finite groups. On above occasion, we want to emphasize that

monolithic characters are important constituent of the set of irreducible characters. Therefore, this study may be considered as a pioneering work for classifying finite groups having more nonlinear monolithic character kernels.

Acknowledgment

The authors of this paper would like to thank the Scientific and Technological Research Council of Turkey for supporting their research. (The grant number of the support is 119F295.).

Conflicts of interest

The authors state that did not have conflict of interests.

References

- [1] Isaacs I. M., Character Theory of Finite Groups, Academic Press, New York, (1976).
- [2] Seitz G.M., Finite groups having only one irreducible representation of degree greater than one. *Proc. Am. Math. Soc.*, (19) (1968) 459-461.
- [3] Manz O., Wolf T.R., Representations of Solvable Groups, London Mathematical Society Lecture Note Series, (185), Cambridge University Press, Cambridge (1993).
- [4] Berkovich Y., Zhmud E. M., Characters of Finite Groups. Part 2, American Mathematical Society, (1999).
- [5] Berkovich Y., On Isaacs' three character degrees theorem, *Proc. Am. Math. Soc.* 125 (3) (1997) 669-677.

Constant Mean Curvature Surfaces Along a Spacelike Curve

Ergin Bayram^{1,a,*}

¹ Department of Mathematics, Faculty of Science, Ondokuz Mayıs University, Samsun, Türkiye.

*Corresponding author

Research Article

History

Received: 27/01/2022

Accepted: 01/08/2022

Copyright



©2022 Faculty of Science,
Sivas Cumhuriyet University

ABSTRACT

We construct constant mean curvature surfaces along a given spacelike curve in 3 dimensional Minkowski space. We parametrically present these surfaces using the famous Frenet frame of the curve in question. We give the sufficient conditions for the so called marching scale functions, which are the coefficients of the Frenet frame fields. We show that it is possible to obtain such surfaces for any given spacelike curve. Finally, the validity of the presented method is supported with illustrative examples.

Keywords: Spacelike curve, Constant mean curvature surfaces, Minkowski 3-space

erginbayram@yahoo.com

<https://orcid.org/0000-0003-2633-0991>

Introduction

The Gaussian and the mean curvature are a measure of how a surface curves. As an intrinsic quantity, the Gaussian curvature is one of the foundations of Riemannian geometry. In contrast, the mean curvature is an extrinsic quantity which measures how the surface lies in space. As the mean curvature is closely related to the character of the surface of a solid material, it is deeply connected to other sciences.

The mean curvature of a surface is half of the sum of principal curvatures at every point of the surface. A minimal surface is a surface which has zero mean curvature at every point. A surface with non-vanishing constant mean curvature is obtained by minimizing the area of the surface while preserving its volume. It can be physically modeled by a soap bubble.

We see surfaces almost in every differential geometry book [1-3]. There are several techniques to characterize surfaces. However, the construction of a surface is also an important issue. Current studies on surfaces have focused on finding surfaces with a common special curve [4 - 14]. Recently, Coşanoğlu and Bayram [15] obtained sufficient conditions for constant mean curvature surfaces through a prescribed curve in 3 dimensional Euclidean space. Mert and Karlığa [16] investigated timelike surfaces with constant angle in de-Sitter space. Mert and Atçeken [17] studied normal and binormal surfaces in hyperbolic 3-space.

In the present paper, analogous to Coşanoğlu and Bayram [15], we obtain parametric constant mean curvature surfaces through a given spacelike curve in 3 dimensional Minkowski space. We present constraints for these types of surfaces. The method is validated with several examples.

Materials and Methods

Apparatus

The real vector space \mathbb{R}^3 endowed with the metric tensor

$$\langle X, Y \rangle = -x_1y_1 + x_2y_2 + x_3y_3$$

is called the Minkowski 3-space and denoted by \mathbb{R}_1^3 , where $X = (x_1, x_2, x_3)$, $Y = (y_1, y_2, y_3) \in \mathbb{R}^3$ [1] The Lorentzian vectorial product is defined by

$$X \times Y = (x_2y_3 - x_3y_2, x_1y_3 - x_3y_1, x_2y_1 - x_1y_2).$$

A vector $X \in \mathbb{R}_1^3$ is called timelike, spacelike or lightlike (null) if

$$\begin{cases} \langle X, X \rangle < 0, \\ \langle X, X \rangle > 0 \text{ or } X = \vec{0}, \\ \langle X, X \rangle = 0, \end{cases}$$

respectively. Similarly, a curve in \mathbb{R}_1^3 is called a timelike, spacelike or lightlike curve if its tangent vector field is always timelike, spacelike or lightlike, respectively.

The set $\{T, N, B\}$ denotes the moving Frenet-Serret frame through a curve α , where T , N and B are the tangent vector field, the principal normal vector field and the binormal vector field of the curve α , respectively.

The unit speed spacelike curve α with timelike normal has spacelike vector fields T and B and timelike vector field N . For this setting we have,

$$T = -N \times B, N = B \times T, B = -T \times N.$$

$B(s)$ is the unique spacelike unit vector field orthogonal to the timelike plane $\{T(s), N(s)\}$ at every point $\alpha(s)$, such that the orientation of \mathbb{R}_1^3 and $\{T, N, B\}$ are the same. Then, we have the following Frenet formulas [18]

$$T' = \kappa N, \quad N' = \kappa T + \tau B, \quad B' = \tau N.$$

The arc-length spacelike curve α with spacelike normal has spacelike vector fields T and N and timelike vector field B . In this case,

$$T = -N \times B, \quad N = -B \times T, \quad B = T \times N.$$

The vector field $B(s)$ is the unique timelike unit vector field orthogonal to the spacelike plane $\{T(s), N(s)\}$ at each point $\alpha(s)$ so that the orientation of \mathbb{R}_1^3 and $\{T, N, B\}$ are the same. Then, we obtain the following Frenet formulas [19]

$$T' = \kappa N, \quad N' = -\kappa T + \tau B, \quad B' = \tau N.$$

The mean curvature of the surface $P(s, t)$ is given as

$$H(s, t) = - \left(\frac{\det(P_s, P_t, P_{ss})G - 2 \det(P_s, P_t, P_{st})F + \det(P_s, P_t, P_{tt})E}{2(-\varepsilon W)^{\frac{3}{2}}} \right) (s, t),$$

where E, F, G are the coefficients of the first fundamental form of the surface $P(s, t)$, $W = EG - F^2$ and

$$\varepsilon = \begin{cases} 1, & \text{if } P(s, t) \text{ is timelike,} \\ -1, & \text{if } P(s, t) \text{ is spacelike,} \end{cases}$$

[19].

Results and Discussion

Constant Mean Curvature Surfaces Along A Spacelike Curve

Let $\alpha(s)$ be a spacelike curve with timelike normal arc-length regular curve with curvature $\kappa(s)$ and torsion $\tau(s)$. Also, assume that $\alpha''(s) \neq \vec{0}, \forall s$. Parametric surfaces possessing $\alpha(s)$ can be written as

$$P(s, t) = \alpha(s) + u(s, t)T(s) + v(s, t)N(s) + w(s, t)B(s), \tag{1}$$

$L_1 \leq s \leq L_2, T_1 \leq t \leq T_2$, where $\{T(s), N(s), B(s)\}$ is the Frenet-Serret frame of $\alpha(s)$. C^2 functions $u(s, t), v(s, t), w(s, t)$ are known as marching-scale functions. Note that, choosing distinct marching-scale functions corresponds to distinct surfaces along the curve $\alpha(s)$.

To simplify the calculations, we suppose that the curve $\alpha(s)$ is a t -parameter curve on the surface in Eqn. (1). So, we have

$$u(s, t_0) \equiv 0, \quad v(s, t_0) \equiv 0, \quad w(s, t_0) \equiv 0$$

for some $t_0 \in [T_1, T_2]$.

We make the following calculations required for the mean curvature.

$$\begin{aligned} P_s(s, t) &= (1 + u_s(s, t) + \kappa(s)v(s, t))T(s) \\ &\quad + (\kappa(s)u(s, t) + v_s(s, t) + \tau(s)w(s, t))N(s) \\ &\quad + (\tau(s)v(s, t) + w_s(s, t))B(s), \end{aligned}$$

$$P_t(s, t) = u_t(s, t)T(s) + v_t(s, t)N(s) + w_t(s, t)B(s),$$

$$P_s(s, t_0) = T(s),$$

$$P_t(s, t_0) = u_t(s, t_0)T(s) + v_t(s, t_0)N(s) + w_t(s, t_0)B(s),$$

$$P_{ss}(s, t_0) = \kappa(s)N(s),$$

$$P_{st}(s, t_0) = P_{ts}(s, t_0) = (u_{ts}(s, t_0) + \kappa(s)v_t(s, t_0))T(s) + (\kappa(s)u_t(s, t_0) + v_{ts}(s, t_0) + \tau(s)w_t(s, t_0))N(s) + (\tau(s)v_t(s, t_0) + w_{ts}(s, t_0))B(s)$$

$$P_{tt}(s, t_0) = u_{tt}(s, t_0)T(s) + v_{tt}(s, t_0)N(s) + w_{tt}(s, t_0)B(s),$$

$$\det(P_s(s, t_0), P_t(s, t_0), P_{ss}(s, t_0)) = -\kappa(s)w_t(s, t_0),$$

$$\det(P_s(s, t_0), P_t(s, t_0), P_{st}(s, t_0)) = v_t(s, t_0)(v_t(s, t_0)\tau(s) + w_{ts}(s, t_0)) - w_t(s, t_0)(u_t(s, t_0)\kappa(s) + v_{ts}(s, t_0) + \tau(s)w_t(s, t_0)),$$

$$\det(P_s(s, t_0), P_t(s, t_0), P_{tt}(s, t_0)) = v_t(s, t_0)w_{tt}(s, t_0) - w_t(s, t_0)v_{tt}(s, t_0),$$

where subscript denotes the partial derivative with respect to the parameter in question. Hence, the surface $P(s, t)$ in Eqn. (1) has the following mean curvature along the curve $\alpha(s)$

$$H(s, t_0) = \frac{\kappa w_t(u_t^2 - v_t^2 + w_t^2) + 2u_t[v_t(v_t\tau + w_{ts}) - w_t(\kappa u_t + v_{ts} + \tau w_t)] + w_t v_{tt} - v_t w_{tt}}{2(\varepsilon(v_t^2 - w_t^2))^{\frac{3}{2}}}(s, t_0).$$

Theorem 1 : The surface $P(s, t)$ in Eqn. (1) has constant mean curvature along the spacelike curve $\alpha(s)$ with spacelike binormal if one of the following conditions is satisfied:

- i) $u(s, t_0) = v(s, t_0) = w(s, t_0) = w_t(s, t_0) = w_{tt}(s, t_0) \equiv 0 \neq u_t(s, t_0) = v_t(s, t_0), \tau(s) = \text{constant}$,
- ii) $u(s, t_0) = v(s, t_0) = w(s, t_0) = v_t(s, t_0) = v_{tt}(s, t_0) \equiv 0 \neq u_t(s, t_0) = w_t(s, t_0), \tau(s) = \text{constant}$,
- iii) $v_t(s, t_0) \neq 0 \equiv u(s, t_0) = v(s, t_0) = w(s, t_0) = u_t(s, t_0) = w_t(s, t_0) = w_{tt}(s, t_0)$,
- iv) $w_t(s, t_0) \neq 0 \equiv u(s, t_0) = v(s, t_0) = w(s, t_0) = u_t(s, t_0) = v_t(s, t_0) = v_{tt}(s, t_0), \kappa(s) = \text{constant}$,

If $\alpha(s), L_1 \leq s \leq L_2$ is a spacelike curve with timelike binormal arc-length regular curve having curvature $\kappa(s)$ and torsion $\tau(s)$, then we have the theorem below.

Theorem 2 : The surface $P(s, t)$ in Eqn. (1) has constant mean curvature along the spacelike curve $\alpha(s)$ with timelike binormal if one of the following conditions is satisfied :

- i) $u(s, t_0) = v(s, t_0) = w(s, t_0) = w_t(s, t_0) = w_{tt}(s, t_0) \equiv 0 \neq u_t(s, t_0) = v_t(s, t_0), \tau(s) = \text{constant}$,
- ii) $u(s, t_0) = v(s, t_0) = w(s, t_0) = v_t(s, t_0) = v_{tt}(s, t_0) \equiv 0 \neq u_t(s, t_0) = w_t(s, t_0), \kappa(s) + \tau(s) = \text{constant}$,
- iii) $v_t(s, t_0) \neq 0 \equiv u(s, t_0) = v(s, t_0) = w(s, t_0) = u_t(s, t_0) = w_t(s, t_0) = w_{tt}(s, t_0)$,
- iv) $w_t(s, t_0) \neq 0 \equiv u(s, t_0) = v(s, t_0) = w(s, t_0) = u_t(s, t_0) = v_t(s, t_0) = v_{tt}(s, t_0), \kappa(s) = \text{constant}$,

Example 1 : In this example, we construct surfaces with constant mean curvature along a given spacelike curve with timelike normal vector field. The unit speed spacelike curve with timelike normal $\alpha(s) = \left(\frac{1}{2}\cosh(\sqrt{2}s), \frac{\sqrt{2}s}{2}, \frac{1}{2}\sinh(\sqrt{2}s)\right)$ has the following Frenet apparatus :

$$T(s) = \left(\frac{\sqrt{2}}{2}\sinh(\sqrt{2}s), \frac{\sqrt{2}}{2}, \frac{\sqrt{2}}{2}\cosh(\sqrt{2}s)\right),$$

$$N(s) = \left(\cosh(\sqrt{2}s), 0, \sinh(\sqrt{2}s)\right),$$

$$B(s) = \left(-\frac{\sqrt{2}}{2}\sinh(\sqrt{2}s), \frac{\sqrt{2}}{2}, -\frac{\sqrt{2}}{2}\cosh(\sqrt{2}s)\right),$$

$$\kappa(s) = 1, \quad \tau(s) = -1.$$

Marching-scale functions $u(s, t) = v(s, t) = t, w(s, t) \equiv 0$ and $t_0 = 0$, satisfies Theorem 1 (i) and the surface

$$P_1(s, t) = \left(\left(t + \frac{1}{2}\right)\cosh(\sqrt{2}s) + \frac{t\sqrt{2}}{2}\sinh(\sqrt{2}s), \frac{\sqrt{2}}{2}(s+t), \left(t + \frac{1}{2}\right)\sinh(\sqrt{2}s) + \frac{t\sqrt{2}}{2}\cosh(\sqrt{2}s)\right),$$

$-1 \leq s \leq 1, 0 \leq t \leq 1$ with constant mean curvature $H(s, 0) = -1$ along the spacelike curve $\alpha(s)$ is obtained (Figure 1).

Choosing marching-scale functions $u(s, t) = w(s, t) = t, v(s, t) \equiv 0$ and $t_0 = 0$, satisfies Theorem 1 (ii) and we immediately get the surface

$$P_2(s, t) = \left(\frac{1}{2}\cosh(\sqrt{2}s), \frac{\sqrt{2}}{2}(s+2t), \frac{1}{2}\sinh(\sqrt{2}s)\right),$$

with constant mean curvature $H(s, 0) = 1$ along the curve $\alpha(s)$ (Figure 2).

Example 2 The spacelike curve with timelike binormal

$$\alpha(s) = \left(\frac{4}{9}\sinh(3s), \frac{4}{9}\cosh(3s), \frac{5}{3}s\right)$$

has the following Frenet apparatus :

$$T(s) = \left(\frac{4}{3}\cosh(3s), \frac{4}{3}\sinh(3s), \frac{5}{3}s\right),$$

$$N(s) = \left(\sinh(3s), \cosh(3s), 0\right),$$

$$B(s) = \left(-\frac{5}{3}\cosh(3s), -\frac{5}{3}\sinh(3s), -\frac{4}{3}\right),$$

$$\kappa(s) = 4, \quad \tau(s) = -5.$$

Choosing marching-scale functions $v(s, t) = t, u(s, t) = w(s, t) \equiv 0$ and $t_0 = 0$, satisfies Theorem 2 (iii) and we obtain the surface

$$P_3(s, t) = \left(\left(\frac{4}{9} + t\right)\sinh(3s), \left(\frac{4}{9} + t\right)\cosh(3s), \frac{5}{3}s\right),$$

$-1 \leq s \leq 1, 0 \leq t \leq 1$ with constant mean curvature $H(s, 0) = 0$ along the curve $\alpha(s)$ (Figure 3) .

If we choose $u(s, t) = v(s, t) \equiv 0, w(s, t) = t$ and $t_0 = 0$, Theorem 2 (iv) is satisfied and we obtain the surface

$$P_4(s, t) = \left(\frac{4}{9}\sinh(3s) - \frac{5}{3}t\cosh(3s), \frac{4}{9}\cosh(3s) - \frac{5}{3}t\sinh(3s), \frac{5s-4t}{3}\right),$$

$-1 \leq s \leq 1, 0 \leq t \leq 1$ with constant mean curvature $H(s, 0) = -2$ along the curve $\alpha(s)$ (Figure 4).

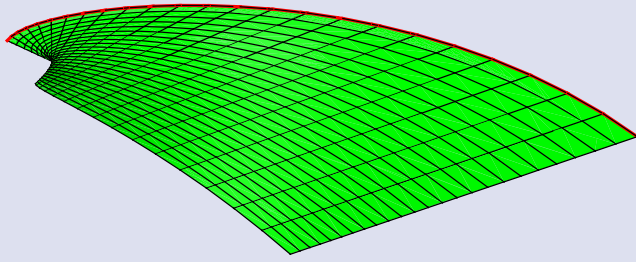


Figure 1. Constant mean curvature surface $P_1(s,t)$ along the spacelike curve $\alpha(s)$

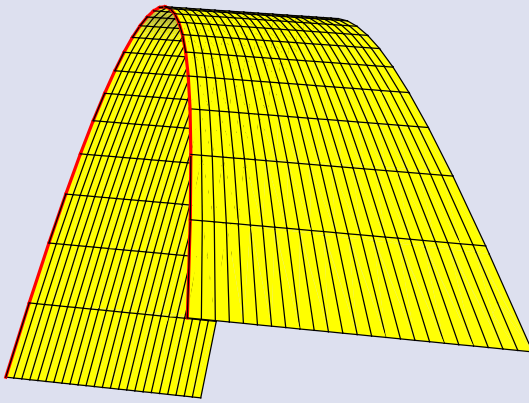


Figure 2. Constant mean curvature surface $P_2(s,t)$ along the spacelike curve $\alpha(s)$

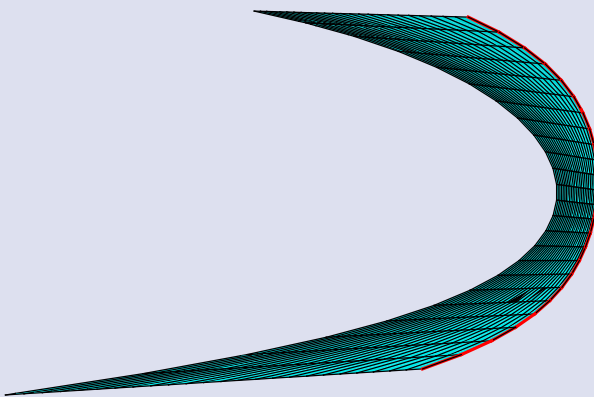


Figure 3. Constant mean curvature surface $P_3(s,t)$ along the spacelike curve $\alpha(s)$

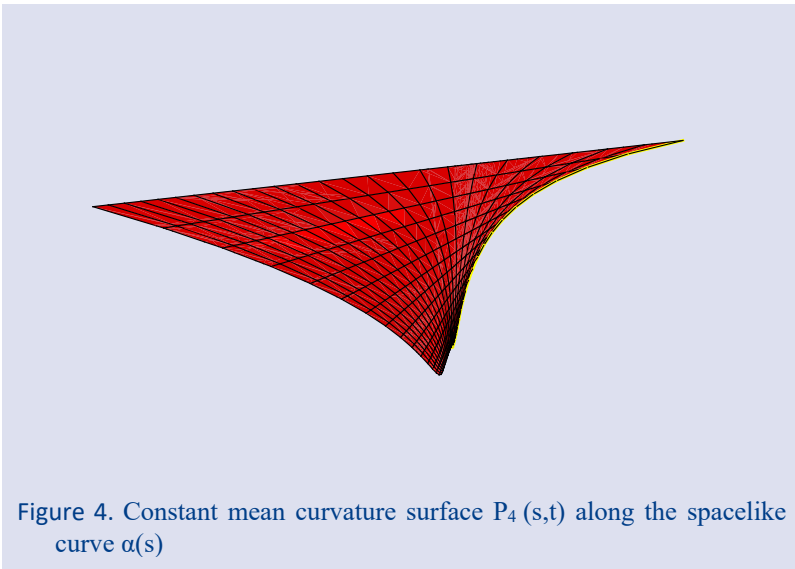


Figure 4. Constant mean curvature surface $P_4(s,t)$ along the spacelike curve $\alpha(s)$

Acknowledgment

The author would like to present his sincere appreciation to the Editor and referees for their time and efforts.

Conflicts of interest

The authors state that there is no conflict of interests.

References

- [1] O'Neill B., Semi-Riemannian geometry with applications to relativity, Academic Press Lim., London, (1983).
- [2] Willmore T.J., An introduction to differential geometry, Oxford University Press, Delhi, (1959).
- [3] Carmo M.P., Differential geometry of curves and surfaces, Englewood Cliffs, Prentice Hall, (1976).
- [4] Wang G.J., Tang K., Tai C.L., Parametric representation of a surface pencil with a common spatial geodesic, *Comput. Aided Design*, 36 (2004) 447-459.
- [5] Kasap E., Akyıldız F.T., Surfaces with common geodesic in Minkowski 3-space, *Appl. Math. Comput*, 177 (2006) 260-270.
- [6] Li C.Y., Wang R.H., Zhu C.G., Parametric representation of a surface pencil with a common line of curvature, *Comput. Aided Design*, 43 (2011) 1110-1117.
- [7] Bayram E., Güler F., Kasap E., Parametric representation of a surface pencil with a common asymptotic curve, *Comput. Aided Design*, 44 (2012) 637-643.
- [8] Bayram E., Bilici M., Surface family with a common involute asymptotic curve, *Int. J. Geom. Methods Modern Phys.*, 13 (2016) 1650062.
- [9] Güler F., Bayram E., Kasap E., Offset surface pencil with a common asymptotic curve, *Int. J. Geom. Methods Modern Phys.*, 15 (2018) 1850195.
- [10] Şaffak Atalay G., Kasap E., Surfaces family with common null asymptotic, *Appl. Math. Comput.*, 260 (2015) 135-139.
- [11] Yüzbaşı Z.K., On a family of surfaces with common asymptotic curve in the Galilean space G_3 , *J. Nonlinear Sci. Appl.*, 9 (2016), 518-523.
- [12] Şaffak Atalay G., Bayram E., Kasap E., Surface family with a common asymptotic curve in Minkowski 3-space, *Journal of Science and Arts*, 2 (43) (2018) 357-368.
- [13] Yoon D.W., Yüzbaşı Z.K., Bektaş M., An approach for surfaces using an asymptotic curve in Lie Group, *Journal of Advanced Physics*, 6 (4) (2017) 586-590.
- [14] Bayram E., Surface pencil with a common adjoint curve, *Turkish Journal of Mathematics*, 44 (2020) 1649 -1659.
- [15] Coşanoğlu H., Bayram E., Surfaces with constant mean curvature along a curve in 3-dimensional Euclidean space, Süleyman Demirel University, *Journal of Natural and Applied Sciences*, 24 (3) (2020) 533-538.
- [16] Mert T., Karlığa B., Timelike surfaces with constant angle in de-Sitter space, *Boletim da Sociedade Paranaense de Matemática*, 35 (2017), 79-93.
- [17] Mert T., Atçeken M., Some special ruled surfaces in hyperbolic 3-space, *Konuralp Journal of Mathematics*, 9 (2), (2021), 298-309.
- [18] Walrave J., Curves and surfaces in Minkowski space, PhD. Thesis, K. U. Leuven Faculteit Der Wetenschappen, 1995.
- [19] Lopez R., Differential geometry of curves and surfaces in Lorentz-Minkowski space, *Int. El. J. of Geometry*, 7 (1) (2014) 44-107.

(k,μ)-Paracontact Manifolds and Their Curvature Classification

Pakize Uygun^{1,a,*}

¹ Department Of Mathematics, Faculty Of Arts And Sciences, Tokat Gaziosmanpaşa University, Tokat, Türkiye.

*Corresponding author

Research Article

History

Received: 25/04/2022

Accepted: 01/08/2022

Copyright



©2022 Faculty of Science,
Sivas Cumhuriyet University

^a pakizeuygun@hotmail.com

^{id} <https://orcid.org/0000-0001-8226-4269>

ABSTRACT

The aim of this paper is to study (k, μ) -Paracontact metric manifold. We introduce the curvature tensors of a (k, μ) -paracontact metric manifold satisfying the conditions $R \cdot P_* = 0, R \cdot L = 0, R \cdot W_1 = 0, R \cdot W_0 = 0$ and $R \cdot M = 0$. According to these cases, (k, μ) -paracontact manifolds have been characterized such as η -Einstein and Einstein. We get the necessary and sufficient conditions of a (k, μ) -paracontact metric manifold to be η -Einstein. Also, we consider new conclusions of a (k, μ) -paracontact metric manifold contribute to geometry. We think that some interesting results on a (k, μ) -paracontact metric manifold are obtained.

Keywords: (k, μ) – Paracontact manifold, η – Einstein manifold, Riemannian curvature tensor.

Introduction

In 1985, Kaneyuki and Williams initiated the notion of paracontact geometry [1]. Zamkovoy achieved systematic research on paracontact metric manifolds and some remarkable subclasses named para-Sasakian manifolds [2]. Recently, B. Cappeletti-Montano, I. Küpeli Erken and C. Murathan introduced a new type of paracontact geometry so-called paracontact metric (k, μ) –space, where k and μ are constants [3]. This is known [4] about the contact case $k \leq 1$, but in the paracontact case there is no restriction of k .

Zamkovoy studied paracontact metric manifolds and some remarkable subclasses named para-Sasakian manifolds. In particular, many authors have pointed to the importance of paracontact geometry and para-Sasakian geometry in recent years. A normal paracontact metric manifold is a para-Sasakian manifold. An almost paracontact metric manifold is a para-Sasakian manifold if and only if [2]

$$(\nabla_{\beta_1} \phi)\beta_2 = -g(\beta_1, \beta_2)\xi + \eta(\beta_2)\beta_1.$$

As a generalization of locally symmetric spaces, many authors have studied semi-symmetric spaces and in turn their generalizations. A semi-Riemannian manifold (M^{2n+1}, g) , $n \geq 1$, is said to be semi-symmetric if its curvature tensor R satisfies $R \cdot R = 0$ for all vector fields β_1, β_2 on M^{2n+1} , where $R(\beta_1, \beta_2)$ acts as a derivation on [5,6]. D. Kowalezyk researched some subclass of semi-symmetric manifolds [5].

On the other hand, B. Prasad introduced a pseudo projective curvature tensor on a Riemannian manifold [6]. S. Ivanov, D. Vassilev and S. Zamkovoy studied a tensor invariant characterizing locally the integrable paracontact Hermitian structures which are paracontact

conformally equivalent to the flat structure on $G(P)$ [7]. Since then several geometers studied curvature conditions and obtain various important properties [8,9,19].

The object of this paper is to study properties of the some certain curvature tensor in a (k, μ) –paracontact metric manifold we research $R \cdot P_* = 0, R \cdot L = 0, R \cdot W_1 = 0, R \cdot W_0 = 0$ and $R(X, Y) \cdot M = 0$, where R, P_*, L, W_1, W_0 and M denote the Riemannian, pseudo-projective, conharmonic, W_1, W_0 and M –projective curvature tensors of manifold, respectively.

Preliminaries

An $(2n + 1)$ -dimensional manifold M is called to have a paracontact structure if it admits a $(1,1)$ –tensor field ϕ , a vector field ξ and a 1-form η satisfying the following conditions [1]:

$$(i) \quad \phi^2 \beta_1 = \beta_1 - \eta(\beta_1)\xi,$$

for any vector field $\beta_1 \in \chi(M)$, where $\chi(M)$ the set of all differential vector fields on M ,

$$(ii) \quad \eta(\xi) = 1, \eta \circ \phi = 0, \phi\xi = 0,$$

an almost paracontact manifold equipped with a pseudo-Riemannian metric g such that

$$\begin{aligned} g(\phi\beta_1, \phi\beta_2) &= -g(\beta_1, \beta_2) + \eta(\beta_1)\eta(\beta_2), \\ g(\beta_1, \xi) &= \eta(\beta_1) \end{aligned} \quad (1)$$

for all vector fields $\beta_1, \beta_2 \in \chi(M)$. An almost paracontact structure is called a paracontact structure if $g(\beta_1, \phi\beta_2) = d\eta(\beta_1, \beta_2)$ with the associated metric g

[2]. We now define a (1,1) tensor field h by $h = \frac{1}{2}L_\xi\phi$, where L denotes the Lie derivative. Then h is symmetric and satisfies the conditions

$$h\phi = -\phi h, \quad h\xi = 0, \quad Tr.h = Tr.\phi h = 0 \quad (2)$$

If $\tilde{\nabla}$ denotes the Levi-Civita connection of g , then we have the following relation

$$\tilde{\nabla}_{\beta_1}\xi = -\phi\beta_1 + \phi h\beta_1 \quad (3)$$

for any $\beta_1 \in \chi(M)$ [2]. For a paracontact metric manifold $M^{2n+1}(\phi, \xi, \eta, g)$, if ξ is a killing vector field or equivalently, $h = 0$, then it is called a K-paracontact manifold.

An almost paracontact manifold is said to be para-Sasakian if and only if the following condition holds

$$(\tilde{\nabla}_{\beta_1}\phi)\beta_2 = -g(\beta_1, \beta_2)\xi + \eta(\beta_2)\beta_1$$

for all $\beta_1, \beta_2 \in \chi(M)$ [2]. A normal paracontact metric manifold is para-Sasakian and satisfies

$$R(\beta_1, \beta_2)\xi = -(\eta(\beta_2)\beta_1 - \eta(\beta_1)\beta_2) \quad (4)$$

for all $\beta_1, \beta_2 \in \chi(M)$, but this is not a sufficient condition for a para-contact manifold to be para-Sasakian. It is clear that every para-Sasakian manifold is K-paracontact. But the converse is not always true [16].

A paracontact manifold M is said to be η -Einstein if its Ricci tensor S of type (0,2) is of the form $S(\beta_1, \beta_2) = ag(\beta_1, \beta_2) + b\eta(\beta_1)\eta(\beta_2)$, where a, b are smooth functions on M . If $b = 0$, then the manifold is also called Einstein [11].

A paracontact metric manifold is said to be a (k, μ) -paracontact manifold if the curvature tensor \tilde{R} satisfies

$$\tilde{R}(\beta_1, \beta_2)\xi = k[\eta(\beta_2)\beta_1 - \eta(\beta_1)\beta_2] + \mu[\eta(\beta_2)h\beta_1 - \eta(\beta_1)h\beta_2] \quad (5)$$

for all $\beta_1, \beta_2 \in \chi(M)$, where k and μ are real constants.

This class is very wide containing the para-Sasakian manifolds as well as the paracontact metric manifolds satisfying $R(\beta_1, \beta_2)\xi = 0$ [12].

$$L(\beta_1, \beta_2) = R(\beta_1, \beta_2)\beta_3 - \frac{1}{2n-1}[S(\beta_2, \beta_3)\beta_1 - S(\beta_1, \beta_3)\beta_2 + g(\beta_2, \beta_3)Q\beta_1 - g(\beta_1, \beta_3)Q\beta_2], \quad (14)$$

$$P_*(\beta_1, \beta_2)\beta_3 = aR(\beta_1, \beta_2)\beta_3 + b[S(\beta_2, \beta_3)\beta_1 - S(\beta_1, \beta_3)\beta_2] - \frac{r}{2n+1}\left(\frac{a}{2n} + b\right)[g(\beta_2, \beta_3)\beta_1 - g(\beta_1, \beta_3)\beta_2], \quad (15)$$

$$M(\beta_1, \beta_2)\beta_3 = R(\beta_1, \beta_2)\beta_3 - \frac{1}{4n}[S(\beta_2, \beta_3)\beta_1 - S(\beta_1, \beta_3)\beta_2 + g(\beta_2, \beta_3)Q\beta_1 - g(\beta_1, \beta_3)Q\beta_2], \quad (16)$$

$$W_0(\beta_1, \beta_2)\beta_3 = R(\beta_1, \beta_2)\beta_3 - \frac{1}{2n}[S(\beta_2, \beta_3)\beta_1 - g(\beta_1, \beta_3)Q\beta_2], \quad (17)$$

$$W_1(\beta_1, \beta_2)\beta_3 = R(\beta_1, \beta_2)\beta_3 + \frac{1}{2n}[S(\beta_2, \beta_3)\beta_1 - S(\beta_1, \beta_3)\beta_2], \quad (18)$$

for all $\beta_1, \beta_2, \beta_3 \in \chi(M)$ [14].

(k, μ) -Paracontact Manifolds and Their Curvature Classification in

In this part, we will give the major results for this paper.

In particular, if $\mu = 0$, then the paracontact metric manifold is called paracontact metric $N(k)$ -manifold. Thus, for a paracontact metric $N(k)$ -manifold the curvature tensor satisfies the following relation

$$R(\beta_1, \beta_2)\xi = k(\eta(\beta_2)\beta_1 - \eta(\beta_1)\beta_2) \quad (6)$$

for all $\beta_1, \beta_2 \in \chi(M)$. Though the geometric behavior of paracontact metric (k, μ) -spaces is different according as $k < -1$, or $k > -1$, but there are some common results for $k < -1$ and $k > -1$ [3].

Lemma 2.1 There does not exist any paracontact (k, μ) -manifold of dimension greater than 3 with $k > -1$ which is Einstein whereas there exist such manifolds for $k < -1$ [3].

In a paracontact metric (k, μ) -manifold $(M^{2n+1}, \phi, \xi, \eta, g)$, $n > 1$, the following relation hold:

$$h^2 = (k + 1)\phi^2, \text{ for } k \neq -1, \quad (7)$$

$$(\tilde{\nabla}_{\beta_1}\phi)\beta_2 - g(\beta_1 - h\beta_1, \beta_2)\xi + \eta(\beta_2)(\beta_1 - h\beta_1), \quad (8)$$

$$S(\beta_1, \beta_2) = [2(1 - n) + n\mu]g(\beta_1, \beta_2) + [2(n - 1) + \mu]g(h\beta_1, \beta_2) + [2(n - 1) + n(2k - \mu)]\eta(\beta_1)\eta(\beta_2), \quad (9)$$

$$S(\beta_1, \xi) = 2nk\eta(\beta_1), \quad (10)$$

$$Q\beta_2 = [2(1 - n) + n\mu]\beta_2 + [2(n - 1) + \mu]h\beta_2 + [2(n - 1) + n(2k - \mu)]\eta(\beta_2)\xi \quad (11)$$

$$Q\xi = 2nk\xi, g(Q\beta_1, \beta_2) = S(\beta_1, \beta_2), \quad (12)$$

$$Q\phi - \phi Q = 2[2(n - 1) + \mu]h\phi \quad (13)$$

for any vector fields β_1, β_2 on M^{2n+1} , where Q and S denotes the Ricci operator and Ricci tensor of (M^{2n+1}, g) , respectively [3].

The concept of conharmonic curvature tensor was defined by Y. Ishii [13]. Conharmonic, pseudo-projective, M -projective, W_0 -curvature tensor and W_1 -curvature tensor of a $(2n + 1)$ -dimensional Riemannian manifolds are, respectively, defined

Let M be $(2n + 1)$ –dimensional (k, μ) –paracontact metric manifold and we denote conharmonic curvature tensor by L , then from (14), we have for later

$$L(\beta_1, \beta_2)\xi = \frac{k}{2n-1} [\eta(\beta_1)\beta_2 - \eta(\beta_2)\beta_1] + \mu[\eta(\beta_2)h\beta_1 - \eta(\beta_1)h\beta_2] - \frac{1}{2n-1} [\eta(\beta_2)Q\beta_1 - \eta(\beta_1)Q\beta_2]. \tag{19}$$

Putting $\beta_1 = \xi$, in (19)

$$L(\xi, \beta_2)\xi = \frac{k}{2n-1} [\beta_2 - \eta(\beta_2)\xi] - \mu h\beta_2 - \frac{1}{2n-1} [2nk\eta(\beta_2)\xi - Q\beta_2]. \tag{20}$$

In (15), choosing $\beta_3 = \xi$ and using (5), we obtain

$$P_*(\beta_1, \beta_2)\xi = \left[ak + 2nkb - \frac{r}{2n+1} \left(\frac{a}{2n} + b \right) \right] (\eta(\beta_2)\beta_1 - \eta(\beta_1)\beta_2) + a\mu(\eta(\beta_2)h\beta_1 - \eta(\beta_1)h\beta_2). \tag{21}$$

In (21), it follows

$$P_*(\xi, \beta_2)\xi = [ak + 2nkb - \frac{r}{2n+1} (\frac{a}{2n} + b)] (\eta(\beta_2)\xi - \beta_2) - a\mu h\beta_2. \tag{22}$$

In the same way, putting $\beta_3 = \xi$ in (16) and using (5), we have

$$M(\beta_1, \beta_2)\xi = \frac{k}{2} (\eta(\beta_2)\beta_1 - \eta(\beta_1)\beta_2) + \mu(\eta(\beta_2)h\beta_1 - \eta(\beta_1)h\beta_2) - \frac{1}{4n} (\eta(\beta_2)Q\beta_1 - \eta(\beta_1)Q\beta_2). \tag{23}$$

Using $\beta_1 = \xi$ in (23), we get

$$M(\xi, \beta_2)\xi = \frac{1}{4n} Q\beta_2 - \frac{k\beta_2}{2} - \mu h\beta_2. \tag{24}$$

In (17), choosing $\beta_3 = \xi$, we obtain

$$W_0(\beta_1, \beta_2)\xi = \frac{1}{2n} \eta(\beta_1)Q\beta_2 - k\eta(\beta_1)\beta_2 + \mu(\eta(\beta_2)h\beta_1 - \eta(\beta_1)h\beta_2). \tag{25}$$

and

$$W_0(\xi, \beta_2)\xi = \frac{1}{2n} Q\beta_2 - k\beta_2 - \mu h\beta_2. \tag{26}$$

In (18), choosing $\beta_3 = \xi$ and using (5), we obtain

$$W_1(\beta_1, \beta_2)\xi = 2k(\eta(\beta_2)\beta_1 - \eta(\beta_1)\beta_2) + \mu(\eta(\beta_2)h\beta_1 - \eta(\beta_1)h\beta_2). \tag{27}$$

Setting $\beta_1 = \xi$ in (27), we get

$$W_1(\xi, \beta_2)\xi = 2k(\eta(\beta_2)\xi - \beta_2) - \mu h\beta_2. \tag{28}$$

From (5), we can derive

$$R(\xi, \beta_2)\beta_3 = k(g(\beta_2, \beta_3)\xi - \eta(\beta_3)\beta_2) + \mu(g(h\beta_2, \beta_3)\xi - \eta(\beta_3)h\beta_2), \tag{29}$$

Choosing $\beta_3 = \xi$, in (29)

$$R(\xi, \beta_2)\xi = k(\eta(\beta_2)\xi - \beta_2) - \mu h\beta_2. \tag{30}$$

Theorem 3.1 Let $M^{2n+1}(\phi, \xi, \eta, g)$ be a (k, μ) -paracontact space. Then M is a conharmonic semi-symmetric if and only if M is an η –Einstein manifold.

Proof. Suppose that M is a conharmonic semi-symmetric. This implies that

$$(R(\beta_1, \beta_2)L)(\beta_3, \beta_4)\beta_5 = R(\beta_1, \beta_2)L(\beta_3, \beta_4)\beta_5 - L(R(\beta_1, \beta_2)\beta_3, \beta_4)\beta_5 - L(\beta_3, R(\beta_1, \beta_2)\beta_4)\beta_5 - L(\beta_3, \beta_4)R(\beta_1, \beta_2)\beta_5 = 0, \tag{31}$$

for any $\beta_1, \beta_2, \beta_3, \beta_4, \beta_5 \in \chi(M)$. Taking $\beta_1 = \beta_5 = \xi$ in (31), making use of (19), (29) and (30), for $B = -\frac{1}{2n-1}$, we have

$$(R(\xi, \beta_2)L)(\beta_3, \beta_4)\xi = R(\xi, \beta_2)(Bk(\eta(\beta_4)\beta_3 - \eta(\beta_3)\beta_4) + \mu(\eta(\beta_4)h\beta_3 - \eta(\beta_3)h\beta_4) + B(\eta(\beta_4)Q\beta_3 - \eta(\beta_3)Q\beta_4) - L(k(g(\beta_2, \beta_3)\xi - \eta(\beta_3)\beta_2) + \mu(g(h\beta_2, \beta_3)\xi - \eta(\beta_3)h\beta_2, \beta_4)\xi - L(\beta_3, k(g(\beta_2, \beta_4)\xi - \eta(\beta_4)\beta_2) + \mu(g(h\beta_2, \beta_4)\xi - \eta(\beta_4)h\beta_2)\xi - L(\beta_3, \beta_4)(k(\eta(\beta_2)\xi - \beta_2) - \mu h\beta_2) = 0. \tag{32}$$

Taking into account (19), (20), (29) and inner product both sides of (32) by $\beta_5 \in \chi(M)$

$$kg(L(\beta_3, \beta_4)\beta_2, \beta_5) + \mu g(L(\beta_3, \beta_4)f\beta_2, \beta_5) + k\mu(\eta(\beta_4)\eta(\beta_5)g(\beta_2, h\beta_3) - \eta(\beta_3)\eta(\beta_5)g(\beta_2, h\beta_4)) + \mu^2(1 + k)(\eta(\beta_4)\eta(\beta_5)g(\beta_2, \beta_3) - \eta(\beta_3)\eta(\beta_5)g(\beta_2, \beta_4)) + B\mu(\eta(\beta_4)\eta(\beta_5)S(\beta_2, h\beta_3) - \eta(\beta_3)\eta(\beta_5)S(\beta_2, h\beta_4)) + Bk(\eta(\beta_4)\eta(\beta_5)S(\beta_2, \beta_3) - \eta(\beta_3)\eta(\beta_5)S(\beta_2, \beta_4)) + 2nk\mu B(\eta(\beta_3)\eta(\beta_5)g(h\beta_2, \beta_4) - g(h\beta_2, \beta_3)\eta(\beta_4)\eta(\beta_5)) + 2nk^2B(g(\beta_2, \beta_4)\eta(\beta_3)\eta(\beta_5) - g(\beta_2, \beta_3)\eta(\beta_4)\eta(\beta_5)) + Bk(g(\beta_2, \beta_3)S(\beta_4, \beta_5) - g(\beta_2, \beta_4)S(\beta_3, \beta_5)) + Bk^2(g(h\beta_2, \beta_3)S(\beta_4, \beta_5) + g(h\beta_2, \beta_4)S(\beta_3, \beta_5)) + \mu^2(g(h\beta_2, \beta_3)g(h\beta_4, \beta_5) - g(h\beta_2, \beta_4)g(h\beta_3, \beta_5)) + k\mu(g(\beta_2, \beta_3)g(h\beta_4, \beta_5) + g(\beta_2, \beta_4)g(h\beta_3, \beta_5)) = 0. \tag{33}$$

Putting (7), (10), (14) and choosing $\beta_4 = \beta_2 = e_i, \xi$, in (33), $1 \leq i \leq n$, for orthonormal basis of $\chi(M)$, we arrive

$$k(1 - B)S(\beta_3, \beta_5) + \mu(1 - B)S(\beta_3, h\beta_5) + (Bkr + 2n(1 + k)[2(n - 1) + \mu] + \mu^2(1 + k) - 2nk^2B)g(\beta_3, \beta_5) + (k\mu B - 2nk\mu)g(\beta_3, h\beta_5) + (\mu^2(1 + k)(2n + 1) - Bkr - 2n\mu B(1 + k)[2(n - 1) + \mu] + 2nk^2B(2n + 1))\eta(\beta_3)\eta(\beta_5) = 0. \tag{34}$$

Using (7) and replacing $h\beta_5$ of β_5 in (34), we get

$$k(1 - B)S(\beta_3, h\beta_5) + \mu(1 - B)(1 + k)S(\beta_3, \beta_5) - 2nk\mu(1 + k)(1 - B)\eta(\beta_2)\eta(\beta_3) + (Bkr + 2n(1 + k)[2(n - 1) + \mu] + \mu^2(1 + k) - 2nk^2B)g(\beta_3, h\beta_5) + (1 + k)(k\mu B - 2nk\mu)g(\beta_3, \beta_5) - (1 + k)(k\mu B - 2nk\mu)\eta(\beta_3)\eta(\beta_5) = 0. \tag{35}$$

From (34), (35) and also using (9), for the sake of brevity we set

$$p_1 = \frac{2nk}{2n-1},$$

$$p_2 = \frac{2n\mu}{2n-1},$$

$$p_3 = \left(-\frac{kr}{2n-1} + 2n(1 + k)[2(n - 1) + \mu] + \mu^2(1 + k) + \frac{2nk^2}{2n-1}\right),$$

$$p_4 = \left(-\frac{k\mu}{2n-1} - 2nk\mu\right),$$

$$p_5 = (\mu^2(1 + k)(2n + 1) + \frac{kr}{2n-1} + \frac{2n\mu}{2n-1}(1 + k)[2(n - 1) + \mu] - \frac{2nk^2}{2n-1}(2n + 1),$$

and

$$q_1 = (p_4p_2(1 + k) - p_3p_1)[2(n - 1) + \mu] + (p_4p_1 - p_3p_2)[2(1 - n) + n\mu],$$

$$q_2 = (p_1^2 - p_2^2(1 + k))[2(n - 1) + \mu] + (p_4p_1 - p_3p_2),$$

$$q_3 = (p_4p_2 - p_3p_2)[2(n - 1) + n(2k - \mu)] - (p_1p_5 + 2nkp_2^2(1 + k) + p_4p_2(1 + k))[2(n - 1) + \mu],$$

we conclude

$$q_2S(\beta_3, \beta_5) = q_1g(\beta_3, \beta_5) + q_3\eta(\beta_3)\eta(\beta_5).$$

So, M is an η -Einstein manifold. Conversely, let $M^{2n+1}(\varphi, \xi, \eta, g)$ be an η -Einstein manifold, i.e. $q_2S(\beta_3, \beta_5) = q_1g(\beta_3, \beta_5) + q_3\eta(\beta_3)\eta(\beta_5)$, then from equations (35), (34), (33), (32) and (31) we obtain M is a conharmonic semi-symmetric.

Theorem 3.2 Let $M^{2n+1}(\phi, \xi, \eta, g)$ be a (k, μ) -paracontact space. Then M is a pseudo-projective semi-symmetric if and only if M is an Einstein manifold.

Proof. Assume that M is a pseudo-projective semi-symmetric. This yields to

$$(R(\beta_1, \beta_2)P_*)(\beta_3, \beta_4)\beta_5 = R(\beta_1, \beta_2)P_*(\beta_3, \beta_4)\beta_5 - P_*(R(\beta_1, \beta_2)\beta_3, \beta_4)\beta_5 - P_*(\beta_3, R(\beta_1, \beta_2)\beta_4)\beta_5 - P_*(\beta_3, \beta_4)R(\beta_1, \beta_2)\beta_5 = 0, \tag{36}$$

for any $\beta_1, \beta_2, \beta_3, \beta_4, \beta_5 \in \chi(M)$. Taking $\beta_1 = \beta_5 = \xi$ in (36) and using (21), (29), (30), for $A = [ak + 2nkb - \frac{r}{2n+1}(\frac{a}{2n} + b)]$, we obtain

$$(R(\xi, \beta_2)P_*)(\beta_3, \beta_4)\xi = R(\xi, \beta_2)(A(\eta(\beta_4)\beta_3 - \eta(\beta_3)\beta_4) + \mu(\eta(\beta_4)h\beta_3 - \eta(\beta_3)h\beta_4) - P_*(k(g(\beta_2, \beta_3)\xi - \eta(\beta_3)\beta_2) + \mu(g(h\beta_2, \beta_3)\xi - \eta(\beta_3)h\beta_2)), \beta_4)\xi - P_*(\beta_3, k(g(\beta_2, \beta_4)\xi - \eta(\beta_4)\beta_2) + \mu(g(h\beta_2, \beta_4)\xi - \eta(\beta_4)h\beta_2))\xi - P_*(\beta_3, \beta_4)k(\eta(\beta_2)\xi - \beta_2) - \mu h\beta_2 = 0. \tag{37}$$

Again, taking into account that (21), (22), (29) in (37), we get

$$kP_*(\beta_3, \beta_4)\beta_2 + \mu P_*(\beta_3, \beta_4)h\beta_2 + ak\mu(\eta(\beta_4)g(\beta_2, h\beta_3)\xi - \eta(\beta_3)g(\beta_2, h\beta_4)\xi) + a\mu^2(1+k)(\eta(\beta_4)g(\beta_2, \beta_3)\xi - \eta(\beta_3)g(\beta_2, \beta_4)\xi) + Ak(g(\beta_2, \beta_3)\beta_4 - g(\beta_2, \beta_4)\beta_3) + A\mu(g(h\beta_2, \beta_3)\beta_4 - g(h\beta_2, \beta_4)\beta_3) + a\mu^2(g(h\beta_2, \beta_3)h\beta_4 - g(h\beta_2, \beta_4)h\beta_3) + ak\mu(g(\beta_2, \beta_3)h\beta_4 - g(\beta_2, \beta_4)h\beta_3) = 0. \tag{38}$$

Putting $\beta_3 = \xi$, using (7), (21) and inner product both sides of in (38) by $\xi \in \chi(M)$, we get

$$bkS(\beta_2, \beta_4) + b\mu S(\beta_4, h\beta_2) - 2nk^2bg(\beta_2, \beta_4) - 2nkb\mu g(\beta_4, h\beta_2) = 0 \tag{39}$$

Replacing $h\beta_4$ of β_4 in (39) and making use of (7), we have

$$bkS(\beta_2, h\beta_4) + b\mu(1+k)S(\beta_2, \beta_4) - 2nkb\mu(1+k)\eta(\beta_2)\eta(\beta_4) - 2nk^2bg(\beta_2, h\beta_4) - 2nkb\mu(1+k)g(\beta_2, \beta_4) + 2nkb\mu(1+k)\eta(\beta_2)\eta(\beta_4) = 0. \tag{40}$$

From (39) and (40), we obtain

$$S(\beta_2, \beta_4) = 2nkg(\beta_2, \beta_4).$$

Thus, M is an Einstein manifold. Conversely, let $M^{2n+1}(\phi, \xi, \eta, g)$ be an Einstein manifold, i.e., $S(\beta_2, \beta_4) = 2nkg(\beta_2, \beta_4)$, then from equations (40), (39), (38), (37) and (36), we arrive M is a pseudo-projective semi-symmetric. This implies that

$$\mu = 2(k + 1 - \frac{1}{n}).$$

Theorem 3.3 Let $M^{2n+1}(\phi, \xi, \eta, g)$ be a (k, μ) -paracontact space. Then M is a M -projective semi-symmetric if and only if M is an Einstein manifold.

Proof. Suppose that M is a M -projective semi-symmetric. This implies that

$$(R(\beta_1, \beta_2)M)(\beta_3, \beta_4)\beta_5 = R(\beta_1, \beta_2)M(\beta_3, \beta_4)\beta_5 - M(R(\beta_1, \beta_2)\beta_3, \beta_4)\beta_5 - M(\beta_3, R(\beta_1, \beta_2)\beta_4)\beta_5 - M(\beta_3, \beta_4)R(\beta_1, \beta_2)\beta_5 = 0, \tag{41}$$

for any $\beta_1, \beta_2, \beta_3, \beta_4, \beta_5 \in \chi(M)$. Setting $\beta_1 = \beta_5 = \xi$ in (41) and making use of (23), (29), (30), for $A = \frac{k}{2}, B = -\frac{1}{4n}$, we obtain

$$(R(\xi, \beta_2)M)(\beta_3, \beta_4)\xi = R(\xi, \beta_2)(A(\eta(\beta_4)\beta_3 - \eta(\beta_3)\beta_4) + \mu(\eta(\beta_4)h\beta_3 - \eta(\beta_3)h\beta_4) + B(\eta(\beta_4)Q\beta_3 - \eta(\beta_3)Q\beta_4) - M(k(g(\beta_2, \beta_3)\xi - \eta(\beta_3)\beta_2) + \mu(g(h\beta_2, \beta_3)\xi - \eta(\beta_3)h\beta_2)), \beta_4)\xi - M(\beta_3, k(g(\beta_2, \beta_4)\xi - \eta(\beta_4)\beta_2) + \mu(g(h\beta_2, \beta_4)\xi - \eta(\beta_4)h\beta_2))\xi - M(\beta_3, \beta_4)(k(\eta(\beta_2)\xi - \beta_2) - \mu h\beta_2) = 0. \tag{42}$$

Inner product both sides of (42) by $\beta_5 \in \chi(M)$, using of (23), (24) and (29), we get

$$kg(M(\beta_3, \beta_4)\beta_2, \beta_5) + \mu g(M(\beta_3, \beta_4)h\beta_2, \beta_5) + Ak(\eta(\beta_4)\eta(\beta_5)g(\beta_2, h\beta_3) - \eta(\beta_3)\eta(\beta_5)g(\beta_2, \beta_4)) + \mu^2(1+k)(\eta(\beta_4)\eta(\beta_5)g(\beta_3, \beta_2) - \eta(\beta_3)\eta(\beta_5)g(\beta_2, \beta_4)) + A\mu(\eta(\beta_4)\eta(\beta_5)g(h\beta_2, \beta_3) - \eta(\beta_5)\eta(\beta_3)g(h\beta_2, \beta_4)) + k\mu(\eta(\beta_4)\eta(\beta_5)g(h\beta_2, \beta_3) - \eta(\beta_5)\eta(\beta_3)g(h\beta_2, \beta_4)) + Bk(\eta(\beta_4)\eta(\beta_5)S(\beta_2, \beta_3) - \eta(\beta_5)\eta(\beta_3)S(\beta_2, \beta_4)) + \mu B(\eta(\beta_4)\eta(\beta_5)S(h\beta_2, \beta_3) - \eta(\beta_5)\eta(\beta_3)S(h\beta_2, \beta_4)) + ak(g(\beta_2, \beta_3)g(\beta_5, \beta_4) - g(\beta_2, \beta_4)g(\beta_3, \beta_5)) + k\mu(g(\beta_3, \beta_2)g(h\beta_4, \beta_5) - g(\beta_2, \beta_4)g(h\beta_3, \beta_5)) + \mu^2(g(h\beta_4, \beta_5)g(h\beta_2, \beta_3) - g(h\beta_2, \beta_4)g(h\beta_3, \beta_5)) + A\mu(g(\beta_5, \beta_4)g(h\beta_2, \beta_3) - g(\beta_3, \beta_5)g(\beta_2, h\beta_4)) = 0. \tag{43}$$

Making use of (7), (16) and choosing $\beta_3 = \beta_5 = e_i, \xi, 1 \leq i \leq n$, for orthonormal basis of $\chi(M)$ in (43), we have

$$kS(\beta_4, \beta_2) + \mu S(\beta_4, h\beta_2) - 2nk^2g(\beta_4, \beta_2) - 2nkb\mu g(\beta_4, h\beta_2) = 0. \tag{44}$$

Replacing $h\beta_2$ of β_2 in (44) and taking into account (7), we get

$$kS(\beta_4, h\beta_2) + \mu(1 + k)S(\beta_4, \beta_2) - 2nk^2g(\beta_4, h\beta_2) - 2nk\mu(1 + k)g(\beta_4, \beta_2) = 0. \tag{45}$$

From (44), (45) and by using (9), we set

$$S(\beta_4, \beta_2) = 2nk g(\beta_4, \beta_2),$$

This tell us M is an Einstein manifold. Conversely, let $M^{2n+1}(\varphi, \xi, \eta, g)$ be an Einstein manifold, i.e., $S(\beta_4, \beta_2) = 2nk g(\beta_4, \beta_2)$, then from equations (45), (44), (43), (42) and (41), we get M is a M –projective semi-symmetric.

Theorem 3.4 Let $M^{2n+1}(\phi, \xi, \eta, g)$ be a (k, μ) -paracontact space. Then M is a W_0 -semi-symmetric if and only if M is an η –Einstein manifold.

Proof. Assume that M is a W_0 -semi-symmetric. This means that

$$(R(\beta_1, \beta_2)W_0)(\beta_3, \beta_4, \beta_5) = R(\beta_1, \beta_2)W_0(\beta_3, \beta_4)\beta_5 - W_0(R(\beta_1, \beta_2)\beta_3, \beta_4)\beta_5 - W_0(\beta_2, R(\beta_1, \beta_2)\beta_4)\beta_5 - W_0(\beta_3, \beta_4)R(\beta_1, \beta_2)\beta_5 = 0, \tag{46}$$

for any $\beta_1, \beta_2, \beta_3, \beta_4, \beta_5 \in \chi(M)$. Setting $\beta_1 = \beta_5 = \xi$ in (46) and making use of (25), (29), (30), for $A = -\frac{1}{2n}$, we obtain

$$(R(\xi, \beta_2)W_0)(\beta_3, \beta_4)\xi = R(\xi, \beta_2)(-A\eta(\beta_3)Q\beta_4 - k\eta(\beta_3)\beta_4 + \mu(\eta(\beta_4)h\beta_3 - \eta(\beta_3)h\beta_4)) - W_0(k(g(\beta_2, \beta_3)\xi - \eta(\beta_3)\beta_4) + \mu(g(h\beta_2, \beta_3)\xi - \eta(\beta_3)h\beta_2, \beta_4)\xi - W_0(\beta_3, k(g(\beta_2, \beta_4)\xi - \eta(\beta_4)\beta_2) + \mu(g(h\beta_2, \beta_4)\xi - \eta(\beta_4)h\beta_2)))\xi - W_0(\beta_3, \beta_4)(k(\eta(\beta_2)\xi - \beta_2) - \mu h\beta_2) = 0. \tag{47}$$

Using (25), (26), (29) and inner product both sides of (47) by $\beta_5 \in \chi(M)$, we get

$$kg(W_0(\beta_3, \beta_4)\beta_2, \beta_5) + \mu g(W_0(\beta_3, \beta_4)h\beta_2, \beta_5) + k\mu(\eta(\beta_4)\eta(\beta_5)g(\beta_2, h\beta_3) - \eta(\beta_3)\eta(\beta_5)g(\beta_2, h\beta_4)) + \mu^2(1 + k)(\eta(\beta_4)\eta(\beta_5)g(\beta_2, \beta_3) - \eta(\beta_3)\eta(\beta_5)g(\beta_2, \beta_4)) + 2nkA(k\eta(\beta_3)\eta(\beta_4)g(\beta_2, \beta_5) - \mu\eta(\beta_4)\eta(\beta_3)g(h\beta_2, \beta_5)) + Ak(S(\beta_4, \beta_5)g(\beta_2, \beta_3) - \eta(\beta_3)\eta(\beta_5)S(\beta_2, \beta_4)) + k^2(g(\beta_2, \beta_3)g(\beta_5, \beta_4) - g(\beta_2, \beta_4)g(\beta_3, \beta_5)) + k\mu(g(\beta_2, \beta_3)g(h\beta_4, \beta_5) - g(\beta_2, \beta_4)g(h\beta_3, \beta_5)) + A\mu(g(h\beta_2, \beta_3)S(\beta_4, \beta_5) - g(h\beta_2, \beta_4)S(\beta_3, \beta_5)) + k\mu(g(h\beta_2, \beta_3)g(\beta_4, \beta_5) + g(h\beta_2, \beta_4)g(\beta_3, \beta_5)) + \mu^2(g(h\beta_2, \beta_3)g(h\beta_4, \beta_5) - g(h\beta_2, \beta_4)g(h\beta_3, \beta_5)) - A\mu(S(h\beta_2, \beta_4)\eta(\beta_3)\eta(\beta_5) + \eta(\beta_3)\eta(\beta_4)S(h\beta_2, \beta_5)) - kA(S(\beta_2, \beta_5)\eta(\beta_3)\eta(\beta_4) + S(\beta_3, \beta_5)g(\beta_2, \beta_4)) - k(\eta(\beta_5)\eta(\beta_3)g(\beta_2, \beta_4) - \mu\eta(\beta_5)\eta(\beta_3)g(\beta_2, h\beta_4)) = 0. \tag{48}$$

Making use of (7), (17) and choosing $\beta_2 = \beta_4 = e_i, \xi, 1 \leq i \leq n$, for orthonormal basis of $\chi(M)$ in (48), we have

$$k(1 - A(2n + 1))S(\beta_3, \beta_5) + \mu S(\beta_3, h\beta_5) + (kAr + 2n\mu A(1 + k)[2(n - 1) + \mu] - 2nk^2 + \mu^2(1 + k))g(\beta_3, \beta_4) + k\mu(1 - 2n)g(\beta_3, h\beta_5) + (-k^2(2n + 1) - Akr - \mu^2(1 + k)(2n + 1)(-k^2(2n + 1) - Akr - \mu^2(1 + k)(2n + 1))\eta(\beta_3)\eta(\beta_5) = 0. \tag{49}$$

Replacing $h\beta_5$ of β_5 in (49) and taking into account (7), it follows

$$k(1 - A(2n + 1))S(\beta_3, h\beta_5) + \mu(1 + k)S(\beta_3, \beta_5) - 2nk\mu(1 + k)\eta(\beta_3)\eta(\beta_5) + (kAr + 2n\mu A(1 + k)[2(n - 1) + \mu] - 2nk^2 + \mu^2(1 + k))g(\beta_3, h\beta_5) + k\mu(1 + k)(1 - 2n)g(\beta_3, \beta_5) - k\mu(1 + k)(1 - 2n)\eta(\beta_3)\eta(\beta_5) = 0. \tag{50}$$

From (49), (50) and by using (9), for the sake of brevity we set

$$p_1 = k\left(2 + \frac{1}{2n}\right),$$

$$p_2 = \left(-\frac{kr}{2n} - \mu(1 + k)[2(n - 1) + \mu] - 2nk^2 + \mu^2(1 + k)\right),$$

$$p_3 = k\mu(1 - 2n),$$

$$p_4 = (-k^2(2n + 1) + \frac{kr}{n} - \mu^2(1 + k)(2n + 1) - k^2(2n + 1) - \mu^2(1 + k)(2n + 1)),$$

and

$$q_1 = (p_3\mu(1 + k) - p_1p_2)[2(n - 1) + \mu] + (p_1p_3 - p_2\mu)[2(1 - n) + n\mu],$$

$$q_2 = (p_1^2 - \mu^2(1 + k))[2(n - 1) + \mu] + (p_1p_3 - p_2\mu),$$

$$q_3 = (p_1p_3 - p_2\mu)[2(n - 1) + n(2k - \mu)] - (p_1p_4 + 2nk\mu^2(1 + k) + p_3\mu(1 + k))[2(n - 1) + \mu],$$

we have

$$q_2S(\beta_3, \beta_5) = q_1g(\beta_3, \beta_5) + q_3\eta(\beta_3)\eta(\beta_5).$$

Thus, M is an η –Einstein manifold. Conversely, let $M^{2n+1}(\varphi, \xi, \eta, g)$ be an η –Einstein manifold, i.e., $q_2S(\beta_3, \beta_5) = q_1g(\beta_3, \beta_5) + q_3\eta(\beta_3)\eta(\beta_5)$, then from equations (50), (49), (48), (47) and (46) we obtain M is a W_0 -semi-symmetric.

Theorem 3.5 Let $M^{2n+1}(\phi, \xi, \eta, g)$ be a (k, μ) -paracontact space. Then M is a W_1 -semi-symmetric if and only if M is an Einstein manifold.

Proof. Suppose that M is a W_1 -semi-symmetric. This means that

$$(R(\beta_1, \beta_2)W_1)(\beta_3, \beta_4, \beta_5) = R(\beta_1, \beta_2)W_1(\beta_3, \beta_4)\beta_5 - W_1(R(\beta_1, \beta_2)\beta_3, \beta_4)\beta_5 - W_1(\beta_3, R(\beta_1, \beta_2)\beta_4)\beta_5 - W_1(\beta_3, \beta_4)R(\beta_1, \beta_2)\beta_5 = 0, \tag{51}$$

for any $\beta_1, \beta_2, \beta_3, \beta_4, \beta_5 \in \chi(M)$. Setting $\beta_1 = \beta_5 = \xi$ in (51) and making use of (27), (29) and (30), we obtain

$$(R(\xi, \beta_2)W_1)(\beta_3, \beta_4)\xi = R(\xi, \beta_2)(2k(\eta(\beta_4)\beta_3 - \eta(\beta_3)\beta_4) + \mu(\eta(\beta_4)h\beta_3 - \eta(\beta_3)h\beta_4)) - W_1(k(g(\beta_2, \beta_3)\xi - \eta(\beta_3)\beta_2) + \mu(g(h\beta_2, \beta_3)\xi - \eta(\beta_3)h\beta_2), \beta_4)\xi - W_1(\beta_3, k(g(\beta_2, \beta_4)\xi - \eta(\beta_4)\beta_2) + \mu(g(h\beta_2, \beta_4)\xi - \eta(\beta_4)h\beta_2))\xi - W_1(\beta_3, \beta_4)(k(\eta(\beta_2)\xi - \beta_2) - \mu h\beta_2) = 0. \tag{52}$$

Using (27) and (29), we get

$$kW_1(\beta_3, \beta_4)\beta_2 + \mu W_1(\beta_3, \beta_4)h\beta_2 + k\mu(\eta(\beta_4)g(\beta_2, h\beta_3)\xi - \eta(\beta_3)g(\beta_2, h\beta_4)\xi) + \mu^2(1 + k)(\eta(\beta_4)g(\beta_2, \beta_3)\xi - \eta(\beta_3)g(\beta_2, \beta_4)\xi) + 2k^2(g(\beta_2, \beta_3)\beta_4 - g(\beta_2, \beta_4)\beta_3) + k\mu(g(\beta_2, \beta_3)h\beta_4 - g(\beta_2, \beta_4)h\beta_3) + 2k\mu(g(h\beta_2, \beta_3)\beta_4 - g(h\beta_2, \beta_4)\beta_3) + \mu^2(g(h\beta_2, \beta_3)h\beta_4 + g(h\beta_2, \beta_4)h\beta_3) = 0. \tag{53}$$

Making use of (10), (18) and choosing $\beta_3 = \xi$ and inner product both sides of in (53) by $\xi \in \chi(M)$, we have

$$kS(\beta_4, \beta_2) + \mu S(\beta_4, h\beta_2) - 2nk^2g(\beta_4, \beta_2) - 2nk\mu g(h\beta_2, \beta_4) = 0. \tag{54}$$

Replacing $h\beta_2$ of β_2 in (54) and by using (7), we get

$$kS(\beta_4, h\beta_2) + \mu(1 + k)S(\beta_4, h\beta_2) - 2nk^2g(\beta_4, h\beta_2) - 2nk\mu(1 + k)g(\beta_4, \beta_2) = 0. \tag{55}$$

From (54) and (55), we obtain

$$S(\beta_2, \beta_4) = 2nkg(\beta_2, \beta_4).$$

So, M is an Einstein manifold. Conversely, let $M^{2n+1}(\varphi, \xi, \eta, g)$ be an Einstein manifold, i.e., $S(\beta_2, \beta_4) = 2nkg(\beta_2, \beta_4)$, then from equations (55), (54), (53), (52) and (51) we get M is a W_1 -semi-symmetric.

Conflicts of interest

There are no conflicts of interest in this work.

References

[1] Kaneyuki S., Williams F.L., Almost paracontact and parahodge structures on manifolds, *Nagoya Math. J.*, 99 (1985), 173-187.

[2] Zamkovoy S., Canonical connections on paracontact manifolds, *Ann. Global Anal. Geom.*, 36 (2009), 37-60.

[3] Cappelletti-Montano B., Küpeli Erken I., Murathan C., Nullity conditions in paracontact geometry, *Differential Geom. Appl.*, 30 (2012), 665-693.

[4] Blair D.E., Koufogiorgos T., Papatoniou B.J., Contact metric manifolds satisfying a nullity condition, *Israel J. Math.*, 91 (1995), 189-214.

[5] Kowalezyk D., On some subclass of semi-symmetric manifolds, *Soochow J. Math.*, 27 (2001), 445-461.

[6] Prasad B., A pseudo projective curvature tensor on a Riemannian manifold, *Bull. Calcutta Math. Soc.*, 94 (3) (2002), 163-166.

[7] Ivanov S., Vassilev D., Zamkovoy S., Conformal paracontact curvature and the local flatness theorem, *Geom. Dedicata*, 144 (2010), 79-100.

[8] Mert T., Characterization of some special curvature tensor on Almost C(a)-manifold, *Asian Journal of Math. and Computer Research*, 29 (1) (2022), 27-41.

[9] Mert T., Atçeken M., Almost C(a)-manifold on W_0^* -curvature tensor, *Applied Mathematical Sciences*, 15 (15) (2021), 693-703.

[10] O'Neill B., *Semi-Riemannian Geometry with Applications to Relativity*, Academic Press, New York, (1983).

[11] Boothby W.M., *An Introduction to Differentiable Manifolds and Riemannian Geometry*, Academic Press, Inc. London, (1986).

[12] Zamkovoy S., Tzanov V., Non-existence of flat paracontact metric structures in dimension greater than or equal to five, *Annuaire Univ. Sofia Fac. Math. Inform.*, 100 (2011), 27-34.

[13] Ishii Y., On conharmonic transformations, *Tensor N. S.*, 7 (1957), 73-80.

[14] Pokhariyal G.P., Mishra R.S., Curvature tensors and their relativistic significance II, *Yokohama Math. J.*, 19 (2) (1971), 97-103.

[15] Atçeken M., Uygun P., Characterizations for totally geodesic submanifolds of (k, μ) -paracontact metric manifolds, *Korean J. Math.*, 28 (2020), 555-571.

[16] Calvaruso G., Homogeneous paracontact metric three-manifolds, *Illinois J. Math.*, 55 (2011), 697-718.

- [17] Szabo Z.I., Structure theorems on Riemannian spaces satisfying $R(X,Y) \cdot R=0$, I: The local version, *J. Differential Geom.*, 17 (4) (1982), 531-582.
- [18] Tripathi M.M., Gupta P., T-curvature tensor on a semi-Riemannian manifold, *J. Adv. Math. Studies.*, 4 (2011), No. 1, 117-129.
- [19] Uygun P., Atçeken M., On (k,μ) -paracontact metric spaces satisfying some conditions on the W_0^* -curvature tensor, *NTMSCI*, 9 (2), (2021), 26-37.

Solutions of Time Fractional fKdV Equation Using the Residual Power Series Method

Sevil Çulha Ünal^{1,a,*}

¹ Department of Avionics, School of Civil Aviation, Suleyman Demirel University, Isparta, Türkiye.

*Corresponding author

Research Article

History

Received: 14/03/2022

Accepted: 02/08/2022

Copyright



©2022 Faculty of Science,
Sivas Cumhuriyet University

ABSTRACT

The fifth-order Korteweg-de Vries (fKdV) equation is a nonlinear model in various long wave physical phenomena. The residual power series method (RPSM) is used to gain the approximate solutions of the time fractional fKdV equation in this study. Basic definitions of fractional derivatives are described in the Caputo sense. The solutions of the time fractional fKdV equation with easily computable components are calculated as a quick convergent series. When compared to exact solutions, the RPSM provides good accuracy for approximate solutions. The reliability of the proposed method is also illustrated with the aid of table and graphs. Clearly observed from the results that the suggested method is suitable and simple for similar type of the time fractional nonlinear differential equations.

Keywords: Fractional partial differential equation, Fifth-order Korteweg-de Vries equation, Residual power series method, Caputo derivative, Approximate solutions.

 sevilunal@sdu.edu.tr

 <https://orcid.org/0000-0001-7447-9219>

Introduction

Nonlinear phenomena modeled as nonlinear partial differential equations occur in many fields of science such as, mathematical biology, plasma physics, nonlinear optics, quantum mechanics, hydrodynamics, fluid dynamics, and chemical kinetics. Among these equations, the fKdV equation has utilized to investigate numerous significant issues in nonlinear physical phenomena. The fKdV equation has emerged in important physical systems such as in the theory of shallow water waves, gravity capillary waves, large interior waves in densely layered oceans, ion sound waves in plasma, and sound waves in a crystal lattice. Besides, the most well-known fKdV equations are the Sawada-Kotera equation, the Lax equation, the Caudrey-Dodd-Gibbon equation, the Ito equation, and the Kaup-Kuperschmidt equation. So far, several methods have used for solving the fKdV equations. These methods are Adomian decomposition [1], Laplace decomposition [2], variational iteration [3], Hirota direct [4], extended direct algebraic [5], homotopy perturbation transform [6], modified variational iteration algorithm-I [7], and modified variational iteration algorithm-II [8].

In recent years, mathematicians and scientists have been interested in studying the solutions of fractional differential equations because of their various applications in fields such as physics, biology, mathematics, chemistry, viscoelasticity, ecology, turbulence, nanotechnology, ecology, aerodynamics, control theory, and so on [9-11]. In the literature, the homotopy analysis method [12, 13], the operational collocation method [13], the finite difference method [13], the homotopy analysis transform method [14], the

generalized Adams-Bashforth Moulton method [15], and the Euler method [16] have been used in solving many fractional differential equations. So far, the time fractional fKdV equation is investigated by utilized homotopy perturbation transform [17], simplest equation [18], trial equation [19], Lie group analysis [20], generalized exp(- $\phi(\xi)$)-expansion [21], novel hyperbolic and exponential ansatz [22] methods. However, the RPSM has not yet been used in the literature to solve the fractional fKdV equation. Hence, the goal of this study is to get approximate solutions of the time fractional fKdV equation

$$D_t^\alpha v(x, t) + v(x, t)v_x(x, t) - v(x, t)v_{xxx}(x, t) + v_{xxxxx}(x, t) = 0, \quad 0 < \alpha \leq 1 \quad (1)$$

by utilizing the RPSM. Here, D_t^α represents the Caputo derivative of $v(x, t)$. The RPSM is offered by Abu Arqub [23] is an efficient method to find the values of the power series solution for fuzzy differential equations. Without perturbation, discretization, or linearization, the proposed method suggests a powerful and simple power series solution for differential equations. RPSM has also fewer processing requirements, require less time, and is more reliable compared to the Taylor series method. Besides, this method does not require comparing the coefficients of the corresponding terms or a recursion relationship. Moreover, the proposed method does not perform any transformation in the transition from simple linearity to complex nonlinearity and from the low order to higher order. In the literature, many fractional

differential equations have also been solved by suggested method, for example, the Zakharov-Kuznetsov equation [24], the Klein-Gordon equation [25], the Boussinesq-Burger's equation [26], the foam drainage equation [27],

the Swift-Holenberg equation [28], the Sharma-Tasso-Olever equation [29], the Fisher equation [30], the Vibration equation [31], the Navier-Stokes equation [32], and the biological population diffusion equations [33].

Preliminaries

In this section, we examine some definitions and theorems for the fractional power series and the Caputo derivative. More detailed information about these can be found in [34,35].

Definition 2.1. [34] The Riemann-Liouville fractional integral operator with order α is expressed as

$$J^\alpha f(x) = \begin{cases} \frac{1}{\Gamma(\alpha)} \int_0^x (x-t)^{\alpha-1} f(t) dt, & \alpha > 0, x > 0 \\ f(x), & \alpha = 0. \end{cases}$$

Definition 2.2. [34] The Caputo fractional derivative with order α is defined as

$$D^\alpha f(x) = J^{n-\alpha} D^n f(x) = \frac{1}{\Gamma(n-\alpha)} \int_0^x (x-t)^{n-\alpha-1} \frac{d^n}{dt^n} f(t) dt, \quad x > 0, \quad n-1 < \alpha < n \in \mathbb{Z}^+$$

where D^n is the classic differential operator. Utilizing the Caputo derivative, the following is also gained

$$D^\alpha x^\beta = 0, \quad \beta < \alpha, \\ D^\alpha x^\beta = \frac{\Gamma(\beta+1)}{\Gamma(\beta+1-\alpha)} x^{\beta-\alpha}, \quad \beta \geq \alpha.$$

Definition 2.3. [34] For n is the smallest integer which exceeds α , the Caputo time fractional differential operator of order α of $v(x, t)$ is defined as

$$D_t^\alpha v(x, t) = \begin{cases} \frac{1}{\Gamma(n-\alpha)} \int_0^t (t-\tau)^{n-\alpha-1} \frac{\partial^n v(x, \tau)}{\partial \tau^n} d\tau, & n-1 < \alpha < n \\ \frac{\partial^n v(x, t)}{\partial t^n}, & \alpha = n \in \mathbb{N}. \end{cases}$$

Definition 2.4. [35] A power series expanding which is called a fractional power series at $t = t_0$ of the form

$$\sum_{n=0}^{\infty} c_n (t-t_0)^{n\alpha} = c_0 + c_1 (t-t_0)^\alpha + c_2 (t-t_0)^{2\alpha} + \dots, \quad 0 \leq n-1 < \alpha \leq n, \quad t \geq t_0,$$

where the constants c_n 's are called the coefficients of the series and t is a variable.

Theorem 2.1. [35] Assume that f has a fractional power series at $t = t_0$ of the manner

$$f(t) = \sum_{n=0}^{\infty} c_n (t-t_0)^{n\alpha}, \quad 0 \leq n-1 < \alpha \leq n, \quad t_0 \leq t < t_0 + R.$$

If $D^{n\alpha} f(t)$ are continuous on $(t_0, t_0 + R)$, then

$$c_n = \frac{D^{n\alpha} f(t_0)}{\Gamma(n\alpha + 1)}, \quad n = 0, 1, 2, \dots,$$

where $D^{n\alpha} = D^\alpha \dots D^\alpha$, and R is the radius of convergence.

Theorem 2.2. [35] Assume that $v(x, t)$ is a multiple fractional power series at $t = t_0$ of the form

$$v(x, t) = \sum_{n=0}^{\infty} f_n(x) (t-t_0)^{n\alpha}, \quad x \in I, \quad 0 \leq n-1 < \alpha \leq n, \quad t_0 \leq t < t_0 + R.$$

When $D_t^{n\alpha}v(x, t)$ are continuous on $I \times (t_0, t_0 + R)$, $f_n(x)$ are described by

$$f_n(x) = \frac{D_t^{n\alpha}v(x, t_0)}{\Gamma(n\alpha + 1)}, \quad n = 0, 1, 2, \dots$$

Here, $D_t^{n\alpha} = \frac{\partial^{n\alpha}}{\partial t^{n\alpha}} = \frac{\partial^\alpha}{\partial t^\alpha} \cdot \frac{\partial^\alpha}{\partial t^\alpha} \dots \frac{\partial^\alpha}{\partial t^\alpha}$, and $R = \min_{c \in I} R_c$, that R_c is effect domain of convergency of the fractional power series $\sum_{n=0}^{\infty} f_n(c)(t - t_0)^{n\alpha}$.

Basic Idea of Suggested Method

In this part of the paper, we examine a solution procedure for the suggested method. To present the basic idea of proposed method, we study the nonlinear fractional differential equation in the form

$$D_t^\alpha v(x, t) = N(v) + R(v), \quad 0 < \alpha \leq 1, \quad t > 0, \tag{2}$$

by the initial condition

$$v(x, 0) = f(x).$$

Here, $D_t^\alpha v(x, t)$ represents the Caputo derivative of $v(x, t)$, $N(v)$ and $R(v)$ denote nonlinear and linear terms, respectively. The RPSM proposes the solution for Eq. (2) with a fractional power series at $t = 0$,

$$v(x, t) = \sum_{n=0}^{\infty} f_n(x) \frac{t^{n\alpha}}{\Gamma(n\alpha + 1)}, \quad x \in I, \quad 0 < \alpha \leq 1, \quad 0 \leq t < R.$$

Then, the k th truncated series of $v(x, t)$, that is $v_k(x, t)$ can be given as

$$v_k(x, t) = \sum_{n=0}^k f_n(x) \frac{t^{n\alpha}}{\Gamma(n\alpha + 1)}, \quad x \in I, \quad 0 < \alpha \leq 1, \quad 0 \leq t < R, \tag{3}$$

where $v_0 = f_0(x) = v(x, 0) = f(x)$. Eq. (3) can be also expressed as

$$v_k(x, t) = f(x) + \sum_{n=1}^k f_n(x) \frac{t^{n\alpha}}{\Gamma(n\alpha + 1)}, \quad x \in I, \quad 0 < \alpha \leq 1, \quad 0 \leq t < R, \quad k = 1, 2, \dots \tag{4}$$

In order to obtain the $f_n(x)$ in series expansion (4), the residual function for Eq. (1) is given below:

$$Res_v(x, t) = D_t^\alpha v(x, t) - N(v) - R(v).$$

Therefore, the k -th residual function $Res_{v,k}$ is

$$Res_{v,k}(x, t) = D_t^\alpha v_k(x, t) - N(v_k) - R(v_k). \tag{5}$$

As in [23, 36-39], some effective relations of RPSM are described as follows:

$$Res_v(x, t) = 0,$$

$$\lim_{k \rightarrow \infty} Res_{v,k}(x, t) = Res_v(x, t) \text{ for } x \in I \text{ and } t \geq 0,$$

$$D_t^{n\alpha} Res_v(x, 0) = D_t^{n\alpha} Res_{v,k}(x, 0) = 0, \quad n = 0, 1, \dots, k. \tag{6}$$

The RPSM and its applications are based on these relations.

The RPSM is clarified by substituting k th truncated series of $v(x, t)$ in Eq. (5) and computing the fractional derivative $D_t^{(k-1)\alpha}$ of $Res_{v,k}(x, t)$ for $k = 1, 2, \dots$. Then, utilizing the relation (6), the algebraic equation in the form

$$D_t^{(k-1)\alpha} Res_{v,k}(x, 0) = 0, \quad 0 < \alpha \leq 1, \quad 0 \leq t < R, \quad t = 0, \quad k = 1, 2, \dots \tag{7}$$

Solutions of the Time Fractional fKdV Equation

In this section, we consider Eq. (1) by the initial condition

$$v(x, 0) = e^x. \tag{8}$$

The exact solution for Eq. (1) when $\alpha = 1$ is [1]

$$v(x, t) = e^{x-t}.$$

For Eq. (1), we express the following residual function as

$$Res_v(x, t) = D_t^\alpha v(x, t) + v(x, t) \frac{\partial}{\partial x} v(x, t) - v(x, t) \frac{\partial^3}{\partial x^3} v(x, t) + \frac{\partial^5}{\partial x^5} v(x, t),$$

and k -th residual function $Res_{v,k}$,

$$Res_{v,k}(x, t) = D_t^\alpha v_k(x, t) + v_k(x, t) \frac{\partial}{\partial x} v_k(x, t) - v_k(x, t) \frac{\partial^3}{\partial x^3} v_k(x, t) + \frac{\partial^5}{\partial x^5} v_k(x, t). \tag{9}$$

In order to gain coefficient $f_1(x)$, we consider $k = 1$ in Eq. (9) and we get

$$Res_{v,1}(x, t) = D_t^\alpha v_1(x, t) + v_1(x, t) \frac{\partial}{\partial x} v_1(x, t) - v_1(x, t) \frac{\partial^3}{\partial x^3} v_1(x, t) + \frac{\partial^5}{\partial x^5} v_1(x, t),$$

where

$$v_1(x, t) = f(x) + f_1(x) \frac{t^\alpha}{\Gamma(\alpha + 1)},$$

for

$$v_0 = f_0(x) = f(x) = v(x, 0) = e^x.$$

Hence, we gain

$$Res_{v,1}(x, t) = f_1(x) + \left(f(x) + f_1(x) \frac{t^\alpha}{\Gamma(\alpha + 1)} \right) \left(f'(x) + f_1'(x) \frac{t^\alpha}{\Gamma(\alpha + 1)} \right) - \left(f(x) + f_1(x) \frac{t^\alpha}{\Gamma(\alpha + 1)} \right) \left(f'''(x) + f_1'''(x) \frac{t^\alpha}{\Gamma(\alpha + 1)} \right) + f^{(5)}(x) + f_1^{(5)}(x) \frac{t^\alpha}{\Gamma(\alpha + 1)}.$$

From Eq. (7), we get $Res_{v,1}(x, 0) = 0$, and thus

$$f_1(x) = -e^x.$$

Therefore, the first RPS solution of Eq. (1) is

$$v_1(x, t) = e^x - e^x \frac{t^\alpha}{\Gamma(\alpha + 1)}.$$

Similarly, substituting $k = 2$ in Eq. (9) to yield the coefficient $f_2(x)$, we get

$$Res_{v,2}(x, t) = D_t^\alpha v_2(x, t) + v_2(x, t) \frac{\partial}{\partial x} v_2(x, t) - v_2(x, t) \frac{\partial^3}{\partial x^3} v_2(x, t) + \frac{\partial^5}{\partial x^5} v_2(x, t),$$

where

$$v_2(x, t) = f(x) + f_1(x) \frac{t^\alpha}{\Gamma(\alpha + 1)} + f_2(x) \frac{t^{2\alpha}}{\Gamma(2\alpha + 1)}.$$

Therefore, we have

$$\begin{aligned}
 Res_{v_2}(x, t) = & f_1(x) + f_2(x) \frac{t^\alpha}{\Gamma(\alpha + 1)} \\
 & + \left(f(x) + f_1(x) \frac{t^\alpha}{\Gamma(\alpha + 1)} + f_2(x) \frac{t^{2\alpha}}{\Gamma(2\alpha + 1)} \right) \left(f'(x) + f_1'(x) \frac{t^\alpha}{\Gamma(\alpha + 1)} + f_2'(x) \frac{t^{2\alpha}}{\Gamma(2\alpha + 1)} \right) \\
 & - \left(f(x) + f_1(x) \frac{t^\alpha}{\Gamma(\alpha + 1)} + f_2(x) \frac{t^{2\alpha}}{\Gamma(2\alpha + 1)} \right) \left(f'''(x) + f_1'''(x) \frac{t^\alpha}{\Gamma(\alpha + 1)} + f_2'''(x) \frac{t^{2\alpha}}{\Gamma(2\alpha + 1)} \right) \\
 & + f^{(5)}(x) + f_1^{(5)}(x) \frac{t^\alpha}{\Gamma(\alpha + 1)} + f_2^{(5)}(x) \frac{t^{2\alpha}}{\Gamma(2\alpha + 1)}.
 \end{aligned}$$

From Eq. (7), we gain $D_t^\alpha Res_{v_2}(x, 0) = 0$, and hence

$$f_2(x) = e^x.$$

Therefore, the second RPS solution of Eq. (1) is

$$v_2(x, t) = e^x - e^x \frac{t^\alpha}{\Gamma(\alpha + 1)} + e^x \frac{t^{2\alpha}}{\Gamma(2\alpha + 1)}.$$

Likewise, substituting $k = 3$ in Eq. (9) to obtain the coefficient $f_3(x)$, we have

$$Res_{v_3}(x, t) = D_t^\alpha v_3(x, t) + v_3(x, t) \frac{\partial}{\partial x} v_3(x, t) - v_3(x, t) \frac{\partial^3}{\partial x^3} v_3(x, t) + \frac{\partial^5}{\partial x^5} v_3(x, t),$$

where

$$v_3(x, t) = f(x) + f_1(x) \frac{t^\alpha}{\Gamma(\alpha + 1)} + f_2(x) \frac{t^{2\alpha}}{\Gamma(2\alpha + 1)} + f_3(x) \frac{t^{3\alpha}}{\Gamma(3\alpha + 1)}.$$

Therefore, we get

$$\begin{aligned}
 Res_{v_3}(x, t) = & f_1(x) + f_2(x) \frac{t^\alpha}{\Gamma(\alpha + 1)} + f_3(x) \frac{t^{2\alpha}}{\Gamma(2\alpha + 1)} \\
 & + \left(f(x) + f_1(x) \frac{t^\alpha}{\Gamma(\alpha + 1)} + f_2(x) \frac{t^{2\alpha}}{\Gamma(2\alpha + 1)} + f_3(x) \frac{t^{3\alpha}}{\Gamma(3\alpha + 1)} \right) \left(f'(x) + f_1'(x) \frac{t^\alpha}{\Gamma(\alpha + 1)} \right. \\
 & \left. + f_2'(x) \frac{t^{2\alpha}}{\Gamma(2\alpha + 1)} + f_3'(x) \frac{t^{3\alpha}}{\Gamma(3\alpha + 1)} \right) \\
 & - \left(f(x) + f_1(x) \frac{t^\alpha}{\Gamma(\alpha + 1)} + f_2(x) \frac{t^{2\alpha}}{\Gamma(2\alpha + 1)} + f_3(x) \frac{t^{3\alpha}}{\Gamma(3\alpha + 1)} \right) \left(f'''(x) + f_1'''(x) \frac{t^\alpha}{\Gamma(\alpha + 1)} \right. \\
 & \left. + f_2'''(x) \frac{t^{2\alpha}}{\Gamma(2\alpha + 1)} + f_3'''(x) \frac{t^{3\alpha}}{\Gamma(3\alpha + 1)} \right) + f^{(5)}(x) + f_1^{(5)}(x) \frac{t^\alpha}{\Gamma(\alpha + 1)} + f_2^{(5)}(x) \frac{t^{2\alpha}}{\Gamma(2\alpha + 1)} \\
 & + f_3^{(5)}(x) \frac{t^{3\alpha}}{\Gamma(3\alpha + 1)}.
 \end{aligned}$$

From Eq. (7), we gain $D_t^{2\alpha} Res_{v_3}(x, 0) = 0$, and hence

$$f_3(x) = -e^x.$$

Therefore, the third RPS solution of Eq. (1) is

$$v_3(x, t) = e^x - e^x \frac{t^\alpha}{\Gamma(\alpha + 1)} + e^x \frac{t^{2\alpha}}{\Gamma(2\alpha + 1)} - e^x \frac{t^{3\alpha}}{\Gamma(3\alpha + 1)}.$$

Using the same process for $k = 4$, the following is obtained as

$$\begin{aligned}
 f_4(x) = & e^x, \\
 v_4(x, t) = & e^x - e^x \frac{t^\alpha}{\Gamma(\alpha + 1)} + e^x \frac{t^{2\alpha}}{\Gamma(2\alpha + 1)} - e^x \frac{t^{3\alpha}}{\Gamma(3\alpha + 1)} + e^x \frac{t^{4\alpha}}{\Gamma(4\alpha + 1)}.
 \end{aligned}$$

To validate the accuracy and efficiency of the suggested method, the numerical comparisons of the fourth RPS solution with the exact solution for $\alpha = 1$ and different values of x and t are illustrated in Table 1. Clearly observed from Table 1 that the absolute error is being smaller when the value of the t is decreasing

Table 1. Comparison between the solutions $v_4(x,t)$ and the exact solution for $\alpha=1$.

x	t	$v_4(x,t)$	Exact solution	Absolute error
-10	0	4.53999×10^{-5}	4.53999×10^{-5}	0
	0.2	3.71704×10^{-5}	3.71703×10^{-5}	$1. \times 10^{-10}$
	0.4	3.04361×10^{-5}	3.04325×10^{-5}	3.6299×10^{-9}
	0.6	2.49427×10^{-5}	2.4916×10^{-5}	2.67117×10^{-8}
	0.8	2.05087×10^{-5}	2.03995×10^{-5}	1.09158×10^{-7}
	1	1.7025×10^{-5}	1.67017×10^{-5}	3.23273×10^{-7}
-5	0	6.73795×10^{-3}	6.73795×10^{-3}	0
	0.2	5.51658×10^{-3}	5.51656×10^{-3}	1.73856×10^{-8}
	0.4	4.51712×10^{-3}	4.51658×10^{-3}	5.38726×10^{-7}
	0.6	3.70183×10^{-3}	3.69786×10^{-3}	3.96436×10^{-6}
	0.8	3.04376×10^{-3}	3.02755×10^{-3}	1.62005×10^{-5}
	1	2.52673×10^{-3}	2.47875×10^{-3}	4.79779×10^{-5}
0	0	1	1	0
	0.2	8.18733×10^{-1}	8.18731×10^{-1}	2.58026×10^{-6}
	0.4	6.704×10^{-1}	6.7032×10^{-1}	7.9954×10^{-5}
	0.6	5.494×10^{-1}	5.48812×10^{-1}	5.88364×10^{-4}
	0.8	4.51733×10^{-1}	4.49329×10^{-1}	2.40437×10^{-3}
	1	3.75×10^{-1}	3.67879×10^{-1}	7.12056×10^{-3}
5	0	1.48413×10^2	1.48413×10^2	0
	0.2	1.21511×10^2	1.2151×10^2	3.82944×10^{-4}
	0.4	9.94962×10^1	9.94843×10^1	1.18662×10^{-2}
	0.6	8.15382×10^1	8.14509×10^1	8.73209×10^{-2}
	0.8	6.70432×10^1	6.66863×10^1	3.5684×10^{-1}
	1	5.56549×10^1	5.45982×10^1	1.05678×10^0
10	0	2.20265×10^4	2.20265×10^4	0
	0.2	1.80338×10^4	1.80337×10^4	5.68339×10^{-2}
	0.4	1.47665×10^4	1.47648×10^4	1.7611×10^0
	0.6	1.21013×10^4	1.20884×10^4	1.29596×10^1
	0.8	9.95009×10^3	9.89713×10^3	5.29598×10^1
	1	8.25992×10^3	8.10308×10^3	1.56841×10^2

In Figure 1, for $-10 \leq x \leq 10$ and $0 \leq t \leq 1$ when $\alpha = 1$, the comparison between the $v_4(x, t)$ solution and the exact solution is illustrated. When equal parameters are selected, the fourth RPS solutions have similar shapes to the exact solutions, as seen in Figure 1.

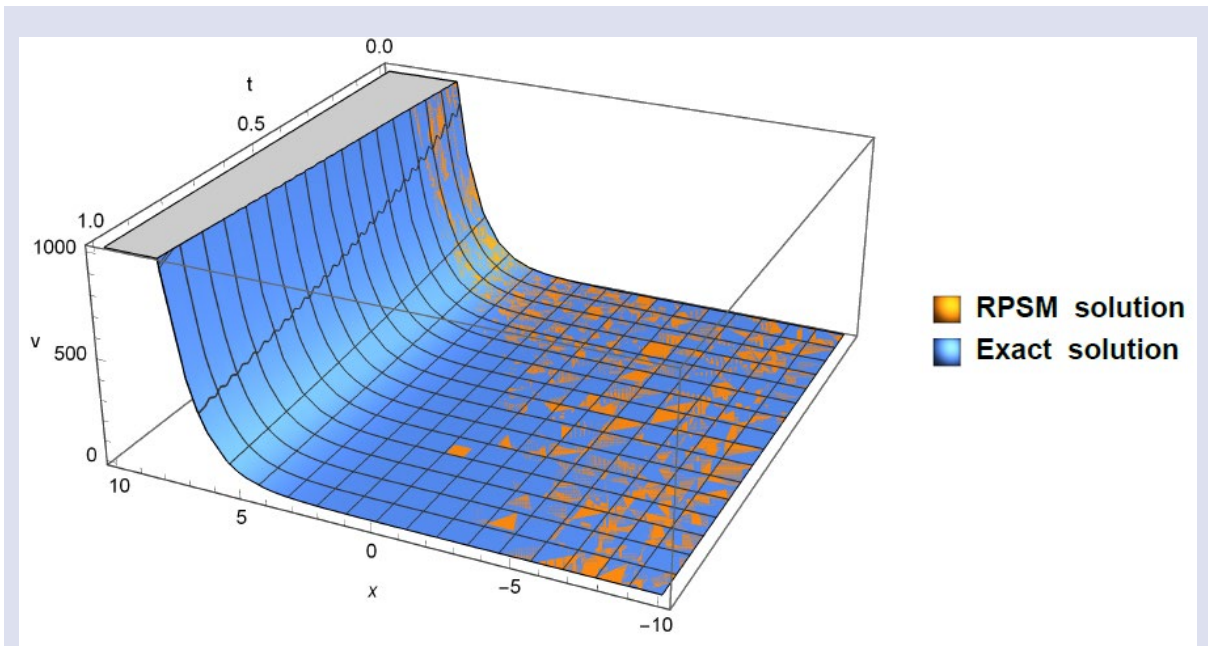


Figure 1. The graph of the exact solution and the $v_4(x, t)$ of Eq. (1) when $\alpha = 1$.

The RPS solution $v_4(x, t)$ is illustrated in Figure 2, for $-20 \leq x \leq 20$ and $0 \leq t \leq 25$ when $\alpha = 0.2, \alpha = 0.5, \alpha = 0.8, \alpha = 1$. When $\alpha = 1$ is chosen among the different values of α , the $v_4(x, t)$ is closest to the exact solution.

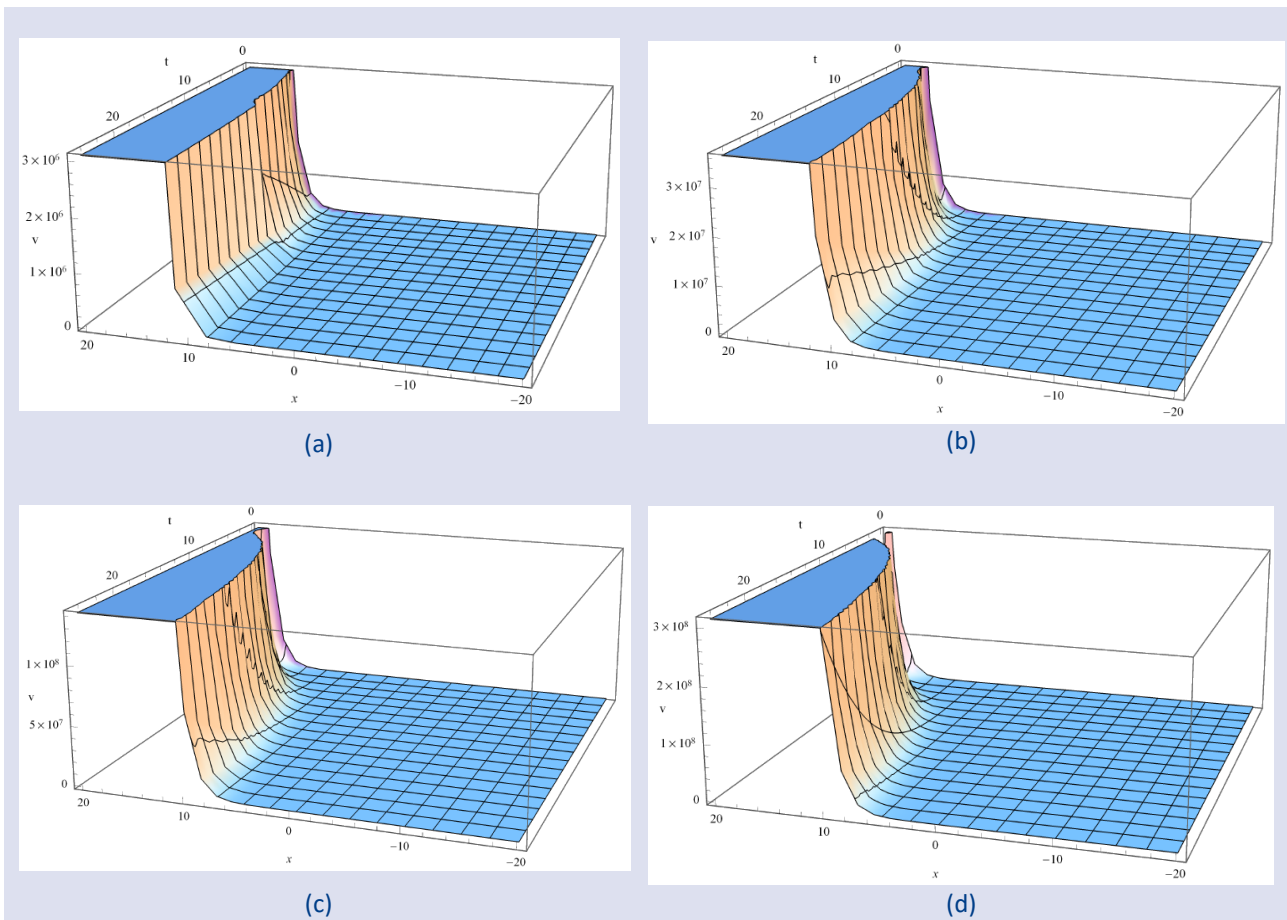


Figure 2. 3D graph of the fourth RPS solution of Eq. (1): (a) $v_4(x, t)$ when $\alpha = 0.2$, (b) $v_4(x, t)$ when $\alpha = 0.5$, (c) $v_4(x, t)$ when $\alpha = 0.8$, (d) $v_4(x, t)$ when $\alpha = 1$.

For $-20 \leq x \leq 20$ and $t = 15$ at the different α values, the $v_4(x, t)$ is demonstrated in Figure 3. In this figure, the line with dots represents the solution at $\alpha = 0.2$, the unitary line represents the solution at $\alpha = 0.5$, the line with dashes represents the solution at $\alpha = 0.8$, and the line with dot-dash represents the solution at $\alpha = 1$. It is clear that from Figure 3, the frequency increases as x approaches to zero. Besides, clearly seen from Figure 3 that the $v_4(x, t)$ solution approaches the exact solution as the value of the α increases.

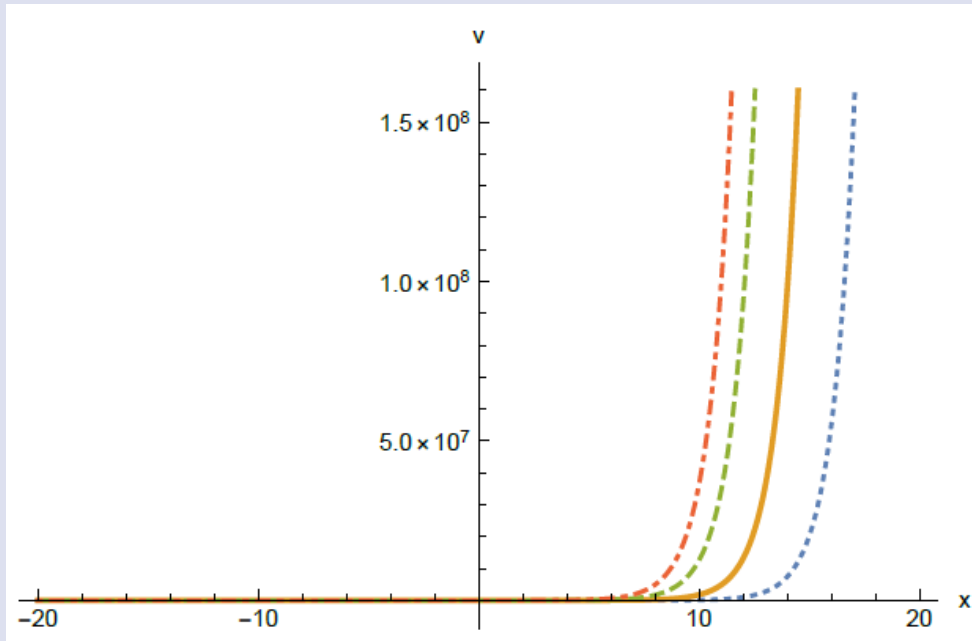


Figure 3. 2D graph of the $v_4(x, 15)$ for $\alpha = 0.2$, $\alpha = 0.5$, $\alpha = 0.8$, and $\alpha = 1$.

Conclusions

In this study, the RPSM was utilized to gain approximate solutions of the time fractional fKdV equation. These solutions were numerically compared to the exact solutions in Table 1. In this table, for $\alpha = 1$ and different values of x and t , the absolute errors of the RPS solutions were also introduced. In Table 1, when the numerical results were examined, the reliability of the proposed method for the time fractional fKdV equation had emerged. Besides, the fourth RPS solutions were demonstrated by 2D and 3D graphs. It could be seen in Figure 1 that the fourth RPS solution has similar shapes to the exact solution when equal parameters were chosen. The RPS solution $v_4(x, t)$ was illustrated for the different values of α in Figure 2 and Figure 3. All graphics were showed by the help of Mathematica. In addition, it was seen that RPSM achieved a high accuracy when the numerical results were analyzed in this paper.

When the RPSM is studied, it has more advantages than other methods in the literature. The RPSM is useful and effective method for solving nonlinear partial differential equations. The suggested method also does not require any linearization, transformation, discretization, or perturbation. Besides, this method does not need any small parameter for iterative solution. Moreover, by minimizing the residual error, the RPSM provides convergence of the series solution. Furthermore,

by selecting a suitable initial estimate approximation, the proposed method can be used in nonlinear problems. As a result, the RPSM can be utilized to solve a wide range of fractional differential equations in mathematics and science.

Conflicts of interest

The author declares that there are no conflicts of interest.

References

- [1] Kaya D., An Explicit and Numerical Solutions of Some Fifth-Order KdV Equation by Decomposition Method, *Appl. Math. Comput.*, 144 (2003) 353-363.
- [2] Handibag S., Karande B.D., Existence the Solutions of Some Fifth-Order KdV Equation by Laplace Decomposition Method, *American J. Comput. Math.*, 3 (2013) 80-85.
- [3] Saravi M., Nikkar A., Promising Technique for Analytic Treatment of Nonlinear Fifth-Order Equations, *World J. Model. Simul.*, 10 (1) (2014) 27-33.
- [4] Wazwaz A.W., A Fifth-Order Korteweg-de Vries Equation for Shallow Water with Surface Tension: Multiple Soliton Solutions, *Acta Physica Polonica A*, 130 (3) (2016) 679-682.
- [5] Seadawy A.R., Lu D., Yue C., Travelling Wave Solutions of the Generalized Nonlinear Fifth-Order KdV Water Wave Equations and Its Stability, *J. Taibah Uni. Sci.*, 11 (2017) 623-633.

- [6] Goswami A., Singh J., Kumar D., Numerical Simulation of Fifth Order KdV Equations Occurring in Magneto-Acoustic Waves, *Ain Shams Eng. J.*, 9 (2018) 2265-2273.
- [7] Ahmad H., Khan T.A., Stanimirovic, P.S., Ahmad, I., Modified Variational Iteration Technique for the Numerical Solution of Fifth Order KdV-type Equations, *J. Appl. Comput. Mech.*, 6 (2020) 1220-1227.
- [8] Ahmad H., Khan T.A., Yao S-W., An Efficient Approach for the Numerical Solution of Fifth-Order KdV Equations, *Open Math.*, 18 (2020) 738-748.
- [9] Ahmad B., Nieto J.J., Existence of Solutions for Nonlocal Boundary Value Problems of Higher-Order Nonlinear Fractional Differential Equations, *Hindawi*, Doi:10.1155/2009/494720 (2009) 1-9.
- [10] Wang Y., Liang S., Wang Q., Existence Results for Fractional Differential Equations with Integral and Multi-point Boundary Conditions, *Boundary Val. Probl.*, Doi:10.1186/s13661-017-0924-4 (2018) 1-11.
- [11] Şenol M., Ata A., Approximate Solution of Time-fractional KdV Equations by Residual Power Series Method, *J. Balıkesir Uni. Ins. Sci. Tech.*, 20 (1) (2018) 430-439.
- [12] Hosseini, K., Ilie, M., Mirzazadeh, M., Yusuf, A., Sulaiman, T.A., Baleanu, D., and Salahshour, S., An Effective Computational Method to deal ith a Time-fractional Nonlinear Water Wave Equation in the Caputo Sense, *Math. Comp. Simul.*, 187 (2021) 248-260.
- [13] Hosseini, K., Sadri, K., Mirzazadeh, M., Ahmadian, A., Chu, Y-M., and Salahshour, S., Reliable Methods to Look for Analytical and Numerical Solutions of a Nonlinear Differential Equation Arising in Heat Transfer with the Conformable Derivative, *Math. Methods Appl. Sci.*, Doi: 10.1002/mma.7582 (2021) 1-13.
- [14] Hosseini, K., Ilie, M., Mirzazadeh, M., and D., Baleanu, An Analytic Study on the Approximate Solution of a Nonlinear Time-fractional Cauchy Reaction-diffusion Equation with the Mittag-Leffler Law, *Math. Methods Appl. Sci.*, 44 (2021) 6247-6258.
- [15] Tuan, N.H., Mohammadi, H., and Rezapour, S., A Mathematical Model for COVID-19 Transmission by Using the Caputo Fractional Derivative, *Chaos Soliton. Fract.*, 140 (2020) 1-11.
- [16] Mohammadi, H., Rezapour, S., and Jajarmi, A., On the Fractional SIRD Mathematical Model and Control for the Transmission of COVID-19: The First and the Second Waves of the Disease in Iran and Japan, *ISA Trans.*, 124 (2022) 103-114.
- [17] Karunakar P., Chakraverty S., Solutions of Time-fractional Third and Fifth-Order Korteweg-de Vries equations Using Homotopy Perturbation Transform Method, *Eng. Comput.*, 36 (7) (2019) 2309-2326.
- [18] Chen C., Jiang Y-L., Simplest Equation Method for Some Time-fractional Partial Differential Equations with Conformable Derivative, *Comp. Math. Appl.*, 75 (2018) 2978-2988.
- [19] Liu T., Exact Solutions to Time-fractional Fifth Order KdV Equation by Trial Equation Method Based on Symmetry, *Symmetry*, 11 (742) (2019) 1-8.
- [20] Wang G. W., Yu T.Z., Feng T., Lie Symmetry Analysis and Explicit Solutions of the Time Fractional Fifth-Order KdV Equation, *Plos One*, 9 (2) (2014) 1-6.
- [21] Lu D., Yue C., Arshad M., Traveling Wave Solutions of Space-time Fractional Generalized Fifth-order KdV equation, *Adv. Math. Phys.*, Article ID 6743276 (2017) 1-6.
- [22] Park C., Nuruddeen R.I., Ali K.K., Muhammad L., Osman M.S., Baleanu D., Novel Hyperbolic and Exponential Ansatz Methods to the Fractional Fifth-order Korteweg-de Vries Equations, *Adv. Diff. Equ.*, 627 (2020) 1-12.
- [23] Arqub A., Series Solution of Fuzzy Differential Equations Under Strongly Generalized Differentiability, *J. Adv. Res. Appl. Math.*, 5 (1) (2013) 31-52.
- [24] Şenol M., Alquran M., Kasmaei H.D., On the Comparison of Perturbation-iteration Algorithm and Residual Power Series Method to Solve Fractional Zakharov-Kuznetsov Equation, *Results Phys.*, 9 (2018) 321-327.
- [25] Körpınar Z., The Residual Power Series Method for Solving Fractional Klein-Gordon Equation, *Sakarya Uni. J. Sci.*, 21 (3) (2017) 285-293.
- [26] Kumar S., Kumar A., Baleanu D., Two Analytical Methods for Time-fractional Nonlinear Coupled Boussinesq-Burger's Equations Arise in Propagation of Shallow Water Waves, *Nonlinear Dyn*, 85 (2016) 699-715.
- [27] Alquran M., Analytical Solutions of Fractional Foam Drainage Equation by Residual Power Series Method, *Math. Sci.*, 8 (2014) 153-160.
- [28] Prakasha D.G., Veerasha P., Baskonus H.M., Residual Power Series Method for Fractional Swift-Hohenberg Equation, *Fractal and Fractional*, 3 (9) (2019) 1-16.
- [29] Kumar A., Kumar S., Singh M., Residual Power Series Method for Fractional Sharma-Tasso-Olevers Equation, *Comm. Numer. Anal.*, 1 (2016) 1-10.
- [30] Qurashi M.M.A., Korpınar Z., Baleanu D., Inc, M., A New Iterative Algorithm on the Time-fractional Fisher Equation: Residual Power Series Method, *Adv. Mech. Eng.*, 9 (9) (2017) 1-8.
- [31] Jena R.M., Chakraverty S., Residual Power series Method for Solving Time-fractional Model of Vibration Equation of Large Membranes, *J. Appl. Comput. Mech.*, 5 (4) (2019) 603-615.
- [32] Jaber K.K., Ahmad R.S., Analytical Solution of the Time Fractional Navier-Stokes Equation, *Ain Shams Eng. J.*, 9 (4) (2018) 1917-1927.
- [33] Zhang, J., Chen, X, and Li, L., and Zhou, C., Elzaki Transform Residual Power Series Method for the Fractional Population Diffusion Equations, *Eng. Let.*, 29 (4) (2021) 1-12.
- [34] Podlubny I., Fractional differential equations, New York: Academic Press, (1999).
- [35] El-Ajou A., Arqub O.A., Zhou Z.A., Momani S., New Results on Fractional Power Series: Theories and Applications, *Entropy*, 15 (2013) 5305-5323.
- [36] Arqub O.A., Abo-Hammour Z., Al-Badarneh R., Momani S., A Reliable Analytical Method for Solving Higher-order Initial Value Problems, *Hindawi*, Doi:10.1155/2013/673829 (2013) 1-12.
- [37] Arqub O.A., El-Ajou A., Zhou Z.A., Momani S., Multiple Solutions of Nonlinear Boundary Value Problems of Fractional Order: A New Analytic Iterative Technique, *Entropy*, 16 (2014) 471-493.
- [38] Arqub O.A., El-Ajou A., Bataineh A.S., Hashim I., A Representation of the Exact Solution of eGeneralized Lane-Emden Equations Using a New Analytical method, *Hindawi*, Doi:10.1155/2013/378593 (2013) 1-10.
- [39] El-Ajou A., Arqub O.A., Momani S., Approximate Analytical Solution of the Nonlinear Fractional KdV-Burgers Equation: A New Iterative Algorithm, *J. Comput. Phys.*, 293 (2015) 81-95.

A Note on Fractional Midpoint Type Inequalities for Co-ordinated (s_1, s_2) -Convex Functions

Fatih Hezenci ^{1,a,*}

¹ Department of Mathematics, Faculty of Arts and Science, Düzce University, Düzce, Türkiye.

*Corresponding author

Research Article

History

Received: 17/03/2022

Accepted: 03/08/2022

Copyright




©2022 Faculty of Science,
Sivas Cumhuriyet University

ABSTRACT

In the present paper, some Hermite-Hadamard type inequalities in the case of differentiable co-ordinated (s_1, s_2) -convex functions are investigated. Namely, the generalizations of the midpoint type inequalities in the case of differentiable co-ordinated (s_1, s_2) -convex functions in the second sense on the rectangle from the plain are established. In addition to this, it is presented several inequalities to the case of Riemann-Liouville fractional integrals and k-Riemann-Liouville fractional integrals by choosing the special cases of our obtained main results.

Keywords: Midpoint inequality, Co-ordinated (s_1, s_2) -convex function, Generalized fractional integrals.

 fatihhezenci@duzce.edu.tr

 <https://orcid.org/0000-0003-1008-5856>

Introduction

The theory of inequality is a considerable topic and remains an interesting research area with numerous number of applications in many mathematical fields. Additionally, convex functions have also an important place in the theory of inequality. One of the most famous inequalities for the case of convex functions is the Hermite-Hadamard inequality. Therefore, many mathematicians have established Hermite-Hadamard-type inequalities and related inequalities such as trapezoid, midpoint, and Simpson's inequality. Furthermore, Fractional calculus has increased interest owing to the its demonstrated applications in a range of the inequality theory on convex functions in recent years. Because of the importance of fractional calculus, mathematicians have investigated distinct fractional integral inequalities.

The inequalities, established by C. Hermite and J. Hadamard for convex functions, are significant topic in the literature. These inequalities state that if $F : I \rightarrow \mathbb{R}$ is a convex function on the interval I of real numbers and $a, b \in I$ with $a < b$, then the following double inequality holds:

$$F\left(\frac{a+b}{2}\right) \leq \frac{1}{b-a} \int_a^b F(x) dx \leq \frac{F(a)+F(b)}{2}. \quad (1)$$

In recent years, remarkable number of papers have been investigated to trapezoid and midpoint type inequalities which give bounds for the right-hand side and left-hand side of the inequality (1), respectively. For instance, Dragomir and Agarwal first established to trapezoid inequalities in the case of convex functions in

the [1] and Kirmacı first investigated to midpoint inequalities to the case of convex functions in the [2]. Iqbal et al. presented some fractional midpoint type inequalities for convex functions in [3]. On the other hand, Dragomir established Hermite-Hadamard inequalities in the case of co-ordinated convex mappings in [4]. The midpoint and trapezoid type inequalities for co-ordinated convex functions were presented in the papers [5] and [6], respectively. Moreover, some fractional midpoint type inequalities for co-ordinated convex functions were presented in the paper [7].

In [8], Sarikaya and Ertuğral first investigated new fractional integrals which are called generalized fractional integrals. Moreover, several trapezoids and midpoint type inequalities for generalized fractional integrals are proved by the authors. In addition to these, Turkyay et al. described the generalized fractional integrals in the case of functions with two variables. These authors investigated Hermite-Hadamard inequalities for this kind of fractional integrals in [9]. For more information about these type of inequalities, we refer to [10-12].

Premiliaries & Generalized Fractional and Double Fractional Integrals

In this section, some definitions and notations which are used frequently in main section are presented.

Definition 1. A function $F: \Delta \rightarrow \mathbb{R}$ will be called s -convex in the second sense on Δ if the following inequality

$$F(tx + (1 - t)z, ty + (1 - t)w) \leq t^s F(x, y) + (1 - t)^s F(z, w)$$

is valid for all $s, t \in [0, 1]$ and $(x, y), (z, w) \in \Delta$.

Modifications to the case of convex and s -convex functions on Δ , which are also known as co-ordinated convex and co-ordinated s -convex functions on Δ , respectively, were introduced by Dragomir [5], Sarikaya [6] and Latif [13].

In the paper [6,14], classical definition in the case of co-ordinated s -convex functions in the second sense can be stated as follows:

Definition 2. A function $F: \Delta \rightarrow \mathbb{R}^2$ is called co-ordinated s -convex in the second sense on Δ if the following inequality holds

$$F(tx + (1 - t)z, \lambda y + (1 - \lambda)w) \leq t^s \lambda^s F(x, y) + (1 - t)^s \lambda^s F(z, y) + t^s (1 - \lambda)^s F(x, w) + (1 - t)^s (1 - \lambda)^s F(z, w) \tag{2}$$

for all $t, \lambda \in [0, 1]$

and $(x, y), (z, w) \in \Delta$, and for fixed $s \in (0, 1]$.

Let us consider $s = 1$ in inequality (2). Then, the function F is said to be co-ordinated convex on Δ . If the inequality (2) is in reversed order, then F will be called a co-ordinated s -concave in the second sense on Δ .

Definition 3. A function $F: \Delta \rightarrow \mathbb{R}^2$ is said to be co-ordinated (s_1, s_2) -convex in the second sense on Δ if the following inequality

$$F(tx + (1 - t)z, \lambda y + (1 - \lambda)w) \leq t^{s_1} \lambda^{s_2} F(x, y) + (1 - t)^{s_1} \lambda^{s_2} F(z, y) + t^{s_1} (1 - \lambda)^{s_2} F(x, w) + (1 - t)^{s_1} (1 - \lambda)^{s_2} F(z, w)$$

is valid for all $t, \lambda \in [0, 1]$ and $(x, y), (z, w) \in \Delta$, and for fixed $s_1, s_2 \in (0, 1]$.

The well-known gamma and beta are defined as follows: For $0 < x, y < \infty$, and $x, y \in \mathbb{R}$,

$$\Gamma(x) := \int_0^\infty t^{x-1} e^{-t} dt$$

and

$$\mathfrak{B}(x, y) := \int_0^1 t^{x-1} (1 - t)^{y-1} dt = \frac{\Gamma(x) \Gamma(y)}{\Gamma(x + y)}$$

The generalized fractional integrals were introduced by Sarikaya and Ertugral as follows:

Definition 4. [8] Let us define a function $\varphi: [0, \infty) \rightarrow [0, \infty)$ satisfying the following condition:

$$\int_0^1 \frac{\varphi(\eta)}{\eta} d\eta < \infty.$$

Let us consider the following left-sided and right-sided generalized fractional integral operators

$${}_{a+}I_\varphi F(x) = \int_a^x \frac{\varphi(x - \eta)}{x - \eta} F(\eta) d\eta, \quad x > a \tag{3}$$

and

$${}_{b-}I_\varphi F(x) = \int_x^b \frac{\varphi(\eta - x)}{\eta - x} F(\eta) d\eta, \quad x < b, \tag{4}$$

respectively.

Some shapes of fractional integrals, namely, Riemann-Liouville fractional integral, k -Riemann-Liouville fractional integral, conformable fractional integral, Hadamard fractional integrals, Katugampola fractional integrals, etc are generalized as the most significant feature of generalized fractional integrals. These significant special cases of the integral operators (3) and (4) are presented as follows:

Let us consider $\varphi(\eta) = \eta$. Then, the operators (3) and (4) become to the Riemann integral.

If we select $\varphi(\eta) = \frac{\eta^\alpha}{\Gamma(\alpha)}$ and $\alpha > 0$, the operators (3) and (4) reduce to the Riemann-Liouville fractional integrals $J_{a+}^\alpha F(x)$ and $J_{b-}^\alpha F(x)$, respectively. Here, Γ is Gamma function.

Let us note that $\varphi(\eta) = \frac{1}{k\Gamma_k(\alpha)}\eta^{\frac{\alpha}{k}}$ and $\alpha, k > 0$. Then, the operators (3) and (4) become to the k -Riemann-Liouville fractional integrals $J_{a+,k}^{\alpha}F(x)$ and $J_{b-,k}^{\alpha}F(x)$, respectively. Here, Γ_k is k -Gamma function.

There are several papers on inequalities for generalized fractional integrals in the literature. In [8], Sarikaya and Ertuğral also established Hermite-Hadamard inequalities in the case of generalized fractional integrals. Moreover, Budak et al. proved midpoint type inequalities and extensions of Hermite-Hadamard inequalities in the papers [15] and [16], respectively. There have been a several number of research papers written on these subjects, (see, [17-19] and the references therein.

In [18], the authors are presented the generalized double fractional integrals as follows:

Definition 5. The Generalized double fractional integrals ${}_{a+,c+}I_{\varphi,\psi}$, ${}_{a+,d-}I_{\varphi,\psi}$, ${}_{b-,c+}I_{\varphi,\psi}$, ${}_{b-,d-}I_{\varphi,\psi}$, are described by

$${}_{a+,c+}I_{\varphi,\psi} F(x, y) = \int_a^x \int_c^y \frac{\varphi(x-\eta)\psi(y-\tau)}{x-\eta} \frac{1}{y-\tau} F(\eta, \tau) d\tau d\eta, \quad x > a, y > c, \tag{5}$$

$${}_{a+,d-}I_{\varphi,\psi} F(x, y) = \int_a^x \int_y^d \frac{\varphi(x-\eta)\psi(\tau-y)}{x-\eta} \frac{1}{\tau-y} F(\eta, \tau) d\tau d\eta, \quad x > a, y < d, \tag{6}$$

$${}_{b-,c+}I_{\varphi,\psi} F(x, y) = \int_x^b \int_c^y \frac{\varphi(\eta-x)\psi(y-\tau)}{\eta-x} \frac{1}{y-\tau} F(\eta, \tau) d\tau d\eta, \quad x < b, y > c, \tag{7}$$

and

$${}_{b-,d-}I_{\varphi,\psi} F(x, y) = \int_x^b \int_y^d \frac{\varphi(\eta-x)\psi(\tau-y)}{\eta-x} \frac{1}{\tau-y} F(\eta, \tau) d\tau d\eta, \quad x < b, y < d, \tag{8}$$

respectively. Here, $F \in L_1([a, b] \times [c, d])$ and the functions $\varphi, \psi : [0, \infty) \rightarrow [0, \infty)$ satisfy $\int_0^1 \frac{\varphi(\eta)}{\eta} d\eta < \infty$ and $\int_0^1 \frac{\psi(\tau)}{\tau} d\tau < \infty$, respectively.

By using Definition 5, well-known fractional integrals can be obtained by some special choices. For instance;

If we assign $\varphi(\eta) = \eta$ and $\psi(\tau) = \tau$, then the operators (5), (6), (7) and (8) become to the double Riemann integral.

For $\varphi(\eta) = \frac{\eta^{\alpha}}{\Gamma(\alpha)}$, $\psi(\tau) = \frac{\tau^{\beta}}{\Gamma(\beta)}$, $\alpha, \beta > 0$, the operators (5), (6), (7) and (8) reduce to the Riemann-Liouville fractional integrals $J_{a+,c+}^{\alpha,\beta}F(x, y)$, $J_{a+,d-}^{\alpha,\beta}F(x, y)$, $J_{b-,c+}^{\alpha,\beta}F(x, y)$ and $J_{b-,d-}^{\alpha,\beta}F(x, y)$, respectively.

Let us consider $\varphi(\eta) = \frac{\eta^{\frac{\alpha}{k}}}{k\Gamma_k(\alpha)}$ and $\psi(\tau) = \frac{\tau^{\frac{\beta}{k}}}{k\Gamma_k(\beta)}$, for $\alpha, \beta, k > 0$. Then, the operators (5), (6), (7) and (8) reduce to the k -Riemann-Liouville fractional integrals $J_{a+,c+}^{\alpha,\beta,k}F(x, y)$, $J_{a+,d-}^{\alpha,\beta,k}F(x, y)$, $J_{b-,c+}^{\alpha,\beta,k}F(x, y)$ and $J_{b-,d-}^{\alpha,\beta,k}F(x, y)$, respectively. For more information and unexplained subjects, the reader is referred to [20-31], and the references therein.

In the paper [32], an identity for twice partially differentiable mappings involving the double generalized fractional integral is established as follows:

Lemma 1. [32] Let $F: \Delta \rightarrow \mathbb{R}$ be an absolutely continuous function on Δ such that the partial derivative of order $\frac{\partial^2 F(\eta, \tau)}{\partial \eta \partial \tau}$ exist for all $(\eta, \tau) \in \Delta$. Then, the following equality for generalized fractional integrals holds:

$$\begin{aligned} & \Phi(a, b, x; c, d, y) \\ &= \frac{(x-a)(y-c)}{Y(x, y)} \int_0^1 \int_0^1 \Lambda_1(x, \eta) \Lambda_2(y, \tau) \frac{\partial^2}{\partial \eta \partial \tau} F(\eta b + (1-\eta)(a+b-x), \tau d + (1-\tau)(c+d-y)) d\tau d\eta \\ & \quad - \frac{(x-a)(d-y)}{Y(x, y)} \int_0^1 \int_0^1 \Lambda_1(x, \eta) \Lambda_2(y, \tau) \frac{\partial^2}{\partial \eta \partial \tau} F(\eta b + (1-\eta)(a+b-x), \tau c + (1-\tau)(c+d-y)) d\tau d\eta \\ & \quad - \frac{(b-x)(y-c)}{Y(x, y)} \int_0^1 \int_0^1 \Delta_1(x, \eta) \Delta_2(y, \tau) \frac{\partial^2}{\partial \eta \partial \tau} F(\eta a + (1-\eta)(a+b-x), \tau d + (1-\tau)(c+d-y)) d\tau d\eta \\ & \quad + \frac{(b-x)(d-y)}{Y(x, y)} \int_0^1 \int_0^1 \Delta_1(x, \eta) \Delta_2(y, \tau) \frac{\partial^2}{\partial \eta \partial \tau} F(\eta a + (1-\eta)(a+b-x), \tau c + (1-\tau)(c+d-y)) d\tau d\eta, \end{aligned}$$

where $\Delta := [a, b] \times [c, d]$,

$$\begin{aligned} \Phi(a, b, x; c, d, y) &= F(a + b - x, c + d - y) \\ &- \frac{1}{\chi_2(y)} \left[{}_{a-}I_{\psi}F(a + b - x, c + d - y) + {}_{c+}I_{\psi}F(a + b - x, c + d - y) \right] \\ &- \frac{1}{\chi_1(x)} \left[{}_{b-}I_{\varphi}F(a + b - x, c + d - y) + {}_{a+}I_{\varphi}F(a + b - x, c + d - y) \right] \\ &+ \frac{1}{Y(x, y)} \left[{}_{b-,d-}I_{\varphi, \psi}F(a + b - x, c + d - y) + {}_{b-,c+}I_{\varphi, \psi}F(a + b - x, c + d - y) \right. \\ &\left. + {}_{a+,d-}I_{\varphi, \psi}F(a + b - x, c + d - y) + {}_{a+,c+}I_{\varphi, \psi}F(a + b - x, c + d - y) \right], \end{aligned}$$

and

$$\begin{cases} \chi_1(x) = \Lambda_1(x, 0) + \Delta_1(x, 0), \\ \chi_2(y) = \Lambda_2(y, 0) + \Delta_2(y, 0), \\ Y(x, y) = \chi_1(x)\chi_2(y). \end{cases}$$

Throughout this paper for brevity, let us consider

$$\Lambda_1(x, \eta) = \int_{\eta}^1 \frac{\varphi((b-x)u)}{u} du, \quad \Delta_1(x, \eta) = \int_{\eta}^1 \frac{\varphi((x-a)u)}{u} du,$$

and

$$\Lambda_2(y, \tau) = \int_{\tau}^1 \frac{\psi((d-y)u)}{u} du, \quad \Delta_2(y, \tau) = \int_{\tau}^1 \frac{\psi((y-c)u)}{u} du.$$

Midpoint Inequalities for Co-ordinated (s_1, s_2) -Convex Function Involving Generalized Fractional Integrals Discussion

Theorem 1. Suppose that the assumptions of Lemma 1 hold. Suppose also that the function $\left| \frac{\partial^2 F}{\partial \eta \partial \tau} \right|$ is co-ordinated (s_1, s_2) -convex on Δ . Then, we have the following inequality for generalized fractional integrals

$$\begin{aligned} &|\Phi(a, b, x; c, d, y)| \\ &\leq \frac{(x-a)(y-c)}{Y(x, y)} \left[\lambda_1 \mu_1 \left| \frac{\partial^2}{\partial \eta \partial \tau} F(b, d) \right| + \lambda_1 \mu_2 \left| \frac{\partial^2}{\partial \eta \partial \tau} F(b, c + d - y) \right| \right. \\ &\quad \left. + \lambda_2 \mu_1 \left| \frac{\partial^2}{\partial \eta \partial \tau} F(a + b - x, d) \right| + \lambda_2 \mu_2 \left| \frac{\partial^2}{\partial \eta \partial \tau} F(a + b - x, c + d - y) \right| \right] \\ &+ \frac{(x-a)(d-y)}{Y(x, y)} \left[\lambda_1 \mu_4 \left| \frac{\partial^2}{\partial \eta \partial \tau} F(b, c) \right| + \lambda_1 \mu_3 \left| \frac{\partial^2}{\partial \eta \partial \tau} F(b, c + d - y) \right| \right. \\ &\quad \left. + \lambda_2 \mu_4 \left| \frac{\partial^2}{\partial \eta \partial \tau} F(a + b - x, c) \right| + \lambda_2 \mu_3 \left| \frac{\partial^2}{\partial \eta \partial \tau} F(a + b - x, c + d - y) \right| \right] \\ &+ \frac{(b-x)(y-c)}{Y(x, y)} \left[\lambda_4 \mu_1 \left| \frac{\partial^2}{\partial \eta \partial \tau} F(a, d) \right| + \lambda_4 \mu_2 \left| \frac{\partial^2}{\partial \eta \partial \tau} F(a, c + d - y) \right| \right. \\ &\quad \left. + \lambda_3 \mu_1 \left| \frac{\partial^2}{\partial \eta \partial \tau} F(a + b - x, d) \right| + \lambda_3 \mu_2 \left| \frac{\partial^2}{\partial \eta \partial \tau} F(a + b - x, c + d - y) \right| \right] \\ &+ \frac{(b-x)(d-y)}{Y(x, y)} \left[\lambda_4 \mu_4 \left| \frac{\partial^2}{\partial \eta \partial \tau} F(a, c) \right| + \lambda_4 \mu_3 \left| \frac{\partial^2}{\partial \eta \partial \tau} F(a, c + d - y) \right| \right. \\ &\quad \left. + \lambda_3 \mu_4 \left| \frac{\partial^2}{\partial \eta \partial \tau} F(a + b - x, c) \right| + \lambda_3 \mu_3 \left| \frac{\partial^2}{\partial \eta \partial \tau} F(a + b - x, c + d - y) \right| \right]. \end{aligned}$$

Here,

$$\begin{cases} \lambda_1 = \int_0^1 \eta^{s_1} \Lambda_1(x, \eta) d\eta, & \lambda_2 = \int_0^1 (1 - \eta)^{s_1} \Lambda_1(x, \eta) d\eta, \\ \lambda_3 = \int_0^1 (1 - \eta)^{s_1} \Delta_1(x, \eta) d\eta, & \lambda_4 = \int_0^1 \eta^{s_1} \Delta_1(x, \eta) d\eta, \end{cases} \tag{9}$$

and

$$\begin{cases} \mu_1 = \int_0^1 \tau^{s_2} \Lambda_2(y, \tau) d\tau, & \mu_2 = \int_0^1 (1 - \tau)^{s_2} \Lambda_2(y, \tau) d\tau, \\ \mu_3 = \int_0^1 (1 - \tau)^{s_2} \Delta_2(y, \tau) d\tau, & \mu_4 = \int_0^1 \tau^{s_2} \Delta_2(y, \tau) d\tau. \end{cases} \tag{10}$$

Proof. Let us take the modulus in Lemma 1. Then, it follows:

$$\begin{aligned} & |\Phi(a, b, x; c, d, y)| \\ & \leq \frac{(x - a)(y - c)}{Y(x, y)} \int_0^1 \int_0^1 \Lambda_1(x, \eta) \Lambda_2(y, \tau) \left| \frac{\partial^2}{\partial \eta \partial \tau} F(\eta b + (1 - \eta)(a + b - x), \tau d + (1 - \tau)(c + d - y)) \right| d\tau d\eta \\ & \quad + \frac{(x - a)(d - y)}{Y(x, y)} \int_0^1 \int_0^1 \Lambda_1(x, \eta) \Delta_2(y, \tau) \left| \frac{\partial^2}{\partial \eta \partial \tau} F(\eta b + (1 - \eta)(a + b - x), \tau c + (1 - \tau)(c + d - y)) \right| d\tau d\eta \\ & \quad + \frac{(b - x)(y - c)}{Y(x, y)} \int_0^1 \int_0^1 \Delta_1(x, \eta) \Lambda_2(y, \tau) \left| \frac{\partial^2}{\partial \eta \partial \tau} F(\eta a + (1 - \eta)(a + b - x), \tau d + (1 - \tau)(c + d - y)) \right| d\tau d\eta \\ & \quad + \frac{(b - x)(d - y)}{Y(x, y)} \int_0^1 \int_0^1 \Delta_1(x, \eta) \Delta_2(y, \tau) \left| \frac{\partial^2}{\partial \eta \partial \tau} F(\eta a + (1 - \eta)(a + b - x), \tau c + (1 - \tau)(c + d - y)) \right| d\tau d\eta. \end{aligned} \tag{11}$$

Since $\left| \frac{\partial^2 F}{\partial \eta \partial \tau} \right|$ is co-ordinated (s_1, s_2) -convex, we have

$$\begin{aligned} & \int_0^1 \int_0^1 \Lambda_1(x, \eta) \Lambda_2(y, \tau) \left| \frac{\partial^2}{\partial \eta \partial \tau} F(\eta b + (1 - \eta)(a + b - x), \tau d + (1 - \tau)(c + d - y)) \right| d\tau d\eta \\ & \leq \int_0^1 \int_0^1 \Lambda_1(x, \eta) \Lambda_2(y, \tau) \left(\eta^{s_1} \tau^{s_2} \left| \frac{\partial^2}{\partial \eta \partial \tau} F(b, d) \right| + \eta^{s_1} (1 - \tau)^{s_2} \left| \frac{\partial^2}{\partial \eta \partial \tau} F(b, c + d - y) \right| \right. \\ & \quad \left. + (1 - \eta)^{s_1} \tau^{s_2} \left| \frac{\partial^2}{\partial \eta \partial \tau} F(a + b - x, d) \right| + (1 - \eta)^{s_1} (1 - \tau)^{s_2} \left| \frac{\partial^2}{\partial \eta \partial \tau} F(a + b - x, c + d - y) \right| \right) d\tau d\eta \tag{12} \\ & = \lambda_1 \mu_1 \left| \frac{\partial^2}{\partial \eta \partial \tau} F(b, d) \right| + \lambda_1 \mu_2 \left| \frac{\partial^2}{\partial \eta \partial \tau} F(b, c + d - y) \right| \\ & \quad + \lambda_2 \mu_1 \left| \frac{\partial^2}{\partial \eta \partial \tau} F(a + b - x, d) \right| + \lambda_2 \mu_2 \left| \frac{\partial^2}{\partial \eta \partial \tau} F(a + b - x, c + d - y) \right|. \end{aligned}$$

Similarly, it follows

$$\begin{aligned} & \int_0^1 \int_0^1 \Lambda_1(x, \eta) \Delta_2(y, \tau) \left| \frac{\partial^2}{\partial \eta \partial \tau} F(\eta b + (1 - \eta)(a + b - x), \tau c + (1 - \tau)(c + d - y)) \right| d\tau d\eta \\ & \leq \lambda_1 \mu_4 \left| \frac{\partial^2}{\partial \eta \partial \tau} F(b, c) \right| + \lambda_1 \mu_3 \left| \frac{\partial^2}{\partial \eta \partial \tau} F(b, c + d - y) \right| \\ & \quad + \lambda_2 \mu_4 \left| \frac{\partial^2}{\partial \eta \partial \tau} F(a + b - x, c) \right| + \lambda_2 \mu_3 \left| \frac{\partial^2}{\partial \eta \partial \tau} F(a + b - x, c + d - y) \right|, \end{aligned} \tag{13}$$

$$\begin{aligned} & \int_0^1 \int_0^1 \Delta_1(x, \eta) \Lambda_2(y, \tau) \left| \frac{\partial^2}{\partial \eta \partial \tau} F(\eta a + (1 - \eta)(a + b - x), \tau d + (1 - \tau)(c + d - y)) \right| d\tau d\eta \\ & \leq \lambda_4 \mu_1 \left| \frac{\partial^2}{\partial \eta \partial \tau} F(a, d) \right| + \lambda_4 \mu_2 \left| \frac{\partial^2}{\partial \eta \partial \tau} F(a, c + d - y) \right| \\ & \quad + \lambda_3 \mu_1 \left| \frac{\partial^2}{\partial \eta \partial \tau} F(a + b - x, d) \right| + \lambda_3 \mu_2 \left| \frac{\partial^2}{\partial \eta \partial \tau} F(a + b - x, c + d - y) \right|, \end{aligned} \tag{14}$$

and

$$\begin{aligned} & \int_0^1 \int_0^1 \Delta_1(x, \eta) \Delta_2(y, \tau) \left| \frac{\partial^2}{\partial \eta \partial \tau} F(\eta a + (1 - \eta)(a + b - x), \tau c + (1 - \tau)(c + d - y)) \right| d\tau d\eta \\ & \leq \lambda_4 \mu_4 \left| \frac{\partial^2}{\partial \eta \partial \tau} F(a, c) \right| + \lambda_4 \mu_3 \left| \frac{\partial^2}{\partial \eta \partial \tau} F(a, c + d - y) \right| \\ & \quad + \lambda_3 \mu_4 \left| \frac{\partial^2}{\partial \eta \partial \tau} F(a + b - x, c) \right| + \lambda_3 \mu_3 \left| \frac{\partial^2}{\partial \eta \partial \tau} F(a + b - x, c + d - y) \right|. \end{aligned} \tag{15}$$

If it is substituted the inequalities (12)-(15) in (11), then the desired results are obtained. This finishes the proof of Theorem 1.

Corollary 1. Let us consider $\varphi(\eta) = \eta$ and $\psi(\tau) = \tau$ for all $(\eta, \tau) \in \Delta$ in Theorem 1. Let us also consider $s_1 = s_2 = s$, $x = \frac{a+b}{2}$ and $y = \frac{c+d}{2}$. Then, we have the following midpoint type inequality for Riemann-Liouville fractional integrals

$$\begin{aligned} & \left| F\left(\frac{a+b}{2}, \frac{c+d}{2}\right) - \frac{1}{d-c} \left[{}_{d-}I_{\psi}F\left(\frac{a+b}{2}, \frac{c+d}{2}\right) + {}_{c+}I_{\psi}F\left(\frac{a+b}{2}, \frac{c+d}{2}\right) \right] \right. \\ & \quad \left. - \frac{1}{b-a} \left[{}_{b-}I_{\varphi}F\left(\frac{a+b}{2}, \frac{c+d}{2}\right) + {}_{a+}I_{\varphi}F\left(\frac{a+b}{2}, \frac{c+d}{2}\right) \right] \right. \\ & \quad \left. + \frac{1}{(b-a)(d-c)} \left[{}_{b-,d-}I_{\varphi,\psi}F\left(\frac{a+b}{2}, \frac{c+d}{2}\right) + {}_{b-,c+}I_{\varphi,\psi}F\left(\frac{a+b}{2}, \frac{c+d}{2}\right) \right. \right. \\ & \quad \left. \left. + {}_{a+,d-}I_{\varphi,\psi}F\left(\frac{a+b}{2}, \frac{c+d}{2}\right) + {}_{a+,c+}I_{\varphi,\psi}F\left(\frac{a+b}{2}, \frac{c+d}{2}\right) \right] \right| \\ & \leq \frac{(b-a)(d-c)}{16} \left[\frac{1}{(s+1)^2(s+2)^2} \left(\left| \frac{\partial^2}{\partial \eta \partial \tau} F(a, c) \right| + \left| \frac{\partial^2}{\partial \eta \partial \tau} F(b, d) \right| + \left| \frac{\partial^2}{\partial \eta \partial \tau} F(b, c) \right| + \left| \frac{\partial^2}{\partial \eta \partial \tau} F(a, d) \right| \right) \right. \\ & \quad \left. + \frac{2}{(s+1)(s+2)^2} \left(\left| \frac{\partial^2}{\partial \eta \partial \tau} F\left(a, \frac{c+d}{2}\right) \right| + \left| \frac{\partial^2}{\partial \eta \partial \tau} F\left(b, \frac{c+d}{2}\right) \right| \right) \right. \\ & \quad \left. + \left| \frac{\partial^2}{\partial \eta \partial \tau} F\left(\frac{a+b}{2}, c\right) \right| + \left| \frac{\partial^2}{\partial \eta \partial \tau} F\left(\frac{a+b}{2}, d\right) \right| \right) + \frac{4}{(s+2)^2} \left(\left| \frac{\partial^2}{\partial \eta \partial \tau} F\left(\frac{a+b}{2}, \frac{c+d}{2}\right) \right| \right) \right] \\ & \leq \frac{(b-a)(d-c)}{16} \left(\frac{2^{2s} + 2^{s+2}(s+1) + 4(s+1)^2}{2^{2s}(s+1)^2(s+2)^2} \right) \\ & \quad \times \left[\left| \frac{\partial^2}{\partial \eta \partial \tau} F(a, c) \right| + \left| \frac{\partial^2}{\partial \eta \partial \tau} F(b, d) \right| + \left| \frac{\partial^2}{\partial \eta \partial \tau} F(b, c) \right| + \left| \frac{\partial^2}{\partial \eta \partial \tau} F(a, d) \right| \right]. \end{aligned}$$

Remark 1. Let us consider $s_1 = s_2 = 1$ in Corollary 1. Then, Corollary 1 reduces to [5, Theorem 2].

Corollary 2. In Theorem 1, if we assign $\varphi(\eta) = \frac{\eta^\alpha}{\Gamma(\alpha)}$ and $\psi(\tau) = \frac{\tau^\beta}{\Gamma(\beta)}$ for all $(\eta, \tau) \in \Delta$ and if we choose $s_1 = s_2 = s$, and $y = \frac{c+d}{2}$, then we have the following midpoint type inequality for Riemann-Liouville fractional integrals

$$\begin{aligned}
 & \left| F\left(\frac{a+b}{2}, \frac{c+d}{2}\right) - \frac{2^{\beta-1}\Gamma(\beta+1)}{(d-c)^\beta} \left[J_{d^-}^\beta F\left(\frac{a+b}{2}, \frac{c+d}{2}\right) + J_{c^+}^\beta F\left(\frac{a+b}{2}, \frac{c+d}{2}\right) \right] \right. \\
 & \left. - \frac{2^{\alpha-1}\Gamma(\alpha+1)}{(b-a)^\alpha} \left[J_{b^-}^\alpha F\left(\frac{a+b}{2}, \frac{c+d}{2}\right) + J_{a^+}^\alpha F\left(\frac{a+b}{2}, \frac{c+d}{2}\right) \right] \right. \\
 & \left. + \frac{2^{\alpha+\beta-2}\Gamma(\alpha+1)\Gamma(\beta+1)}{(b-a)^\alpha(d-c)^\beta} \left[J_{b^-,d^-}^{\alpha,\beta} F\left(\frac{a+b}{2}, \frac{c+d}{2}\right) + J_{b^-,c^+}^{\alpha,\beta} F\left(\frac{a+b}{2}, \frac{c+d}{2}\right) \right. \right. \\
 & \left. \left. + J_{a^+,d^-}^{\alpha,\beta} F\left(\frac{a+b}{2}, \frac{c+d}{2}\right) + J_{a^+,c^+}^{\alpha,\beta} F\left(\frac{a+b}{2}, \frac{c+d}{2}\right) \right] \right| \\
 & \leq \frac{(b-a)(d-c)}{16} \left[\frac{\alpha\beta}{(s+1)^2(s+\alpha+1)(s+\beta+1)} \right. \\
 & \times \left(\left| \frac{\partial^2}{\partial\eta\partial\tau} F(a,c) \right| + \left| \frac{\partial^2}{\partial\eta\partial\tau} F(a,d) \right| + \left| \frac{\partial^2}{\partial\eta\partial\tau} F(b,c) \right| + \left| \frac{\partial^2}{\partial\eta\partial\tau} F(b,d) \right| \right) \\
 & + \frac{2\alpha \left(\frac{1}{s+1} - \mathfrak{P}(\beta+1, s+1) \right)}{(s+1)(s+\alpha+1)} \left(\left| \frac{\partial^2}{\partial\eta\partial\tau} F\left(a, \frac{c+d}{2}\right) \right| + \left| \frac{\partial^2}{\partial\eta\partial\tau} F\left(b, \frac{c+d}{2}\right) \right| \right) \\
 & + \frac{2\beta \left(\frac{1}{s+1} - \mathfrak{P}(\alpha+1, s+1) \right)}{(s+1)(s+\beta+1)} \left(\left| \frac{\partial^2}{\partial\eta\partial\tau} F\left(\frac{a+b}{2}, c\right) \right| + \left| \frac{\partial^2}{\partial\eta\partial\tau} F\left(\frac{a+b}{2}, d\right) \right| \right) \\
 & + 4 \left(\frac{1}{s+1} - \mathfrak{P}(\alpha+1, s+1) \right) \left(\frac{1}{s+1} - \mathfrak{P}(\beta+1, s+1) \right) \left| \frac{\partial^2}{\partial\eta\partial\tau} F\left(\frac{a+b}{2}, \frac{c+d}{2}\right) \right| \Bigg] \\
 & \leq \frac{(b-a)(d-c)}{16} \left[\frac{\alpha\beta}{(s+1)^2(s+\alpha+1)(s+\beta+1)} + \frac{2\alpha \left(\frac{1}{s+1} - \mathfrak{P}(\beta+1, s+1) \right)}{2^s(s+1)(s+\alpha+1)} \right. \\
 & \left. + \frac{2\beta \left(\frac{1}{s+1} - \mathfrak{P}(\alpha+1, s+1) \right)}{2^s(s+1)(s+\beta+1)} + \frac{4}{2^{2s}} \left(\frac{1}{s+1} - \mathfrak{P}(\alpha+1, s+1) \right) \left(\frac{1}{s+1} - \mathfrak{P}(\beta+1, s+1) \right) \right] \\
 & \times \left(\left| \frac{\partial^2}{\partial\eta\partial\tau} F(a,c) \right| + \left| \frac{\partial^2}{\partial\eta\partial\tau} F(a,d) \right| + \left| \frac{\partial^2}{\partial\eta\partial\tau} F(b,c) \right| + \left| \frac{\partial^2}{\partial\eta\partial\tau} F(b,d) \right| \right)
 \end{aligned}$$

Remark 2. If it is chosen $s_1 = s_2 = 1$ in Corollary 2, then Corollary 2 becomes to [32, Corollary 1].

Corollary 3. In Theorem 1, if we assign $\varphi(\eta) = \frac{\eta^\alpha}{k\Gamma_k(\alpha)}$ and $\psi(\tau) = \frac{\tau^\beta}{k\Gamma_k(\beta)}$ for all $(\eta, \tau) \in \Delta$ and if we choose $s_1 = s_2 = s$, $x = \frac{a+b}{2}$ and $y = \frac{c+d}{2}$, then we have the following midpoint type inequality for k -Riemann-Liouville fractional integrals

$$\begin{aligned}
 & \left| F\left(\frac{a+b}{2}, \frac{c+d}{2}\right) - \frac{2^{\frac{\beta}{k}-1} \Gamma_k(\beta+k)}{(d-c)^{\frac{\beta}{k}}} \left[J_{d-,k}^{\beta} F\left(\frac{a+b}{2}, \frac{c+d}{2}\right) + J_{c+,k}^{\beta} F\left(\frac{a+b}{2}, \frac{c+d}{2}\right) \right] \right. \\
 & \left. - \frac{2^{\frac{\alpha}{k}-1} \Gamma_k(\alpha+k)}{(b-a)^{\frac{\alpha}{k}}} \left[J_{b-,k}^{\alpha} F\left(\frac{a+b}{2}, \frac{c+d}{2}\right) + J_{a+,k}^{\alpha} F\left(\frac{a+b}{2}, \frac{c+d}{2}\right) \right] \right. \\
 & \left. + \frac{2^{\frac{\alpha+\beta}{k}-2} \Gamma_k(\alpha+k) \Gamma_k(\beta+k)}{(b-a)^{\frac{\alpha}{k}} (d-c)^{\frac{\beta}{k}}} \left[J_{b-,d-}^{\alpha,\beta,k} F\left(\frac{a+b}{2}, \frac{c+d}{2}\right) + J_{b-,c+}^{\alpha,\beta,k} F\left(\frac{a+b}{2}, \frac{c+d}{2}\right) \right. \right. \\
 & \left. \left. + J_{a+,d-}^{\alpha,\beta,k} F\left(\frac{a+b}{2}, \frac{c+d}{2}\right) + J_{a+,c+}^{\alpha,\beta,k} F\left(\frac{a+b}{2}, \frac{c+d}{2}\right) \right] \right| \\
 & \leq \frac{(b-a)(d-c)}{16} \left[\frac{\alpha\beta}{(s+1)^2 (sk+\alpha+k)(sk+\beta+k)} \right. \\
 & \times \left(\left| \frac{\partial^2}{\partial\eta\partial\tau} F(a,c) \right| + \left| \frac{\partial^2}{\partial\eta\partial\tau} F(a,d) \right| + \left| \frac{\partial^2}{\partial\eta\partial\tau} F(b,c) \right| + \left| \frac{\partial^2}{\partial\eta\partial\tau} F(b,d) \right| \right) \\
 & + \frac{2\alpha \left(\frac{1}{s+1} - \mathfrak{P}\left(\frac{\beta}{k} + 1, s+1\right) \right)}{(s+1)(sk+\alpha+k)} \left(\left| \frac{\partial^2}{\partial\eta\partial\tau} F\left(a, \frac{c+d}{2}\right) \right| + \left| \frac{\partial^2}{\partial\eta\partial\tau} F\left(b, \frac{c+d}{2}\right) \right| \right) \\
 & + \frac{2\beta \left(\frac{1}{s+1} - \mathfrak{P}\left(\frac{\alpha}{k} + 1, s+1\right) \right)}{(s+1)(sk+\beta+k)} \left(\left| \frac{\partial^2}{\partial\eta\partial\tau} F\left(\frac{a+b}{2}, c\right) \right| + \left| \frac{\partial^2}{\partial\eta\partial\tau} F\left(\frac{a+b}{2}, d\right) \right| \right) \\
 & + 4 \left(\frac{1}{s+1} - \mathfrak{P}\left(\frac{\alpha}{k} + 1, s+1\right) \right) \left(\frac{1}{s+1} - \mathfrak{P}\left(\frac{\beta}{k} + 1, s+1\right) \right) \left| \frac{\partial^2}{\partial\eta\partial\tau} F\left(\frac{a+b}{2}, \frac{c+d}{2}\right) \right| \right] \\
 & \leq \frac{(b-a)(d-c)}{16} \left[\frac{\alpha\beta}{(s+1)^2 (sk+\alpha+k)(sk+\beta+k)} + \frac{2\alpha \left(\frac{1}{s+1} - \mathfrak{P}\left(\frac{\beta}{k} + 1, s+1\right) \right)}{2^s (s+1)(sk+\alpha+k)} \right. \\
 & \left. + \frac{2\beta \left(\frac{1}{s+1} - \mathfrak{P}\left(\frac{\alpha}{k} + 1, s+1\right) \right)}{2^s (s+1)(sk+\beta+k)} + \frac{4}{2^{2s}} \left(\frac{1}{s+1} - \mathfrak{P}\left(\frac{\alpha}{k} + 1, s+1\right) \right) \left(\frac{1}{s+1} - \mathfrak{P}\left(\frac{\beta}{k} + 1, s+1\right) \right) \right] \\
 & \times \left(\left| \frac{\partial^2}{\partial\eta\partial\tau} F(a,c) \right| + \left| \frac{\partial^2}{\partial\eta\partial\tau} F(a,d) \right| + \left| \frac{\partial^2}{\partial\eta\partial\tau} F(b,c) \right| + \left| \frac{\partial^2}{\partial\eta\partial\tau} F(b,d) \right| \right).
 \end{aligned}$$

Remark 3. Let us consider $s_1 = s_2 = 1$ in Corollary 3. Then, Corollary 3 reduces to [32, Corollary 2].

Theorem 2. Assume that the assumptions of Lemma 1 are valid. Assume also that the mapping $\left| \frac{\partial^2 F}{\partial\eta\partial\tau} \right|^q, q > 1$ is co-ordinated (s_1, s_2) -convex on Δ . Then, the following inequality for generalized fractional integrals holds:

$$\begin{aligned}
 |\Phi(a, b, x; c, d, y)| &\leq \frac{(x-a)(y-c)}{\Upsilon(x, y)} \left(\int_0^1 \int_0^1 [\Lambda_1(x, \eta)\Lambda_2(y, \tau)]^p d\tau d\eta \right)^{\frac{1}{p}} \\
 &\times \left(\frac{\left| \frac{\partial^2}{\partial\eta\partial\tau} F(b, d) \right|^q + \left| \frac{\partial^2}{\partial\eta\partial\tau} F(b, c+d-y) \right|^q + \left| \frac{\partial^2}{\partial\eta\partial\tau} F(a+b-x, d) \right|^q + \left| \frac{\partial^2}{\partial\eta\partial\tau} F(a+b-x, c+d-y) \right|^q}{(s_1+1)(s_2+1)} \right)^{\frac{1}{q}} \\
 &+ \frac{(x-a)(d-y)}{\Upsilon(x, y)} \left(\int_0^1 \int_0^1 [\Lambda_1(x, \eta)\Delta_2(y, \tau)]^p d\tau d\eta \right)^{\frac{1}{p}} \\
 &\times \left(\frac{\left| \frac{\partial^2}{\partial\eta\partial\tau} F(b, c) \right|^q + \left| \frac{\partial^2}{\partial\eta\partial\tau} F(b, c+d-y) \right|^q + \left| \frac{\partial^2}{\partial\eta\partial\tau} F(a+b-x, c) \right|^q + \left| \frac{\partial^2}{\partial\eta\partial\tau} F(a+b-x, c+d-y) \right|^q}{(s_1+1)(s_2+1)} \right)^{\frac{1}{q}} \\
 &+ \frac{(b-x)(y-c)}{\Upsilon(x, y)} \left(\int_0^1 \int_0^1 [\Delta_1(x, \eta)\Lambda_2(y, \tau)]^p d\tau d\eta \right)^{\frac{1}{p}} \\
 &\times \left(\frac{\left| \frac{\partial^2}{\partial\eta\partial\tau} F(a, d) \right|^q + \left| \frac{\partial^2}{\partial\eta\partial\tau} F(a, c+d-y) \right|^q + \left| \frac{\partial^2}{\partial\eta\partial\tau} F(a+b-x, d) \right|^q + \left| \frac{\partial^2}{\partial\eta\partial\tau} F(a+b-x, c+d-y) \right|^q}{(s_1+1)(s_2+1)} \right)^{\frac{1}{q}} \\
 &+ \frac{(b-x)(d-y)}{\Upsilon(x, y)} \left(\int_0^1 \int_0^1 [\Delta_1(x, \eta)\Delta_2(y, \tau)]^p d\tau d\eta \right)^{\frac{1}{p}} \\
 &\times \left(\frac{\left| \frac{\partial^2}{\partial\eta\partial\tau} F(a, c) \right|^q + \left| \frac{\partial^2}{\partial\eta\partial\tau} F(a, c+d-y) \right|^q + \left| \frac{\partial^2}{\partial\eta\partial\tau} F(a+b-x, c) \right|^q + \left| \frac{\partial^2}{\partial\eta\partial\tau} F(a+b-x, c+d-y) \right|^q}{(s_1+1)(s_2+1)} \right)^{\frac{1}{q}}.
 \end{aligned}$$

Here, $\frac{1}{p} + \frac{1}{q} = 1$ and $\Phi(a, b, x; c, d, y)$ are defined as in Lemma 1.

Proof. With the help of Hölder inequality and co-ordinated (s_1, s_2) -convexity of $\left| \frac{\partial^2 F}{\partial\eta\partial\tau} \right|^q$, it follows

$$\begin{aligned}
 &\int_0^1 \int_0^1 \Lambda_1(x, \eta)\Lambda_2(y, \tau) \left| \frac{\partial^2}{\partial\eta\partial\tau} F(\eta b + (1-\eta)(a+b-x), \tau d + (1-\tau)(c+d-y)) \right| d\tau d\eta \\
 &\leq \left(\int_0^1 \int_0^1 [\Lambda_1(x, \eta)\Lambda_2(y, \tau)]^p d\tau d\eta \right)^{\frac{1}{p}} \\
 &\times \left(\int_0^1 \int_0^1 \left| \frac{\partial^2}{\partial\eta\partial\tau} F(\eta b + (1-\eta)(a+b-x), \tau d + (1-\tau)(c+d-y)) \right|^q d\tau d\eta \right)^{\frac{1}{q}} \tag{16} \\
 &\leq \left(\int_0^1 \int_0^1 [\Lambda_1(x, \eta)\Lambda_2(y, \tau)]^p d\tau d\eta \right)^{\frac{1}{p}} \\
 &\times \left(\frac{\left| \frac{\partial^2}{\partial\eta\partial\tau} F(b, d) \right|^q + \left| \frac{\partial^2}{\partial\eta\partial\tau} F(b, c+d-y) \right|^q + \left| \frac{\partial^2}{\partial\eta\partial\tau} F(a+b-x, d) \right|^q + \left| \frac{\partial^2}{\partial\eta\partial\tau} F(a+b-x, c+d-y) \right|^q}{(s_1+1)(s_2+1)} \right)^{\frac{1}{q}}.
 \end{aligned}$$

Similarly, we obtain

$$\int_0^1 \int_0^1 \Lambda_1(x, \eta) \Lambda_2(y, \tau) \left| \frac{\partial^2}{\partial \eta \partial \tau} F(\eta b + (1 - \eta)(a + b - x), \tau c + (1 - \tau)(c + d - y)) \right| d\tau d\eta$$

$$\leq \left(\int_0^1 \int_0^1 [\Lambda_1(x, \eta) \Lambda_2(y, \tau)]^p d\tau d\eta \right)^{\frac{1}{p}}$$

$$\times \left(\frac{\left| \frac{\partial^2}{\partial \eta \partial \tau} F(b, c) \right|^q + \left| \frac{\partial^2}{\partial \eta \partial \tau} F(b, c + d - y) \right|^q + \left| \frac{\partial^2}{\partial \eta \partial \tau} F(a + b - x, c) \right|^q + \left| \frac{\partial^2}{\partial \eta \partial \tau} F(a + b - x, c + d - y) \right|^q}{(s_1 + 1)(s_2 + 1)} \right)^{\frac{1}{q}}, \tag{17}$$

$$\int_0^1 \int_0^1 \Delta_1(x, \eta) \Delta_2(y, \tau) \left| \frac{\partial^2}{\partial \eta \partial \tau} F(\eta a + (1 - \eta)(a + b - x), \tau d + (1 - \tau)(c + d - y)) \right| d\tau d\eta$$

$$\leq \left(\int_0^1 \int_0^1 [\Delta_1(x, \eta) \Delta_2(y, \tau)]^p d\tau d\eta \right)^{\frac{1}{p}}$$

$$\times \left(\frac{\left| \frac{\partial^2}{\partial \eta \partial \tau} F(a, d) \right|^q + \left| \frac{\partial^2}{\partial \eta \partial \tau} F(a, c + d - y) \right|^q + \left| \frac{\partial^2}{\partial \eta \partial \tau} F(a + b - x, d) \right|^q + \left| \frac{\partial^2}{\partial \eta \partial \tau} F(a + b - x, c + d - y) \right|^q}{(s_1 + 1)(s_2 + 1)} \right)^{\frac{1}{q}}, \tag{18}$$

and

$$\int_0^1 \int_0^1 \Delta_1(x, \eta) \Delta_2(y, \tau) \left| \frac{\partial^2}{\partial \eta \partial \tau} F(\eta a + (1 - \eta)(a + b - x), \tau c + (1 - \tau)(c + d - y)) \right| d\tau d\eta$$

$$\leq \left(\int_0^1 \int_0^1 [\Delta_1(x, \eta) \Delta_2(y, \tau)]^p d\tau d\eta \right)^{\frac{1}{p}}$$

$$\times \left(\frac{\left| \frac{\partial^2}{\partial \eta \partial \tau} F(a, c) \right|^q + \left| \frac{\partial^2}{\partial \eta \partial \tau} F(a, c + d - y) \right|^q + \left| \frac{\partial^2}{\partial \eta \partial \tau} F(a + b - x, c) \right|^q + \left| \frac{\partial^2}{\partial \eta \partial \tau} F(a + b - x, c + d - y) \right|^q}{(s_1 + 1)(s_2 + 1)} \right)^{\frac{1}{q}}. \tag{19}$$

If it is substituted the inequalities (16)-(19) in (11), then the required results are obtained. This ends of the proof of Theorem 2.

Corollary 4. Let us consider $\varphi(\eta) = \eta$ and $\psi(\tau) = \tau$ for all $(\eta, \tau) \in \Delta$ in Theorem 2. Let us also consider $s_1 = s_2 = s$, $x = \frac{a+b}{2}$ and $y = \frac{c+d}{2}$. Then, we have the following midpoint type inequality for Riemann-Liouville fractional integrals

$$\left| F\left(\frac{a+b}{2}, \frac{c+d}{2}\right) - \frac{1}{d-c} \left[{}_a-I_\psi F\left(\frac{a+b}{2}, \frac{c+d}{2}\right) + {}_{c+}I_\psi F\left(\frac{a+b}{2}, \frac{c+d}{2}\right) \right] \right.$$

$$\left. - \frac{1}{b-a} \left[{}_b-I_\varphi F\left(\frac{a+b}{2}, \frac{c+d}{2}\right) + {}_{a+}I_\varphi F\left(\frac{a+b}{2}, \frac{c+d}{2}\right) \right] \right.$$

$$\left. + \frac{1}{(b-a)(d-c)} \left[{}_{b-,a-}I_{\varphi,\psi} F\left(\frac{a+b}{2}, \frac{c+d}{2}\right) + {}_{b-,c+}I_{\varphi,\psi} F\left(\frac{a+b}{2}, \frac{c+d}{2}\right) \right] \right.$$

$$\left. + \left| {}_{a+,d-}I_{\varphi,\psi} F\left(\frac{a+b}{2}, \frac{c+d}{2}\right) + {}_{a+,c+}I_{\varphi,\psi} F\left(\frac{a+b}{2}, \frac{c+d}{2}\right) \right| \right|$$

$$\begin{aligned}
 &\leq \frac{(b-a)(d-c)}{16(p+1)^{\frac{2}{p}}(s+1)^{\frac{2}{q}}} \\
 &\times \left[\left(\left| \frac{\partial^2}{\partial\eta\partial\tau} F(b,d) \right|^q + \left| \frac{\partial^2}{\partial\eta\partial\tau} F\left(b, \frac{c+d}{2}\right) \right|^q + \left| \frac{\partial^2}{\partial\eta\partial\tau} F\left(\frac{a+b}{2}, d\right) \right|^q + \left| \frac{\partial^2}{\partial\eta\partial\tau} F\left(\frac{a+b}{2}, \frac{c+d}{2}\right) \right|^q \right)^{\frac{1}{q}} \right. \\
 &+ \left(\left| \frac{\partial^2}{\partial\eta\partial\tau} F(b,c) \right|^q + \left| \frac{\partial^2}{\partial\eta\partial\tau} F\left(b, \frac{c+d}{2}\right) \right|^q + \left| \frac{\partial^2}{\partial\eta\partial\tau} F\left(\frac{a+b}{2}, c\right) \right|^q + \left| \frac{\partial^2}{\partial\eta\partial\tau} F\left(\frac{a+b}{2}, \frac{c+d}{2}\right) \right|^q \right)^{\frac{1}{q}} \\
 &+ \left(\left| \frac{\partial^2}{\partial\eta\partial\tau} F(a,d) \right|^q + \left| \frac{\partial^2}{\partial\eta\partial\tau} F\left(a, \frac{c+d}{2}\right) \right|^q + \left| \frac{\partial^2}{\partial\eta\partial\tau} F\left(\frac{a+b}{2}, d\right) \right|^q + \left| \frac{\partial^2}{\partial\eta\partial\tau} F\left(\frac{a+b}{2}, \frac{c+d}{2}\right) \right|^q \right)^{\frac{1}{q}} \\
 &\left. + \left(\left| \frac{\partial^2}{\partial\eta\partial\tau} F(a,c) \right|^q + \left| \frac{\partial^2}{\partial\eta\partial\tau} F\left(a, \frac{c+d}{2}\right) \right|^q + \left| \frac{\partial^2}{\partial\eta\partial\tau} F\left(\frac{a+b}{2}, c\right) \right|^q + \left| \frac{\partial^2}{\partial\eta\partial\tau} F\left(\frac{a+b}{2}, \frac{c+d}{2}\right) \right|^q \right)^{\frac{1}{q}} \right] \\
 &\leq \frac{(b-a)(d-c)}{16(p+1)^{\frac{2}{p}}(s+1)^{\frac{2}{q}}} \\
 &\times \left[\left(\frac{1+2^{s+1}+2^{2s}}{2^{2s}} \left| \frac{\partial^2}{\partial\eta\partial\tau} F(b,d) \right|^q + \frac{1+2^s}{2^{2s}} \left(\left| \frac{\partial^2}{\partial\eta\partial\tau} F(b,c) \right|^q + \left| \frac{\partial^2}{\partial\eta\partial\tau} F(a,d) \right|^q \right) + \frac{1}{2^s} \left| \frac{\partial^2}{\partial\eta\partial\tau} F(a,c) \right|^q \right)^{\frac{1}{q}} \right. \\
 &+ \left(\frac{1+2^{s+1}+2^{2s}}{2^{2s}} \left| \frac{\partial^2}{\partial\eta\partial\tau} F(b,c) \right|^q + \frac{1+2^s}{2^{2s}} \left(\left| \frac{\partial^2}{\partial\eta\partial\tau} F(b,d) \right|^q + \left| \frac{\partial^2}{\partial\eta\partial\tau} F(a,c) \right|^q \right) + \frac{1}{2^s} \left| \frac{\partial^2}{\partial\eta\partial\tau} F(a,d) \right|^q \right)^{\frac{1}{q}} \\
 &+ \left(\frac{1+2^{s+1}+2^{2s}}{2^{2s}} \left| \frac{\partial^2}{\partial\eta\partial\tau} F(a,d) \right|^q + \frac{1+2^s}{2^{2s}} \left(\left| \frac{\partial^2}{\partial\eta\partial\tau} F(a,c) \right|^q + \left| \frac{\partial^2}{\partial\eta\partial\tau} F(b,d) \right|^q \right) + \frac{1}{2^s} \left| \frac{\partial^2}{\partial\eta\partial\tau} F(b,c) \right|^q \right)^{\frac{1}{q}} \\
 &\left. + \left(\frac{1+2^{s+1}+2^{2s}}{2^{2s}} \left| \frac{\partial^2}{\partial\eta\partial\tau} F(a,c) \right|^q + \frac{1+2^s}{2^{2s}} \left(\left| \frac{\partial^2}{\partial\eta\partial\tau} F(a,d) \right|^q + \left| \frac{\partial^2}{\partial\eta\partial\tau} F(b,c) \right|^q \right) + \frac{1}{2^s} \left| \frac{\partial^2}{\partial\eta\partial\tau} F(b,d) \right|^q \right)^{\frac{1}{q}} \right].
 \end{aligned}$$

Theorem 3. Let us note that the assumptions of Lemma 1 hold. If the function $\left| \frac{\partial^2 F}{\partial\eta\partial\tau} \right|^q$, $q \geq 1$ is co-ordinated convex on Δ , then the following inequality for generalized fractional integral holds:

$$\begin{aligned}
 & |\Phi(a, b, x; c, d, y)| \\
 & \leq \frac{(x-a)(y-c)}{\Upsilon(x, y)} \left(\int_0^1 \int_0^1 \Lambda_1(x, \eta) \Lambda_2(y, \tau) d\tau d\eta \right)^{1-\frac{1}{q}} \\
 & \quad \times \left[\lambda_1 \mu_1 \left| \frac{\partial^2}{\partial \eta \partial \tau} F(b, d) \right|^q + \lambda_1 \mu_2 \left| \frac{\partial^2}{\partial \eta \partial \tau} F(b, c+d-y) \right|^q \right. \\
 & \quad \left. + \lambda_2 \mu_1 \left| \frac{\partial^2}{\partial \eta \partial \tau} F(a+b-x, d) \right|^q + \lambda_2 \mu_2 \left| \frac{\partial^2}{\partial \eta \partial \tau} F(a+b-x, c+d-y) \right|^q \right]^{\frac{1}{q}} \\
 & \quad + \frac{(x-a)(d-y)}{\Upsilon(x, y)} \left(\int_0^1 \int_0^1 \Lambda_1(x, \eta) \Delta_2(y, \tau) d\tau d\eta \right)^{1-\frac{1}{q}} \\
 & \quad \times \left[\lambda_1 \mu_4 \left| \frac{\partial^2}{\partial \eta \partial \tau} F(b, c) \right|^q + \lambda_1 \mu_3 \left| \frac{\partial^2}{\partial \eta \partial \tau} F(b, c+d-y) \right|^q \right. \\
 & \quad \left. + \lambda_2 \mu_4 \left| \frac{\partial^2}{\partial \eta \partial \tau} F(a+b-x, c) \right|^q + \lambda_2 \mu_3 \left| \frac{\partial^2}{\partial \eta \partial \tau} F(a+b-x, c+d-y) \right|^q \right]^{\frac{1}{q}} \\
 & \quad + \frac{(b-x)(y-c)}{\Upsilon(x, y)} \left(\int_0^1 \int_0^1 \Delta_1(x, \eta) \Lambda_2(y, \tau) d\tau d\eta \right)^{1-\frac{1}{q}} \\
 & \quad \times \left[\lambda_4 \mu_1 \left| \frac{\partial^2}{\partial \eta \partial \tau} F(a, d) \right|^q + \lambda_4 \mu_2 \left| \frac{\partial^2}{\partial \eta \partial \tau} F(a, c+d-y) \right|^q \right. \\
 & \quad \left. + \lambda_3 \mu_1 \left| \frac{\partial^2}{\partial \eta \partial \tau} F(a+b-x, d) \right|^q + \lambda_3 \mu_2 \left| \frac{\partial^2}{\partial \eta \partial \tau} F(a+b-x, c+d-y) \right|^q \right]^{\frac{1}{q}} \\
 & \quad + \frac{(b-x)(d-y)}{\Upsilon(x, y)} \left(\int_0^1 \int_0^1 \Delta_1(x, \eta) \Delta_2(y, \tau) d\tau d\eta \right)^{1-\frac{1}{q}} \\
 & \quad \times \left[\lambda_4 \mu_4 \left| \frac{\partial^2}{\partial \eta \partial \tau} F(a, c) \right|^q + \lambda_4 \mu_3 \left| \frac{\partial^2}{\partial \eta \partial \tau} F(a, c+d-y) \right|^q \right. \\
 & \quad \left. + \lambda_3 \mu_4 \left| \frac{\partial^2}{\partial \eta \partial \tau} F(a+b-x, c) \right|^q + \lambda_3 \mu_3 \left| \frac{\partial^2}{\partial \eta \partial \tau} F(a+b-x, c+d-y) \right|^q \right]^{\frac{1}{q}}.
 \end{aligned}$$

Here, $\Phi(a, b, x; c, d, y)$ is defined as in Lemma 1, $A_i, i = 1, 2, 3, 4$ are described as in (9) and $B_i, i = 1, 2, 3, 4$ are defined as in (10).

Proof. Power mean inequality and co-ordinated (s_1, s_2) -convexity of $\left| \frac{\partial^2 F}{\partial \eta \partial \tau} \right|^q$ yield

$$\begin{aligned}
 & \int_0^1 \int_0^1 A_1(x, \eta) A_2(y, \tau) \left| \frac{\partial^2}{\partial \eta \partial \tau} F(\eta b + (1 - \eta)(a + b - x), \tau d + (1 - \tau)(c + d - y)) \right| d\tau d\eta \\
 & \leq \left(\int_0^1 \int_0^1 A_1(x, \eta) A_2(y, \tau) d\tau d\eta \right)^{1 - \frac{1}{q}} \\
 & \quad \times \left(\int_0^1 \int_0^1 A_1(x, \eta) A_2(y, \tau) \left| \frac{\partial^2}{\partial \eta \partial \tau} F(\eta b + (1 - \eta)(a + b - x), \tau d + (1 - \tau)(c + d - y)) \right|^q d\tau d\eta \right)^{\frac{1}{q}} \\
 & \leq \left(\int_0^1 \int_0^1 A_1(x, \eta) A_2(y, \tau) d\tau d\eta \right)^{1 - \frac{1}{q}} \\
 & \quad \times \left(\int_0^1 \int_0^1 A_1(x, \eta) A_2(y, \tau) \left[\eta \tau \left| \frac{\partial^2}{\partial \eta \partial \tau} F(b, d) \right|^q + \eta(1 - \tau) \left| \frac{\partial^2}{\partial \eta \partial \tau} F(b, c + d - y) \right|^q \right. \right. \\
 & \quad \left. \left. + (1 - \eta) \tau \left| \frac{\partial^2}{\partial \eta \partial \tau} F(a + b - x, d) \right|^q + (1 - \eta)(1 - \tau) \left| \frac{\partial^2}{\partial \eta \partial \tau} F(a + b - x, c + d - y) \right|^q \right] d\tau d\eta \right)^{\frac{1}{q}} \tag{20} \\
 & = \left(\int_0^1 \int_0^1 A_1(x, \eta) A_2(y, \tau) d\tau d\eta \right)^{1 - \frac{1}{q}} \\
 & \quad \times \left(\lambda_1 \mu_1 \left| \frac{\partial^2}{\partial \eta \partial \tau} F(b, d) \right|^q + \lambda_1 \mu_2 \left| \frac{\partial^2}{\partial \eta \partial \tau} F(b, c + d - y) \right|^q \right. \\
 & \quad \left. + \lambda_2 \mu_1 \left| \frac{\partial^2}{\partial \eta \partial \tau} F(a + b - x, d) \right|^q + \lambda_2 \mu_2 \left| \frac{\partial^2}{\partial \eta \partial \tau} F(a + b - x, c + d - y) \right|^q \right)^{\frac{1}{q}}.
 \end{aligned}$$

Similarly, we obtain

$$\begin{aligned}
 & \int_0^1 \int_0^1 A_1(x, \eta) A_2(y, \tau) \left| \frac{\partial^2}{\partial \eta \partial \tau} F(\eta b + (1 - \eta)(a + b - x), \tau c + (1 - \tau)(c + d - y)) \right| d\tau d\eta \\
 & \leq \left(\int_0^1 \int_0^1 A_1(x, \eta) A_2(y, \tau) d\tau d\eta \right)^{1 - \frac{1}{q}} \\
 & \quad \times \left(\lambda_1 \mu_4 \left| \frac{\partial^2}{\partial \eta \partial \tau} F(b, c) \right|^q + \lambda_1 \mu_3 \left| \frac{\partial^2}{\partial \eta \partial \tau} F(b, c + d - y) \right|^q \right. \\
 & \quad \left. + \lambda_2 \mu_4 \left| \frac{\partial^2}{\partial \eta \partial \tau} F(a + b - x, c) \right|^q + \lambda_2 \mu_3 \left| \frac{\partial^2}{\partial \eta \partial \tau} F(a + b - x, c + d - y) \right|^q \right)^{\frac{1}{q}}, \tag{21}
 \end{aligned}$$

$$\begin{aligned}
 & \int_0^1 \int_0^1 A_1(x, \eta) A_2(y, \tau) \left| \frac{\partial^2}{\partial \eta \partial \tau} F(\eta a + (1 - \eta)(a + b - x), \tau d + (1 - \tau)(c + d - y)) \right| d\tau d\eta \\
 & \leq \left(\int_0^1 \int_0^1 A_1(x, \eta) A_2(y, \tau) d\tau d\eta \right)^{1 - \frac{1}{q}} \\
 & \quad \times \left(\lambda_4 \mu_1 \left| \frac{\partial^2}{\partial \eta \partial \tau} F(a, d) \right|^q + \lambda_4 \mu_2 \left| \frac{\partial^2}{\partial \eta \partial \tau} F(a, c + d - y) \right|^q \right. \\
 & \quad \left. + \lambda_3 \mu_1 \left| \frac{\partial^2}{\partial \eta \partial \tau} F(a + b - x, d) \right|^q + \lambda_3 \mu_2 \left| \frac{\partial^2}{\partial \eta \partial \tau} F(a + b - x, c + d - y) \right|^q \right)^{\frac{1}{q}}, \tag{22}
 \end{aligned}$$

and

$$\begin{aligned}
 & \int_0^1 \int_0^1 A_1(x, \eta) A_2(y, \tau) \left| \frac{\partial^2}{\partial \eta \partial \tau} F(\eta a + (1 - \eta)(a + b - x), \tau c + (1 - \tau)(c + d - y)) \right| d\tau d\eta \\
 & \leq \left(\int_0^1 \int_0^1 A_1(x, \eta) A_2(y, \tau) d\tau d\eta \right)^{1 - \frac{1}{q}} \\
 & \quad \times \left(\lambda_4 \mu_4 \left| \frac{\partial^2}{\partial \eta \partial \tau} F(a, c) \right|^q + \lambda_4 \mu_3 \left| \frac{\partial^2}{\partial \eta \partial \tau} F(a, c + d - y) \right|^q \right. \\
 & \quad \left. + \lambda_3 \mu_4 \left| \frac{\partial^2}{\partial \eta \partial \tau} F(a + b - x, c) \right|^q + \lambda_3 \mu_3 \left| \frac{\partial^2}{\partial \eta \partial \tau} F(a + b - x, c + d - y) \right|^q \right)^{\frac{1}{q}}. \tag{23}
 \end{aligned}$$

If we substitute the inequalities (20)-(23) in (11), then we establish desired result. This completes the proof of Theorem 3.

Corollary 5. Let us consider $\varphi(\eta) = \eta$ and $\psi(\tau) = \tau$ for all $(\eta, \tau) \in \Delta$ in Theorem 3. Let us also consider $s_1 = s_2 = s$, $x = \frac{a+b}{2}$ and $y = \frac{c+d}{2}$. Then, we have the following midpoint type inequality for Riemann-Liouville fractional integrals

$$\begin{aligned} & \left| \Phi \left(a, b, \frac{a+b}{2}; c, d, \frac{c+d}{2} \right) \right| = F \left(\frac{a+b}{2}, \frac{c+d}{2} \right) \\ & - \frac{1}{d-c} \left[{}_a-I_\psi F \left(\frac{a+b}{2}, \frac{c+d}{2} \right) + {}_{c+}I_\psi F \left(\frac{a+b}{2}, \frac{c+d}{2} \right) \right] \\ & - \frac{1}{b-a} \left[{}_b-I_\phi F \left(\frac{a+b}{2}, \frac{c+d}{2} \right) + {}_{a+}I_\phi F \left(\frac{a+b}{2}, \frac{c+d}{2} \right) \right] \\ & + \frac{1}{(b-a)(d-c)} \left[{}_{b-,a-}I_{\phi,\psi} F \left(\frac{a+b}{2}, \frac{c+d}{2} \right) + {}_{b-,c+}I_{\phi,\psi} F \left(\frac{a+b}{2}, \frac{c+d}{2} \right) \right. \\ & \left. + {}_{a+,d-}I_{\phi,\psi} F \left(\frac{a+b}{2}, \frac{c+d}{2} \right) + {}_{a+,c+}I_{\phi,\psi} F \left(\frac{a+b}{2}, \frac{c+d}{2} \right) \right] \\ & \leq \frac{4^{\frac{1}{q}}(b-a)(d-c)}{64} \\ & \times \left[\left(\frac{\left| \frac{\partial^2}{\partial \eta \partial \tau} F(b, d) \right|^q}{(s+1)^2(s+2)^2} + \frac{\left| \frac{\partial^2}{\partial \eta \partial \tau} F \left(b, \frac{c+d}{2} \right) \right|^q}{(s+1)(s+2)^2} + \frac{\left| \frac{\partial^2}{\partial \eta \partial \tau} F \left(\frac{a+b}{2}, d \right) \right|^q}{(s+1)(s+2)^2} + \frac{\left| \frac{\partial^2}{\partial \eta \partial \tau} F \left(\frac{a+b}{2}, \frac{c+d}{2} \right) \right|^q}{(s+2)^2} \right)^{\frac{1}{q}} \right. \\ & + \left(\frac{\left| \frac{\partial^2}{\partial \eta \partial \tau} F(b, c) \right|^q}{(s+1)^2(s+2)^2} + \frac{\left| \frac{\partial^2}{\partial \eta \partial \tau} F \left(b, \frac{c+d}{2} \right) \right|^q}{(s+1)(s+2)^2} + \frac{\left| \frac{\partial^2}{\partial \eta \partial \tau} F \left(\frac{a+b}{2}, c \right) \right|^q}{(s+1)(s+2)^2} + \frac{\left| \frac{\partial^2}{\partial \eta \partial \tau} F \left(\frac{a+b}{2}, \frac{c+d}{2} \right) \right|^q}{(s+2)^2} \right)^{\frac{1}{q}} \\ & + \left(\frac{\left| \frac{\partial^2}{\partial \eta \partial \tau} F(a, d) \right|^q}{(s+1)^2(s+2)^2} + \frac{\left| \frac{\partial^2}{\partial \eta \partial \tau} F \left(a, \frac{c+d}{2} \right) \right|^q}{(s+1)(s+2)^2} + \frac{\left| \frac{\partial^2}{\partial \eta \partial \tau} F \left(\frac{a+b}{2}, d \right) \right|^q}{(s+1)(s+2)^2} + \frac{\left| \frac{\partial^2}{\partial \eta \partial \tau} F \left(\frac{a+b}{2}, \frac{c+d}{2} \right) \right|^q}{(s+2)^2} \right)^{\frac{1}{q}} \\ & \left. + \left(\frac{\left| \frac{\partial^2}{\partial \eta \partial \tau} F(a, c) \right|^q}{(s+1)^2(s+2)^2} + \frac{\left| \frac{\partial^2}{\partial \eta \partial \tau} F \left(a, \frac{c+d}{2} \right) \right|^q}{(s+1)(s+2)^2} + \frac{\left| \frac{\partial^2}{\partial \eta \partial \tau} F \left(\frac{a+b}{2}, c \right) \right|^q}{(s+1)(s+2)^2} + \frac{\left| \frac{\partial^2}{\partial \eta \partial \tau} F \left(\frac{a+b}{2}, \frac{c+d}{2} \right) \right|^q}{(s+2)^2} \right)^{\frac{1}{q}} \right]. \end{aligned}$$

Remark 4. If we consider suitable choices of $\varphi(\eta)$ and $\psi(\tau)$ then the new inequalities can be obtained for some forms of fractional integrals, namely, Riemann-Liouville fractional integral, k -Riemann-Liouville fractional integral, conformable fractional integral, Hadamard fractional integrals, Katugampola fractional integrals, etc.

Conclusion

In this paper, some Hermite-Hadamard type inequalities are established for the case of differentiable co-ordinated (s_1, s_2) -convex functions. In other words, the generalizations of the midpoint type inequalities are proved for the case of differentiable co-ordinated (s_1, s_2) -convex functions in the second sense on the rectangle from the plain. Moreover, several inequalities are given for the case of Riemann-Liouville fractional integrals and k -Riemann-

Liouville fractional integrals by choosing the special cases of our obtained main results. In future studies, improvements or generalizations of our results can be investigated by using different kinds of convex function classes or other types of fractional integral operators. Furthermore, the authors can extend the results by choosing bounded functions and also try to give discrete versions of the findings for the future studies.

Author contributions

The author read and approved the final manuscript.

Funding

There is no funding.

Availability of Data Materials

Data sharing not applicable to this paper as no data sets were generated or analysed during the current study.

Acknowledgments

The author would like to express their sincere thanks to the editor and the anonymous reviewers for their helpful comments and suggestions.

Conflicts of interest

The author declare that they have no competing interests.

References

- [1] Dragomir S.S., Agarwal R.P., Two inequalities for differentiable mappings and applications to special means of real numbers and to trapezoidal formula, *Appl. Math. Lett.*, 11 (5) (1998) 91-95.
- [2] Kirmaci U.S., Inequalities for differentiable mappings and applications to special means of real numbers to midpoint formula, *Appl. Math. Comput.*, 147 (5) (2004) 137-146.
- [3] Iqbal M., Bhatti M.I., Nazeer K., Generalization of inequalities analogous to Hermite-Hadamard inequality via fractional integrals, *Bull. Korean Math. Soc.*, 52 (3) (2015) 707-716.
- [4] Dragomir S.S., On Hadamard's inequality for convex functions on the co-ordinates in a rectangle from the plane, *Taiwanese J. Math.*, 4 (2001) 775-788.
- [5] Latif M.A., Dragomir S.S., On some new inequalities for differentiable co-ordinated convex functions, *J. Inequal. Appl.*, 2012 (1) (2012) 1-13.
- [6] Sarikaya M.Z., Set E., Ozdemir M. E., Dragomir S.S., New some Hadamard's type inequalities for coordinated convex functions, *Tamsui Oxford Journal of Information and Mathematical Sciences*, 28 (2) (2012) 137-152.
- [7] Tunç T., Sarikaya M.Z., Yaldiz H., Fractional Hermite-Hadamard's type inequality for co-ordinated convex functions, *TWMS J. Pure Appl. Math.*, 11 (1) (2020) 3-29.
- [8] Sarikaya M.Z., Ertugral F., On the generalized Hermite-Hadamard inequalities, *Annals of the University of Craiova, Mathematics and Computer Science Series*, 47 (1) (2020) 193-213.
- [9] Turkay M.E., Sarikaya M.Z., Budak H., Yildirim H., Some Hermite-Hadamard type inequalities for co-ordinated convex functions via generalized fractional integrals, *Journal of Applied Mathematics and Computing with application*, 2 (1) (2021) 1-21.
- [10] Budak H., Hezenci F., Kara H., On generalized Ostrowski, Simpson and Trapezoidal type inequalities for co-ordinated convex functions via generalized fractional integrals, *Adv. Difference Equ.*, 2021 (1) (2021) 1-32.
- [11] Chen F., A note on the Hermite-Hadamard inequality for convex functions on the co-ordinates, *J. Math. Inequal.*, 8 (4) (2014) 915-923.
- [12] Ozdemir M.E., Yildiz C., Akdemir A.O., On some new Hadamard-type inequalities for co-ordinated quasi-convex functions, *Hacet. J. Math. Stat.*, 41 (5) (2012) 697-707.
- [13] Latif M.A., Alomari M., On the Hadamard-type inequalities for h-convex functions on the co-ordinates, *Int. J. of Math. Anal.*, 3 (33) (2009) 1645-1656.
- [14] Park J., On the Hermite-Hadamard-type inequalities for co-ordinated (s, r) -convex mappings, *Inter. J. of Pure and Applied Math.*, 74 (2) (2012) 251-263.
- [15] Budak H., Kara, H., Kapucu R., New midpoint type inequalities for generalized fractional integral, *Computational Methods for Differential Equations*, 10 (1) (2022) 93-108.
- [16] Budak H., Pehlivan E., Kösem P., On new extensions of Hermite-Hadamard inequalities for generalized fractional integrals, *Sahand Communications in Mathematical Analysis*, 18 (1) (2021) 73-88.
- [17] Han J., Mohammed P.O., Zeng H., Generalized fractional integral inequalities of Hermite-Hadamard-type for a convex function, *Open Math.*, 18 (1) (2020) 794-806.
- [18] Qi F., Mohammed P. O., Yao J.C., Yao Y.H., Generalized fractional integral inequalities of Hermite-Hadamard type for (α, m) -convex functions, *J Inequal Appl*, 2019 (135) (2019).
- [19] Zhao D., Ali M.A., Kashuri A., Budak H., Sarikaya M.Z., Hermite-Hadamard-type inequalities for the interval-valued approximately h-convex functions via generalized fractional integrals, *J. Inequal. Appl.*, 2020 (1) 1-38.
- [20] Agarwal, P., Dragomir, S.S., Jleli, M., Samet, B., *Advances in mathematical inequalities and applications*, Springer Singapore, 2018.
- [21] Agarwal, P., Vivas-Cortez, M., Rangel-Oliveros, Y., Ali, M.A., New Ostrowski type inequalities for generalized s-convex functions with applications to some special means of real numbers and to midpoint formula, *AIMS Mathematics*, 7 (1) (2022) 1429-1444.
- [22] Budak H., Agarwal, P., New generalized midpoint type inequalities for fractional integral, *Miskolc Math. Notes*, 20 (2) (2019) 781-793.
- [23] Butt, S.I., Umar, M., Rashid, S., Akdemir, A.O., Chu, Y.M., New Hermite-Jensen-Mercer-type inequalities via k-fractional integrals, *Adv. Difference Equ.*, 2020 (1) (2020) 1-24.
- [24] Butt, S.I., Nadeem, M., Farid, G., On Caputo fractional derivatives via exponential s-convex functions, *Turkish Journal of Science*, 5 (2) (2020) 140-146.
- [25] Ekinci, A., Özdemir, M.E., Set, E., New integral inequalities of Ostrowski type for quasi-convex functions with applications, *Turkish Journal of Science*, 5 (3) (2020) 290-304.
- [26] Ekinci, A. Ozdemir, M., Some new integral inequalities via Riemann-Liouville integral operators, *Appl. Comput. Math.*, 18 (3) (2019) 288-295.
- [27] Kızıl, Ş. Avcı Ardiç, M., Inequalities for strongly convex functions via Atangana-Baleanu Integral Operators, *Turkish Journal of Science*, 6 (2) (2021) 96-109.
- [28] Mohammed, P.O., Abdeljawad, T., Alqudah, M.A., Jarad, F., New discrete inequalities of Hermite-Hadamard type for convex functions, *Adv. Difference Equ.*, 2021 (1) (2021) 1-10.
- [29] Neang, P., Nonlaopon, K., Tariboon, J., Ntouyas, S.K., Agarwal, P., Some trapezoid and midpoint type inequalities via fractional (p, q) -calculus, *Adv. Difference Equ.*, 2021 (1) (2021) 1-22.
- [30] Özdemir, M.E., Latif, M.A., and Akdemir, A.O., On some Hadamard-type inequalities for product of two s-convex functions on the co-ordinates, *J. Inequal. Appl.*, 2012 (1) (2012) 1-13.
- [31] Sitthiwirattam, T., Murtaza, G., Ali, M.A., Promsakon, C., Sial, I. B., Agarwal, P., Post-quantum midpoint-type inequalities associated with twice-differentiable functions, *Axioms*, 11 (2) (2022) 46.
- [32] Kara H., Budak H., Hezenci F., On Midpoint Type Inequalities for Co-Ordinated Convex Functions via Generalized Fractional Integrals, *7th Int. Ifs And Contemporary Mathematiccs Conference, conference proceeding book*, (2021) 133-148.

Robust Stability and Stable Member Problems for Multilinear Systems

Şerife Yılmaz^{1,a,*}

¹ Department of Mathematics and Science Education, Faculty of Education, Burdur Mehmet Akif Ersoy University, Istiklal Campus 15030 Burdur, Türkiye.

*Corresponding author

Research Article

History

Received: 06/03/2022

Accepted: 05/08/2022

Copyright



©2022 Faculty of Science,
Sivas Cumhuriyet University

ABSTRACT

In this paper, we consider robust stability and stable member problems for linear systems whose characteristic polynomials are nonmonic polynomials with multilinear uncertainty. For both problems, the results are given by using the reflection (box) coefficients and the extreme point property of multilinear functions defined on the box. Finding stable member in a polynomial family is one of the hard problems of linear control theory. This issue is considered by visualizing the cases $n - l = 2$ and $n - l = 3$. Necessary and sufficient conditions for robust stability and the existence of a stable member of the multilinear polynomial family using the reflection coefficients are obtained. Several examples are provided.

Keywords: Schur stability, Multilinear function, Stable member, Box coefficients.

serifeyilmaz@mehmetakif.edu.tr  <https://orcid.org/0000-0002-7561-3288>

Introduction

Consider the following polynomial with real coefficients

$$p(z) = a_1 + a_2z + \dots + a_nz^{n-1} + a_{n+1}z^n \quad (1)$$

where $a_{n+1} \neq 0$. If $a_{n+1} = 1$ the obtained polynomial

$$p(z) = a_1 + a_2z + \dots + a_nz^{n-1} + z^n \quad (2)$$

is called a monic polynomial which corresponds to n -dimensional vector $a = (a_1, a_2, \dots, a_n)^T \in \mathbb{R}^n$. The polynomial (1) is called Schur stable polynomial if all roots lie in the open unit disc of the complex plane. The set of all monic Schur stable polynomials defines the set

$$\mathcal{D}_n = \{a \in \mathbb{R}^n : p(z) \text{ is Schur stable polynomial}\}. \quad (3)$$

\mathcal{D}_n is open, bounded and nonconvex subset in \mathbb{R}^n . The closure of \mathcal{D}_n is

$$\overline{\mathcal{D}_n} = \{a \in \mathbb{R}^n : p(z) \text{ has all roots in the closed unit disc}\}.$$

Given a non-monic polynomial family \mathcal{P} with multilinear uncertainty

$$\mathcal{P} = \{p(z, q) = a_1(q) + a_2(q)z + \dots + a_n(q)z^{n-1} + a_{n+1}(q)z^n : q \in Q \subset \mathbb{R}^l\}. \quad (4)$$

Here Q is a box and $a_i(q) : Q \rightarrow \mathbb{R}$ ($i = 1, 2, \dots, n + 1$) are multilinear functions, that are affine linear with respect to each component. Without loss of generality assume that $a_{n+1}(q) > 0$ for all $q \in Q$. If for $q \in Q$ the polynomial (4) is Schur stable the family (4) is said to be robust Schur stable. From now on the term stable will mean Schur stable.

It is well known that a multilinear polynomial family appears quite frequently in practical applications [1]. In [2], some conditions for the Schur stability of this family are given. In [3,4], sufficient conditions are given for ensuring Schur stability by using the Edge Theorem. In [5], it is suggested a simple algorithm for testing Schur stability of a multilinear family and given a result on Schur stability of a compact matrix family.

In Section 2 we discussed the robust stability of non-monic multilinear polynomial families using the reflection coefficients in [6,7] and give a necessary and sufficient condition for robust stability of the multilinear polynomial family.

The existence of a stable member in a matrix polytope and other related problems has been considered in many works (see [1,8,9] and references therein). Finding stable member in a polynomial family is one of the hard problems of linear control theory (see [10]). In Section 3, the necessary and sufficient condition for the existence of a stable member in the multilinear non-monic polynomial family is given. An application of this condition is shown in the example. In Section 4, a method is given for the presence of the stable element when the difference between degree and the number of uncertain parameters is 2 and 3.

In [6] a multilinear map $f(k_1, k_2, \dots, k_n) = (f_1(k_1, k_2, \dots, k_n), \dots, f_n(k_1, k_2, \dots, k_n))^T$ has been defined by the multiplication of second and first order factors;

If n is even

$$\begin{aligned}
 & f_1(k_1, k_2, \dots, k_n) + f_2(k_1, k_2, \dots, k_n)z + \dots \\
 & \quad + f_n(k_1, k_2, \dots, k_n)z^{n-1} + z^n \\
 & = [z^2 + (k_1k_2 + k_1)z + k_2] \\
 & \quad \cdot [z^2 + (k_3k_4 + k_3)z + k_4] \dots [z^2 \\
 & \quad + (k_{n-1}k_n + k_{n-1})z + k_n],
 \end{aligned}$$

if n is odd

$$\begin{aligned}
 & f_1(k_1, k_2, \dots, k_n) + f_2(k_1, k_2, \dots, k_n)z + \dots \\
 & \quad + f_n(k_1, k_2, \dots, k_n)z^{n-1} + z^n \\
 & = [z^2 + (k_1k_2 + k_1)z + k_2] \dots [z^2 \\
 & \quad + (k_{n-2}k_{n-1} + k_{n-2})z + k_{n-1}] \\
 & \quad \cdot (z + k_n).
 \end{aligned}$$

Proposition 1 ([6]): $p(z)$ is a Schur polynomial if and only if there exist numbers $k_j \in (-1,1)$ such that $a_i = f_i(k_1, k_2, \dots, k_n)$ ($i, j = 1, 2, \dots, n$).

From Proposition 1 follows the following

Proposition 2: $a \in \overline{\mathcal{D}_n}$ if and only if there exist numbers $k_j \in [-1,1]$ such that $a_i = f_i(k_1, k_2, \dots, k_n)$ ($i, j = 1, 2, \dots, n$). The defined above map f is a multilinear. The set $Q = \{(q_1, q_2, \dots, q_l)^T : q_i^- \leq q_i \leq q_i^+, i = 1, 2, \dots, l\}$ is called a box. The following theorem shows that a multilinear image of a box is a polytope, that is convex hull of a finite number of points.

Theorem 1 (The mapping theorem [3], p.247): Let $f: Q \rightarrow \mathbb{R}^n$ be a multilinear map, where Q is a box with the set of extreme points $\{q^i\}$, then convex hull of the image $f(Q)$ equals $co\{f(q^i)\}$, where co stands for the convex hull.

Let K be the n -dimensional cube defined by

$$K = \{(k_1, k_2, \dots, k_n) : -1 \leq k_1 \leq 1, \dots, -1 \leq k_n \leq 1\}.$$

Proposition 3: $f(\partial K) = \partial \mathcal{D}_n$, where ∂K is the boundary of the set K .

Proof. Take any $x \in f(\partial K)$. Then there exists $(k_1^0, k_2^0, \dots, k_n^0) \in \partial K$ such that $f(k_1^0, k_2^0, \dots, k_n^0) = x$. Without loss of generality assume that $x \in \{k \in K : k_1 = 1\}$, then $x = f(1, k_2^0, \dots, k_n^0)$. Three cases are possible.

$f(1, k_2^0, \dots, k_n^0) \in \mathcal{D}_n$. This case is impossible, since the second order factor $[s^2 + (k_2^0 + 1)s + k_2^0]$ from the definition of f has unstable factor $(s + 1)$.

$f(1, k_2^0, \dots, k_n^0)$ is an exterior point of \mathcal{D}_n . This case is impossible as well, since any neighbourhood of $(1, k_2^0, \dots, k_n^0)$ contains element from K^0 (the set of interior point of K) and we obtain a contradiction to Proposition 1.

It remains the case $x \in \partial \mathcal{D}_n$ which proves $f(\partial K) \subset \partial \mathcal{D}_n$.

Conversely, assume that $x \in \partial \mathcal{D}_n$. Then there exists a sequence $x^m \in \mathcal{D}_n$ such that $x^m \rightarrow x$ as $m \rightarrow \infty$. By Proposition 1 there exists $k^m \in K^0$ such that $f(k^m) = x^m$. The set K is compact and without loss of generality assume that $k^m \rightarrow k \in K$. Then $f(k) = x$. The inclusion $k \in K^0$ is impossible due to Proposition 1 and equality $f(k) = x$ and openness of \mathcal{D}_n (Recall that any vector $y \in \partial \mathcal{D}_n$ is unstable.). Consequently $k \in \partial K$ and $x \in f(\partial K)$.

Stability of a Non-monic Multilinear Family

Consider the set \mathcal{D}_n (see equation (3)). The boundary set $\partial \mathcal{D}_n$ of \mathcal{D}_n consists of three parts ([7])

$$\partial \mathcal{D}_n = B_1 \cup B_{-1} \cup B_c$$

where

$$\begin{aligned}
 B_1 &= \{a \in \mathbb{R}^n : p(z) \text{ has all roots in the closed disc } |z| \leq 1 \text{ and has at least one root } z = 1\}, \\
 B_{-1} &= \{a \in \mathbb{R}^n : p(z) \text{ has all roots in the closed disc } |z| \leq 1 \text{ and has at least one root } z = -1\}, \\
 B_c &= \{a \in \mathbb{R}^n : p(z) \text{ has all roots in the closed disc } |z| \leq 1 \text{ and has at least one complex root } z = e^{j\theta}, 0 < \theta < \pi\}.
 \end{aligned}$$

The following proposition has been proved in [6]. It gives parametric description of the boundary set $\partial \mathcal{D}_n$.

Proposition 4 ([6]): a) Let n be even. Then the surface B_1 has the parametric equation

$$\begin{aligned}
 x_i &= f_i(-1, k_2, \dots, k_n), i = 1, 2, \dots, n \\
 -1 &\leq k_2 \leq 1, \dots, -1 \leq k_n \leq 1
 \end{aligned}$$

and the surface B_{-1} has the parametric equation

$$\begin{aligned}
 x_i &= f_i(1, k_2, \dots, k_n), i = 1, 2, \dots, n, \\
 -1 &\leq k_2 \leq 1, \dots, -1 \leq k_n \leq 1.
 \end{aligned}$$

b) Let n be odd. Then the surface B_1 has the parametric equation

$$\begin{aligned}
 x_i &= f_i(k_1, k_2, \dots, k_{n-1}, -1), i = 1, 2, \dots, n \\
 -1 &\leq k_1 \leq 1, \dots, -1 \leq k_{n-1} \leq 1,
 \end{aligned}$$

and the surface B_{-1} has the parametric equation

$$\begin{aligned}
 x_i &= f_i(k_1, k_2, \dots, k_{n-1}, 1), i = 1, 2, \dots, n \\
 -1 &\leq k_1 \leq 1, \dots, -1 \leq k_{n-1} \leq 1.
 \end{aligned}$$

c) The surface has the parametric equation

$$\begin{aligned}
 x_i &= f_i(k_1, 1, k_3, \dots, k_{n-1}, k_n), i = 1, 2, \dots, n \\
 -1 &\leq k_1 \leq 1, -1 \leq k_3 \leq 1, \dots, -1 \leq k_n \leq 1.
 \end{aligned}$$

Now we give stability condition of the family (4).

Define the functions ($i = 1, 2, \dots, n$)

$$F_i(q_1, \dots, q_l, k_1, k_2, \dots, k_n) = F_i(q, k) = a_{n+1}(q)f_i(k) - a_i(q) \tag{5}$$

Theorem 2: Assume that the family (4) is given, where n is even, $a_i(q): Q \rightarrow \mathbb{R}$ ($i = 1, 2, \dots, n + 1$) are multilinear functions, $Q \subset \mathbb{R}^l$ is a box and $a_{n+1}(q) > 0$ for all $q \in Q$. Assume also that this family has a stable member $p(z, q^*)$. Then (4) is robust stable if and only if the following conditions a), b), c) are satisfied simultaneously.

a) The system

$$F_i(q_1, q_2, \dots, q_l, -1, k_2, \dots, k_n) = 0 \tag{6}$$

has no solution on the box $Q \times [-1,1]^{n-1}$ ($i = 1, 2, \dots, n$).

b) The system

$$F_i(q_1, q_2, \dots, q_l, 1, k_2, \dots, k_n) = 0 \tag{7}$$

has no solution on the box $Q \times [-1,1]^{n-1}$ ($i = 1, 2, \dots, n$).

c) The system

$$F_i(q_1, q_2, \dots, q_l, k_1, 1, k_3, \dots, k_n) = 0 \tag{8}$$

has no solution on the box $Q \times [-1,1]^{n-1}$ ($i = 1, 2, \dots, n$).

Proof. Assume that the family (4) is robust stable. From the condition $a_{n+1}(q) > 0$ it follows that the family

$$\tilde{\mathcal{P}} = \left\{ \frac{a_1(q)}{a_{n+1}(q)} + \frac{a_2(q)}{a_{n+1}(q)}z + \dots + \frac{a_n(q)}{a_{n+1}(q)}z^{n-1} + z^n; q \in Q \right\}$$

is robust stable as well. Consequently for all $q \in Q$ the vector $v(q) = \left(\frac{a_1(q)}{a_{n+1}(q)}, \dots, \frac{a_n(q)}{a_{n+1}(q)} \right)$ is not contained in the boundary $\partial \mathcal{D}_n = B_1 \cup B_{-1} \cup B_c$ of the open set \mathcal{D}_n . By Proposition 1 and 4

$v(q) \notin B_1 \Rightarrow$ The system (6) has no solution on $Q \times [-1,1]^{n-1}$,

$v(q) \notin B_{-1} \Rightarrow$ The system (7) has no solution on $Q \times [-1,1]^{n-1}$,

$v(q) \notin B_c \Rightarrow$ The system (8) has no solution on $Q \times [-1,1]^{n-1}$.

Conversely, if the systems (6), (7) and (8) have no solutions then $\tilde{\mathcal{P}} \subset \mathcal{D}_n$ or $\tilde{\mathcal{P}} \subset \mathcal{D}_n^c$, where \mathcal{D}_n^c is the complementary of \mathcal{D}_n . Since the family \mathcal{P} and consequently the family $\tilde{\mathcal{P}}$ has a stable member then $\tilde{\mathcal{P}} \subset \mathcal{D}_n$, from this it follows that the family (4) is robust stable.

The systems (6), (7), (8) can be investigated by using The Mapping Theorem (Theorem 1) and splitting evaluation algorithm (see [5]). Divide the box $Q \times [-1,1]^{n-1}$ into small subboxes and if the convex hull of the images of vertices does not include the zero then eliminate this small subbox.

Example 1: Consider robust stability problem for the following multilinear family

$$p(z, q) = (7 - q_1q_2 - 2q_1)z^6 + (2 + q_1 + 0.5q_2)z^5 + (2.5 + q_1 + 0.1q_2 - q_1q_2)z^4 + (1.5 + q_1q_2)z^3 + (0.5 + q_1 - q_1q_2)z^2 + (-0.7 + q_1 + 0.5q_2)z + 0.4 - q_1 + q_2 - 0.5q_1q_2,$$

$q_1 \in [6,10]$, $q_2 \in [3,5]$. For $q_1 = 6$, $q_2 = 3$ the polynomial is stable. Using the equations of the boundary $\partial \mathcal{D}_n$ in the parametric forms ((6), (7), (8)) write three multilinear systems of equations

$$F_i(q, k) = a_{n+1}(q)f_i(k) - a_i(q)$$

$$a_7(q_1, q_2)f_i(1, k_2, k_3, \dots, k_6) - a_i(q_1, q_2) = 0 \quad (9) \quad (i = 1, \dots, 6)$$

$$a_7(q_1, q_2)f_i(-1, k_2, k_3, \dots, k_6) - a_i(q_1, q_2) = 0 \quad (10) \quad (i = 1, \dots, 6)$$

$$a_7(q_1, q_2)f_i(k_1, 1, k_3, \dots, k_6) - a_i(q_1, q_2) = 0 \quad (11) \quad (i = 1, \dots, 6)$$

where $a_i(q_1, q_2)$ are the coefficients of $p(z, q)$ and $(q_1, q_2, k_1, \dots, k_6) \in B = [6,10] \times [3,5] \times [-1,1] \times \dots \times [-1,1]$.

We have to show that all three systems (9)-(11) have no solutions. Here we use splitting-elimination algorithm (see [5]) with the use of The Mapping Theorem (divide the box B into small subboxes, if for a subbox the zero is not contained in the convex hull of the images of vertices, then eliminate this subbox).

For the systems (9), (10) and (11) all subboxes are eliminated after 2, 2 and 418 steps totally 16 sec, respectively. Therefore the given family does not intersect the boundary of \mathcal{D}_n and has a stable member. Consequently the family is robust stable.

Example 2: Consider the given multilinear family

$$p(z, q) = (1 - q_1 + 3q_2 + 3q_1q_2)z^7 + (q_1q_2 + q_1 - q_2 - 6)z^6 + (-5q_1q_2 - 6q_1 + 5q_2 + 12)z^5 + (8q_1q_2 + 13q_1 - 7q_2 - 8)z^4 + (-4q_1q_2 - 11q_1 - q_2)z^3 + (q_1q_2 + 8q_2 - 1)z^2 + (4q_1 - 4q_2 + 4)z - 4 + q_1 - q_2,$$

$q_1 \in [-1, 4]$, $q_2 \in [-2, 5]$. Using the equations of the boundary $\partial \mathcal{D}_n$ we obtain three multilinear systems of equations that correspond to the multilinear family.

For the equation systems, all subboxes are eliminated after 78, 122 and 256 steps totally 63 sec, respectively. There are no solutions. Therefore the given family does not intersect the boundary of \mathcal{D}_n . For $q_1 = 0$, $q_2 = 0$ the polynomial is not stable. As a result the family has no stable member.

Existence of a Stable Member

Consider the family (4), we are interested in the existence of $q^* \in Q$ such that $p(z, q^*)$ becomes Schur stable. This problems of such types are important in the control theory ([11]).

Theorem 3: There exists a stable member in \mathcal{P} if and only if the following multilinear system

$$F_i(q_1, \dots, q_l, k_1, \dots, k_n) = a_{n+1}(q)f_i(k) - a_i(q) = 0 \quad (12) \quad (i = 1, 2, \dots, n)$$

has a solution in $Q \times (-1,1)^n$.

Proof. There exists a stable member in \mathcal{P} if and only if there exists a stable member in $\tilde{\mathcal{P}}$. By Proposition 1 for a given $q^* \in Q$ the polynomial $\tilde{p}(z, q^*) \in \tilde{\mathcal{P}}$ is stable if and only if there exists $k^* \in (-1,1)^n$ such that

$$\frac{a_i(q^*)}{a_{n+1}(q^*)} = f_i(k^*) \quad (i = 1, 2, \dots, n)$$

By the definition of F_i this means that the system (12) has solution $(q^*, k^*) \in Q \times (-1,1)^n$. System (12) is a multilinear system defined on a box. Its solution can be searched by splitting-elimination algorithm:

Divide $Q \times (-1,1)^n$ into small subboxes and for a small subbox the convex hull of vertices does not include the zero then the eliminate this subbox by the Mapping Theorem. By this way we eliminate a great number of subboxes. If a remaining subbox has small volume then check its center for stability, i.e. if (q^c, k^c) is a center then check the polynomial $p(z, q^c)$ for stability.

Example 3: Consider the given multilinear family

$p(z, q) = (q_1 - 0.2q_2 + 3.6)z^5 + (q_1 + 0.3q_2 + 1.1)z^4 + (0.5q_1q_2 - 1.5q_1 + q_2 - 3)z^3 + (q_1q_2 - 3q_1 + 1.25q_2 - 3.75)z^2 + (q_2 - q_1 - 5)z + q_1 + q_2 - 1,$
 $q_1 \in [-4, -1], q_2 \in [2, 5].$ The splitting-elimination algorithm gives 388 remaining subboxes of

$$B = [-1, 1]^5 \times [-4, -1] \times [2, 5].$$

When the centers of the remaining 388 subboxes are examined, for the center $q_1^c = -\frac{17}{8}, q_2^c = \frac{25}{8}$ of the box

$$[0.5, 1] \times [-0.5, 0] \times [-1, -0.5] \times [0, 1] \times [0, 1] \times \left[-\frac{5}{2}, -\frac{7}{4}\right] \times \left[\frac{11}{4}, \frac{7}{2}\right]$$

the polynomial is stable.

Stable Member for the Cases $n - l = 2$ and $n - l = 3$

As pointed out in [5] stabilization problem for unstable plant can be reduced to the following:

Let A be $n \times l$ matrix with full rank, $U^0 \in \mathbb{R}^n, c = (c_1, c_2, \dots, c_l)^T$ and $k = (k_1, k_2, \dots, k_n)^T$. Is there exists $(c, k) \in \mathbb{R}^l \times \mathbb{R}^n$ such that

$$Ac + U^0 = f(k) \tag{13}$$

where $f: \mathbb{R}^n \rightarrow \mathbb{R}^n$ is defined in Introduction and $l < n$? By solving the first l equations in (13) with respect to c_1, c_2, \dots, c_l and inserting into the lost $n - l$ equations the obtained $c_1 = b_1(k), \dots, c_l = b_l(k)$ a multilinear system consisting of $(n - l)$ equations

$$\begin{aligned} g_1(k_1, k_2, \dots, k_n) &= 0 \\ &\vdots \\ g_{n-l}(k_1, k_2, \dots, k_n) &= 0 \end{aligned} \tag{14}$$

is obtained. Consequently there exists a stabilizing vector c if and only if the system (14) has a solution in $[-1, 1]^n$. Here we consider the cases $n - l = 2$ and $n - l = 3$.

In this case, it is possible to display rough image of $(-1, 1)^n$ under map g .

From the equation (14) it follows that there exists a stabilizing vector if and only if the zero is contained in the image

$g((-1, 1)^n) = \{g(k) : k \in (-1, 1)^n\}$ where $g = (g_1, \dots, g_{n-1})^T$. Gridding and displaying this image for the cases $n - l = 2$ and $n - l = 3$ may give positive results.

The following procedure can be suggested.

By gridding, display the "rough" image $g((-1, 1)^n)$. This "rough" image gives a hint of the existence (or nonexistence) of a solution of (14).

Choose sufficient small $\varepsilon > 0$. Consider for a point $g(k^*)$ for which the distance between $g(k^*)$ and the origin is less than ε .

Calculate $c^* = b(k^*)$ and check c^* for a stabilizing parameter.

Example 4: Let the family (2) be as

$$p(z, c) = z^5 + (c_3 - 0.4)z^4 + (c_2 - 0.1c_3 - 1.19)z^3 + (c_1 - 0.1c_2 - 0.06c_3 + 0.876)z^2 + (-0.1c_1 - 0.06c_2)z - 0.06c_1.$$

Here

$$A = \begin{bmatrix} -0.06 & 0 & 0 \\ -0.1 & -0.06 & 0 \\ 1 & -0.1 & -0.06 \\ 0 & 1 & -0.1 \\ 0 & 0 & 1 \end{bmatrix}, U^0 = \begin{bmatrix} 0 \\ 0 \\ 0.876 \\ -1.19 \\ -0.4 \end{bmatrix}.$$

Therefore $n = 5, l = 3, n - l = 2$. After corresponding calculations we conclude that $g_1(k_1, \dots, k_5)$ has 27 terms whereas $g_2(k_1, \dots, k_5)$ has 22 terms.

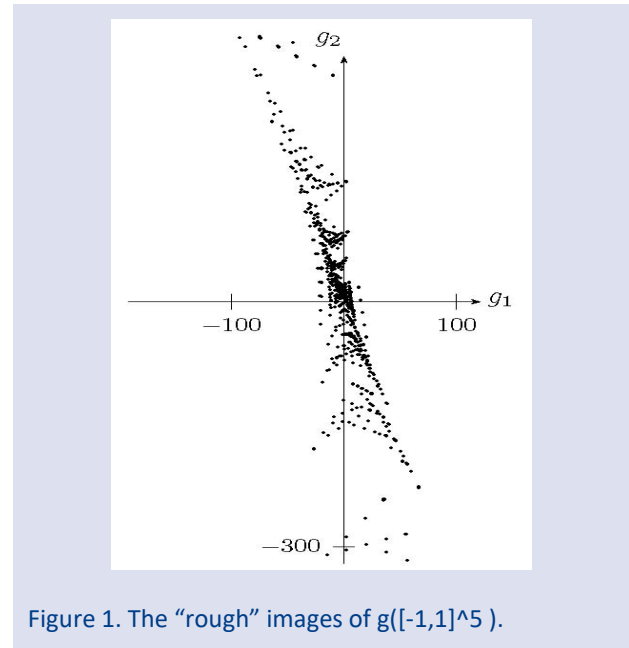


Figure 1. The "rough" images of $g([-1, 1]^5)$.

Gridding the cube $[-1, 1]^5$ with step size $h = 0.25$ and displaying the image $g([-1, 1]^5)$ gives the Fig. 1.

For $\varepsilon = 0.5, k^*$ is calculated as $k^* = (-0.75, -0.5, 0.75, -0.25, 0.5)^T$ which gives stabilizing vector $c^* = (-1.041, 1.215, 0.877)^T$.

Example 5: Consider the following "famous" example from [9,10];

$$p(z, c) = p_0(z) + c_1p_1(z) + c_2p_2(z),$$

where $p_0(z) = z^5 - 0.1z^4 - 1.9825z^3 + 0.1772z^2 + 0.8211z, p_1(z) = z^2 - 0.5z + 0.8, p_2(z) = z^3 - 0.5z^2 + 0.8z.$

Here

$$A = \begin{bmatrix} 0.8 & 0 \\ -0.5 & 0.8 \\ 1 & -0.5 \\ 0 & 1 \\ 0 & 0 \end{bmatrix}, U^0 = \begin{bmatrix} 0 \\ 0.8211 \\ 0.1772 \\ -1.9825 \\ -0.1 \end{bmatrix}$$

and

$$\begin{aligned} g_1(k_1, k_2, k_3, k_4, k_5) &= 0.625(k_1k_2k_4k_5 + k_2k_3k_4k_5 \\ &\quad - k_1k_4k_5 - k_2k_3k_5 - k_2k_4) \\ &\quad + 0.859375k_2k_4k_5 - k_1k_2k_3k_4k_5 \\ &\quad + k_1k_2k_3k_5 + k_1k_3k_4k_5 + k_1k_2k_4 \\ &\quad - k_1k_3k_5 + k_2k_3k_4 - k_1k_4 - k_2k_3 \\ &\quad + k_2k_5 + k_4k_5 + 0.6903875, \end{aligned}$$

$$\begin{aligned}
 g_2(k_1, k_2, k_3, k_4, k_5) &= 1.25(-k_1k_2k_4k_5 - k_2k_3k_4k_5 \\
 &+ k_1k_4k_5 + k_2k_3k_5 + k_2k_4) \\
 &- k_1k_2k_3k_4 + 0.78125k_2k_4k_5 \\
 &- 3.008875 + k_1k_2k_3 - k_1k_2k_5 \\
 &+ k_1k_3k_4 - k_3k_4k_5 - k_1k_3 + k_1k_5 \\
 &+ k_3k_5 + k_2 + k_4
 \end{aligned}$$

$$\begin{aligned}
 g_3(k_1, k_2, k_3, k_4, k_5) &= -0.1 - k_1k_2 - k_3k_4 + k_1 + k_3 \\
 &- k_5.
 \end{aligned}$$

Gridding $[-1,1]^5$ with step size $h = 0.03$ and displaying the image $g([-1,1]^5)$ gives the Fig. 2.

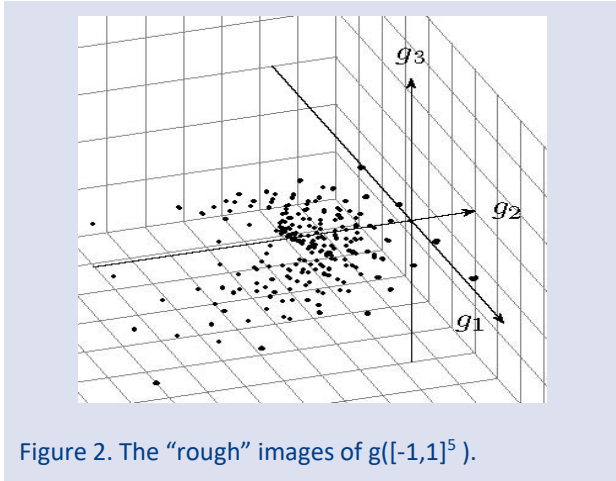


Figure 2. The “rough” images of $g([-1,1]^5)$.

For $\varepsilon = 0.1$, k^* is calculated as $k^* = (-0.99, -0.96, 0.99, -0.96, -0.03)^T$ and the corresponding $c^* = (-0.03456, 0.104025)^T$ is stabilizing vector.

Conclusion

In this study, determining the robust stability of families of nonmonic multilinear polynomials and searching for stable member in these families are discussed. Reflection (box) coefficients have been used to analyze these problems. The set of n -th order Schur stable polynomials can be characterized by the reflection coefficients. For these problems, the results are given by using the reflection coefficients and the multilinear functions' extreme point property. Hence a multilinear equations system is obtained. Solution of this system of equations can be investigated with the division-elimination algorithm. One of the hard problems in linear control theory is considered by visualizing for the cases $n - l = 2$ and $n - l = 3$. A number of examples are given to illustrate the results.

Conflicts of interest

The author declared there is no conflict of interest associated with this work.

References

- [1] Bhattacharyya S.P., Chapellat H., Keel L., Robust control: The parametric approach, Prentice-Hall, New Jersey, (1995) 432-459.
- [2] Nürges Ü., New Stability Conditions via Reflection Coefficients of Polynomials, *IEEE Transactions on Automatic Control*, 50 (9) (2005) 1354-1360.
- [3] Anderson B.D.O., Kraus F., Mansour M., Dasgupta S., Easily Testable Sufficient Conditions for the Robust Stability of Systems with Multilinear Parameter Dependence, *Automatica*, 31 (1) (1995) 25-40.
- [4] Tsing N.K., Tits A.L., When is the Multiaffine Image of a Cube a Convex Polygon?, *Systems & Control Letters*, 20 (6) (1993) 439-445.
- [5] Akyar H., Büyükköroğlu T., Dzhafarov V., On Stability of Parametrized Families of Polynomials and Matrices, *Abstract and Applied Analysis*, Article ID 687951 (2010) 1-16.
- [6] Dzhafarov V., Büyükköroğlu T., Akyar H., Stability Region for Discrete Time Systems and Its Boundary, *Trudy Instituta Matematiki i Mekhaniki UrO RAN*, 27 (3) (2021) 246-255.
- [7] Yılmaz Ş., Stable Polytopes for Discrete Systems by Using Box Coefficients, *Circuits, Systems, and Signal Processing*, 41 (2) (2022) 789-804.
- [8] Barmish B.R., New tools for robustness of linear systems, Macmillan, New York, (1994) 237-256.
- [9] Yılmaz Ş., Büyükköroğlu T., Dzhafarov V., Random Search of Stable Member in a Matrix Polytope, *Journal of Computational and Applied Mathematics*, 308 (2016) 59-68.
- [10] Polyak B.T., Shcherbakov P.S., Hard Problems in Linear Control Theory: Possible Approaches to Solution, *Automation and Remote Control*, 66 (2005) 681-718.
- [11] Fam A.T., Meditch J.S., A Canonical Parameter Space for Linear Systems Design, *IEEE Transactions on Automatic Control*, 23 (3) (1978) 454-458.
- [12] Büyükköroğlu T., Çelebi G., Dzhafarov V., Stabilisation of Discrete-Time Systems via Schur Stability Region, *International Journal of Control*, 91 (7) (2018) 1620-1629.
- [13] Nürges Ü., Avanesov S., Fixed-Order Stabilising Controller Design by a Mixed Randomized/Deterministic Method, *International Journal of Control*, 88 (2) (2015) 335-346.
- [14] Petrikevich Y.I., Randomized Methods of Stabilization of the Discrete Linear Systems, *Automation and Remote Control*, 69 (11) (2008) 1911-1921.

Generalization of Some Integral Inequalities for Arithmetic Harmonically Convex Functions

Huriye Kadakal^{1,a,*}

¹ Department of Primary Education, Faculty of Education, Bayburt University, Bayburt, Türkiye.

*Corresponding author

Research Article

History

Received: 27/04/2022

Accepted: 15/09/2022

Copyright



©2022 Faculty of Science,
Sivas Cumhuriyet University

ABSTRACT

In this study, by using an integral identity, Hölder integral inequality and modulus properties we obtain some new general inequalities of the Hermite-Hadamard and Bullen type for functions whose derivatives in absolute value at certain power are arithmetically harmonically (AH) convex. In the last part of the article, applications including arithmetic mean, geometric mean, harmonic mean, logarithmic mean and p-logarithmic mean, which are some special means of real numbers, are given by using arithmetic harmonically convex functions.

Keywords: Convex function, Arithmetic-harmonically convex function, Hermite-Hadamard and Bullen type inequality.

huriyekadakal@hotmail.com

<https://orcid.org/0000-0002-0304-7192>

Introduction

Definition 1.1. A function $\mathfrak{R}: I \subseteq \mathbb{R} \rightarrow \mathbb{R}$ is said to be convex if the inequality

$$\mathfrak{R}(t\mathfrak{m} + (1-t)\mathfrak{n}) \leq t\mathfrak{R}(\mathfrak{m}) + (1-t)\mathfrak{R}(\mathfrak{n})$$

valid for all $\mathfrak{m}, \mathfrak{n} \in I$ and $t \in [0,1]$. If this inequality reverses, then \mathfrak{R} is said to be concave on interval $I \neq \emptyset$.

Theorem 1.2. (Hermite-Hadamard integral inequality) Let $\mathfrak{R}: I \subseteq \mathbb{R} \rightarrow \mathbb{R}$ be a convex function defined on I of real numbers and $\mathfrak{m}, \mathfrak{n} \in I$ with $\mathfrak{m} < \mathfrak{n}$. The following inequality

$$\mathfrak{R}\left(\frac{\mathfrak{m}+\mathfrak{n}}{2}\right) \leq \frac{1}{\mathfrak{n}-\mathfrak{m}} \int_{\mathfrak{m}}^{\mathfrak{n}} \mathfrak{R}(x) dx \leq \frac{\mathfrak{R}(\mathfrak{m})+\mathfrak{R}(\mathfrak{n})}{2}. \quad (1)$$

holds.

Some of inequalities for means can be derived from (1) for appropriate choices of \mathfrak{R} . See [1-4], for the results of the generalization and improvement of (1).

Theorem 1.3. (Bullen's inequality) Suppose that $\mathfrak{R}: [\mathfrak{m}, \mathfrak{n}] \rightarrow \mathbb{R}$ is a convex function on $[\mathfrak{m}, \mathfrak{n}]$. Then we get:

$$\begin{aligned} \mathfrak{R}\left(\frac{\mathfrak{m}+\mathfrak{n}}{2}\right) &\leq \frac{1}{2} \left[\mathfrak{R}\left(\frac{3\mathfrak{m}+\mathfrak{n}}{4}\right) + \mathfrak{R}\left(\frac{\mathfrak{m}+3\mathfrak{n}}{4}\right) \right] \\ &\leq \frac{1}{\mathfrak{n}-\mathfrak{m}} \int_{\mathfrak{m}}^{\mathfrak{n}} \mathfrak{R}(x) dx \\ &\leq \frac{1}{2} \left[\mathfrak{R}\left(\frac{\mathfrak{m}+\mathfrak{n}}{2}\right) + \frac{\mathfrak{R}(\mathfrak{m})+\mathfrak{R}(\mathfrak{n})}{2} \right] \\ &\leq \frac{\mathfrak{R}(\mathfrak{m})+\mathfrak{R}(\mathfrak{n})}{2}. \quad (2) \end{aligned}$$

Definition 1.4. [5, 6] A function $\mathfrak{R}: I \subset \mathbb{R} \rightarrow (0, \infty)$ is said to be AH convex function if for all $\mathfrak{m}, \mathfrak{n} \in I$ and $t \in [0,1]$ the equality

$$\mathfrak{R}(t\mathfrak{m} + (1-t)\mathfrak{n}) \leq \frac{\mathfrak{R}(\mathfrak{m})\mathfrak{R}(\mathfrak{n})}{t\mathfrak{R}(\mathfrak{m}) + (1-t)\mathfrak{R}(\mathfrak{n})} \quad (3)$$

holds.

For further details and proofs on both AH convex functions and other kinds of convexity, we refer the reader to [7-21] and references there in.

To derive main results for AH convex functions, we need the following Lemma 1.5.

Lemma 1.5. Let $\mathfrak{R}: I^\circ \subset \mathbb{R} \rightarrow \mathbb{R}$ be a differentiable function on I° where $\mathfrak{m}, \mathfrak{n} \in I^\circ$ with $\mathfrak{m} < \mathfrak{n}$. If $\mathfrak{R}' \in L[a, b]$, then the following identity holds:

$$\begin{aligned} I_n(\mathfrak{R}, \mathfrak{m}, \mathfrak{n}) &= \sum_{i=0}^{n-1} \frac{\mathfrak{m}-\mathfrak{n}}{2n^2} \left[\int_0^1 (1-2t) \mathfrak{R}'\left(t \frac{(n-i)\mathfrak{m}+i\mathfrak{n}}{n}\right) \right. \\ &\quad \left. + (1-t) \frac{(n-i-1)\mathfrak{m}+(i+1)\mathfrak{n}}{n} \right] dt \end{aligned} \quad (4)$$

where

$$\begin{aligned} I_n(\mathfrak{R}, \mathfrak{m}, \mathfrak{n}) &= \sum_{i=0}^{n-1} \frac{1}{2n} \left[f\left(\frac{(n-i)\mathfrak{m}+i\mathfrak{n}}{n}\right) \right. \\ &\quad \left. + f\left(\frac{(n-i-1)\mathfrak{m}+(i+1)\mathfrak{n}}{n}\right) \right] \\ &\quad - \frac{1}{\mathfrak{n}-\mathfrak{m}} \int_{\mathfrak{m}}^{\mathfrak{n}} \mathfrak{R}(x) dx. \end{aligned}$$

In this study, we use Hölder integral inequality and (4) in order to provide inequality for functions whose first derivatives in absolute value at certain power are AH-convex.

Throughout this paper, the following notations will be used for nonnegative numbers m, m ($m > m$):

1. $A := A(m, m) = \frac{m+m}{2}$, $m, m > 0$, (arithmetic mean)
2. $G := G(m, m) = \sqrt{mm}$, $m, m \geq 0$, (geometric mean)
3. $H := H(m, m) = \frac{2mm}{m+m}$, $m, m > 0$, (harmonic mean)
4. $L := L(m, m) = \begin{cases} \frac{m-m}{\ln m - \ln m}, & m \neq m; \\ m, & m = m \end{cases}$ $m, m > 0$, (logarithmic mean)
5. $L_p := L_p(m, m) = \begin{cases} \left(\frac{m^{p+1} - m^{p+1}}{(p+1)(m-m)} \right)^{\frac{1}{p}}, & m \neq m, p \in \mathbb{R} \setminus \{-1, 0\}; \\ m, & m = m \end{cases}$ $m, m > 0$ (p - logarithmic mean).

L_p is monotonically increasing over $p \in \mathbb{R}$, denoting $L_0 = I$ and $L_{-1} = L$. In addition,

$$A_{n,i} = A_{n,i}(m, m) = \frac{(n-i)m + im}{n}.$$

Main results

Theorem 2.1. Let $\mathfrak{R}: I \subset (0, \infty) \rightarrow (0, \infty)$ be a differentiable mapping on I° , and $m, m \in I^\circ$ with $m < m$. If $|\mathfrak{R}'|$ is an AH convex function on $[m, m]$, then the following inequalities hold:

i) If $|\mathfrak{R}'(A_{n,i+1})| - |\mathfrak{R}'(A_{n,i})| \neq 0$, then

$$|I_n(\mathfrak{R}, m, m)| \leq \sum_{i=0}^{n-1} \left\{ \frac{m-m}{2n^2} \frac{|\mathfrak{R}'(A_{n,i})||\mathfrak{R}'(A_{n,i+1})|}{(|\mathfrak{R}'(A_{n,i+1})| - |\mathfrak{R}'(A_{n,i})|)^2} \ln \frac{A(|\mathfrak{R}'(A_{n,i+1})|, |\mathfrak{R}'(A_{n,i})|)}{H(|\mathfrak{R}'(A_{n,i+1})|, |\mathfrak{R}'(A_{n,i})|)} \right\} \quad (5)$$

ii) If $|\mathfrak{R}'(A_{n,i+1})| - |\mathfrak{R}'(A_{n,i})| = 0$, then

$$|I_n(\mathfrak{R}, m, m)| \leq \sum_{i=0}^{n-1} \frac{m-m}{4n^2} |\mathfrak{R}'(A_{n,i})|. \quad (6)$$

Proof. i) Let $|\mathfrak{R}'(A_{n,i+1})| - |\mathfrak{R}'(A_{n,i})| \neq 0$. From the properties of modulus and the Lemma 1.5, we write

$$\begin{aligned} |I_n(\mathfrak{R}, m, m)| &= \left| \sum_{i=0}^{n-1} \frac{m-m}{2n^2} \left[\int_0^1 (1-2t)\mathfrak{R}'(tA_{n,i} + (1-t)A_{n,i+1})dt \right] \right| \\ &\leq \sum_{i=0}^{n-1} \frac{m-m}{2n^2} \left| \left[\int_0^1 (1-2t)\mathfrak{R}'(tA_{n,i} + (1-t)A_{n,i+1})dt \right] \right| \\ &\leq \sum_{i=0}^{n-1} \frac{m-m}{2n^2} \left[\int_0^1 |1-2t| |\mathfrak{R}'(tA_{n,i} + (1-t)A_{n,i+1})| dt \right]. \end{aligned} \quad (7)$$

Since $|\mathfrak{R}'|$ is an AH convex function on $[m, m]$, then we have

$$|\mathfrak{R}'(tA_{n,i} + (1-t)A_{n,i+1})| \leq \frac{|\mathfrak{R}'(A_{n,i})||\mathfrak{R}'(A_{n,i+1})|}{t|\mathfrak{R}'(A_{n,i+1})| + (1-t)|\mathfrak{R}'(A_{n,i})|}$$

If we use the inequality in (7), we obtain

$$\begin{aligned} |I_n(\mathfrak{R}, m, m)| &\leq \sum_{i=0}^{n-1} \frac{m-m}{2n^2} \int_0^1 |1-2t| \frac{|\mathfrak{R}'(A_{n,i})||\mathfrak{R}'(A_{n,i+1})|}{t|\mathfrak{R}'(A_{n,i+1})| + (1-t)|\mathfrak{R}'(A_{n,i})|} dt \\ &= \sum_{i=0}^{n-1} \frac{m-m}{2n^2} |\mathfrak{R}'(A_{n,i})||\mathfrak{R}'(A_{n,i+1})| \int_0^1 \frac{|1-2t|}{t|\mathfrak{R}'(A_{n,i+1})| + (1-t)|\mathfrak{R}'(A_{n,i})|} dt \end{aligned}$$

$$= \sum_{i=0}^{n-1} \frac{m - mn}{2n^2} |\mathfrak{R}'(A_{n,i})| |\mathfrak{R}'(A_{n,i+1})| \left[\int_0^{\frac{1}{2}} \frac{1-2t}{t|\mathfrak{R}'(A_{n,i+1})| + (1-t)|\mathfrak{R}'(A_{n,i})|} dt + \int_{\frac{1}{2}}^1 \frac{2t-1}{t|\mathfrak{R}'(A_{n,i+1})| + (1-t)|\mathfrak{R}'(A_{n,i})|} dt \right]. \quad (8)$$

By changing variable as $u = t|\mathfrak{R}'(A_{n,i+1})| + (1-t)|\mathfrak{R}'(A_{n,i})|$ in the last two integrals, it is easily seen that

$$\int_0^{\frac{1}{2}} \frac{1-2t}{t|\mathfrak{R}'(A_{n,i+1})| + (1-t)|\mathfrak{R}'(A_{n,i})|} dt = \frac{1}{(|\mathfrak{R}'(A_{n,i+1})| - |\mathfrak{R}'(A_{n,i})|)^2} [|\mathfrak{R}'(A_{n,i+1})| - |\mathfrak{R}'(A_{n,i})| + (|\mathfrak{R}'(A_{n,i+1})| + |\mathfrak{R}'(A_{n,i})|) \ln \frac{|\mathfrak{R}'(A_{n,i+1})| + |\mathfrak{R}'(A_{n,i})|}{2|\mathfrak{R}'(A_{n,i})|}] \quad (9)$$

$$\int_{\frac{1}{2}}^1 \frac{2t-1}{t|\mathfrak{R}'(A_{n,i+1})| + (1-t)|\mathfrak{R}'(A_{n,i})|} dt = \frac{1}{(|\mathfrak{R}'(A_{n,i+1})| - |\mathfrak{R}'(A_{n,i})|)^2} \times \left[(|\mathfrak{R}'(A_{n,i+1})| + |\mathfrak{R}'(A_{n,i})|) \ln \frac{|\mathfrak{R}'(A_{n,i+1})| + |\mathfrak{R}'(A_{n,i})|}{2|\mathfrak{R}'(A_{n,i+1})|} - (|\mathfrak{R}'(A_{n,i+1})| - |\mathfrak{R}'(A_{n,i})|) \right]. \quad (10)$$

By substituting the equalities (9) and (10) in (8), we have

$$|I_n(\mathfrak{R}, mm, m)| \leq \sum_{i=0}^{n-1} \left\{ \frac{m - mn}{2n^2} \frac{|\mathfrak{R}'(A_{n,i})| |\mathfrak{R}'(A_{n,i+1})|}{(|\mathfrak{R}'(A_{n,i+1})| - |\mathfrak{R}'(A_{n,i})|)^2} \ln \frac{A(|\mathfrak{R}'(A_{n,i+1})|, |\mathfrak{R}'(A_{n,i})|)}{H(|\mathfrak{R}'(A_{n,i+1})|, |\mathfrak{R}'(A_{n,i})|)} \right\}$$

which is the desired result.

ii) Let $|\mathfrak{R}'(A_{n,i+1})| - |\mathfrak{R}'(A_{n,i})| = 0$. Then, substituting $|\mathfrak{R}'(A_{n,i+1})| = |\mathfrak{R}'(A_{n,i})|$ in the inequality (8), we obtain

$$|I_n(\mathfrak{R}, mm, m)| \leq \sum_{i=0}^{n-1} \frac{m - mn}{4n^2} |\mathfrak{R}'(A_{n,i+1})|.$$

Remark 2.2. Using the arithmetic harmonically convexity of the function $|\mathfrak{R}'|$ in the Theorem 2.1, we get

i) If $|\mathfrak{R}'(A_{n,i+1})| - |\mathfrak{R}'(A_{n,i})| \neq 0$, then

$$|I_n(\mathfrak{R}, mm, m)| \leq \sum_{i=0}^{n-1} \frac{m - mn}{2n^2} \frac{[(n-i-1)|\mathfrak{R}'(m)| + (i+1)|\mathfrak{R}'(m)] [|(n-i)|\mathfrak{R}'(m)| + i|\mathfrak{R}'(m)|]}{(|\mathfrak{R}'(m)| + |\mathfrak{R}'(m)|)^2} \times \ln \frac{[(2n-2i-1)|\mathfrak{R}'(m)| + (2i+1)|\mathfrak{R}'(m)]^2}{4[|(n-i)|\mathfrak{R}'(m)| + i|\mathfrak{R}'(m)|] [|(n-i-1)|\mathfrak{R}'(m)| + (i+1)|\mathfrak{R}'(m)|]}$$

ii) If $|\mathfrak{R}'(A_{n,i+1})| - |\mathfrak{R}'(A_{n,i})| = 0$, then

$$|I_n(\mathfrak{R}, mm, m)| \leq \sum_{i=0}^{n-1} \frac{m - mn}{2n} \frac{|\mathfrak{R}'(m)| |\mathfrak{R}'(m)|}{(n-i-1)|\mathfrak{R}'(m)| + (i+1)|\mathfrak{R}'(m)|}$$

Corollary 2.3. By choosing $n = 1$ in Remark 2.2, we obtain the following inequalities:

i) If $|\mathfrak{R}'(m)| - |\mathfrak{R}'(m)| \neq 0$, then

$$\left| \frac{\mathfrak{R}(m) + \mathfrak{R}(m)}{2} - \frac{1}{m - mn} \int_m^m \mathfrak{R}(x) dx \right| \leq \frac{m - mn}{2} \frac{|\mathfrak{R}'(m)| |\mathfrak{R}'(m)|}{(|\mathfrak{R}'(m)| + |\mathfrak{R}'(m)|)^2} \ln \frac{[|\mathfrak{R}'(m)| + |\mathfrak{R}'(m)|]^2}{4|\mathfrak{R}'(m)| |\mathfrak{R}'(m)|} = \frac{m - mn}{8} \frac{H(|\mathfrak{R}'(m)|, |\mathfrak{R}'(m)|)}{A(|\mathfrak{R}'(m)|, |\mathfrak{R}'(m)|)} \ln \frac{A(|\mathfrak{R}'(m)|, |\mathfrak{R}'(m)|)}{H(|\mathfrak{R}'(m)|, |\mathfrak{R}'(m)|)}$$

ii) If $|\mathfrak{R}'(m)| - |\mathfrak{R}'(m)| = 0$, then

$$\left| \frac{\mathfrak{R}(m) + \mathfrak{R}(m)}{2} - \frac{1}{m - mn} \int_m^m \mathfrak{R}(x) dx \right| \leq \frac{m - mn}{4} |\mathfrak{R}'(m)|.$$

Corollary 2.4. By choosing $n = 2$ in Remark 2.2, we get the following Bullen type inequalities:

i) If $|\mathfrak{R}'(A_{n,i+1})| - |\mathfrak{R}'(A_{n,i})| \neq 0$ for all $i = 0, 1$, then

$$\left| \frac{1}{2} \left[\frac{\mathfrak{R}(\mathfrak{m}\mathfrak{m}) + \mathfrak{R}(\mathfrak{m})}{2} + \mathfrak{R}\left(\frac{\mathfrak{m}\mathfrak{m} + \mathfrak{m}}{2}\right) \right] - \frac{1}{\mathfrak{m} - \mathfrak{m}\mathfrak{m}} \int_{\mathfrak{m}\mathfrak{m}}^{\mathfrak{m}} \mathfrak{R}(x) dx \right| \leq \frac{\mathfrak{m} - \mathfrak{m}\mathfrak{m}}{8} \frac{|\mathfrak{R}'(\mathfrak{m}\mathfrak{m})| H(|\mathfrak{R}'(\mathfrak{m}\mathfrak{m})|, |\mathfrak{R}'(\mathfrak{m})|)}{\left[\left| \mathfrak{R}'\left(\frac{\mathfrak{m}\mathfrak{m} + \mathfrak{m}}{2}\right) \right| - |\mathfrak{R}'(\mathfrak{m}\mathfrak{m})| \right]^2}$$

$$\times \ln \frac{A[H(|\mathfrak{R}'(\mathfrak{m}\mathfrak{m})|, |\mathfrak{R}'(\mathfrak{m})|), |\mathfrak{R}'(\mathfrak{m}\mathfrak{m})|]}{H\left(|\mathfrak{R}'\left(\frac{\mathfrak{m}\mathfrak{m} + \mathfrak{m}}{2}\right)|, |\mathfrak{R}'(\mathfrak{m}\mathfrak{m})|\right)} + \frac{\mathfrak{m} - \mathfrak{m}\mathfrak{m}}{8} \frac{|\mathfrak{R}'(\mathfrak{m})| H(|\mathfrak{R}'(\mathfrak{m}\mathfrak{m})|, |\mathfrak{R}'(\mathfrak{m})|)}{\left[|\mathfrak{R}'(\mathfrak{m})| - \left| \mathfrak{R}'\left(\frac{\mathfrak{m}\mathfrak{m} + \mathfrak{m}}{2}\right) \right| \right]^2} \ln \frac{A[H(|\mathfrak{R}'(\mathfrak{m}\mathfrak{m})|, |\mathfrak{R}'(\mathfrak{m})|), |\mathfrak{R}'(\mathfrak{m})|]}{H\left(|\mathfrak{R}'\left(\frac{\mathfrak{m}\mathfrak{m} + \mathfrak{m}}{2}\right)|, |\mathfrak{R}'(\mathfrak{m})|\right)}$$

ii) If $|f'(A_{n,i+1})| - |f'(A_{n,i})| = 0$ for all $i = 0, 1$, then

$$\left| \frac{1}{2} \left[\frac{\mathfrak{R}(\mathfrak{m}\mathfrak{m}) + \mathfrak{R}(\mathfrak{m})}{2} + \mathfrak{R}\left(\frac{\mathfrak{m}\mathfrak{m} + \mathfrak{m}}{2}\right) \right] - \frac{1}{\mathfrak{m} - \mathfrak{m}\mathfrak{m}} \int_{\mathfrak{m}\mathfrak{m}}^{\mathfrak{m}} \mathfrak{R}(x) dx \right| \leq \frac{\mathfrak{m} - \mathfrak{m}\mathfrak{m}}{8} A[H(|\mathfrak{R}'(\mathfrak{m}\mathfrak{m})|, |\mathfrak{R}'(\mathfrak{m})|), |\mathfrak{R}'(\mathfrak{m}\mathfrak{m})|].$$

Theorem 2.5. Let $\mathfrak{R}: I \subset (0, \infty) \rightarrow (0, \infty)$ be a differentiable mapping on I° , and $\mathfrak{m}\mathfrak{m}, \mathfrak{m} \in I^\circ$ with $\mathfrak{m}\mathfrak{m} < \mathfrak{m}$. If $|\mathfrak{R}'|^q$ is an AH convex function on $[\mathfrak{m}\mathfrak{m}, \mathfrak{m}]$ for some fixed $q > 1$, then the following inequalities hold:

i) If $|\mathfrak{R}'(A_{n,i+1})|^q - |\mathfrak{R}'(A_{n,i})|^q \neq 0$, then

$$|I_n(\mathfrak{R}, \mathfrak{m}\mathfrak{m}, \mathfrak{m})| \leq \sum_{i=0}^{n-1} \frac{b-a}{2n^2} \left(\frac{1}{p+1}\right)^{\frac{1}{p}} \frac{|\mathfrak{R}'(A_{n,i})| |\mathfrak{R}'(A_{n,i+1})|}{L^{\frac{1}{q}}(|\mathfrak{R}'(A_{n,i})|^q, |\mathfrak{R}'(A_{n,i+1})|^q)}, \tag{11}$$

ii) If $|\mathfrak{R}'(A_{n,i+1})|^q - |\mathfrak{R}'(A_{n,i})|^q = 0$, then

$$|I_n(\mathfrak{R}, \mathfrak{m}\mathfrak{m}, \mathfrak{m})| \leq \sum_{i=0}^{n-1} \frac{\mathfrak{m} - \mathfrak{m}\mathfrak{m}}{2n^2} \left(\frac{1}{p+1}\right)^{\frac{1}{p}} |\mathfrak{R}'(A_{n,i+1})|. \tag{12}$$

where $\frac{1}{p} + \frac{1}{q} = 1$.

Proof. i) Let $|\mathfrak{R}'(A_{n,i+1})|^q - |\mathfrak{R}'(A_{n,i})|^q \neq 0$. From the properties of modulus and the Lemma 1.5, we write

$$|I_n(\mathfrak{R}, \mathfrak{m}\mathfrak{m}, \mathfrak{m})| \leq \sum_{i=0}^{n-1} \frac{\mathfrak{m} - \mathfrak{m}\mathfrak{m}}{2n^2} \left[\int_0^1 |1 - 2t| |\mathfrak{R}'(tA_{n,i} + (1-t)A_{n,i+1})| dt \right] \tag{13}$$

Since $|\mathfrak{R}'|^q$ is an AH convex function on $[\mathfrak{m}\mathfrak{m}, \mathfrak{m}]$, the following inequality

$$|\mathfrak{R}'(tA_{n,i} + (1-t)A_{n,i+1})|^q \leq \frac{|\mathfrak{R}'(A_{n,i})|^q |\mathfrak{R}'(A_{n,i+1})|^q}{t |\mathfrak{R}'(A_{n,i+1})|^q + (1-t) |\mathfrak{R}'(A_{n,i})|^q} \tag{14}$$

holds. If we use the inequality in (13) and consider the Hölder integral inequality, we get

$$|I_n(\mathfrak{R}, \mathfrak{m}\mathfrak{m}, \mathfrak{m})| \leq \sum_{i=0}^{n-1} \frac{\mathfrak{m} - \mathfrak{m}\mathfrak{m}}{2n^2} \left(\int_0^1 |1 - 2t|^p dt \right)^{\frac{1}{p}} \left(\int_0^1 |f'(tA_{n,i} + (1-t)A_{n,i+1})|^q dt \right)^{\frac{1}{q}}$$

$$\leq \sum_{i=0}^{n-1} \frac{\mathfrak{m} - \mathfrak{m}\mathfrak{m}}{2n^2} \left(\frac{1}{p+1}\right)^{\frac{1}{p}} \left(\int_0^1 \frac{|f'(A_{n,i})|^q |f'(A_{n,i+1})|^q}{t |f'(A_{n,i+1})|^q + (1-t) |f'(A_{n,i})|^q} dt \right)^{\frac{1}{q}} \tag{15}$$

$$= \sum_{i=0}^{n-1} \frac{\mathfrak{m} - \mathfrak{m}\mathfrak{m}}{2n^2} \left(\frac{1}{p+1}\right)^{\frac{1}{p}} \frac{|f'(A_{n,i})| |f'(A_{n,i+1})|}{L^{\frac{1}{q}}(|f'(A_{n,i})|^q, |f'(A_{n,i+1})|^q)}, \tag{16}$$

where

$$\int_0^1 |1 - 2t|^p dt = \frac{1}{p+1}$$

$$\int_0^1 \frac{1}{t |f'(A_{n,i+1})|^q + (1-t) |f'(A_{n,i})|^q} dt = L^{-1}(|f'(A_{n,i})|^q, |f'(A_{n,i+1})|^q).$$

ii) Let $|\mathfrak{R}'(A_{n,i+1})|^q - |\mathfrak{R}'(A_{n,i})|^q = 0$. Then, substituting $|\mathfrak{R}'(A_{n,i+1})|^q = |\mathfrak{R}'(A_{n,i})|^q$ in the inequality (15), we have

$$|I_n(\mathfrak{R}, \mathfrak{m}, \mathfrak{m})| \leq \sum_{i=0}^{n-1} \frac{\mathfrak{m} - \mathfrak{m}\mathfrak{m}}{2n^2} \left(\frac{1}{p+1}\right)^{\frac{1}{p}} |\mathfrak{R}'(A_{n,i+1})|.$$

Remark 2.6. By using the arithmetic harmonically convexity of the function $|\mathfrak{R}'|^q$ in (16), we get the following for $|\mathfrak{R}'(A_{n,i+1})|^q - |\mathfrak{R}'(A_{n,i})|^q \neq 0$,

$$|I_n(\mathfrak{R}, \mathfrak{m}, \mathfrak{m})| \leq \sum_{i=0}^{n-1} \frac{\mathfrak{m} - \mathfrak{m}\mathfrak{m}}{2} \left(\frac{1}{p+1}\right)^{\frac{1}{p}} |\mathfrak{R}'(A_{n,i})| |\mathfrak{R}'(A_{n,i+1})| \left(n \frac{\ln[(n-i)|\mathfrak{R}'(\mathfrak{m})|^q + i|\mathfrak{R}'(\mathfrak{m}\mathfrak{m})|^q]}{-\ln[(n-i-1)|\mathfrak{R}'(\mathfrak{m}\mathfrak{m})|^q + (i+1)|\mathfrak{R}'(\mathfrak{m})|^q]} \right)^{\frac{1}{q}}.$$

Corollary 2.7. By choosing $n = 1$ in Remark 2.6, we obtain the following inequalities

i) If $|\mathfrak{R}'(\mathfrak{m}\mathfrak{m})|^q - |\mathfrak{R}'(\mathfrak{m})|^q \neq 0$, then

$$\left| \frac{\mathfrak{R}(\mathfrak{m}\mathfrak{m}) + \mathfrak{R}(\mathfrak{m})}{2} - \frac{1}{\mathfrak{m} - \mathfrak{m}\mathfrak{m}} \int_{\mathfrak{m}\mathfrak{m}}^{\mathfrak{m}} \mathfrak{R}(x) dx \right| \leq \frac{\mathfrak{m} - \mathfrak{m}\mathfrak{m}}{2} \left(\frac{1}{p+1}\right)^{\frac{1}{p}} \frac{G^2(|\mathfrak{R}'(\mathfrak{m}\mathfrak{m})|, |\mathfrak{R}'(\mathfrak{m})|)}{L^{\frac{1}{q}}(|\mathfrak{R}'(\mathfrak{m}\mathfrak{m})|^q, |\mathfrak{R}'(\mathfrak{m})|^q)}.$$

ii) If $|\mathfrak{R}'(\mathfrak{m}\mathfrak{m})|^q - |\mathfrak{R}'(\mathfrak{m})|^q = 0$, then

$$\left| \frac{\mathfrak{R}(\mathfrak{m}\mathfrak{m}) + \mathfrak{R}(\mathfrak{m})}{2} - \frac{1}{\mathfrak{m} - \mathfrak{m}\mathfrak{m}} \int_{\mathfrak{m}\mathfrak{m}}^{\mathfrak{m}} \mathfrak{R}(x) dx \right| \leq \frac{\mathfrak{m} - \mathfrak{m}\mathfrak{m}}{2} \left(\frac{1}{p+1}\right)^{\frac{1}{p}} |\mathfrak{R}'(\mathfrak{m})|.$$

Corollary 2.8. By choosing $n = 2$ in Remark 2.6, we obtain the following Bullen type inequalities:

i) If $|\mathfrak{R}'(A_{2,i+1})|^q - |\mathfrak{R}'(A_{2,i})|^q \neq 0$ for all $i = 0, 1$, then

$$\begin{aligned} & \left| \frac{1}{2} \left[\frac{\mathfrak{R}(\mathfrak{m}\mathfrak{m}) + \mathfrak{R}(\mathfrak{m})}{2} + \mathfrak{R}\left(\frac{\mathfrak{m}\mathfrak{m} + \mathfrak{m}}{2}\right) \right] - \frac{1}{\mathfrak{m} - \mathfrak{m}\mathfrak{m}} \int_{\mathfrak{m}\mathfrak{m}}^{\mathfrak{m}} \mathfrak{R}(x) dx \right| \\ & \leq \frac{\mathfrak{m} - \mathfrak{m}\mathfrak{m}}{8} \left(\frac{1}{p+1}\right)^{\frac{1}{p}} \left[\frac{G^2(|\mathfrak{R}'(\mathfrak{m}\mathfrak{m})|, |\mathfrak{R}'(\frac{\mathfrak{m}\mathfrak{m} + \mathfrak{m}}{2})|)}{L^{\frac{1}{q}}(|\mathfrak{R}'(\frac{\mathfrak{m}\mathfrak{m} + \mathfrak{m}}{2})|^q, |\mathfrak{R}'(\mathfrak{m}\mathfrak{m})|^q)} + \frac{G^2(|\mathfrak{R}'(\frac{\mathfrak{m}\mathfrak{m} + \mathfrak{m}}{2})|, |\mathfrak{R}'(\mathfrak{m}\mathfrak{m})|)}{L^{\frac{1}{q}}(|\mathfrak{R}'(\frac{\mathfrak{m}\mathfrak{m} + \mathfrak{m}}{2})|^q, |\mathfrak{R}'(\mathfrak{m})|^q)} \right], \end{aligned}$$

ii) If $|f'(A_{2,i+1})|^q - |f'(A_{2,i})|^q = 0$ for all $i = 0, 1$, then

$$\left| \frac{1}{2} \left[\frac{\mathfrak{R}(\mathfrak{m}\mathfrak{m}) + \mathfrak{R}(\mathfrak{m})}{2} + \mathfrak{R}\left(\frac{\mathfrak{m}\mathfrak{m} + \mathfrak{m}}{2}\right) \right] - \frac{1}{\mathfrak{m} - \mathfrak{m}\mathfrak{m}} \int_{\mathfrak{m}\mathfrak{m}}^{\mathfrak{m}} \mathfrak{R}(x) dx \right| \leq \frac{\mathfrak{m} - \mathfrak{m}\mathfrak{m}}{4} \left(\frac{1}{p+1}\right)^{\frac{1}{p}} A \left(\left| \mathfrak{R}'\left(\frac{\mathfrak{m}\mathfrak{m} + \mathfrak{m}}{2}\right) \right|, |\mathfrak{R}'(\mathfrak{m})| \right).$$

Applications for special means

$\mathfrak{R}(x) = x^p, x > 0$ is an AH convex function for $p \in (-1, 0)$ [5]. Using this function we have the following propositions:

Proposition 3.1. Let $0 < a < b$ and $p \in (-1, 0)$. Then we get:

$$\frac{1}{p+1} \left| \sum_{i=0}^{n-1} \frac{1}{n} A((A_{n,i})^{p+1}, (A_{n,i+1})^{p+1}) - L_{p+1}^{p+1}(\mathfrak{m}, \mathfrak{m}) \right| \leq \sum_{i=0}^{n-1} \left\{ \frac{\mathfrak{m} - \mathfrak{m}\mathfrak{m}}{2n^2} \frac{(A_{n,i})^p (A_{n,i+1})^p}{[(A_{n,i+1})^p - (A_{n,i})^p]^2} \ln \frac{A((A_{n,i+1})^p, (A_{n,i})^p)}{H((A_{n,i+1})^p, (A_{n,i})^p)} \right\}.$$

Proof. For $p \in (-1, 0)$, the function $f(x) = \frac{x^{p+1}}{p+1}, x > 0$ is AH convex. Therefore, the assertion follows from (5) in Theorem 2.1, for $\mathfrak{R}: (0, \infty) \rightarrow \mathbb{R}, \mathfrak{R}(x) = \frac{x^{p+1}}{p+1}$.

Corollary 3.2. If we take $n = 1$ in Proposition 3.1, we get:

$$\left| A \left((A_{1,0})^{p+1}, (A_{1,1})^{p+1} \right) - L_{p+1}^{p+1}(\mathbb{m}, \mathbb{m}) \right| \leq \frac{\mathbb{m} - \mathbb{m}\mathbb{m}}{2} \frac{(A_{1,0})^p (A_{1,1})^p}{\left[(A_{1,1})^p - (A_{1,0})^p \right]^2} \ln \frac{A \left((A_{1,1})^p, (A_{1,0})^p \right)}{H \left((A_{1,1})^p, (A_{1,0})^p \right)},$$

that is,

$$\frac{1}{p+1} \left| A(a^{p+1}, b^{p+1}) - L_{p+1}^{p+1}(\mathbb{m}, \mathbb{m}) \right| \leq \frac{\mathbb{m} - \mathbb{m}\mathbb{m}}{2} \frac{\mathbb{m}^p \mathbb{m}^p}{\left[\mathbb{m}^p - \mathbb{m}^p \right]^2} \ln \frac{A(\mathbb{m}^p, \mathbb{m}^p)}{H(\mathbb{m}^p, \mathbb{m}^p)}.$$

Proposition 3.3. Let $\mathbb{m}, \mathbb{m} \in (0, \infty)$ with $\mathbb{m} < \mathbb{m}$, $q > 1$ and $m \in (-1, 0)$. Then, we have:

$$\frac{q}{q+m} \left| \sum_{i=0}^{n-1} \frac{1}{n} A \left((A_{n,i})^{\frac{q}{m+q}}, (A_{n,i+1})^{\frac{q}{m+q}} \right) - L_{\frac{m}{q}+1}^{\frac{m}{q}+1}(\mathbb{m}, \mathbb{m}) \right| \leq \sum_{i=0}^{n-1} \frac{\mathbb{m} - \mathbb{m}\mathbb{m}}{2n^2} \left(\frac{1}{p+1} \right)^{\frac{1}{p}} \frac{(A_{n,i})^{\frac{m}{q}} (A_{n,i+1})^{\frac{m}{q}}}{L^{\frac{1}{q}} \left((A_{n,i})^m, (A_{n,i+1})^m \right)}.$$

Proof. The assertion follows from (11) in Theorem 2.5. Let $\mathfrak{R}(x) = \frac{q}{m+q} x^{\frac{m}{q}+1}$, $x \in (0, \infty)$. Then $|\mathfrak{R}'(x)|^q = x^m$ is AH convex on $(0, \infty)$ and the result follows from Theorem 2.5.

Corollary 3.4. Taking $n = 1$ in Proposition 3.3, we get:

$$\frac{q}{q+m} \left| A \left(a^{\frac{q}{m+q}}, b^{\frac{q}{m+q}} \right) - L_{\frac{m}{q}+1}^{\frac{m}{q}+1}(\mathbb{m}, \mathbb{m}) \right| \leq \frac{\mathbb{m} - \mathbb{m}\mathbb{m}}{2} \left(\frac{1}{p+1} \right)^{\frac{1}{p}} \frac{\mathbb{m}^{\frac{m}{q}} \mathbb{m}^{\frac{m}{q}}}{L^{\frac{1}{q}}(\mathbb{m}^m, \mathbb{m}^m)}.$$

Conclusion

In this paper, by using the definition of arithmetically-harmonically functions and some simple mathematical inequalities, we obtained some new inequalities related to Hermite-Hadamard and Bullen type.

Acknowledgment

This study was supported by Bayburt University BAP [2022/69002-03] Unit. The author is grateful to referees for careful reading, suggestions, and valuable comments, which have substantially improved the paper.

Conflicts of interest

There are no conflicts of interest in this work.

References

[1] Dragomir S.S., Pearce C.E.M., Selected Topics on Hermite-Hadamard Inequalities and Applications, RGMIA Monographs, Victoria University, (2000).
 [2] Kadakal H., New Inequalities for Strongly r-Convex Functions, *Journal of Function Spaces*, 2019 (2019) 10 p.
 [3] Maden S., Kadakal H., Kadakal M., İşcan İ., Some new integral inequalities for n-times differentiable convex and concave functions, *J. Nonlinear Sci. Appl.*, 10(12) (2017) 6141-6148.
 [4] Sarikaya M.Z., Aktan N., On the generalization of some integral inequalities and their applications, *Mathematical and Computer Modelling*, 54 (2011) 2175-2182.

[5] Dragomir S.S., Inequalities of Hermite-Hadamard type for AH-convex functions, *Stud. Univ. Babeş-Bolyai Math.* 61(4) (2016) 489-502.
 [6] Zhang T.Y., Qi F., Integral Inequalities of Hermite-Hadamard Type for m-AH Convex Functions, *Turkish Journal of Analysis and Number Theory*, 2(3) (2014) 60-64.
 [7] Agarwal P., Kadakal M., İşcan İ., Chu Y.M., Better approaches for n-times differentiable convex functions, *Mathematics*, 8(6) (2020) 950.
 [8] Bekar K., Inequalities for three-times differentiable arithmetic-harmonically functions, *Turkish Journal of Analysis and Number Theory*, 7(3) (2019) 85-90.
 [9] İşcan İ., Kadakal H., Kadakal M., Some new integr l inequalities for n-times differentiable quasi-convex functions, *Sigma Journal of Engineering and Natural Sciences*, 35(3) (2017) 363-368.
 [10] İşcan İ., Toplu T. and Yetgin F., Some new inequalities on generaliation of hermite-Hadamard and Bullen type inequalities, applications to trapezoidal and midpoint formula, *Kragujevac Journal of Mathematics*, 45(4) (2021) 647-657.
 [11] Kadakal H., Hermite-Hadamard type inequalities for two times differentiable arithmetic-harmonically convex functions, *Cumhuriyet Science Journal*, 40(3) (2019) 670-678.
 [12] Kadakal H., (α, m_1, m_2) -convexity and some inequalities of Hermite-Hadamard type, *Communications Faculty of Sciences University of Ankara Series A1 Mathematics and Statistics*, 68(2) (2019) 2128-2142.
 [13] Kadakal H., On refinements of some integral inequalities using improved power-mean integral inequalities, *Numerical Methods for Partial Differential Equations*, 36(6) (2020) 1555-1565.
 [14] Kadakal H., Hermite-Hadamard type inequalities for subadditive functions, *AIMS Mathematics*, 5(2) (2020) 930-939.

- [15] Kadakal M., Geometric trigonometrically convexity and better approximations, *Numerical Methods for Partial Differential Equations*, 36(6) (2020) 1830-1844.
- [16] Kadakal M., İşcan İ., Exponential type convexity and some related inequalities, *Journal of Inequalities and Applications*, 2020(1) (2020) 1-9.
- [17] Kadakal M., et al. On improvements of some integral inequalities, *Honam Mathematical Journal*, 43(3) (2021) 441-452.
- [18] Kadakal H., Kadakal M., İşcan İ., Some new integral inequalities for N-times differentiable R-convex and R-concave functions, *Miskolc Mathematical Notes*, 20(2) (2019) 997-1011.
- [19] Özcan S., İşcan İ., Some new Hermite-Hadamard type inequalities for s-convex functions and their applications, *Journal of inequalities and applications*, 2019(1) (2019) 1-11.
- [20] Özcan S., Some integral inequalities for harmonically-convex functions, *Journal of Function Spaces*, 2019 (2019).
- [21] Toplu T., Kadakal M., İşcan İ., On n-polynomial convexity and some related inequalities, *AIMS Math.*, 5(2) (2020) 1304-1318.

Does Electron Spectrum Affect TLD-100 Dose Response in 6 MV Photon Beam Irradiation?

Neslihan Sarigül^{1,a,*}

¹ Institute of Nuclear Science, Hacettepe University, Ankara, Türkiye.

*Corresponding author

Research Article

History

Received: 12/03/2022

Accepted: 29/06/2022

Copyright



©2022 Faculty of Science,
Sivas Cumhuriyet University

ABSTRACT

In this study, the electron spectrum effect on the TLD-100 dosimeter response to a 6 MV photon beam in different media like water, aluminum, polystyrene, iron, copper, and lead using Monte Carlo and Burlin cavity theory was evaluated. To calculate and compare the dose to medium to dose to cavity correction factors (f), the electronic equilibrium spectrum produced by the 6 MV photon beam and its maximum electron energy in different media were used. The electronic equilibrium spectra were obtained using Beamdp Monte Carlo Simulation. Using two different methods, the cavity theory was applied to obtain the response of the TLD-100 to 6 MV photon beam in the media considered. In the first method, the average mass collision stopping power ratios and the average mass effective attenuation coefficients were calculated using the electron spectrum of 6 MV. In the second method, these parameters were calculated based on the maximum energy value of 6 MV. The maximum difference between the f values obtained using the two methods was about 10 % for lead, while it was less than 2.5 % for other media. Consequently, the differences between f factors calculated using these two methods were insignificant except for lead.

Keywords: MC, LiF: MgTi, Cavity theory, Lead.

nsarigul@hacettepe.edu.tr

<https://orcid.org/0000-0002-5371-7924>

Introduction

Thermoluminescence dosimeters (TLDs) are one of the most effective materials used to measure the absorbed dose in many fields such as medicine and industry. TLD-100 (LiF: MgTi) chip dosimeters are preferred because of their near tissue equivalence effective number, wide linear response range, and low signal fading [1,2]. Also, they have a very small size for point dose measurements. Moreover, TLD-100 can even be used for in vivo measurement of dose in proton or intraoperative electron radiation therapy [3,4]. TLD-100 detectors are constructed of a different material than the medium. This creates a cavity where the TLDs are used to measure a dose. The general cavity theory is used the relationship between the absorbed dose and the dose in the medium (D_{med}) and the average absorbed dose in the cavity (D_{cav}) [5].

Monte Carlo (MC) simulations report dose-to-medium. MC simulations give more realistic results, an important reason why MC is suggested to be the gold standard. Especially, in or near heterogeneities, it has been used to get an accurate estimation of absorbed dose [6–8]. In the literature, the general cavity theory was examined using MC for LiF, $Li_2B_4O_7$, $CaSO_4$, CaF_2 , and dosimeters inside perspex, water, aluminum, copper, and lead after ^{60}Co gamma rays and megavoltage photon beams exposures [9,10]. In these studies, it has been shown that the mass collision stopping-power ratio and the mass energy-absorption coefficient ratio of the water to the phantom material change more rapidly with energy in materials with high atomic numbers. The electron spectrum effect was examined on LiF for ^{60}Co

gamma-rays in the same media that is presented in this paper using electronic equilibrium spectra and its maximum energy [10]. However, in these studies, it was not specified how the TLD-100 dose-response was affected by the electron spectrum obtained from a 6 MV photon beam, which is frequently used in clinics.

In clinical applications, the TLD-100 dosimeter is commonly irradiated with the 6 MV photon beam. Therefore, evaluating the effect of the electron spectrum on the TLD-100 dosimeter response is necessary for the 6 MV photon beam. The main aim of the following study is to observe the electron spectrum effect on the TLD-100 response to media considered using effective mass attenuation coefficient and mass collision stopping power from electron spectrum and maximum energy of the 6 MV photon beam. In summary, the effect of electron spectrum on TLD-100 response was investigated in different densities by using MC simulation and Burlin cavity theory.

Materials and Methods

Monte Carlo

The Monte Carlo EGSnrc package was used for all simulations. EGSnrc/Beamnrc was used to generate phase space data, which are on the surface of slabs. The spectral distribution simulation tool in the BeamDp from phase space data was used to calculate spectrum weighted mass stopping power ratios. The phantom set-ups were created using BEAMnrc, having TLD-100 inserted into the six different

materials as shown in Fig.1. The TLD-100 chip was simulated in different depths as shown in Table 1. The placements of the TLD-100 chip were calculated using water equivalent depths and ensured that the depths were beyond the maximum depth dose (d_{max}).

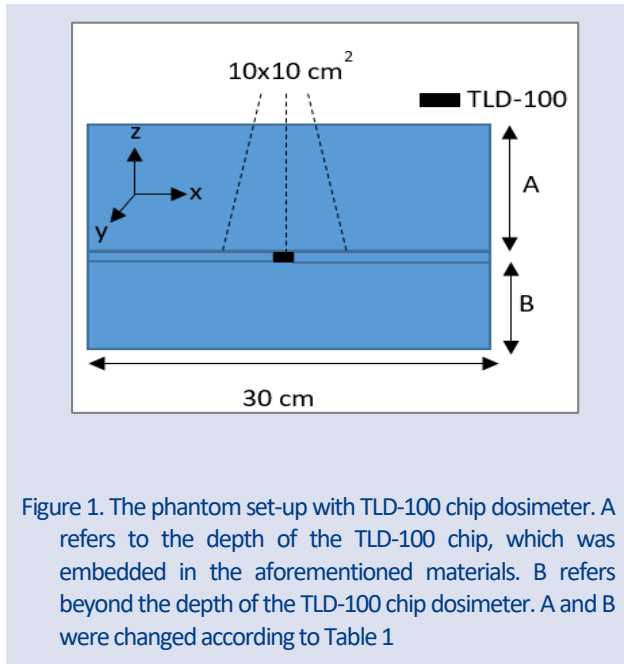


Figure 1. The phantom set-up with TLD-100 chip dosimeter. A refers to the depth of the TLD-100 chip, which was embedded in the aforementioned materials. B refers beyond the depth of the TLD-100 chip dosimeter. A and B were changed according to Table 1

The field size was 10x10 cm² and the source-axis distance (SAD) was set to 100 cm. The phantom material was chosen 30 cm cube of material. H2O700ICRU, AL700ICRU, POLYSTY700ICRU, CU700ICRU, FE700ICRU, and PB700ICRU were assigned to water, aluminum, polystyrene, copper, iron, and lead. The density of TLD-100 is 2.64 gcm⁻³. It consists of Li (26.70%), F (73.28%), with Mg (0.001%) and Ti (0.025%) dopant [11]. Pegs4, which is used to create material in the EGSnrc package, was also used to construct TLD-100.

Table 1: Material depth where the TLD-100 chip was placed for considered media.

Phantom Materials	Density (g/cm ³)	Depth (cm)	Beyond the depth of TLD-100 chip (cm)
Water	1.00	10	5
Polystyrene	1.06	9.43	4.72
Aluminum	2.7	3.71	1.85
Iron	7.87	1.27	0.64
Copper	8.96	1.12	0.56
Lead	11.35	0.88	0.44

For the particles' transport model, AE, AP, ECUT, and PCUT were characterized. AP and AE are the threshold energy for the production of photons and secondary electrons, respectively. ECUT and PCUT are used as cut-off energies for electron and photon transport, respectively. The parameters ECUT and AE were terminated at 0.7 MeV. The parameter AP and PCUT were set to 0.01 MeV. The parameter ESTEPE, which is fractional energy loss per electron step, was 2.5%. The parameters ESAVE is electron range rejection technique was set to 2 MeV and the parameter SBS, which is selective bremsstrahlung

splitting, were $N_{min}=10$, $N_{max}=100$. SBS and ESAVE parameters were chosen for increasing simulation speed. A total 10⁷ histories were simulated and statistical uncertainty was less than 1%.

Cavity Theory

Tmax-based calculation

Detectors (cavity) are used to measure dose in a medium. Generally, detector and medium have different atomic numbers and densities. The relationship between the D_{med} and the D_{cav} is given by Burlin's general cavity theory as follows:[12]

$$f = \frac{D_{cav}}{D_{med}} = d s / \rho_{med}^{cav} + (1 - d) \left(\frac{\mu_{en}}{\rho} \right)_{med}^{cav} \tag{1}$$

where f is known as the dose to the cavity to dose to the medium conversion factor. The parameter f varies with energy and radiation type. And also it varies with the size and composition of the cavity in the medium. $\left(\frac{\mu_{en}}{\rho} \right)_{med}^{cav}$ is the ratio of average mass-energy absorption coefficients of the cavity to the medium and s / ρ_{med}^{cav} is the ratio of the mean mass collisional stopping power of the cavity to that of the medium. The parameter d is the weighting factor. It is related to cavity size and it is given by;

$$d \equiv \frac{\phi_m}{\phi_m^e} = \frac{\int_0^g \phi_m^e e^{-\beta l} dl}{\int_0^g \phi_m^e dl} = \frac{1 - e^{-\beta g}}{\beta g} \tag{2}$$

$$1 - d \equiv \frac{\phi_c}{\phi_c^e} = \frac{\int_0^g \phi_c^e (1 - e^{-\beta l}) dl}{\int_0^g \phi_c^e dl} = \frac{\beta g + e^{-\beta g} - 1}{\beta g} \tag{3}$$

where, ϕ_m^e and ϕ_m represent the electron fluence in medium with and without CPE (charged particle equilibrium), respectively. $1-d$ is defined as the dose component resulting from photon interactions in the cavity. It is the ratio of the electron fluence created by the photons in the cavity to that created under electronic equilibrium [10]. l represents the distance between a point in the cavity and the wall. The mean cord length, in other words, the average path length of electrons across the cavity is given by g ; often determined as;

$$g = \frac{4V}{S} \tag{4}$$

V represents the cavity volume. The surface area of the cavity is given by S . Different sizes of TLD-100 dosimeters are used in clinical applications. The size of 0.32x0.32x0.09 cm³ is frequently used in clinics. When the g parameter is calculated for these dimensions according to Eqn.4, the result is approximately 0.3[13]. In literature, the g parameter has been calculated for different TLD chip sizes using different equations [9,14]. This value ranges from 0.1 to 1 for the TLD-100 chip. To compare the results with the literature, the g value was chosen as 0.1, 0.3, 0.5, and 1.

β represents the effective mass attenuation coefficient of the electrons. The electrons here are those that penetrate the cavity material originating from the wall. In the literature, different calculations have been made for β . There are many formulas proposed for calculating the value of β (see Table 2) from the maximum energy (T_{max}) of the electron spectrum from a head-on Compton collision of a photon with energy $h\nu$ or the extrapolated range (R) of T_{max} [15].

$$T_{max} = \frac{2(h\nu)^2}{2h\nu + 0.511 \text{ MeV}} \quad (5)$$

Eqn. 5 is for monochromatic energy photon beams. For a 6 MV photon beam, the mean energy of the photons ($h\nu_{mean}$) is approximately 1/3 of the kinetic energy of the incoming electrons [16]. In this study, $h\nu_{mean}$ is chosen as 2 MeV. From Eqn. 5, T_{max} is 1.77 MeV.

Table 2: Equations for calculating β . The subscript number refers author of the study.

Author	Formula
Evans[17]	$\beta_1 = \frac{17}{(T_{max})^{1.14} \cdot 18 \cdot 6}$
Loevinger[18]	$\beta_2 = \frac{16}{(T_{max} - 0.036)^{1.37}}$
Burlin[12]	$\beta_3 = \frac{16}{(T_{max} - 0 \cdot 036)^{1.4}}$
Chan and Burlin[19]	$e^{(-\beta_4 R)} = 0.01$
Janssens[20]	$e^{(-\beta_5 R)} = 0.04$
Paliwal and Almond[21]	$\beta_6 = \frac{14}{(T_{max})^{1.09}}$

f factor (Eqn.1) was calculated using the $(\frac{\mu_{en}}{\rho})_{med}^{cav}$, the s/ρ_{med}^{cav} , and the parameter d . The parameter d is obtained from β and g (Eqn.2). R and $(\frac{\mu_{en}}{\rho})_{med}^{cav}$ are calculated from the $h\nu_{mean}$ value [22] using NIST (National Institute of Standards and Technology) [23,24]. s/ρ_{med}^{cav} is calculated from average equilibrium-spectrum electron energies ($\frac{T_{av}}{2}$) [25]. The parameter T_{av} is given by:

$$\frac{T_{av}}{h\nu_{mean}} = \frac{\sigma_{tr}^e}{\sigma^e} \quad (6)$$

where σ_{tr}^e represents the energy transfer cross-section for Compton interaction. σ^e is the Klein-Nishina cross-section per electron [26]. To obtain σ_{tr}^e and σ^e , the literature was used [15]. In this part, the calculated f factors were named as $f_{\beta_1}, f_{\beta_2}, f_{\beta_3}, f_{\beta_4}, f_{\beta_5}, f_{\beta_6}$ for Evans[17], Loevinger [18], Burlin [12], Chan and Burlin [19], Janssens [20] and Paliwal and Almond [21] equations, respectively.

Spectrum weighted calculation

Generally, the parameter β is assumed that the same for medium and cavity since it is the maximum energy of the spectrum which determines the β value. It is supposed that the electron spectra have the same maximum photon

energy in the medium and cavity [10]. However, the medium and the cavity have different materials. And the electron spectra are not identical. Therefore, Silva [10] suggests the following equations:

$$f = d(\frac{s}{\rho})_{med}^{cav} + d'(\mu_{en}/\rho)_{med}^{cav} \quad (7)$$

$$d' = \frac{1 - e^{-\beta_{avg} g}}{\beta_{avg}} \quad (8)$$

$$d'' = 1 - \frac{1 - e^{\beta'_{avg} g}}{\beta'_{avg}} \quad (9)$$

β_{av} and β'_{av} represent the averaged values of the electron mass attenuation coefficients for the medium and cavity, respectively. The electron spectra were analyzed to calculate s/ρ_{med}^{cav} , β_{av} and β'_{av} . The β values for each energy were obtained from Janssens [20] equation. The β and s/ρ were multiplied by the spectrum value corresponding to each energy to obtain the average effective mass attenuation coefficient and average mass collision stopping power, respectively. From full-spectrum, 0.04 MeV - T_{max} ((from eqn.5) = ~1.77 MeV) energy range was chosen to calculate these parameters. $(\mu_{en}/\rho)_{med}^{cav}$ was calculated from humean. The value of $f^{janssens}$ was calculated using Eqn. 7, 8, and 9.

Results and Discussion

In this study, to observe the electron spectrum effect on TLD-100 response in water, polystyrene, aluminium, iron, copper, and lead, the effective mass attenuation coefficient and mass collision stopping power were calculated using two different methods. Firstly, these parameters were calculated using the electron spectrum of the 6 MV photon beam in the aforementioned media. The electron spectra were obtained using BEAMnrc MC simulation with 0.1 % statistical error. Fig. 2 shows the electron energy versus spectrum from 0.01 to 6 MeV.

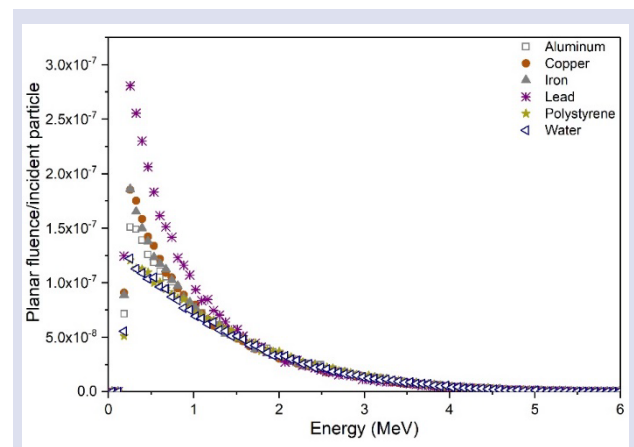


Figure 2. Planar electron spectral distribution of 6 MV photon beam in aluminum, copper, lead, iron, polystyrene, and water.

In the second method, the effective mass attenuation coefficient and mass collision stopping power were calculated from NIST [24] table using T_{max} ((from eqn.5) = ~ 1.77 MeV) value. The electron ranges and mass collision stopping power have a 1 % relative error.

Table 3 presents the s/ρ obtained using spectrum weighted and NIST. It also presents mass energy-absorption coefficients.

Table 3: The $(\mu_{en}/\rho)_{med}^{cav}$ and s/ρ_{med}^{cav} for TLD-100 chip dosimeter in the media studied, considering both the spectrum weighted and NIST

Medium	$(s/\rho)_{Material}^{TLD-100}$	$(s/\rho)_{Material}^{TLD-100}$	$(\mu_{en}/\rho)_{Material}^{TLD-100}$
	(from spectrum)	(NIST)	(NIST)
Water	0.808±1%	0.807	0.833
Polystyrene	0.827±1%	0.828	0.861
Aluminum	1.028±1%	1.029	0.959
Iron	1.156±1%	1.154	0.988
Copper	1.195±1%	1.196	1.006
Lead	1.548±1%	1.552	0.921

As seen in Table 3, the difference between the $s/\rho_{med}^{TLD-100}$ from NIST and spectrum weighted approximation was no more than 0.3% for all media. The values of β were calculated using Table 1 and the results are shown in Table 4.

Table 4: Calculated β values, using Table 1, for the media considered.

β (cm ² g ⁻¹)	TLD-100	Water	Aluminum	Iron	Copper	Lead	Polystyrene
B_1	8.867	8.867	8.867	8.867	8.867	9.397	8.867
B_2	8.750	8.750	8.750	8.750	8.750	9.397	8.750
B_3	7.404	7.404	7.404	7.404	7.404	7.964	7.404
B_4	4.345	5.418	4.304	3.903	3.775	3.361	5.233
B_5	3.037	3.787	3.008	2.728	2.638	2.350	3.658
B_6	7.513	7.513	7.513	7.513	7.513	7.943	7.513

As seen in Table 4, the β values varied among themselves in the same material. While the β_{1-3} and β_6 values did not change with material density except lead, β_4 and β_5 changed. β_{av} and β'_{av} were calculated using the spectrum of 6 MV photon beam. Table 5 displays β_{av} and β'_{av} values using spectrum weighted approximation for the TLD-100 chip which was in the considered media.

Table 5: The β_{av} and β'_{av} values were obtained using spectrum weighted approximation for the TLD-100 chip which was in the considered media.

Medium	β_{av} and β'_{av} (cm ² g ⁻¹)	β'_{av} (cm ² g ⁻¹)
Water	16.819	13.612
Polystyrene	16.554	13.314
Aluminum	13.607	14.488
Iron	12.771	15.494
Copper	12.569	15.519
Lead	10.369	16.557

As seen in Table 5, while the value of β_{av} was more than β'_{av} , in water and polystyrene, it was the opposite for aluminum, iron, copper, and lead, and the maximum difference between the two parameters was seen in lead.

d and $1-d$ were calculated using Table 4 and Eqn.2-3 to obtain $f_{\beta_1}, f_{\beta_2}, f_{\beta_3}, f_{\beta_4}, f_{\beta_5}, f_{\beta_6}$. d' and d'' were calculated using Table 5 and Eqn.8-9 for $f^{d'anssens}$. Table 6 shows the d and $1-d$ values are considered media for g values from 0.1 to 1 gcm⁻².

Table 6: d and $1-d$ for different g (0.1, 0.3, 0.5, 1 g/cm^2) values using Eqns. 2-3 in considered media.

Medium	$g(\text{g/cm}^2)$							
	0.1		0.3		0.5		1.0	
	d	$1-d$	d	$1-d$	d	$1-d$	d	$1-d$
Water	0.83	0.17	0.60	0.40	0.45	0.55	0.26	0.74
Polystyrene	0.84	0.16	0.61	0.39	0.46	0.54	0.27	0.73
Aluminium	0.86	0.14	0.66	0.34	0.52	0.48	0.32	0.68
Iron	0.88	0.13	0.68	0.32	0.55	0.45	0.34	0.66
Copper	0.88	0.12	0.69	0.31	0.56	0.44	0.35	0.65
Lead	0.90	0.10	0.74	0.26	0.62	0.38	0.42	0.58

Table 7 shows the d' and d'' for different g (0.1, 0.3, 0.5, 1 g/cm^2) values using Eqn. 8-9 in media considered

Table 7: d' and d'' for different g (0.1, 0.3, 0.5, 1 g/cm^2) values using Eqns. 8-9 in considered media.

Medium	$g(\text{g/cm}^2)$							
	0.1		0.3		0.5		1.0	
	d'	d''	d'	d''	d'	d''	d'	d''
Water	0.49	0.45	0.20	0.76	0.12	0.85	0.06	0.93
Polystyrene	0.49	0.45	0.20	0.75	0.12	0.85	0.06	0.93
Aluminium	0.55	0.47	0.24	0.77	0.15	0.86	0.07	0.93
Iron	0.57	0.49	0.26	0.79	0.16	0.87	0.08	0.94
Copper	0.57	0.49	0.26	0.79	0.16	0.87	0.08	0.94
Lead	0.62	0.51	0.31	0.80	0.19	0.88	0.10	0.94

As seen in Table 6 and 7, the d and d' decreases while the $1-d$ and d'' increases as the cavity gets larger. Values in both tables are also affected by the density of the media. The parameters have maximum values in lead.

Fig. 3 shows that the f values for the TLD-100 chip in considered media as a function of g .

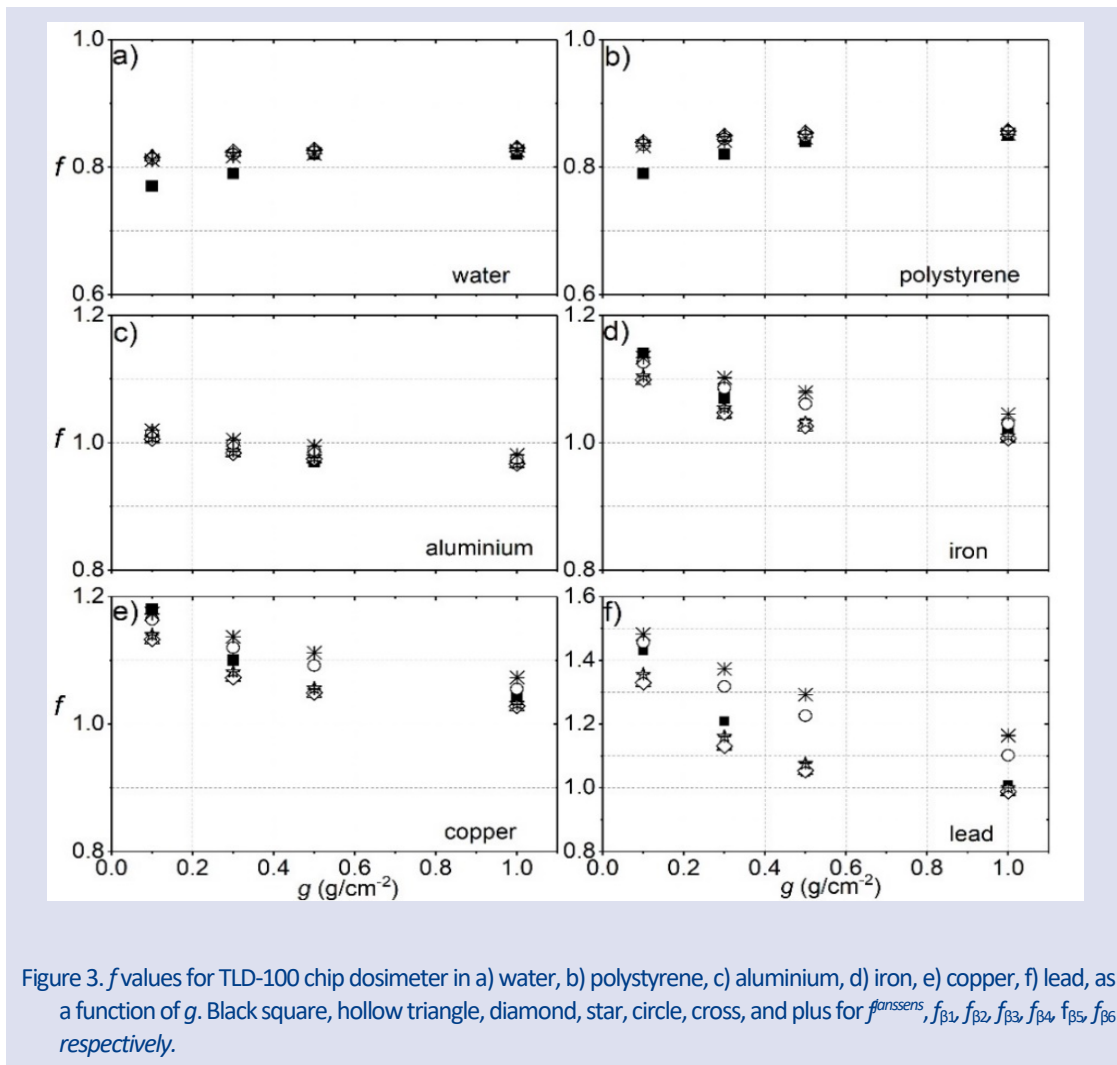


Figure 3. f values for TLD-100 chip dosimeter in a) water, b) polystyrene, c) aluminium, d) iron, e) copper, f) lead, as a function of g . Black square, hollow triangle, diamond, star, circle, cross, and plus for f_{amssens} , $f_{\beta 1}$, $f_{\beta 2}$, $f_{\beta 3}$, $f_{\beta 4}$, $f_{\beta 5}$, $f_{\beta 6}$ respectively.

The estimated relative errors in this study are μ_{en}/ρ (2%), s/ρ (1%), and R (1%) [24]. This relative error is less than 3% in the calculated f values. As seen in Fig. 3, when the density of the medium increased, the f values increased. The f values were affected by the density of the medium. The f values were very close to each other in the same media except lead despite the β values being very different from each other. The standard deviation between f values was less than 2.5% except lead for different g (0.1, 0.3, 0.5 and 1 g/cm²) values. It was 5.6%, 9%, 9%, 6.2% for 0.1, 0.3, 0.5 and 1 g/cm², respectively. In the literature, the difference between f values for ⁶⁰Co gamma-rays is not more than 5% in lead.

Conclusion

In this study, the Burlin General Cavity Theory was applied to obtain the response of the TLD-100 chip to 6 MV in different media using two different methods. T_{max} -based calculations and the electron spectrum weighted were used to calculate the response of the TLD-100 chip. At 6 MV, the maximum difference between the f values obtained using the two methods was about 10 % for lead, while it was less than 2.5 % for other media. The results indicated that the differences between f factors calculated using these two methods were insignificant except for lead. When the energy was increased from ⁶⁰Co to 6 MV photon beam, the difference between f values calculated from the two methods increased for lead material. It was shown that the f values increased as the density of the medium increased.

Conflicts of interest

The authors state that did not have a conflict of interests.

References

- [1] Chen R. and Leung P. L., Nonlinear dose dependence and dose-rate dependence of optically stimulated luminescence and thermoluminescence, *Radiation Measurements*, 33 (5) (2001) 475-481.
- [2] Montaña-García C. and Gamboa-deBuen I., Measurements of the optical density and the thermoluminescent response of LiF:Mg,Ti exposed to high doses of ⁶⁰Co gamma rays, *Radiation Protection Dosimetry*, 119 (1-4) (2006) 230-2.
- [3] Hsi W. C., Fagundes M., Zeidan O., Hug E., and Schreuder N., Image-guided method for TLD-based in vivo rectal dose verification with endorectal balloon in proton therapy for prostate cancer, *Medical Physics*, 40 (5) (2013) 051715.
- [4] Liuzzi R., Savino F., D'Avino V., Pugliese M., and Cella L., Evaluation of LiF:Mg,Ti (TLD-100) for Intraoperative Electron Radiation Therapy Quality Assurance, *PLoS ONE*, 10 (10) (2015) 0139287.
- [5] Carlsson G. A., Theoretical Basis for Dosimetry, 1 st ed. USA: Academic Press, Inc., (1985) 2-77.
- [6] Haraldsson P., Knöös T., Nyström H., and Engström P., Monte Carlo study of TLD measurements in air cavities, *Physics in Medicine and Biology*, 48 (18) (2003) 253-9.
- [7] Ma C. M. and Li J., Dose specification for radiation therapy: Dose to water or dose to medium?, *Physics in Medicine and Biology*, 56 (10) (2011) 3073-89.
- [8] Alashrah S., Kandaiya S., Maalej N., and El-Taher A., Skin dose measurements using radiochromic films, TLDs and ionisation chamber and comparison with Monte Carlo simulation, *Radiation Protection Dosimetry*, 162 (3) (2014) 338-44.
- [9] Mobit P. N., Nahum A. E., and Mayles P., An EGS4 Monte Carlo examination of general cavity theory An EGS4 Monte Carlo examination of general cavity theory, *Physics in Medicine and Biology*, 42 (7) (1997) 1319-34
- [10] Silva H., An analysis of the electron spectrum effect on LiF response to cobalt-60 gamma-rays, *Nuclear Inst. and Methods in Physics Research B*, 44 (1989) 166-171.
- [11] Davis S. D., High Sensitivity Lithium Fluoride As a Detector for Environmental Dosimetry, M.Sc Thesis, McGill University, Medical Physics Unit, (2003).
- [12] Burlin T. E., A general theory of cavity ionisation, *The British Journal of Radiology*, 39 (466) (1966) 727-34.
- [13] Sarigül N., Surucu M., Reft C., Yegingil Z., and Aydogan B., Examination of general cavity theory for magnesium and titanium doped lithium fluoride (TLD-100) of varying thicknesses in bone and lung, *Radiation Measurements*, 94 (2016) 1-7.
- [14] Horowitz Y. S., Photon general cavity theory, *Radiation Protection Dosimetry*, 9 (1) (1984) 5-18.
- [15] Attix F. H., Introduction to Radiological Physics and Radiation Dosimetry, 2nd ed. New York: Wiley-VCH, (1986).
- [16] Edwards C. R. and Mountford P. J., Near surface photon energy spectra outside a 6 MV field edge, *Physics in Medicine and Biology*, 49 (18) (2004) 293-301.
- [17] Evans R. D., The Atomic Nucleus, 1 st edition, New Delhi: Tata McGraw-Hill, (1955).
- [18] Loevinger R., The dosimetry of beta sources in tissue; the point-source function, *Radiology*, 66 (1) (1956) 55-62.
- [19] Burlin T. E. and Chan F. K., The effect of the wall on the Fricke dosimeter, *The International Journal of Applied Radiation and Isotopes*, 20 (11) (1969) 767-775.
- [20] Janssens A., Eggermont G., Jacobs R., and Thielens G., Spectrum perturbation and energy deposition models for stopping power ratio calculations in general cavity theory, *Physics in Medicine and Biology*, 19 (5) (1974) 619-30.
- [21] Paliwal B. R. and Almond P. R., Applications of cavity theories for electrons to LiF dosimeters, *Physics in Medicine and Biology*, 20 (4) (1975) 547-58.
- [22] Podgorsak E. B. and Kainz K., Radiation Oncology Physics: A Handbook for Teachers and Students, *Medical Physics*, 33 (6) (2006) 1920.
- [23] Berger M.J., Coursey J.S., Zucker M.A., and Chang J., ESTAR, PSTAR, and ASTAR: Computer Programs for Calculating Stopping-Power and Range Tables for Electrons, Protons, and Helium Ions (version 1.2.3), National Institute of Standards and Technology, Available at: <http://physics.nist.gov/PhysRefData/Star/Text/ESTAR.html> Retrieved April 7, 2022.
- [24] Hubbel J. H. and Seltzer S. M., Tables of X-Ray Mass Attenuation Coefficients and Mass Energy-Absorption Coefficients (version 1.4), National Institute of Standards and Technology, Available: <https://www.nist.gov/pml/x-ray-mass-attenuation-coefficients> Retrieved April 7, 2022
- [25] Bull R. K., Stopping powers for electrons and positrons, *International Journal of Radiation Applications and Instrumentation. Part D. Nuclear Tracks and Radiation Measurements*, 11 (4-5) (1986) 273.
- [26] Horowitz Y. S., The theoretical and microdosimetric basis of thermoluminescence and applications to dosimetry., *Physics in Medicine and Biology*, 26 (5) (1981) 765-824.

Rx, Ry and Rz Rotation Operators of Spin 4 Systems in Quantum Information Theory

Mehpeyker Kocakoç^{1,a,*}, Recep Tapramaz^{2,b}

¹ Vocational Scholl of İmamoğlu, Çukurova University, Adana, Türkiye.

² Department of Physics, Faculty of Arts and Sciences, Ondokuz Mayıs University, Samsun, Türkiye.

*Corresponding author

Research Article

History

Received: 05/03/2022

Accepted: 01/07/2022

Copyright




©2022 Faculty of Science,
Sivas Cumhuriyet University

ABSTRACT

Quantum computing requires use of various physical techniques together with quantum theory. One of the promising systems is spin systems as applied and seen in pulsed nuclear magnetic resonance (NMR) and pulsed electron paramagnetic resonance (EPR) spectroscopies and hence spin-based quantum information technology. Construction of higher spin systems and related rotation operators is important for the theoretical infrastructure that can be used in quantum information theory. It is expected that as the value of spin increases, it will give way to longer time in the computation with bigger data.

Spin operators up to spin-4 have been published in previous studies. In this work, explicit symbolic expressions of x, y and z components of rotation operators for spin-4 were worked out via exponential operator for each element of related spin operator matrices and simple linear curve fitting process. The procedures gave out exact expressions of each element of the rotation operators. It can be predicted that quantum rotation operators for higher spins, like spin-4, will theoretically and practically contribute to spin-based quantum information technology.

Keywords: Rotation operator, Spin, Quantum computers, Quantum information theory, Linear curve fitting process.

 mpeyker@gmail.com

 <https://orcid.org/0000-0001-7966-1482>

 recept@omu.edu.tr

 <https://orcid.org/0000-0002-7051-1717>

Introduction

Quantum computing combines computer science with quantum mechanics and it is a fast-growing research field[1-5]. Feynman [6,7] pointed out that only the computers working with quantum mechanical principles can simulate a quantum mechanical system, or one needs a quantum computer utilizing quantum mechanical processes can succeed such sophisticated and time-consuming works. One system of such computers utilizes spins and hence spin rotation operators, also known as completely quantum mechanical rotation operators and have no classical counterpart.

Spin rotation operators are one of the processes in quantum mechanical applications like pulsed magnetic resonance spectroscopy. In the literature only rotation operators of spin-1/2 system $R_x(\theta), R_y(\theta), R_z(\theta)$ can be found related with quantum information theory. Wigner[8] introduced expressions of rotation matrices or Wigner-d matrices for orbital angular momenta on the standard Euler angles basis. Real rotation operators for total angular momenta of spin-1/2, 1, 3/2 and 2 were generated from Wigner-d formula in some quantum mechanics textbooks[9-12] and in some published papers [13-19]. A recently published paper on rotation operators by Curtright et al. [20] and Curtright and Van Korftrik[21] give rotation operator expressions in polynomial form for all spins in Cartesian components. In order to find out the rotation operators in a matrix form one has to sum up the

polynomial terms given, which includes powers of related angular momentum operators.

Pulsed nuclear magnetic resonance (pulsed-NMR), pulsed electron paramagnetic resonance (pulsed-EPR) and pulsed electron nuclear double resonance (pulsed-ENDOR) spectroscopies, however, utilize rotation operators in rotating coordinate system or laboratory coordinate system where the spins are polarized along a definite orientation by an external magnetic field. The direction of the external magnetic field is defined as z-axis and a series of magnetic pulses are applied consequently along laboratory x and/or y axes to rotate the polarized spins around related axes. Spin-based quantum-computation systems, where pulsed magnetic resonances are leading techniques which utilize pulse sequences, use the rotation operators intensively in the rotating coordinate system[22-28].

Electron spin has attracted renewed interest towards the development of various new devices that depend on combined logic, storage and sensor applications. Another important application of these spin-based devices is in the computation depending on the quantum logic. Spin-based quantum computation depending on electronic solid-state devices are shifting gradually toward the prospective information technology [28].

In this work, explicit rotation operator expressions of spin-4 are constructed from exponential operators given in Eqn. (1) for x, y and z components of angular momenta

for a series of angles θ between interval θ_{-1} and θ_N with certain steps, e.g between 0 and 360o with 10o steps, and fitting the obtained values to suitable functions by linear curve fitting procedure.

Obtaining Rotation Processors

Matrix representations of rotation operators and their effect on quantum states are essential part of the quantum mechanics of microscopic systems [3-8] and these matrices, in turn, can be widely used in a variety of applications. In order to be able to perform processes with exponential rotation operators given in Eqn. (1), it is necessary to form this operator for processing as linear operator, in other words, this operator should be linearized by making series expansions given as

$$\hat{R}_\alpha = \exp(i\theta_p \hat{J}_\alpha), \quad \alpha = x, y, z \tag{1}$$

which is derived from time dependent Schrödinger equation $-i\hbar \frac{\partial \psi}{\partial t} = \hat{H} \psi$ for a rotating magnetic field pulse B_1 , where $\hat{H} = g\beta B_1 \hat{J}_\alpha$ is pulse Hamiltonian applied to a spin system polarized by an external magnetic field along laboratory x or y axis and \hat{J}_α ($\alpha = x, y, z$) are Pauli spin matrices representing electron spin S or nuclear spin I , coupled S and I systems. The constants g and β are Landé- g factor and Bohr magneton respectively. Here θ_p is the angle of rotation and t_p is rotating pulse duration. Thus θ_p can be written as $\theta_p = g\beta B_1 t_p / \hbar = \omega_p t_p$.

Eqn. (1) can be rewritten by definition

$$R_\alpha = \exp(i\theta_p \hat{J}_\alpha) = \cos(\theta_p \hat{J}_\alpha) + i \sin(\theta_p \hat{J}_\alpha), \quad \alpha = x, y, z \tag{2}$$

Where

$$\cos(\theta_p \hat{J}_\alpha) = \mathbb{I} - \frac{1}{2!} \theta_p^2 \hat{J}_\alpha^2 + \frac{1}{4!} \theta_p^4 \hat{J}_\alpha^4 - \frac{1}{6!} \theta_p^6 \hat{J}_\alpha^6 + \dots = \sum_{n=0}^{\infty} \frac{1}{(2n)!} \theta_p^{2n} \hat{J}_\alpha^{2n} \tag{3}$$

$$\begin{aligned} \sin(\theta_p \hat{J}_\alpha) &= \frac{1}{1!} \theta_p \hat{J}_\alpha - \frac{1}{3!} \theta_p^3 \hat{J}_\alpha^3 + \frac{1}{5!} \theta_p^5 \hat{J}_\alpha^5 - \dots \\ &= \sum_{n=0}^{\infty} \frac{1}{(2n+1)!} \theta_p^{2n+1} \hat{J}_\alpha^{2n+1} \end{aligned}$$

As the spin value increases evaluation of power series given in Eqn. (3) requires intensive calculation due to the powers of spin operator matrices. Pauli matrices for spin-1/2 and corresponding explicit rotation operators are borrowed from textbooks [11-13] and are given in Eqn. (4).

$$\hat{I}_x = \frac{1}{2} \begin{bmatrix} 0 & 1 \\ 1 & 0 \end{bmatrix}, \hat{I}_y = \frac{i}{2} \begin{bmatrix} 0 & -1 \\ 1 & 0 \end{bmatrix}, \hat{I}_z = \frac{1}{2} \begin{bmatrix} 1 & 0 \\ 0 & -1 \end{bmatrix} \tag{4}$$

$$\hat{R}_x(\theta) = \begin{bmatrix} c & i s \\ i s & c \end{bmatrix}, \hat{R}_y(\theta) = \begin{bmatrix} c & s \\ -s & c \end{bmatrix}, \hat{R}_z(\theta) = \begin{bmatrix} z & 0 \\ 0 & z^* \end{bmatrix}$$

where c, s and z are defined as $c = \cos(\theta/2), s = \sin(\theta/2), z = c + is$. The rotation operators for spin-1/2 systems are rather easy because the elements of the powers of Pauli spin matrices are either zero or unity multiplied by a coefficient.

One of the way of obtaining explicit expressions of the rotation operators for the spins greater than 1/2 can be done two-step numerical calculation. In the first step the sine and cosine series given in Eqn. (3) are summed up numerically to highest possible precision for each element of a spin matrix for certain angles between e.g. 0° and 360° with definite intervals like 10°. Variations of real and imaginary elements of rotation matrices are numerical values obtained after sums obtained for each angle. In the second step, variations of each element of the rotation matrices as functions of rotation angles are fitted to a linear function. The exact fitting function $r_{ij}(\theta)$, found after some trials, are determined and given in Eqn. (5),

$$r_{ij}(\theta) = \sum_{p=1}^K \xi_p^{(ij)} \cos^{K-p} \left(\frac{\theta}{2} \right) \sin^{p-1} \left(\frac{\theta}{2} \right) \tag{5}$$

where $K = 2(J + 1); i, j = 1, 2, 3 \dots K, \theta$ is rotation angle around x, y or z axis and J is the value of spin (nuclear, electronic or coupled spins) and K is the number of terms of fitting function and ξ_p is the coefficient of p 'th term of linear fitting function which is determined by linear curve fitting process. The accuracies of all fitting processes were controlled by the value r which is known as goodness of fitting, and visually on simultaneous plots of original and fitted curves. The operators corresponding to spins smaller than 4 were published previously [29-30]. All rotation operator matrices obtained were tested by comparing to corresponding operators obtained from Wigner-d formula [8,19] and operators in polynomial equations given by Curtright *et al.* [20] and Curtright and Van Korftrik [21].

Results and Discussion

Rotation operator elements corresponding to spin-4 operators are calculated using Eqns. (3) and (5), as discusses in the text above. The compact fit function given in Eqn. (5) can be expanded as given below,

$$\begin{aligned} r_{ij} = & \xi_0 c^8 + \xi_1 c^7 s^1 + \xi_2 c^6 s^2 + \xi_3 c^5 s^3 + \xi_4 c^4 s^4 \\ & + \xi_5 c^3 s^5 + \xi_6 c^2 s^6 + \xi_7 c^1 s^7 + \xi_8 s^8 \end{aligned} \tag{6}$$

Angular variation of rotation operator element r_{26} of operator matrix $R_x(\theta)$ and as an example, is given in Figure 1a. Angular variation of rotation operator element r_{46} of operator matrix $R_y(\theta)$, as an example, is given in Figure 1b.

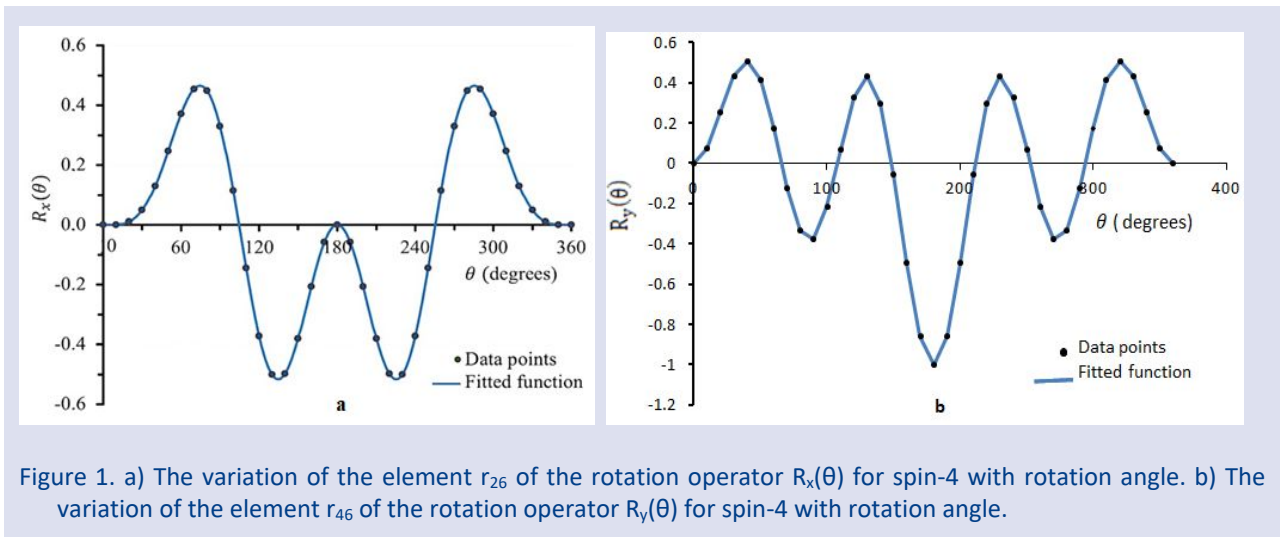


Figure 1. a) The variation of the element r_{26} of the rotation operator $R_x(\theta)$ for spin-4 with rotation angle. b) The variation of the element r_{46} of the rotation operator $R_y(\theta)$ for spin-4 with rotation angle.

The variation and graph of these elements according to the angle are given in Figure 1 a and b. As can be seen in Figure 1, the agreement was found to be perfect in the operations performed with the least squares method. Figure 1 shows the solid line fit function in a and b.

where other coefficients are zero. All nonzero elements of rotation operator matrices $R_x(\theta)$, $R_y(\theta)$ and $R_z(\theta)$ were calculated similarly. Calculations were performed with the precision of $\varepsilon = 10^{-9}$ and elements of rotation operators were given in Eqn. (8) and Table1.

$$r_{26} = \sqrt{175} c^4 s^4 - \sqrt{63} c^2 s^6 \quad (7)$$

$$R_x = \begin{bmatrix} r_{11} & ir_{12} & r_{13} & ir_{14} & r_{15} & ir_{16} & r_{17} & ir_{18} & r_{19} \\ ir_{12} & r_{22} & ir_{23} & r_{24} & ir_{25} & r_{26} & ir_{27} & r_{28} & ir_{18} \\ r_{13} & ir_{23} & r_{33} & ir_{34} & r_{35} & ir_{36} & r_{37} & ir_{27} & r_{17} \\ ir_{14} & r_{24} & ir_{34} & r_{44} & ir_{45} & r_{46} & ir_{36} & r_{26} & ir_{16} \\ r_{15} & ir_{25} & r_{35} & ir_{45} & r_{55} & ir_{45} & r_{35} & ir_{25} & r_{15} \\ ir_{16} & r_{26} & ir_{36} & r_{46} & ir_{45} & r_{44} & ir_{34} & r_{24} & ir_{14} \\ r_{17} & ir_{27} & r_{37} & ir_{36} & r_{35} & ir_{34} & r_{33} & ir_{23} & r_{13} \\ ir_{18} & r_{28} & ir_{27} & r_{26} & ir_{25} & r_{24} & ir_{23} & r_{22} & ir_{12} \\ r_{19} & ir_{18} & r_{17} & ir_{16} & r_{15} & ir_{14} & r_{13} & ir_{12} & r_{11} \end{bmatrix}$$

$$R_y = \begin{bmatrix} r_{11} & r_{12} & -r_{13} & -r_{14} & r_{15} & r_{16} & -r_{17} & -r_{18} & r_{19} \\ -r_{12} & r_{22} & r_{23} & -r_{24} & -r_{25} & r_{26} & r_{27} & -r_{28} & -r_{18} \\ -r_{13} & -r_{23} & r_{33} & r_{34} & -r_{35} & r_{36} & r_{37} & r_{27} & -r_{17} \\ r_{14} & -r_{24} & -r_{34} & r_{44} & r_{45} & -r_{46} & r_{36} & r_{26} & r_{16} \\ r_{15} & r_{25} & -r_{35} & -r_{45} & r_{55} & r_{45} & -r_{35} & -r_{25} & r_{15} \\ -r_{16} & r_{26} & -r_{36} & -r_{46} & -r_{45} & r_{44} & r_{34} & -r_{24} & -r_{14} \\ -r_{17} & -r_{27} & r_{37} & -r_{36} & -r_{35} & -r_{34} & r_{33} & r_{23} & -r_{13} \\ r_{18} & -r_{28} & -r_{27} & r_{26} & r_{25} & -r_{24} & -r_{23} & r_{22} & r_{12} \\ r_{19} & r_{18} & -r_{17} & -r_{16} & r_{15} & r_{14} & -r_{13} & -r_{12} & r_{11} \end{bmatrix}$$

$$R_z = \begin{bmatrix} z_{11} & 0 & 0 & 0 & 0 & 0 & 0 & 0 & 0 \\ 0 & z_{22} & 0 & 0 & 0 & 0 & 0 & 0 & 0 \\ 0 & 0 & z_{33} & 0 & 0 & 0 & 0 & 0 & 0 \\ 0 & 0 & 0 & z_{44} & 0 & 0 & 0 & 0 & 0 \\ 0 & 0 & 0 & 0 & z_{55} & 0 & 0 & 0 & 0 \\ 0 & 0 & 0 & 0 & 0 & z_{44}^* & 0 & 0 & 0 \\ 0 & 0 & 0 & 0 & 0 & 0 & z_{33}^* & 0 & 0 \\ 0 & 0 & 0 & 0 & 0 & 0 & 0 & z_{22}^* & 0 \\ 0 & 0 & 0 & 0 & 0 & 0 & 0 & 0 & z_{11}^* \end{bmatrix}$$

Table 1. Elements of rotation operators for spin 4

$r_{11} = c^8$	$r_{28} = s^8 - \sqrt{49}c^2s^6$
$r_{12} = \sqrt{7}c^7$	$r_{33} = c^8 - \sqrt{144}c^6s^2$
$r_{13} = -\sqrt{28}c^6s^2$	$r_{34} = \sqrt{18}c^7s - \sqrt{450}c^5s^3 + \sqrt{200}c^3s^5$
$r_{14} = -\sqrt{56}c^5s^3$	$r_{35} = \sqrt{640}c^4s^4 - \sqrt{90}(c^6s^2 + c^2s^6)$
$r_{15} = \sqrt{70}c^4s^4$	$r_{36} = \sqrt{200}c^5s^3 + \sqrt{450}c^3s^5 - \sqrt{18}cs^7$
$r_{16} = \sqrt{56}c^3s^5$	$r_{37} = \sqrt{225}c^4s^4 - \sqrt{144}c^2s^6 + s^8$
$r_{17} = -\sqrt{28}c^2s^6$	$r_{44} = c^8 - \sqrt{225}c^6s^2 + \sqrt{900}c^4s^4 - \sqrt{100}c^2s^6$
$r_{18} = -\sqrt{7}cs^7$	$r_{45} = \sqrt{20}(c^7s + cs^7) + \sqrt{720}(c^3s^5 - c^5s^3)$
$r_{19} = s^8$	$r_{46} = s^8 - \sqrt{100}c^6s^2 + \sqrt{900}c^4s^4 - \sqrt{225}c^2s^6$
$r_{22} = c^8 - \sqrt{49}c^6s^2$	$r_{55} = c^8 - \sqrt{256}(c^6s^2 + c^2s^6) + s^8$
$r_{23} = \sqrt{14}c^7s - \sqrt{126}c^5s^3$	$z_{11} = c^8 - 28(c^6s^2 + c^2s^6) + 70c^4s^4 + s^8$
$r_{24} = \sqrt{175}c^4s^4 - \sqrt{63}c^6s^2$	$+ 8i(c^7s - cs^7)$
$r_{25} = \sqrt{140}(c^3s^5 - c^5s^3)$	$+ 56i(c^3s^5 - c^5s^3)$
$r_{26} = \sqrt{175}c^4s^4 - \sqrt{63}c^2s^6$	$z_{22} = c^8 + 14(c^2s^6 - c^6s^2) - s^8 + 6i(c^7s + cs^7)$
$r_{27} = \sqrt{126}c^3s^5 - \sqrt{14}cs^7$	$- 14i(c^5s^3 + c^3s^5)$
	$z_{33} = c^8 - 4(c^6s^2 + c^2s^6) - 10c^4s^4 + s^8$
	$+ 4i(c^7s + c^5s^3 - c^3s^5 - cs^7)$
	$z_{44} = c^8 + 2(c^6s^2 - c^2s^6) - s^8 + 2i(c^7s + cs^7)$
	$+ 6i(c^5s^3 + c^3s^5)$
	$z_{55} = 1$

Conclusions

Spin-based quantum computing uses qubit systems (spin-1/2, single electron or proton), qutrit systems (spin-1, electron pair or nuclei), and qudit systems (spin>1). Present studies on spin-based quantum computation system concentrate mainly on qubit system, but higher spin system also seem to be promising. Besides the nuclei with higher spins, carbon nanotubes or fullerenes may contain two, three or more unpaired electrons therefore, it seems necessary to establish the theoretical foundations of large spin systems. Since EPR spectroscopy can work in different spin systems, it is evident that quantum mechanical spin operators, some basic quantum gates corresponding quantum rotation operators will encourage investigation for spin systems greater than spin-1/2.

Quantum mechanical rotation operators $R_x(\theta)$, $R_y(\theta)$ and $R_z(\theta)$ corresponding to spin-4 were formed by series expansion of exponential operator and variations generated for each element of rotation operator were fitted by least squares procedure to linear functions of sines and cosines. The operators $R_x(\theta)$ and $R_z(\theta)$ in matrix forms are symmetric, and $R_y(\theta)$ is antisymmetric. The rotation operators found can be used to determine the rotations of the corresponding spins or dipoles around three Cartesian coordinates. It is expected that it can form a basis for its implementation for spin-4 or equivalent magnetic dipole systems.

Conflicts of interest

The authors state that did not have conflict of interests.

References

- [1] Gruska, J., Quantum Computing, McGraw-Hill Publishing Company. UK, (1999) 439.
- [2] Bellac, M.A., A short Introduction To Quantum Information and Computation, (translated from French). Cambridge University Press. Berlin, (2006).
- [3] McMahon, D., Quantum computing, Explained. John Wiley & Sons. Inc. Publication. USA, (2008) 332.
- [4] Nakahara, M., Ohmi T., Quantum Computing From Linear Algebra to Physical Realizations, Taylor and Francis Books. Boca Raton, (2008).
- [5] Nielsen, M.A., Chuang I. L., Quantum Computation and Quantum Information, 10th Anniversary Ed, Cambridge University Press. Cambridge, New York, (2010).
- [6] Feynman R., Simulating physics with computers, Int. J. Theor. Phys., 21 (1982) 467–488.
- [7] Feynman, R., Quantum Mechanical Computers, *Foundation of Physics*, 16(6) (1986)507.
- [8] Wigner, E.P., Group theory and its applications to the quantum mechanics of atomic spectra, Academic Press. Los Mexico. Alamos, (1959).
- [9] Messiah, A., Quantum Mechanics Vol. 2., North-Holland John Wiley & Sons. Orsay, France, (1966).
- [10] Sakurai J.J., Napolitano J.J., Modern Quantum Mechanics. Cambridge University Press, United States of America, (2011).
- [11] Schiff, L.I., Quantum Mechanics, Third Ed. New York, (1968).
- [12] Merzbacher, E., Quantum Mechanics, Second Ed. New York, (1970).
- [13] Morrison M.A., Parker G.A., A Guide to Rotations in Quantum Mechanics, *J. Aust. Phys.*, 40 (1987) 465–498.
- [14] Shu-Shen L., Gui-Lu L., Feng-Shan B., Song-Lin F., Hou-Zhi Z., Quantum computing, *Proceedings of the Academy of Sciences of the United States of America*, 98(21) (2001) 11847-11848.

- [15] Blanca M.A., Flórez M., Bermejo M., Evaluation of the rotation matrices in the basis of real spherical harmonics, *Journal of Molecular Structure Theochem*, 419 (1997) 19-27.
- [16] Dachsel, H., Fast and accurate determination of the Wigner rotation matrices in the fast multipole method, *J. Chem.Phys.*, 124 (2006) 144115–1-144115–6.
- [17] Gimbutas, Z., Greengard, L., A fast and stable method for rotating spherical harmonic expansions, *J. Comput. Phys.*, 228 (2009) 5621–5627.
- [18] Aubert, G., An alternative to Wigner d-matrices for rotating real spherical harmonics, *AIP Advances*, 3 (2013) 062121–1-062121–25.
- [19] Tilma T., Everitt M. J., Samson J.H., Munro W.J., Nemoto K., Wigner Functions for Arbitrary Quantum Systems, *Phys. Rev. Letters*, 117 (2016) 180401.
- [20] Curtright, T.L., Fairlie, D.B., Zachos, C.K., Compact Formula for Rotations as Spin Matrix Polynomials, *Sigma*, 10 (2014) 1–15.
- [21] Curtright, T.L., Van Korftryk, T.S., On Rotations as Spin Matrix Polynomials, *Journal of Physics A: Mathematical and Theoretical*, 48 (2014) 1-15.
- [22] Fukushima, E., Roeder, S.B.W., Experimental pulse NMR: a nuts and bolts approach, Wesley Publishing Company, Massachusetts, (1981).
- [23] Rule, G.S., Hitchens, T.K., Fundamentals of Protein NMR Spectroscopy, Springer. New Delhi, India, (2006).
- [24] Oliviera I.S., Bonagamba T.J., Sarthour, R.S., Freitas, J.C.C., deAzevedo, E.R., NMR Quantum Information Processing. ElsevierScience. Netherlands, (2007).
- [25] Jones, J.A., NMR Quantum Computation, *Prog. Nucl. Magn. Reson. Spectroscopy*, 38 (2001) 326–360.
- [26] Schweiger, A., Jeschke, G., Principles of Pulse Electron Paramagnetic Resonance. Oxford University Press. UK, (2001).
- [27] Price M.D., Fortunato E.M., Pravia M.A., Breen C., Kumaresean S., Rosenberg G., Cory D.G., Information Transfer on an NMR Quantum Information Processor, *Concepts in Magnetic Resonance Part A*, 13(3) (2001) 151-158.
- [28] Govind Joshi, S.K., Spintronics and quantum computation, *Indian J. Phys.*, 78A (3) (2004) 299-308.
- [29] Kocakoc M., Tapramaz R., Formation of Matrices of $S = 1$, $S = 3/2$ Spin Systems in Quantum Information Theory Formation of Matrices Some Spin Systems, *J. New Research in Science*, 7(2) (2018) 9-12.
- [30] Kocakoc M., Tapramaz R., Some Transactions Made with Hadamard Gate in Qutrit Systems, *Journal of New Results in Engineering and Natural Science*, 8 (2018) 6-10.

The Effect of Experimental Cycles on the Traps Depths of Dosimetric Traps of Natural Calcite Minerals

Dilek Toktamış^{1,a,*}

¹ Department of Physics Engineering, Faculty of Science, Gaziantep University, Gaziantep, Türkiye.

*Corresponding author

Research Article

History

Received: 23/02/2021

Accepted: 29/03/2022

Copyright





©2022 Faculty of Science,
Sivas Cumhuriyet University

ABSTRACT

A trap found in a solid state radiation dosimetry is characterized by kinetic parameters such as trap depth (E_a), frequency factor (s), kinetic order (b) and carrier concentration (n_0). Trap depth (Activation energy) is the required energy to release carriers in the trap. In this study, it is investigated that how the dosimetric trap depths of the traps found in the four natural calcite minerals are affected by reusable of them as a dosimeter. All samples were irradiated about 36 Gy beta dose and read out by a thermoluminescence dosimeter (TLD) reader. A computer glow curve deconvolution program (CGCD) was used to get the kinetic parameters. And the results are compared for the four calcite samples.

Keywords: Thermoluminescence, Dosimetry, Radiation, Calcite.

 dilektoktamis@hotmail.com

 <https://orcid.org/0000-0002-0333-1740>

Introduction

Some insulators and semiconductors emit light when they are stimulated by heat after absorbing radiation dose from some radiation source such as beta source. This special emitting light is called as thermoluminescence (TL). The energy of the emitted TL light is different from the absorbed energy due to radiative transition between localized and delocalized band in the structure. In the TL process, an insulator absorbs radiation energy then electron-hole pairs are generated in conduction and valance band. The charge carriers (electrons and holes) are trapped by electron and hole traps (also known as localized energy levels) found in forbidden bandgap. The traps are metastable states in the forbidden bandgap. These are defects such as vacancy, dislocations and impurity atoms. Without applying thermal energy, the charge carries stay in the traps. When enough thermal energy is given to the solid, these charge carriers release from traps and moves into the delocalized bands (conduction and valance band). Finally they recombine radiatively with their opposite charges in the recombination center and thermoluminescence light emits. In the TL studies, the variation of TL light intensity as a function of temperature is obtained to know informations about structure of the material. The graph given in figure1 is called as TL glow curve. And also, in dosimetric studies, the absorbed radiation dose is calculated by calculating area under the TL glow curve.

In the Figure1, each peak generally represents a trap. The TL glow curve has four peaks in the Figure1. Each trap is evicted completely at specific peak temperature.

A trap found in the sample is characterized by kinetic parameters such as activation energy (E_a), frequency factor (s), kinetic order (b) and carrier concentration (n_0). Activation energy, also known as trap depth, is the required energy to release carriers in the trap. Kinetic order gives the relation

between the rate of retrapping and recombination. Frequency factor is the number of attempt of carrier to escape from the trap. The carrier concentration gives the number of trapped carrier and peak integral generally gives it. Trap depth or activation energy (E_a) is required energy, expressed in electronvolt, to release charge carrier (electron or hole) from trap to conduction or valance band of a crystal. These traps are metastable state or level within the forbidden bandgap.

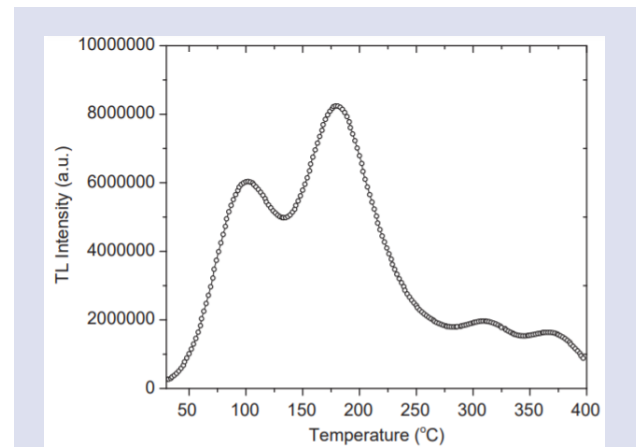


Figure 1. An example of TL glow curve [1]

The metastable state can be electron trap near to the conduction band or hole trap near to the valance band, or a luminescence center (recombination center) near to the middle of bandgap [2-5]. The trap depth for electron trap is measured from the trap to the bottom of conduction band and for the hole trap from trap to top of the valance band.

In the dosimetric studies, reusability (also known as reproducibility) effect plays important role. At every usage of radiation dosimeter, different TL glow curve may be obtained and this is undesired result. For a good dosimeter, same TL glow curve is desired at the end of each reading.

In this study, it is investigated that how the dosimetric trap depths of the traps found in the four natural calcite minerals are affected by reusable of them as a dosimeter.

Samples and Methods

Four different natural calcite minerals were used in this work. They are tagged as sample1, sample2, sample3

and sample4. The TL glow curves of the four samples were obtained after irradiation sample by a beta source and read out by a TLD reader. All examples were irradiated about 36 Gy at room temperature with a point beta source (^{90}Sr - ^{90}Y) which delivers 0.040 Gy/s. Its activity is about 3.7 GBq (100 mCi). Glow curve measurements were made using a Harshaw TLD System 3500 Manual TLD Reader at 1 °C/s heating rate experiment. The irradiator and the TLD Reader were shown in Figure 2. The kinetic parameters of the traps found in the samples were obtained by a computerised glow curve deconvolution (CGCD) method developed by Afouxenidis et al [6]



Figure 2. (a) Irradiator and (b) TLD Reader

When the glow curve has overlapping peaks it is suitable to use Computer Glow Curve Deconvolution Method program, which become popular way to study the trapping parameters parameters such as trap depth (E_a), frequency factor (s), and kinetic order (b) from thermoluminescence glow curves in recent years [7]. In this method, the TL intensity-Temperature data is imported to the program and several satellite peaks are simulated by entering kinetic parameters. Due to the suitable simulated satellite peaks, a simulated TL glow curve is created. The main aim in the program that superimpose experimental TL glow curve and simulated TL glow curve on each other. Then this simulated curve is fitted to experimental curve.

Results and Discussion

In the results part the fitted glow curves of the four samples and their variation of trap depth as a function of reusability were given.

Calcite sample1

In the Figure 3 (a) the fitted TL glow curve of one of the repeat experiment for the sample1 is given. The TL glow curve is fitted with six satellite peaks which locate at different temperatures. The Figure of merit (FOM) for this cycle of measurement was found 0.947%. The variation of the activation energies of two main satellite peaks located at ~ 140 °C and at ~ 320 °C are given in the Figure 3(b). The activation energy of the peak at ~ 140 °C does not affected by the repeat of experiment and found 0.6 eV but there is a change for the activation energy of the peak at ~ 320 °C. Its value fluctuates from 1.8 eV to 2.1 eV. Besides these, the FOM values for the fitted TL glow curves of each cycle is given Table 1. The standard deviation for the peak at ~ 140 °C and at ~ 320 °C are 1.57% and 7.07%, respectively.

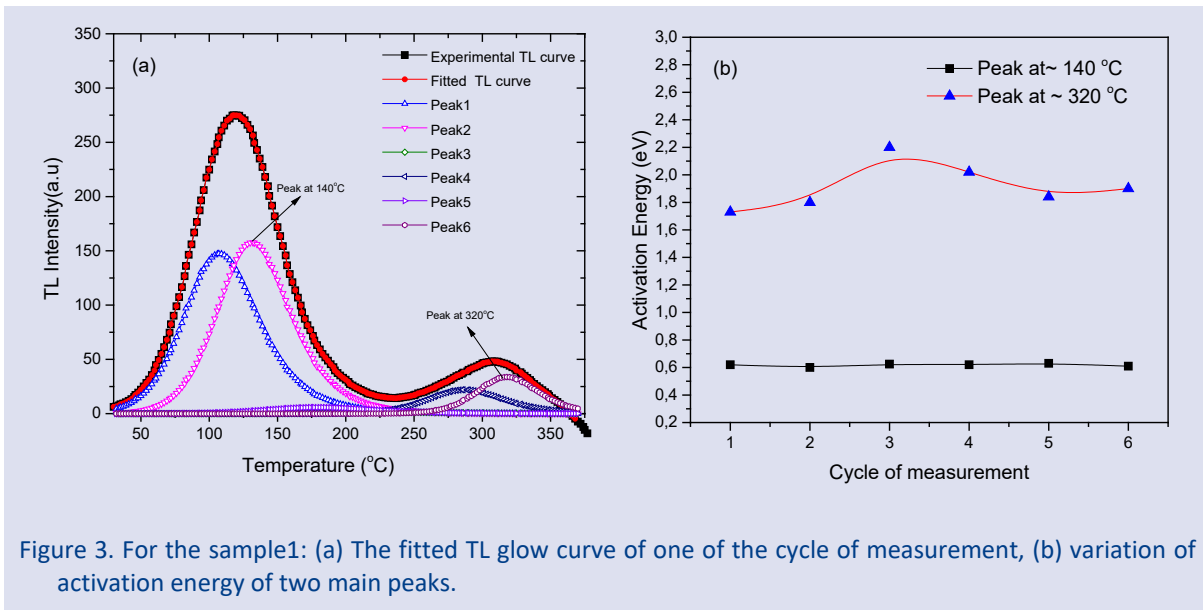


Table 1. The values of Figure of merit (FOM) for the six cycle of measurements

	Cycle 1	Cycle 2	Cycle 3	Cycle 4	Cycle 5	Cycle 6
FOM (%)	1.29	1.06	1.2	1.01	1.26	1.05

Calcite sample2

The fitted TL glow curve and their five satellite peaks for the second calcite sample are shown in Figure 4 (a). The reusability of this sample is investigated via three trap depths located at ~90 oC, ~140 oC and ~245 oC shown in Figure 4(b). It is seen that the peak at ~90 oC is more stable than others at ~140 oC and ~245 oC. The standard deviation for the peak at ~90 oC, ~140 oC and ~245 oC are 5%, 6.2%, and 5.2%, respectively. For the second calcite sample, the FOM values for the fitted TL glow curves of each cycle is given Table 2

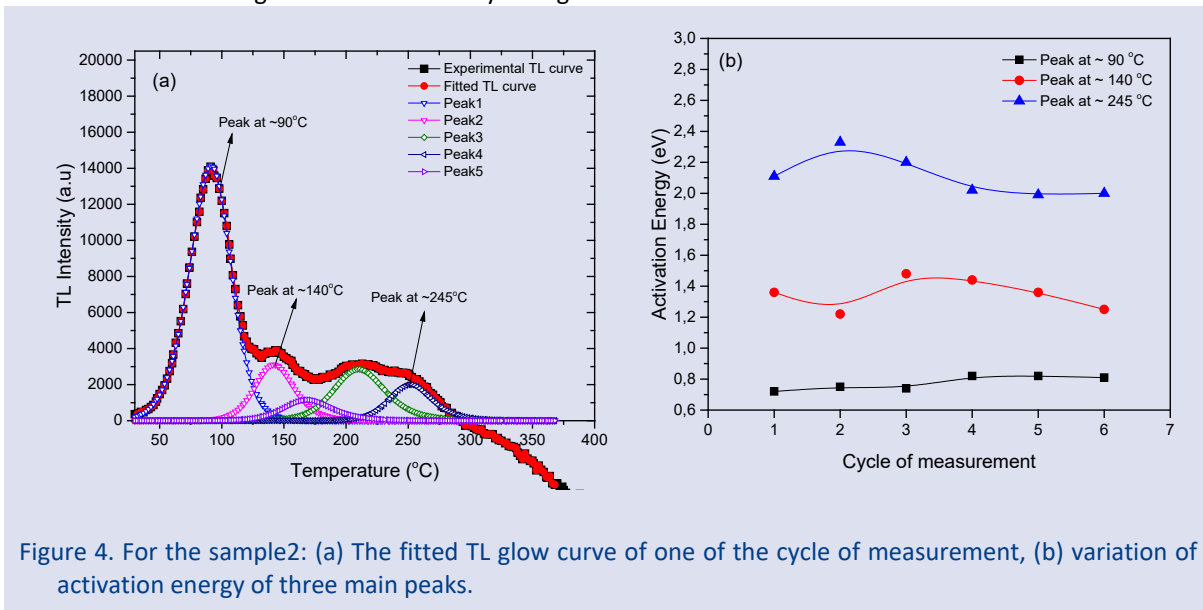


Table 2. The values of Figure of merit (FOM) for the six cycle of measurements

	Cycle 1	Cycle 2	Cycle 3	Cycle 4	Cycle 5	Cycle 6
FOM (%)	1.74	2.23	2.38	2.2	1.35	1.55

Calcite sample3

The TL glow curve of the third calcite sample is fitted by six satellite peaks shown in Figure 5(a). The FOM values of the each cycle is given in the Table 3. The variation of the traph depths of three main peaks at ~115 oC, ~245 oC and ~290 oC as a function of repeat of experiment is drawn in Figure 5(b). The stabilities of the peak at ~115 oC and ~245 oC are better than the peak at ~290 oC. The standard deviation for the peak at ~115 oC, ~245 oC and ~290 oC are 0%, 3.8%, and 12.5%, respectively.

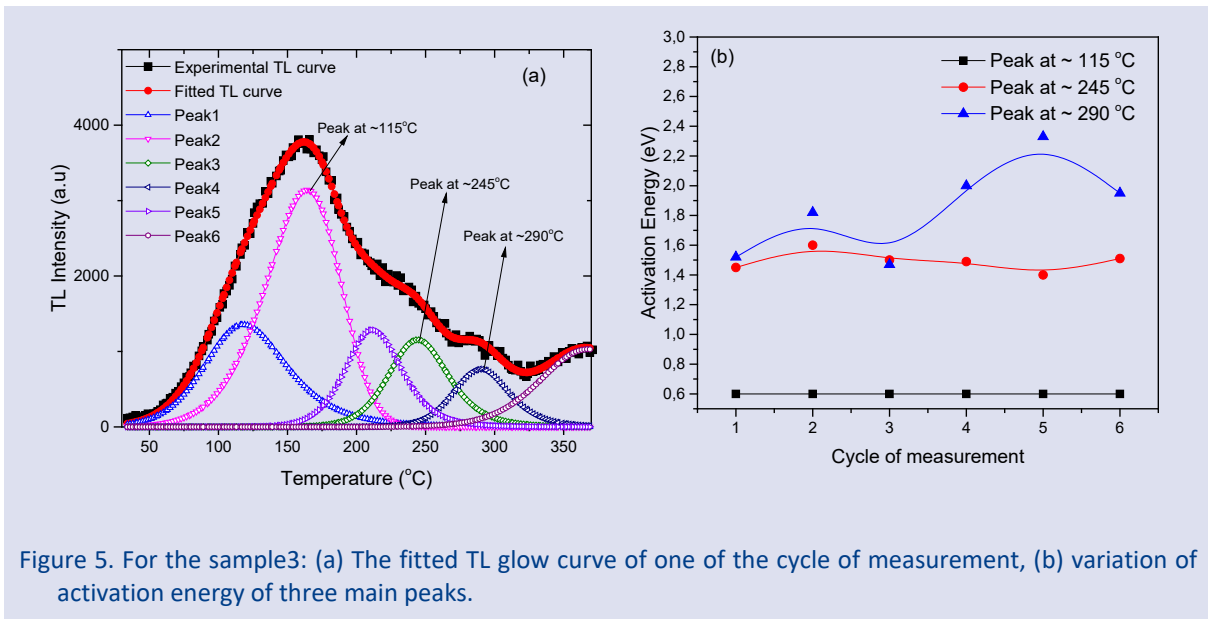


Figure 5. For the sample3: (a) The fitted TL glow curve of one of the cycle of measurement, (b) variation of activation energy of three main peaks.

Table 3. The values of Figure of merit (FOM) for the six cycle of measurements

	Cycle 1	Cycle 2	Cycle 3	Cycle 4	Cycle 5	Cycle 6
FOM (%)	3.03	2.91	2.89	2.74	2.49	2.32

Calcite sample4

For the last calcite sample, the fitted TL glow curve of one of the cycles is obtained by using five satellite peaks shown in Figure 6(a). In the Table 4, all FOM values for each cycle of the fourth calcite sample are tabulated. Like other samples, the stabilities of the trap depths of three main traps located at ~115 °C, ~225 °C and ~340 °C are investigated in Figure 6(b). It is seen that the trap depth of the trap at ~115 °C is more stable than of the traps at ~225 °C and ~340 °C. The standard deviation for the peak at ~115 °C, ~225 °C and ~340 °C are 0.6%, 12.7%, and 6.3%, respectively.

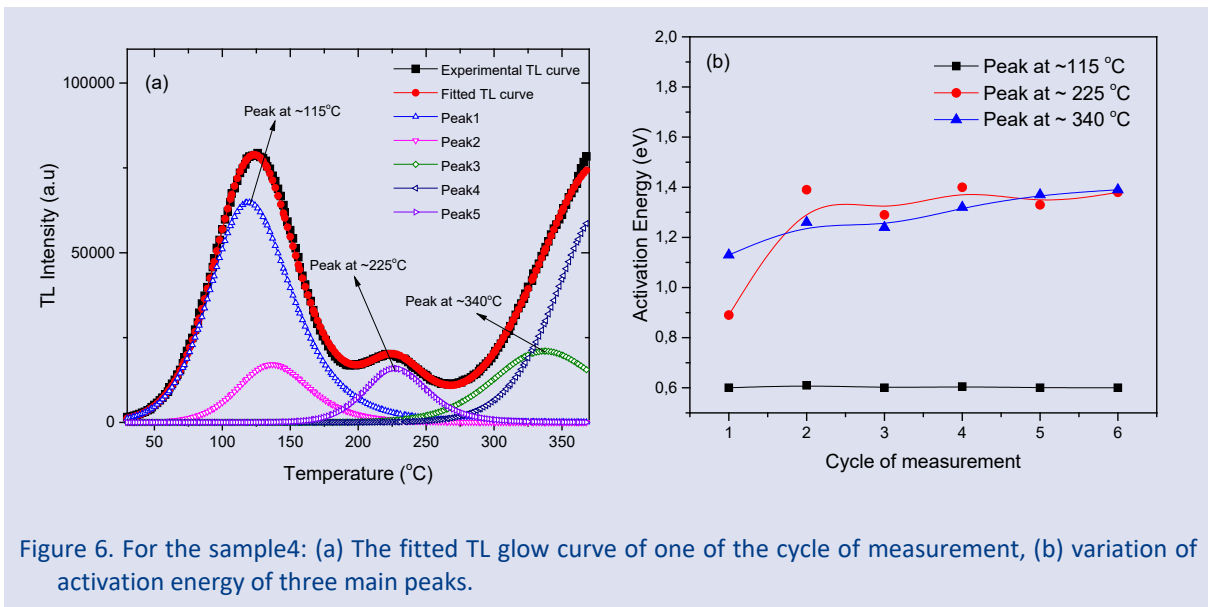


Figure 6. For the sample4: (a) The fitted TL glow curve of one of the cycle of measurement, (b) variation of activation energy of three main peaks.

Table 4. The values of Figure of merit (FOM) for the six cycle of measurements

	Cycle 1	Cycle 2	Cycle 3	Cycle 4	Cycle 5	Cycle 6
FOM (%)	1.23	1.86	1.31	1.63	1.74	1.24

Conclusion

Trap depth (activation energy) is one of the kinetic parameters of a trap. It is the required stimulation energy to evict all trapped charge carriers from the trap. The kinetic parameters are found by several methods. Computer glow

curve deconvolution (CGCD) or computerised curve deconvolution (CCD) is a analysis program to get kinetic parameters of traps. The computerised curve deconvolution (CCD) analysis of thermoluminescence (TL) glow curves and optically stimulated luminescence (OSL) decay curves into their individual glow peaks and

components respectively have been recognised over the last 30 years to be of major importance [6, 8-12]. The main aim in the program that superimpose experimental TL glow curve and simulated TL glow curve on each other. Then this simulated curve is fitted to experimental curve. The goodness of fit is tested by using the figure of merit (FOM) [13,14]. Generally, in the cases of experimental TL glow-curves the fit is acceptable for FOM% values less than 2%.

The FOM is a very convenient expression to take as a measure of goodness of fit:

$$FOM[\%] = \sum_{j_i}^{j_f} \frac{100|y_j - y(x_j)|}{A} \times 100\% \quad (1)$$

where j_i = first channel in the region of interest, j_f = last channel in the region of interest, y_j = information content j , $y(x_j)$ = value of the fitting function in channel j , A = integral of the fitted glow curve in the region of interest. It can be said that if the values of the FOM are between 0.0% and 2.5% the fit is good, 2.5 % and 3.5% the fit is fair, and > 3.5% it is bad fit [1,3]. In this study, the effects of repeat of experiment on the trap depth of the main traps found in four different natural calcite (CaCO_3) samples were investigated. For the four samples, a simulated TL glow curve with several satellite peaks is fitted to the experimental TL glow curve. Their FOM values are given in table 1, 2, 3 and 4. The FOM values of all cycles (repeat) for the sample1 and 4 are in the range of acceptable value (< 2%). Although some of cycles for the sample2 and all of the cycles for the sample3 have bigger FOM values but they are very close to 2%. Generally, the trap depth of the trap found at $\sim 100^\circ\text{C}$ is not affected by the cycle of measurement (repeat of experiment) for all samples. Its value is about 0.6eV with very small standard deviation. However, the trap depths of the traps found at higher temperature region between 200°C and $\sim 350^\circ\text{C}$ fluctuate between 1.4eV and 2.1eV. It means repeat of experiment with higher temperature changes the structure of the traps. In the other words, there is a trap conversion between too close traps with repeat of experiment due to the higher temperature [2,15]. The stabilizing the trap structure can be achieved by annealing preparation. In order to prepare a thermoluminescent material for use, it is needed to perform a thermal treatment, usually called annealing, carried out in oven or/and furnace, which consists of heating up the TL samples to a predetermined temperature, keeping them at that temperature for a predetermined period of time and then cooling down the samples to room temperature [16,17].

In conclusion, the trap depths of shallow traps are almost unaffected by the repeat of experiment but the reusage of the sample changes the trap depths of deeper traps.

Conflicts of interest

The authors state that did not have conflict of interests.

References

- [1] Toktamış D., Toktamış H., Yazıcı A. N., The Effects of Thermal Treatments on the Thermoluminescence Properties of Biogenic Minerals Present in the Seashells, *Radiation Effects and Defects in Solids*, 171 (11–12) (2016) 951–964.
- [2] Furetta C., Handbook of Thermoluminescence, World Scientific Publishing Co.Pte.Ltd. Singapore, (2003).
- [3] Abdel-Razek Y.A., Thermoluminescence dosimetry using natural calcite, *Journal of Taibah University for Science*, 10 (2) (2016) 286-295.
- [4] Khanlary M.R., Townsend P.D., TL spectra of single crystals and crushed calcite, *Nucl. Tracks Radiat. Meas.*, 18(1-2) (1991) 29-35.
- [5] Yüksel M., Thermoluminescence and dosimetric characteristics study of quartz samples from Seyhan Dam Lake Terraces, *Canadian Journal of Physics*, 96 (7) (2018) 779-783.
- [6] Afouxenidis D., Polymeris G. S., Tsirliganis N.C., Kitis G., Computerized Curve Deconvolution of TL/OSL Curves Using a Popular Spreadsheet Program, *Radiation Protection Dosimetry*, 149 (2012) 363–370.
- [7] Halperin A., Braner A. A., Evaluation of Thermal Activation Energies from Glow Curves, *Physical Review Letters*, 117 (1960) 408-415.
- [8] Horowitz Y. S., Moscovitch M., Computerized Glow Curve Deconvolution Applied to High Dose (102 – 105 Gy) TL Dosimetry, *Nuclear Instruments and Methods in Physics Research*, A243(1) (1986) 207 – 214.
- [9] Horowitz Y. S., Moscovitch M., Wilt M., Computerized Glow Curve Deconvolution Applied to Ultralow Dose LiF Thermoluminescence Dosimetry, *Nuclear Instruments and Methods in Physics Research*, A244 (3) (1986) 556 – 564.
- [10] Horowitz Y. S., Yossian D., Computerized Glow Curve Deconvolution: The Case of LiF TLD-100, *Journal Physics D: Applied Physics*, 26(8) (1993) 1331 – 1332.
- [11] Horowitz Y. S., Yossian D., Computerized Glow Curve Deconvolution: Application to Thermoluminescence Dosimetry, *Radiation Protection Dosimetry*, 60(1) (1995) 1 – 114.
- [12] Furetta C., Kitis G., Kuo C.-H., Kinetics Parameters of CVD Diamond by Computerized Glow-curve Deconvolution (CGCD), *Nuclear Instruments Methods in Physics Research B: Beam Interactions with Materials and Atoms*, 160(1) (2000) 65 – 72.
- [13] Balian H. G., Eddy N. W., Figure-of-merit (FOM): An Improved Criterion over the Normalized Chi-squared Test for Assessing Goodness-of-fit of Gamma-ray Spectral Peaks, *Nuclear Instruments Methods*, 145 (1977) 389-395.
- [14] Kitis G., Chen R., Pagonis V., Carinou E., Ascounis P., Kamenopoulou V., Thermoluminescence under an Exponential Heating Function: II. Glow-curve Deconvolution of Experimental Glow-curves, *Journal of Physics D: Applied Physics*, 39 (2006) 1508-1514.
- [15] Toktamış H., Ünsal Ö. L., Toktamış D., A. Necmeddin Yazıcı, Thermoluminescence properties of unique Rosso Levanto marble, *Luminescence*, 36 (1) (2021) 142-148.
- [16] Busuoli G., Applied Thermoluminescence Dosimetry, Adam Hilger Ltd Ispra, (1981).
- [17] Drisoll C. M. H., Barthe J. R., Oberhofer M., Busuoli G., Hickman C., Annealing Procedures for Commonly Used Radiothermoluminescent Materials, *Radiation Protection Dosimetry*, 14(1) (1986) 17-32

Investigation of Gamma Ray Buildup Factor for some Shielding Absorber

Hiwa Mohammad Qadr^{1,a,*}¹ Department of Physics, College of Science, University of Raparin, Sulaimanyah, Iraq.

*Corresponding author



Research Article

History

Received: 04/04/2022

Accepted: 06/08/2022

Copyright

©2022 Faculty of Science,
Sivas Cumhuriyet University hiwa.physics@uor.edu.krd <https://orcid.org/0000-0001-5585-3260>

ABSTRACT

The purpose of this research is to observe and understand the processes by which gamma rays are attenuated in passing through absorber, and the effects of shielding geometry. Gamma ray linear attenuation coefficient, mass attenuation coefficient, mean free path, half value layer and buildup factor were evaluated for different absorbers, by using ⁶⁰Co source with energy value 1.332 MeV. The linear attenuation coefficient of the absorber such as aluminium was (0.1485 cm⁻¹), whereas it was observed (0.4359 cm⁻¹) for iron, and stainless steel was (0.463 cm⁻¹). The obtained results have been compared to the other absorbers. As a result of that, linear attenuation coefficient and the mass attenuation coefficient are higher for stainless steel and better radiation shielding compared with other absorbers. The results of theoretical and experimental for all parameters are a good agreement. Moreover, it is found that the buildup factor increases with thickness of the absorber increasing.

Keywords: Scintillation detector, Shielding absorber, Buildup factor, Broad-beam geometry, Mean free path.

Introduction

There are two main types of ionizing radiation. First, the directly ionizing radiations such as the alpha particle, beta particles and many other charged particles ionize atoms of their target material due to coulombic interactions with the electrons of the material, and the amount of kinetic energies of these particles determines the amount of this coulombic force [1-5]. Second, indirectly ionizing radiations are neutral particles such as high energy photons and neutrons which do not directly ionize atoms but undergo interactions to eject an energetic electron called the secondary electron. Despite the fact that a large number of possible interaction mechanisms of gamma rays with matter are known, three processes are most important in the attenuation of gamma rays by matter [6-9]. These processes of interaction are photoelectric effect, Compton scattering and pair production. In each of these processes an ionizing particle, usually an electron, is produced which can subsequently be detected. Photoelectric interactions are dominate at low energies (up to several hundred keV) and pair production at high energies (more than 5 MeV) with Compton scattering being most important in the mid-energy range [10-12]. Compton scattering refers to an inelastic scatter between a photon and a particle (usually electron). When an incident photon of relative high energy comes to interact with an atom, the bond between electron and nuclei is weak, indicating that we can regard the electron as nearly free and use the Compton scattering model [13-15].

Nowadays, there are a large number of experimental, theoretical and simulation studies have been applied on the absorbed dose and radiation shielding parameters in different ways [16-24]. Therefore, the linear attenuation

coefficient, the mass attenuation coefficient, Half Value Layer, Tenth Value Layer and Mean Free Path are a useful parameters that must be known to design and choose a shielding material. Furthermore, gamma ray buildup factor is a useful parameter for calculating radiation shielding, absorbed dose and protection, have been usually studied by practical measurements and theoretical calculation [25-28].

In this research, ⁶⁰Co source used in this work should be transported in its carrying brick, always handle remotely and requires appropriate shielding to reduce the dose rate at all exposed areas to less than 2.5 mSv/hr [6]. The linear attenuation coefficient and gamma ray buildup factors were determined for three shielding absorbers. Then, obtained values of the parameters compared with the theoretical values.

Theoretical Calculation

This section summarize theoretical relations which have been used for the determination linear attenuation coefficient μ , mass attenuation coefficient μ_m , half value layer HVL, mean free path MFP and buildup factor B. Basically, According to Lambert-Beer's law, gamma rays are attenuated passing through an absorber [18]. Probability, some of the gamma rays travel through the thickness without interaction leading to the transmission of the gamma rays. The intensity of the transmitted beam at any thickness of the absorber can be described in the following equation:

$$I = I_0 e^{-\mu x} \quad (1)$$

Where μ , cm⁻¹ is the linear attenuation coefficient of the absorber. I_0 is the initial intensity of the gamma ray, I is transmitted intensity of the gamma ray and x , cm is thickness. Rearrange of equation (1) gives the following equation for linear attenuation coefficient.

$$\mu = \frac{1}{x} \ln \left(\frac{I_0}{I} \right) \quad (2)$$

The linear attenuation coefficient is the sum of the contributions to attenuation coefficient for each type of interaction, as [10];

$$\mu = \mu_{ph} + \mu_C + \mu_P \quad (3)$$

Here μ_{ph} , μ_C and μ_P denote photoelectric absorption, Compton scattering and pair production, respectively.

Mass attenuation coefficient can be described as a ratio of the linear attenuation coefficient to unit density (ρ) of the absorber with unit (cm²/g) [29]. It can be a useful coefficient due to only the atomic composition of the attenuator is taken into account and not the individual density of the absorber. Thus, using equation (4), mass attenuation coefficient from linear attenuation coefficient can be calculated as:

$$\mu_m = \frac{(\mu)}{(\rho)} \quad (4)$$

The half value layer (HVL) with unit cm is also called the half value thickness. It can be defined as the thickness of the absorber at which the transmitted intensity is one-half the incident intensity for the gamma ray [30, 31]. The HVL depends on the linear attenuation coefficient values and can be calculated by the following formula:

$$HVL = \frac{\ln 2}{\mu} \quad (5)$$

The linear attenuation coefficient is inversely related to mean free path (MFP) which is the average distance between two successive collisions during gamma ray travels in matter [32], it can be expressed as:

$$MFP = \frac{1}{\mu} \quad (6)$$

Buildup factor (B) is a useful parameter that shows the ratio of the total radiation quantity at a given point to the number un-collided photons [33]. So, this parameter depends on energy of the photon, linear attenuation and thickness of the absorber. The schematic arrangement of the narrow-beam geometry is shown in figure (1). It shows the thickness of the absorber which placed between the source and the detector. In this circumstance, the detector is able to detect only those photons that suffers no collision with the absorber. The narrow-beam geometry can be expressed in the following expression.

$$\frac{I_{good}}{I_0} = e^{-\mu x} \quad (7)$$

Figure 2 shows broad- beam geometry which scattered photons in the absorber are able to reach the detector. The broad-beam geometry can be written in the following expression.

$$\frac{I_{bad}}{I_0} = e^{-\mu x} \quad (8)$$

Hence, based on equations 6 and 7, the buildup factor can be calculated in the following relation [34].

$$B = \frac{I_{bad \text{ geometry}}}{I_{good \text{ geometry}}} \quad (9)$$

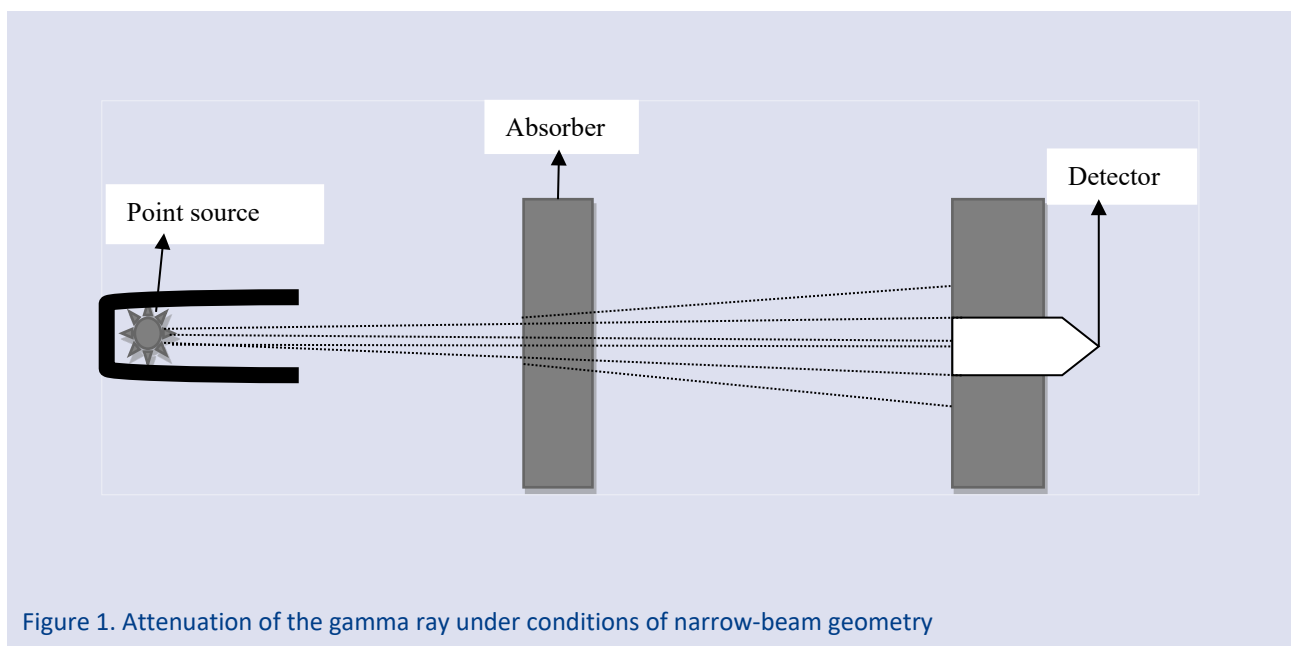


Figure 1. Attenuation of the gamma ray under conditions of narrow-beam geometry

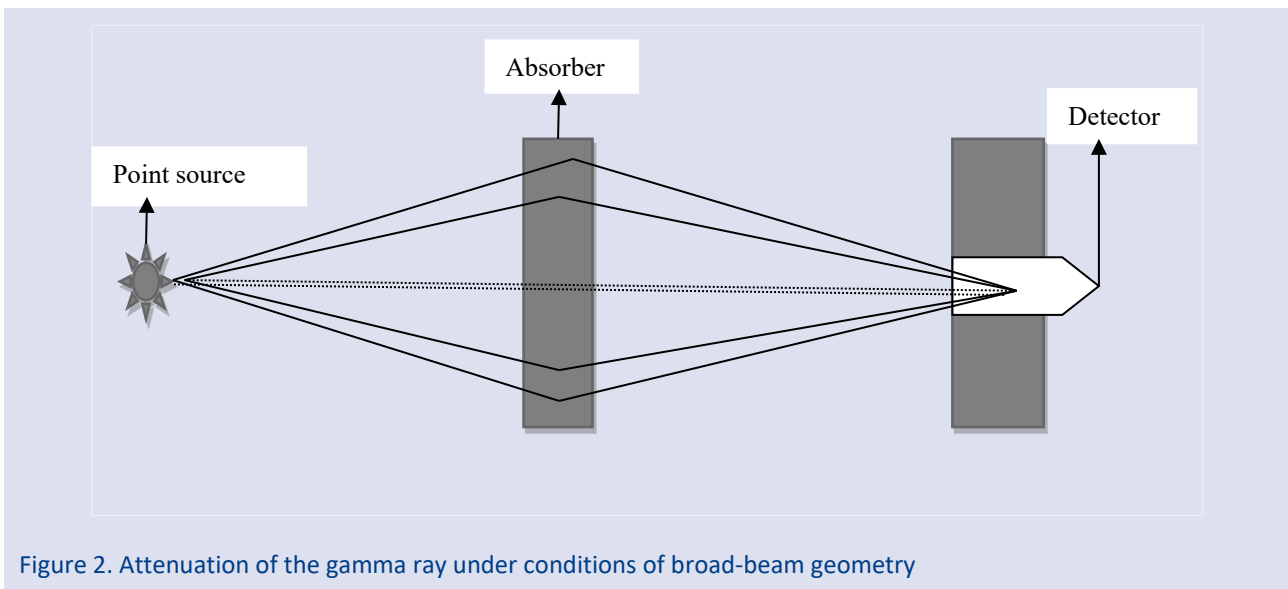


Figure 2. Attenuation of the gamma ray under conditions of broad-beam geometry

Methodology

Figure 3 shows schematic picture for the electric system which used in this paper. The absorbers used as shield are iron, concrete and aluminium. Start by building a well shielded enclosure and inserting the 7 MBq ^{60}Co source at one end. The radioactive source emits gamma rays with energies value 1.332 MeV. The energy spectra in this work obtained from NaI(Tl) scintillation detector were analyzed by the maestro program. Place absorber between the source and the detector, and measure gamma ray attenuation versus absorber thickness.

Buildup factor is measured by two methods. First, for narrow-beam geometry, the distance between the point source and the absorber was 14 cm and the distance between the detector and the point source is 47 cm. At

the beginning, an initial measurement was recorded without using any absorber. Then, this step was repeated for different thickness of the absorber and Data acquisition time was chosen as 120 seconds for each shielding absorber. As a result of that, only those gamma rays are allowed to reach the detector which traverse the absorber without undergoing any collision.

Second, for broad-beam geometry, the distance between the point source and the detector was increased in which scattered gamma rays in the thickness absorber are also able to reach the detector after collisions. So, using different absorber in both narrow-beam and broad-beam geometry, we can count number of gamma rays passed through these absorbers for various absorber thickness.

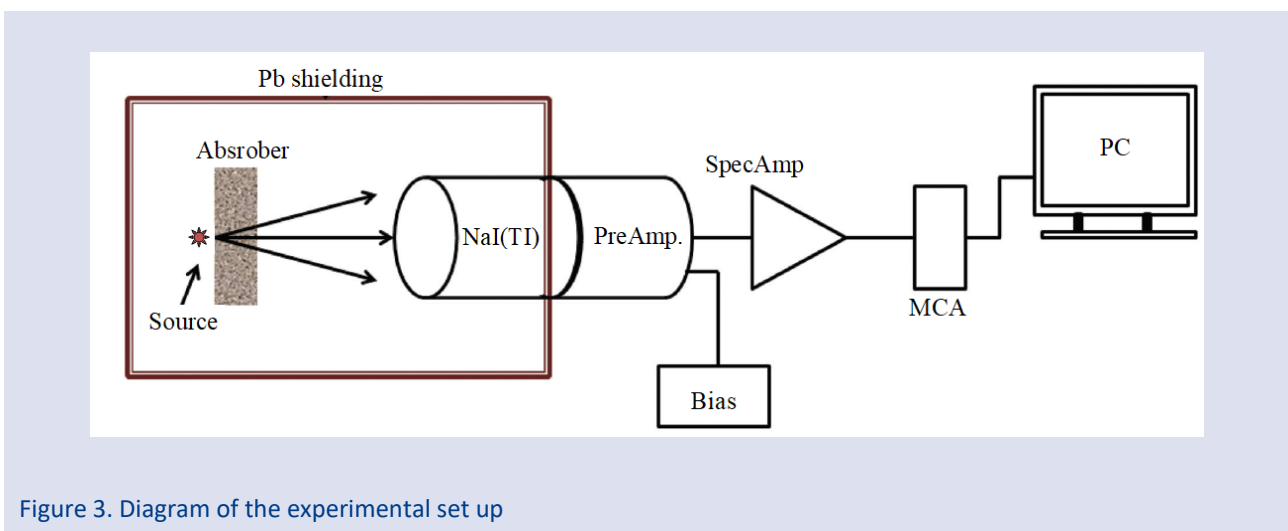


Figure 3. Diagram of the experimental set up

Results and Analysis

Calculation of the gamma ray attenuation coefficient for aluminium, iron and stainless steel are carried out using both narrow-beam and broad-beam geometries to calculate $\ln(I/I_0)$. Figures 4 obviously shows the $\ln(I/I_0)$ as

functions of the absorber thickness for both narrow-beam and broad-beam geometrical arrangement using ^{60}Co source

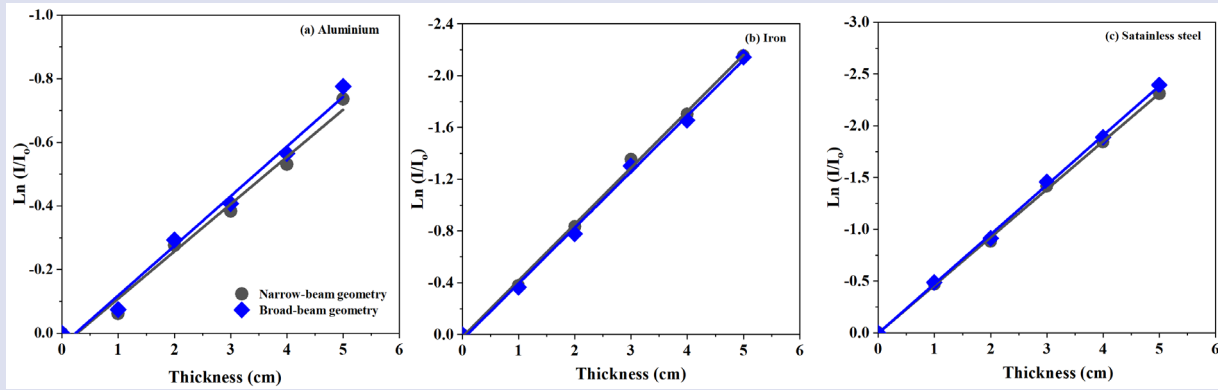


Figure 4. Comparison $\ln(I/I_0)$ as a function of the absorber thickness for both narrow-beam and broad-beam geometries using (a) aluminium (b) iron (c) stainless steel

Table 1 demonstrates the experimental values of the gamma ray linear and mass attenuation coefficients for three types shielding absorber. They were obtained by measuring the intensities of gamma rays passed through the various absorbers. It is evident from this table the linear and mass attenuation coefficient for aluminum has the lowest value, and for stainless steel it is the highest. The highest linear and mass attenuation coefficient are

due to its containment of high atomic number and high density that are more effective for gamma ray attenuation. On other hand, the lowest values of the linear and mass attenuation coefficient indicate higher penetration depth. The experimental μ and μ_m values were compared the theoretical μ and μ_m values [35, 36]. It is clearly demonstrate that the experimental results agree with the theoretical values

Table 1. Values of the experimental and theoretical linear and mass attenuation coefficient for three types shielding absorber.

Source	Atomic number	ρ (g/cm ³)	Experimental μ (cm ⁻¹)	Theoretical μ (cm ⁻¹)	Experimental μ_m (cm ² /g)	Theoretical μ_m (cm ² /g)
Aluminium	13	2.74	0.1485	0.137	0.0542	0.052
Iron	26	7.86	0.4359	0.421	0.0554	0.0535
Stainless steel	28	7.9	0.463	0.462	0.0586	0.0585

Another parameters measured in this work for the gamma ray interaction with absorbers are half value layers and mean free path. The experimental and theoretical gamma ray half value layers and mean free path of shielding absorbers are shown in Table 2. It is clear that the stainless steel has the lowest values of both half

value layer and mean free path. While, aluminium has the highest value of both parameters due to it is has poor atomic number. It is also showed that the experimental results and theoretical values for both parameters are a good agreement.

Table 2. Values of the experimental and theoretical half value layer and mean free path for three types shielding absorber

Source	Experimental HVL (cm)	Theoretical HVL (cm)	Experimental MFP (cm)	Theoretical MFP (cm)
Aluminium	4.668	5.059	6.734	7.299
Iron	1.59	1.646	2.294	2.475
Stainless steel	1.497	1.5003	2.16	2.1645

Buildup factor is also useful parameter in designing any radiation shielding. Buildup factor of shielding absorbers are measured using narrow-beam and broad-beam geometry and are given in Table 3. It is observed that as the thickness shielding absorber increases, the buildup factor increases. Hence, buildup factor values rely on the atomic number.

Nevertheless, the table indicates that broad-beam geometry values are bigger than narrow-beam geometry values due to there are no scattered gamma rays for narrow-beam geometry. Figure 5 shows comparison buildup factor as a function of penetration depth.

Table 3. Values of broad-beam geometry and narrow-beam geometry and buildup factor for three shielding absorber

Source	Thickness (cm)	Broad-beam geometry	Narrow-beam geometry	Buildup factor
Aluminum	0	292.6033	148.7733	1
	1	271.67	127.87	1.080236367
	2	218.1233	100.89	1.0992582
	3	194.675	86.34	1.146420427
	4	166.3867	73.53	1.150534958
	5	134.6722	54.226	1.262746466
Iron	0	351.18	195.9067	1
	1	236.7533	122.53667	1.07782805
	2	149.25	76.34	1.090640696
	3	88.31667	43.49667	1.132677283
	4	62.11333	30.5	1.136068422
	5	39.155	17.41	1.254607767
Stainless steel	0	323.09	189.677	1
	1	198.89	109.5433	1.06590447
	2	129.75	70.436	1.081443507
	3	75.22	39.928	1.10597912
	4	48.91	25.433	1.128992943
	5	30.65	14.96	1.202790644

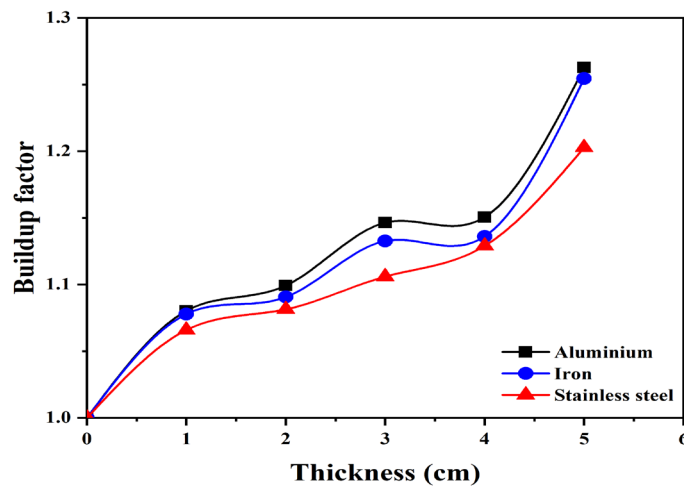


Figure 5. Buildup factor as a function of absorber thickness for aluminium, iron and stainless steel

Conclusion

In this paper, gamma ray attenuation parameters of three types shielding absorbers have been investigated and discussed in terms of gamma ray attenuation coefficient and buildup factor at 1.332 MeV energy. The result shows that the linear and mass attenuation coefficient decrease with increasing atomic number and density of the absorber. Thus, stainless steel appears to be the best gamma ray absorber among the three absorbers under consideration due to its higher value for linear and mass attenuation coefficient. The results of HVL, and MFP were also determined for three absorbers. Clearly, aluminium absorber has the highest value of the above

parameters and stainless steel absorber has the lowest values. The lower HVL and MFP values of any shielding absorber are better for shielding purposes.

Furthermore, the data shows that broad-beam geometry values are always greater than narrow-beam geometry values. It is noticed that the buildup factor for aluminium has higher value due to it has a lower atomic number compared to other absorbers. So, it is easy for gamma ray to scatter and pass through this absorber.

Conflicts of interest

The authors state that did not have conflict of interests

References

- [1] Qadr, H. M., Pressure Effects on Stopping Power of Alpha Particles in Argon Gas, *Physics of Particles and Nuclei Letters*, 18(2) (2021) 185-189.
- [2] Hiwa, M. Q., Stopping power of alpha particles in helium gas, Bulletin of the Moscow State Technical University. NE Bauman. Series "Natural Sciences", (2) (2020) 117-125.
- [3] Qadr, H. M., Hamad, A. M., Using of Stopping and Range of Ions in Matter Code to Study of Radiation Damage in Materials, *RENSIT* 12(4) (2020) 451-456.
- [4] Qadr, H. M., A molecular dynamics calculation to cascade damage processes, The Annals of "Dunarea de Jos" University of Galati. Fascicle IX, *Metallurgy and Materials Science*, 43(4) (2020) 13-16.
- [5] Mohammad, Q., Maghdid, H., Alpha-particle stopping powers in air and argon, *Journal of pure and applied physics*, 5 (2017) 22-28.
- [6] Knoll, G. F., Radiation detection and measurement, John Wiley & Sons 2010.
- [7] Sengupta, B., Generation and Modeling of Radiation for Clinical and Research Applications, (2019).
- [8] Qadr, H. M., Proportional Counter in X-Ray Fluorescence, *Aksaray University Journal of Science and Engineering*, 5(1) (2021) 1-7.
- [9] Qadr, H. M., Mamand, D., A Review on DPA for computing radiation damage simulation, *Journal of Physical Chemistry and Functional Materials*, 5(1) (2022) 30-36.
- [10] Hamad, A. M., Qadr, H. M., Gamma-Rays Spectroscopy by Using a Thallium Activated Sodium Iodide NaI (TI), *Eurasian Journal of Science and Engineering*, 4(1) (2018) 99-111.
- [11] Qadr, H. M., Comparison of energy resolution and efficiency of NaI (TI) and HPGe detector using gamma-ray spectroscopy, *Journal of Physical Chemistry and Functional Materials*, 3(1) (2020) 24-27.
- [12] Parks, J. E., The Compton effect-Compton scattering and gamma ray spectroscopy, Department of Physics, University of Tennessee, Knoxville, TN (2009) 37.
- [13] Bergstrom Jr, P., Surić, T., Pisk, K., Pratt, R., Compton scattering of photons from bound electrons: full relativistic independent-particle-approximation calculations, *Physical Review A*, 48(2) (1993) 1134.
- [14] Xiong, M., Activity Estimation Method of Linear Gamma-Ray Source under Shield Based on Single Compton Scattering, *Open Access Library Journal*, 7(07) (2020) 1.
- [15] Qadr, H. M., Experimental Study of the Pressure Effects on Stopping Power for Alpha Particles in Air, *Gazi University Journal of Science*, (2022) 272-279.
- [16] Qadr, H., Effect of Ion Irradiation on the Mechanical Properties of High and Low Copper, *Atom Indonesia*, 46(1) (2020) 47-51.
- [17] Tekin, H. O., Manici, T., Simulations of mass attenuation coefficients for shielding materials using the MCNP-X code, *Nuclear Science and Techniques*, 28(7) (2017) 1-4.
- [18] Alavian, H., Tavakoli-Anbaran, H., Comparative study of mass attenuation coefficients for LDPE/metal oxide composites by Monte Carlo simulations, *The European Physical Journal Plus*, 135(1) (2020) 82.
- [19] Sayyed, M., Agar, O., Kumar, A., Tekin, H., Gaikwad, D., Obaid, S. S., Shielding behaviour of $(20+x)$ Bi₂O₃-20BaO-10Na₂O-10MgO-(40-x) B₂O₃: an experimental and Monte Carlo study, *Chemical Physics*, 529 (2020) 110571.
- [20] Hiwa, M. Q., The use of the MCNP Code for Radiation Damage Calculations, *Mathematical Physics and Computer Modeling*, 24(1) (2021).
- [21] Qadr, H. M., Radiation damage and dpa in iron using mcnp5, *European Journal of Materials Science and Engineering*, 5(3) (2020) 109-114.
- [22] Qadr, H. M., Mamand, D. M., Molecular Structure and Density Functional Theory Investigation Corrosion Inhibitors of Some Oxadiazoles, *Journal of Bio- and Tribo-Corrosion*, 7(4) (2021) 140.
- [23] Qadr, H. M., A Molecular Dynamics Study of Temperature Dependence of the Primary State of Cascade Damage Processes, *Russian Journal of Non-Ferrous Metals* 62(5) (2021) 561-567.
- [24] Qadr, H. M., Hamad, A. M., MECHANICAL PROPERTIES OF FERRITIC MARTENSITIC STEELS: A REVIEW, Scientific Bulletin of 'Valahia' University, *Materials & Mechanics*, 17(16) (2019).
- [25] Susoy, G., Guclu, E. A., Kilicoglu, O., Kamislioglu, M., Al-Buriahi, M., Abuzaid, M., Tekin, H., The impact of Cr₂O₃ additive on nuclear radiation shielding properties of LiF-SrO-B₂O₃ glass system, *Materials Chemistry and Physics* 242 (2020) 122481.
- [26] Kurudirek, M., Kurucu, Y., Investigation of some nuclear engineering materials in terms of gamma ray buildup factors at experimental energies used in nuclear physics experiments, *Radiation Effects and Defects in Solids* (2020) 1-17.
- [27] Manić, V., Manić, G., Nikezić, D., Krstić, D., Effect of Buildup Factors on Indoor Gamma Dose Rate, *Radiation Protection Dosimetry* (2020).
- [28] Sriwongsa, K., Coconut dust gypsums board for shielding radiation and buildup factors building material, *Walailak Journal of Science and Technology (WJST)* (2020).
- [29] Akman, F., Enez, B., Fincan, S. A., Akdemir, F., Geçibesler, I., Investigation of some radiation interaction parameters for bacteria isolated from the soil in the low energy region, *Canadian Journal of Physics*, 98(3) (2020) 251-259.
- [30] Alim, B., A comprehensive study on radiation shielding characteristics of Tin-Silver, Manganin-R, Hastelloy-B, Hastelloy-X and Dilver-P alloys, *Applied Physics A*, 126(4) (2020) 1-19.
- [31] Akkaş, A., Determination of the tenth and half value layer thickness of concretes with different densities, *Acta Physica Polonica, A* 129(4) (2016) 770-772.
- [32] Qadr, H. M., Calculation of gamma-ray attenuation parameters for aluminium, iron, zirconium and tungsten, *Problems of Atomic Science and Technology, Ser. Thermonuclear Fusion*, 43(2) (2020) 25-30.
- [33] Jubair, S., Calculation of the Buildup Factors for Ceramic Materials, *Iraqi Journal of Applied Physics*, 7(1) (2011) 23-26.
- [34] Qadr, H. M., Calculation for gamma ray buildup factor for aluminium, graphite and lead, *International Journal of Nuclear Energy Science and Technology*, 13(1) (2019) 61-69.
- [35] Hubbell, J. H., Seltzer, S. M., Tables of X-ray mass attenuation coefficients and mass energy-absorption coefficients 1 keV to 20 MeV for elements Z= 1 to 92 and 48 additional substances of dosimetric interest, National Inst. of Standards and Technology-PL, Gaithersburg, MD (United ..., 1995).
- [36] Hubbell, J., Photon cross sections, attenuation coefficients and energy absorption coefficients, National Bureau of Standards Report NSRDS-NBS29, Washington DC (1969).

Chemical and Radiological Characterizations of the Desert Dust Coming from Northern Africa to Batman (Southeastern Turkey)

Ümit Işık^{1,a,*}, Uğur Çevik^{2,b}, Dicle Bal Akkoca^{3,c}, Kahraman Oğuz^{4,d}, Nevzat Damla^e

¹Batman Provincial Disaster and Emergency Directorate, Batman, Türkiye.

²Department of Physics, Faculty of Science, Karadeniz Technical University, Trabzon, Türkiye.

³Department of Geological Engineering, Faculty of Engineering, Fırat University, Elazığ, Türkiye.

⁴Turkish State Meteorological Service, Ankara / Türkiye.

*Corresponding author

Research Article

ABSTRACT

This work investigates the chemical and radiological characterizations of the dust coming from Sahara in North Africa to Batman city in the southeastern region of Turkey on 20 May 2017. According to meteorological maps, the source region of the dust storm that took place in Batman was found to be Libya, which is supported by the NOAA HYSPLIT model's back trajectory analysis. XRD analyses show that the common minerals of the dust samples are quartz, feldspars, calcite, dolomite, hematite and rutile. Chemical patterns of some major, minor and trace elements in dust samples are generally consistent with those of Saharan Dust composition. The heavy metals in the dust follow the decreasing concentration order: Mn > Zn > Cr > Ni > Cu > Pb. The enrichment factors (EF) of these elements show anthropogenic contamination effects with regard to Zn, Cr and S elements in dust samples. The corresponding values of the radionuclides, the absorbed dose rates in the air and the annual effective doses in the samples were also evaluated and compared to the internationally recommended values. The findings are supposed to be beneficial for tracking and evaluating any environmental pollution inventory in this area.

Keywords: Dust, Chemical analysis, Radioactivity, Enrichment factor, Trajectory analysis.

History

Received: 02/01/2022

Accepted: 08/08/2022

Copyright



©2022 Faculty of Science,
Sivas Cumhuriyet University

^aumit.isik@afad.gov.tr

^bdbal@firat.edu.tr

^enevzatdamla@hotmail.com

^{1d} <https://orcid.org/0000-0003-2889-2832>

^{1d} <https://orcid.org/0000-0002-6567-7739>

^{1d} <https://orcid.org/0000-0003-1253-597X>

^{1d} ugurc@ktu.edu.tr

^{1d} koguz@mgm.gov.tr

^{1d} <https://orcid.org/0000-0002-9797-0294>

^{1d} <https://orcid.org/0000-0001-5305-6145>

Introduction

Dust storms are important source of dispersal of suspended dust. Mineral-containing dusts are the most common type of aerosol having a wide range of effects on human health [1]. The Sahara Desert (North Africa) is the most important source of mineral dust-containing aerosols in the world [2]. The Saharan Desert is a 9.000.000 km² desert located in the north of Africa, separating the middle and the north of the continent (Figure 1).

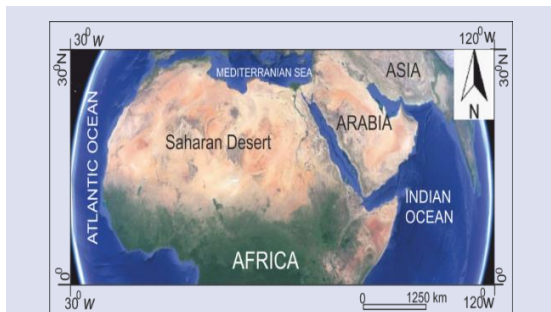


Figure 1. The Location of Sahara Desert.

Turkey faces dust events originating from the African desert frequently. Every year, dust from the neighbouring and even far away countries comes to Turkey at certain

periods. Especially in spring in March, April, May. On an annual average, 20 million tons of dust as wet or dry precipitate in our country either wet or dry. This red sand is thought to have emerged as a result of the erosion in the Great Sahara, Arabia, Iran and Syria around Turkey. The transported desert dust from different countries has significant effects on both human health and the flourishing parts of plants such as branches, leaves and flowers. The transport of dust aerosols from deserts (such as Sahara, Arabia) and semi-arid areas into and around Turkey is of great importance in terms of climate, land and marine ecosystems, and human activities and health. The main reason for dust transport is stated to be drought and desertification.

Dust storms are generally occur in dry and arid areas. Dust particles transfer into the atmosphere due to vertical winds; and through these winds, they can be transported thousands of kilometers away. Most of these mineral-containing dusts cause a great deal of damage to the environment and human health. On the other hand, these dusts cause a decrease in soil fertility and harm plants. These dust storms have an impact on human health because fine dust particles reach the airways and lungs, increasing the risk of chronic respiratory and lung diseases [3-5].

The effect of the Saharan dust storms on chemistry has been observed in the literature [6, 7-8]. In the literature, the dust has also been investigated for its radioactive content, which may effect human health [9]. However, Earth's radiation balance, which comes from the Saharan dust storms has been difficult to assess, due to limited observations from the surface in literature. No attempt about chemistry and radiological characterizations has been made yet to deal with dust storms in Turkey. In this study, the first observations were presented about the effect of a major dust storm having occurred on 20 May 2017 on the chemistry and radiation balance in Batman city (southeastern Turkey) (Figure 2). This study aims to provide information about the origins, the behaviors and the distributions of chemical and radiological

characterizations in dust samples, which can be useful for epidemiological, geological and environmental management studies. In addition, soil samples from the same region were analyzed for comparison purposes.

Materials and Methods

The dust samples were collected from different locations on the roofs of the houses from the urban area of Batman (Figure 2). X-ray diffraction (XRD) analyses of three dust samples were carried out with Rigaku D/Max-III C X-ray diffractometer. The Cu K α radiation over the range was 10°–70°.

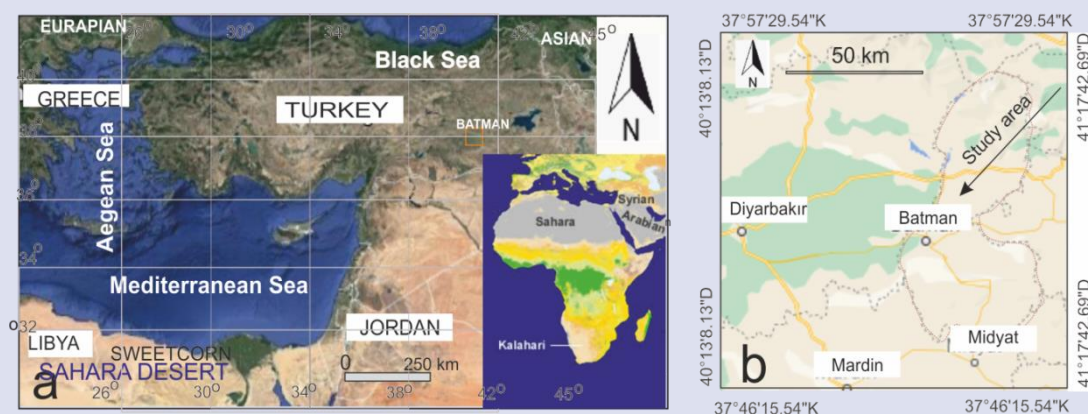


Figure 2. a) The location of the study area in Turkey. b) Sampled Batman city.

Five dust samples were made ready in pressed pellet forms for energy-dispersive x-ray fluorescence (EDXRF) analysis (Epsilon 5, PANalytical, Almelo, The Netherlands). The powder was dried at 105 °C for 4 hours. The dried pellets, which had a diameter of 40 mm and a uniform mass of 400 ± 2 mg, were prepared.

The soil samples were collected from the locations close to where the dust samples were taken. The samples were powdered and dried for a full day at 110 °C so that the moisture they had could be removed and a uniform weight could be attained. Approximately 160 g of sample was transferred in gas-tight plastic polyethylene containers. Afterward, the containers were fully sealed for 28 days to attain a secular equilibrium between ^{226}Ra and ^{222}Rn with their daughter nuclei.

The activities of ^{238}U , ^{232}Th , ^{40}K and ^{137}Cs in the samples were employed utilizing a coaxial germanium detector (HPGe) supplied by Canberra, USA. The energy resolution was 1.9 keV for 1332 keV gamma-ray peaks of ^{60}Co with a relative efficiency of 15%. The detector was shielded in a 10 cm lead shield to lessen the background radiation and was concentric with a thin layer of copper. An empty container was counted in the same manner and geometry as the samples in order to determine the background distribution around the detector. The background spectra were utilized so as to correct the net peak area of the gamma rays of the measured natural radionuclides [10,

11-12]. The calibrations of the detector were described in detail in earlier works [13-14].

The activities of ^{238}U and ^{232}Th were determined using the characteristic γ -lines of 351.9 keV from ^{214}Pb and 609.3 keV from ^{214}Bi and γ -lines of 583.1 keV from ^{208}Tl and 911.1 keV from ^{228}Ac , respectively. The contents of ^{40}K and ^{137}Cs were estimated via its characteristic gamma-ray emission line at 1460.8 keV and 661.6 keV, respectively.

The activity concentration of radionuclides in the sample units in Becquerel per kilograms (Bq.kg $^{-1}$) were calculated by the Equation below;

$$A=C/(\epsilon \times P \times W \times t) \quad (1)$$

where A is the activity of a radionuclide, C is the net count of a peak at energy E, ϵ is the measured photo-peak efficiency, P is the probability of the gamma-ray line in a radionuclide, W is the weight of the sample in kilograms and t is the counting live time

Results and Discussion

Meteorological Conditions and Trajectory Analysis

Meteorological conditions on the Mediterranean Basin and surrounding continents vary seasonally and often cause the transport of air masses through different

regions. The Mediterranean region is known as the region where cyclonic activities occur frequently all year round. Figure 3 presents 850 Mb geopotential height maps to demonstrate atmospheric circulation in the region and the transport of the air mass between 17-20 May 2017. The meteorological condition, which caused dust transport to Turkey, is associated with a deep low-pressure center located between the northeast of Libya and the southwest of Turkey on 17 and 18 May 2017. This

low-pressure center moved towards the interior of Turkey on 19 May 2017 and reached northeast of Turkey on 20 May 2017. The high-pressure center located over Algeria and Libya on 19 May 2017 deepened on 20 May 2017. The transport of the air mass takes place from the high-pressure center to the low-pressure center. In this case, the transport of the air mass containing dust was carried out from Libya to Turkey.

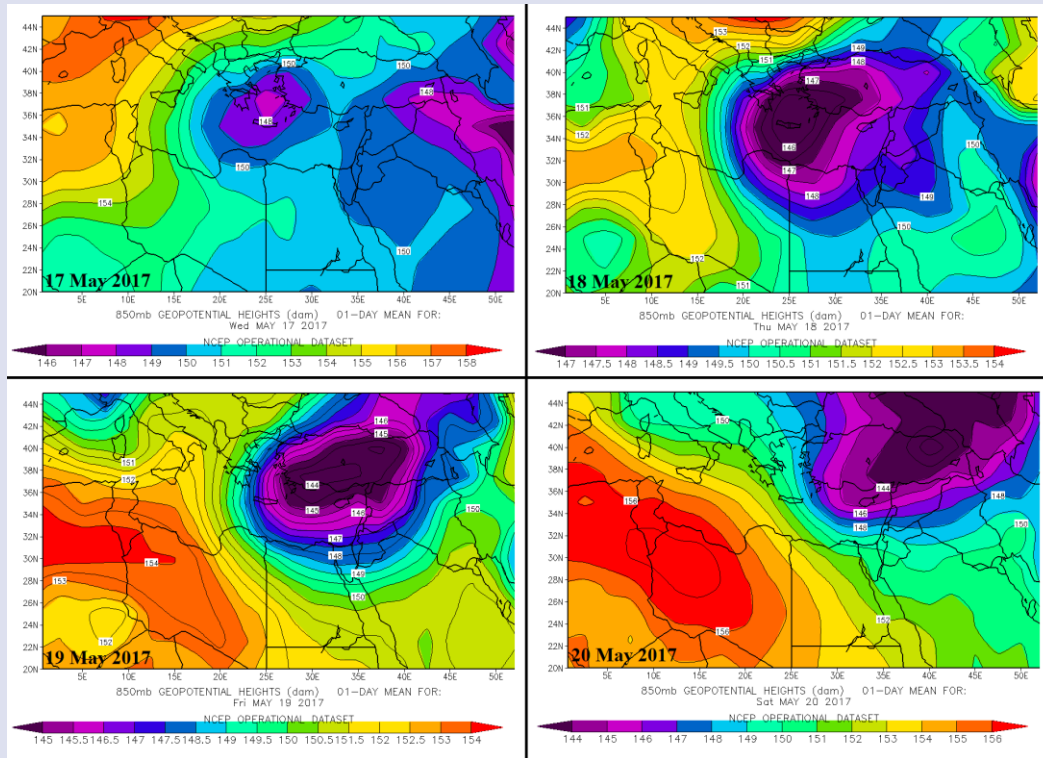


Figure 3. Atmospheric circulation in the lower (850 hPa geopotential height) troposphere on 17-20 May 2017.

To examine this movement in detail, The Hybrid Single-Particle Lagrangian Integrated Trajectory (HYSPLIT) model of NOAA was examined. HYSPLIT model is one of the models that is used to determine trajectories of air masses. To determine the source region of air masses reaching to Batman province (37.55 N and 41.05 E coordinates), back trajectory analysis was performed with the HYSPLIT model. HYSPLIT model was run for 96 hours duration at 12 UTC on 20 May 2017 at 10 m level (Figure 4). The red line on the map shows the source and trajectory of the air mass reaching Batman. It is clear that the source of air mass coming to Batman province is from the northern region of Libya. The air mass passed Syria and then reached the province of Batman.

Mineralogical and chemical composition of the samples

The whole-rock X-ray diffraction patterns (XRD) of D1, D5 and D9 dust samples are shown in Figure 5. In whole-rock XRD analysis, clay 4.47 Å ($2\theta = 19^\circ$), quartz 3.34 Å ($2\theta = 26^\circ$), feldspar 3.20 Å ($2\theta = 28^\circ$), dolomite 2.90 Å ($2\theta = 31^\circ$), calcite 3.03 Å ($2\theta = 30^\circ$), hematite 3.66 Å ($2\theta = 24^\circ$), rutile 3.25 Å ($2\theta = 28^\circ$) main peaks were identified (Figure 5 a-b-c). Results of XRD analysis revealed that almost all minerals observed in the samples were of feldspars, quartz, dolomite, calcite, hematite and rutile in dust samples (Figure 5). Scheuven et al. (2013) [15], Formenti et al. (2011) [16], Journet et al. (2014) [17] stated that quartz, feldspars, calcite, dolomite, hematite and rutile minerals are common to all northern African dust source areas.

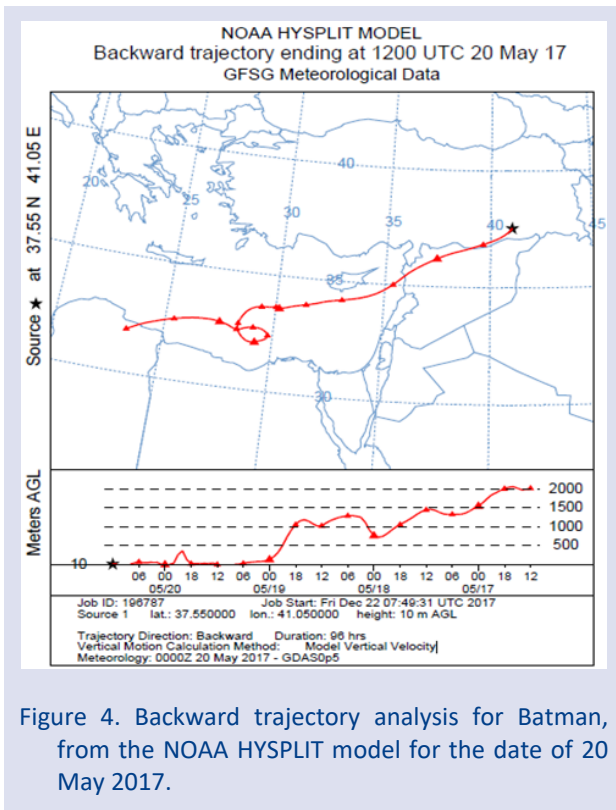


Figure 4. Backward trajectory analysis for Batman, from the NOAA HYSPLIT model for the date of 20 May 2017.

The chemical compositions of the dust samples are shown in Table 1. Silicon and aluminum are dominant in the dust samples. Average data of the desert dust from Sahara by Rodrigues-Navarro are included as a reference. The concentrations of Si, Fe, Mg, K, Ti and P, V, Mn, Zn, Cr, Ni, Pb are similar in the dust samples and Sahara dust (Table 1, Figure 6). Ca and Al have higher content in dust samples than Saharan dust, which shows higher calcite and clay contents in the investigated dust samples. Results of XRD analysis revealed that there were important amount of calcite minerals in the dust samples (Figure 5). Ca values are very high in dust samples. Scheuven et al. (2013) [15] suggested that the (Ca+Mg)/Fe ratios are between 4.29 and 8.40. This ratio is between 3.25 and 4.77, very close to this ratio in dust samples, which is consistent with north-eastern Africa (Egypt, Libya).

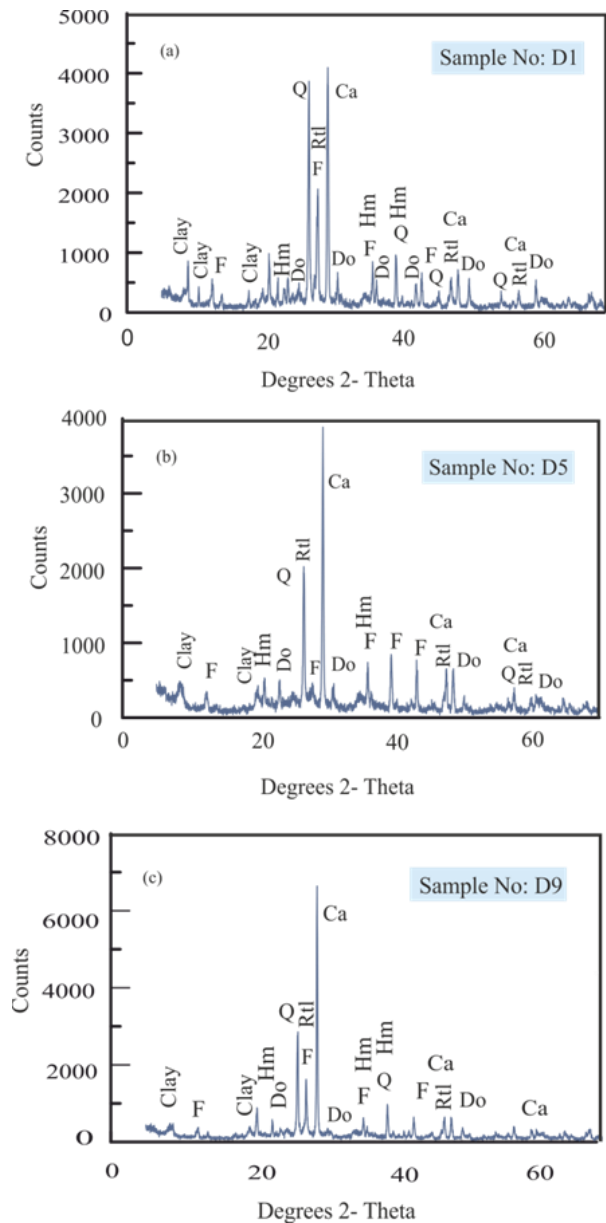


Figure 5. XRD analysis of (a) D1 (b) D5 (c) D9 dust samples showing the presence of quartz (Q), feldspar (F), calcite (Ca), dolomite (Do), rutile (Rtl), and hematite (Hm). The general reflection of clay minerals (Clay) at 4.49 Å is shown.

Table 1. The chemical composition of the dust samples S.Dust: Sahara Dust, from Rodrigues-Navarro et al. (XRF determination, only * ICP determination).

	D1	D3	D5	D7	D9	Max	Min	Average	St Dev.	S.Dust	
Major/Minor Elements (%)	Si	24.11	24	23.78	24.26	23.87	24.26	23.78	24	0.19	24.05
	Al	17.01	11.04	11.41	11.4	10.93	17.01	10.93	12.36	2.61	6.62
	Fe	3.27	3.4	4.78	3.19	3.46	4.78	3.19	3.62	0.66	3.69
	Mg	1.23	1.23	2.06	1.25	1.22	2.06	1.22	1.4	0.37	1.24
	Ca	12.18	12.22	17.04	11.77	12.66	17.04	11.77	13.17	2.18	5.72
	K	1.78	1.83	2.11	1.76	1.84	2.11	1.76	1.86	0.14	1.53
	Ti	0.60	0.61	0.58	0.6	0.64	0.64	0.58	0.61	0.02	0.45
	(Ca+Mg)/Fe	3.35	3.36	4.77	3.25	3.47	3.25	4.77	3.46	0.63	1.74
Minor/Trace Elements (ppm)	P	0.06	2.29	0.06	0.1	0.07	2.29	0.06	0.52	0.99	0.04
	Ba	338	293.39	472.53	302.01	313.48	472.53	293.39	343.88	73.84	529*
	Sr	337	350.93	313.58	322.79	372.35	372.35	313.58	339.33	23.28	162
	V	136.33	167.77	128.5	130.76	140.79	167.77	128.5	140.83	15.81	103*
	Mn	556	582.98	539.36	540.65	597.13	597.13	539.36	563.22	25.84	400
	Zn	343.87	116.67	110.29	117.03	206.97	343.87	110.29	178.97	100.51	367
	Cr	165.85	167.77	158.09	154.75	184.63	184.63	154.75	166.22	11.61	78
	Ni	91.43	93.51	90.52	83.76	108.31	108.31	83.76	93.5	9.05	51
	Cu	40.38	40.31	34.54	38.38	54.48	54.48	34.54	41.618	7.57	...
	Pb	25.8	23.31	35.4	25.16	26.29	35.4	23.31	27.19	4.73	27*
	S	2915	3574	2931.73	1907.63	2759.04	3574	1907.63	2817.48	597.1	390

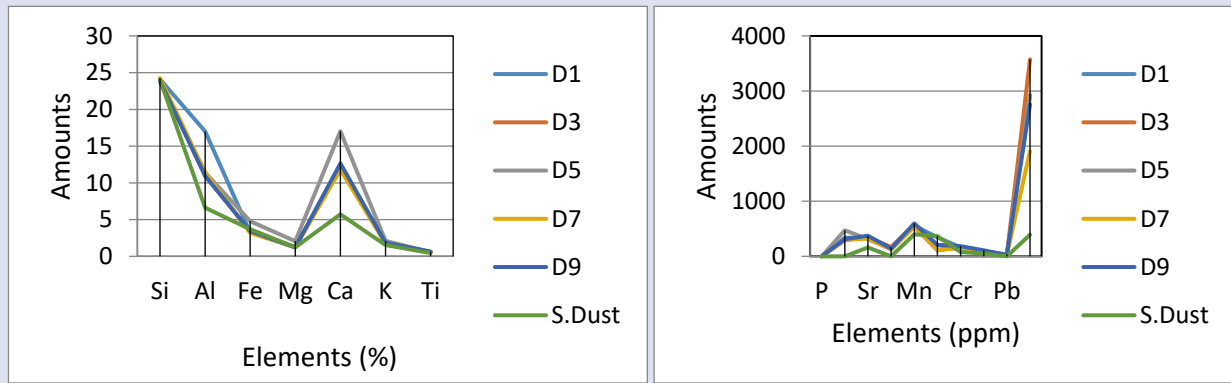


Figure 6. Element distributions relative to Sahara Dust (S.Dust) composition (data from Rodrigues Navarro) for dust samples.

Desert dust and its effects on human health have been studied in the recent years. Dust with anthropogenic pollution occurs with condensation of organic and inorganic compounds, particle-phase reactions [18]. Enrichment factor functions in its assessment and heavy metal is also very frequent in its anthropogenic contribution whose value is used. In order to decide whether heavy metals are of natural or anthropogenic origin, normalized enrichment factor (EF) is commonly used [19]. The EF is defined by Equation (2):

$$EF = \frac{\frac{C_n(\text{sample})}{C_{ref}(\text{sample})}}{\frac{B_n(\text{background})}{B_{ref}(\text{background})}} \quad (2)$$

where EF is the enrichment factor, C_n (sample) is the element content of soil sample, C_{ref} (sample) is the concentration of element in soil sample taken as reference, B_n (background) is the background value of the same element in the earth crust and B_{ref} (background) is the background value of reference element for normalization in the earth crust.

In normalization geochemical such as iron, zircon and titanium inactive elements are used. In this study, the normalization process is calculated according to Fe (Table 2). EF values of $0.5 \leq EF \leq 1.5$ indicate that the element is of lithogenic origin, whereas $EF > 1.5$ indicates there is an enrichment in the environment. $EF = 1.5-3$ is minor enrichment; $EF = 3-5$ is moderate enrichment; $5-10$ is moderately severe enrichment; $10-25$ is severe enrichment; $25-50$ is very severe enrichment; and $EF > 50$ is extremely severe enrichment. EF values do not suggest an anthropogenic effect for Cu and Mn in desert samples, however, Ni and Cr show minor, S shows moderate and Pb and Zn show highly anthropogenic effects. These results demonstrate that the rapid, intense dust advection during the incident led to a great deal of contamination of the environment. In fact, Schaule and Patterson (1981) [20] and Lyamani et al., (2005) [21], and Sholkovitz et al., (2009) [22] suggested an anthropogenic combustion of lead and Ni in Saharan soils. Garrison et al. (2014) [23] reported that in the African dust, great majority of enriched metals/metalloids could be emitted from biomass burning, oil combustion, mining activities and vehicle traffic.

Table 2. The enrichment factors (EF) for heavy metals for dust samples.

Samples	Mn	Ni	Cu	Zn	Cr	Pb	S
D1	0.89	1.86	1.12	7.51	2.52	7.89	4.68
D3	0.90	1.83	1.08	2.45	2.47	6.86	5.52
D5	0.59	1.26	0.66	1.65	1.65	7.41	3.22
D7	0.89	1.75	1.09	2.62	2.43	7.89	3.14
D9	0.91	2.09	1.43	4.27	2.67	7.60	4.18
Average	0.84	1.76	1.08	3.70	2.35	7.53	4.15
St Dev.	0.14	0.30	0.28	2.33	0.40	0.43	1.00

Radiological Characterization of the Dust Samples

The activities of ^{40}K , ^{137}Cs , ^{238}U and ^{232}Th were estimated to be 375, below detection limit (BDL), 72 and 17 Bq.kg^{-1} , respectively in the soil sample and 240, 9, 84 and 10 Bq.kg^{-1} respectively in the dust sample. The absorbed dose rate in the air (D) depends on the activities

of these radionuclides in the samples. D was computed in units of nano gray per hour (nGy.h^{-1}) utilizing Equation (3) [24]:

$$D = 0.462x A_U + 0.621x A_{Th} + 0.0417x A_K \quad (3)$$

where A_K , A_{Th} and A_U are the activities of ^{40}K , ^{232}Th and ^{238}U (in $Bq.kg^{-1}$), respectively. The calculated absorbed dose rates in the air were found to be $59 nGy.h^{-1}$ for soil sample and $55 nGy.h^{-1}$ for dust sample, respectively, which is lower than the world mean ($60 nGy.h^{-1}$). In order to assess the annual effective dose rate (AEDR); the conversion coefficient 0.7 sievert per gray ($Sv.Gy^{-1}$) from the absorbed dose in the air to the effective dose and the outdoor occupancy factor (0.2) recommended by UNSCEAR was utilized [24]. Accordingly, AEDR was computed in units of mili sievert per year ($mSv.y^{-1}$) utilizing Equation (4):

$$AEDR = D \times T \times F \quad (4)$$

where D is the computed dose rate (in $nGy.h^{-1}$), T is the outdoor occupancy time ($0.2 \times 24 h \times 365.25 d = 1753.2 h.y^{-1}$), and F is the conversion factor ($0.7 \times 10^{-6} Sv.Gy^{-1}$). The computed value of the annual effective dose is $0.073 mSv.y^{-1}$ in the soil sample and it is $0.068 mSv.y^{-1}$ in the dust sample. These values are compatible with the world mean of $0.070 mSv.y^{-1}$ [24].

Conclusions

In this study, the dust storm occurred on 20 May 2017 in Batman city was investigated in terms of mineralogical, chemical and radiological characterizations. The results were assessed for compliance with the international values. Meteorological maps showed that there was a high-pressure center over Algeria and Libya, but a low-pressure center over Turkey on 20 May 2017. Therefore, dust transportation occurred from Libya towards Turkey. XRD analysis showed that quartz, feldspars, calcite, dolomite, hematite and rutile minerals were present in dust samples. Si, Fe, Mg, K, Ti and P, V, Mn, Zn, Cr, Ni, Pb contents are similar in the investigated samples and Sahara dust. The computed value of the annual effective dose rate is in line with the world mean content. The results are anticipated to contribute to the improvement of monitoring of the environment and estimations of today's climate models related to the dust impact on climate.

Acknowledgment

The authors would courteously like to appreciate the contributions of experienced English lecturer of Batman University, Ihsan Pilatin, for editing the manuscript from the beginning till the end.

Conflicts of interest

There are no conflicts of interest in this work.

References

- [1] De Longueville Florence, Ozer P., Doumbia S., Henry S., Desert Dust Impacts on Human Health: An Alarming Worldwide Reality and a Need for Studies in West Africa, *Int J Biometeorol.*, 57(1) (2013)1–19.
- [2] Kim Hyun-Sun, Kim Dong-Sik, Kim Ho, Yi Seung-Muk., Relationship between mortality and fine particles during Asian dust, smog–Asian dust, and smog days in Korea, *Int J Environ Health Res.*, 22(6) (2012) 518–530.
- [3] Chung Yong-Seung, Yoon Ma-Beong., On the occurrence of yellow sand and atmospheric loadings, *Atmos. Environ.*, 30(13) (1996) 2387–2397.
- [4] Goudie A.S., Middleton N. J., Saharan dust storms: nature and consequences, *Earth. Sci. Rev.*, 56 (1-4) (2001) 179–204.
- [5] Ababneh Z.Q., Ababneh A.M., Alsaqabi S., Almasoud F.I., A study of the radioactivity in the dust storm event of April 2015 in Arabian Peninsula, *Radiat. Prot. Dosim.*, 179 (2) (2018) 108-118.
- [6] Avila A., Queralt-Mitjans I., Alarcón M., Mineralogical composition of African dust delivered by red rains over northeastern Spain, *J Geophys Res.*, 102 (D18) (1997) 21977-21996.
- [7] Guieu C., Loÿe-Pilot M.D., Ridame C., Thomas C., Chemical characterization of the Saharan dust end-member: Some biogeochemical implications for the western Mediterranean Sea, *J. Geophys. Res.*, 107(D15) (2002) 4258-4268.
- [8] Morales-Baquero R., Pulido-Villena E., Reche I, Atmospheric inputs of phosphorus and nitrogen to the southwest Mediterranean region: Biogeochemical responses of high mountain lakes, *Limnol. Oceanogr.*, 51(2) (2006) 830–837.
- [9] Abdallah M.J, Eyadeh M.M., Hamadneh H.H., Akour A.N., Hawamdeh M. M., Almaaitah I. F., Radiological Characterization of Settled Dust during a Severe Dust Episode in Jordan, *Jordan Journal of Physics.*, 12 (2) (2019) 183-189.
- [10] Damla N., Cevik U., Kobya A. I., Celik A., Van Grieken R., Kobya Y., Radiological characterization of gas concrete used in building materials in Turkey, *J. Hazard. Mater.* 168 (2009) 681-687.
- [11] Isik U., Damla N., Bal Akkoca D., Cevik U., Mineralogical, geochemical and radiological characterisation of Selmo Formation in Batman area, Turkey, *Isot Environ Health Stud.*, 48(2) (2012) 302–312.
- [12] Radulescu I., Blebea-Apostu A.M., Margineanu R.M., Mocanu N., Background radiation reduction for a high-resolution gamma-ray spectrometer used for environmental radioactivity measurements, *Nucl. Instrum. Methods. Phys. Res A.*, 715(2013)112–118.
- [13] Damla N., Cevik U., Kobya A.I., Ataksor B., Isik U., Assessment of environmental radioactivity for Batman, Turkey, *Environ. Monit. Assess.*, 160 (1-4) (2010) 401-412.
- [14] Damla N., Aldemir K., Radon survey and soil gamma doses in primary schools of Batman, Turkey, *Isot Environ Health Stud.*, 50 (2) (2014) 226-234.
- [15] Scheuvens D., Schütz L., Kandler K., Ebert M., Weinbruch S., Bulk composition of northern African dust and its source sediments – A compilation, *Earth, Sci. Rev.*, 116 (2013) 170–194.
- [16] Formenti P., Schütz L., Balkanski Y., Desboeufs K., Ebert M., Kandler K., Petzold A., Scheuvens D., Weinbruch S., Zhang D., Recent progress in understanding physical and chemical properties of African and Asian mineral dust, *Atmos. Chem. Phys.*, 11(16) (2011) 8231–8256.
- [17] Journet E., Balkanski Y., Harrison S. P., A new data set of soil mineralogy for dust-cycle modelling, *Atmos. Chem. Phys.*, 14 (8) (2014) 3801–3816.

- [18] Zhang X., Zhao L., Tong D. Q., Wu G., Dan M., Teng B., A systematic review of global desert dust and associated human health effects, *Atmosphere.*, 7(12) (2016) 158.
- [19] Hornung H., Krom M.D., Cohen Y., Trace metal distribution on sediments and benthic fauna of Haifa Bay, Israel, *Estuar Coast Shelf Sci.*, 29(1) (1989) 43-56.
- [20] Schaule B. K., Patterson C. C., Lead concentrations in the northeast Pacific: Evidence for global anthropogenic perturbations., *Earth Planet. Sci. Lett.*, 54(1) (1981) 97 – 116.
- [21] Lyamani H., Olmo F.J, Alados-Arboledas L., Saharan dust outbreak over southeastern Spain as detected by sunphotometer, *Atmos. Environ.*, 39(38) (2005) 7276- 7284.
- [22] Sholkovitz E. R., Sedwick P. N., Church T.M., Influence of anthropogenic combustion emissions on the atmospheric deposition of soluble aerosol iron to the oceans: Empirical estimates for island sites in the North Atlantic, *Geochim. Cosmochim. Acta.*, 73(14) (2009) 3981-4003.
- [23] Garrison V.H., Majewski M. S., Konde L., Wolf R. E., Otto R. D., Tsuneoka Y., Inhalable desert dust, urban emissions, and potentially biotoxic metals in urban Saharan-Saharan air, *Sci. Total Environ.*, 500-501 (2014) 383-394.
- [24] UNSCEAR. Sources and effects of ionizing radiation. New York: *United Nations Scientific Committee on the Effects of Atomic Radiation*; 2000.

A new Lifetime Distribution Based on the Transmuted First Two Lower Records

Tenzile Erbayram^{1,a,*}, Ümmügülsüm Yıldırım^{1,b}, Yunus Akdoğan^{1,c}

¹ Department of Statistics, Faculty of Science, Selçuk University, Konya, Türkiye

*Corresponding author

Research Article

History

Received: 28/03/2022

Accepted: 16/06/2022

Copyright



©2022 Faculty of Science,
Sivas Cumhuriyet University

ABSTRACT

This article introduces a new lifetime distribution by merging the first two lower records based on exponential distribution and discusses the different features of the distribution. Statistical inferences about the distribution parameters are discussed with three estimation methods, namely maximum likelihood, least squares, and weighted least squares. Monte Carlo simulation study is performed to evaluate of these estimators based on mean square errors estimation, mean absolute deviation, and mean relative errors of estimation for a sample of different sizes. A distribution simulation analysis based on real data is provided to demonstrate the adaptability of the proposed model.

Keywords: Lower record value, Lifetime distribution, Monte Carlo simulation, Estimation.

^a tenzile.erbayram@selcuk.edu.tr
^c yakdogan@selcuk.edu.tr

^b <https://orcid.org/0000-0002-3275-120X>
^d <https://orcid.org/0000-0003-3520-7493>

^e acargulsum466@gmail.com ^f <https://orcid.org/0000-0001-6780-6373>

Introduction

Over the past two decades, many discrete and continuous statistical distributions have been introduced into the literature. These distributions are saved as members of a distribution family. Some distribution families in the literature can be ordered as follows: Azzalini [1] obtained the skew normal distribution, Mudholkar and Srivastava [2] described exponential distribution family, Marshall and Olkin [3] proposed a new family of continuous distribution, namely the Marshall and Olkin family. Eugene et al. [4] proposed another family of distribution titled beta-generated family. Recently, Mahdavi and Kundu [5] introduced a new family titled α -power transformation (APT) and Karakaya et. al. [6] obtained alpha logarithmic transformation (ALT) family.

An example of a distribution family is transmuted families. Generally, transmuted families are reported based on order statistics. Transformed distributions were introduced by Shaw and Buckley [7,8] using a quadratic transformation. The order statistics of the transformed distributions can be sorted as [9,10]. Recently, Balakrishnan [11] proposed a new family of transformed distributions based on datasets. Tanış and Saraçoğlu [12] studied a special model based on the Weibull distribution of a family of transformed record-based distributions. Both in terms of distribution properties and statistical inference parallel to the study [11]. Tanış et al. [13], introduced a transmutation lower record type and suggested a sub-model for Fréchet distribution, moreover Tanış [14], suggested transmutation lower record type

inverse Rayleigh and Tanış [15], suggested transmutation lower record type power function distribution.

Let $X_{L(1)}$ and $X_{L(2)}$ be the first two lower record values from a population with cumulative distribution function (cdf) $F(x)$.

$$\begin{aligned} G(x) &= pP(X_{L(1)} \leq x) + (1-p)P(X_{L(2)} \leq x) \\ &= pF(x) + (1-p)[F(x)(1 - \log(F(x)))] \\ &= F(x)[1 - p \log(F(x))] \end{aligned} \quad (1)$$

The distribution family with cdf in Equation (1) is called transmuted lower record type (TLRT) and using TLRT, the probability density function (pdf) of distribution is given by

$$g(x) = f(x)[1 - p(1 + \log(F(x)))]. \quad (2)$$

In this paper, we obtained the TLRT version of the exponential distribution in Section 2. In Section 3, the unknown parameters are estimated by estimation methods. A simulation study is performed in order to compare the performance of these estimators in terms of mean squared errors (MSEs), mean absolute deviations (ABBs) and mean relative errors estimates (MREs). Two applications with real data are made to show the applicability of introduced distribution.

Transmuted Lower Record Type Exponential Distribution

Let X be a random variable having exponential distribution. The cdf and pdf of X as follows,

$$F(x) = 1 - \exp(-\lambda x), \tag{3}$$

and

$$f(x) = \lambda \exp(-\lambda x) \tag{4}$$

where $\lambda > 0$. Substituting the cdf (3) and pdf (4) into TLRT family the following cdf and pdf are obtained as

$$F(x; \lambda) = (1 - \exp(-\lambda x))(1 - p \log(1 - \exp(-\lambda x))) \tag{5}$$

and

$$f(x; \lambda) = \lambda \exp(-\lambda x) (1 - p \log(1 - \exp(-\lambda x)) - p \lambda \exp(-\lambda x)) \tag{6}$$

where $\lambda > 0, p \in (0,1)$. The distribution with cdf is called TLRT – Exp(p, λ) distribution. Figure 1 presents the plots of the TLRT – Exp(p, λ) pdf for some choices of parameters. From Figure 1, we observe that the probabilities are decreasing when x is increasing.

The mean of the TLRT – Exp(p, λ) distribution is obtained as

$$E(X) = -\frac{6p - 6 + p\pi^2}{6\lambda} \tag{7}$$

The second moment of distribution cannot be obtained. It is a rare distribution whose variance and other moments cannot be obtained due to the non-finite integral solution. The survival function and hazard function TLRT – Exp(p, λ) distribution is given by respectively

$$S(x) = 1 - F(x) = -p(-1 + \exp(-\lambda x)) \log(1 - \exp(-\lambda x)) + \exp(-\lambda x) \tag{8}$$

And

$$h(x) = \frac{f(x)}{S(x)} = \frac{\lambda \exp(-\lambda x) (-1 + p \log(1 - \exp(-\lambda x)) + p)}{p(-1 + \exp(-\lambda x)) \log(1 - \exp(-\lambda x)) - \exp(-\lambda x)} \tag{9}$$

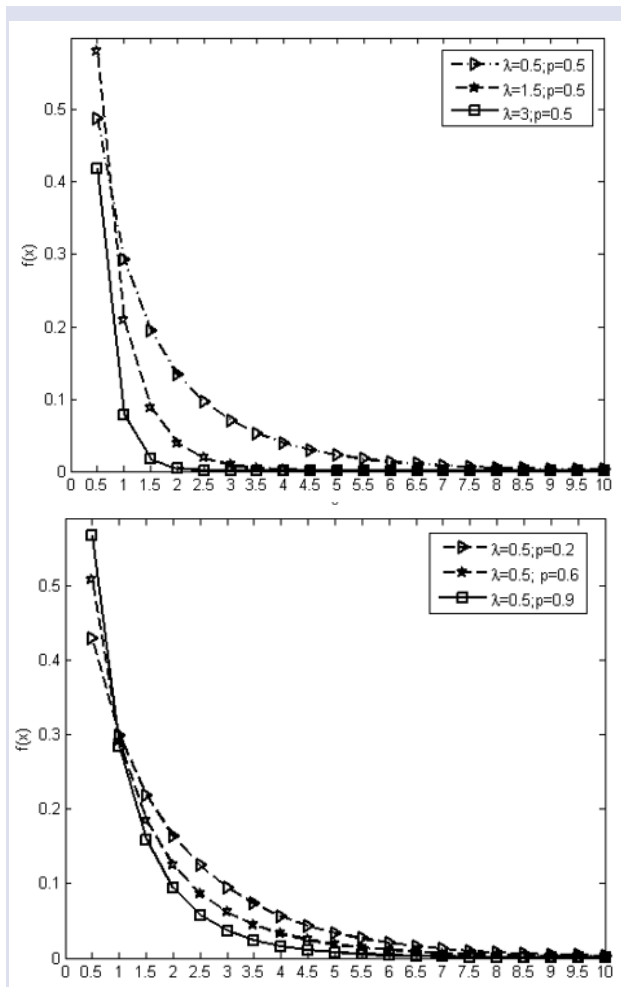


Figure 1. The pdf of TLRT – Exp(p, λ) distribution for some choices of p and λ .

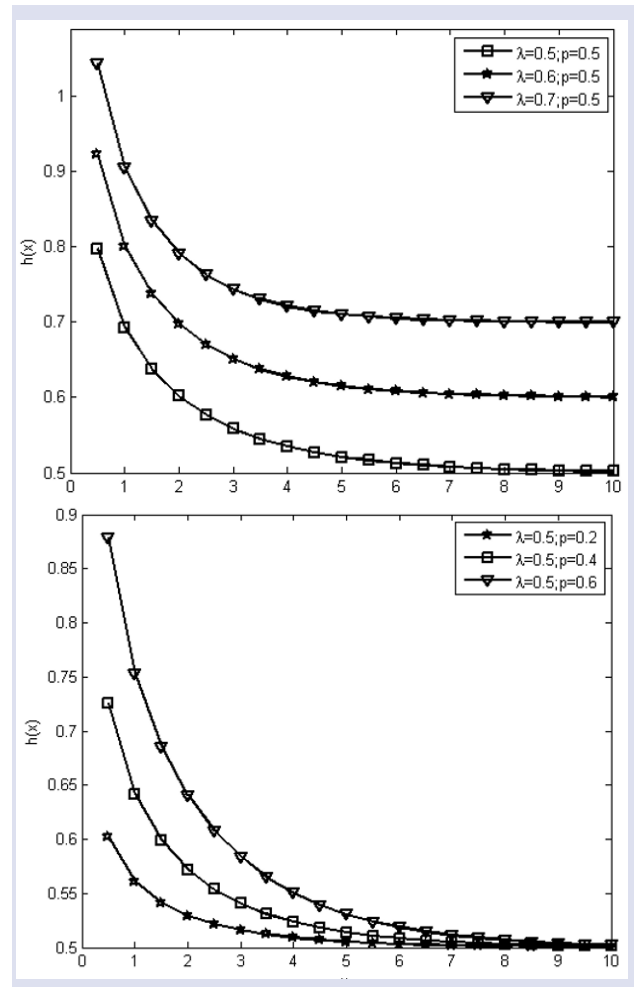


Figure 2. The hf of TLRT – Exp(p, λ) distribution for some choices of p and λ

Estimation

In this section, estimations of TLRT – Exp parameters have been examined using some classical methods.

Method of Maximum Likelihood

Let $x_1; x_2; \dots; x_n$ be the observations of n independent and identically random variable $X_1; X_2; \dots; X_n$ from the TLRT – Exp distribution. Such that, the log likelihood function has the following formula:

$$\ell_n(p, \lambda) = n \log(\lambda) - \lambda \sum_{i=1}^n x_i + \sum_{i=1}^n \log\{1 - p \log(1 - \exp(\lambda x_i)) - p\}. \tag{10}$$

By differentiating Equation (9) with respect to p and λ respectively, and equating to zero, we have

$$\frac{\partial \ell_n(p, \lambda)}{\partial p} = \frac{\log(1 - \exp(-\lambda x_i))}{(-1 + p \log(1 - \exp(-\lambda x_i)))} - 1 = 0 \tag{11}$$

and

$$\frac{\partial \ell_n(p, \lambda)}{\partial \lambda} = \frac{n}{\lambda} - \sum_{i=1}^n x_i - \sum_{i=1}^n \frac{p x_i \exp(-\lambda x_i)}{(1 - \exp(-\lambda x_i))(1 - p \log(1 - \exp(-\lambda x_i)))} = 0 \tag{12}$$

We have the maximum likelihood (ML) estimators of the TLRT – Exp parameters p and λ by maximizing the Equations 10-11. These equations cannot be solved analytically for p and λ . Therefore, they can be obtained by numerical methods. The “optim” command in R is used for this purpose.

Method of least square and weighted least square

Let $x_{1:n}; x_{2:n}; \dots; x_{n:n}$ be the order statistics of a random sample from the TLRT – Exp distribution. Hence, we have the least square (LS) estimators of the TLRT – Exp parameters p and λ by minimizing the following equation:

$$S(p, \lambda) = \sum_{j=1}^n \left[F(x_{j:n}|p, \lambda) - \frac{j}{n+1} \right]^2$$

with respect to p and λ , where $F(\cdot)$ is the cdf in Equation (5). Equivalently, they can be obtained by solving:

$$\sum_{j=1}^n \left[F(x_{j:n}|p, \lambda) \frac{j}{n+1} \right] \eta_1(x_{j:n}|p, \lambda) = 0,$$

$$\sum_{j=1}^n \left[F(x_{j:n}|p, \lambda) \frac{j}{n+1} \right] \eta_2(x_{j:n}|p, \lambda) = 0,$$

where,

$$\eta_1(x_{j:n}|p, \lambda) = \frac{\partial F(x_{j:n})}{\partial p} = (-1 + \exp(\lambda)) \log(1 - \exp(-\lambda))$$

and

$$\eta_2(x_{j:n}|p, \lambda) = \frac{\partial F(x_{j:n})}{\partial \lambda} = -\exp(-\lambda) (-1 + p \log(1 - \exp(-\lambda)) + p)$$

The weighted least square (WLS) estimators, \hat{p}_{WLS} and $\hat{\lambda}_{WLS}$, can be obtained by minimizing

$$W(p, \lambda) = \sum_{j=1}^n \frac{(n+1)^2(n+2)}{j(n-j+1)} \left[F(x_{j:n}|p, \lambda) - \frac{j}{n+1} \right]^2$$

These estimators can also be obtained by solving:

$$\sum_{j=1}^n \frac{(n+1)^2(n+2)}{j(n-j+1)} F \left[(x_{j:n}|p, \lambda) \frac{j}{n+1} \right] \eta_1(x_{j:n}|p, \lambda) = 0$$

And

$$\sum_{j=1}^n \frac{(n+1)^2(n+2)}{j(n-j+1)} F \left[(x_{j:n}|p, \lambda) \frac{j}{n+1} \right] \eta_2(x_{j:n}|p, \lambda) = 0$$

Simulation Study

To obtain information about the performance of estimators, we conducted an appropriate simulation study. The results are given in the Tables 1-6. We calculated the average absolute biases (ABBs), mean square errors (MSEs), and mean relative errors of the estimates (MREs) for all methods. The ABBs, MREs, and MSEs are calculated by

$$\widehat{ABBS}_\varphi = \frac{1}{N} \sum_{i=1}^N |\hat{\varphi}_i - \varphi|$$

$$\widehat{MSES}_\varphi = \frac{1}{N} \sum_{i=1}^N (\hat{\varphi}_i - \varphi)^2$$

And

$$\widehat{MRES}_\varphi = \frac{1}{N} \sum_{i=1}^N |\hat{\varphi}_i - \varphi| / \varphi,$$

where, $\varphi = (p, \lambda)$ and $\hat{\varphi} = (\hat{p}, \hat{\lambda})$. The “optim” BFGS routine in the R program were adopted to generate 5000 trials to estimate these indices of the ML, LS and WLS estimates. The sample sizes are considered as $n = 50, 100, 250, 500$ and two-parameter settings were considered, $(p = 0.5, \lambda = 0.5), (p = 0.5, \lambda = 1.5), (p = 0.5, \lambda = 3), (p = 0.6, \lambda = 1.5), (p = 0.9, \lambda = 1.5)$.

Table 1. The averages of estimates, MSEs, ABBs, and MREs of the TLRT-Exp model for $\lambda = 0.5$ and $p = 0.5$

n		MLE estimate		EKK estimate		WEKK estimate	
		$\hat{\lambda}$	\hat{p}	$\hat{\lambda}$	\hat{p}	$\hat{\lambda}$	\hat{p}
50	Averages	0.5255	0.4511	0.5226	0.5355	0.5191	0.5415
	MSEs	0.0100	0.0356	0.0099	0.0414	0.0096	0.0416
	ABBs	0.0100	0.1887	0.0997	0.2036	0.0979	0.2041
	MREs	0.2000	0.3774	0.1993	0.4072	0.1957	0.4081
100	Averages	0.5144	0.4596	0.5166	0.4763	0.5166	0.4763
	MSEs	0.0081	0.0292	0.0092	0.0400	0.0925	0.0400
	ABBs	0.0899	0.1709	0.0961	0.2000	0.0962	0.2000
	MREs	0.1799	0.3419	0.1922	0.3999	0.1923	0.4000
200	Averages	0.5093	0.4761	0.5075	0.4834	0.5077	0.4832
	MSEs	0.0052	0.0181	0.0074	0.0342	0.0075	0.0344
	ABBs	0.0721	0.1347	0.0865	0.1852	0.0868	0.1854
	MREs	0.1442	0.2694	0.1729	0.3703	0.1736	0.3708
300	Averages	0.5042	0.4862	0.4999	0.4923	0.4998	0.4923
	MSEs	0.0037	0.0130	0.0062	0.0277	0.0062	0.0278
	ABBs	0.0611	0.1140	0.0787	0.1663	0.0788	0.1666
	MREs	0.1221	0.2280	0.1573	0.3326	0.1575	0.3332
500	Averages	0.5018	0.4928	0.4999	0.4977	0.5009	0.4969
	MSEs	0.0023	0.0077	0.0052	0.0180	0.0052	0.0177
	ABBs	0.0480	0.0879	0.0720	0.1341	0.0721	0.1330
	MREs	0.0960	0.1758	0.1441	0.2681	0.1441	0.2660

Table 2. The averages of estimates, MSEs, ABBs, and MREs of the TLRT-Exp model for $\lambda = 1.5$ and $p = 0.5$

n		MLE estimate		EKK estimate		WEKK estimate	
		$\hat{\lambda}$	\hat{p}	$\hat{\lambda}$	\hat{p}	$\hat{\lambda}$	\hat{p}
50	Averages	1.5455	0.4610	1.5613	0.5484	1.5699	0.5375
	MSEs	0.0860	0.0347	0.0889	0.0419	0.0928	0.0419
	ABBs	0.2933	0.1864	0.2982	0.2049	0.3047	0.2048
	MREs	0.1955	0.3728	0.1988	0.4098	0.2031	0.4095
100	Averages	1.5335	0.4733	1.5231	0.5039	1.5190	0.4042
	MSEs	0.0680	0.0260	0.0800	0.0400	0.0810	0.0405
	ABBs	0.2600	0.1611	0.2830	0.2002	0.2840	0.2005
	MREs	0.1733	0.3223	0.1890	0.4004	0.1895	0.4011
200	Averages	1.5364	0.4747	1.5155	0.4879	1.5144	0.4884
	MSEs	0.0460	0.0165	0.0672	0.0350	0.0673	0.0351
	ABBs	0.2145	0.1283	0.2593	0.1871	0.2595	0.1874
	MREs	0.1430	0.2567	0.1729	0.3742	0.1729	0.3747
300	Averages	1.5127	0.4873	1.5052	0.4880	1.5055	0.4879
	MSEs	0.0303	0.0117	0.0581	0.0271	0.0582	0.0271
	ABBs	0.1741	0.1083	0.2412	0.1647	0.2413	0.1647
	MREs	0.1160	0.2165	0.1608	0.3293	0.1608	0.3294
500	Averages	1.5168	0.4871	1.4949	0.4959	1.4950	0.4959
	MSEs	0.0185	0.0071	0.0471	0.0175	0.0471	0.0175
	ABBs	0.1361	0.0847	0.2171	0.1325	0.2171	0.1326
	MREs	0.0907	0.1695	0.1448	0.2650	0.1448	0.2652

Table 3. The averages of estimates, MSEs, ABBs, and MREs of the TLRT-Exp model for $\lambda = 3$ and $p = 0.5$

n		MLE estimate		EKK estimate		WEKK estimate	
		$\hat{\lambda}$	\hat{p}	$\hat{\lambda}$	\hat{p}	$\hat{\lambda}$	\hat{p}
50	Averages	3.0904	0.4595	3.0227	0.6044	3.0384	0.5910
	MSEs	0.3136	0.0321	0.2973	0.0412	0.3022	0.0410
	ABBs	0.5600	0.1793	0.5452	0.2030	0.5497	0.2025
	MREs	0.1867	0.3585	0.1817	0.4059	0.1832	0.4050
100	Averages	3.0425	0.4813	3.0036	0.5246	2.9886	0.5315
	MSEs	0.2503	0.0256	0.2932	0.0395	0.2978	0.0397
	ABBs	0.5003	0.1599	0.5414	0.1987	0.5457	0.1993
	MREs	0.1668	0.3197	0.1805	0.3974	0.1819	0.3986
200	Averages	3.0763	0.4725	3.0461	0.4772	3.0457	0.4773
	MSEs	0.1778	0.0169	0.2580	0.0334	0.2592	0.0336
	ABBs	0.4216	0.1301	0.5079	0.1827	0.5091	0.1834
	MREs	0.1405	0.2602	0.1693	0.3654	0.1697	0.3667
300	Averages	3.0289	0.4874	2.9849	0.5009	2.9848	0.5015
	MSEs	0.1273	0.0124	0.2324	0.0280	0.2331	0.0282
	ABBs	0.3568	0.1112	0.4821	0.1673	0.4828	0.1680
	MREs	0.1189	0.2223	0.1607	0.3346	0.1609	0.3359
500	Averages	3.0083	0.4930	3.0150	0.4917	3.0143	0.4917
	MSEs	0.0794	0.0074	0.1888	0.0167	0.1892	0.0168
	ABBs	0.2818	0.0862	0.4345	0.1294	0.4349	0.1296
	MREs	0.0939	0.1723	0.1448	0.2588	0.1450	0.2592

Table 4. The averages of estimates, MSEs, ABBs, and MREs of the TLRT-Exp model for $\lambda = 1.5$ and $p = 0.2$.

n		MLE estimate		EKK estimate		WEKK estimate	
		$\hat{\lambda}$	\hat{p}	$\hat{\lambda}$	\hat{p}	$\hat{\lambda}$	\hat{p}
50	Averages	1.4239	0.2517	1.3787	0.2944	1.3702	0.2947
	MSEs	0.0459	0.0142	0.0746	0.0205	0.0777	0.0206
	ABBs	0.2143	0.1193	0.2730	0.1433	0.2787	0.1435
	MREs	0.1429	0.5968	0.1820	0.7163	0.1858	0.7175
100	Averages	1.4639	0.2199	1.4445	0.2415	1.4444	0.2415
	MSEs	0.0235	0.0090	0.0387	0.0125	0.0387	0.0124
	ABBs	0.1532	0.0949	0.1968	0.1116	0.1968	0.1116
	MREs	0.1022	0.4748	0.1312	0.5581	0.1312	0.5581
200	Averages	1.4953	0.2004	1.4893	0.2085	1.4893	0.2085
	MSEs	0.0133	0.0057	0.0209	0.0079	0.0209	0.0079
	ABBs	0.1152	0.7553	0.1449	0.0888	0.1449	0.0888
	MREs	0.0768	0.3763	0.0966	0.4442	0.0966	0.4442
300	Averages	1.5004	0.1968	1.4971	0.2005	1.4971	0.2005
	MSEs	0.0092	0.0045	0.0145	0.0056	0.0145	0.0056
	ABBs	0.0959	0.0673	0.1204	0.0747	0.1204	0.0747
	MREs	0.0639	0.3365	0.0803	0.3737	0.0803	0.3737
500	Averages	1.5036	0.1972	1.5025	0.1996	1.5025	0.1996
	MSEs	0.0055	0.0027	0.0087	0.0036	0.0087	0.0036
	ABBs	0.0740	0.0518	0.0931	0.0611	0.0931	0.0601
	MREs	0.0494	0.2592	0.0620	0.3006	0.0620	0.3007

Table 5. The averages of estimates, MSEs, ABBs, and MREs of the TLRT-Exp model for $\lambda = 1.5$ and $p = 0.6$

n		MLE estimate		EKK estimate		WEKK estimate	
		$\hat{\lambda}$	\hat{p}	$\hat{\lambda}$	\hat{p}	$\hat{\lambda}$	\hat{p}
50	Averages	1.6103	0.5344	1.6363	0.6806	1.6630	0.6622
	MSEs	0.0943	0.0274	0.0769	0.0141	0.0859	0.0140
	ABBs	0.3072	0.1657	0.2772	0.1190	0.2932	0.1184
	MREs	0.2048	0.2762	0.1848	0.1983	0.1954	0.1974
100	Averages	1.5811	0.5519	1.5953	0.6567	1.5884	0.6758
	MSEs	0.0775	0.0251	0.0635	0.0141	0.0668	0.0147
	ABBs	0.2785	0.1585	0.2520	0.1188	0.2584	0.1211
	MREs	0.1856	0.2642	0.1680	0.1979	0.1730	0.2019
200	Averages	1.5618	0.5667	1.5658	0.5908	1.5527	0.6057
	MSEs	0.6111	0.0208	0.0487	0.0129	0.0488	0.0130
	ABBs	0.2472	0.1442	0.2208	0.1136	0.2210	0.1144
	MREs	0.1648	0.2404	0.1472	0.1893	0.1473	0.1907
300	Averages	1.5361	0.5754	1.5366	0.5943	1.5307	0.6105
	MSEs	0.0468	0.0167	0.0432	0.0123	0.0453	0.0126
	ABBs	0.2163	0.1294	0.2078	0.1109	0.2129	0.1122
	MREs	0.1442	0.2156	0.1386	0.1849	0.1419	0.1869
500	Averages	1.5170	0.5889	1.5135	0.5945	1.5042	0.6107
	MSEs	0.0338	0.0116	0.0360	0.0114	0.0387	0.0117
	ABBs	0.1838	0.1079	0.1898	0.1069	0.1968	0.1083
	MREs	0.1226	0.1799	0.1265	0.1782	0.1312	0.1804

Table 6. The averages of estimates, MSEs, ABBs, and MREs of the TLRT-Exp model for $\lambda = 1.5$ and $p = 0.9$

n		MLE estimate		EKK estimate		WEKK estimate	
		$\hat{\lambda}$	\hat{p}	$\hat{\lambda}$	\hat{p}	$\hat{\lambda}$	\hat{p}
50	Averages	1.9066	0.7185	2.0446	0.7123	2.0508	0.7112
	MSEs	0.1700	0.0329	0.2968	0.0352	0.3039	0.0353
	ABBs	0.4124	0.1815	0.5448	0.1877	0.5512	0.1880
	MREs	0.2749	0.2017	0.3631	0.2086	0.3675	0.2089
100	Averages	1.8762	0.7339	1.9471	0.7122	1.9535	0.7116
	MSEs	0.1419	0.0276	0.2023	0.0353	0.2085	0.0355
	ABBs	0.3767	0.1661	0.4498	0.1878	0.4566	0.1884
	MREs	0.2511	0.1846	0.2998	0.2087	0.3044	0.2093
200	Averages	1.7546	0.7840	1.9006	0.7143	1.9016	0.7141
	MSEs	0.0724	0.0134	0.1605	0.0345	0.1613	0.0345
	ABBs	0.2690	0.1159	0.4006	0.1857	0.4016	0.1859
	MREs	0.1793	0.1288	0.2670	0.2063	0.2677	0.2065
300	Averages	1.7156	0.8046	1.8707	0.7180	1.8728	0.7174
	MSEs	0.0542	0.0094	0.1379	0.0331	0.1391	0.0333
	ABBs	0.2329	0.0971	0.3714	0.1819	0.3730	0.1826
	MREs	0.1553	0.1079	0.2476	0.2022	0.2487	0.2028
500	Averages	1.6551	0.8313	1.7963	0.7566	1.8031	0.7497
	MSEs	0.0380	0.0067	0.0897	0.0206	0.0940	0.0226
	ABBs	0.1951	0.0816	0.2995	0.1434	0.3066	0.1503
	MREs	0.1300	0.0907	0.1997	0.1593	0.2044	0.1670

From Tables 1-6, it was concluded that the averages estimates, ABBs, MREs and MSEs of all estimates decrease when n increases as expected. The ML, LS and WLS estimates are almost identical in terms of ABBs, MSEs, and MREs criteria.

Real Data Applications

In this section, the TLRT – Exp distribution is applied to the two real data sets. For the comparison issue, we consider transmuted lower record type Fréchet (TLRT-F), Exponential (Exp), Fréchet (Fr), transmuted log-logistic (TLL), transmuted Weibull (TW) and transmuted exponential (TE) distributions. The pdfs of these distributions are given in the ML estimates, log-likelihood

value, Akaike's information criteria (AIC), corrected Akaike information criterion (AICc), Kolmogorov-Smirnov test statistic (KS), p-values based on the statistic for all distributions given in Table 7-8. Different discrimination criterion methods based on log-likelihood function evaluated at the ML estimates were also considered. The discrimination criterion methods are respectively: $AIC = -2l(\hat{\theta}, x) + 2k$, $AICc = AIC + (2k(k + 1))/((n - k - 1))$ and $BIC = -2l(\theta, x) + k \log(n)$ where k is the number of parameters to be fitted $\hat{\theta}$ and is the estimates of θ .

First data set: These data were reported in by Chouklain and Stephens [16]. The data are $n = 72$ exceedances of flood peaks (in m3/s) of the Wheaton River near Carcross in Yukon Territory, Canada. The 72 exceedances, for the years 1958 to 1984, rounded to one decimal place.

Table 7. MLEs and selection criteria statistics for first data set

	TLRT-Exp	TLRT-F	TLL	TW	TE	Fr	Exp
α	0.2248	0.6521	1.1609	0.9017	24.408	0.6521	12.204
p	0.0703	2.8834	16.405	25.109	-0.1345	2.8790	
λ		0.0016	0.5275	1.000			
$-l_n$	251.23	267.02	257.64	251.50	253.36	267.02	253.66
KS	0.0993	0.1530	0.1286	0.1052	0.1278	0.1532	0.9539
p-value	0.4770	0.0686	0.1846	0.4035	0.3037	0.0682	0.0000
AIC	506.46	540.04	521.28	509.00	510.72	538.04	509.32
AICc	506.63	540.39	521.63	509.35	510.89	538.21	509.38
BIC	506.17	539.61	520.85	508.57	510.43	537.75	509.18

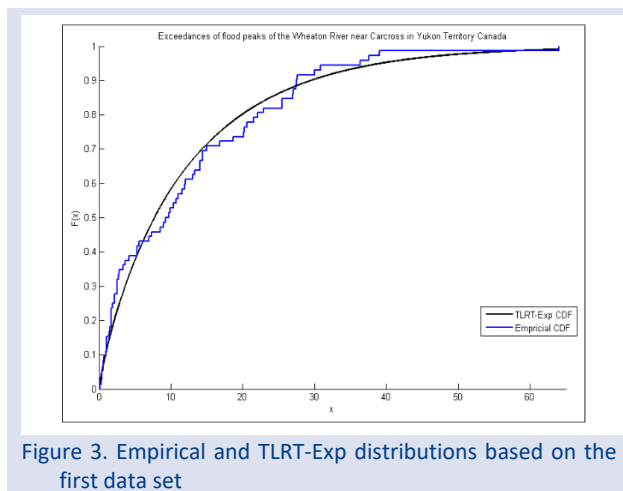


Figure 3. Empirical and TLRT-Exp distributions based on the first data set

Second data set

These data were reported in by Riffi et.al [17]. The data was collected from a group of 46 patients, per years, upon the recurrence of leukemia who received autologous marrow. The data set is listed below which is about leukemia free-survival times (in years) for the 46 autologous transplant patients.

According to the results in Table 7-8, TLRT-Exp has minimum KS and maximum p-value. In addition, when the discrimination criteria are examined, it is seen that it has minimum values in three criteria (AIC, AICc and BIC).

Table 8. MLEs and selection criteria statistics for second data set

Test	TLRT-Exp	TLRT-F	TLL	TW	TE	Fr	Exp
α	0.3884	0.4887	1.0127	0.8403	1.7678	0.7017	1.5172
p	0.4985	1.7313	1.9256	3.1614	0.3206	0.3371	
λ		1.0000	1.0000	1.0000			
$-l_n$	63.72	67.80	65.32	63.99	64.65	69.45	65.18
KS	0.0964	0.1204	0.0972	0.1001	0.1431	0.1399	0.2701
p-value	0.7864	0.5170	0.7781	0.7460	0.5073	0.3288	0.0024
AIC	131.44	141.60	136.64	133.98	133.30	142.90	132.36
AICc	131.72	142.17	137.21	134.55	133.58	143.18	132.45
BIC	130.77	140.59	135.63	132.97	132.63	142.23	132.02

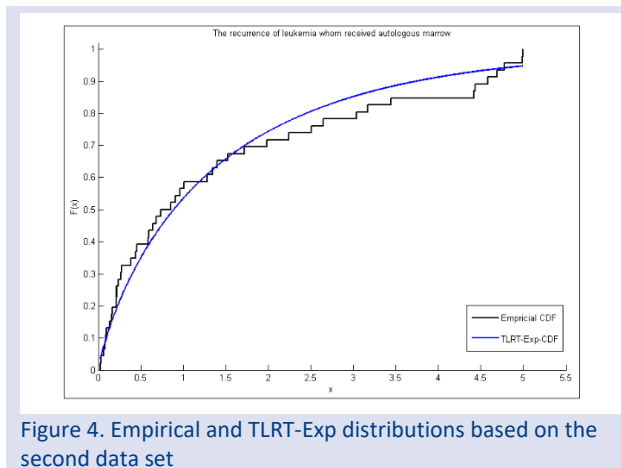


Figure 4. Empirical and TLRT-Exp distributions based on the second data set

From Figure 3-4, it can be said that TLRT-Exp can be a good alternative to modeling real data.

Conclusions

In this study, we proposed a new model via the transmuted lower record type family using exponential distribution and examined the properties of the new model such as survival, cumulative distribution, hazard rate functions, and expected value. In the literature review, it can be seen that the family so far have been applied to the Fréchet, power function and inverse Rayleigh distributions. Statistical inferences about the distribution parameters are discussed with three estimation methods, namely maximum likelihood, least squares, and weighted least squares. A detailed Monte Carlo simulation study is conducted to examine the performance of given estimation methods. In addition, the new model is examined in two real data sets with regard to discrimination criteria. It was observed that the obtained model is more flexible than the known distributions such as transmuted lower record type Fréchet, exponential, Fréchet, transmuted log-logistic, transmuted Weibull, and transmuted exponential

distributions. Considering that the variety of data is increasing, the family used in this study can be applied to other existing and primarily newly obtained continuous distributions for future studies.

Acknowledgement

The authors are thankful to the referees for their valuable remarks, comments and suggestions that led to the improvement of the presentation of the research work to this form.

Conflicts of interest

The authors declare that they have no conflicts of interest.

References

- [1] Azzalini A., A class of distributions which includes the normal ones, *Scandinavian Journal of Statistics*, 12 (1985) 171-178.
- [2] Mudholkar G.S., Srivastava D.K., Exponentiated Weibull family for analyzing bathtub failure-rate data, *IEEE Transactions on Reliability*, 42 (1993) 299-302.
- [3] Marshall A.W., Olkin I., A new method for adding a parameter to a family of distributions with application to the exponential and Weibull families, *Biometrika*, 84 (1997) 641-652.
- [4] Eugene N., Lee C., Famoye F., Beta-normal distribution and its applications, *Communications in Statistics-Theory and Methods*, 31 (2002) 497-512.
- [5] Mahdavi A., Kundu D., A new method for generating distributions with an application to exponential distribution, *Communications in Statistics-Theory and Methods*, 46 (2017) 6543-6557.
- [6] Karakaya K., Kınacı I., Akdoğan Y., Kuş C., A new family of distributions, *Hacettepe Journal of Mathematics and Statistics*, 46 (2017) 303-314.

- [7] Shaw W.T., Buckley I.R., The alchemy of probability distributions: Beyond gram-charlier & cornish-fisher expansions, and skew-normal or kurtotic-normal distributions, (2007) Submitted, Feb, 7, 64.
- [8] Shaw W.T., Buckley I.R., The alchemy of probability distributions: beyond Gram-Charlier expansions, and a skew-kurtotic-normal distribution from a rank transmutation map, arXiv preprint arXiv:0901.0434. (2009).
- [9] Alizadeh M., Merovci F., Hamedani G.G., Generalized transmuted family of distributions: properties and applications, *Hacet. J. Math. Stat.*, 46 (2017) 645–667.
- [10] Granzotto D.C.T., Louzada F., Balakrishnan N., Cubic rank transmuted distributions: inferential issues and applications, *Journal Statistical Computation and Simulation*, 87(14) (2017) 2760–2778.
- [11] Balakrishnan N., He M., A Record-Based Transmuted Model, Under review, Advance Online Publication (2019).
- [12] Taniş C., Saraçoğlu B., On the record-based transmuted model of Balakrishnan and He based on Weibull distribution, *Communications in Statistics - Simulation and Computation*, In press, (2020).
- [13] Taniş C., Saraçoğlu B., Kuş C., Pekkör A., Karakaya, K., Transmuted lower record type Fréchet distribution with lifetime regression analysis based on type I-censored data, *Journal of Statistical Theory and Applications*, 20(1) (2021) 86-96.
- [14] Taniş C., Transmuted lower record type inverse rayleigh distribution: estimation, characterizations and applications, *Ricerche di Matematica*, In press, (2022)
- [15] Taniş C., Transmuted lower record type power function distribution, *Journal of Science and Arts*, 21(4) (2021) 951-960.
- [16] Choulakian V., Stephens M.A., Goodness-of-fit tests for the generalized Pareto distribution, *Technometrics*, 43(4) (2001) 478-484.
- [17] Riffi M.I., Ansari S.I., Hamdan M.S., A generalized transmuted Frechet distribution, *Journal of Statistics Applications & Probability*, 8(2) (2019) 1-10.

Classification of Students' Mathematical Literacy Score Using Educational Data Mining: PISA 2015 Turkey Application

Hasan Aykut Karaboğa^{1,a}, Serkan Akogul^{2,b,*}, Ibrahim Demir^{3,c}

¹ Department of Educational Science, Faculty of Education, Amasya University, Amasya, Türkiye

² Department of Statistics, Faculty of Sciences, Pamukkale University, Denizli, Türkiye

³ Turkish Statistical Institute, Ankara, Türkiye.

*Corresponding author

Research Article

History

Received: 27/06/2022

Accepted: 12/09/2022

Copyright



©2022 Faculty of Science,
Sivas Cumhuriyet University


ABSTRACT

PISA 2015 mathematical literacy score of Turkey is 420 while the average score of all countries is 461. It is understood that; Turkish students' PISA 2015 mathematical literacy score was lower than the average. The basic reasons for the below average score need to be truly examined and developmental activities should be revealed. The aim of this study is to classify students according to the factors affecting their mathematical literacy score and to reveal the effects of these factors in classification. The data of the study is obtained from 5895 students who participated in PISA 2015. In this study, we used Random Forest, Naïve Bayes Classifier, Logistic Regression, Decision Tree Algorithm and Discriminant Analysis as classifiers. According to the results, Random Forest method produced more accurate scores than other methods with 76.32% accuracy. We also calculated the correct classification rate and determined the factors that positively and negatively affect the classification with discriminant analysis. According to the discriminant analysis home possessions, information and computer technology resources at home and students' expected occupational status were the most positive effective variables on mathematical literacy score. On the other hand, family wealth possessions, student-related factors affecting school climate and anxiety have negative effect on mathematical literacy score.

Keywords: Classification, Educational data mining, PISA 2015, Mathematics education, Discriminant analysis.

^a h.aykut.karaboga@amasya.edu.tr  <https://orcid.org/0000-0001-8877-3267>

^c idemir@gmail.com

 <https://orcid.org/0000-0002-2734-4116>

^b sakogul@pau.edu.tr

 <https://orcid.org/0000-0002-0346-4308>

Introduction

Countries continue their existence with educational investments. Because high qualified people ensure keeping up with industrial competitions, developments and global changes in the world. The protection of the interests of the countries depends on such highly-educated citizens. In order to reveal the effectiveness of education, it is needed to be evaluated objectively at national and international level. For this reason, according to certain evaluations like PISA, it is necessary to determine educational level of country and to take measures to eliminate deficiencies. As an OECD member, Turkey regularly participates in the PISA program to assess the quality of education [1].

Mathematical literacy, science literacy, reading literacy, computer skills, students' motivations, opinions about themselves, the school environment and their families are collected in the PISA exam. Mathematical literacy focuses on measuring the capacity to use, formulate and interpret mathematics. While Turkey's PISA 2015 mathematical literacy score is 420, the average score of OECD countries is 490. The results of Turkey's PISA average mathematical literacy score between 2003 and 2015 are given in Table 1. It is seen that PISA 2015 score is the lowest. The basic dynamics of this decrease should be correctly identified, examined and prevented. For this purpose, we classified students' mathematical literacy

score with the factors that affecting success using Educational Data Mining (EDM) techniques and discriminant analysis.

Table 1. PISA Turkey ranking - average score of mathematics

Years	2003	2006	2009	2012	2015
All Country Average	489	484	465	470	461
OECD Average	500	494	495	494	490
Turkey Average	423	424	445	448	420
Number of Participating Countries	41	57	65	65	70
Turkey Ranking	35	43	43	44	49

Overall, the EDM shows us an evaluation process with advantages for educational development and assessment. Researchers prefer EDM techniques to classical statistical methods due to the increase in data type and amount [2]. Because data mining techniques are easy to use and the number of methods is high according to different data types. Also these methods generate efficient results faster than classical methods. The most commonly used data mining methods in education are clustering, classification, regression and association analysis [3]. In addition, against to classical statistical techniques the absence of constraints such as normality, covariance, linearity and

normal distribution is also give advantage to the EDM [3]. However, since the methods have certain advantages over each other in some conditions, they should be used together or the comparative results should be examined too. In this study, taking this into account, different classification techniques were compared. Our research aims to contribute the EDM centred literature of PISA studies. For this purpose, mainly two research questions are addressed: (1) which factors have positive or negative impact of students mathematical success, (2) and which EDM method or discriminant analysis is more appropriate for classifying data for PISA 2015 Turkish mathematical dataset.

This study differs from other studies in the literature on PISA in terms of the EDM methods and variables used [4-7]. Random Forest [4,7], Discriminant Analysis [8], Decision Tree [5,7,9], Logistic Regression [10], Naïve Bayes [11,12] studies are encountered in the literature. However, no article was found using these methods and the data set mentioned in the article. In this respect, it is thought that the study will contribute to the literature.

Literature

In the literature, the EDM is used in many different applications. Slater et al. [13] reviewed 40 research tools for the EDM and learning analytics (LA). Reviewers pointed out that it is not a suitable tool for end-to-end the EDM and the LA analysis. Therefore, the combination of the EDM tools is more useful for complex analysis.

In a different study, Devasia, Vinushree and Hegde [14] conducted an experiment to predict students' performance with proposed web based application. According to the paper Naïve Bayes technique produced more accurate results from the other techniques. To get faster and more efficient accreditation process Tastimur, Karakose, and Akin [15] performed an IT-based accreditation model for engineering education. They suggested 10 criteria and used Genetic Algorithm method to train k-Nearest Neighbor classifier. Different methods have been developed for classification based on variable and/or model selection [16]. Agaoglu [17] appraised, instructors' performance with seven different classification methods. He used support vector machines, C5.0, CART, Discriminant Analysis and Artificial Neural Network methods to analyse 2850 course evaluation scores. C5.0 classifier gave the best classification result.

Shahiri and Husain [9] reviewed literature systematically to find most successive students' performance prediction methods from 2002 to 2015. They found that the most used prediction methods are Neural Network, Decision Tree, Support Vector Machine, k-Nearest Neighbor and Naïve Bayes respectively. Osmanbegović and Suljić [12] compared data mining applications for student success prediction at the University of Tuzla. Developing learners' creativity was the most important part of web based learning system.

One of the EDM application study for higher education prediction in Turkey is conducted by Tekin [18]. In that

study, it was aimed to prevent the students who determined to give up the school. Artificial Neural Networks, Support Vector Machines and Extreme Learning Machine methods used to predict students' graduation grades. Using PISA and TIMSS data Kiray, Gok and Bozkir [19] identified the affective variables on mathematics and science with decision trees and clustering algorithms. In their study, they found out reading and problem solving skills affect mathematical achievement and, so on science achievement is affective variable on mathematical achievement.

Aksu and Güzeller [5], classified PISA 2012 mathematical literacy scores of Turkish students with CHAID method. As a result of their study, it was determined that attitude towards the course, perception of self-efficacy and anxiety were important variables on mathematical literacy score. Dolu [20] examined science performance and economic, social and cultural status index (ESCS) relation for PISA 2015 Turkey survey with Hierarchical Linear Models. As a result of her study, she found that ESCS had a low positive effect on science achievement. Aksu and Keceoglu [10] compared prediction results of mathematical success with logistic regression, CHAID and REPTree methods.

Gure et al. [21] used Multilayer Perceptron and Random Forest methods to estimate PISA 2015 mathematical literacy score. As a result of the study, it was stated that the Random Forest algorithm produced more successful results. Toprak and Gelbal [8] compared classification performances of artificial neural networks, decision trees and discriminant analysis at PISA 2012 mathematical literacy score for different sample sizes. They used all student data for analysis with 17 mathematical success related variables. Koyuncu and Gelbal [11] tested performance of Naïve Bayes, k-Nearest Neighbor, Neural Network, and Logistic Regression methods under different sample size conditions for PISA 2012 dataset. As it's seen in literature, different EDM methods give different results [10]. In this study, analyzes were made with some of the algorithms that produced the most successful results, considering the superiority of the methods to classify PISA 2015 mathematical literacy success of the Turkish students.

Materials and Methods

As indicated by Romero and Ventura [3], the "Educational Data Mining" term was first introduced in 2005. EDM is combination of education, statistics and computer sciences [3]. We can describe data mining models in two ways; predictive or descriptive. Predictive models contain Prediction, Classification, Time Series Analysis and Regression. Descriptive models generally used for summarizing the data, clustering, discovering Association Rules and Sequence Discovery [3,22]. The EDM applications are expanding in traditional and computer-based education. These applications are helpful to education designer and pedagogues [23].

The EDM is a lodestar for educators and managers to obtain educational expert knowledge about learning systems and student behaviours. It is crucial that defining the problem and converting the data to a suitable form for curing an educational problem [23]. So, there is an immense opportunity to judge all pedagogical paradigms and educational approaches with the EDM applications [24].

On detecting factor related performance analysis, compared to other data analytic techniques the EDM give detailed and more efficient results. Furthermore, in human sciences these results adapt to needs better than other techniques. It is often stated that evaluating the results by using a combination of several data mining methods is healthier instead of using data mining algorithms alone [18]. Because depend on the data structure and data size, the EDM methods have some advantages [23].

For this reason, weakness of the data mining techniques should be decrease with comparative studies to classical methods [7]. The EDM applications are not separated by sharp lines [25]. But in our literature, it seems to be a deficiency in this subject. One of the purposes of our paper is contributing the usage of these powerful methods in our literature.

Research Sample

Academic success is a complex issue because, academic achievement are composite of a variety of family-related variables, school-related variables, personal variables and social or environmental variables. Family-related variables include socioeconomic and sociocultural variables, parents' education and occupation, parents' support, family structure, and parents' relation in school. School-related variables are relevant with school assessment, teacher support and assessment, learning opportunities, class size, and schools' social and cultural support. Social variables based on student' living era and schools' social environment [7].

Personal factors like school related variables and demographic variables are indicative on students' academic achievement [7]. Mathematic skills are not only important for high school performance, but also determinative of undergraduate success [26]. Socio-demographic variables, studying attitudes and previous achievements have positive effect on success [12]. A lot of studies have shown that demographic variables, past academic achievements, family income are effective variables on academic achievement [27]. Other highly correlated factor with student performance is qualification of parents [14].

As a result, mathematical achievement is closely related to these internal and external factors. By identifying the factors that lead to mathematical achievement or failure, and by removing negative situations, the overall academic achievement will turn into motivation with an increasing effect. In this study, we selected variables from the PISA 2015 dataset given in Table 2.

Table 2. Mathematical Achievement Related Factors

#	Variable Name	Explanation of variables
1	BSMJ	Students' Expected Occupational Status
2	HISEI	Highest Occupational Status of Parents
3	OUTHOURS	Out-of-School Study Time Per Week
4	MMINS	Mathematics Learning Time (minutes per week)
5	TMINS	Total Learning Time (minutes per week)
6	BELONG	Sense of Belonging to School
7	ANXTEST	Test Anxiety
8	MOTIVAT	Students' Achievement Motivation
9	CPSVALUE	Value of Co-Operation
10	EMOSUPS	Parents Emotional Support
11	CULTPOSS	Cultural possessions at Home
12	HEDRES	Home Educational Resources
13	HOMEPOS	Home Possessions
14	ICTRES	Information and Computer Technology Resources
15	WEALTH	Family Wealth Possessions
16	ESCS	Index of Economic, Social and Cultural Status
17	EDUSHORT	Shortage of Educational Material
18	STAFFSHORT	Shortage of Educational Staff
19	STUBEHA	Student-related Factors Affecting School Climate
20	TEACHBEHA	Teacher-related Factors Affecting School Climate
21	STRATIO	Student Teacher Ratio

The research sample is 5895 Turkish students who participated in the PISA 2015 Program. Indices were chosen instead of variables affecting the mathematical literacy score. Some selected variables have positive effect on mathematical literacy score, while some factors have negative effect on mathematical literacy score. The target variable was coded with (0= not successful,1= successful). On this variable 0 means under average mathematical literacy score and 1 means above average mathematical literacy score.

Classification Algorithms

In this study, we used C4.5, Logistic Regression, Naïve Bayes and Random Forest, which is the most widely used EDM methods in the literature. In addition, discriminant analysis was used to examine the factors affecting success.

Discriminant Analysis is one of the statistical technique that give canonical functions for classification of cases into two or more mutually exclusive groups or scores about two or more variables. Furthermore, Discriminant Analysis help to detect most powerful discriminators' characteristics named discriminating variables. In summary Discriminant Analysis find linear combination of group discriminators, membership prediction of new cases with discrimination functions, evaluating the group differences based on variables [28].

Classification with Discriminant Analysis has two main concepts. Firstly, to differentiate classes using canonical discriminant functions or discriminating variables. Secondly, predicting group membership of the future observations. For each group classification function is a linear combination of variables [28].

C4.5 is a type of classification algorithm which is a member of decision tree family. This algorithm is one of the most popular machine learning method. This method was developed by Quinlan [29] to overcome some

deficiencies of ID3 algorithm. C4.5 algorithm handles both continuous and discrete data.

Relationships between dependent and independent variables can be investigated using Logistic Regression. The most important assumption in standard regression is that the dependent variable must be continuous. If the dependent variable takes the value 0 or 1, binary Logistic Regression should be applied to predict or classify the dependent variable of the observable independent variables [30].

Naïve Bayes is in the supervised learning subclass of machine learning. In other words, it is clear which class the sample data in the data set belongs to. This statistical method is based on calculating the conditional probability of the effect of each attribute on the outcome. Naïve Bayes has stands out as one of the most efficient and effective inductive learning algorithms for machine learning methods and data mining [2,22].

In the Random Forest method, many decision trees are created using different variations of a training data. New versions of the training data are obtained by randomly selecting a sample from the original training dataset by displacement. Every tree in the forest should be advanced to the greatest imaginable level without pruning. To classify a new test substance, each tree in the forest is allowed to make a classification decision. As a result, the classification decision is made for the majority among these situations [2]. In addition, it is a method that gives better results compared to its corresponding algorithms [5].

Performance Criteria

Various criteria are used to evaluate the results in machine learning studies. In this study, some commonly used criteria were taken into account as comparison criteria. These classification measures were determined as accuracy (ACC), F-measure, Kappa and mean absolute error (MAE) statistics, respectively.

ACC is determined by the ratio of all correctly classified samples in the model to the total number of samples. The ACC formula is given in equation (1).

$$ACC = \frac{TP + TN}{TP + TN + FP + FN} \tag{1}$$

Here, depending on the results, it is expressed as True positive (TP): true positive estimate, False positive (FP): false positive estimate, True negative (TN): true negative estimate, and False negative (FN): false negative estimate [22].

The F-measure, also called the F-score, is a measure of a model’s accuracy on a dataset. It is used to evaluate binary classification systems, which classify examples into ‘positive’ or ‘negative’. The F-measure is a way of combining the precision and recall of the model, and it is defined as the harmonic mean of the model’s precision and recall. A perfect model has an F-measure of 1. Mathematical definition of the F-measure is given in equation (2).

$$F - measure = \frac{2}{\frac{1}{precision} + \frac{1}{recall}} = \frac{2 * TP}{2 * TP + FP + FN} \tag{2}$$

Kappa statistics (κ) investigates the predictive performance of a classification model. It is a convenient statistic to measure the evaluation of categorical variables. It is also a value based on the chi-square table [31]. Those whose κ value is close to 1 are closer to the solution. P_o and P_e show the relationship between two categorical variables [32].

$$\kappa = \frac{p_o - p_e}{1 - p_e} \tag{3}$$

Mean absolute error (MAE) statistics help to reveal the differences between predicted and observed values of a model [33]. The MAE calculates the average of the absolute differences between the predicted and observed values. Here, the MAE statistic is calculated as follows to show the predicted and observed values of P_i and O_i [33].

$$MAE = n^{-1} \sum_{i=1}^n |P_i - O_i| \tag{4}$$

Accuracy and Kappa, which are used extensively in EDM studies, should be calculated too instead of using only f-measure to show effectiveness [34]. Table 5 shows the classification performances of algorithms based on the previously mentioned classification criteria (ACC, F-Measure, κ statistic and MAE). The best algorithm was accepted based on the ACC criterion. Other classification criteria were also used to support the final result.

Results

Discriminant Analysis was first applied in the study. At the end of the analysis, the students were classified according to their mathematical literacy score. Classification rates according to discriminant analysis are given in Table 3.

Table 3. Classification Results of Discriminant Analysis

Category	Total	Predicted Group Membership	
		Unsuccessful	Successful
Unsuccessful	3245 (100%)	2361 (72.8%)	884 (27.2%)
Successful	2650 (100%)	835 (31.5%)	1815 (68.5%)

According to the results given in the table, the accuracy of our model was found to be 70.8%. In addition, the weights of the factors for the separation function are as in Table 4. According to these weights, the most effective variables are understood.

Table 4. Standardized Canonical Discriminant Function Coefficients

No	Variable Name	Score	No	Variable Name	Score
1	HOMEPOS	0.955	1	WEALTH	-0.592
2	BSMJ	0.336	2	STUBEHA	-0.396
3	ICTRES	0.335	3	ANXTEST	-0.247
4	HISEI	0.287	4	OUTHOURS	-0.210
5	MOTIVAT	0.231	5	CULTPOSS	-0.172
6	MMINS	0.169	6	HEDRES	-0.172
7	STRATIO	0.146	7	STAFFSHORT	-0.172
8	TEACHBEHA	0.126	8	ESCS	-0.140
9	TMINs	0.058	9	EDUSHORT	-0.117
10	CPSVALUE	0.041			
11	BELONG	0.040			
12	EMOSUPS	0.036			

As its seen in Table 4, BSMJ, HISEI, MMINS, TMINs, BELONG, MOTIVAT, CPSVALUE, EMOSUPS, HOMEPOS, ICTRES, TEACHBEHA, STRATIO have positive effect on mathematical literacy score. However, OUTHOURS, ANXTEST, CULTPOSS, HEDRES, WEALTH, ESCS, EDUSHORT, STAFFSHORT and STUBEHA have negative effect on mathematical literacy score.

According to these results, home possessions the most positive effective variable on mathematical literacy score. Second effective variable was ICT resources at home. Also ‘students’ expected occupational status’ and ‘highest occupational status of parents’ had positive effect on mathematical literacy score. On the other hand, ‘family wealth possessions’, ‘student-related factors affecting school climate’ and ‘test anxiety’ had negative effect on mathematical literacy score.

Table 5. Comparison of Classification Achievements of the Methods

Classifier	ACC	F-Measure	κ statistic	MAE
Random Forest	76.57%	0.764	0.521	0.348
C4.5 Classifier	71.23%	0.712	0.416	0.317
Logistic Regression	71.09%	0.709	0.411	0.378
Discriminant Analysis	70.80%	0.708	0.412	0.294
Naïve Bayes	68.36%	0.684	0.365	0.332

As it was seen, Random Forest was the best algorithm according to ACC (76.57%), F-Measure (0.764), κ statistic (0.521) and MAE (0.348). According to the results, Random Forest method produced more accurate scores than other EDM methods.

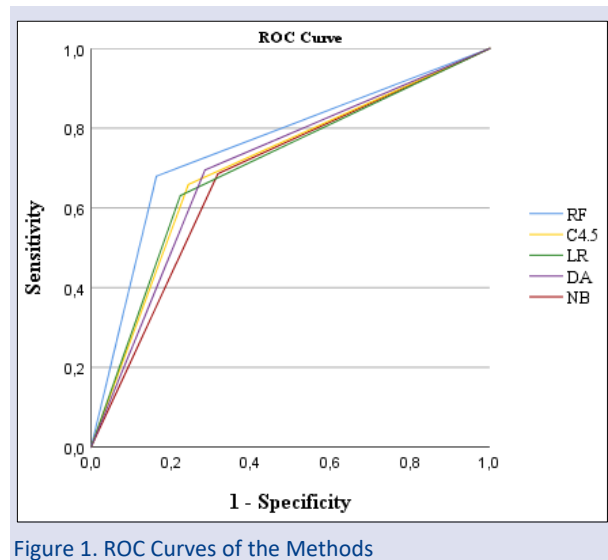


Figure 1. ROC Curves of the Methods

RF, C4.5, LR, DA, NB have compared with ROC area. As it seen, RF has the greatest ROC area than other methods ($AUC_{RF} = 0.758$; $AUC_{C4.5} = 0.707$; $AUC_{LR} = 0.704$; $AUC_{DA} = 0.705$; $AUC_{NB} = 0.684$). As can be seen from the ROC curve, the difference between the methods is not very high. However, it is still seen that EDM methods produce slightly better results than Discriminant Analysis.

Discussion, Conclusion and Recommendations

Actual topics of EDM are prediction, clustering, outlier detection, relationship mining, social network analysis, process mining, text mining and data refinement for human judgement, discovery with models, knowledge tracing and nonnegative matrix factorization [3]. On detecting factor related performance analysis, compared to other data analytic techniques EDM techniques give detailed and more efficient results. So, in human sciences these results adapt to needs better than other techniques. But weakness of the data mining techniques should be decrease with comparative studies with classical methods [7].

In our study, Discriminant Analysis from classical methods and Random Forest, Decision Tree, Logistic Regression and Naïve Bayes algorithms from data mining methods were compared. The aim of this study is to determining the factors affecting PISA 2015 mathematical literacy score by using Discriminant Analysis and comparing the classification capabilities of this method with Random Forest, C4.5, Logistic Regression, and Naïve Bayes algorithms. As a result of the analysis, random forest method was found to be the most successful classification method in PISA 2015 Turkey data.

When the results are examined, it is seen that the ‘Home Possessions’ variable has a positive effect on mathematics achievement [6,20]. The ‘Highest Occupation Status of Parents’ variable also has a positive effect on student success. Highly educated parents’ children are more successful than other students [6]. In addition, ‘Students’ Expected Occupation Status’ also has a positive effect on success. It can be assumed that this

variable also increases the motivation of the student and high motivation increases success [6]. ICT Resources, which can be used for the course, have a positive effect on academic success [35]. Also, mathematics learning time increase one of the most influential variables on mathematics achievement is the mathematical achievement [6,36]. Furthermore, 'Student Teacher Ratio' and 'Teacher-related Factors Affecting School Climate' [37] have positive effects on mathematical achievement.

On the other hand, unlike many studies in the literature [20] 'family wealth possessions', 'cultural possessions at home', 'home educational resources' and 'Index of Economic, Social and Cultural Status' variables has a negative effect on mathematical literacy score. Accordingly, family wealth has not a positive effect on success. As it is known, the negative student behaviour decreases the academic achievement. For this reason, the student-related factors affecting school climate variable is also one of the variables that negatively affect mathematical literacy score [38]. In addition, the anxiety has also negative effect on academic achievement [5,6]. 'Out-of-School study time' is another variable that negatively affects academic achievement. Working hard outside of school has not increased mathematical literacy score. This may be due to the anxiety-enhancing effect and the fact that students get bored and lose motivation. Also it is known that lack of material have negative effects on achievement [39]. In this study, 'Shortage of Educational Staff' and 'Shortage of Educational Material' variables, similar to the literature, had a negative effect on mathematics achievement. It can be assumed that the results obtained may be due to the research sample. For this, work can be repeated with different countries.

As a result, family wealthy is not an indicator of academic achievement. On the other hand, the education level of the family and the professional expectations of the student had positive effects on achievement. Students' expectations can motivate them and make it easier for them to achieve. ICT resources have made a positive contribution to achievement as a means of finding solutions for academic problems. In our education system, students can get higher scores by creating multimedia-supported learning environments with projects such as the FATİH project. These projects eliminate educational inequality and enriching the learning environment for all learning types [40]. In addition, motivated students contribute to their mathematical literacy score with the study time they allocate to the mathematics lesson. In addition, it is expected that reducing student anxiety and eliminating the lack of educational materials, which are obstacles to success, will contribute to mathematics achievement.

This research has some limitations. The results of this research are based only on the PISA 2015 Turkey data set and only mathematics achievement was used in this study. Another limitation is that this dataset measures 15-year-old students' ability to use their mathematical knowledge and skills to cope with real-life challenges. The

study can be repeated in comparison with the mathematics achievements of different countries.

Conflicts of interest

There are no conflicts of interest in this work.

References

- [1] Taş U.E., Arici Ö., Ozarkan H.B., Özgürlük B., PISA 2015 ulusal raporu, *Ankara: Milli Eğitim Bakanlığı*, (2016).
- [2] Witten I.H., Frank E., Data mining: practical machine learning tools and techniques with Java implementations, *Acm Sigmod Record*, 31(1) (2002) 76-77.
- [3] Romero C., Ventura S., Educational Data Mining: A Review of the State of the Art, *IEEE Trans. Syst., Man, Cybern. C*, 40(6) (2010) 601-618.
- [4] Aksu G., Doğan N., Veri madenciliğinde kullanılan öğrenme yöntemlerinin farklı koşullar altında karşılaştırılması, *Ankara University Journal of Faculty of Educational Sciences (JFES)*, 51(3) (2018) 71-100.
- [5] Aksu G., Güzeller C.O., Classification of PISA 2012 mathematical literacy scores using Decision-Tree Method: Turkey sampling, *Eğitim ve Bilim*, 41(185) (2016) 101-122.
- [6] Dos Santos R.A., Paulista C.R., da Hora, H.R.M., Education Data Mining on PISA 2015 Best Ranked Countries: What Makes the Students go Well, *Technology, Knowledge and Learning*, (2021) 1-32.
- [7] Martínez Abad F., Chaparro Caso López A.A., Data-mining techniques in detecting factors linked to academic achievement, *School Effectiveness and School Improvement*, 28(1) (2017) 39-55.
- [8] Toprak E., Gelbal S., Comparison of Classification Performances of Mathematics Achievement at PISA 2012 with the Artificial Neural Network, Decision Trees and Discriminant Analysis, *International Journal of Assessment Tools in Education*, 7(4) (2020) 773-799.
- [9] Shahiri A.M., Husain W., Rashid N.A., A Review on Predicting Student's Performance Using Data Mining Techniques, *Procedia Computer Science*, 72 (2015) 414-422.
- [10] Aksu G., Keceoglu C.R., Comparison of Results Obtained from Logistic Regression, CHAID Analysis and Decision Tree Methods, *EJER*, 19 (84) (2019) 1-20.
- [11] Koyuncu İ., Gelbal S., Comparison of Data Mining Classification Algorithms on Educational Data under Different Conditions, *Journal of Measurement and Evaluation in Education and Psychology*, 11(4) (2020) 325-345.
- [12] Osmanbegovic E., Suljic M., Data Mining Approach for Predicting Student Performance, *Economic Review: Journal of Economics and Business*, 10(1) (2012) 3-12.
- [13] Slater S., Joksimović S., Kovanovic V., Baker R.S., Gasevic D., Tools for Educational Data Mining: A Review, *Journal of Educational and Behavioral Statistics*, 42(1) (2017) 85-106.
- [14] Devasia T., Vinushree T.P., Hegde V., Prediction of students performance using Educational Data Mining. In 2016 International Conference on Data Mining and Advanced Computing (SAPIENCE), (2016) 91-95.
- [15] Tastimur C., Karakose M., Akin E., Improvement of relative accreditation methods based on data mining and artificial intelligence for higher education, *15th International Conference on Information Technology Based Higher Education and Training (ITHET)*, (2016) 1-7.

- [16] Gogebakan M., A Novel Approach for Gaussian Mixture Model Clustering Based on Soft Computing Method, *IEEE Access*, 9 (2021) 159987–160003.
- [17] Agaoglu M., Predicting Instructor Performance Using Data Mining Techniques in Higher Education, *IEEE Access*, 4(1) (2016) 2379–2387.
- [18] Tekin A., Early Prediction of Students' Grade Point Averages at Graduation: A Data Mining Approach, *EJER*, 14(54) (2014) 207–226.
- [19] Kiray S.A., Gok B., Bozkir A.S., Identifying the Factors Affecting Science and Mathematics Achievement Using Data Mining Methods, *JESEH*, 1(1) (2015) 28.
- [20] Dolu A., Sosyoekonomik Faktörlerin Eğitim Performansı Üzerine Etkisi: PISA 2015 Türkiye Örneği, *Yönetim ve Ekonomi Araştırmaları Dergisi*, 18(2) (2020) 41-58.
- [21] Güre Ö.B., Kayri M., Erdoğan F., Analysis of Factors Effecting PISA 2015 Mathematics Literacy via Educational Data Mining, *Education & Science/Eğitim ve Bilim*, 45(202) (2020).
- [22] Tan P.N., Steinbach M., Kumar V., *Introduction to data mining*, Second edition, Global edition, New York, (2020).
- [23] Romero C., Ventura S., Data mining in education, *WIREs Data Mining and Knowledge Discovery*, 3(1) (2013) 12–27.
- [24] Peña-Ayala A., Educational data mining: A survey and a data mining-based analysis of recent works, *Expert Systems with Applications*, 41(4) (2014) 1432–1462.
- [25] Bakhshinategh B., Zaiane O.R., ElAtia S., Ipperciel D., Educational data mining applications and tasks: A survey of the last 10 years, *Educ Inf Technol*, 23(1) (2018) 537–553.
- [26] Chong S., Mak M., Loh W.M., Data-mining applications with the admission data of adult learners in higher education: a pilot study, *IJMIE*, 10(2) (2016) 131.
- [27] Mishra T., Kumar D., Gupta S., Students' Performance and Employability Prediction through Data Mining: A Survey, *Indian Journal of Science and Technology*, 10(24) (2017) 1-6.
- [28] Izenman A.J., *Modern multivariate statistical techniques: regression, classification, and manifold learning*. New York, Springer, (2008).
- [29] Quinlan J.R., *C4.5: Programs for Machine Learning*. San Mateo, California: Morgan Kaufmann Publishers, (1993).
- [30] Hosmer Jr D.W., Lemeshow S., Sturdivant R.X., *Applied logistic regression*, John Wiley & Sons, 398 (2013).
- [31] Donner A. Klar N., The statistical analysis of kappa statistics in multiple samples, *Journal of Clinical Epidemiology*, 49(9) (1996) 1053–1058.
- [32] Turanoglu-Bekar E., Ulutagay G., Kantarcı-Savas S., Classification of Thyroid Disease by Using Data Mining Models: A Comparison of Decision Tree Algorithms, *The Oxford Journal of Intelligent Decision and Data Science*, 2016(2) (2016) 13–28.
- [33] Willmott C. Matsuura K., Advantages of the mean absolute error (MAE) over the root mean square error (RMSE) in assessing average model performance, *Clim. Res.*, 30 (2015) 79–82.
- [34] Costa E.B., Fonseca B., Santana M.A., de Araújo F.F., Rego J., Evaluating the effectiveness of educational data mining techniques for early prediction of students' academic failure in introductory programming courses, *Computers in Human Behavior*, 73 (2017) 247–256.
- [35] Skryabin M., Zhang J., Liu L., Zhang D., How the ICT development level and usage influence student achievement in reading, mathematics, and science, *Computers & Education*, 85 (2015) 49–58.
- [36] Martínez-Abad F., Gamazo A., Rodríguez-Conde M.-J., Educational Data Mining: Identification of factors associated with school effectiveness in PISA assessment, *Studies in Educational Evaluation*, 66 (2020) 100875.
- [37] Topçu M.S., Arıkan S., Erbilgin E., Turkish Students' Science Performance and Related Factors in PISA 2006 and 2009, *Aust. Educ. Res.*, 42 (1) 117–132.
- [38] Altun A., Kalkan Ö.K., Cross-national study on students and school factors affecting science literacy, *Educational Studies*, 47(4) (2021) 403-421.
- [39] Arends F., Winnaar L., Mosimege M., Teacher classroom practices and Mathematics performance in South African schools: A reflection on TIMSS 2011, *South African Journal of Education*, 37(3) (2017).
- [40] Zhao Y., Lu Z., Study on the Application of Multimedia Network Teaching Platform in College Physical Education Teaching, *International Journal of Signal Processing, Image Processing and Pattern Recognition*, 9(4) (2016) 193–202.

AUTHOR GUIDELINES

Thank you for choosing to submit your paper to Cumhuriyet Science Journal. The following instructions will ensure we have everything required so your paper can move through pre-evaluating, peer review, production and publication smoothly. Please take the time to read and follow them as closely as possible, as doing so will ensure your paper matches the journal's requirements.

Submission

Cumhuriyet Science Journal is an international, peer-reviewed, free of charge journal covering the full scope of both natural and engineering sciences. Manuscripts should be submitted by one of the authors of the manuscript as online submission after registration to the Cumhuriyet Sciences Journal. Microsoft Word (.doc, .docx, .rtf), files can be submitted. There is no page limit. If there is a problem while uploading the files of manuscript, please try to reduce their file size, especially manuscripts including embedded figures. Submissions by anyone other than one of the authors will not be accepted. The submitting author takes responsibility for the paper during submission and peer review. If for some technical reason submission through the online submission system is not possible, the author can contact csj@cumhuriyet.edu.tr for support.

Submission or processing charges

Cumhuriyet Science Journal does not charge any article submission, processing charges, and printing charge from the authors.

Terms of Submission

Papers must be submitted on the understanding that they have not been published elsewhere (except in the form of an abstract or as part of a published lecture, review, or thesis) and are not currently under consideration by another journal. The submitting author is responsible for ensuring that the article's publication has been approved by all the other coauthors. It is also the authors' responsibility to ensure that the articles emanating from a particular institution are submitted with the approval of the necessary institution. Only an acknowledgment from the editorial office officially establishes the date of receipt. Further correspondence and proofs will be sent to the author(s) before publication unless otherwise indicated. It is a condition of submission of a paper that the corresponding author permit editing of the paper for readability. All enquiries concerning the publication of accepted papers should be addressed to csj@cumhuriyet.edu.tr. Please note that Cumhuriyet Science Journal uses iThenticate software to screen papers for unoriginal material. By submitting your paper to Cumhuriyet Science Journal are agreeing to any necessary originality checks your paper may have to undergo during the peer review and production processes. Upon receiving a new manuscript, the Editorial office conducts initial pre-refereeing checks to ensure the article is legible, complete, correctly formatted, original, within the scope of the journal in question, in the style of a scientific article and written in clear English. Any article that has problems with any of the journal criteria may be rejected at this stage.

Peer Review

This journal operates a single blind review process. All contributions will be initially assessed by the editor for suitability for the journal. Papers deemed suitable are then typically sent to a minimum of two independent expert reviewer to assess the scientific quality of the paper. The author is required to upload the revised article to the system within 15 days by making the corrections suggested by the referee. The article will be rejected if there are no fixes in it. The Editor is responsible for the final decision regarding acceptance or rejection of articles. The Editor's decision is final

Title and Authorship Information

The following information should be included

Paper title

Full author names

Full institutional mailing addresses

Corresponding address

Email address

Abstract

The manuscript should contain an abstract. The researchers who are native speakers of Turkish have to add Turkish title and abstract as well. The abstract should be self-contained and citation-free and should be 250-300 words.

Keywords

Keywords of the scientific articles should be selected from the web address of www.bilimadresleri.com

Introduction

This section should be succinct, with no subheadings.

Materials and Methods

This part should contain sufficient detail so that all procedures can be repeated. It can be divided into subsections if required.

Conflicts of interest

Sample sentence if there is no conflict of interest: The authors stated that did not have conflict of interests.

Acknowledgements

Sample sentences for acknowledgements: The work was supported by grants from CUBAP (T-1111). We would like to acknowledge Prof. Mehmet Sözer, MD, for his precious technical and editorial assistance. We would like to thank

References

References to cited literature should be identified by number in the text in square brackets and grouped at the end of the paper in numerical order of appearance. Each reference must be cited in the text. Always give inclusive page numbers for references to journal articles and a page range or chapter number for books. References should be styled and punctuated according to the following examples

- [1] Karaca E., Ulusoy S., Morgül Ü., Ulusoy H.I., Development of Analytical Method for Sensitive Determination of Streptozotocin based on Solid Phase Extraction, Cumhuriyet Sci. J., 41 (4) (2020) 826-831. (sample reference for journals)
- [2] Keskin B., Ozkan A.S., Inverse Spectral Problems for Dirac Operator with Eigenvalue Dependent Boundary and Jump Conditions, Acta Math. Hungar., 130 (2011) 150-159(sample reference for journals)
- [3] Mazur M.T., Kurman R.J., Dysfunctional Uterine Bleeding. In: Mazur M.T., Kurman R.J., (Eds). Diagnosis of endometrial biopsies and curettings, A practical approach. 2nd ed. Berlin: Springer, (2005) 100-120. (sample reference for book chapters)
- [4] Mazur M.T., Kurman R.J.,Diagnosis of endometrial biopsies and curettings, A practical approach. 2nd ed. Berlin, (2005) 100-120. (sample reference for book)
- [5] National Cancer Institute, Surveillance Epidemiology and End Results. Cancer of the Corpus and Uterus, NOS. Available at: http://seer.cancer.gov/statfacts/html/corp.html?statfacts_page=corp. Retrieved March 2, 2008. (sample reference for websites)
- [6] Surname N., Title of thesis, PD or master thesis, Name of university, name of institue, year. (sample reference for thesis)
- [7] Surname N., Title of fulltext conference paper, name of conference, city, year, pages. (sample reference for Abstratcs in conferences are not accepted as a valid reference except full text)

Preparation of Figures

Each figure can be integrated in the paper body or separately uploaded and should be cited in a consecutive order. Figure widths can be 4-6 inch as 300 dpi. The labels of the figures should be clear and informative. The name and the subtitles of the figures must be 9-point font.

Preparation of Tables

Tables should be cited consecutively in the text. Every table must have a descriptive title and if numerical measurements are given, the units should be included in the column heading. Tables should be simple with simple borders and text written as left text. The name and the subtitle of the tables must be 9-point font

Proofs

Corrected proofs must be returned to the publisher within 2 weeks of receipt. The publisher will do everything possible to ensure prompt publication. It will therefore be appreciated if the manuscripts and figures conform from the outset to the style of the journal.

Copyright

Open Access authors retain the copyrights of their papers, and all open access articles are distributed under the terms of the Creative Commons Attribution license, which permits unrestricted use, distribution and reproduction in any medium, provided that the original work is properly cited.

The use of general descriptive names, trade names, trademarks, and so forth in this publication, even if not specifically identified, does not imply that these names are not protected by the relevant laws and regulations.

While the advice and information in this journal are believed to be true and accurate on the date of its going to press, neither the authors, the editors, nor the publisher can accept any legal responsibility for any errors or omissions that may be made. The publisher makes no warranty, express or implied, with respect to the material contained herein.

Ethical Guidelines

New methods and ethically relevant aspects must be described in detail, bearing in mind the following:

Human Experiments. All work must be conducted in accordance with the Declaration of Helsinki (1964). Papers describing experimental work on human subjects who carry a risk of harm must include:

A statement that the experiment was conducted with the understanding and the consent of the human subject.

A statement that the responsible Ethical Committee has approved the experiments.

Animal Experiments. Papers describing experiments on living animals should provide:

A full description of any anaesthetic and surgical procedure used.

Evidence that all possible steps were taken to avoid animal suffering at each stage of the experiment. Papers describing experiments on isolated tissues must indicate precisely how the donor tissues were obtained.

Submission Preparation Checklist

As part of the submission process, authors are required to check off their submission's compliance with all of the following items, and submissions may be rejected that do not adhere to these guidelines.

The submission has not been previously published, nor is it before another journal for consideration (or an explanation has been provided in Comments to the Editor).

The submission file is in Microsoft Word document file (Times New Roman) format.

Where available, URLs for the references have been provided.

The text is single-spaced; uses a 11-point font; employs italics, rather than underlining (except with URL addresses); and all illustrations, figures, and tables are placed within the text at the appropriate points, rather than at the end.

The text adheres to the stylistic and bibliographic requirements outlined in the Author Guidelines, which is found in About the Journal.

If submitting to a peer-reviewed section of the journal, the instructions in Ensuring a Double-Blind Review have been followed.